DYNA

Journal of theFacultad de Minas, Universidad Nacional de Colombia - Medellin Campus
DYNA 91 (234), October - December, 2024 - ISSN 0012-7353

Imagen creada a partir de IA, en: https://designer.microsoft.com/image-creator

Facultad de Minas
Sede Medellín

UNIVERSIDAD NACIONAL DE COLOMBIA

DYNA
http://dyna.medellin.unal.edu.co/

DYNA is an international journal published by the Facultad de Minas, Universidad Nacional de Colombia, Medellín Campus since 1933. DYNA publishes peer-reviewed scientific articles covering all aspects of engineering. Our objective is the dissemination of original, useful and relevant research presenting new knowledge about theoretical or practical aspects of methodologies and methods used in engineering or leading to improvements in professional practices. All conclusions presented in the articles must be based on the current state-of-the-art and supported by a rigorous analysis and a balanced appraisal. The journal publishes scientific and technological research articles, review articles and case studies.

DYNA publishes articles in the following areas:

Organizational Engineering
Civil Engineering
Materials and Mines Engineering
Geosciences and the Environment
Systems and Informatics
Chemistry and Petroleum
Mechatronics
Bio-engineering
Other areas related to engineering

Publication Information

DYNA (ISSN 0012-73533, Printed; 2346-2183, online).
Is published by the Facultad de Minas, Universidad Nacional de Colombia, with a quarterly periodicity (January - March, April - June, July - September and October - December).
Circulation License Resolution 000584 de 1976 from the Ministry of the Government.

Contact information:
Web page: https://revistas.unal.edu.co/index.php/dyna
E-mail: dyna@unal.edu.co
Mail address:
Revista DYNA
Facultad de Minas
Universidad Nacional de Colombia - Medellín Campus
Carrera 80 No. 65-223 Bloque M9 - Of.:107
Telephone: (574) (604) 4255343
Medellín - Colombia

Notice
All statements, methods, instructions and ideas are only responsibility of the authors and not necessarily represent the view of the Universidad Nacional de Colombia. The publisher does not accept responsibility for any injury and/or damage for the use of the content of this journal.
The concepts and opinions expressed in the articles are the exclusive responsibility of the authors.

Institutional Exchange Request
DYNA may be requested as an institutional exchange through the e-mail: canjebib_med@unal.edu.co or to the postal address:

Biblioteca Central “Efe Gómez”
Universidad Nacional de Colombia, Sede Medellín
Calle 59A No 63-20
Teléfono: (574) (604) 430 97 86
Medellín - Colombia

Indexing and Databases

DYNA is admitted in:

The National System of Indexation and Homologation of Specialized Journals CT+I-PUBLINDEX, Category C

Science Citation Index Expanded
SCImago Journal & Country Rank - SJR
SCOPUS
SciELO Scientific Electronic Library Online
Chemical Abstract - CAS
Scientific Electronic Library on Line - SciELO
GEOREF
PERIÓDICA Data Base
Latindex
Actualidad Iberoaméricana
Redalyc - Scientific Information System
Directory of Open Acces Journals - DOAJ
PASCAL
CAPES
UN Digital Library - SINAB
EBSCO Host Research Databases

Publisher’s Office
Luz Alexandra Montoya Restrepo, Director
Mónica del Pilar Rada T., Editorial Coordinator
Catalina Cardona A., Editorial Assistant
Manuela González C., Editorial Assistant

Todograficas Ltda., Diagramming

Reduced Postal Fee
Tarifa Postal Reducida # 2014-287 4-72.
La Red Postal de Colombia, expires Dec. 31st, 2024

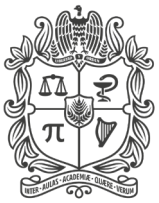

UNIVERSIDAD
NACIONAL
DE COLOMBIA

DYNA

DYNA
http://dyna.medellin.unal.edu.co/

Universidad Nacional de Colombia

DYNA
http://dyna.medellin.unal.edu.co/

Universidad Nacional de Colombia

Journal DYNA, 91 (234), October - December, 2024. Medellín. ISSN 0012-7353 Printed, ISSN 2346-2183 Online

CONTENTS

DYNA
http://dyna.medellin.unal.edu.co/

Universidad Nacional de Colombia

Our Cover
Image created with Artificial Intelligence AI at https://designer.microsoft.com/image-creator.

Authors
David Álvarez C., Designer - Todográficas Ltda.

DYNA
http://dyna.medellin.unal.edu.co/

Universidad Nacional de Colombia

Revista DYNA, 91 (234), Octubre - Diciembre. Medellín. ISSN 0012-7353 Printed, ISSN 2346-2183 Online

CONTENIDO

DYNA
http://dyna.medellin.unal.edu.co/

Universidad Nacional de Colombia

Nuestra carátula
Imagen creada con Inteligencia Artificial IA en https://designer.microsoft.com/image-creator.

Autores
David Álvarez C., Diseñador - Todográficas Ltda.

DYNA
http://dyna.medellin.unal.edu.co/

UNIVERSIDAD NACIONAL DE COLOMBIA

Production of hydroxyapatite from phosphoric rock

Gloria Soto-Calle [a], Adrián Gómez- Zapata [b], Néstor Rojas-Reyes [a] & Sandra Díaz-Bello [c]

[a] *Universidad Nacional de Colombia, Sede Medellín, Facultad de Minas, Instituto de Minerales -CIMEX, Medellín, Colombia. gmsotoc@unal.edu.co, nrrojasr@unal.edu.co*
[b] *Institución Universitaria Pascual Bravo, Facultad de Ingeniería, Medellín, Colombia. adrian.gomez@pascualbravo.edu.co*
[c] *Facultad de Ingeniería Ambiental- Grupo de investigación GICAN- CITECDES, Universidad Santo Tomás, Tunja, Colombia. sandra.diazb@usantoto.edu.co*

Received: March 6th, 2024. Received in revised form: May 29th, 2024. Accepted: June 7th, 2024.

Abstract
The article focuses on processes used to obtain hydroxyapatite from phosphate rock in the municipality of Pesca (Department of Boyacá, Colombia) by leaching with nitric acid. An analysis was carried out to evaluate the influence of different concentrations of leaching acid and treatment time on the recovery of phosphorus and calcium ions. The results indicated that maximum recovery of phosphorus and calcium ions was achieved by increasing concentration to 5M. The influence of the concentration of the precipitating agent was also analyzed and it was found that, although increased concentrations improve the pH adjustment rate, the purity of the HAp obtained decreases at higher concentrations, possibly due to the formation of other species associated with sodium hydroxide. Following washing with deionized water, pure HAp was obtained as a final product, which was characterized using XPR, XRD, SEM/EDS and FTIR.

Keywords: phosphate rock; acid leaching; hydroxyapatite.

Obtención de hidroxiapatita a partir de roca fosfórica

Resumen
El presente trabajo se centra en la obtención de hidroxiapatita (HAp) a partir de roca fosfórica proveniente del municipio de Pesca del departamento de Boyacá, por medio de la lixiviación con ácido nítrico. Se llevo a cabo un análisis para evaluar la influencia de la concentración del ácido lixiviante y el tiempo del tratamiento en la recuperación de iones de fósforo y calcio. Los resultados indicaron que al incrementar la concentración ácida hasta 5*M* se logró la máxima recuperación de dichos iones. También se analizó la influencia de la concentración del agente precipitador y se encontró que, si bien, el aumento en la concentración mejora la velocidad de ajuste del pH, se observa una disminución en la pureza de la HAp obtenida, esto posiblemente debido a la formación de otras especies asociadas al hidróxido de sodio. Después de un lavado con agua desionizada se obtuvo como producto final, HAp pura, la cual fue caracterizada por FRX, DRX, SEM/EDS y FTIR.

Palabras clave: roca fosfórica; lixiviación ácida; hidroxiapatita.

1 Introduction

Hydroxyapatite (HAp) is a calcium phosphate that, due to its composition and mechanical properties, is considered one of the most versatile and effective biomaterials with application, in particular, in bone tissue regeneration, in particular in dental coating and orthopedic devices [1,2]. However, its uses are not limited to these specific areas. Research has shown HAp to have potential applications in the fields of aesthetic medicine, water treatment filters and the manufacture of carbon dioxide sensors [3].

The most commonly used method in the manufacture of HAp is hydrothermal synthesis, which relies on using chemical precursors under basic pH conditions to precipitate HAp and its associated compounds from aqueous solutions enriched in phosphate (PO_4^{-3}) and calcium (Ca^{+2}) ions [3-5]. In the present work hydrometallurgical processes were used only.

Phosphorus pentoxide (P_2O_5) can be obtained from

How to cite: Soto-Calle, G., Gómez-Zapata, A., Rojas-Reyes, N., and Díaz-Bello, S., Production of hydroxyapatite from phosphoric rock. DYNA, 91(234), pp. 9-15, October - December, 2024.

phosphate rock (PR), which is considered to be the raw material for the production of elemental phosphorus (P) and other elements including calcium (Ca), sodium (Na) and magnesium (Mg) [6,7]. PR is generally found in the form of natural fluorapatite ($Ca1_0(PO_4)_6(F)_2$) in apatite deposits [8].

Generally, phosphoric acid is obtained by leaching PR to obtain P-enriched solutions [9,10]. Other elements, such as Ca, are also leached during this process, because of the nature of PR [11]. Leaching is a chemical process used to recover soluble substances; it frequently involves the use of acids to dissolve the components of interest [12]. Although PR deposits are the principal natural source used to extract elemental P, information on its processing as a raw material to obtain HAp remains scarce.

Some deposits with the capacity to support the exploitation of PR are found in Colombia. In 2022, the Colombian Geological Service (SGC) identified three areas of interest in the department of Boyacá [13].

The objective of this study is to establish a laboratory-based hydrometallurgical processing route by examining different leaching conditions for obtaining HAp from PR. These conditions include acid concentration levels and treatment time. In addition, an analysis was also carried out of the impacts of sodium hydroxide (NaOH) concentrations when used as agents for precipitating the species found.

2 Materials and methods

2.1 Materials

A sample of PR from the municipality of Pesca was prepared. The sample was crushed and ground to a particle size of less than 103 µm and then sieved to ensure that 80% of the total complied with the standardized granulometry. This sample was characterized chemically and mineralogically using Epsilon 13V 1.5 Malvern Panalytical X-ray fluorescence and Empyrean Panalytical XRD equipment respectively. The operating conditions for the latter were set for a sweep in the 2θ axis from 5° to 70° with steps of 0. 02° and a time of 0.5 s/step. In addition, Cu radiation with wavelength -λ- of 1.5406 Å was employed, along with X'pert High Score Plus software for data processing.

2.2 Leaching tests

The PR sample was subjected to leaching processes at laboratory scale, in solutions of nitric acid (HNO_3) between 2 and 7 M and leaching times of 24 h, in order to analyze the dissolution behavior of P and Ca ions as a function of the acid concentration. The leaching process was carried out in beakers with mechanical agitation at fixed speed and maintaining a constant 1/3 sample(solid)/solution(liquid) ratio. The P and Ca present in the acid leaching solution was analyzed using the semiquantitative XRF characterization technique.

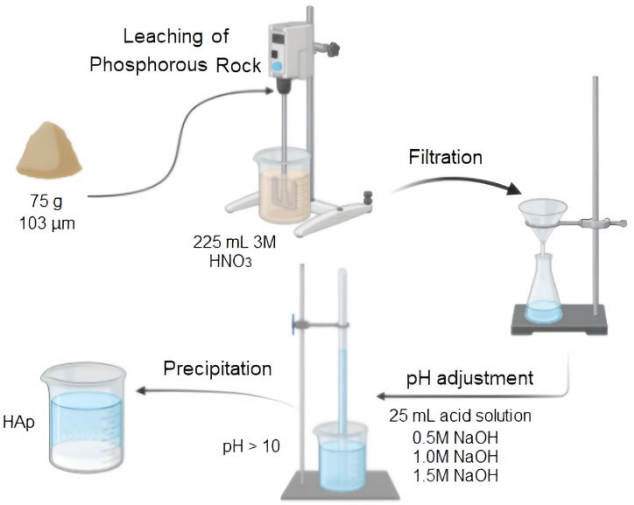

Figure 1: Schematic diagram of the process used to obtain hydroxyapatite from phosphate rock.
Source: the authors

2.3 Precipitation of HAp

NaOH solutions at concentrations of 0.5, 1 and 1.5 M were added as precipitating agents to 25 mL of the 3M HNO_3 solution obtained from the acid leaching of the PR, until a pH greater than 10 was reached (see Fig. 1). During the reaction, a precipitate forms as the alkalinity of the solution increases. Once the pH reached a desired value, the agitation was suspended. The product obtained, composed of a colorless liquid phase and a white solid phase, was left to stand for 24 h, after which the two phases were separated by filtration.

The solid phases were dried using a heating plate at a temperature of 70°C for 30 min. The samples obtained were labeled H05, H10 and H15 and prepared for XRF and XRD analysis. In this study, the reference samples obtained during the process were washed with deionized water in order to eliminate water-soluble species.

2.4 Characterization of the HAp

A compositional characterization of the samples obtained was carried out using XRF and an Oxford Instruments energy dispersive X-ray spectroscopy probe (EDS) coupled to a JEOL JSM-5910LV SEM. Structural characterization was carried out using XRD.

3 Results and Discussion

The different characterization techniques performed on the PR sample showed that the predominant species were fluorapatite (FA), which accounted for 59% of the total, quartz (Qz) with 34% and calcite (CaC) with 7%. The principal amplification peaks for each of these minerals are presented on the right side of Fig. 2. XRD analysis is semi-quantitative and assumes an error of approximately ±5% by

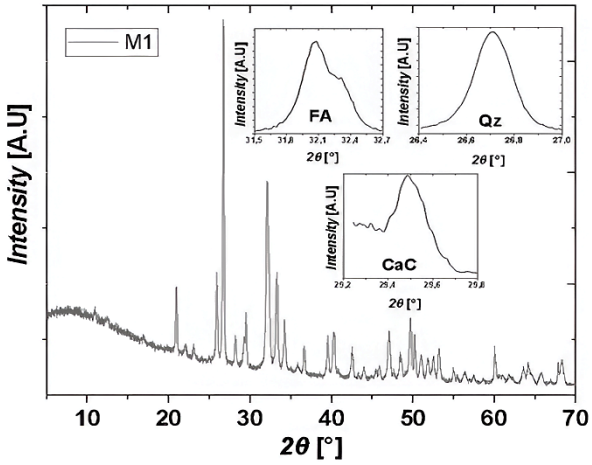

Figure 2. X-ray diffraction spectra for the PR sample. FA is fluorapatite, Qz is quartz and CaC is calcite.
Source: the authors

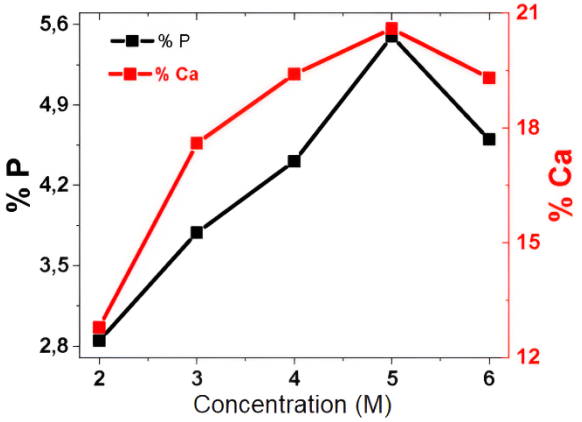

Figure 3. Extraction of P and Ca ions over 24 h at different acid concentrations.
Source: the authors

Table 1.
Elemental and oxide composition of the PR sample

Element	[%]	Oxide	[%]
P	13.44	P_2O_5	26.81
Ca	36.76	CaO	37.00
Si	12.48	SiO_2	25.67
Mg	3.54	MgO	6.89
Al	1.29	Al_2O_3	2.45
K	0.23	K_2O	0.21
Ti	0.09	TiO_2	0.09
Mn	0.02	MnO	0.02
Fe	1.06	Fe_2O_3	0.92

Source: the authors

weight. The elemental chemical analysis of the PR sample rendered the following percentages for P and Ca: 13.44% and 36.76%, respectively, with a P_2O_5 content of 26.81% and CaO content of 37%, as shown in Table 1. It should be noted that the error reported by the XRF equipment is less than 0.05%. The deposit may therefore be classified as a good source for the obtention of by-products with higher added value such as HAp. It is, in other words, a high-grade deposit [14].

3.1 Effects of acid concentrations

Fig. 3 presents the leaching behavior of P and Ca. The enriched solutions were analyzed using XRF. The PR sample showed an increase in the release of ions of interest when dissolved using concentrations of 2 to 5M HNO_3, with the highest extraction levels occurring at 5M. As the acid concentration of the solution increased above this value, recovery rates decreased, a finding that may be associated with the degree of solubility of the RP. Furthermore, increased concentrations did not result in higher levels of dissolution of P and Ca, possibly due to the formation of insoluble compounds that reduce the efficiency of the process. [15].

3.2 The effects of time

Fig. 4 shows that for periods exceeding 18 h, time has no significant effect on the leaching of P and Ca. It was determined that 18 h after the leaching process began, a leached fraction of 0.281 P was obtained in the solution, while at 48 h only a further 0.008 was obtained (X = M dissolved/M total, where M is P or Ca).

The behavior of Ca during extraction was similar to that of P, maximum recovery having occurred by 24 h (X = 0.466) and extraction remained stable after this time. It is probable that the reaction might reactivate the extraction of P and Ca. However, to validate this hypothesis the duration of the protocol would have to be extended, which might lead to the formation of insoluble compounds and further decrease the efficiency of the process. [15].

An upward tendency in the percentage of P and Ca ions, similar to that presented in Fig.s 3 and 4, was also reported by Tekin et al. (2001) [16] and Taha et al., (2013) [17], who studied the effects of ultrasound on the kinetics of the dissolution of PR in HNO_3 at molar concentrations between 0.01 and 0.1 M for durations of up to 5 min, and of PR from the western Abu Tartur Desert in the same acid at different agitation conditions.

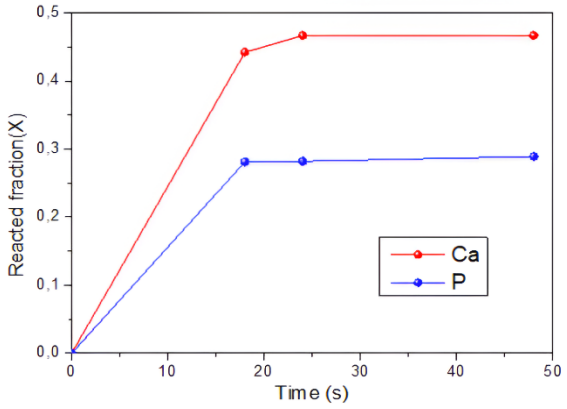

Figure 4. Dissolution of P and Ca ions in a 3 M HNO_3 solution.
Source: the authors

3.3 The effect of NaOH concentration on HAp precipitation

NaOH is a common and effective agent used to modify pH levels during the precipitation of HAp [9]. After varying the concentrations in order to adjust pH, XRD and XRF showed that increased concentrations favor the formation of sodium nitrate ($NaNO_3$), decreasing the percentage of P present in the precipitate. Table 2 presents the values, in % wt, of the results of the compositional analysis of the samples obtained from HAp, for NaOH concentrations of 0.5; 1 and 1.5 M, respectively.

The Ca/P molar ratio is close to 1.6 for the pure HAp species, a finding that makes it possible to establish potential uses it might be put to or the biological needs it could meet [18]. However, when the molar ratios for the samples obtained in the laboratory were calculated, the Ca/P ratio of 1.6 was not found, probably because of an excess of Ca, most likely associated with the presence of mineralogical species associated with this element. Thus, in order to enhance the use of these materials in biological applications, the Ca/P molar relation must be adjusted using additional processes.

The analysis of the crystalline phase of the HAp samples was performed using XRD assays. The diffraction spectra (diffractograms) for the powders, synthesized with different concentrations of NaOH, are presented in Fig. 5.

Fig. 5 shows the characteristic triple peak of monoclinic HAp, which is presented in the range of 31° to 33° in the 2θ axis with the main Miller indices (h k l) (221), (-222) and (-360), for the peaks, with intensities of 100, 52.6, and 61.4 %, respectively. Some studies have reported that in the monoclinic phase, HAp displays piezoelectric properties [20], which has led this species to be considered suitable for bone tissue regeneration, since it can remain electrically active and stimulate the tissues at a controllable rate [21,22].

Table 2.
Elemental analysis of HAp samples.

Element	Composition [%]		
	H05	H10	H15
P	13.01	10.21	12.71
Ca	37.68	34.62	37.88
Mg	6.83	6.22	7.00
Si	0.53	0.50	0.37
Al	0.54	0.41	0.47
Cl	0.22	0.22	0.21
Ti	0.01	0.01	0.01
Mn	0.02	0.01	0.01
Fe	0.34	0.262	0.28

Source: the authors

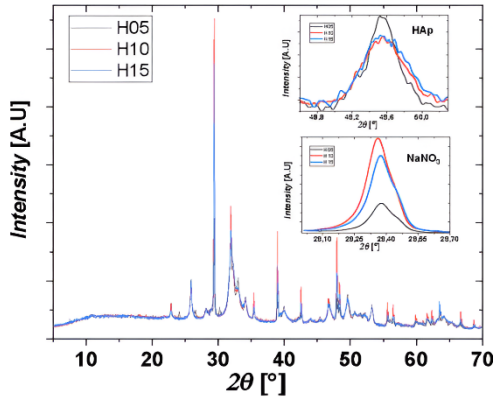

Figure 5. XRD spectra for the different HAp samples
Source: the authors

Table 3.
Mineralogical phases present in the synthesized samples (in percentages).

Phase	Percentage		
	H05	H10	H15
HAp	73	51	54
$NaNO_3$	27	49	46

Source: the authors

Table 4.
Network parameters for the patterns of the mineralogical phases found in the synthesized of hydroxyapatite samples.

Phase	Sample	Network parameters			
		Å			Å³
		a	b	c	V
HAp	H05 H10 H15	9.421	18.843	6.881	1057.96
$NaNO_3$	H05 (A)	5.070	5.070	16.820	374.43
	H10 (B)	5.070	5.070	16.829	374.63
	H15 (C)	5.072	5.072	16.835	375.08

Source: the authors

Table 3 reports the values, in percentages, for the two main mineralogical phases detected in the samples at the different molar concentrations at which they were treated. These phases correspond to HAp, which belongs to the monoclinic crystalline system (code 01-076-0694) in the database consulted [19] and $NaNO_3$, which belongs to the rhombohedral crystalline system (codes 01-076-2243 (A), 01-072-1213 (B) and 01-079-2056 (C)). Table 4 reports the values for the lattice parameters and unit cell volumes for each of the phases.

The data recorded in Table 4 indicate a slight variation in the lattice parameters for the $NaNO_3$ phase that leads in addition to a variation in the volume of the unit cell. This may be associated with the forces or intensity of the chemical interactions that occur during the reactions as the molarity of the solution increases.

The concentration of NaOH is an important variable, considering that there is a significant increase in the formation of $NaNO_3$ species and a decrease in the volume of the solution and the time required for pH conditions to adjust. This finding is evident in both the XRD and XRF results as the purity of the HAp obtained decreases.

3.4 Obtaining pure HAp

The solid phase product obtained was washed using deionized water in order to increase the purity of the HAp and increase the Ca/P ratio to bring it closer to a value of 1.6 for biological applications [23]. This is a figure informed by the percentages that favor the formation HAp and the fact that $NaNO_3$ is highly soluble in water. In the morphological analysis, polyhedral agglomerates of variable size and homogeneous diameter were observed. Fig. 6 shows an SEM image of the product obtained after the washing process.

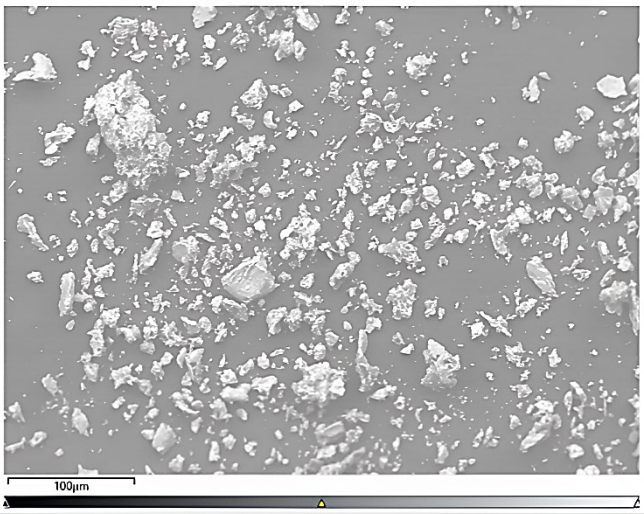

Figure 6. Powdered material obtained following washing with deionized water.
Source: the authors

Table 5.
Ca/P ratio for HAp sample.

Element	HAp sample	
	% weight	g/mol
Ca	54.39	40.08
P	24.75	30.97
Ca/P	1.7	

Source: the authors

The analysis of elemental composition showed P, Ca and Mg percentages of 16.140 %, 44.85 % and 7.40 %, respectively.

Fig. 7A) illustrates to the SEM/EDS analysis in in false-color scale for the elements found in higher concentrations in a particular part of the sample. Fig. 7B) gives the Ca distribution and Fig. 7C) gives the P distribution. The EDS data obtained for the Ca/P molar ratio are recorded in Table 5 shows the Ca/P ratio for HAp sample was 1.7, possibly because the HAp was calcium-rich [24]. There is evidence that the Ca/P molar ratio calculated from EDS data may lie in a range between 1.5 and 2.0. [24].

Fig. 8 shows the diffraction pattern of the HAp sample. It may be observed that following washing, the only detected species was HAp, in unaltered monoclinic phase, which displayed the characteristic triad in the peaks 31.77(1)°, 32.19(1)° and 32.90(6)°, corresponding to the Miller indices (h k l) (221), (-222) and (-360), respectively, of which an enlarged view is presented in the upper right section of the figure.

Fig. 9 illustrates the infrared spectrum, showing the fundamental bands of the principal hydroxyl (OH^-) and phosphate (PO_4^{-3}) groups of the HAp. The hydroxyl group is responsible for the bands centered around 630 cm^{-1} and 3,448 cm^{-1}. For the phosphate group, bands were present at 963 cm^{-1}, corresponding to a stretching vibration (1.046 cm^{-1} and 1.098 cm^{-1}) associated with asymmetric stretching, and 568 cm^{-1}, associated with bending vibration [26]. A very well-defined fringe was also observed at 1639 cm^{-1}, which is attributed to water absorption.

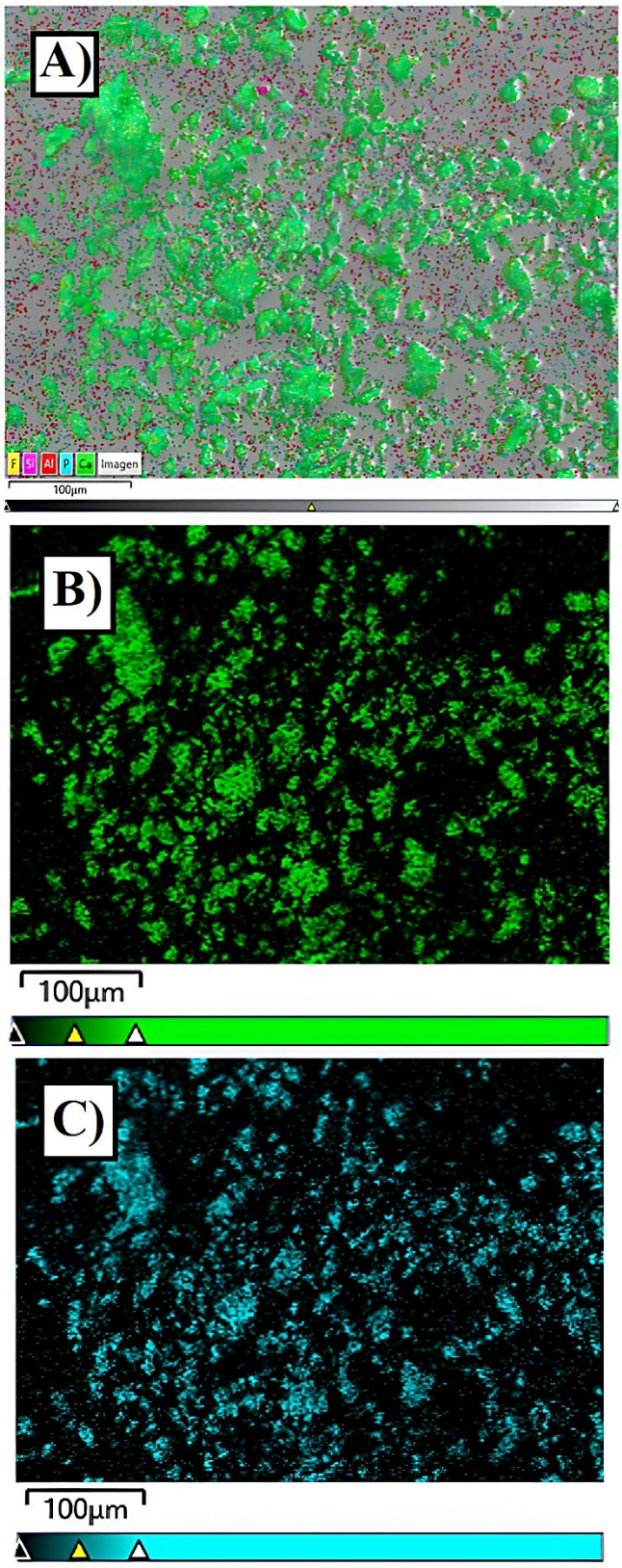

Figure 7. SEM/EDS images for HAp sample. A) False-colour map for F (yellow), Si (magenta), Al (red), P (turquoise) and Ca (green). B) False-colour map, green for Ca. C) False-colour map, turquoise for P.
Source: the authors

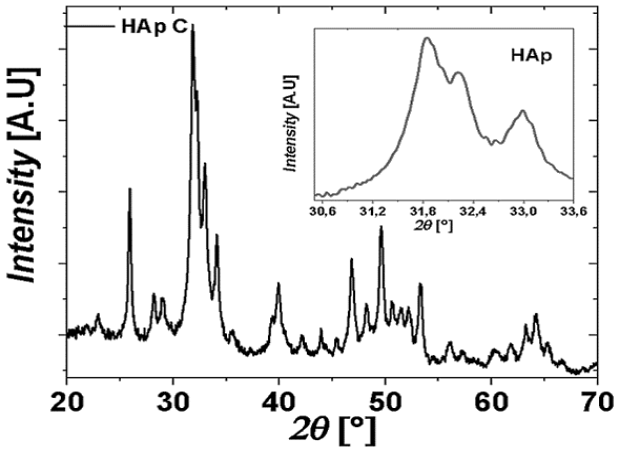

Figure 8. XRD spectra for the HAp sample following washing with deionized water.
Source: the authors

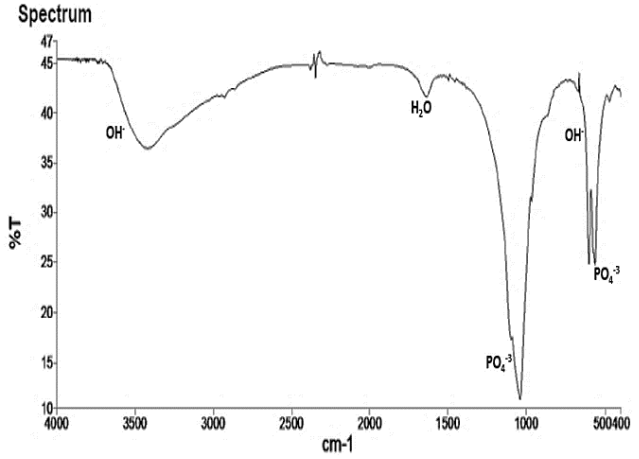

Figure 9. Infrared spectrum for the HAp sample
Source: the authors

4 Conclusion

This article has explored the potential of PR as a raw material for obtaining HAp by acid leaching of P and Ca ions, and their subsequent precipitation with NaOH. The analysis of P and Ca dissolution behavior permitted an evaluation of the availability of these elements in solution. It was observed that agitation time did not significantly affect the recovery of P and Ca. In addition, for acid solution concentrations higher than 5 M, it was not possible to obtain solutions enriched in the ions of interest. The results indicated that it was possible to obtain the species under the established conditions. However, the concentration of the precipitating agent influenced the purity of the HAp obtained.

The addition of NaOH solution above 0.5 M favored the formation of $NaNO_3$, a highly water-soluble compound. This property facilitates the cleaning of the species of interest by washing with deionized water. Adjustment of pH to values above 10 indicated that HAp is the most stable calcium phosphate under this condition. Although HAp is considered to be a high potential biomaterial, complementary studies should be carried out because of the nature of the rock. These should include long-term biocompatibility tests in order to determine the potential biological applications of this material obtained from PR.

Bibliography

[1] Garrido-Hernández, A., García-Domínguez, G., Reyes-Miranda, J., Camacho-González, M. A., Chávez-Güitrón, L., and Castillo-Minjárez J.M., Evaluation de la citotoxicidad de fosfatos de calcio sintetizados a diferentes relations molares de Ca/P por la vía hidrotermal. Pädi Boletín Científico de Ciencias Básicas e Ingenierías del ICBI, 10 (Esp.7), pp. 183-188, 2022. DOI: https://doi.org/10.29057/icbi.v10iEspecial7.9957

[2] Chávez, M.L., and Lourdes, Reyes, A.B., Síntesis por coprecipitation del bifosfato de calcio con base en hidroxiapatita y β-fosfato tricálcico. Revista Tendencias en Docencia e Investigation en Química. [online]. 5(5), pp. 355-361, 2019. [date of reference July 25th of 2023]. Available at: http://zaloamati.azc.uam.mx/bitstream/handle/11191/7843/Sintesis_por_coprecipitacion_2019.pdf?sequence=1&isAllowed=y

[3] Sánchez-Campos, D., Salado-Leza, D., Pérez-López, J.E., Rodríguez-Lugo, V., and Mendoza-Anaya, D., Curiosidades e implications tecnológicas de la hidroxiapatita sintética. Pädi Boletín Científico de Ciencias Básicas e Ingenierías del ICBI, 10(19), pp. 50-54, 2022. DOI: https://doi.org/10.29057/icbi.v10i19.9231

[4] Tamimi, F., Sheikh, Z., and Barralet, J., Dicalcium phosphate cements: Brushite and Monetite. Acta Biomaterialia, 8(2), pp. 474–487, 2012. DOI: https://doi.org/10.1016/j.actbio.2011.08.005.

[5] Le, H.R., Chen, K.Y., and Wang, C.A., Effect of pH and temperature on the morphology and phases of co-precipitated hydroxyapatite. J Solgel Sci Technol, 61(3), pp. 592–599, 2012. DOI: https://doi.org/10.1007/s10971-011-2665-7.

[6] Munir, M.U., Salman, S., Ihsan A., and Elsaman, T., Synthesis, characterization, functionalization and bio-applications of hydroxyapatite nanomaterials: an overview. Int. J. Nanomedicine. 2(17), pp. 1903-1925, 2022. DOI: https://doi.org/10.2147/IJN.S360670.

[7] Castro, L.N. and Melgar, R.J., Rocas fosfóricas. Capítulo Bolivia. Minerales para la Agricultura en Latinoamérica Capítulo III-3, Eds. Nielson y Sarudiansky Coordinadores Generales: Castro, L. y Melgar, R., 2005, pp. 74-82.

[8] Ptáček, P., Apatites and their synthetic analogues - synthesis, Structure, Properties and Applications. In: Tech, Apr. 13, 2016. DOI: https://doi.org/10.5772/59882.

[9] Avşar, C., and Gezerman, O., An evaluation of phosphogypsum (PG)-derived nanohydroxyapatite (HAP) synthesis methods and waste management as a phosphorus source in the agricultural industry. Medziagotyra, 29(2), pp. 247–254, 2023. DOI: https://doi.org/10.5755/j02.ms.31695.

[10] Bouchkira, I., Latifi, A.M., Khamar, L., and Benjelloun, S., Modeling and multi-objective optimization of the digestion tank of an industrial process for manufacturing phosphoric acid by wet process. Comput. Chem. Eng. 156, art. 107536, 2022. DOI: https://doi.org/10.1016/j.compchemeng.2021.107536.

[11] Ryszko, U., Rusek, P., and Kołodyńska, D., Quality of phosphate rocks from various deposits used in wet phosphoric acid and P-fertilizer production. Materials, 16(2), art. 20793, 2023. DOI: https://doi.org/10.3390/ma16020793.

[12] Calgaro, C.O., Tanabe, E.H., Bertuol, D.A., Silvas, F.P.C., Espinosa, D.C.R., and Tenório, J.A.S., Leaching processes. In: Veit, H., Moura Bernardes, A., eds., Electronic waste. Topics in mining, metallurgy and materials engineering. Springer, Cham., 2015. DOI: https://doi.org/10.1007/978-3-319-15714-6_5

[13] Martínez, G., Rojas, N., Terraza, R., Martín, C., and Rojas, S., Geological mapping for phosphate in the central region of the Eastern Cordillera, Department of Boyacá, Colombia. Boletín Geológico, 50(1), art. 666, 2023. DOI: https://doi.org/10.32685/0120-1425/bol.geol.50.1.2023.666

[14] Hikmet-Sengul, A., Kadir-Ozer, M., and Sahin G., Beneficiation of

Mardin-Mazıdağı (Turkey) calcareous phosphate rock using dilute acetic acid solutions. Chemical Engineering Journal. 122(3), pp. 135-140, 2006. DOI: https://doi.org/10.1016/j.cej.2006.06.005.
[15] Argotte-Ibarra, L., Barreiro-Quino, O.F., Ríos-Reyes, C.A., Henao-Martínez, J.A. and Castro-Salazar, H.T., Analysis of the solubility of phosphate rock from Aipe (Colombia) via formation of 2Na-EDTA complex. Chemosphere, 286(3), art. 131786, 2022. DOI: https://doi.org/10.1016/j.chemosphere.2021.131786.
[16] Tekin, T., Tekin, D., and Bayramoğlu, M., Effect of ultrasound on the dissolution kinetics of phosphate rock in HNO_3. Ultrasonics Sonochemistry, 8(4), pp. 373-377, 2001. DOI: https://doi.org/10.1016/S1350-4177(00)00078-X
[17] Taha, M.H., Aly, H.F., and Aly, M.M., Dissolution kinetics of western deseret phosphate rocks, Abu Tartur with hydrochloric acid. Arab Journal of Nuclear Science and Applications. [online]. 46(5), pp. 1-16, 2013. [date of reference July 25th of 2023]. Available at: https://www.researchgate.net/publication/309900618_Dissolution_kinetics_of_Western_Desert_phosphate_rocks_Abu_Tartur_with_hydrochloric_acid
[18] Guastaldi, C., and Herrera-Aparecida, A., Fosfatos de cálcio de interesse biológico: importância como biomateriais, propriedades e métodos de obtenção de recobrimentos. Revisão Quím. Nova 33(6), art. 600025, 2010. DOI: https://doi.org/10.1590/S0100-40422010000600025
[19] International Centre for Diffraction Data. PDF-2, [online]. 2007. [date of reference Jan. 10th of 2024]. Available at: https://www.icdd.com/
[20] Lang, B.S., Tofail, S.M.A., Gandhi, A.A., Gregor, M., Wolf-Brandstetter, C., Kost, J., Bauer, S., and Krause, M., Pyroelectric, piezoelectric, and photoeffects in hydroxyapatite thin films on silicon. Appl. Phys. Lett., 98(2), art. 123703, 2011. DOI: https://doi.org/10.1063/1.3571294.
[21] Shi, H., Zhou, Z., Li, W., Fan, Y., Li, Z., and Wei, J., Hydroxyapatite based materials for bone tissue engineering: a brief and comprehensive introduction. Crystals, 11(2), art. 149, 2021. DOI: https://doi.org/10.3390/cryst11020149
[22] Huerta, V., Influencia de los defectos cristalinos en las propiedades opto-eléctricas de nanocintas de hidroxiapatita. Tesis de Doctorado en Ciencias. Centro de Investigation Científica y de Education Superior de Ensenada, Baja California. [online]. 2023. [date of reference Dec. 20th of 2023]. Available at: http://cicese.repositorioinstitucional.mx/jspui/handle/1007/3858
[23] Rojas, E., Simulación y caracterización experimental de las propiedades vibracional óptico no lineal Glicina nitrado de sodio. Tesis de Licenciatura. Departamento de Física, Universidad de Sonora, México, [online]. 2011. [date of reference Jul. 10th of 2023]. Available at: http://hdl.handle.net/20.500.12984/8067
[24] Prihanto, A., Muryanto, S., Ismail, R., Jamari, J., and Bayuseno, A.P., Batch hydrothermal synthesis of nanocrystalline, thermostable hydroxyapatite at various pH and temperature levels. Inorg. Chem. Commun. 157, art. 1301, 2023. DOI: https://doi.org/10.1016/j.inoche.2023.111301.
[25] Akram, M., Ahmed, R., Shakir, I., Ibrahim, W.A., and Hussain, R., Extracting hydroxyapatite and its precursors from natural resources. Journal of Materials Science, 49(4), pp. 1461–1475, 2014. DOI: https://doi.org/10.1007/s10853-013-7864-x.
[26] Mirta, M., Lima-Leite, F., Sérgio de Paula, P., Luiz-Pissetti, F., Malta-Rossi, A., Lima-Moreira, E., and Primerano-Mascarenha Y., XRD, AFM, IR and TGA study of nanostructured hydroxyapatite. Mat. Res. 15(4), art. 5000069, 2012. DOI: https://doi.org/10.1590/S1516-14392012005000069

G.M. Soto-Calle, is a BSc. Eng.in Mining and Metallurgical Engineering and is a Master's student in Materials and Process Engineering from the Universidad Nacional de Colombia, Medellín campus. She belongs to the research group at the CIMEX Minerals Institute at the same university. Her research interests focus on mining safety and extractive metallurgy. ORCID: ORCID: 0009-0007-4175-2208.

A.A. Gómez-Zapata, is an Industrial Instrumentation Technologist and BSc. Eng. in Instrumentation and Control Engineer all of them from the Politécnico Colombiano Jaime Isaza Cadavid, Medellín, Colombia. He has a MSc. and PhD in Engineering, Materials and Processes, and Materials Science and Technology from the Universidad Nacional de Colombia, Medellín campus. He is an Occasional Full Time Professor at the Institutción Universitaria Pascual Bravo, Medellín. He is particularly interested and experienced in the synthesis and characterization of nanostructured materials for applications in energy, mining, biomaterials, alternative energies, agro-industrial waste, environmental and -in general- the solution or mitigation of negative environmental effects.
ORCID: 0000-0002-3536-1629

N.R. Rojas-Reyes, is a BSc. Eng. in Metallurgical Engineering from the Universidad Pedagógica y Tecnológica de Colombia. He earned his MSc. in Engineering Sciences, with a specialization in Extractive Metallurgy, from the Universidad de Concepción, Chile, and completed his DSc. in Engineering Sciences with a focus on Materials Science at the Universidad Nacional de Colombia. He is currently a Full Professor at the Universidad Nacional de Colombia, Medellín campus, and is a researcher at the CIMEX Mineral Institute. His research interests encompass the characterization of minerals, the hydrometallurgy of precious metals, the recovery of metals from waste materials, and the rheology of mineral suspensions.
ORCID: 0000-0002-1644-471X.

S.C. Díaz-Bello, is BSc. Eng. in Metallurgical Engineering from the Universidad Pedagógica y Tecnológica de Colombia, Tunja, Colombia. She has a MSc. in Metallurgy and Materials science and a PhD in Engineering, Materials Science and Materials Technology. She teaches in the Faculty of Environmental Engineering and is a member of the CIGAN research group, all at the Universidad Santo Tomás, Tunja, Colombia. Her research focuses on new construction materials, renewable energies, circular economies and extractive metallurgy.
ORCID: 0000-0002-8114-6655

DYNA
http://dyna.medellin.unal.edu.co/

UNIVERSIDAD NACIONAL DE COLOMBIA

Synthesis and evaluation of the antibacterial activity of Cu(II) and Ni(II) complexes with mixed ligands based on glycine and dicarboxylic acids

Luisa Fernanda Múnera-Gómez [a], Juan Carlos Muñoz-Acevedo [b] & Elizabeth Pabón-Gelves [a]

[a] *Universidad Nacional de Colombia, Sede Medellín, Facultad de Ciencias, Departamento de Química. Medellín, Colombia. lfmunerag@unal.edu.co, epabon@unal.edu.co*
[b] *Instituto de Química. Universidad de Antioquia, Medellín, Colombia. juan.munoz1@udea.edu.co*

Received: December 15th, 2023. Received in revised form: June 21st, 2024. Accepted: July 5th, 2024.

Abstract
A large number of metal complexes have the ability to inhibit bacterial growth. Cu(II) and Ni(II) complexes based on glycine (Gly), itaconic acid (Ita), and oxalic acid (Ox) were synthesized by conventional methods and evaluated for their antibacterial activity. The metal complexes were characterized by TGA, FTIR, UV-vis spectroscopy, and XRD. The metal: ligands ($M:L_1:L_2$) stoichiometry of these complexes is 1:2:2, and coordination around Cu(II) and Ni(II) seems to be octahedral, with the ligands bound through the N atom of the amino group and O atoms of the bridging carboxylate group. These compounds are crystalline and stable at temperatures between 250 to 300°C. The metal complexes were screened for their antibacterial activity against the bacterial species *Staphylococcus aureus*, *Bacillus cereus*, *Listeria monocytogenes*, *Salmonella*, and *Escherichia coli*. These compounds were shown to have antibacterial activity mainly against gram-positive strains, with a minimum inhibitory concentration of 20 ppm.

Keywords: complexes; amino acids; glycine; itaconic acid; oxalic acid.

Síntesis y evaluación de la actividad antibacteriana de complejos de Cu(II) y Ni(II) con ligandos mixtos basados en glicina y ácidos dicarboxílicos

Resumen
Un gran número de complejos metálicos tienen la capacidad de inhibir el crecimiento bacteriano. Se sintetizaron complejos de Cu(II) y Ni(II) basados en glicina (Gly), ácido itacónico (Ita) y ácido oxálico (Ox) mediante métodos convencionales y se evaluó su actividad antibacteriana. Los complejos metálicos se caracterizaron por TGA, FTIR, espectroscopia UV-vis y XRD. La estequiometría metal:ligandos ($M:L_1:L_2$) de estos complejos es 1:2:2, y la coordinación alrededor de Cu(II) y Ni(II) parece ser octaédrica, con los ligandos unidos a través del átomo de N del grupo amino y los átomos de O del grupo carboxilato puente. Estos compuestos son cristalinos y estables a temperaturas entre 250 y 300°C. Los complejos metálicos se probaron para su actividad antibacteriana contra las especies bacterianas *Staphylococcus aureus*, *Bacillus cereus*, *Listeria monocytogenes*, *Salmonella* y *Escherichia coli*. Estos compuestos demostraron tener actividad antibacteriana principalmente contra cepas gram-positivas, con una concentración mínima inhibitoria de 20 ppm.

Palabras clave: complejos; aminoácidos; glicina; ácido itacónico; ácido oxálico.

1 Introduction

Metal complexes with biological ligands are of great interest since they allow us to find new alternatives to combat and/or control diseases [1]. Aminoacids (AA) are molecules of great importance for human health; they are necessary for the formation of proteins that allow the organism to carry out fundamental activities such as tissue repair, metabolic

How to cite: Múnera-Gómez, L.F., Muñoz-Acevedo, J.C., and Pabón-Gelves, E., Synthesis and evaluation of the antibacterial activity of Cu(II) and Ni(II) complexes with mixed ligands based on glycine and dicarboxylic acids. DYNA, 91(234), pp. 16-23, October - December, 2024.

processes, growth, and energy production, among others. These biomolecules used as ligands have become an attractive alternative to synthesize metal complexes, as they provide high biological activity and are biocompatible and safe for the organism [2,3]. Complexes derived from different AA are used as antibacterial, antifungal and antioxidant agents [4,5]. The use of AA theoretically allows the use of any of them since they have two functional groups that can interact with the metal. Glycine (Gly) is the simplest aminoacid that has facilitated the study of metal-ligand interactions and the determination of the parameters that affect the formation of stable compounds. Likewise, the aminoacids methionine and cysteine have been used as ligands to enhance the antioxidant capacity and the use of histidine has allowed the polymerization of the chain in 2D and 3D [6,7]. The AA in complexes improved antibacterial activity against various strains of health concern, mainly those associated with foodborne diseases and water pollution [8]. However, the use of AA as the only ligand implies in most cases, that the complexes have low thermal stability and form 1D or 2D networks [9,10], very few complexes using only AA have the ability to form 3D networks and these mostly achieved with aromatic AA that allow the formation of hydrogen bonds to form supramolecular networks [11]. The use of ancillary ligands in metal complexes with AA is a necessary route to improve the properties exhibited by the compounds with AA, which degrade at temperatures between 150 to 250°C [12]. Dicarboxylic acids are used as ancillary ligands that act as a bridge between metal cations, which in theory allows improving the structural properties of the complex. Additionally, the functional groups that these acids contain can confer other chemical properties to the complex [13] Cao et al. (2020) used Ag(I) and 1,4-benzenedicarboxylic acid (BDC or terephthalic acid) to synthesize complexes with activity against oral bacterial strains [14]. The sustained release of ions is related to the chemical stability possessed by the complex due to the two -COOH groups that bind to the metal and extend the network. The use of pyridin-3,5-dicarboxylic acid with Ag (I) was studied by Alisir et al. (2015), the thermal stability of the synthesized complex was 190°C showing antibacterial activity against a wide variety of gram-positive and gram-negative strains, the complex showed reduced activity against fungi such as *Candida albicans* [15]. Meanwhile, Lucena et al. (2018) succeeded in synthesizing a porous complex for the transport and subsequent release of diclofenac sodium from Zn(II), biphenyl-4,4'-dicarboxylic acid and adenine linkers. It has been shown that drug delivery systems integrating biological components can be used to reduce adverse effects due to biological compatibility [16]. Undoubtedly, dicarboxylic acids are ligands that allow obtain complexes with a wide variety of properties, also improve thermal stability and dimensionality, while presenting good antibacterial activity against a wide variety of species of clinical and industrial interest [8,17,18]. The use of biological molecules helps to generate greater stability and compatibility with living systems. Because of these properties, the use of dicarboxylic acids and AA in metal complexes can improve the antibacterial activity against a wide variety of pathogenic species. Cu and Ni complexes with amino acids as single ligands have been shown to have antibacterial activity, greater stability and faster and more efficient syntheses. In contrast, other metals such as Zn, Ag and Co, although they have good antibacterial activity, have synthesis methods that are less efficient, more polluting and yield lower amounts [25].

In the present study, four complexes with Cu(II) and Ni(II) metal cations were synthesized using glycine (Gly) as amino acid and oxalic (Ox) and itaconic (Ita) acids as ligands, in order to determine their antibacterial properties. For this purpose, the antibacterial activity and the minimum inhibitory concentration (MIC) of the complexes against several gram-positive and gram-negative species were evaluated.

2 Experimental

2.1 Materials and reagents

All chemicals used were of the analytical reagent grade without further purification. $Cu(CH_3COO)_2H_2O$ >98%, $Ni(CH_3COO)_2$ $4H_2O$ >98%, NaOH 0.1 M 98%, methanol were acquired from Merck; itaconic acid 99% (Sigma-Aldrich); glycine 99.5%, oxalic acid 99% and pure absolute ethanol 99.5% were obtained of PanReac.

2.2 Synthesis of the metal complexes

A schematic of the synthesis procedure can be seen in Fig. 1, which was carried out following a molar ratio $M:L_1:L_2$ 1:2:2, where ligand 1 (L_1) is the amino acid and ligand 2 (L_2) is the dicarboxylic acid. The procedure is as follows: a mixture of copper acetate monohydrate or nickel acetate tetrahydrate in deionized water was heated at 70°C in a water bath for about 15 min with constant stirring. A small amount of ethanol was added to help with the homogenization of the solution and then the AA was incorporated.

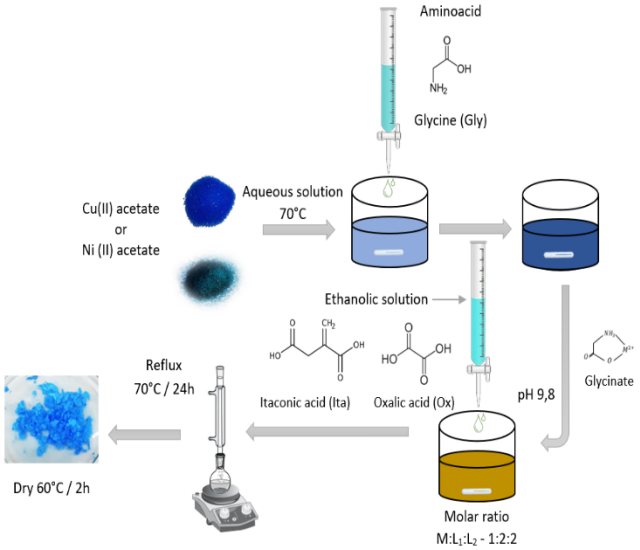

Figure 1. Scheme of the synthesis of metal complexes $M:L_1:L_2$
Source: Self-made image

The reaction mixture was left in agitation under controlled temperature (not exceeding 70°C). After approximately five minutes the formation of blue crystals could be appreciated. The pH was adjusted to 9.8 with the addition of 0.1M NaOH to obtain the glycinate species. Subsequently, an ethanolic solution with dicarboxylic acid (Ita or Ox) was added, preferably at 70°C to avoid thermal shock with the solution containing the AA, and stirred for 10 minutes. The solution was transferred to a two-necked round-bottom balloon and the system was refluxed at 70°C for 24 hours. Finally, after the reaction time, the system was filtered, dried at 60°C for 2 hours and finally stored for further analysis

2.3 Antibacterial activity

The standardized diffusion method in semi-solid agar wells was followed to evaluate the antimicrobial activity of the synthesized compounds against gram-positive ATCC bacteria: *Staphylococcus aureus, Bacillus cereus* and *Listeria monocytogenes* and gram-negative species: *Salmonella* and *Escherichia Coli*. The species were cultured at 37 °C for 24 h in nutrient broth. The cultures were adjusted with the McFarland standard and the petri dishes were prepared with 20 mL of the semisolid culture Müller Hinton (MH) and 50 µL of pathogen. In the petri dishes, 10 mm diameter wells were made to deposit the coordination compounds and the positive (oxytetracycline) and negative (peptone water) controls. The concentrations of the compounds were 5 mg/L, 10 mg/L and 15 mg/L. The cultures were incubated at 37 °C for 48 h, subsequently the diameter of the inhibition zone was measured to compare it with that of the antibiotic disks. The minimum inhibitory concentration (MIC) test was performed in a 96-well plate with the compounds that showed antibacterial activity against any of the strains studied. The technique used was half dilutions analyzing concentrations of 20 to 5 mg/L in duplicate. The bacteria were placed in liquid MH medium and shaken at 37 °C for 25 h. The growth of the pathogen was taken as a target. To adjust the McFarland standard to 106 CFU/mL (CFU= colony forming units) and the contamination controls of the medium and the compounds were carried out in duplicate [19]. The MIC values were determined in a UV-Vis spectrometer by the optical density method at 620 nm (OD_{620}), the bacterial growth curves were determined by scheduling readings every hour. All OD_{620} data were the average values of duplicate tests [20].

2.4 Characterization

The thermogravimetric analysis (TGA) was carried out on the TA Instruments model SDT 650 with a nitrogen atmosphere (20 mL/min), a heating ramp of 10 °C/min and a temperature range of 25 °C to 600 °C. The samples did not require additional preparation to the drying performed in the synthesis method. The infrared spectra of the coordination compounds were obtained on the Perkin Elmer Spectrum two series 93881 IR spectrometer equipped with an ATR diamond crystal performing 16 scans in a range between 4000 to 400 cm^{-1}. The UV-Vis studies of the coordination compounds were carried out in the Boeco S-220 spectrophotometer in a range between 200 to 900 nm. For measurement in the visible range, solutions of the compounds were prepared at a concentration of 0.002 M in methanol. While, for the measurement in the ultraviolet range, the concentrations were 0.001 M. The diffractograms were obtained on a Malvern-PANalytical device model Empyrean 2012 with Pixel 3D detector and Cu source (λ=1.541874 Å) at 40 kV and 40 Ma, Goniometer: Omega/2θ and platform configuration: Reflection transmission spinner rotating at 4 rpm. The step was 0.05° and a time per step was 50 s. Scanning electron microscopy images were taken on the JEOL JSM-5910LV equipment.

3 Results and discussion

3.1 Characterization of metal complexes

Four metal complexes were synthesized, Cu-Gly-Ita, Cu-Gly-Ox, Ni-Gly-Ita and Ni-Gly-Ox. The synthesis method was described in Fig. 1 following a 1:2:2 molar ratio $M:L_1:L_2$. The SEM images (Fig. 2) of some of these compounds show acicular crystals for the compounds with copper and laminar crystals for the compounds with nickel. It is also observed that the copper compounds are larger compared to the nickel compounds and have smooth and uniform surfaces.

Fig. 3 shows the thermal analysis of the complexes synthesized. The complex with itaconic acid Cu-Gly-Ita loses coordination waters around 150 °C, this generates a mass loss that does not exceed 10%. Subsequently, the complex remains stable up to 250 °C, at this temperature the degradation of the amino acid begins, generating a mass loss of approximately 40%, finally the respective metal oxide is obtained. On the other hand, the complex with oxalic acid Ni-Gly-Ox reaches temperatures close to 200°C before releasing coordination water. In this case, the released water generates a mass loss of 20%, slightly more than twice the mass lost by the Cu-Gly-Ita complex. The complex with oxalic acid remains stable up to 335°C, temperature at which the degradation of the amino acid begins. According to the studies reported by Sevgi F. et al (2018), the decomposition

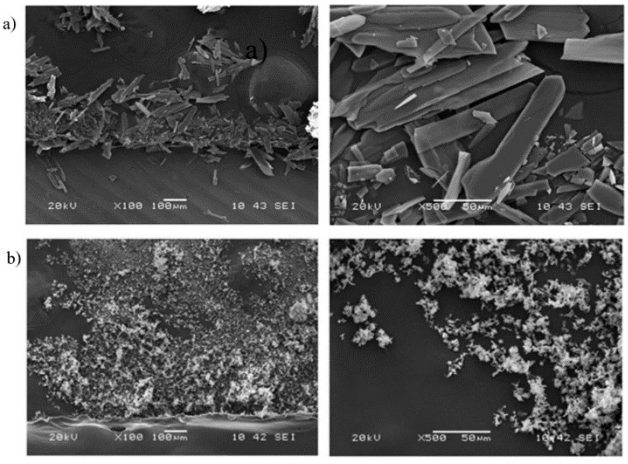

Figure 2. SEM images for a) Cu-Gly-Ita and b) Ni-Gly-Ita
Source: Self-made image

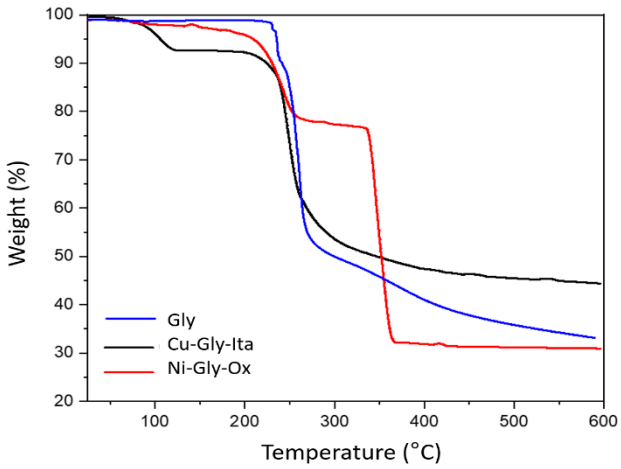

Figure 3. TGA of some selected metal complexes
Source: Self-made image

of Schiff base complexes from glycine and phenylalanine with copper and nickel occurred in three stages, loss of coordination waters between 100-180°C, degradation of the organic part between 320-360 °C and between 360-400 °C degradation of aromatic units [21]. For the complexes reported in this study, the third step is not expected, however, the temperature ranges for the other processes are very similar with those found in the literature. On the other hand, it can be observed that for processes requiring temperatures above 200 °C, it is ideal to use a complex having oxalic acid. It can also be observed that these complexes are more efficient because up to 80% of the material can be used, which is not the case with complexes synthesized with itaconic acid, of which only 50 to 60% can be used.

The FTIR spectra (Fig. 4) shows defined bands between 3400 to 3200 cm^{-1} characteristics for the frequencies of the NH_2 amino group of amino acids due to the asymmetric and symmetric tension of the N-H bonds [22]. The shifts in the carboxyl bands that are between 1700 and 1400 cm^{-1} (Table 1) allow determining a change in the coordination environment due to the interactions of this functional group with the metal. Additionally, the difference between the asymmetric and symmetric vibrations of the carboxyl (Δv $COOH_{as-s}$) shows the way in which the ligand is bonded to the metal. Glycine has a Δv of 99 cm^{-1}, which allows predicting for the amino acid a monodentate coordination of the carboxyl group, the amino group is also linked to the metal since the characteristic M-N bands can be seen in the region between 400 to 600 cm^{-1} [23,24]. This allows us to establish that Gly binds to the metal through the two active sites, evidencing the successful formation of the glycinate complex in the step after adjusting the pH during the synthesis. Moreover, itaconic and oxalic acids have a Δv of 101 cm^{-1} and 72 cm^{-1} respectively; this indicates that the ancillary ligands also bind to the metal in a monodentate manner, leaving a carboxyl group free to bridge with another unit neighbor. Köse D. et al (2016) reported for the complex formed with the metals Co, Ni, Cu and Zn with the ligand glycine, the carboxyl of the amino acid also acts in a monodentate manner, and the bands reported by them for the main groups are also seen in this study [25]. The changes occur mainly in the vibrations of the -COOH groups which in the case of this study, by having the ancillary ligand (Ita or Ox) competing to bind to the metal, generate displacements and changes in the environment coordination.

The XRD pattern (Fig. 5), shows that the four complexes are crystalline, as evidenced by the sharp peaks. All the compounds appear as dense phases. Tipically, peaks below 10° are indicators of possible micropores, however, this behavior is not observed in any of these compounds. [26–28].

In the UV-Vis spectra for the complexes with Cu(II), a single absorption band of *d-d* transitions was observed (Fig. 6a), for the Cu-Gly-Ita complex the transition is ($^2E_g \rightarrow {}^2T_{2g}$) 15576 cm^{-1} (642 nm). However, the Cu-Gly-Ox complex presents several bands that overlap each other in the region

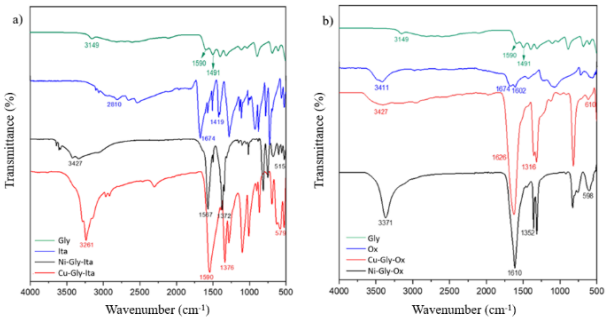

Figure 4. FTIR spectra of the metal complexes a) Cu-Gly-Ita; Ni-Gly-Ita and b) Cu-Gly-Ox; Ni-Gly-Ox
Source: Self-made image

Table 1.
Most representative vibration modes in cm^{-1} of the IR spectrum of the synthesized metal complexes

Assignation	*Gly*	*Ita*	*Ox*	*Cu-Gly-Ita*	*Cu-Gly-Ox*	*Ni-Gly-Ita*	*Ni-Gly-Ox*
$vas\,NH_2$	3153	--	--	3261	3427	3427	3371
$vas\,COO^-$	1590	1674	1674	1590	1626	1567	1610
$vs\,COO^-$	1491	1573	1062	1376	1316	1372	1352
$v\,C-N$	1020	--	--	1140	1112	1009	909
$v\,M-N$	--	--	--	579	610	515	598
$\Delta V\ COOH_{as-s}$	99	101	72	214	310	195	258

Source: Self-made table

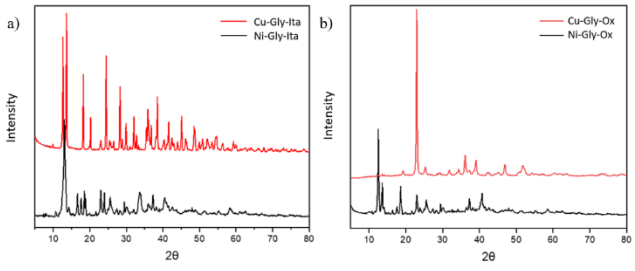

Figure 5. DRX pattern of the metal complexes a) Cu-Gly-Ita, Ni-Gly-Ita and b) Cu-Gly-Ox, Ni-Gly-Ox
Source: Self-made image

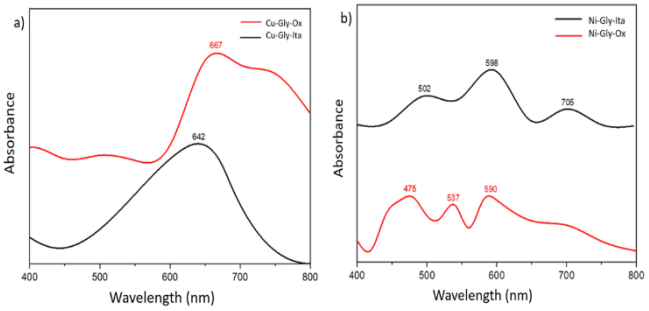

Figure 6. UV-Vis spectra of metal complexes. a) Cu-Gly-Ita and Cu-Gly-Ox. b) Ni-Gly-Ita and Ni-Gly-Ox
Source: Self-made image

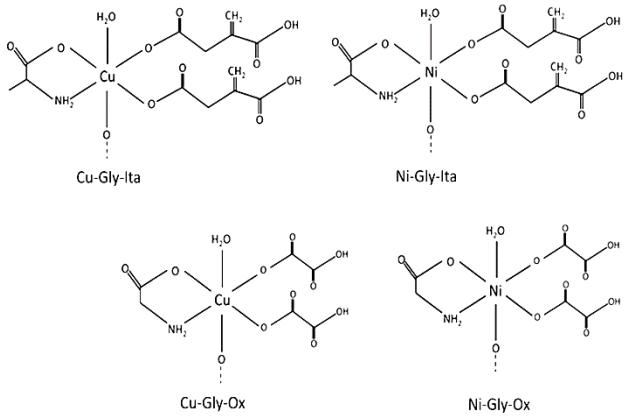

Figure 7. Proposed structures of metal complexes
Source: Self-made image

between 22123 and 13333 cm^{-1} (452 and 750 nm), according to Köse D. et al (2016) this is due to that Cu(II) complexes present octahedra distorted by the Jahn-Teller effect and the structure of the complex is pseudo-octahedral [25]. In these cases, the upper peak is designated as the absorption band and the d-d transition is set ($^2E_g \rightarrow {}^2T_{2g}$) 14992 cm^{-1} (667 nm). On the other hand, for the Ni-Gly-Ita and Ni-Gly-Ox complexes, three absorption bands of d-d transitions were observed (Fig. 6b). The first transition ($^3A_{2g} \rightarrow {}^3T_{2g}$)(F) 19920 and 21052 cm^{-1} (502 and 475 nm), the second transition ($^3A_{2g} \rightarrow {}^3T_{1g}$)(F) 16722 and 18621 cm^{-1} (598 and 537 nm) and the last transition ($^3A_{2g} \rightarrow {}^3T_{1g}$)(P) 16949 and 14184 cm^{-1} (590 and 705 nm) respectively. All transitions are low energy (from 400 nm onwards) which indicates interactions between *d* orbitals of transition metals or between orbitals of metals and ligands, as is the case.

Based on the characterization studies, the possible structures (Fig. 7) of the synthesized complexes can be proposed. The FTIR spectra showed the characteristic vibrations between the metal and the nitrogen or oxygen atoms of the amino acids and dicarboxylic acids; it was also possible to establish the coordination mode of the carboxyl group. The UV-Vis spectra allowed us to determine that the coordination environments are distorted octahedral for the complexes with copper and octahedral for the complexes with nickel due to the low energy signals obtained in the range of 400 to 900 nm that indicate interactions between *d* orbitals or between metal and ligand, as is the case.

3.2 Antibacterial activity of metal complexes

The synthesized metal complexes were tested against five bacterial species including gram-positive genera: *Staphylococcus aureus, Bacillus cereus* and *Listeria monocytogenes* and gram-negative genera: *Salmonella* and *Escherichia* Coli. The activity was determined by measuring the zone of inhibition. The Ni-Gly-Ox complex did not present inhibition against the genera under study and the Cu-Gly-Ox complex only presented activity against *Listeria*. As mentioned before, all synthesized complexes are dense phases; the antibacterial activity of the complexes occurs by diffusion of ions of the respective metal [29,30]. If the complex is very dense, it interferes with the release of the ions, which directly affects the antibacterial capacity. In contrast, complexes with itaconic acid presented good activity against 4 of the 5 genera under study (Table 2). The Ni-Gly-Ita complex did not show activity against *Staphylococcus aureus* and its maximum activity was against *Listeria*. On the other hand, the complexes synthesized with copper presented better activity against the bacterial genera under study. Notably the compound Cu-Gly-Ita showed significant activity against *Listeria monocytogenes.* This bacterium causes serious diseases due to the consumption of foods contaminated with this pathogen. Listeriosis can cause septicemia, meningitis, encephalitis, pneumonia and intrauterine or cervical infection in pregnant women that can lead to spontaneous abortion [31].

In general, the best activity was against gram-positive species. This is because bacteria of this type do not have an outer membrane, which facilitates the penetration of metal ions through the peptidoglycan, causing cell lysis and subsequent bacterial death. In contrast, gram-negative bacteria have an outer membrane that provides an extra

Table 2.
Antibacterial activity of metal complexes

Compounds	Antibacterial activity (Zones of inhibition in cm)						
	Bacillus	*Staphylococcus*	*E. coli*	*Salmonella*	*Listeria*	*Control +*	*Control -*
Cu-Gly-Ita	0.60±1.00	0.50±1.00	1.00±1.00	0.60±1.00	2.00±1.00	3.00±1.00	--
Cu-Gly-Ox	--	--	--	--	0.50±1.00	3.00±1.00	--
Ni-Gly-Ita	0.50±1.00	--	0.70±1.00	0.40±1.00	0.80±1.00	3.00±1.00	--
Ni-Gly-Ox	--	--	--	--	--	3.00±1.00	--

Control + : Oxitetraciclyne, Control - : Peptone water
Source: Self-made image

protective barrier, making the antibacterial action of some coordination complexes more difficult [32]. Fan et al. (2023) state that the mortality rate is between 20% and 30% in high-risk communities, such as the elderly, pregnant women, young children, and immunosuppressed people [33]. These same compounds have good activity against *Escherichia Coli*, another pathogen that causes food poisoning that can be very serious, mainly in children and vulnerable populations. The most common infections caused by *Escherichia Coli* are traveler's diarrhea, neonatal meningitis, cholangitis, urinary tract infection, cholecystitis, and pneumonia [34].

3.1 Minimum inhibitory concentration

The MIC test was performed for the complexes that showed significant activity against sensitive pathogens, these compounds were Cu-Gly-Ita and Ni-Gly-Ita against *Listeria*, *E-coli* and *Bacillus* bacteria. The MIC was determined using the optical density method measured at 620 nm. The MIC values for the copper compounds were around 20 mg/L and the nickel compounds between 5 to 10 mg/L. These results agree with those reported by authors such as Liu et al. (2012) whose coordination compounds with nickel and 5-phenyl-1H-pyrazole-3-carboxylic acid report MIC values between 15 to 20 ppm [35]. Jo et al. (2019) describes the minimum bactericidal concentration of compounds synthesized with copper, bipyridyl ligands and glutaric acid at values around 20 ppm [36]. Against *Listeria* (Fig. 8), the Cu-Gly-Ita complex presents minimum inhibitory activity at 20 ppm, during the first 750 minutes the inhibition activity is fast, however, after 1000 minutes an increase in the curve is observed. This indicates that the activity of the complex against the pathogen begins to decrease and the population of viable cells increases. On the other hand, the Ni-Gly-Ita complex presents inhibition at the concentration of 10 ppm during the first 1250 minutes; the antibacterial activity is sustained during these minutes for 20 and 10 ppm but the viable cells increase after 1250 minutes for the concentration of 10 ppm.

For the Cu-Gly-Ita complex against *E-Coli* (Fig. 9), the antibacterial activity occurs at 20 ppm. At the concentrations of 10 and 5 ppm, the complex reduces bacterial growth, but does not maintain this trend. However, the Ni-Gly-Ita complex at 10 ppm shows inhibition during the first 500 minutes, after that time an increase in the optical density is observed, indicating, an increase in viable cells.

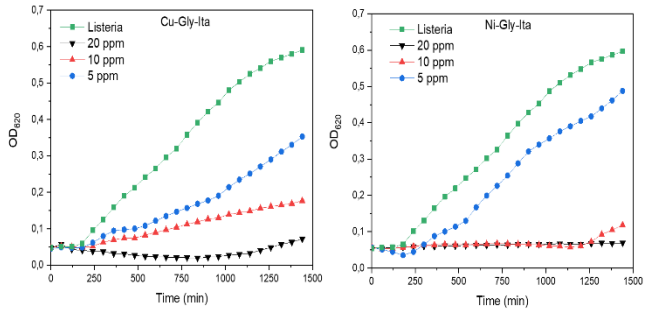

Figure 8. Growth curves of *Listeria* with 5, 10 and ppm.
Source: Self-made image

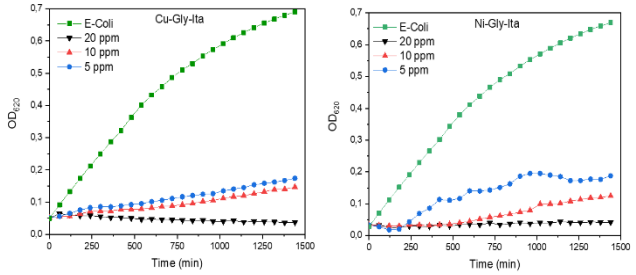

Figure 9. Growth curves of *E-Coli* with 5, 10 and 20 ppm.
Source: Self-made image

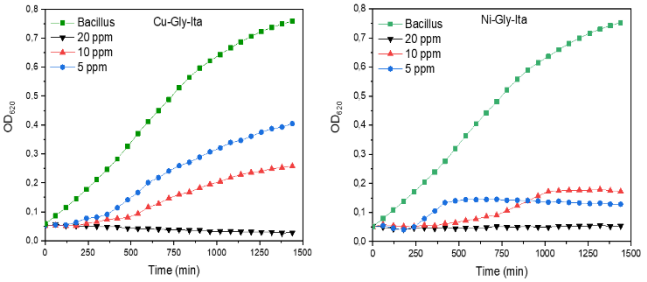

Figure 10. Growth curves of *Bacillus* with 5, 10 and 20 ppm.
Source: Self-made image

Against *Bacillus* (Fig. 10), the Cu-Gly-Ita complex presents inhibition at a concentration of 20 ppm, this activity is sustained over time showing the same pattern for the copper complexes described in this study. The behavior of the Ni-Gly-Ita complex during the first 250 minutes is inhibitory at the 3 concentrations (5, 10 and 20 ppm) however, bacterial growth is activated for the lower concentrations and is only maintained for 20 ppm.

4 Conclusions

The metal complexes synthesized with glycine present a monodentate coordination mode of the carboxyl group. This allows the ligand to have a free group to interact with neighboring molecules and act as a bridge. The improvement in thermal capacity occurs in the complexes with oxalic acid due to the formation of dense phases, making them more stable at temperatures ranging between 250 and 350°C, depending on the metal and the amino acid. However, the complexes synthesized with this acid do not exhibit significant antibacterial activity against the species studied. The biological activity of the complexes occurs mainly against gram-positive genera. The diffusion of metal ions through the peptidoglycan of the bacteria is favored, as they do not have an outer layer for additional protection. On the other hand, while the complexes with nickel show smaller zones of inhibition compared to those with copper, they have a lower MIC, around 10 ppm compared to the MIC of copper complexes, which is 20 ppm. This implies that less of the nickel complex is needed to achieve optimal and low-polluting results. However, the literature reports MICs around 40 ppm. The Cu-Gly-Ita complex exhibits greater antibacterial activity, particularly against the gram-positive species *Listeria monocytogenes*.

References

[1] Subramaniyam, A., Ravi, P.V. and Pichumani, M. Structure co-ordination of solitary amino acids as ligands in metal-organic frameworks (MOFs): A comprehensive review. J Mol Struct, 1251 (3) 131931, 2022. https://doi.org/10.1016/j.molstruc.2021.131931

[2] An, J., Geib, S.J. and Rosi, N.L. High and Selective CO_2 Uptake in a Cobalt Adeninate Metal−Organic Framework Exhibiting Pyrimidine- and Amino-Decorated Pores. J Am Chem Soc, 132 (1), pp. 38–39, 2010. https://doi.org/10.1021/ja909169x

[3] Anderson, S.L., Boyd, P.G., Gładysiak, A., Nguyen, T.N., Palgrave, R.G., Kubicki, D., Emsley, L., Bradshaw, D., Rosseinsky, M.J., Smit,B. and Stylianou, K.C. Nucleobase pairing and photodimerization in a biologically derived metal-organic framework nanoreactor. Nat Commun, 10, (1), 2019. https://doi.org/10.1038/s41467-019-09486-2

[4] Saikumari, N. Synthesis and characterization of amino acid Schiff base and its copper (II) complex and its antimicrobial studies. Materials Today: Proceedings, 47, pp. 1777–1781. 2021. https://doi.org/10.1016/j.matpr.2021.02.607

[5] Siddiki, N.A., Islam, S., Begum, S. and Salam, M.A. Synthesis, spectral characterization, thermal behavior and biological activities study of ternary metal complexes of alanine and 1,8-diaminonapthalene with Co(III), Ni(II), Cu(II), Zn(II) and Cd(II). Materials Today: Proceedings, 46, pp. 6374–6381, 2019. https://doi.org/10.1016/j.matpr.2020.06.126

[6] An, J., Geib, S.J. and Rosi, N.L. Cation-Triggered Drug Release from a Porous Zinc-Adeninate Metal-Organic Framework. J Am Chem Soc, 131 (24), pp. 8376–8377, 2009. https://doi.org/10.1021/ja902972w

[7] İnci, D., Aydın, R. and Zorlu, Y. Biomacromolecular interactions and radical scavenging activities of one-dimensional (1D) copper(II) glycinate coordination polymer. Journal of the Iranian Chemical Society, 18 pp. 3017-3030, 2021. https://doi.org/10.1007/s13738-021-02249-1

[8] Aljahdali, M. Synthesis, characterization and equilibrium studies of some potential antimicrobial and antitumor complexes of Cu(II), Ni(II), Zn(II) and Cd(II) ions involving 2-aminomethylbenzimidazole and glycine. Spectrochim Acta A Mol Biomol Spectrosc, 112, pp. 364–376, 2013. https://doi.org/10.1016/j.saa.2013.03.057

[9] Li, B., Luo, Y., Zheng, Y., Liu, X., Tan, L. and Wu, S. Two-dimensional antibacterial materials. Prog Mater Sci, 130 (10), p. 100976 2022. https://doi.org/10.1016/j.pmatsci.2022.100976

[10] [Akbar. S.A. and Morsali, A. Linker functionalized metal-organic frameworks. Coord Chem Rev, 399, p. 213023, 2019. https://doi.org/10.1016/j.ccr.2019.213023

[11] MacLaren, J.K. and Janiak, C. Amino-acid based coordination polymers. Inorganica Chim Acta, 389, (7) pp. 183–190, 2012. https://doi.org/10.1016/j.ica.2012.03.010

[12] Weiss, I.M., Muth, C., Drumm, R. and Kirchner, H. Thermal decomposition of the aminoacids glycine, cysteine, aspartic acid, asparagine, glutamic acid, glutamine, arginineand histidine. BMC Biophys, 2018. https://doi.org/10.1186/s13628-018-0042-4

[13] Yablokov, V.Y., Smel'tsova, I.L., Zelyaev, I.A. and Mitrofanova, S.V. Studies of the rates of thermal decomposition of glycine, alanine, and serine. Russ J Gen Chem, 79 (8), pp. 1704–1706, 2009. https://doi.org/10.1134/S1070363209080209

[14] Cao, P., Wu, X., Zhang, W., Zhao, L., Sun, W. and Tang, Z. Killing Oral Bacteria Using Metal-Organic Frameworks. Ind Eng Chem Res, 59 (4), pp. 1559–1567, 2020. https://doi.org/10.1021/acs.iecr.9b05659

[15] Alisir, S.H., Demir, S., Sariboga, B. and Buyukgungor, O. A disparate 3-D silver (I) coordination polymer of pyridine-3,5-dicarboxylate and pyrimidine with strong intermetallic interactions: X-ray crystallography, photoluminescence and antimicrobial activity. J Coord Chem, 68 (1), pp. 155–168, 2015. https://doi.org/10.1080/00958972.2014.978307

[16] Lucena, G.N., Alves, R.C., Abuçafy, M.P., Chiavacci, L.A., da Silva, I.C., Pavan, F.R. and Galvão, R.C. Zn-based porous coordination solid as diclofenac sodium carrier. J Solid State Chem, 260, pp. 67–72, 2018. https://doi.org/10.1016/j.jssc.2018.01.011

[17] Yuan, K., Ye, X., Liu, W., Liu, K., Wu, D., Zhao, W., Qian, Z., Li, S., Huang, C., Yu, Z. and Chen, Z. Preparation, characterization and antibacterial activity of a novel Zn(II) coordination polymer derived from carboxylic acid. J. Mol Struct, 1241, p. 130624, 2021. https://doi.org/10.1016/j.molstruc.2021.130624

[18] Akbarzadeh, F., Motaghi, M., Singh Chauhan, N.P. and Sargazi, G. A novel synthesis of new antibacterial nanostructures based on Zn-MOF compound: design, characterization and a high-performance application. Heliyon, 6 (1), pp. e03231, 2020. https://doi.org/10.1016/J.HELIYON.2020.E03231

[19] Wiegand, I., Hilpert, K. and Hancock, R.E.W. Agar and broth dilution methods to determine the minimal inhibitory concentration (MIC) of antimicrobial substances. Nat Protoc, 3 (2), pp. 163–175, 2008. https://doi.org/10.1038/nprot.2007.521

[20] Liu, A., Wang, C.C., Wang, C.Z., Fu, H.F., Peng, W., Cao, Y.L., Chu, H.Y. and Du, A.F. Selective adsorption activities toward organic dyes and antibacterial performance of silver-based coordination polymers. J Colloid Interface Sci, 512, pp. 730–739, 2018. https://doi.org/10.1016/j.jcis.2017.10.099

[21] Sevgi, F., Bagkesici, U., Kursunlu, A.N. and Guler, E. Fe (III), Co(II), Ni(II), Cu(II) and Zn(II) complexes of schiff bases based-on glycine and phenylalanine: Synthesis, magnetic/thermal properties and antimicrobial activity. J Mol Struct, 1154, pp. 256–260, 2018. https://doi.org/10.1016/j.molstruc.2017.10.052

[22] Chávez, N.K., Ramírez, R.I., Sheen, P., Zimic, M.J. and Valderrama, A.C. Síntesis, caracterización y evaluación de la actividad biológica de compuestos de coordinación de cobalto con pirazinamida. Rev Soc Quím Perú, 86 (3), pp. 315–328, 2020. https://doi.org/10.37761/rsqp.v86i3.303

[23] Deacon, G.B. and Phillips, R.J. Relationships between the carbon-oxygen stretching frequencies of carboxylato complexes and the type of carboxylate coordination. Coord. Chem. Rev., 33, pp. 227–250, 1980. https://doi.org/10.1016/S0010 8545(00)80455-5.

[24] El-Newehy, M.H., Osman, S.M., Refat, M.S., Al-Deyab, S.S and El-Faham, A. Microwave synthesis of copolymers based on itaconic acid moiety and their utility for scavenging of copper (II) and lead (II). Journal of Macromolecular Science, Part A: Pure and Applied Chemistry, 52 (7), pp. 561–576, 2015. https://doi.org/10.1080/10601325.2015.1039335

[25] Köse, D.A., Toprak, E., Kasąrci, A., Avci, E., Avci, G.A., Sąhin, O. and Buyükgüngör, O. Synthesis, Spectral, and Thermal Studies of Co(II), Ni(II), Cu(II), and Zn(II)-Glycinato Complexes and Investigation of Their Biological Properties: Crystal Structure of $[Cu(\mu\text{-gly})2(H_2O)]n$. Synthesis and Reactivity in Inorganic, Metal-Organic and Nano-Metal Chemistry, 46 (7), pp. 1109–1118, 2016. https://doi.org/10.1080/15533174.2013.801855

[26] Nguyen, H.G.T., Tao, R. and Van Zee, R.D. Porosity, Powder X-Ray Diffraction Patterns, Skeletal Density, and Thermal Stability of NIST Zeolitic Reference Materials RM 8850, RM 8851, and RM 8852. J Res Natl Inst Stand Technol, 126, (126047), pp. 1–10, 2021. https://doi.org/10.6028/jres.126.047

[27] Newsam, J.M., Yang, C.Z., King, H.E., Jones, R.H. and Xie, D. Experiences in studying zeolites and related microporous materials by synchrotron x-ray diffraction. Journal of Physics and Chemistry of Solids, 52 (10), pp. 1281–1288, 1991. https://doi.org/10.1016/0022-3697(91)90204-D

[28] Eswaramoorthy, M., Neeraj, S. and Rao, C.N.R. Synthesis of hexagonal microporous silica and aluminophosphate by supramolecular templating of a short-chain amine. Microporous and Mesoporous Materials, 28 (1), pp. 205–210, 1999. https://doi.org/10.1016/S1387-1811(98)00309-6

[29] Dharmaraja, J., Esakkidurai, T., Subbaraj, P. and Shobana, S. Mixed ligand complex formation of 2-aminobenzamide with Cu(II) in the presence of some amino acids: Synthesis, structural, biological, pH-metric, spectrophotometric and thermodynamic studies. Spectrochim Acta A Mol Biomol Spectrosc, 114, pp. 607–621, 2013. https://doi.org/10.1016/j.saa.2013.05.043

[30] Wyszogrodzka, G., Marszałek, B., Gil, B. and Dorozyński, P. Metal-organic frameworks: Mechanisms of antibacterial action and potential applications. Drug Discov Today, 21 (6), pp. 1009–1018, 2016. https://doi.org/10.1016/j.drudis.2016.04.009

[31] Agboola, T.D. and Bisi-Johnson, M.A. Occurrence of Listeria monocytogenes in irrigation water and irrigated vegetables in selected areas of Osun State, Nigeria. Sci Afr, 19, p. e01503, 2023. https://doi.org/10.1016/j.sciaf.2022.e01503

[32] Rojas, S., Arenas, A. and Horcajada, P. Metal-organic frameworks: A novel platform for combined advanced therapies. Coordination Chemistry Reviews, 388, pp. 202–226, 2019. https://doi.org/10.1016/j.ccr.2019.02.032
[33] Fan, X., Gurtler, J.B. and Mattheis, J.P. Possible sources of *Listeria monocytogenes* contamination of fresh-cut apples and antimicrobial interventions during antibrowning treatments: A review," J Food Prot, 86 (6) p. 100100, 2023. https://doi.org/10.1016/j.jfp.2023.100100
[34] Doyle, M.E., Archer, J., Kaspar, C.W. and Weiss, R. Human Illness Caused by E. coli O157: H7 from Food and Non-food Sources. FRI Briefings [Online]. 10, pp. 1–37, 2006, [Date of reference October 18 of 2023]. Available: https://fri.wisc.edu/files/Briefs_File/FRIBrief_EcoliO157H7humanillness.pdf
[35] Liu, C.B., Gong, Y.N., Chen, Y. and Wen, H.L. Self-assembly and structures of new transition metal complexes with phenyl substituted pyrazole carboxylic acid and N-donor co-ligands. Inorganica Chim Acta, 383, pp. 277–286, 2012. https://doi.org/10.1016/J.ICA.2011.11.015
[36] Jo, J.H., Kim, H.C., Huh, S., Kim, Y. and Lee, D.N. Antibacterial activities of Cu-MOFs containing glutarates and bipyridyl ligands. Dalton Transactions, 48 (23), pp. 8084–8093, 2019. https://doi.org/10.1039/c9dt00791a

L.F. Múnera-Gómez, is Biological Engineer in 2021, and MSc. in Chemistry in 2024, both degrees from the Universidad Nacional de Colombia, Medellín, Colombia. Her research interests include coordination chemistry and biochemistry.
ORCID: 0009-0006-3097-2849

J.C. Muñoz-Acevedo, is a PhD from the Universidad de Chile, Santiago, Chile. Since 2007 is working as a full-time professor at the Universidad de Antioquia, Colombia. Was the Director of the Institute of Chemistry, between december 2018 and march 2023. His actual research field is in Inorganic synthesis of porous materials, MOF, and other inorganic complexes.
ORCID: 0000-0001-7543-0644.

E. Pabón-Gelves, received her PhD from the Universidad de Chile, Santiago, Chile. She is currently a full professor at the Department of Chemistry, Faculty of Sciences, Universidad Nacional de Colombia, Sede Medellín. Her current research interest is in materials chemistry
ORCID: 0000-0001-8108-7635

DYNA
http://dyna.medellin.unal.edu.co/

UNIVERSIDAD NACIONAL DE COLOMBIA

Colombian monthly energy inflows predictability

Andrés Felipe Hurtado-Montoya [a] & Nicolás Alberto Moreno-Reyes [b]

[a] *ISAGEN, Medellín, Colombia. afhurtado@isagen.com.co*
[b] *Universidad EAFIT, Medellín, Colombia. namorenor@eafit.edu.co*

Received: May 6th, 2024. Received in revised form: September 13th, 2024. Accepted: September 27th, 2024.

Abstract
Streamflow forecasting is essential for water resources management in several social and economic strategic sectors, involving space-temporal variability modeling of the hydrological processes and the influence of several climatic phenomena. Furthermore, high water-dependent sectors such as the Colombian electricity market, require not only the expected streamflow values but also the occurrence probability or reliability bands of such forecast inflows necessary in robust risk analyses. We propose a mathematical approach for monthly streamflow forecasting in Colombia and quantify its predictability, incorporating climate model outcomes as a time series of macroclimatic indexes and punctual hydro-climatological stations. The methodology integrates parametric and non-parametric models, exogenous variables analysis, and uncertainty estimation through stochastic modeling. This research will contribute to the Colombian hydrology understanding and provide elements for risk analysis, planning, and decision-making in social and economic sectors involved with water resources management.

Keywords: streamflow forecasting; uncertainty; Colombian streamflow's predictability.

Predictibilidad de los aportes mensuales de energía en Colombia

Resumen
El pronóstico de caudales es esencial en la gestión de los recursos hídricos en varios sectores sociales y económicos estratégicos e involucra la modelación de variabilidad espacio temporal de los procesos hidrológicos y la influencia de varios fenómenos climáticos. Además, la alta dependencia del agua en sectores como el mercado eléctrico colombiano requiere (solo los valores de caudal esperados, sino también su probabilidad de ocurrencia o bandas de confianza de tales pronósticos necesaria en análisis robustos de riesgo. Se propone un enfoque matemático para el pronóstico mensual de caudales en Colombia y la cuantificación de su predictibilidad, incorporando resultados de modelos climáticos como series temporales de índices macroclimáticos y estaciones hidroclimatológicas puntuales. La metodología integra la aplicación de modelos paramétricos y (paramétricos, el análisis de variables exógenas y la estimación de la incertidumbre mediante modelos estocásticos. Esta investigación contribuirá en el entendimiento de la hidrología colombiana y brindará elementos para el análisis de riesgo, la planificación y la toma de decisiones en los sectores sociales y económicos involucrados con la gestión de los recursos hídricos.

Palabras clave: pronóstico de caudales; incertidumbre; predictibilidad de los caudales colombianos.

1 Introduction

Space-temporal variability understanding of the hydrological process is an imperative goal because of its environmental, social, economic, and cultural implications. Research in hydro-climatological topics is necessary to improve the water resource management of the country, where future water availability estimation through streamflow forecasting is a central task for the strategic planning of electrical, agricultural, tourist, and drinking water distribution sectors. Water resources management relies on hydrological historical data and future projections, where precipitation and streamflow time series, statistical analysis, and modeling have allowed a better understanding of the country's hydro-climatological processes. Furthermore, hydrological forecasting is an essential task for planning, and improving it is a continuous challenge to gain confidence in the decision-making process involving strategic national sectors.

Thanks to its abundant water resources, hydroelectricity makes up about 70% of the generation matrix, where different reservoirs help manage the natural inter-annual

How to cite: Hurtado-Montoya, A.F., and Moreno-Reyes, N.A., Colombian monthly energy inflows predictability. DYNA, 91(234), pp. 24-33, October - December, 2024.

variability linked to the hydro-climatological behavior. This high dependence on water availability and the uncertainty associated with the evolution of the climatic system led to significant levels of vulnerability to deal with through reservoir management, streamflow forecasting, and uncertainty quantification. Government planning institutions, the system operator, and the hydroelectric power plant owners perform the monthly streamflow forecasting for the Colombian electricity market to guarantee reliability through energetic resources management (mainly water, coal, and gas). Despite the availability of climate data and monthly streamflow time series of rivers used for the hydroelectricity generation in Colombia, streamflow forecasting uncertainty estimation is still subject to improvement. A mathematical approach incorporating elements such as the time of the year, the prediction horizon, and the climatic events will improve the forecasting activities using probabilistic methodologies.

This research starts with the importance of improving water availability forecasting and determining the reliability of the results. Both are essential tasks for planning in different highly water-dependent sectors, where not only the expected values are necessary but also the probability of occurrence of other plausible scenarios. Moreover, apart from the practical applications of this research, another goal is related to the continuous efforts to understand the Colombian hydro-climatological processes through mathematical modeling.

The next two subsections present an overview of the Colombian hydro-climatology variability and the mathematical modeling applied to hydrological time series. Then, section 2 describes the data and procedure to obtain the time series of interest. Section 3 corresponds with the methodology, and describes the models evaluated and the forecasting process. Finally, analysis and conclusions about the model performance and forecasting uncertainty in Colombia are given in sections 4 and 5.

1.1 Colombian hydro-climatology

Several factors modulate Colombian hydro-climatology, such as the tropical dynamics, the Intertropical Convergence Zone (ITCZ) displacement during the year [1,21], the humidity inflow from the Amazon basin and the Pacific and Atlantic oceans, the hydrological surface process, and the Andes physiography. Additionally, various climatic phenomena operating in different spatial and temporal scales affect the Colombian hydro-climatology, like the Pacific Decadal Oscillation (PDO), the North Atlantic Oscillation (NAO), the Quasi-Bienal Oscillation (QBO), El Niño-Southern Oscillation (ENSO), the Chocó low-level jet, the Mesoscale Convective Systems (MCS), the Madden-Julian Oscillation (MJO), and the tropical easterly waves [23,26]. The influence of this hydroclimatic complexity in water resources distribution, the access to numerous hydro-climatological databases, and the computational capabilities justify the research efforts to shape a better conceptual framework of the hydrological processes and their predictability using mathematical modeling. This research aims to contribute to the knowledge of Colombian hydrology through monthly streamflow predictability estimation using probability theory approaches.

Various hydrology and climate research form the conceptual framework for streamflow characterization and modeling in Colombia. Although ITCZ characterizes the streamflow annual cycle in the Colombian regions, other climate phenomena also influence the space-temporal variability. Associated with the trade winds, the Chocó low-level jet [25] is a wind current with considerable influence on Colombian climatology, specifically in the central and western zones. Furthermore, the Chocó jet interacts dynamically and thermodynamically with the MCS [17] in the region [23,27,29-31]. Another significant jet stream for the hydrological characterization is the San Andrés jet [27,31], which is also associated with the trade wind transporting humidity from the Atlantic Ocean to Colombia. Climate change due to natural variability and anthropogenic actions, the PDO, and the NAO [23,35] operate on the interdecadal scale. The QBO (26 months) [14,30] and the ENSO, the main phenomena, operate on the interannual scale. The MJO (40-60 days) [32] and the weekly variability (5-7 days) relate to tropical westerly waves operate on the intra-annual scale. Finally, the tropical dynamics and the country's physiographic are relevant on the diurnal scales [23,26]. The influence of these phenomena acting at different temporal scales shows the level of complexity related to the water resources distribution study and modeling in Colombia.

The ENSO [1] is the global scale climate event that affects the most the Colombian hydro-climatology, from the monthly to interannual scales [25-28,33]. The ENSO is a quasi-periodic phenomenon with an average recurrence of four years that varies between two and seven years [40]. Most of the research regarding Colombian water resources incorporate the ENSO as the most important predictive variable [9-11,28,42]. However, The ENSO forecasting has limitations due to the climate system complexity, which are higher when forecasting goes further the northern hemisphere spring, time of the year known as the spring barrier [39,43] when there is high uncertainty about the evolution of the climate tropical system. Nevertheless, new approaches, more data, and better computational resources continuously improve the ENSO forecast [8], as modeling incorporating Machine Learning [13], information theory [22], and including some climatic variables [20] to overpasses the spring barrier.

1.2 Mathematical modeling

Streamflow forecasting is one of the most relevant tasks in water resources management [9,11,36,44], letting us anticipate the hydrological processes with a certain level of reliability. Physically-based hydrological and mathematical models are two ways to approach monthly streamflow forecasting. In the first case, simulation of the physical processes inside the basin demands high computational resources and amounts of information unavailable most of the time. In the second case, even though physical laws govern the hydrological processes, their non-linear complexities involving many variables justify the use of mathematical models, achieving versatility and including many more basins in the analysis. Hydrological forecasting

studies typically use mathematical or data-driven models, but most do not incorporate adequate measures of uncertainty [18].

Between statistical models, linear regression and autoregressive models have been traditionally used in streamflow prediction. Autoregressive models, which preserve the mean, variance, and autocorrelation structures of the series for a defined number of lags, have been widely used since the beginning of the sixties to the generation of time series [37], and Box and Jenkins [5] improved the mathematical framework since 1970. Fulfilling the model assumptions, they become parsimonious models suitable for time series modeling through a simple mathematical approach like in [1], where an autoregressive model is more accurate than a neural network model.

Mathematical models are functional at incorporating efficiently secondary data like macroclimatic index time series from climate models' outcomes. Most of the streamflow forecasting research in Colombia involves exogenous variables related to the ENSO characterization, and among the mathematical models used are those based on linear regression, neural networks, Multivariate Adaptive Regression Spline (MARS), autoregression, spectral analysis, and entropy [7,36]. It is also relevant to highlight the limitations of the analogous-based models [41], the importance of multivariate series when using dynamic system theory [6], and the usefulness and versatility of Machine Learning [45]. Otherwise, non-parametric forecasting is an appropriate methodology to deal with error propagation when using exogenous variables [34].

Despite the number of methodologies and models used to forecast the water resources in Colombia, limitations in uncertainty modeling justify investigative efforts to improve water resources management. Some common approaches to estimate the uncertainty are probabilistic methods based on historical models' performance [19], the construction of confident bands using independent components [44], the use of autoregressive modeling to generate probabilistic scenarios [16], autoregressive residual representation using the t-student distribution [12], parental methods [2], and bootstrap-based models [1,24,38]. However, it is necessary to improve and develop methodologies to quantify the uncertainty in the forecasting process. It requires considering the geographical zone, the spatial and temporal scales, the month at the beginning of the forecast, the forecasting horizon, and the active climatic phenomena. Stochastic modeling and the estimation of confidence intervals will provide more and better elements for risk analysis, planning, and decision-making in the sectors involved with water resources management.

The ENSO is the most influential climate event in Colombian hydrology, and most of the monthly streamflow forecasting models incorporate it through projected data of the Pacific Ocean temperature. However, climate forecasting also involves high uncertainty, which propagates to streamflow forecasting that usually is not quantified. This research aims to quantify monthly streamflow forecasting uncertainty in Colombia by incorporating measuring station data, secondary time series, modeling, and evaluation using efficiency, parsimony, and physical representability criteria. In the short and medium term, streamflow forecasting is commonly a time series where confidence intervals or another uncertainty measure rarely integrate the forecasting values. The lack of knowledge or information about the models' predictive capacity depreciates the forecasting task and increases the risk of making erroneous decisions. Moreover, the hydrological process's complexity and modeling limitations in streamflow forecasting make it essential to include the expected values and the quantification of its uncertainty.

The advantages of probabilistic approaches are related to the need to highlight the uncertainty of the streamflow forecasting process and the importance of having tools for better management of the resources through risk analysis. The methodology proposed will be applicable in different sectors involving hydrological forecasting, specifically in the Colombian electrical market, improving the understanding of spatial and temporal variability of Colombian water resources. The Colombian electrical market is an economic sector with a high dependence on water resources from rivers that flow to several reservoirs in the country. This condition has led to the instrumentation of several basins in the country, with more than 30 monthly streamflow time series available for studying the spatial and temporal water resource distribution. Furthermore, this worthy data and additional climate data justify the mathematical modeling to have more reliable forecasting results.

2. Data

Hydroelectric projects in Colombia (Figs. 1, 2) represent 66% of the power system capacity. We used the data from 41 monthly streamflow time series related to the rivers that supply the main hydroelectric projects in Colombia, accounting for more than 90% of the inflows. Record length varies depending on the time series, ranging from 1938 to 2023 for the longest and from 1982 to 2023 for the shortest series (Figs. 1, 2, Table 1).

Energy inflows, it is hydrological inflows to hydroelectric power plants, are also known as SIN time series and are usually represented in Colombia in GWh units or as a percentage of the historical mean. XM, as administration of the Colombian energy market, updates the SIN time series daily, and it has been available since 2000.

To have a much longer SIN time series necessary for robust statistical analysis, we reconstruct it using the monthly streamflow data since 1950 by converting the streamflow time series (monthly average in cubic meters per second) to power using the conversion factor (energy power and streamflow ratio) associated to each hydropower plant and then to energy according with the seconds of the month,

$$E = s \sum_{i=1}^{n} f_i \cdot Q_i$$

where E is the total monthly energy inflow in $[GWh]$, Q_i is the monthly streamflow value of the river i associated with the hydroelectric power plant i in $[m^3/s]$, f_i is its corresponding energy power and streamflow ratio in $[GW/m^3/s]$, n is the number of rivers, and s is a constant containing the seconds of the month. Fig. 3 shows the multi-annual monthly means calculated in the 1982-2023 period, where all the streamflow series have records.

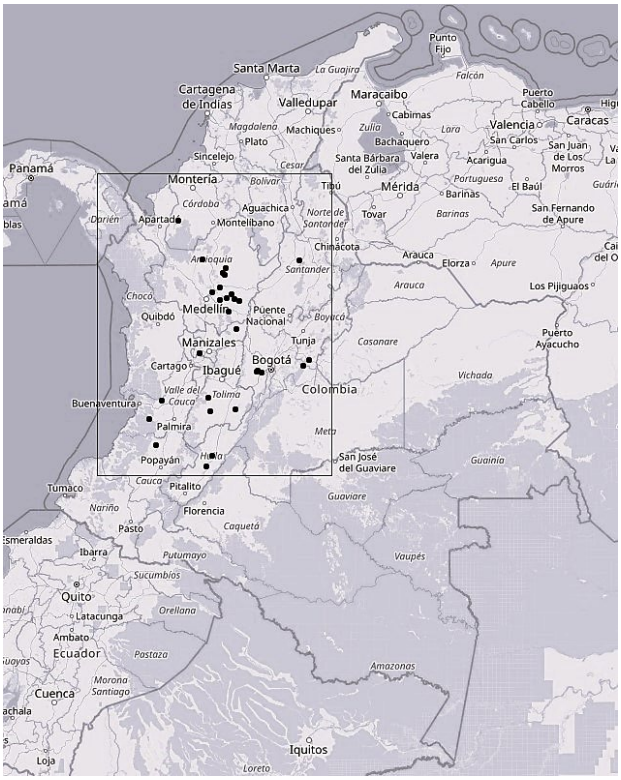

Figure 1. Location of the Colombian hydroelectric projects with installed capacity greater than 20 MW.
Source: The authors.

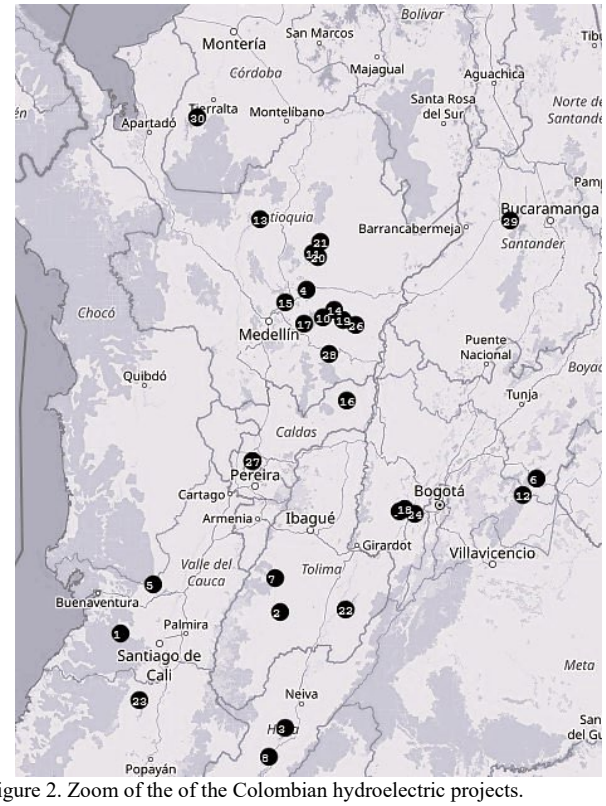

Figure 2. Zoom of the of the Colombian hydroelectric projects.
Source: The authors.

Table 1.
Monthly streamflow time series used.

ID	Hydroelectric Plant	Streamflow time series	Beginning year
1	Albán	Alto Anchicayá	1976
		Digua	1976
2	Amoyá	Amoyá	1974
3	Betania	Betania	1961
4	Carlos Lleras	Carlos Lleras	1972
5	Calima	Calima	1946
6	Chivor	Batá	1978
7	Cucuana	Cucuana	1972
		San Marcos	1972
8	El Quimbo	El Quimbo	1961
9	Esmeralda	Campoalegre	1980
		Chinchina	1961
		Estrella	1972
		San Eugenio	1980
10	Guatapé	Nare	1956
11	Guatrón	Concepción	1955
		Nechí Pajarito Dolores	1955
		Guadalupe	1938
		Tenche	1955
12	Guavio	Guavio	1963
13	Ituango	Ituango	1982
14	Jaguas	San Lorenzo	1956
15	La Tasajera	Grande	1942
16	Miel	Miel	1963
		Guarinó	1980
		Manso	1966
17	Minas	Escuela de Minas	1956
18	Pagua	Bogotá (regulado)	1965
		Blanco	1972
		Chuza	1967
19	Playas	Guatapé	1959
20	Porce 2	Porce 2	1973
		Quebradona	1942
21	Porce 3	Porce 3	1973
22	Prado	Prado	1955
23	Salvajina	Salvajina	1947
24	Salto II	Bogotá (regulado)	1965
25	Samper	Bogotá (regulado)	1965
26	San Carlos	San Carlos	1965
27	San Francisco	San Francisco	1980
28	San Miguel	San Miguel	1974
29	Sogamoso	Sogamoso	1959
30	Urrá	Urrá	1960

Source: The authors.

From January 1950 to December 2023, the SIN inflows time series as a percentage of the average conditions is constructed by dividing each energy month's value by the long-term monthly mean. In months with some missing streamflow data, SIN values in percentage are estimated using available data, and the E value by multiplying it with the corresponding historical monthly mean.

2.1 Standardization

Most of the hydroelectric streamflow time series in Colombia has a clear bimodal annual cycle, with two maximums at April-May and October-November because of the pass of the ZCIT two times in a year through the center of Colombia. Moreover, the east region of Colombian, with two of the largest hydropower plants (Chivor and Guavio), exhibits a unimodal annual cycle with a maximum in June-

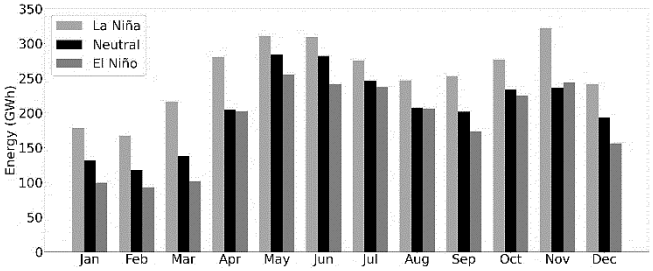

Figure 3. Monthly multi-annual means of the SIN time series for the three ENSO climatological conditions.
Source: The authors.

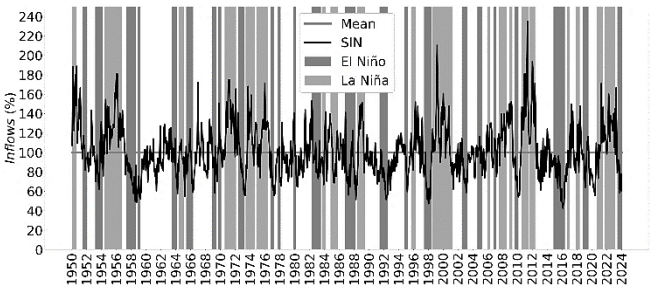

Figure 4. SIN time series in percentage of the average conditions.
Source: The authors.

July, which entails for the total energy inflows one period of high inflows (April-November) and another of low inflows (December-March) which are known as the wet and dry seasons for the Electricity Colombian Market.

To capture not the known intra-annual variability but the inter-annual variability associated with climatic events as the ENSO, the E monthly time series is standardized by removing the multi-annual mean of the month and dividing it by the standard deviation of the month. With this transformation, time series are scaled with zero mean and unit standard deviation without an annual cycle. Fig. 3 shows the reconstructed SIN time series, while Fig. 4 shows the monthly multi-annual means for the three ENSO climatological conditions.

2.2 ENSO time series

The ENSO is the principal climatological phenomenon affecting Colombian water resources availability and should be incorporated in the forecasting models to represent inter-annual climate fluctuations. One of the most common climatic variables used in ENSO monitoring is the Oceanic Niño Index (ONI), calculated by the NOAA (National Oceanic and Atmospheric Administration) agency. The ONI, available since 1950, tracks the running 3-month average sea surface temperatures in the east-central tropical Pacific between 120°-170°W (denominated as El Niño 3.4 region) to estimate the anomaly (deviation from mean conditions). ONI index data is available in https://origin.cpc.ncep.noaa.gov/products/analysis_monitoring/ensostuff/ONI_v5.php.

Along with the ONI, whose data is historical, El Niño 3.4 anomaly forecasts made by different global climate agencies and collected by the Research Institute for Climate and Society (IRI) were used. Every month, the IRI publishes forecasts for the next nine months of about 25 agencies, 16 of which use dynamic climate models and nine statistical models. Historical data on this forecasting activity has been available since 2002 in https://iri.columbia.edu/our-expertise/climate/forecasts/enso/current/?enso_tab=enso-sst_table.

3. Methodology

Different mathematical models commonly used in hydrological time series forecasting and widely employed in Colombia were implemented, as well as the use of the Root Mean Square Error (RMSE) as the error metric for the models' performance analysis. We evaluated simple and multiple linear regression, simple and multiple linear regression using robust techniques, analogous series, non-parametric regression, neural networks, decision trees, and autoregressive models. The SIN time series length is 888 months long (1950-2023), and it was divided into calibration (1950-2012) and test (2013-2023) periods, representing 85% and 15%. We sensitized and adjusted the model parameters in the calibration period and evaluated the model in the test period, estimating the error variance to posterior uncertainty analysis.

Analogous series is the simplest model analyzed and commonly used in Colombia in medium and long-term energetic analysis. The first step is to compare the last τ (model parameter) observed months with the historical record to determine the most similar period with the present condition (last τ months). After that, the forecast is the observed data following that period. We also incorporated the ONI time series to determine the most similar historical period, accounting for the streamflow and the climate signal, and using the Euclidean distance as a similarity criterion.

Robust techniques applied to simple and multiple linear regression involve discarding outliers or atypical data according to different criteria: data points with high residuals or far away according to the Euclidean distance (kNN) or the Mahalanobis distance. Another technique evaluated consists of the estimation of the parameters of the regression through a modification of the covariance matrix, employing statistical measures for the correlation and standard deviation less sensitive to outliers like the Kendall and Spearman for the correlation and the MAD for the standard deviation.

We also fitted autoregressive models to the data. These models are also linear, in which the number and values of the parameters are a function of the linear structure dependence of the data. An autoregressive model $AR(p)$ is defined as:

$$Y_t = \beta + \phi_1 \cdot Y_{t-1} + \cdots + \phi_p \cdot Y_{t-p} + \epsilon_t$$

where β, ϕ_1, $\cdots$, ϕ_p are the model parameters and ϵ_t is assumed to be a white noise process. An autoregressive model with exogenous variable $ARX(p)$ is defined as:

$$Y_t = \beta + \phi_1 \cdot Y_{t-1} + \cdots + \phi_p \cdot Y_{t-p} + \sum_{j=1}^{m} \gamma_j \cdot X_{t,j} + \epsilon_t$$

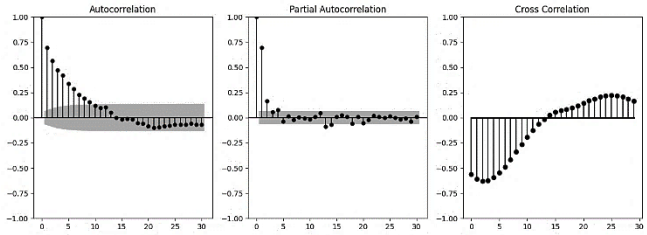

Figure 5. Time series' dependence structure.
Source: The authors.

where $X_{t,j}$ are the exogenous regressors. Model parameters were estimated using Conditional Maximum Likelihood.

Fig. 5 shows the correlation structure of the data. The autocorrelation diagram exhibits a quick decay, with correlations statistically significant observed until ten months. However, the partial autocorrelation diagram suggests that only the first lag represents almost all the linear dependence structure of the series. The pattern observed in the autocorrelation and partial autocorrelation diagrams is typical of AR models, and due to the high correlation between the inflows and the ONI time series, we also evaluated autoregressive models with exogenous variables (ARX). Although analyzed, different autoregressive models like AR with climatically conditioned parameters or SARIMA models using non-standardized data led to a good forecasting performance (results not shown), but AR1 and ARX1 models are superior according to parsimony criteria.

Forecast confidence interval were estimated with two different approaches. In the first one, we used the error variance estimated in the test period, calculated after the Box-Cox transformation used to stabilize the variance over the residuals. Otherwise, in the second one and using the empirical function of the residuals, we used Bootstrap to generate 1000 series of residuals to simulate 1000 possible outputs, re-calibrate the model, and obtain a distribution of the parameters. This methodology starts estimating the autoregressive coefficients β and ϕ in the equation $Y_t = \beta + \phi \cdot Y_{t-1} + \epsilon_t$, the computation of the residuals ϵ_t, and the definition of its empirical distribution function of the centered residuals. If the residuals are not centered, then $\tilde{e}_t = \epsilon_t - \hat{e}$ and $\hat{e} = \frac{1}{n-p}\sum_{t=p+1}^{n} \hat{\epsilon}_t$ equations are used.

Using Bootstrap to draw i.i.d. ϵ_t^* resamples from the empirical distribution of the residuals $\hat{F}_{\tilde{\epsilon}}$ leads to one forecast for each residual resampling defining the recursion $Y_t^* = \beta + \phi \cdot Y_{t-1}^* + \epsilon_t^*$. It allows computing B future observations where the mean represents the future expected value, it is the forecast, and the 5% and 95% percentiles define the confidence band.

Continuing with more sophisticated models capable of capturing the nonlinearities present in the time series, we calibrated non-parametric regressions, neural networks, and decision trees models. In all the cases and according to the train and test periods, optimal parameters estimation using the train data consisted of a bias and variance trade-off. For the case of non-parametric regression, we evaluated different kernels and bandwidth values, in neural networks we considered different configurations varying the number of neurons and layers, while for the decision trees the deep was the hyper-parameter calibrated.

Table 2.
Algorithm.

1:	Estimate β and ϕ in $Y_t = \beta + \phi \cdot Y_{t-1} + \epsilon_t$ using Conditional Maximum Likelihood Estimation
2:	Compute the residuals ϵ_t
3:	Define the empirical distribution function of the centered residuals $\hat{F}_{\tilde{\epsilon}}$
4:	if residuals ϵ_t are centered:
5:	$\tilde{e}_t = \epsilon_t$
6:	if not:
7:	$\tilde{e}_t = \epsilon_t - \hat{e}$ and $\hat{e} = \frac{1}{n-p}\sum_{t=p+1}^{n} \hat{\epsilon}_t$
8:	end if
9:	for $i = 1\ to\ B$:
10:	Draw a i.i.d. ϵ_t^* resample from $\hat{F}_{\tilde{\epsilon}}$
11:	Compute $Y_{ti}^* = \beta + \phi \cdot Y_{t-1}^* + \epsilon_t^*$
12:	end for
13:	$Y_{t\_forecast} = mean(Y_{ti}^*)$
14:	$Y_{t_5\%} = percentile(Y_{ti}^*, 0.05)$
15:	$Y_{t_{95}\%} = percentile(Y_{ti}^*, 0.95)$

Source: The authors.

In all the models described above, the target variable is the standardized energy inflows, and the predictive variables are the past standardized energy inflows and the past and forecast ONI time series. We analyzed different numbers of lags for the predictive variables, especially for the non-linear models, and calibrated monthly models, which is 12 models (one per month), trying to obtain a better forecasting performance.

4. Results

As expected, all the models evaluated (Table 2) presented better results than the simplest forecasting method, the monthly multi-annual mean (RMSE = 0.26 and RMSE = 0.25 for the calibration and test periods). Additionally, the error metric in the test period is higher using non-linear models than simpler linear models. It is due to a high linear dependence between the SIN's time series with its lags and with the exogenous variable, rather than a non-linear dependence, or possibly due to the lack of other variables that adequately represent the non-linear dependence structure. Besides, the monthly models that consider an independent model for each month do not improve the forecasting performance despite increasing the number of parameters 12 times.

4.1 Autoregressive model

Due to the linear dependence structure of the data and the fact that it is a time series, the ARX1 is the best of all the models studied. This model presents better adjustment, has few parameters, and allows simulating the stochastic nature of the SIN time series, preserving the historical dependence structure and incorporating the climate signal through the exogenous variable. Furthermore, the ARX1 model is more suitable since it retains temporal and climate coherence when forecasting ahead of one month.

Table 3.
Results.

Model/RMSE	Standard Model		Monthly Model	
	Calibration	Test	Calibration	Test
Analogous		0.90		
Analogous ONI		0.91		
Simple linear regression	0.71	0.81	0.69	0.82
Multiple linear regression	0.68	0.76	0.64	0.78
Deep data residuals	0.68	0.75	0.65	0.76
Deep data residuals Knn	0.68	0.76	0.65	0.76
Deep data residuals Mahal.	0.68	0.75	0.65	0.77
Robust - Kendall	0.69	0.76	0.66	0.76
Robust - Spearman	0.68	0.76	0.64	0.77
Robust - MAD	0.68	0.76	0.70	0.77
Robust - Kendall-MAD	0.70	0.76	0.69	0.77
Robust - Spearman-MAD	0.68	0.76	0.71	0.77
AR1	0.71	0.81		
ARX1	0.68	0.75		
Non-parametric regression	0.71	0.81	0.63	0.82
Mult. non parametric reg.	1.00	1.02	0.60	0.77
Decision Trees	0.64	0.82	0.52	0.80
Neural Networks	0.70	0.75	0.64	0.77

*CLIMATOLOGICAL RMSE: 0.99 y 1.02
Source: The authors.

Fig. 6 shows the forecasting results in the test period for a horizon of one month. After fitting the ARX1 model with the standardized SIN time series, as described in section 3, the residuals distribution obtained follows a normal distribution (Fig. 7). Similarly, with the Box-Cox transformation, normality in residuals is met (Fig. 8), but the new model is adjusted after two transformations, increasing the complexity of the model. Moreover, the residuals met the non-autocorrelation hypothesis with and without the Box-Cox transformation (Fig. 9).

Neither the Gaussian residual distribution nor data transformation is necessary with the bootstrapping approach, in which the simulations start from the empirical distribution of the residuals. Fig. 6 shows a comparison of the simulation in the test periods. Both forecast values and confidence intervals are similar, making the bootstrapping method more suitable as it is less restrictive. Although not perfectly, the forecast follows the tendency and variability of the observed data, and more importantly, the forecast uncertainty represented by the shaded area adequately contains the observed data for the level of significance assumed (5%).

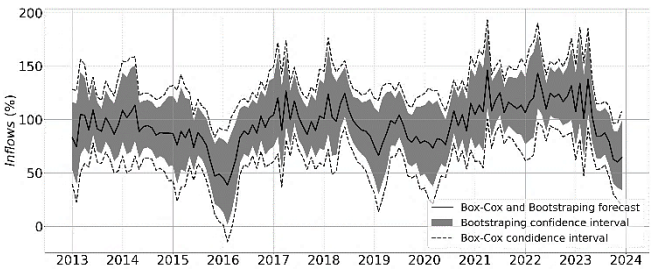

Figure 6. ARX1 forecasting results in the test period.
Source: The authors.

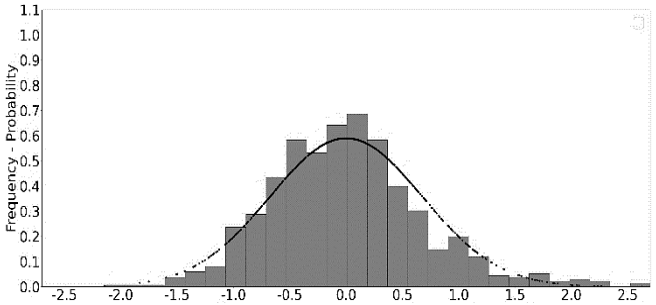

Figure 7. Residuals distribution of the ARX1 model.
Source: The authors.

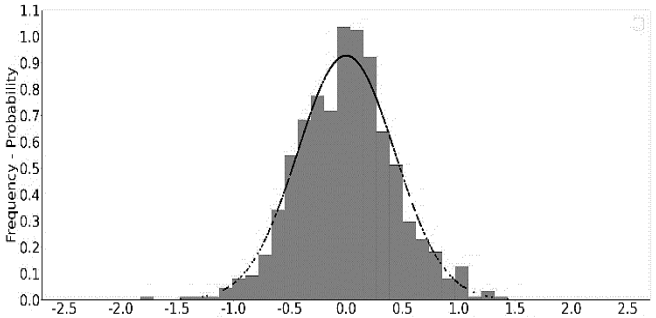

Figure 8. Residuals distribution of the ARX1 model after the Box-Cox transformation.
Source: The authors.

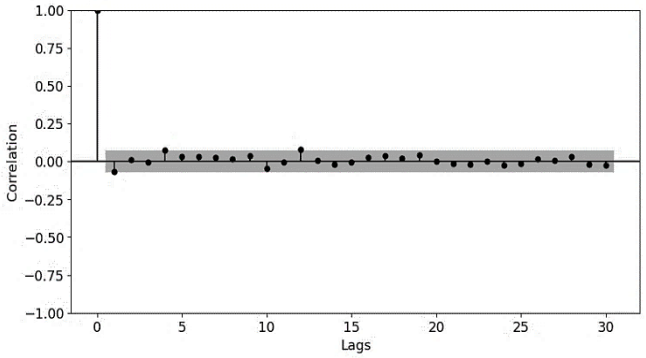

Figure 9. Residuals partial autocorrelation of the ARX1 model after the Box-Cox transformation.
Source: The authors.

Figs. 10 and 11 are related to the uncertainty level of the forecast process. Fig. 8 compares the AR1 and ARX1 models of how the error variance increases with the forecast horizon. Naturally, in both cases, the error variance increases with the time horizon, and it is evident how the exogenous variable influences this increase to be less pronounced, maintaining the error variance significantly lower concerning the AR1 model (without exogenous variables). Moreover, Fig. 9 shows the level of uncertainty according to the target month, estimated as the quotient between the uncertainty length and the multi-annual average value of the forecast month.

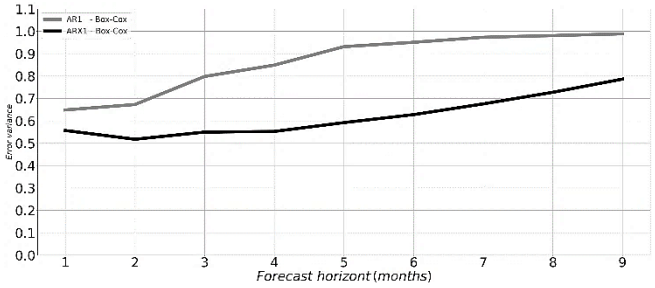

Figure 10. Error variance as a function of the forecast horizon.
Source: The authors.

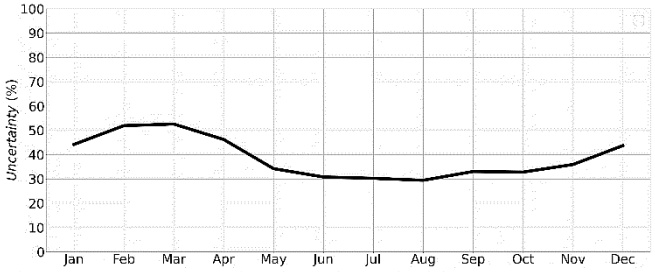

Figure 11. Forecast uncertainty for each month of the year.
Source: The authors.

4.1 El Niño 2023-2024

In May 2023, began one of the strongest El Niño events in recorded history according to the NOAA ONI index. Only five El Niño events have reached two degrees temperature anomaly umbral, and between them is the El Niño 2023-2024 with high global impacts. Particularly in Colombia, since May 2023, a prolonged water availability deficit was observed.

To visualize the model performance in the 2023-2024 event, Fig. 12 shows the one-month ahead forecast for the April-December 2023 period, while Fig. 13 shows the forecasting exercise for the April-December 2023 period using the March 2023 observed inflows and the 9 ONI projected values. The model follows the low streamflow tendency because of the serial dependence and the expected continuity of the El Niño event, as suggested by the climate agencies and incorporated in the exogenous values. As expected in the 9-month forecasting exercise, confidence bands increase with the forecasting horizon, reflecting both the natural uncertainty associated with several months ahead forecast and the duration and intensity of the event.

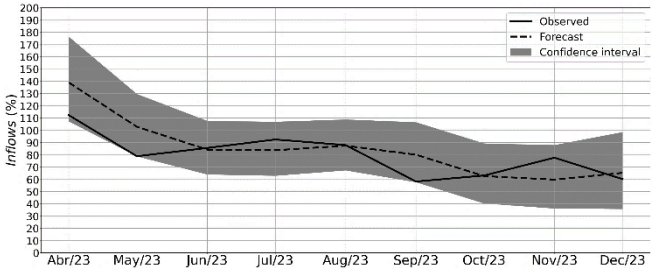

Figure 12. One-month ahead April-December 2023 forecast.
Source: The authors.

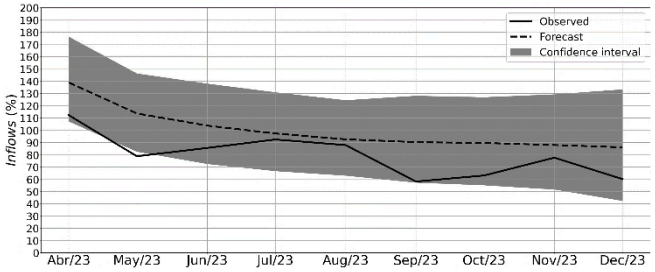

Figure 13. April-December 2023 forecast using the March 2023 observed inflows and the 9 ONI projected values.
Source: The authors.

4.2 La Niña 2024-2025

According with the official CPC ENSO probability forecast, based on a consensus of CPC and IRI forecasters available in https://iri.columbia.edu/our-expertise/climate/forecasts/enso/current/ and published on March 14, El Niño 2023-2024 was expected to finish between April and May, followed by two or three months of neutral conditions and of a La Niña 2024-2025. Fig. 14 shows the December 2023 - August 2024 forecast using the November 2023 observed inflows and the 9 ONI projected values. Consistent with the El Niño event, the forecast suggests system inflow below the historical mean until April. However, the observed inflows have been below forecasted values due to the limitation of the model by not incorporating other variables that could explain the intense system water deficit, such as those related to the Amazon basin and Atlantic Ocean activity. In addition to the above, ENSO patterns and their influence on Colombia may be changing because of the temperature records of the last 2 years, making it more difficult the forecasting exercise. However, the reliability bands capture the variability of the series according to the selected significance level.

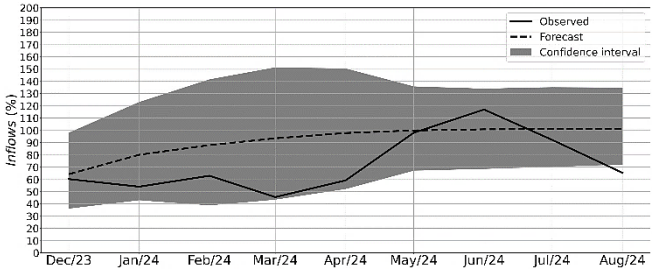

Figure 14. December 2023 - August 2024 forecast using the November 2023 observed inflows and the 9 ONI projected values.
Source: The authors.

5. Conclusions

We studied the Colombian monthly streamflow predictability through the evaluation of different forecasting mathematical models, the use of robust and non-parametric techniques, and the incorporation of exogenous data, trying to extract the maximum amount of information only from the streamflow time series and estimating reliability bands using probabilistic approaches, providing tools for a better water

resources management in the country.

After analyzing the correlation structure of the data employing techniques such as the partial autocorrelation function, monthly energy inflow forecasting through different mathematical models was evaluated. The autoregressive model with exogenous variables presented the best results due to the inflows' high dependence on the previous month, the linear dependence structure of the series, and the climate information contained in the ONI series. Besides, confidence interval estimation using Bootstrap from the empirical distribution of the residuals allows for a reliable estimate of uncertainty without assuming any residual distribution. The stochastic structure of the model finally adopted permits the estimation of multiple plausible scenarios when forecasting, which is an essential condition in the study of uncertainty and risk analysis. The methodology for estimating confidence bands allows us to represent the Colombian hydro-climatology complexity related to its geography, physiography, and hydro-climatological season.

Three aspects determined the viability of incorporating exogenous variables in the forecasting process. Firstly, a statistical analysis of the energy inflow series allowed us to conclude about a significant dependence on the ONI exogenous variable. Secondly, the exogenous data, with predicted ONI values for a horizon of 9 months, significantly impact the energy inflow forecast, especially when predictions are made for horizons longer than three months. Finally, using parsimony criteria, despite having more parameters, the exogenous variable incorporation leads to an increase in the performance or predictability of the model.

Machine learning models implemented did not show better performance than autoregressive models. It could be because the time series does not exhibit nonlinearities, it is much less than the linear dependence, or there is not enough available exogenous data to incorporate in the models. In summary, autoregressive models are more appropriate to capture the time series dynamics.

The results obtained in this research will contribute to the understanding of the hydro-climatological processes in Colombia via mathematical modeling, as the forecasting and reliability bands estimation methodology will provide tools for decision-making in sectors dealing with the uncertainty associated with the distribution of the water resources.

References

[1] Al-Saati, N.H., Omran, I.I., Salman, A.A., Al-Saati, Z., and Hashim, K.S., Statistical modeling of monthly streamflow using time series and artificial neural network models: Hindiya Barrage as a case study. Water Practice & Technology 16(2), pp. 681–691, 2021. DOI: https://doi.org/10.2166/wpt.2021.012.

[2] Bezerra, B., Veiga, A., Barroso, L.A., and Pereira, M., Stochastic long-term hydrothermal scheduling with parameter uncertainty in autoregressive streamflow models. IEEE Transactions on power systems, 32(2), 2017. DOI: https://doi.org/10.119/TPWRS.2016.2572722.

[3] Beyaztas, U., Arikan, B.B., Beyaztas, B.H., and Kahya, E., Construction of prediction intervals for palmer drought severity index using bootstrap. Journal of Hydrology 559, pp. 461-470, 2018. DOI: https://doi.org/10.1016/j.jhydrol.2018.02.021.

[4] Bjerknes, J., Atmospheric teleconnections from the equatorial pacific. Monthly Weather Review, 97(3), pp. 163-172, 1969. DOI: https://doi.org/10.1175/1520-0493(1969)097<0163:ATFTEP>2.3.CO;2

[5] Box, G.E.P., and Jenkins, G.M., Time series analysis: forecasting and control. Holden-Day, 1976. ISBN: 0816211043, 9780816211043.

[6] Cao, L., Mees, A., and Judd, K., Dynamics from multivariate time series. Physica D: Nonlinear Phenomena, 121(1-2), pp. 75–88, 1998. DOI: https://doi.org/10.1016/S0167-2789(98)00151-1.

[7] Carvajal, L.F., Salazar, J.E., Mesa, O.J., y Poveda, G., Predicción hidrológica en Colombia mediante análisis espectral singular y máxima entropía. Ingeniería Hidráulica en México, XIII, (1), pp. 7–16, 1998.

[8] Chen, D., and Cane, M.A., El Niño prediction and predictability. Journal of Computational Physics, 227(7), pp. 3625-3640, 2008. DOI: https://doi.org/10.1016/j.jcp.2007.05.014.

[9] Córdoba, S., Palomino, R., Raquel, Gámiz, S., Castro, Y., and Esteban, M., Influence of tropical Pacific SST on seasonal precipitation in Colombia: prediction using El Niño and El Niño Modoki. Climate Dynamics, 44(5-6), pp. 1293–1310, 2015. DOI: https://doi.org/10.1007/s00382-014-2232-3.

[10] Córdoba, S., Palomino, R., Raquel, Gámiz, S., Castro, Y., and Esteban, M., Seasonal streamflow prediction in Colombia using atmospheric and oceanic patterns. Journal of Hydrology, 538, pp. 1–12, 2016. DOI: https://doi.org/10.1016/j.jhydrol.2016.04.003.

[11] Dracup, J.A., and Gutie, F., An analysis of the feasibility of long-range streamflow forecasting for Colombia using El Niño–Southern Oscillation indicators. Journal of Hydrology, 246, pp. 181–196, 2001. DOI: https://doi.org/10.1016/S0022-1694(01)00373-0.

[12] Favereau, M., Lorca, A., Negrete-Pincetic, M., and Vicuña, S., Robust streamflow forecasting: a student's t-mixture vector autoregressive model. Stochastic Environmental Research and Risk Assessment 36, pp. 3979–3995, 2022. DOI: https://doi.org/10.1007/s00477-022-02241-y.

[13] Ham, Y.G., Kim, J.H., and Luo, J.J., Deep learning for multi-year ENSO forecasts. Nature, 573(7775), pp. 568–572, 2019. DOI: https://doi.org/10.1038/s41586-019-1559-7.

[14] Holton, J.R., and Hakim, G.J., An introduction to dynamic meteorology. 5th Ed., 2012. DOI: https://doi.org/10.1016/C2009-0-63394-8.

[15] Jaramillo, A., y Chaves, B., Distribución de la precipitación en Colombia analizada mediante conglomeración estadística. Cenicafé, 51(2), pp. 102–113, 2000.

[16] Kelman, J., Vieira, A., and Rodriguez, J.E., El Niño influence on streamflow forecasting. Stochastic Environmental Research and Risk Assessment, 14, pp. 123–138, 2000. DOI: https://doi.org/10.1007/PL00009776.

[17] Laing, A.G., and Fritsch, J.M., Mesoscale convective complexes in Africa. Monthly Weather Review, 121(8), pp. 2254–2263, 1993. DOI: https://doi.org/10.1175/1520-0493(1993)121<2254:MCCIA>2.0.CO;2.

[18] Yan, L., Feng, J., Hang, T., and Zhu, Y., Flow interval prediction based on deep residual network and lower and upper boundary estimation method. Applied Soft Computing Journal, 104, art. 107228, 2021. DOI: https://doi.org/10.1016/j.asoc.2021.107228.

[19] L'Heureux, M.L., Tippett, M.K., Takahashi, K., Barnston, A.G., Becker, E.J., Bell, G.D., Di Liberto, T.E., Gottschalck, J., Halpert, M.S., Hu, Z.Z., Johnson, N.C., Xue, Y., and Wang, W., Strength outlooks for the El Niño-Southern oscillation. Weather and Forecasting, 34(1), pp. 165–175, 2019. DOI: https://doi.org/10.1175/WAF-D-18-0126.1.

[20] McPhaden, M.J., Tropical Pacific Ocean heat content variations and ENSO persistence barriers. Geophysical Research Letters, 30(9), pp. 1995–1998, 2003. DOI: https://doi.org/10.1029/2003GL016872.

[21] Mejía, J.F., Mesa, O.J., Poveda, G., Vélez, J.I., Hoyos, C., Mantilla, R., Barco, J., Cuartas, L.A., Montoya, M., y Botero, B., Distribución espacial y ciclos anual y semianual de la precipitación en Colombia. DYNA, 127, pp. 7-26, 1999.

[22] Meng, J., Fan, J., Ludescher, J., Agarwal, A., Chen, X., Bunde, A., Kurths, J., and Schellnhuber, H.J., Complexity-based approach for El Niño magnitude forecasting before the spring predictability barrier. Proceedings of the National Academy of Sciences of the United States of America, 117(1), pp. 177–183, 2020. DOI: https://doi.org/10.1073/pnas.1917007117.

[23] Mesa, O.J., Poveda, G., y Carvajal, L.F., Introducción al clima de Colombia. Universidad Nacional de Colombia, Medellín, primera edición, 1997. ISBN: 9586281442, 9789586281447.
[24] Palm, B.G., Bayer, F.M., and Cintra, R.J., Prediction intervals in the beta autoregressive moving model. Communications in statistics – simulation and computation. 52(8), pp. 3635–3656, 2023. DOI: https://doi.org/10.1080/03610918.2021.1943440.
[25] Poveda, G., Retroalimentación dinámica entre El Niño Oscilación del Sur y la hidrología de Colombia. Tesis de Doctorado, Universidad Nacional de Colombia, sede Medellín, 1998.
[26] Poveda, G., La hidroclimatología de Colombia: una síntesis desde la escala interdecadal hasta la escala diurna. Revista Academia Colombiana de Ciencias, 28(10), pp. 201–222, 2004. DOI: https://doi.org/10.18257/raccefyn.28(107).2004.1991.
[27] Poveda, G., Gil, M.M., and Quiceno, N., El ciclo anual de la hidrología de Colombia en relación con el ENSO y la NAO. Bulletin de l'Institut Français d'Études Andines, 27(3), pp. 721–731, 1998.
[28] Poveda, G., Jaramillo, A., Gil, M.M., Quiceno, N., and Mantilla, R., Seasonality in ENSO-related precipitation, river discharges, soil moisture, and vegetation index in Colombia. Water Resources Research, 37(8), pp. 2169–2178, 2001. DOI: https://doi.org/10.1029/2000WR900395.
[29] Poveda, G., and Mesa, O.J., On the existence of Lloró (the rainiest locality on Earth), Enhanced ocean-land-atmosphere interaction by a low-level jet. Geophysical Research Letters 27(11), pp. 1675-1678, 2000. DOI: https://doi.org/10.1029/1999GL006091.
[30] Poveda, G., and Mesa, O.J., Feedbacks between hydrological processes in tropical South America and large-scale ocean-atmospheric phenomena. Journal of Climate, 10(10), pp. 2690–2702, 1997. DOI: https://doi.org/10.1175/1520-0442(1997)010<2690:FBHPIT>2.0.CO;2.
[31] Poveda, G., y Mesa, O.J., La corriente de chorro superficial del oeste ("del Chocó") y otras dos corrientes de chorro en Colombia climatología y variabilidad durante las fases del ENSO. Ciencias de la Tierra, 23(89), pp. 517–528, 1999. DOI: https://doi.org/10.18257/raccefyn.23(89).1999.2848.
[32] Poveda, G., Mesa, O.J., Salazar, L.F., Arias, P.A., Moreno, H.A., Vieira, S.C., Agudelo, P.A., Toro, V.G., and Álvarez, J.F., The diurnal cycle of precipitation in the tropical Andes of Colombia. Monthly Weather Review, 133(1), pp. 228–240, 2005. DOI: https://doi.org/10.1175/MWR-2853.1.
[33] Poveda, G., Vélez, J.I., and Mesa, O.J., Atlas Hidrológico de Colombia. Universidad Nacional de Colombia, Medellín, 2000.
[34] Rodríguez, N., y Siado, P., Un pronóstico paramétrico de la inflación colombiana. Revista Colombiana de Estadística, 26(2), pp. 89-128, 2003.
[35] Rogers, J.C., The association between the North Atlantic Oscillation and the Southern Oscillation in the Northern Hemisphere. Monthly Weather Review, 112(10), pp. 1999-2015, 1984. DOI: https://doi.org/10.1175/1520-0493(1984)112<1999:TABTNA>2.0.CO;2.
[36] Rojo, J.D., Carvajal, L.F., and Velásquez, J.D., Streamflow prediction using a forecast combining system. IEEE Latin America Transactions, 13(4), pp. 1035–1040, 2015. DOI:10.1109/TLA.2015.7106354.
[37] Thomas, H., and Fiering, M., Mathematical synthesis of streamflow sequences for the analysis of river basins by simulations. Design of Water Resource Systems, Edited by Mass et al., Harvard University Press, Cambridge, pp. 459-493, 1962. DOI: https://doi.org/10.4159/harvard.9780674421042.c15.
[38] Thombs, L.A., and Schucany, W.R., Bootstrap prediction intervals for autoregression. Journal of the American Statistical Association, 85(410), pp. 486-492, 1990. DOI: https://doi.org/10.2307/2289788.
[39] Torrence, C., and Webster, P.J., The annual cycle of persistence in the El Niño/Southern Oscillation. Quarterly Journal of the Royal Meteorological Society 124(550), pp. 1985–2004, 1998. DOI: https://doi.org/10.1002/qj.49712455010.
[40] Trenberth, K.E., General characteristics of El Niño-Southern Oscillation. Teleconnection Linking Worldwide Climate Anomalies. Cambridge University Press, New York, 1991.
[41] Van Den Dool, H.M., Searching for analogues, how long must we wait? Tellus A: Dynamic Meteorology and Oceanography, 46(3), pp. 314-324, 1994. DOI: https://doi.org/10.1034/j.1600-0870.1994.t01-2-00006.x.
[42] Waylen, P., and Poveda, G., El Nino-Southern Oscillation and aspects of western South American hydro-climatology. Hydrological Processes, 16(6), pp. 1247–1260, 2002. DOI: https://doi.org/10.1002/hyp.1060.
[43] Webster, P.J., The annual cycle and the predictability of the tropical coupled Ocean-Atmosphere system. Meteorology and Atmospheric Physics, 56, pp. 33–55, 1995. DOI: https://doi.org/10.1007/BF01022520.
[44] Westra, S., Sharma, A., Brown, C., and Lall, U., Multivariate streamflow forecasting using independent component analysis. Water Resources Research, 44(2), pp. 1–11, 2008. DOI: https://doi.org/10.1029/2007WR006104.
[45] Yang, T., Asanjan, A.A., Welles, E., Gao, X., Sorooshian, S., and Liu, X. Developing reservoir monthly inflow forecasts using artificial intelligence and climate phenomenon information. Water Resources Research. Journal of the American Water Resources Association, (53), pp. 2786–2812, 2017. DOI: https://doi.org/10.1002/2017WR020482.

A.F. Hurtado-Montoya, received the BSc. Eng. in Civil Engineering in 2006 and the MSc. in Engineering (Water Resources) in 1999, both from the Universidad Nacional de Colombia Medellín Campus, and the MSc in Applied Mathematics from the Universidad Eafit Medellin, Colombia. He has a sepecialization in Turbomachenary. As a researcher in the field of hydroclimatology he has published articles related to the spatio-temporal variability of precipitation and climate change in Colombia. He has taught mathematics, hydrology, design of hydraulic structures and general and transient hydraulics. He has participated in the identification, structuring and design of various hydroelectric plants. Currently, he is an energy transactional professional at Isagen. His research interests include time series forecasting and hydroclimatology,
ORCID: 0000-0003-4928-3227.

N.A. Moreno-Reyes, is BSc. in Mathematics, Dr. in statistics conferred by the State University of Campinas. Currently, he serves as a professor at EAFIT University in Medellín, Colombia. His research focus lies within the field of probability and statistics, with a current emphasis on Bayesian inference, stochastic processes, and statistical applications.
ORCID: 0000-0002-9371-1615.

DYNA
http://dyna.medellin.unal.edu.co/

UNIVERSIDAD NACIONAL DE COLOMBIA

Relationship between climate variability and mass removal processes. Tunja-Páez case study

July Katerine Rojas-Mesa, Luis Carlos Leguizamón-Barreto & Luis Alfredo Vega-Báez

Facultad de Ingeniería, Universidad Pedagógica y Tecnológica de Colombia, Tunja, Colombia., july.rojas@uptc.edu.co, luiscarlos.leguizamon@uptc.edu.co, luis.vega@uptc.edu.co

Received: June 7th, 2024. Received in revised form: September 13th, 2024. Accepted: September 30th, 2024.

Abstract
This article focused on the relationship between the influence of climatic variables and seismic activity in the dynamics of slopes that presented mass removal phenomena in the case study: Tunja-Páez Corridor. This analysis was carried out through the application of a probabilistic model that integrated parameters of soil resistance, seismic activity, and accumulated precipitation to establish the definition of rainfall thresholds obtained from the rainfall records preceding each of the removal events. This model used first order, second moment FOSM, and the Poisson distribution of probabilistic foundations to estimate the probability of failure of given slope. Additionally, the change in precipitation in the years 2040, 2070, and 2100 as defined by forecasts of Climate Change (CC) according to IDEAM were used to compare the effects on the probability of soil saturation.

Keywords: climate variability; mass removal; precipitation; seismic activity; road infrastructure.

Relación entre la variabilidad climática con procesos de remoción en masa. Caso de estudio Tunja-Páez

Resumen
El presente artículo tuvo como enfoque relacionar la influencia de variables climáticas y la actividad sísmica en la dinámica de los taludes que presentaron fenómenos de remoción en masa en el caso de estudio: vía Tunja-Páez. Este análisis se realizó mediante la aplicación de un modelo probabilístico que integró parámetros de resistencia del suelo, actividad sísmica y la precipitación acumulada para establecer la definición de umbrales de lluvia obtenidos de los registros de lluvia antecedente a cada uno de los eventos de remoción. Dicho modelo utilizó fundamentos probabilísticos de primer orden y segundo momento FOSM y la distribución de Poisson, con el fin de estimar la probabilidad de falla del talud, además se involucró el cambio de las precipitaciones en el año 2040, 2070 y 2100 definidas por pronósticos del Cambio Climático (CC) según el IDEAM con el propósito de comparar las afectaciones en la probabilidad de saturación del suelo.

Palabras clave: variabilidad climática; remoción en masa; precipitación; actividad sísmica; infraestructura vial.

1 Introduction

The variations presented in the climatic context worldwide have unleashed a series of territorial effects that may impact society in various ways. These impacts include fires, an increase in sea level, extreme weather events, and increases in temperature and precipitation, among others [1]. The change in temperature is shown by the increase of 1°C on a global scale from 1880 to 2017 which is equivalent to a gradual increase of 0.2°C per decade. This scenario is discouraging when the Intergovernmental Panel on Climate Change [2] warns of a global warming of 1.5°C by the year 2040.

Additionally, an average increase of 19 cm in the mean sea level between 1901-2010 was recorded and according to the World Meteorological Organization (WMO) it is expected that this level will reach 58 cm by the year 2100 [3]. These kinds of effects are attributed to greenhouse gas (GHG) emissions discharged into the atmosphere since the industrial revolution as stated by the IPCC. Even though

How to cite: Rojas-Mesa, J.K., Leguizamón-Barreto, L.C., and Vega-Báez, L.A., Relationship between climate variability and mass removal processes. Tunja-Páez case study. DYNA, 91(234), pp. 34-43, October - December, 2024.

Colombia does not contribute significant amounts of emissions into the atmosphere in this type of discharges, it is affected by the climatic variations that this phenomenon implies.

An example of this occurred in 2010 when a rainy event known as the La Niña Phenomenon left 21,300 people affected, 771 homes destroyed, 50 dead, and 52 injured due to mass movements triggered by heavy rainfall throughout Colombia [4]. By taking into consideration the predictions made by the Institute of Hydrology, Meteorology, and Environmental Studies (IDEAM), it is estimated that by 2040 there will be a reduction in precipitation of 30% in the Caribbean region and Amazon, while for the central zone, which includes Cauca, the Coffee Region, Huila, Tolima, and Boyacá, they will increase by more than 30% [5].

The effect of hydroclimatic factors in the activation of historical disasters in Colombia had an incidence of 88% between 1998 and 2016. According with the National Planning Department (DNP), 15% of the incidences corresponded to mass movements throughout the country [6]. Regarding the regional scenario, Boyacá ranks fourth within Colombia as the department with the greatest population exposed to hydroclimatic threats with 59.6% [7]. For the period between 2014 and 2018, 75 mass movements associated with landslides were registered according to a report from the Cámara de Comercio Tunja, Duitama, and Sogamoso [8].

The problems generated by the activation of processes in mass removal brings with it social and economic effects [9], which slow down the development of the territory in terms of transport and connectivity [10]. Colombia has been working on the formulation of strategic risk management plans to mitigate the impact of such events [11]; however, there is no evidence of an analysis in the Department of Boyacá. This is especially true of determining the effects of climatic variables in terms of precipitation and seismic activity on the activation of mass removal phenomena on the slopes that make up the Tunja-Páez road corridor.

The current study incorporates a catalog of mass removal processes obtained from the Mass Movements Information System "SIMMA" from the Colombian Geological Service generated in the study area. This catalog is related to the accumulated daily precipitation and the climate change scenarios of 2040, 2070, and 2100 which allow an estimation of the probability of slope failure. The seismic activity of the area is included through the application of deterministic methods and probabilistic techniques which are represented in Geographic Information Systems [12,13] such as Quantum GIS. The results obtained in this study can be considered an initial phase for estimating the threat in linear projects in the region and provide criteria on the formulation of mitigation and/or adaptation measures for drainage and containment projects related to road infrastructure in the framework of climate change forecasts.

2 Materials and methodology

2.1 Description of the study area

The Tunja-Páez road corridor is 118 km long and is located in the department of Boyacá on the Eastern Cordillera in the An-dean Region and crosses the following municipalities in order from north to south: Tunja, Ramiriquí, Zetaquira, Miraflores, and Páez (Fig. 1). It is identified as Route 60 of the National Road Network and also has a rugged mountainous relief with elevations that vary between 1,300 and 3,000 meters above sea level. These reliefs make it difficult for the geometric layout in some sections and results in areas of instability on the slopes. The Tunja-Páez road corridor has an area of influence of 1,700 km2 and an estimated 53,000 inhabitants. It is currently paved between Tunja and Miraflores according to the National Institute of Roads [14].

2.2 Information collected from mass movements

The information on the mass movements of the department of Boyacá is obtained from the Catalog and Inventory of the Mass Movements Information System (SIMMA) of the Colombian Geological Service (SGC) and the inventory of mass movements of the Georeferencing platform (HERMES) from the National Institute of Roads (INVÍAS). 2174 data points of mass removal events are collected for the department of Boyacá between 1972 and 2020. With the layer of the study road (Tunja-Páez) in QGis, a grid is created that frames the entire corridor road through a rectangular strip 12 km wide and 60 km long, made up of cells of 1 square km. Only mass movements that were limited by the grid are considered which corresponded to 271 events that affect the Tunja-Páez road corridor (Fig.1).

2.3 Information collected about precipitation

A database of the daily precipitation was obtained from the pluviometric stations of IDEAM close to the recorded mass movements as shown in Table 1.

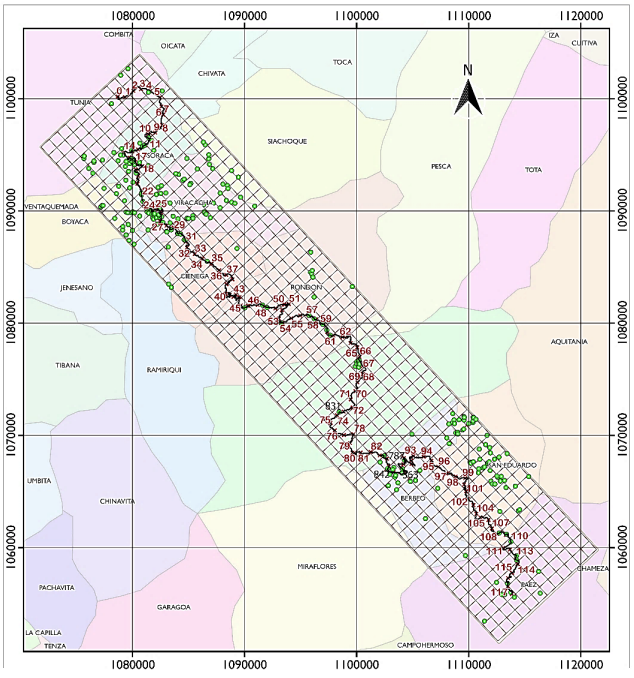

Figure 1. Mass movements recorded in the study area via Tunja-Páez
Source: Authors

Table 1.
Hydroclimatological stations used for the analysis of the precipitation variable

Station	Code	Category*	Latitude (N)	Longitude (O)	Period
Páez	35080050	P	5.096361	-73.053222	1975-2020
Zetaquira	35080010	P	5.282972	-73.169277	1957-2020
Rondón	35085020	CO	5.358416	-73.203611	1970-2020
Ramiriquí	35070010	P	5.399527	-73.332972	1957-2020
Villa Luisa	35075030	CO	5.422222	-73.349416	1981-2020
Teatinos	35070310	P	5.422822	-73.375777	1990-2020
Pila la finca	24030420	P	5.518916	-73.310722	1992-2020
Campo Hermoso	35085050	CO	5.034500	-73.103666	1986-2020
El Vivero	35085040	CO	5.192555	-73.144777	1984-2020
Camp Buenavista	35080030	P	5.183722	-73.086722	1962-2020
UPTC	24035130	CO	5.553611	-73.355277	1962-2020

Category: *P: fluviometric, *CO: Ordinary Climate
Source: The authors

2.4 Geological information collected

The road from the city of Tunja to the Municipality of Zetaquira is located on the Soapaga regional fault and the predominant materials in the area up to the municipality of Páez correspond to colluvial deposits [15]. These masses are composed of clay matrix blocks of colluvial origin. The slopes present undermining events at the base due to the natural channels produced by the high intensity of rainfall in the area. The current study considers the use of the geological units present in the department of Boyacá that frame the study corridor in order to identify the geotechnical parameters that can condition the stability of the soils.

Table 2.
Resistance parameters identified in the Tunja-Páez roadway corridor

Symbol UG	Description	Soil unit weight (KN/m^3)		Internal friction angle (°)		Cohesion (KPa)	
		μ	Σ	μ	σ	μ	σ
Kpgt	Claystones and siltstones with coal seams	19.02	0.95	29.20	2.92	10	5
Ksm	Quartz sandstones, siliceous mudstones, shales and shales. limestone banks.	20.71	1.04	30.18	3.02	10	5
Ngc	Sandstones with intercalations of claystones, conglomerates and locally pyroclastic	19.02	0.95	29.20	2.92	10	5
Pgc	Polymictic conglomerates, quartz sandstones and claystones.	19.02	0.95	29.20	2.92	10	5
Pgt	Claystones with intercalations of clayey to conglomerate sandstones and coal beds.	20.71	1.04	30.18	3.02	10	5
Kim	Limestone and calcareous mudstone, sandstone and claystone conglomerates.	18.63	0.93	28.10	2.81	49.03	24.52
Kit	Quartz sandstones with intercalations of mudstones and limestones.	18.00	0.90	26.00	2.60	35	17.50

Source: The authors

According to the geological map of Boyacá, each type of soil was assigned the resistance parameters corresponding to the unit weight of the soil (γsoil in kN/m3), cohesion (c in kPa), angle of internal friction of the soil (ϕ in degrees), and the average slope of the land (α in degrees) in the areas where landslides occur (Table 2). The values presented in each of the soil properties are obtained from road improvement projects carried out by the Tecnoconsulta Group in INVÍAS studies [14].

2.5 Applied methodology

The current study used the methodology suggested by [16] which considers the infinite slope model that allows forecasting the probability of the failure of a slope (PFT) involving the behavior of accumulated daily rainfall to each slope process mass removal. This method is based on the safety factor equation, whose expression involves the soil resistance parameters of the geological units of the study area, the height of the water table, the topography of the area to be analyzed in terms of inclination of the slopes, and the values of effective peak acceleration (PGA).

Within the bibliographic review of the methodologies that relate rain and seismic activity as triggers of mass removal processes in terms of probability of failure, this methodology turns out to be practical for roads exposed to this type of phenomena because it can be carried out a sensitivity test in the rainfall equations preceding each removal process involving climate change scenarios to try to establish probabilities of saturation and total failure throughout the Vail corridor under study.

The possible relationship of climatic variables with mass removal processes is determined by the probability of total annual failure of a slope (PFA) as applied by [17] by considering the precipitation and earthquake variables. This model estimates the probability that the safety factor (FS) is less than 1.0, indicating a slope failure condition.

The expression evaluates a scenario in dry and saturated conditions by estimating fault surfaces and water tables at different heights. It is limited by the fact that this expression doesn't take into account the effect of soil saturation where these types of movements occur due to the complexity that this implies. Historical rainfall averages in the area of study are included in order to estimate the rainfall threshold that can generate these removal events and therefore give an estimate of soil saturation. The estimation of the probability of slope failure expressed by eq. (1) depends on the mechanical characteristics of the soils and their relationship with the rainfall and seismic activity in the area.

$$P_{ft} = P_{fs} * P_s + P_{ns} * (1 - P_s) \quad (1)$$

Where: Pft = probability of total failure of the slope, Pfs = probability of failure of the slope due to an earthquake in saturated condition, Ps = probability that the soil is saturated, Pns = probability of failure due to earthquake in unsaturated condition, and (1-Ps) = probability that the soil is not saturated.

To determine the probability of total failure of the slope, an estimation of the marginal probability that the soil is saturated, and an emphasis on the estimation is used because the process is carried out empirically to determine the thresholds of rain that can activate mass movements. It is also very complicated to analyze the phenomenon of infiltration and moisture content present in the soils in question. Studies carried out in other areas of Colombia by [18-20] have defined critical rainfall thresholds by considering short-term rainfall and long-term rainfall for each of the mass movements detected.

2.6 Precipitation inference

The generation of rainfall thresholds that can be associated with the appearance of mass movements, are obtained through a mix of short-term rainfall (LA) and long-term rainfall (LAA), which allows dispersion scenarios to be created and compared to rainfall averages and the occurrence of mass removal processes [19].

The relationship between climate variability in terms of precipitation and mass shedding processes lies in the definition of rainfall thresholds for the study area corresponding to the Tunja-Páez roadway corridor. These thresholds were defined by combining short-term rainfall (LA) to the removal event for 1, 3, 5, and 7 days with long-term rainfall (LAA) at 5, 10, 15, 30, 60, and 90 days [21]. These combinations generate 24 scenarios that represent the behavior of rainfall in the area and can be associated with the generation of mass movements. The proposed rainfall threshold for the occurrence of mass movements is represented in Fig. 2.

Fig. 2 contains three representative regions of antecedent rainfall (A, B, and C) for the mass removal events recorded in the study area [18]. Region (A) frames the removal processes possibly activated by little rain; however, these events cannot be related to short-term rainfall, but rather to geological factors in the area.

Region (B) is defined by events triggered by 15 days of accumulated rainfall less than 160mm followed by accumulated rainfall 3 days prior to the activation of the removal process. This condition could signal a dangerous scenario for unstable slopes. Finally, region (C) represents the area where the heaviest precipitation occurs with an accumulation of more than 15 days. The events that occur in this region can be triggered by soil saturation due to a water storage for several days. These regions are described in Table 3.

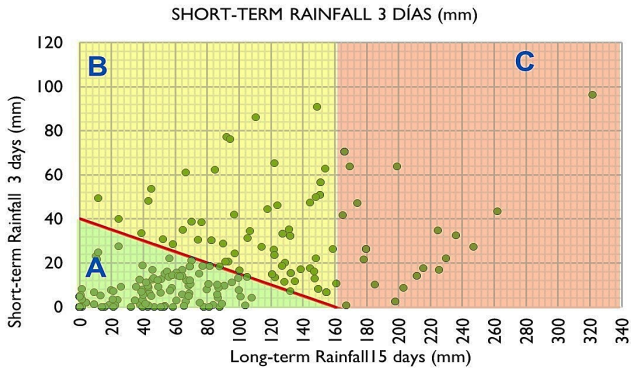

Figure 2. Rain threshold for the Tunja-Páez road
Source: The authors

Table 3.
Description of the representative regions of Fig.2

Region	Description
A	$P_{15} < 40$mm does not exceed threshold
B	$0 < P_{15} < 160$mm exceed threshold
C	$P_{15} > 160$mm exceed threshold

Source: The authors

The behavior of the rains in all the scenarios analyzed allows for the establishment of the definition of thresholds for LA of 3 days and LAA of 15 days, since this combination presents the least dispersion of records of mass removal presented and in turn concentrates the majority of the events (82%) of mass movements between the thresholds of LA of 40 mm and LAA of 160 mm. This indicates that 18% of the events occurred under rainy conditions greater than 40 mm and that the rain on the days prior to the appearance of each of the mass movements can be decisive in the occurrence of surface mass events that are already directly related to the regime of short rainfall. The proposed rainfall threshold Fig. 2 that can cause mass movements in the Tunja-Páez road is expressed by eq. (2).

$$P_3 = -0.25P_{15} + 40mm; \quad con \quad 0 < P_{15} < 160mm \qquad (2)$$

Where: P3: Accumulated rainfall 3 days prior (mm), P15: Accumulated rainfall 15 days prior to the 3 days in (mm).

According to the equation of the straight line, when P15>160mm (defined by the red border line), a very small, accumulated precipitation of 3 days (P3) can trigger a mass removal process. According to [22], it represents a propitious condition for the infiltration of water into the soil layers and generates a critical condition in the event that said accumulated rain increases the pore pressure and therefore reduces the bearing capacity of the soil, thus activating the mass movements. The soil is predicted to be saturated when the 3-day accumulated rainfall exceeds the threshold rainfall calculated by P3 and determined by eq. (3).

$$Ll_{3m} \geq Ll_3 \qquad (3)$$

Where, Ll3m: accumulated rainfall of 3 days LA (mm), Ll3: P3 threshold (mm). In order to fulfill the condition established in eq. (3), a new series is generated that relates the accumulated rainfall of 3 days (LA3) and the preceding accumulated rainfall of 15 days (P15) by means of the mobile rain windows technique. Here, LA3 corresponds to the sum of the precipitation of 3 consecutive days which starts from the first precipitation record including the day on which the event occurs to obtain the first record, the process is repeated adding the following 3 rain records shifting the calculation from day to day to the last record of that series. Finally, Ll3m is the result of the partial summations of the moving rain windows which is repeated for P15.

When the condition of eq. (3) is met, a count is made of the times that the threshold was exceeded in the generated series, which is called occurrences. These occurrences, when divided by the total rainfall records, represents the probability of soil saturation [22]. According to the studies carried out by [17], the probability of soil saturation is related to the probability of annual failure (due to the action of the rains) in

terms of a conditional probability that a landslide occurs at the site (Ls) given that the daily precipitation exceeds the slope failure threshold (RT) as defined by eq. (4).

$$P(L_S|R > R_T) = \frac{ND_S}{ND_T} \quad (4)$$

Where: P(LS | R>RT) = conditional probability that a landslide occurs on the road given that daily precipitation (R) exceeds the critical rainfall threshold, NDS = number of times the threshold is exceeded at the site of the slope, NDT = total number of times the threshold is exceeded in the entire road corridor. This allows us to calculate the temporary probability of failure (PT) expressed by eq. (5) using the Poisson distribution which considers the number of events that exceed said threshold in a time t which refers to the years of record, corresponding to 47 years for the current study.

$$PT = P(X \leq x) * P(L_S|R > R_T) \quad (5)$$

Taking into account that PT= temporal probability of failure of each of the critical slopes and P (X≤x) = Poisson distribution defined as the annual probability of n failures occurring with λ for 47 years of records.

By considering the location of the mass removal points in the road corridor and its area of influence, the conditional probability and the temporary probability of failure of each of the critical points and the probability of saturation of the soil (Ps) can be established. Through the sum of the partial (temporary) probabilities along the Tunja – Páez road, this probability is equivalent to 91.90%.

The determination of the probability of soil saturation exposed in Table 4 is represented in Fig. 3 according to the performance of an interpolation in the Quantum Gis (QGis) software. This allows the probabilistic values in each row of the 1km grid within the area of influence of the Tunja-Páez road.

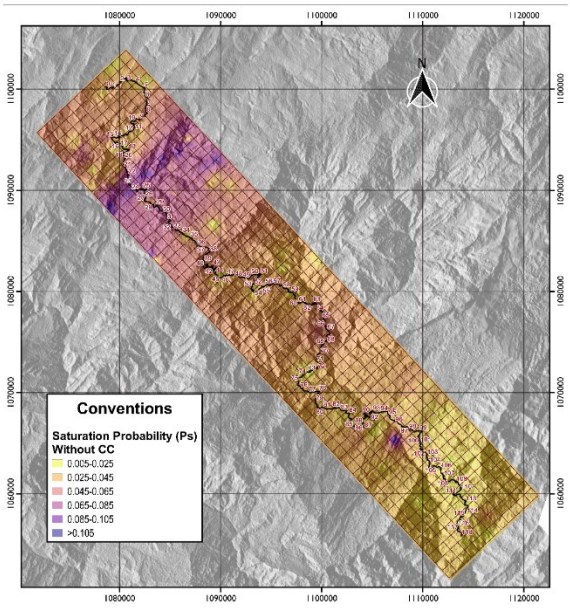

Figure 3. Probability of Saturation without precipitation scenario due to Climate Change (CC)
Source: The authors

Table 4.
Temporary probability of saturation of the Tunja-Páez road by row of the 60 km grid

Number	No. Events	Nf/R>RT	P(Ls/R>RT)	λ	P(X≤x)	PT
1	2	1	0.00629	0.0213	1.00	0.00629
4	4	2	0.01259	0.0426	1.00	0.01259
5	9	8	0.05036	0.1702	1.00	0.05036
6	7	4	0.02518	0.0851	1.00	0.02518
7	2	2	0.01259	0.0426	1.00	0.01259
8	12	3	0.01888	0.0638	1.00	0.01888
9	2	2	0.01259	0.0426	1.00	0.01259
10	15	11	0.06924	0.2340	1.00	0.06924
11	21	16	0.10071	0.3404	1.00	0.10071
12	21	9	0.05665	0.1915	1.00	0.05665
13	4	3	0.01888	0.0638	1.00	0.01888
14	14	10	0.06295	0.2128	1.00	0.06295
15	12	9	0.05665	0.1915	1.00	0.05665
16	3	2	0.01259	0.0426	1.00	0.01259
17	2	2	0.01259	0.0426	1.00	0.01259
18	2	1	0.00629	0.0213	1.00	0.00629
24	5	5	0.03147	0.1064	1.00	0.03147
25	5	4	0.02518	0.0851	1.00	0.02518
26	1	1	0.00629	0.0213	1.00	0.00629
27	2	1	0.00629	0.0213	1.00	0.00629
29	2	1	0.00629	0.0213	1.00	0.00629
30	3	3	0.01888	0.0638	1.00	0.01888
34	7	6	0.03777	0.1277	1.00	0.03777
42	2	2	0.01259	0.0426	1.00	0.01259
43	11	5	0.03147	0.1064	1.00	0.03147
44	16	5	0.03147	0.1064	1.00	0.03147
45	11	1	0.00629	0.0213	1.00	0.00629
46	1	1	0.00629	0.0213	1.00	0.00629
47	7	4	0.02518	0.0851	1.00	0.02518
48	11	2	0.01259	0.0426	1.00	0.01259
49	3	1	0.00629	0.0213	1.00	0.00629
50	8	3	0.01888	0.0638	1.00	0.01888
51	2	2	0.01259	0.0426	1.00	0.01259
53	3	1	0.00629	0.0213	1.00	0.00629
54	1	1	0.00629	0.0213	1.00	0.00629
55	2	2	0.01259	0.0426	1.00	0.01259
56	2	1	0.00629	0.0213	1.00	0.00629
57	2	2	0.01259	0.0426	1.00	0.01259
58	5	5	0.03147	0.1064	1.00	0.03147
59	1	1	0.00629	0.0213	1.00	0.00629
60	1	1	0.00629	0.0213	1.00	0.00629
		TOTAL				**0.919**

Source: The authors

2.7 Climate change scenarios regarding the variability of precipitation

Climate change scenarios in terms of precipitation provide information on the increase or decrease in precipitation in any region of the country. This information was obtained from the IDEAM open data portal in order to observe the areas where these changes are evident in the department of Boyacá. These climate change scenarios correspond to periods of 30 years grouped as follows: from 2011 to 2040; 2041 to 2070, and 2071 to 2100 and were built from the behavior of rainfall in the period between 1976 and 2005. These scenarios present variations ranging from -9% to over 40% depending on the distribution of daily rainfall throughout the department. Considering the above, a new rain series is generated (one series per scenario) using the daily precipitation data modified by the variations that may occur. This allows the thresholds that can trigger movements to be obtained for each climate change scenario and applied to the moving windows process. For the purposes of this study, we intend to analyze the changes presented in the recorded rainfall which affecting them by the critical percentage variation. The results obtained for each scenario are listed in Table 5.

Table 5.
Failure thresholds for each Climate Change scenario

Characteristics	2040	2070	2100
Failure Threshold Equation	P_3= -0.14P_{30}+40mm	P_3= -0.18P_{30}+45mm	P_5= -0.17P_{30}+45mm
No. Data between thresholds	141	147	156
% Data between thresholds	59	54	58
% Probability of roadway saturation Ps	95.40	91.86	97.23

Source: The authors

Table 6.
Temporary probability of saturation of the Tunja-Páez road for each of the climate change precipitation scenarios

Scenario	Ps for the entire roadway (%)	Change (%)
without CC	91.90	
2040	95.40	+3.5
2070	91.86	- 0.04
2100	97.23	+5.3

Source: The authors

To analyze the behavior of precipitation at different time scales and its influence on the Tunja-Páez road, a new series of accumulated daily precipitation has been gathered including this variation for each of the new Climate Change scenarios for the years 2040, 2070, and 2100. This information allows us to compare the probability of saturation in the three scenarios with respect to the current scenario as represented in Table 6.

Each future precipitation scenario presents a marginal change as shown in Table 6. Here, the difference in probabilities for each one with respect to the scenario without Climate Change varies between 0.04% and 5.33%, the latter being the one with the greatest increase in the probability of saturation and corresponding to the year 2100.

2.8 Influence of seismic activity

Seismic activity is associated with the possible occurrence of removal processes on the slopes of unstable areas through the application of the limit equilibrium method [23] in which the safety factor for the infinite slope is considered in each one of the areas of the grid that frames the road corridor. This process allows the probability of slope failure due to seismic action (Pfs) to be calculated by incorporating the parameters of soil resistance, rainfall, and seismic activity [17]. The data on the resistance parameters of the study soils were collected through the layers of the Geographic Information Systems of the Colombian Geological Service, Corpoboyacá, INVÍAS, and other complementary studies. The information to be used corresponds to lithological and geological units obtained from the Geological Map of Boyacá, the Digital Elevation Model DEM, and the seismic hazard layer of Boyacá to obtain the design PGA with respect to the place of each mass movement.

According to the infinite slope methodology, the probabilities of failure of slopes that can present mass movements are calculated according to the return period of the PGA obtained and reported in the General Seismic Hazard Study of Colombia [24]. For the current case study, this corresponds to 475 years with an acceleration value of 0.2g, that is, the multiplying factor will be 1/475 to find the probability of failure of the annual slope given a probability of total failure of the system. Assuming that the resistance parameters and the SF behave according to a standardized normal distribution with a mean of 0 and a standard deviation of 1, eq. (6) is obtained, which relates the aforementioned variables.

$$FS = \frac{c}{\gamma H cos\alpha(sin\alpha + PGA cos\alpha)} + \frac{(\gamma H - \gamma_W Hw) cos\alpha \tan\phi}{\gamma H(sin\alpha + PGA cos\alpha)} \quad (6)$$

Where c= soil cohesion [kPa or kN/m^2], γs= unit weight of soil [KN/m^3], γw= unit weight of water [KN/m^3], H= height of the failing zone [m], Hw= height of the water from the fault surface [m], ϕ = Angle of internal friction of the ground [°], α= average slope of the terrain [°], and PGA= acceleration produced by the earthquake defined by 0.2g. The variables that make up eq. (6), are assumed for H and Hw in the current study in order to analyze the sensitivity of the slope failure probability when failure surface heights (H) of 5m, 10m, and 20m are considered along with water table depths (Hw) of 0m, 3m, and 5m. For the purposes of this analysis, the 5m failure surface is considered since it is related to surface mass movements [25]. As for the heights of water from the failure surface, they are set at 0m and 5m to estimate the probability of failure of the slope during wet conditions and in saturated condition, respectively.

2.9 Slope failure probability

The probability of failure of a slope at a critical point depends on the exceedance of the intrinsic variables of the model. For rainfall, this was calculated through the exceedance of the critical rainfall threshold. However, for the purposes of analyzing the relationship between seismic activity and the generation of mass removal processes, it is determined as the probability that FS is less than 1. This probability is evaluated by means of a reliability index (β) expressed in eq. (7), which considers the effect of the uncertainty of the model representing the number of standard deviations between the most probable value of the factor of safety E(FS) and the factor of safety equal to 1 [FS=1], [17].

$$\beta = \frac{E[FS] - 1}{\sigma[FS]} \quad (7)$$

Where E[FS] = expected value of the factor of safety and σ[FS]= standard deviation of the factor of safety. The estimation of the probability of failure in unsaturated and saturated conditions is determined by the area under the curve of the probability density function of the SF with values less than 1 when applying the normal distribution and the Bae-statistical technique of [26].

The use of the Taylor series to calculate the probability distribution of a function with "n" number of random variables requires the values of the moments of the statistical

distributions of the variables that make up the function, in this case of 1st order and 2nd moment (FOSM), equivalent to the expected value E[FS] and the variance V[FS] of the safety factor. The FOSM method determines the partial derivatives of the variables $\bar{X}i$ =c, ϕ and γ_{soil}, in order to calculate the variance and subsequently the standard deviation [27], as observed in Eq. (8)-(9).

$$E[F] = F(\bar{X}_1, \bar{X}_2, \ldots \bar{X}_N) \quad donde \ \bar{X}_i = E[Xi] \tag{8}$$

$$V[F] = \sum_{i=1}^{N} \left(\frac{\partial F}{\partial X_i}\right)^2 * V(X_i) \tag{9}$$

The function F is evaluated for the mean values of all the variables considered in the calculation of FS. Once the probabilities that make up eq. (1) have been determined, the probability of total slope failure (PFT) can be calculated.

2.10 Results and discussion

The model used for the total probability of slope failure is calculated by determining the E[FS]. This is done by taking the respective average values of the mechanical characteristics of the soils in the area where the Tunja-Páez corridor extends for each of the failure surfaces (H= 5m, 10m, and 20m). Each failure surface (H), in turn contains a calculation of the safety factor for each estimated water table by taking into consideration the different heights of the water level (Hw= 0m, 3m, and 5m). When the failure surface is 5m, the SF decreases in the first 40 kilometers of the road corridor. When the water table rises to 5m with SF values less than 0.5 on the other hand, the last 40 kilometers show values of FS>1.0. The comparison allows for the understanding the variation of the safety factor when it is affected by the water table and the failure surface in the entire road corridor. The changes are presented in Tables 7 and Table 8 taking as reference the failure surface at 5m and the height of the water level of Hw= 0, 3, and 5m respectively.

A decrease in FS is observed on average of 20% when the failure surface is 10m and 30% when this depth is 20m when taking the failure surface at 5m as a reference. For the case of the 5m failure surface, a decrease in the safety factor of 16% is observed when the assumed water table rises to 3m and 26% when the height of the water reaches 5m. This behavior is due to the findings by [28] and other authors when they relate the decrease in the safety factor with the increase in pore pressure and the loss of soil stability caused by the possible saturation of the soil. According to the above, the critical conditions of the soil are evaluated when the water level is 5m corresponding to a saturated condition and in a humid condition when this level is 0m. This allows us to define the probability of slope failure when the soil is saturated and when it is not by applying the normal distribution. This normal probability is calculated taking into account the partial derivatives of the soil resistance parameters through the FOSM method. This determines the variance and standard deviation of the safety factor (eq. 7, 8) in order to evaluate the comparison of this variable with a FS=1.

This process allows us to obtain the probabilities per earthquake for an unsaturated condition (Pfns) in Fig. 4 from which values between 44% and 80% are obtained and for a saturated condition (Pfs) in Fig. 5 with probabilities between 47% and 94%. In critical terms, the probability of failure between 47% and 94% evaluated in a saturated condition (Hw=5m) is related to terrain slopes that range between 38° and 42°. This situation occurs in areas where they present higher probabilities of soil saturation with values close to 30%. Considering that the probability of soil saturation is determined by eq. (4)-(5), a minimum annual saturation probability of 0.63% and a maximum of 10.13% are observed. This corresponds to partial probabilities within the road corridor; however, when evaluated in terms of probability of saturation (Ps) for the entire Tunja – Páez road, it has a value of 91.90% which is considered in the calculation of the Total Failure Probability (PFT) of the slopes in the study area.

Table 7.
Safety factor changes for (H=10m and Hw=0, 3, and 5m)

E [FS] Failure Surface H=10m		
Hw=0m	Hw=3m	Hw= 5m
-0.230	-0.154	-0.104
-24%	-19%	-15%

Source: The authors

Table 8.
Safety factor changes for (H=20m and Hw=0, 3, and 5m)

E [FS] Failure Surface H=20m		
Hw=0m	**Hw=3m**	**Hw= 5m**
-0.344	-0.232	-0.156
-36%	-29%	-22%

Source: The authors

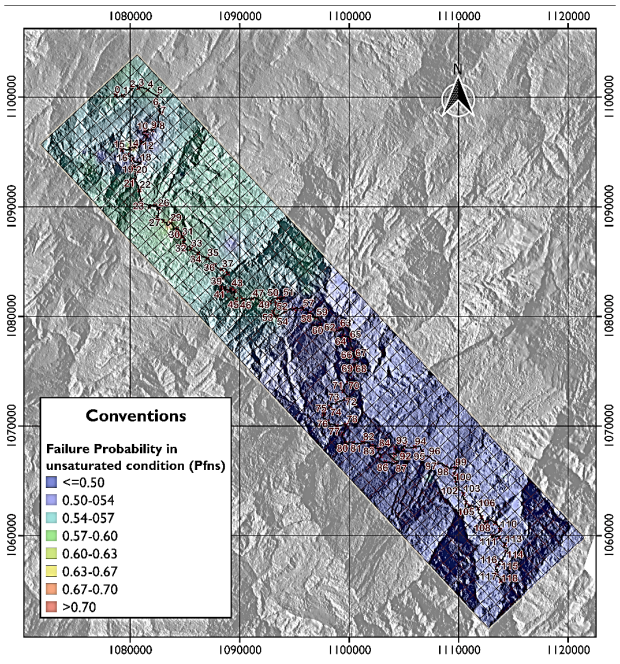

Figure 4. Failure probability due to earthquake in unsaturated condition (Pfns)
Source: The authors

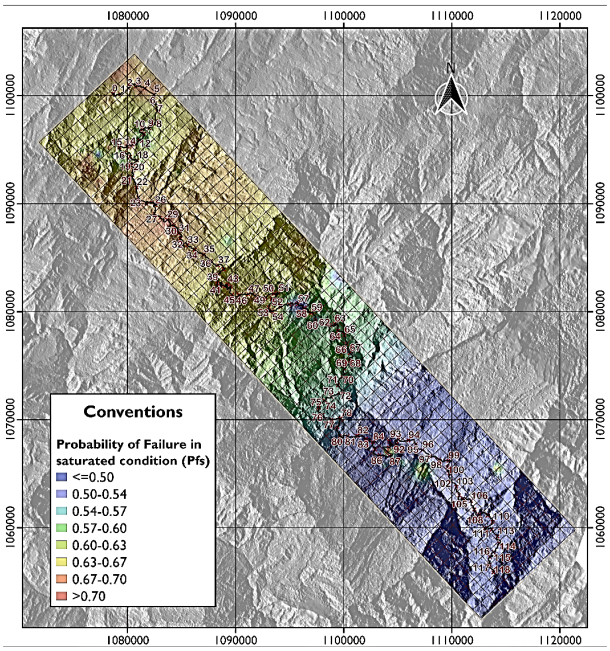

Figure 5. Failure probability due to earthquake in saturated condition (Pfs)
Source: The authors

With the application of eq. (1), the probability of total failure of the PFT slopes present in the Tunja-Páez road is estimated, where values between 46.42% and 93.02% are obtained. When these values are impacted by the annual probability of an earthquake whose value corresponds to 0.2% for a return period of 475 years (design PGA). According to the study from Colombia [24], the annual failure probabilities (PFA) range from 0.0977% to 0.1958% which make up an annual probability of failure in the entire corridor of 32.83%. These annual failure probabilities in terms of landslide hazards can be considered low based on the criteria of [29] and their classification of PFanual for values between 0.2% and 0.02%. According to a diagnosis carried out in the field along the entire Tunja-Páez corridor, 10 critical points are identified that present slopes between 40° and 50° according to the map of slopes from the Lidar images obtained directly in the field using drone flights. These instability zones are presented in Table 9 and the annual failure probability (PFA) is observed for each of the points.

The probabilities of total slope failure (PFT) and total annual slope failure (PFA) presented in Table 9 represent the partial probability of the area where each mass movement was recorded, but not that of the entire road corridor. The probabilities and critical points identified are represented in Fig. 6. According to an interpolation carried out with the PFT results in the QGis program, the behavior of the probability is graphically represented in the entire area of the Tunja-Páez road corridor.

Fig. 6 represents the PFT in the Tunja-Páez road corridor without being affected by the Saturation Probabilities (Ps) of the CC. The highest PFT occurs in the first 55 kilometers of the road belonging to the municipalities of Soracá (PR 4+000), Boyacá – Boyacá (PR 14+000), Ramiriquí (PR 23+000), and Quebrada Honda (PR 54+000) with values above 63%. Meanwhile, PFTs below 47% occur between the municipalities of Miraflores (PR 86+000) and Páez (PR 118+000).

The picture changes when the PFT is recalculated using eq. (1) with the Ps for the three CC scenarios (2040, 2070, and 2100) (Table 5) whose results are presented below (Tables 10 and Table 11).

Table 9.
Critical points obtained in the Tunja-Páez corridor

No.	Marker	Length (m)	Location	PFT (%)	PFA(%)	Contention and/or drainage work
1	PR 13+625	100	Soracá	93.02	0.1958	Failing retaining wall and failing drainage
2	PR 29+583	200	Ciénega	93.02	0.1958	Stone retaining wall and blocked drainage pipes
3	PR 45+581	80	Rondón	64.61	0.1361	No infrastructure
4	PR 57+745	60	Rondón	64.61	0.1361	Box culvert
5	PR 58+925	50	Rondón	54.74	0.1152	Failing retaining wall
6	PR 60+880	220	Zetaquira	48.85	0.1028	Drain in concrete/no retaining wall
7	PR 83+393	50	Zetaquira	46.73	0.0984	Failing retaining wall
8	PR 89+686	40	Miraflores	46.42	0.0977	Box culvert and failing retaining wall
9	PR 108+990	100	Páez	46.83	0.0986	No drainage/retaining wall
10	PR 113+330	200	Páez	46.83	0.0986	No infrastructure

Source: The authors

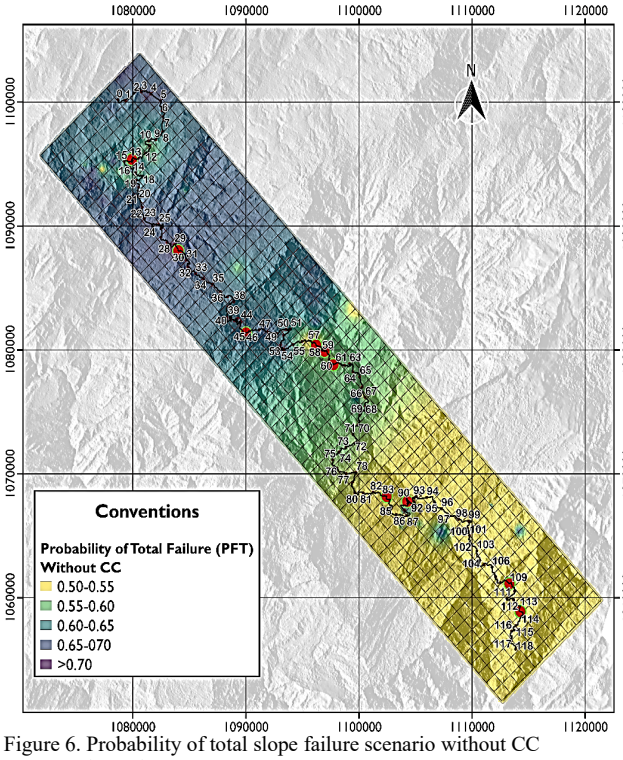

Figure 6. Probability of total slope failure scenario without CC
Source: The authors

Table 10.
Total Failure Probability (PFT) of the Tunja-Páez road for each of the Climate Change (CC) scenarios

Scenario CC	PFT Min. (%)	PFT Max. (%)	PFTA Min. (%)	PFTA Max. (%)
Without	46.42	93.02	0.0977	0.1958
2040	46.50	93.52	0.0979	0.1969
2070	46.42	93.02	0.0977	0.1958
2100	46.54	93.77	0.0980	0.1974

Source: The authors

Table **1**.
Total Failure Probability (PFTA) for the entire Tunja-Páez road in each of the Climate Change (CC) scenarios

Scenario CC	∑ PFTA (%)	Difference (%)
Without	32.83	0.00
2040	32.98	+0.15
2070	32.83	0.00
2100	33.06	+0.23

Source: The authors

Table 10 relates the PFT of each event that occurred in the Tunja-Páez road corridor and in turn the probabilities of total annual failure (PFTA) by involving the annual probability per earthquake. However, Table 11 shows the difference of the PFTA between scenarios referencing the scenario without Climate Change and for the entire road corridor (sum of partial PFTAs of each event).

In Fig. 6, 7, the probability of total failure (PFT) is represented in the area of the study road corridor through the interpolation of the results obtained for the scenario without the effects of Climate Change and the year 2040. The effect of rainfall on the PFT between the scenario without Climate Change and the three CC scenarios (2040, 2070, and 2100) is relatively low. Fig. 7 can represent the behavior of the three CC scenarios since the PFT has a similar behavior.

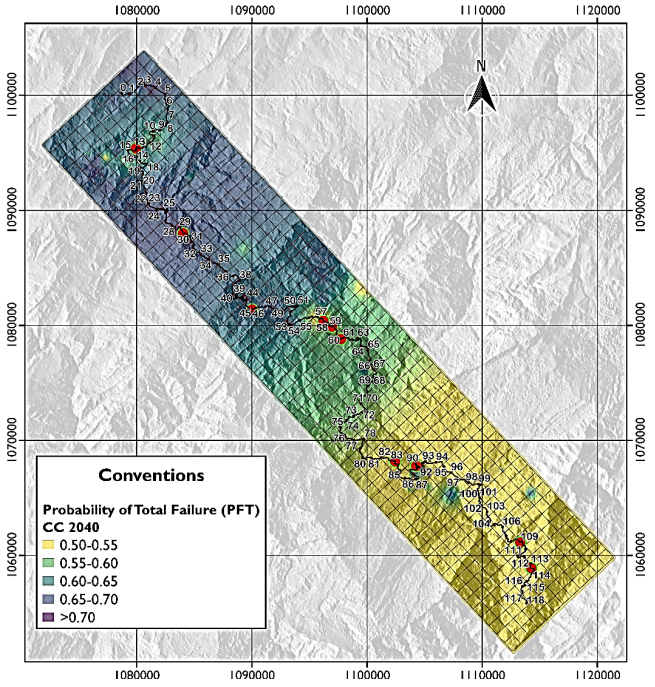

Figure 7. Probability of total slope failure scenario year 2040
Source: The authors

2.11 Conclusions

The probabilistic model based on the limit equilibrium method allows us to determine the existing relationship in a practical way between the climatic variables with mass removal processes and taking into consideration the seismic activity in the deterministic calculation of the safety factor obtained from the mechanical parameters of the soils present in the Tunja-Páez road corridor.

It is important to clarify that these parameters were compiled from previous studies carried out by INVÍAS in the study area and the analysis considers estimated values in order to observe the effects on the geotechnical dynamics of the case study. The applied process aims to approach the behavior of the slopes of the study area when precipitation variables and seismic activity of the area are analyzed. This facilitates failure forecasting in instability zones as long as the history of mass movement records in the study area is available. For the current study, an analysis was carried out at a local scale; however, in order to involve more removal events in the study, it was proposed to frame the road corridor with a grid made up of 1km^2 cells. This generalizes the probabilistic analysis and could reduce the quality of the estimate made due to the size of the cell considered.

The emergence of mass movements triggered by the accumulated rainfall of 3 days and preceding 15 days is possible, according to the fault threshold calculated due to the observation in the behavior of the probability of saturation where the values of greater probability coincide with the critical points identified in the visual inspection carried out in the Tunja-Páez road corridor. When considering the seismic acceleration of 0.2g at all points of mass removal, it was observed that the probabilities due to seismic action in normal humidity or unsaturated conditions had a maximum value of 80% and the scenario becomes critical when the height of the assumed water table (Hw=5m), reaching a probability per action of the earthquake in saturated condition of 94%.

When the probability of total annual failure (PFTA) is recalculated by incorporating the probabilities of saturation (Ps) for each of the Climate Change scenarios, it is observed that the variation of the probability between scenarios is low since the results vary between 0.15% and 0.23% in relation to the scenario without Climate Change. The current study can be considered a preliminary stage of hazard studies due to mass movements in the department of Boyacá and can be improved if the information of all the prevailing soil tests in the region is available. However, it is close to a simulation of the effects of precipitation and earthquakes on the slopes of the analyzed area.

Acknowledgments

This study was supported by the Vicerrectoría de Investigación y Extensión (VIE) of the Universidad Pedagógica y Tecnológica de Colombia (UPTC) Tunja campus in collaboration with public entities such as the Secretaría de Infraestructura de Boyacá and the Instituto Nacional de Vías (INVIAS).

References

[1] Vano, A., Dettinger, M., Cifelli, R., Dufour, A., Miller, K., Olsen, J., and Wilson, A., Hydroclimatic extremes as challenges for the water management community: lessons from Oroville and hurricane Harvey, Explaining extreme events of 2017 from a climate perspective, Bull.

Amer. Meteor. Soc, 100(1), pp. S9-S14, 2019. DOI: https://doi.org/10.1175/BAMS-D-18-0219.1

[2] Panel Intergubernamental de Cambio Climático (IPCC). Calentamiento global de 1.5°C: informe especial sobre los efectos del calentamiento global con respecto a los niveles preindustriales y las trayectorias correspondientes que deberían seguir las emisiones mundiales de gases de efecto invernadero, en el contexto del reforzamiento de la respuesta mundial a la amenaza del cambio climático, el desarrollo sostenible y los esfuerzos por erradicar la pobreza. [en línea]. 2019. ISBN 978-92-9169-351-1. Disponible en: https://www.ipcc.ch/site/assets/uploads/sites/2/2019/09/IPCC-Special-Report-1.5-SPM_es.pdf.

[3] Greenpeace. Así nos afecta el cambio climático. Informe. [en línea]. 2018. Disponible en: https://es.greenpeace.org/es/wp-content/uploads/sites/3/2018/11/GP-cambio-climatico-LR.pdf.

[4] United Nations Office for the Coordination of Humanitarian Affairs (OCHA). Temporada de lluvias 2010 Fenómeno de La Niña. Informe de Situación No 6, pp. 2-7, [en línea]. 2010. Disponible en: https://www.paho.org/disasters/index.php?option=com_docman&view=download&category_slug=colombia&alias=1630-informe-ocha-colombia-ola-invernal&Itemid=1179&lang=en.

[5] Instituto de Hidrología Meteorología y Estudios Ambientales - IDEAM y Universidad Nacional de Colombia - UNAL. La variabilidad climática y el cambio climático en Colombia. IDEAM Bogota, [en línea]. 2018. Disponible en: https://documentacion.ideam.gov.co/cgi-bin/koha/opac-detail.pl?biblionumber=38256.

[6] Departamento Nacional de Planeación DNP. Índice municipal de riesgo de desastres de Colombia. [en línea]. 2018. Disponible en: https://colaboracion.dnp.gov.co/CDT/Prensa/Presentaci%C3%B3n%20%C3%8D%C3%8Dndice%20Municipal%20de%20Riesgo%20de%20Desastres.pdf

[7] Departamento Nacional de Planeación DNP. Índice Municipal de riesgos de desastres ajustado por capacidades. [en línea]. 2019. Disponible en: https://colaboracion.dnp.gov.co/CDT/Prensa/IndiceMunicipaldeRiesgodeDesastres.pdf

[8] Cámara de Comercio de Tunja, Cámara de Comercio de Duitama, Cámara de Comercio de Sogamoso y Fundación Centro de Desarrollo Tecnológico para la Sostenibilidad y Competitividad Regional. Boyacá en cifras. [en línea]. 2019. ISSN: 2539-150X, Disponible en: https://cctunja.org.co/wp-content/uploads/2019/09/Boyaca_Cifras_2019_.pdf

[9] Instituto Distrital de Gestión de Riesgos y Cambio Climático IDIGER. Escenario de Riesgo, Riesgo por Movimientos en Masa. [en línea]. 2020. Disponible en: https://www.idiger.gov.co/rmovmasa.

[10] Mergili, M., Marchant, C.I., y Moreiras, S.M., Causas, características e impacto de los procesos de remoción en masa, en áreas contrastantes de la región Andina. Cuadernos de Geografía. Revista Colombiana de Geografía. 24(2), pp. 113-131, 2014. DOI: https://doi.org/10.15446/rcdg.v24n2.50211.

[11] Banco Mundial Colombia y Global Facility for Disaster Reduction and Recovery (GFDRR). Análisis de la gestión del riesgo de desastres en Colombia: un aporte para la construcción de políticas públicas. 1ra ed. [en línea]. 2012. Disponible en: https://gestiondelriesgo.gov.co/sigpad/archivos/gestiondelriesgoweb.pdf

[12] Bornaetxea, T., Antigüedady, I., y Ormaetxea, O., Mapas de susceptibilidad de deslizamientos a partir del modelo de regresión logística en la cuenca del río Oria (Gipuzcoa). Estrategias de tratamiento de variables. Cuaternario y Geomorfología. 32(2), pp. 7-29, 2018. DOI: https://doi.org/10.17735/cyg.v32i1-2.59493.

[13] Tsangaratos, P., Ilia, I., Hong, H., Chen, W., and Xu, C., Applying information theory and GIS-based quantitative methods to produce landslide susceptibility maps in Nancheng Country, China. Landslides. 14, pp. 1091-1111, 2016. DOI: https://doi.org/10.1007/s10346-016-0769-4.

[14] Instituto Nacional de Vías INVÍAS y TECNOCONSULTA. Actualización de los estudios y diseños para el mejoramiento de la carretera Tunja - Ramiriquí - Miraflores -Páez entre el PR0 y el PR118. Vol. 14, Hito III, 2014, 15 P.

[15] Rojas, J., and Leguizamón, L.C., A review of the relation between climate variability and mass removal processes: Tunja-Páez case study, Ingeniería Solidaria. 18(1), pp. 1-40, 2022. DOI: https://doi.org/10.16925/2357-6014.2022.01.09.

[16] Hidalgo, C. y Vega, J., Estimación de la amenaza por deslizamientos detonados por sismos y lluvia (Valle de Aburrá, Colombia). Revista EIA. [en línea]. 11(22), pp. 103-117, 2014. Disponible en: https://revistas.eia.edu.co/index.php/reveia/article/view/676.

[17] Hidalgo, C., Vega, J., De Assis, A.P. y Villarraga, M.R., Estimación por deslizamiento en proyectos lineales: carreteras en suelos residuales. Conferencia: IV Simposio Panamericano de Deslizamientos. [en línea]. 2012, pp. 1-19, Disponible en: https://www.researchgate.net/publication/294874206.

[18] Moreno, H., Vélez, M.V., Montoya, J. y Rhenals, R.L., La lluvia y los deslizamientos de tierra en Antioquia: análisis de su ocurrencia en las escalas interanual, intra anual y diaria. Revista EIA. [en línea]. (5), pp. 59-69, 2006. Disponible en: https://www.scielo.org.co/pdf/eia/n5/n5a05.pdf.

[19] Aristizábal, E., González, T., Montoya. J., Vélez, J., y Martínez-Guerra, A., Análisis de umbrales empíricos de lluvia para el pronóstico de movimiento en masa en el Valle de Aburrá, Colombia. Revista EIA, [en línea]. (15), pp. 95-111, 2011. Disponible en: https://www.scielo.org.co/pdf/eia/n15/n15a09.pdf

[20] Ramos, A.M., Trujillo, M.G. y Prada, L.F., Niveles umbrales de lluvia que generan deslizamientos: una revisión crítica. Ciencia e Ingeniería Neogranadina. 25(2), pp. 61-80, 2015. DOI: https://doi.org/10.15665/re.v13i1.348.

[21] Althuwaynee, O.F., Asikoglu, O., and Eris, E., Threshold contour production of rainfall intensity that induces landslides in susceptible regions of northern Turkey. Landslides, [online]. 15(8), pp. 1541-1560, 2018. Available at: https://link.springer.com/article/10.1007/s10346-018-0968-2

[22] Vega, J.A., Estimación del riesgo por deslizamientos de laderas generados por eventos sísmicos en la ciudad de Medellín usando herramientas de Geomática. Tesis de Maestría, Universidad Nacional de la Plata, Argentina. [en línea]. 2013. Disponible en: https://comisiones.ipgh.org/CARTOGRAFIA/Premio/Tesis_2015/Tesis_Johnny_Vega.pdf.

[23] Servicio Geológico Colombiano (SGC). Guía metodológica para estudios de amenaza, vulnerabilidad y riesgo por movimientos en masa 1ra ed. ISBN: 978-958-99528-5-6, 2016.

[24] Asociación colombiana de Ingeniería Sísmica AIS. Estudio General de Amenaza Sísmica de Colombia 2009. Comité AIS-300: amenaza sísmica, Bogotá, Colombia. [en línea]. pp. 95-96, 2009. Disponible en: https://www.rcrisis.com/Content/files/EstudioGeneraldeAmenazaSismicadeColombia2009_AIS_lowres.pdf.

[25] Keefer, D.K., Landslides caused by earthquakes. Geological Society of America Bulletin. 95(4), pp. 406–421, 1984.

[26] Baecher, G., and Christian, J., Reliability and Statistics in Geotechnical Engineering. Wiley. ISBN: 978-0-470-87125-6, 2003.

[27] Hidalgo, C. y De Assis, A.P., Herramientas para análisis por confiabilidad en geotecnia: la teoría. Revista Ingenierías Universidad de Medellín. [en línea]. 10(18), pp. 69-78, 2011. Disponible en: https://revistas.udem.edu.co/index.php/ingenierias/article/view/339.

[28] Rosales-Rodríguez, C.A., Hazard maps of shallow landslides associated with infiltration processes in the Sapuyes river basin. Ingeniería e Investigación, 41(1), pp. 1-9, 2021. DOI: https://revistas.unal.edu.co/index.php/ingeinv/article/view/84611/77531

[29] Chowdhury, R., Flentje, P., and Bhattacharya, G., Geotechnical Slope Analysis. 1st ed. Taylor & Francis, 2006. DOI: https://doi.org/10.1201/9780203864203.

J.K. Rojas-Mesa, is BSc. Eng in Transportation and Roads Engineer, Sp. in Road Infrastructure, MSc. in Engineering with emphasis on Road Infrastructure, with experience in analysis in probabilistic estimation of mass movements triggered by precipitation and earthquakes and construction processes. Co-researcher of the Road Infrastructure Research and Development Group of the Universidad Pedagógica y Tecnológica de Colombia (UPTC).
ORCID: 0000-0003-0779-3843

L.C. Leguizamón-Barreto, is Bsc. Eng in in Transport and Roads Engineer, Sp. in Road Infrastructure, MSc., and Dr. in Engineering with emphasis in Geotechnics, with experience in modeling the mechanical behavior of geomaterials and implementation of 3D finite elements. Professor and researcher UPTC.
ORCID: 0000-0002-3316-3768

L.A. Vega-Báez, Transportation and Roads Engineer, Dr. in Engineering, UPM-Madrid – Spain, MSc. in Engineering and research in traffic and transportation, Universidad del Cauca, Sp. in Social evaluation of projects, Universidad de Los Andes. Professor and researcher UPTC.
ORCID: 0000-0001-7343-5791

DYNA
http://dyna.medellin.unal.edu.co/

UNIVERSIDAD NACIONAL DE COLOMBIA

Structure of the production module, production factors and economic performance in Brazilian coffee growth

Matheus Mangia Marques [a], Gustavo Alves de Melo [e], Luiz Gonzaga de Castro Júnior [a], Eduardo Gomes Carvalho [b], Maria Gabriela Mendonça Peixoto [d], Samuel Borges Barbosa [e], Maria Cristina Angélico de Mendonça [a], Patrícia Guarnieri dos Santos [c], André Luiz Marques Serrano [d], Lucas Oliveira Gomes Ferreira [f] & José Baltazar Salgueirinho Osório de Andrade Guerra [g]

[a] *Department of Agroindustrial Management, Federal University of Lavras, Lavras, Minas Gerais, Brazil. matheus.marques3@estudante.ufla.br, gonzaga.ufla@gmail.com, mariacam@ufla.br*
[b] *Department of Administration, Federal University of Lavras, Lavras, Minas Gerais, Brazil. eduardogomes@cefetmg.br*
[c] *Department of Administration, Faculty of Economics, Administration, Accounting and Public Policy Management, University of Brasília, Brasília, Minas Gerais, Brazil, pguarnieri@unb.br*
[d] *Department of Production Engineering, Faculty of Technology, University of Brasília, Brasília, Minas Gerais, Brazil, mgabriela.unb@gmail.com, andrelms@unb.br*
[e] *Institute of Exact Sciences and Technology, Federal University of Viçosa, Rio Paranaíba, Minas Gerais. Brazil. gustavo.a.melo@ufv.br, osamuelbarbosa@gmail.com*
[f] *Department of Accounting and Actuarial Sciences, University of Brasília, Brasília, Minas Gerais, Brazil. lucasoliveira@unb.br*
[g] *Department of Administration, University of the South of Santa Catarina, Florianópolis, Brazil. baltazar.guerra@unisul.br*

Received: February 19th, 2024. Received in revised form: September 12th, 2024. Accepted: October 11th, 2024.

Abstract
Coffee growing is an important activity for Brazilian agribusiness, and several production factors can reflect on economic and productive results. In this sense, the objective of this work was to evaluate, through Structural Equation Modeling, the interactions between property structure and effective operational costs with productivity, product value, and economic performance for coffee growing in Brazil. It was observed that the property structure positively influences productivity, but the hypotheses that they influence product value and economic performance were not validated. As for the effective operating costs, it was only possible to affirm a negative influence on financial performance. In this way, the study contributes to the formation of strategies among producers as well as providing theoretical support on the applicability of the structural equation modeling technique. Finally, it is suggested the use of new managerial indicators to measure economic performance, the evaluation of the impact of coffee beverage quality on costs and ownership structure, in addition to replicating the study for other crops such as oranges, apples, bananas, and papaya.

Keywords: coffee; agribusiness; structural equation modeling.

Estructura del módulo de producción, factores de producción y desempeño económico en el crecimiento del café brasileño

Resumen
El cultivo de café es una actividad importante para la agroindustria brasileña y existen varios factores de producción que pueden reflejarse en los resultados económicos y productivos. En este sentido, el objetivo de este trabajo fue evaluar, a través del Modelo de Ecuaciones Estructurales, las interacciones entre la estructura de propiedad y los costos operativos efectivos con la productividad, el valor del producto y el desempeño económico del cultivo de café en Brasil. Se observó que la estructura de propiedad influye positivamente en la productividad, pero no se validaron las hipótesis de que influyen en el valor del producto y el desempeño económico. En cuanto a los costos operativos efectivos, sólo se pudo afirmar una influencia negativa en el desempeño económico. De esta manera, el estudio contribuye a la formación de estrategias entre los productores, así como brindar sustento teórico sobre la aplicabilidad de la técnica de modelación de ecuaciones estructurales. Finalmente, se sugiere el uso de nuevos indicadores gerenciales para medir el desempeño económico, la evaluación del impacto de la calidad de la bebida de café en los costos y la estructura de propiedad, además de replicar el estudio para otros cultivos como naranja, manzana, plátano y papaya.

Palabras clave: café; agronegocios; modelos de ecuaciones estructurales.

How to cite: Marques, M.M., de Melo, G.A., Júnior, L.G.C., Carvalho, E.G., Peixoto, M.G.M., Barbosa, S.B., de Mendonça, M.C.A., Santos, P.G., Serrano, A.L.M., Ferreira, L.O.G., and Guerra, J.B.S.O.A. Structure of the production module, production factors and economic performance in Brazilian coffee growth. DYNA, 91(234), pp. 44-53, October - December, 2024.

1 Introduction

Brazilian agribusiness is an essential pillar for the country's economic dynamics, ensuring the fulfillment of trade relations in different regions of the world [1]. In addition, the sector is an important source of employment and income generation for disadvantaged classes. According to [2], the Gross Domestic Product (GDP) of Agro grew by 24.31% in 2020, which increased the sector's share of the national GDP. Among the main products, the country has stood out in the production of some commodities such as corn, soybeans, coffee, and meats [3].

Coffee growing is one of the main activities of Brazilian agribusiness and, in this sense, the search for new perspectives of analysis that are capable of making the segment more efficient is characterized as a functional way of identifying production bottlenecks [4]. Coffee is one of the oldest, most popular, and most appreciated beverages around the world and has played an important role in consumer culture since the mid-16th century [4]. In addition, Brazil is the largest producer and largest exporter of coffee in the world [2,5]. In the last ten years, the Brazilian coffee crop grew by 41.6% in production volume, from 43.5 million bags in 2009 [6] to 61.6 million bags in 2020 [5], a 25% increase compared to the previous harvest according to Table 1. About 47.4 million bags come from arabica coffee (Coffea arabica) and 14.3 million bags from conilon coffee (Coffea canephora). The area destined for coffee growing (production and training) is around 2.2 million hectares [5].

Among the main producing states, Minas Gerais is the largest producer, responsible for approximately 33.5 million bags. It is noteworthy that in the state four regions are considered with their specificities, namely: Sul de Minas, Cerrado Mineiro, Zona da Mata Mineira, and Norte de Minas. Espírito Santo is the second largest producer, adding the production of arabica and conilon coffees, the state is responsible for the production of 13.6 million bags. When dealing only with conilon coffee, it becomes the largest producer in the national territory, with about 9.1 million bags [2,5].

Table 1.
Coffee production in Brazil by region and federative units, in thousand bags.

Region/State	Production (thousand bags processed) 2020 harvest
North	2434.10
RO	2434.10
North East	4138.20
BA	4138.20
Midwest	398.90
MT	158.40
GO	240.50
Southeast	53573.70
MG	33460.20
ES	13609.00
RJ	346.00
SP	6158.50
South	937.60
PR	937.60
Others	145.90
Brazil	61628.40

Source: [1]. Note: Estimate in September/2020.

Table 2
Coffee exports in Brazil in 2020

	Arabica	Conilon	Soluble	Roasted	Total
Bags (60kg)	35,599,346	4,924,851	4,124,062	23,765	44,672,024
Exchange Revenue (US$)	4,721,725,831.35	382,863,725.77	539,896,102.20	7,647,076.25	5,652,132,735.57

Source: [3].

São Paulo occupies the third place with the production of 6.2 million bags of Arabica coffee. Then there is Bahia with the production of 4.1 million bags, 2.1 million of which are conilon coffee - the second largest producer of conilon. In the north of the country, the state of Rondônia is the third largest producer of conilon coffee, with around 2.4 million bags, and ranks fifth overall. In the south of the country, the sixth largest producer is Paraná, with the production of 937.6 thousand bags of Arabica coffee. According to the [8], the export volume in 2020 was 44,672,024 bags of 60 kg, according to Table 2, with foreign exchange revenue of US$ 5,652,132,735.57.

Coffee farming has economic and social importance, as it is an activity of great importance and contributes, on a large scale, to the generation of jobs, income, and is of fundamental importance for regional development due to its ability to move the economy in several sectors, from cultivation to processing and marketing of products derived from the field [5]. When it comes to aspects related to productivity, coffee farming has faced difficulties with the occurrence of undesirable climatic events in recent years and that may extend over the next few years if containment measures are not taken [9]. In this sense, long periods of drought associated with the occurrence of frosts have impacted coffee production in the main producing regions. In Brazil, coffee production is divided into two types, namely Arabica and Conilon coffee. The production of Arabica coffee extends to the regions of Minas Gerais, Espirito Santo, Paraná, São Paulo, and Bahia. Conilon production occurs mainly in the states of Rondônia, Bahia, and Espírito Santo [2,5].

Coffee production in Brazil is also influenced by effective operating costs which are linked to production stages ranging from field production, harvest and post-harvest, processing, marketing, and export [5,10]. These costs have a direct impact on the economic performance of the activity. Given this, the objective of this study was to evaluate, through Structural Equation Modeling, the interactions between property structure and effective operating costs with productivity, product value, and economic performance for coffee farming in Brazil.

In this context, it is worth noting that the economic performance of agricultural properties can be measured through the use of economic indicators that use production costs [11]. The identification of production costs of an agricultural company offers a range of possibilities of analysis, among them the analysis of profitability: an indispensable tool when looking to verify the efficiency of a productive activity [12,13].

The calculation of the income of agricultural enterprises, compared to the total costs of production, provides subsidies

to observe the degree to which costs were recovered through the products obtained in the company, products that are marketed, stored, and/or consumed [14]. There are several purposes for which production cost data are used and for each of them, a specific script must be followed, both for calculation and analysis. Thus, the costs serve to verify how the resources used in a production process are being remunerated, making it possible to verify how the profitability of the activity in question is, compared to alternatives for the use of time and capital [15].

The concept of operational cost developed by the Institute of Agricultural Economics [16], is conceptualized as the expenses effectively disbursed by the farmer plus the depreciation of machines and specific improvements of the activity, incorporating other cost components, aiming to obtain the total cost of production and profitability analysis. To calculate the hourly cost of the machines, the concept of variable cost (repairs, fuel, consumables, and operator labor) and fixed cost (depreciation, insurance, garage, and interest on capital) was considered. The sum of these two components constitutes the total cost, per hour, of using the machines, considering the different characteristics of each machine [17].

[17] treats Gross Margin (MB) as a margin about the effective operating cost (COE), that is, the result that remains after the producer pays the effective operating cost and about this same cost (in percentage) considering a certain unit sales price and the yield of the production system for the activity. For [12], the gross margin (MB) is constituted from the difference between total gross revenue and variable costs. The result will demonstrate whether the property under analysis is covering current production costs, without taking into account fixed and opportunity costs. The positive result will determine the survival of the activity, at least in the short term [12].

In a market system, the economic performance of agricultural properties depends mainly on the following factors: i) Structural characteristics of the production unit: combination and organization of production factors and edaphoclimatic characteristics; ii) Nature and degree of production intensification: technological level used in production; iii) Level of technical and managerial efficiency of production: rational use of agricultural techniques and use of managerial tools; and iv) Importance of expenses with obtaining means of production: expenses related to the use of means of production [18].

In addition, good performance management practices associated with coffee production can bring benefits to leverage results in the sector. According to [19] and [20], performance management comprises an important aspect for the strategic planning of organizations. In agribusiness, performance management can occur through performance monitoring mechanisms, for example, with the use of performance indicators [19]. Thus, there are quality, capacity, production, and financial indicators, among others, that can be incorporated into coffee production [19,21].

However, strategic planning is a key element for achieving good results in a given sector [20]. In coffee farming, this planning is present from the initial stages of planting, where producers measure costs, choose indicators, define short and long-term goals and objectives [22]. However, this requires the effort of a group of collaborators, which can initially impact operating costs, being often unfeasible for small producers [23].

In Brazil, about 80% of coffee production comes from areas cultivated by small producers [22,24]. This fact directly reflects on the generation of jobs, where there are more than 8 million people in paid activity. In this way, the possibility of acquiring credit and rural insurance by this class of producers has been an alternative to overcome the difficulties imposed by the economic scenario recently [22]. It is worth mentioning the value added by family production to the quality of the coffee produced since the cultivation of specialty coffees follows unique processes, different from large-scale and mechanized production [22].

Coffee, according to [7], represents the second most consumed beverage in Brazil, and this consumption has grown steadily in recent years. At the same time, the population's interest in coffees of certified origin has also grown, especially for types of coffee of organic origin [22,25]. The presence of certification is an important aspect of proving the attributes of the drink, especially for the lay public, but it prioritizes good eating habits [22].

Thus, the study seeks contributions regarding the unfolding of the financial structure for the coffee trade. In this way, producers based on this knowledge will have greater possibilities within the productive activity, to plan better according to the variables that most impact the economic performance of the activity. In addition, a theoretical contribution constitutes the formation of relevant material on the applicability of the structural equation modeling technique in coffee farming.

Therefore, the study was divided into an introductory section, with the presentation of relevant information that justify the study, followed by the hypothesis section and research model. Thus, the next section corresponded to the methodology, where the study was characterized, and the structural model was validated. Soon after, the results and discussions were presented, followed by the conclusion and section of acknowledgments and references.

2 Research hypothesis and model

2.1 Hypotheses

The study starts from the investigation of the production factors and property structure have a direct impact on the economic performance of the activity. In this sense, Table 3 presents the hypotheses that were tested to interpret the relationships between predictor variables.

The first hypothesis presented seeks to confirm the influence of disbursements with inputs on effective operating costs (COE) since expenses related to the purchase of correctives, fertilizers, and pesticides are components of the indicator [16].

The second hypothesis deals with the verification of the influence of the property structure (productive module), a construct that is composed of predictor variables such as “productive area”, “culture”, “type of production” and “crop

Table 3.
Research hypotheses.

H_1: Disbursements with inputs influence the property's effective operating costs (COE).
H_2: The structure of the productive module influences productivity.
H_3: The structure of the productive module influences the value of the product.
H_4: The structure of the productive module influences economic performance.
H_5: Effective operating costs (COE) influence productivity.
H_6: Effective operating costs (COE) influence the value of the product.
H_7: Effective operating costs (COE) influence financial performance.
H_8: Productivity influences financial performance.
H_9: Product value influences financial performance.

Source: Authors (2022).

system". Hypotheses H2, H3, and H4 test whether the construct influences productivity, product value, and economic performance, respectively. The crop is divided into Arabica coffee or conilon coffee production and the cultivation system into irrigated or rainfed. Meanwhile, the type of production is categorized into i) manual, when mechanized activities are not carried out (use of self-propelled agricultural equipment); ii) semi-mechanized, when there is mechanized activity in carrying out the cultivation, but the harvest is manual; and iii) mechanized, when there are mechanized activities in driving and harvesting [26].

In addition, the influence of the COE is also tested by the hypotheses H5, H6, and H7, which are linked to productivity, product value, and economic performance, respectively. From these, it is sought to verify if the value related to the expenses interferes in an increase in productivity or the quality of the product (value). The relationship with performance (MB) is expected to be negative about economic performance, given that MB=Receita-COE. Hypotheses H8 and H9 aim to confirm the direct impact of productivity and product value with economic performance. Revenue is the product between productivity and the value of the product, so it is expected that both hypotheses will be accepted.

The proposed structural equation model to test these hypotheses was built with the help of SmartPLS3 software, shown in Fig. 1.

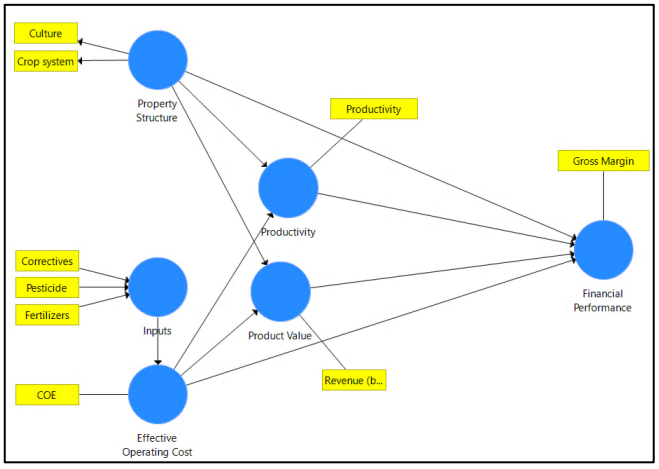

Figure 1. Proposed Structural Equation Model.
Source: Authors (2022)

2.2 Structural equation modeling

Structural equation modeling is a statistical method used to analyze multivariate data sets that use a combination of techniques and procedures [27,28]. According to [29] and [30], structural equation modeling can also be understood as an improved version of path analysis, which allows the investigation direct and indirect causality between variables. According to [31] and [32], the modeling of structural equations can help in the planning of organizational actions. The method involves the development of a structural model that represents the possible paths between the variables, the analysis and adjustment of the measurement model, and the model focuses on minimizing the difference between the covariance matrix and the observed variance [32,33].

In addition, this method allows several models to be tested, and different paths specified, so that the reality under study can be portrayed in more detail [28]. Although the measurement model can reproduce the possible paths and, therefore, allow the analysis of the interrelationship between the variables, it is necessary to verify the fit between the observation data and the hypothetical model [29,33,34]. According to [27] and [30], this verification can be performed through factor analysis. These authors also emphasized that there are two types of factor analysis: exploratory factor analysis, which links unobserved variables from which conclusions are drawn, with observable variables; and confirmatory factor analysis (CFA), which tests a set of variables based on theoretical or empirical observations and evidence and based on that, tests the model's fit against competitive factors.

[35] confirmed this view and the CFA has an important value in the data review and improvement process. Due to the nature of the data and the direct dependence of the distribution, the estimation of the structural model and the measurement model of structural equation modeling is very complicated to perform [28,36]. [37] point out this argument, emphasizing that this estimate analyzes the hypothetical structure of the sample data and then tests how well the observed data fits the measurement model. Also, according to the authors, the analysis is performed by comparing the variance-covariance matrix that represents the relationship between the variables and the estimated variance-covariance matrix of the best-fit model.

According to [33], a structural model can contain formative and/or reflexive constructs. The formative constructs are formed by variables observed and, not necessarily, correlated. The reflexive constructs are formed by observed and correlated variables [32]. In this sense, the use of structural models allows the simultaneous estimation of interrelated dependence relationships, as well as the incorporation of measurement errors in the model estimation process [28,32].

3 Methodology

Data on coffee production costs in Brazil and Brazilian producing states used in this study were collected by the "Campo Futuro" project. This project is made up of several partner institutions, including the Confederation of Agriculture and Livestock of Brazil (CNA), the National Rural Learning Service (SENAR) and the Center for Intelligence in

Management and Markets (CIM) of the Federal University of Lavras (UFLA).

The methodology used for data collection was the Panel. This method consists of meetings with small, medium, and large producers, in which they provide information on labor, crop management, harvest and post-harvest, general expenses, financial values, crop area, inputs, productivity, machines, and equipment, cost interest and inventory [16,38,39].

This study used the basis of the factors that make up the effective operating cost (COE). According to [2], the COE comprises all costs effectively spent in an agricultural year, involving all cost components generated by the relationship between the technical coefficients (amount used) and their prices. As well as the characteristics of the productive modes that portray the productive area, productivity, the species of coffee cultivated, the type of production, the cultivation system, and the value obtained in the commercialization of the product. The time cut used was from 2017 to 2020, totaling 49 samples.

To analyze the financial viability of the different groups, the gross margin was used as an indicator of the financial performance of the milk activity, calculated by the equation: Gross Margin = Revenue (per hectare) – Effective operational cost (per hectare). The measurement of production factors is given by the indicators of costs with inputs (fertilizers, correctives, and pesticides) and effective operating costs.

The first methodological step was to organize the indicators in scales, being necessary to apply the logarithmic scale in base 10 for the indicators defined by unit of area (hectare). After transforming the data into ".txt", inserted the file into the software and mounted the model.

The next step was to verify the discriminant validity using the Heterotrace-Monotrace (HTMT) criterion, as shown in Table 4. Values above 0.90 indicate that discriminant validity is not present and only one construct presented a higher value (in bold).

The next step was to evaluate the reflective models, through the reliability of the indicator, internal consistency, convergent validity, and discriminant validity, as shown in Table 5. Higher external loads indicate how common the indicators are and values above 0.708 are recommended, as they indicate that the construct explains more than 50% of the variance of the indicator. Cronbach's alpha should assume values between 0.7 and 0.95 and composite reliability greater than 0.7. While the convergent validity (AVE) must be greater than 0.50 and with that, the reflexive constructs are validated, confirming the discriminant validity.

Table 4.
Discriminant validity analysis based on the HTMT criterion.

Variables	Operational costs	Property Structure	Productivity	Financial feedback	Product Value
Operational costs					
Property Structure	0.556				
Productivity	0.630	0.985			
Financial feedback	0.381	0.151	0.122		
Product Value	0.402	0.690	0.653	0.341	

Source: Authors (2022).

Table 5.
Validation of reflexive constructs.

Latent variable	Indicators	External loads	Cronbach's alpha	Composite reliability	BIRD	Discriminant validity?
Property structure	Culture	0.946	0.855	0.932	0.873	Yes
	Cultivation System	0.922				

Source: Authors (2022).

Table 6.
Validation of training constructs.

Construct	Indicator	External loads	T value	Value - p
inputs	Concealers	0.351	1,665	0.096
	defensive	0.192	0.561	0.575
	fertilizers	0.999	29,710	0.000*

Source: Prepared by the author (2021).

The evaluation of formative constructs takes place by checking the convergent validity of formative measurement models, evaluating the models in question of collinearity and the significance and relevance of formative indicators. Table 6 verifies the external loads of each indicator with statistical significance with p-value < 0.5. Only the indicator "Fertilizers" was relevant, but the others remained due to proof of participation of the construct in the literature.

Table 7 presents the assessment of the collinearity of the indicators through VIF values. Thus, VIF values above 5 indicate critical problems of collinearity between the indicators of formatively measured constructs. Ideally, VIF values should be close to 3 and below, which is what happened with the data indicated in Table 7.

4 Results and discussion

This study aimed to analyze the influences of production factors and the structure of the productive module on the economic efficiency of coffee farming in Brazil based on the Gross Margin obtained. Fig. 2 presents the result of the proposed Structural Equation Model. In this way, one can verify the strong path coefficients between property structure and productivity, between inputs and costs, between productivity and economic performance, and between product value and economic performance.

Table 7.
Collinearity Analysis.

Variables	VIF
COE	1,000
Concealers	1,117
Culture	2,265
defensive	1.056
fertilizers	1,176
gross margin	1,000
Productivity	1,000
Revenue (bag)	1,000
cultivation system	2,265

Source: Authors (2022).

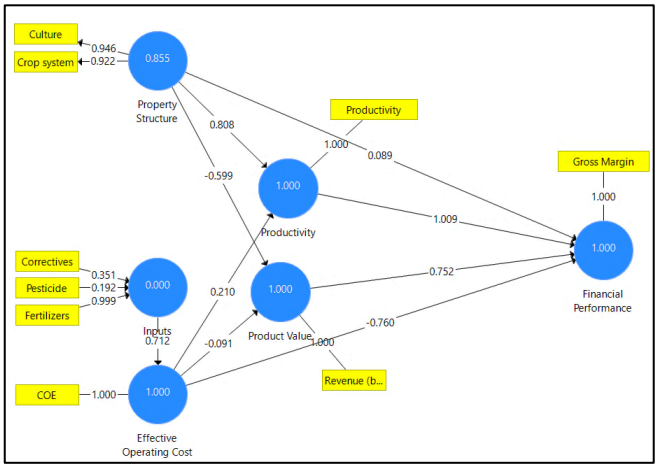

Figure 2. Result of the proposed Structural Equation Model.
Source: Authors (2022).

Still according to Fig. 2, it is possible to observe a predominance of formative constructs in the structural model. Thus, only the construct "Ownership structure" was considered reflexive, where its predictor variables present high correlation. According to [5] and [2], before carrying out a particular planting, issues related to the choice of cultivation and the cultivation system to be used are important to guarantee good productivity and preserve the quality of the crop. ground.

In the field of coffee farming, soil preparation is an important step in the process, since coffee productivity depends on the nutrients present in the soil in specific amounts [40]. Among the producing properties in Brazil, it is common to use strategies for this purpose, such as crop rotation based on the cultivation of corn, soybeans, and cotton, for example, and the later introduction of coffee [41]. In addition, the use of fertilizers is one of the concerns of producers, given the high cost of these elements for production. Thus, a viable alternative is the use of residues generated in production such as coffee husks, which have a high nutritional value for the soil, partially replacing the consumption of fertilizers [40].

Given this, the "Inputs" construct contemplates the predictive variables of fertilizers, correctives, and pesticides. These three elements, when present, guarantee good coffee productivity [41]. However, the excessive use of these can negatively impact both the quality of the product and the soil as well as the operational costs of production, generating an unsatisfactory economic performance of the activity [41]. Furthermore, this study investigates other forms of relationship between the constructs "Inputs", "Productivity" and "Product Value". Productivity in the structural model of Fig. 2 is a first-order construct, as is the value of the product. Productivity represents the amount of coffee bags produced per hectare, while the value of the product corresponds to the product's commercialization price, both are tested in the model based on the impact on "Economic performance".

The relationship between the constructs "Ownership Structure", "Productivity" and "Product Value" are also tested by the structural model. According to [42], there is a difference between the type of soil and the treatment performed in it for the choice of a particular cultivar. In this sense, coffee is characterized as a plant that adapts well to the tropical climate prevailing in Brazil. The relief is also an important aspect of the formation of coffee plantations. That said, the quality of the product is impacted and the variation in product prices can vary according to the processes carried out since planting.

In a recent context, the use of certifications of origin and processes is a measure implemented for producers who produce coffees with a high standard of quality [2]. In addition, certification supports the role of consumer choice by attesting that the product was produced according to a set of specific processes in each region [43]. According to [43], Minas Gerais is one of the largest coffee producers in Brazil, and, above all, it has a denomination of origin certification, which means that this region has specialized and can produce a differentiated and excellent product as in Honduras and Colombia, for example.

The search for better results by coffee producers has been recurrent in Brazil in recent harvests, given the occurrence of undesirable climatic events such as long periods of drought and the occurrence of frosts that hampered the prosperity of production [44,45]. In addition, the global economic context has made it difficult to form good prices and an attractive margin for producers, with the high price of inputs and exchange rate issues with the devaluation of the real [2]. Thus, an alternative has been the commercialization of the product in the foreign market through standardization and increase in the quality of the product. Another alternative line contemplates the organic production of coffee that has grown among the preference of consumers in the country, and reducing costs for producers with inputs [41].

Table 8 presents the results obtained by the hypothesis test, and it can be affirmed that the hypotheses H1, H2, H7, H8, and H9 were accepted. It confirmed that inputs have a direct influence on the behavior of effective operating costs, that the ownership structure has a direct influence on productivity, that effective operating costs negatively influence economic performance, and that both productivity and product value positively influence performance economic.

The hypotheses H3, H4, H5, and H6 had no statistical significance at 0.05 and, therefore, were rejected. Thus, it is not possible to say that the property structure somehow influences the value of the product or economic performance. Likewise, it cannot be said that effective operating costs influence productivity or product value.

The hypothesis H1 was used as a test hypothesis for the model, following the Production Cost Theory, conceptualized as the sum of all resources (inputs) and operations (services) used in the production process of some productive activity [46]. However, the proposed structural model considers only fertilizers, correctives and pesticides as inputs. The result obtained in hypothesis 1 confirms the impact of these elements on the effective operational cost of production. According to [47], expenses with fertilizers were the main responsible for the variation in coffee production costs in Brazil in recent years.

Table 8.
Analysis of the structural model and hypothesis testing.

Hypotheses		T statistic	p-value	Expected signal	Signal found	Result
H1	Inputs → Effective Operating Costs	2,060	0.039**	+	+	Accepted
H2	Property Structure → Productivity	2,615	0.009**	+	+	Accepted
H3	Property Structure → Product Value	1.902	0.057	+	-	reject
H4	Ownership structure → Economic performance	0.118	0.906	+	+	reject
H5	Effective Operating Costs → Productivity	1,730	0.084	+	+	reject
H6	Effective Operating Costs → Product Value	0.178	0.859	+	-	reject
H7	Effective Operating Costs → Economic performance	2,089	0.037**	-	-	Accepted
H8	Productivity → Economic Performance	2.010	0.045**	+	+	Accepted
H9	Product Value → Economic Performance	2,460	0.014**	+	+	Accepted

Source: Authors (2022).

The hypothesis H2 confirmed that the structure of the property has a positive influence on productivity, being considered as components of the structure in the research in question, the species (Coffea arabica or Coffea canephora), and the production system (manual, semi-mechanized or mechanized). The botanical differences between the species predict that Coffea canephora has higher productivity and this fact is reflected in the study. In the work by [26] "the productivity of the coffee crop was not influenced by mechanized harvesting over the years, with the harvester passing once or twice in the crop. The increase in stem vibration promoted a greater amount of harvested grains, but defoliation increased proportionally to the increase in vibration. With two passes of the harvester, defoliation was greater than manual harvesting in all crops studied."

In the hypothesis H3 the property structure was expected to influence the value of the product since Coffea arabica has a higher market value and this factor could be inconsistent with the result. As described by [48] "the price The higher sales price of Arabica coffee can be justified because it is used to produce specialty coffees, or gourmet coffees, it is a differentiated bean that generates more added value and requires greater attention in its cultivation. Conilon coffee is used for blends, that is, blends and for soluble coffee, so it tends to have a lower selling price". In addition, the structure of the property is associated with the quality of the product, since higher-standard coffees require unconventional production processes [48,49]. However, this study, by rejecting this hypothesis, provokes reflections on low-standard productions, where small producers find themselves financially unable to make investments that raise the quality and value of the product. According to the [50], the availability of rural credit is a decisive issue for small producers to remain in coffee farming.

In the hypothesis H4 it was expected that, reflecting the higher valuation of the product proposed in H3, the ownership structure would have a positive impact on economic performance but was also rejected. Again, the study went in a different direction than expected, inferring that the cultivation system and culture do not influence economic performance. However, if the scenario of small producers is considered, the situation is reversed, since there is a lack of resources to have satisfactory impacts on the economic performance of the property [50]. According to [48], the economic performance of a property does not depend solely on the production structure, but on a combination of factors such as productivity, market value, production costs, experience of producers, among others. In hypothesis H5, higher effective operating costs suggest a more developed technological package applied to the activity, more inputs, skilled labor, and more efficient services, which would have an impact on productivity. If we consider in terms of efficiency, unit costs tend to decrease as productivity increases, the results of the work by [18] indicate that the average operating cost of arabica coffee was R$265.00 per bag of coffee produced, being reduced to R$210.00 when potential yields are reached, which justifies the rejection of the hypothesis.

The hypothesis H6 it was an exploratory hypothesis that sought to determine whether the costs could reflect on the price of the product, whether for better quality or added value. However, the hypothesis was rejected. The search for improvements in the quality of the product incurs higher operational costs, however, this does not provide guarantees of good coffee prices for the producer. This is because prices depend on external economic and environmental conditions such as crises, climate in the region, among others [45,47].

The hypothesis H7 it was a hypothesis that sought to understand whether there is an influence of the COE on economic performance, which was confirmed since performance is measured by subtracting the revenue obtained by the COE. However, it is worth mentioning that satisfactory economic performance requires the combination of good product prices and low operating costs. Thus, hypothesis 7 reaffirms the contribution of the COE to economic performance. According to [45], operating costs are related to the processes adopted by producers on their properties, since making wrong decisions can compromise crop productivity and increase costs.

Hypothesis H8 it was a hypothesis accepted as expected since productivity is directly related to total revenue and thus to economic performance, as well as H9, which measures a higher value of the product, influences a better economic

performance. Both hypotheses influence economic performance as a common aspect. But for this to occur, investments must be leveraged in the coffee activity to reach new levels of performance. Given this, the creation of rural credit and insurance programs is justified to provide the necessary support to producers from different social classes and, consequently, the growth of the sector [48, 50].

5 Conclusions

Regarding the general objective of the research, the study between the property structure construct and the effective operating costs influencing economic performance found relevant results. In general, the study revealed that the higher the technological level of the property and the species used, there are positive influences on productivity levels, however it was not possible to observe this relationship in performance. It was also not possible to verify the influence of any construct on the formation of the value of the product, maintaining the specific market relationship for each region.

The study brought important managerial level contributions on the cost structure in coffee production. In this sense, based on this knowledge of the interrelationship of variables, producers will be able to better plan their field operations to increase crop productivity. In addition, the theoretical contributions were associated with the study method (Structural Equation Modeling), to encourage new studies in the area and promote the knowledge of the methodology by scholars.

As for the limitations of the work, data from a period from 2017 to 2020 was used, which can be expanded to older dates and annual updates to investigate changes in behavior. Another point is to increase the number of models or samples that were used to compose the database.

Finally, the study considered proposals for future research agendas. In this scope, a suggestion is to use other management indicators to measure economic performance in addition to the Gross Margin. To test the impact of coffee beverage quality under the influence of costs and ownership structures on economic performance. Another suggestion is to extend the present study to other crops, such as oranges, apples, bananas, and papayas.

Acknowledgments

Acknowledgments to the Federal University of Lavras – UFLA for the contributions, and to the Minas Gerais State Research Support Foundation – FAPEMIG for the support and funding of the search.

References

[1] CEPEA. Perspectivas para o agronegócio em 2022. Centro de Estudos Avançados em Economia Aplicada - CEPEA-Esalq/USP. [online]. 2022. [Accessed: September 15th 2024]. Available at: https://www.cepea.esalq.usp.br/br/opiniao-cepea/perspectivas-para-o-agronegocio-em-2022.aspx.

[2] CNA BRASIL. PIB do agronegócio tem crescimento recorde de 24,31% em 2020. Confederação da Agricultura e Pecuária do Brasil (CNA). [online]. 2022. [Accessed: September 15th 2024]. Available at: https://www.cnabrasil.org.br/noticias/pib-do-agronegocio-tem-crescimento-recorde-de-24-31-em-2020 0.

[3] Ben-Amara, D., Chen, H., and Hafeez, M., Role of entrepreneurial opportunity identification factors in the eco-innovation of agribusiness. Business Strategy & Development, 3(4), pp. 435-448, 2020. DOI: https://doi.org/10.1002/bsd2.107

[4] Samoggia, A., and Riedel, B., Coffee consumption and purchasing behavior review: Insights for further research. Appetite, 129, pp. 70-81. 2018. DOI: https://doi.org/10.1016/j.appet.2018.07.002

[5] CONAB, National Supply Company. Monitoring the Brazilian coffee crop, v. 6 – 2020, Harvest no. 4 - fourth survey, Brasília. 2020.

[6] CONAB, National Supply Company. Monitoring of Brazilian crop – coffee; Second estimate – 2013 Harvest. Brasília, 2013.

[7] CONAB. Conab - Safra Brasileira de Café. Conab - Página inicial. [online]. 2022. [Accessed: September 15th 2024]. Available at: https://www.conab.gov.br/info-agro/safras/cafe.

[8] Council of coffee exporters from Brazil – Cecafé. Annual export. [online]. 2021. [Accessed: February 08th 2024]. Available at: https://www.cecafe.com.br/dados-estatisticos/exportacoes-brasileiras/

[9] CNN Brasil. Mudanças climáticas podem afetar produção de café no Brasil, diz estudo. CNN Brasil. [online]. 2022. [Accessed: February 08th 2024]. Available at: https://www.cnnbrasil.com.br/business/mudancas-climaticas-podem-afetar-producao-de-cafe-no-brasil-diz-estudo/.

[10] Shim, J.M., Lee, W.S., Moon, J., and Song, M., Coffee shop corporate social responsibility (CSR) and reuse intention using triple bottom line theory. British Food Journal, 123(12), pp. 4421-4435, 2021. DOI: https://doi.org/10.1108/BFJ-12-2020-1134

[11] Ntiamoah, E.B., Li, D., and Sarpong, D.B., The effect of innovation practices on agribusiness performance: a structural equation modelling (SEM) approach. African Journal of Science, Technology, Innovation and Development, [online]. 11(6), pp. 671-681, 2019.Available at: https://hdl.handle.net/10520/EJC-18b0b25690

[12] Viana, J.G.A., and Silveira, V.C.P., Production costs and performance indicators: a methodology applied to sheep production systems. CEP, 90050, 2008, 230 P.

[13] dos Santos, P.M., Cirillo, M.Â., and Guimaraes, E.R., Specialty coffee in Brazil: transition among consumers' constructs using structural equation modeling. British Food Journal. 123(5), pp. 1913-1930, 2021. DOI: https://doi.org/10.1108/BFJ-06-2020-0537

[14] Lampert, J.A., Rural administration textbook. In: Rural Administration. Santa Maria: DEAER/UFSM. 2003.

[15] Safras & Cifras. Curso de gerenciamento econômico na agropecuária. FARSUL/SENAR. Rio Pardo, Brasil, 1997.

[16] Matsunaga, M., Bemelmans, P.F., Toledo, P.D., Dulley, R.D., Okawa, H., and Pedroso, I.A., Metodologia de custo de produção utilizada pelo IEA. Agricultura em São Paulo, 23, pp. 123-139, 1976.

[17] Martin, N.B., Serra, R., Oliveira, M.D.M., Ângelo, J.A., and Okawa, H., Integrated system of agricultural and livestock costs-Custagri. Inf. Econ., 28, pp. 7-28, 1998.

[18] Lima, A.L.R. et al., Production costs: the impact of productivity on coffee growing results in the main producing regions in Brazil, 2008.

[19] Mariyono, J., Improvement of economic and sustainability performance of agribusiness management using ecological technologies in Indonesia. International Journal of Productivity and Performance Management. 69(5), pp. 989-1008, 2019. DOI: https://doi.org/10.1108/IJPPM-01-2019-0036

[20] Van Waeyenberg, T., Peccei, R., and Decramer, A., Performance management and teacher performance: the role of affective organizational commitment and exhaustion. The International Journal of Human Resource Management, 33(4), pp. 623-646, 2022. DOI: https://doi.org/10.1080/09585192.2020.1754881

[21] Suárez, A.E., Gutiérrez-Montes, I., Ortiz-Morea, F.A., Suárez, J.C., Di Rienzo, J., and Casanoves, F., Contribution of livelihoods to the well-being of coffee-growing households in southern Colombia: a structural equation modeling approach. Sustainability, 14(2), art. 743, 2022. DOI: https://doi.org/10.3390/su14020743

[22] Pronti, A., and Coccia, M., Multicriteria analysis of the sustainability performance between agroecological and conventional coffee farms in the East Region of Minas Gerais (Brazil). Renewable Agriculture and Food Systems, 36(3), pp. 299-306, 2021. DOI: https://doi.org/10.1017/S1742170520000332

[23] Izquierdo, N.V., Lezama, O.B.P., Dorta, R.G., Viloria, A., Deras, I., and Hernández-Fernández, L., Fuzzy logic applied to the performance

evaluation. Honduran coffee sector case. In: International Conference on Swarm Intelligence Springer, Cham. 2018, pp. 164-173. DOI: https://doi.org/10.1007/978-3-319-93818-9_16
[24] Gosal, G.G., Christian, T.F., and Filbert, V., The Relationship between sensory marketing, packaging, and purchasing decisions. A study of coffesia's coffee product. 2020.
[25] Cruz-Correia, P.F.D., Reis, J.G.M.D., Toloi, R.C., Araújo, F.A.D., Bonilla, S.H., Souza, J.S.D., ... and Souza, A.E.D., Economic and environmental perfomance in coffee supply chains: a Brazilian Case study. In: IFIP International Conference on Advances in Production Management Systems Springer, Cham. 2020, pp. 631-639. DOI: https://doi.org/10.1007/978-3-030-57997-5_73
[26] Oliveira, E. de et al., Influence of mechanized harvesting on coffee production. Rural Science, 37, pp. 1466-1470, 2007.
[27] Marsh, H.W., Morin, A.J., Parker, P.D., and Kaur, G., Exploratory structural equation modeling: an integration of the best features of exploratory and confirmatory factor analysis. Annual review of clinical psychology, 10, pp. 85-110, 2014. DOI: https://doi.org/10.1146/annurev-clinpsy-032813-153700
[28] Tripathi, K.K., and Jha, K.N., Determining success factors for a construction organization: a structural equation modeling approach. J. Manage. Eng, 34(1), art. 04017050, 2018. DOI: https://doi.org/10.1061/(ASCE)ME.1943-5479.0000569
[29] Chandio, F.H., Studying acceptance of online banking information system: a structural equation model. Doctoral dissertation, Brunel University Brunel Business School, United Kingdom, 2011.
[30] Mueller, R.O., and Hancock, G.R., Structural equation modeling. In: The reviewer's guide to quantitative methods in the social sciences. Routledge. 2018, pp. 445-456.
[31] Hair, J.F., Ringle, C.M., and Sarstedt, M., PLS-SEM: Indeed a silver bullet. Journal of Marketing theory and Practice, 19, pp. 139-152, 2011. DOI: https://doi.org/10.2753/MTP1069-6679190202
[32] Zhang, H., Structural equation modeling. In: Models and Methods for Management Science, Springer, Singapore, 2022, pp. 363-381.
[33] Civelek, M.E., Essentials of structural equation modeling. Essentials of Structural Equation Modeling, 2018.
[34] Oliveira, R.R., Marinho-Marlon, F.A., and Days, A.T., A study on the use of structural equation modeling in scientific production in the areas of administration and information systems. Journal of Administration of the Federal University of Santa Maria, 9, pp. 559-578, 2016.
[35] Perry, J.L., Nicholls, A.R., Clough, P.J., and Crust, L., Assessing model fit: caveats and recommendations for confirmatory factor analysis and exploratory structural equation modeling. Measurement in physical education and exercise science, 19, pp. 12-21, 2015. DOI: https://doi.org/10.1080/1091367X.2014.952370
[36] Bagozzi, R.P., and Yi, Y., Specification, evaluation, and interpretation of structural equation models. Journal of the Academy of Marketing Science, 40, pp. 8-34, 2012. DOI: https://doi.org/10.1007/s11747-011-0278-x
[37] Wan-Omar, W.A., and Hussin, F., Transformational leadership style and job satisfaction relationship: a study of structural equation modeling (SEM). International Journal of Academic Research in Business and Social Sciences (IJARBSS), 3, pp. 346-365, 2013.
[38] Pandey, P., and Pandey, M.M., Research methodology tools and techniques, Bridge Center, 2021.
[39] Dźwigoł, H., and Dźwigoł-Barosz, M., Scientific research methodology in management sciences. Financial and credit activity problems of theory and practice, 2(25), pp. 424-437, 2018.
[40] SEBRAE. Como conservar o solo na produção de café. [online]. 2022. [Accessed: September 15th 2024]. Available at: https://www.sebrae.com.br/sites/PortalSebrae/artigos/como-conservar-o-solo-na-producao-de-cafe,a40b9e665b182410VgnVCM100000b272010aRCRD. Accessed: 15 set. 2024.
[41] Hasibuan, A.M., Ferry, Y., and Wulandari, S., Factors affecting farmers' decision to use organic fertilizers on Robusta coffee plantation: a case study in Tanggamus, Lampung. In: IOP Conference Series: Earth and Environmental Science, 974(1), art. 012105, IOP Publishing, 2022. DOI: https://doi.org/10.1088/1755-1315/974/1/012105
[42] Nzeyimana, I., Hartemink, A.E., and de Graaff, J., Coffee farming and soil management in Rwanda. Outlook on Agriculture, 42(1), pp. 47-52, 2013. DOI: https://doi.org/10.5367/oa.2013.0118
[43] Cerrado Mineiro (Brasil). A Região do Cerrado Mineiro. [online]. 2022. [Accessed: December 22th 2024]. Available at: https://www.cerradomineiro.org/index.php?pg=home.
[44] Camargo, M.B.P.D., The impact of climatic variability and climate change on arabic coffee crop in Brazil. Bragantia, 69, pp. 239-247, 2010. DOI: https://doi.org/10.1590/S0006-87052010000100030
[45] Pham, Y., Reardon-Smith, K., Mushtaq, S., and Cockfield, G., The impact of climate change and variability on coffee production: a systematic review. Climatic Change, 156(4), pp. 609-630, 2019. DOI: https://doi.org/10.1007/s10584-019-02538-y
[46] Reis, R.P., Reis, A.J.D., Fontes, R.E., Takaki, H.R.C., and Castro Júnior, L.G.D., Custos de produção da cafeicultura no sul de Minas Gerais, 2001. DOI: https://doi.org/10.22004/ag.econ.43360
[47] Cooxupé. Com altas puxadas pelos fertilizantes, custo de produção na cafeicultura está 50% mais elevado. [online]. 2022. [Accessed: December 22th 2024]. Available at: https://www.cooxupe.com.br/noticias/com-altas-puxadas-pelos-fertilizantes-custo-de-producao-na-cafeicultura-esta-50-mais-elevado/. Acesso em: 22 dez. 2020.
[48] Marques, I.R., Comparability of costs and prices in the cultivation of arabica and conilon coffee, 2021.
[49] Merle, I., Pico, J., Granados, E., Boudrot, A., Tixier, P., Virginio Filho, E.D.M., ..., and Avelino, J., Unraveling the complexity of coffee leaf rust behavior and development in different Coffea arabica agroecosystems. Phytopathology, 110(2), pp. 418-427, 2020. DOI: https://doi.org/10.1094/PHYTO-03-19-0094-R
[50] Ministério da Economia. Crédito rural. Ministério da Economia. [online]. 2022. Available at: https://www.gov.br/fazenda/pt-br/assuntos/politica-agricola-e-meio-ambiente/atuacao-spe/credito-rural

M.M. Marques, is a MSc. in Administration from the Federal University of Lavras-UFLA, in 2022. He is BSc. in Agronomy from the Federal University of Lavras-UFLA in 2020.
ORCID: 0000-0002-0500-4014

G.A. de Melo, is a PhD. in Business Administration from the Federal University of Lavras-UFLA, in 2024. MSc. in Administration from the Federal University of Lavras-UFLA, in 2022. He is BSc. in Production Engineering from the Federal University of Viçosa-UFV-Campus Rio Paranaíba, in 2018.
ORCID: 0000-0001-5635-4180

L.G.C. Júnior, is teacher at the Federal University of Lavras-UFLA, permanent teacher at the Postgraduate Program in Administration at Federal University of Lavras-UFLA. Member of the Management Board of the National Institute of Coffee Science and Technology.
ORCID: 0000-0002-1215-0183

E.G. Carvalho, is teacher at the Federal University of Lavras-UFLA, teacher at the Postgraduate Program in Administration at Federal University of Lavras-UFLA.
ORCID: 0000-0002-5266-375X

M.G.M. Peixoto, is PhD. in Production Engineering from the São Carlos School of Engineering-EESC - University of São Paulo-USP, in 2016. MSc. in Production Engineering from the Federal University of São Carlos-UFSCar, in 2013, and a Business of the Federal University of Lavras-UFLA, in 2010. Teacher at the University of Brasilia-UnB.
ORCID: 0000-0003-1238-2301

S.B. Barbosa, is BSc. Eng. in Industrial Design from the University of Brasilia (UnB). MSc. and PhD in Production Engineering from the Federal University of Santa Catarina (UFSC), Brazil. Teacher at the Federal University of Viçosa-UFV Campus Rio Paranaíba.
ORCID: 0000-0001-5148-2095

M.C.A. de Mendonça, is PhD. in Production Engineering from the Federal University of São Carlos. Teacher of the Department of Agroindustrial Management, Federal University of Lavras-UFLA.
ORCID: 0000-0002-7383-9435

P.G. Santos, is PhD. in Production Engineering from the Federal University of Pernambuco-UFPE, 2012. MSc. in Production Engineering from the Federal University of Paraná-UFPR, in 2007. Teacher at the University of Brasilia-UnB.
ORCID: 0000-0002-7383-9435

A.L.M. Serrano, a PhD in Economy from the University of Brasília-UnB, in 2021. MSc. in Economy from the University of Brasília-UnB, in 2016. Teacher at the University of Brasilia-UnB.
ORCID: 0000-0001-5182-0496

L.O.G. Ferreira, a PhD in Accounting Sciences from the University of Brasília-UnB, in 2021. Msc. in Accounting Sciences from the University of Brasília-UnB, 2012. Teacher at the University of Brasilia-UnB.
ORCID: 0000-0002-8734-4740

J.B.S.O.A. Guerra, is Ph.D. in Political Science/International Relations – Sophia University and New University of Bulgary, Teacher at the University of the South of Santa Catarina, Unisul, Brazil.
ORCID: 0000-0002-6709-406X

DYNA
http://dyna.medellin.unal.edu.co/

UNIVERSIDAD NACIONAL DE COLOMBIA

Extraction of molybdenite concentrates by leaching

Vanesa Bazan [a], Marcela Medina [b] & Ivana Orozco [b]

[a] CONICET-Facultad de Ingeniería, Universidad Nacional de San Juan, San Juan, Argentina. bazan@unsj.edu.ar
[b] Facultad de Ingeniería, Universidad Nacional de San Juan, San Juan, Argentina. iorozco@unsj.edu.ar, marcelacelina@yahoo.com.ar

Received: June 27th, 2024. Received in revised form: September 27th, 2024. Accepted: October 16th, 2024.

Abstract
Molybdenum concentrate, as Molybdenite (MoS_2), is nowadays obtained as a byproduct of the processing of porphyry copper ores, being molybdenite considered a minor component. The procedure for the commercial extraction of molybdenum from such a sulfide ore, involves the operations of roasting the concentrate, purifying the resulting calcination, either by distillation of molybdenum trioxide (MoO_3) or by a hydrometallurgical pathway, and finally reducing the trioxide of molybdenum with hydrogen to obtain the metal.
The objective of the present work is to study the production of molybdenum from molybdenite concentrates using aqueous solution of hydrochloric acid (HCl) as a lixiviant, sodium chloride (NaCl) as a catalyst, sodium hydroxide (NaOH) as a pH regulator, and lastly ferric chloride ($FeCl_3$) as an oxidant. The results show that working pH greater than 8, temperature of 50 °C, hydrochloric acid concentration of 5%, solid/liquid ratio of 10:1, stirring rate of 200-300 rpm and the addition of 2% ferric chloride. Mo leaching was 70% under experimental conditions at a time of 180 minutes, with a complete removal of iron.

Keywords: molybdenite; leaching; ferric chloride

Extracción de concentrados de molibdenita por lixiviación

Resumen
El concentrado de molibdenita (MoS_2) es obtenido actualmente como un subproducto en el procesamiento de minerales provenientes de un pórfido de cobre, siendo la molibdenita considerada un componente menor. El procedimiento para la extracción comercial de molibdeno desde un sulfuro, la molibdenita, implica tostar el concentrado, purificar el calcinado resultante, ya sea por destilación de tiroxido de molibdeno (MoO_3)o por una ruta hidrometalúrgica, y finalmente reducir el trióxido con hidrógeno para obtener el metal
El objetivo del presente trabajo es estudiar la producción de molibdeno desde concentrados de molibdenita usando una solución acuosa de ácido clorhídrico (HCl) como lixiviante, cloruro de sodio (NaCl) como catalizador, hidróxido de sodio (OHNa) como regulador de pH, y por último cloruro férrico ($FeCl_3$) como un oxidante. Los resultados muestran que trabajando en un pH más grande que 8 temperatura de 50ºC, con una concentración de ácido clorhídrico de 5% y una relación solida / liquido de 10:1, velocidad de agitación de 200- 300 rpm y la adición de un 2% de cloruro férrico, La lixiviación de Mo fue del 70% en condiciones experimentales en un tiempo de 180 minutos, con una remoción completa del hierro.

Palabras clave: molibdenita; lixiviación; cloruro férrico.

1 Introduction

Molybdenum, as main component or as a by-product, is found in low-grade ores and before its use as an industrial or metallurgical product, it must undergo in operations of concentration in order to liberate the mineral species, molybdenite (MoS_2), which is the most important one in terms of economics.

The conventional method for extracting Mo involves an oxidation-roasting-leaching process with ammonia. Alternative processes such as oxidative pressure leaching, alkaline melting and alkaline hypochlorite leaching have gained increasing utilization in Mo production. Currently, ammonium molybdate is mainly reached by the ammonia leaching method [1]. This involves roasting molybdenite at high temperatures to obtain molybdenum calcine, which consists mainly of MoO_3 [2-4]. Subsequently, ammonium molybdate is produced through a series of processes, including leaching, purification and crystallization [5-6]. The ammonia leaching method imposes strict quality

How to cite: Bazan, V., Medina, M., and Orozco, I., Extraction of molybdenite concentrates by leaching. DYNA, 91(234), pp. 54-61, October - December, 2024.

requirements on molybdenum calcine due to the weak alkalinity of ammonia. Typically, the Mo content in calcine should exceed 55% (w/w), with iron (Fe) and copper (Cu) content below 2% (w/w). Furthermore, ideally the soluble Mo content should exceed 98% by weight [7]. Deviation from these specifications can result in high Mo content in the leach residue, negatively affecting Mo recovery. The shortage of high-quality molybdenite is increasing due to the continued exploitation of Mo resources, leading to an increasing proportion of low-grade complex molybdenite ore [8]. Typically, pyrite and chalcopyrite accompany low-grade complex molybdenite [9-10,11], easily transforming into insoluble iron molybdate and copper molybdate during the oxidation roasting process [12-14]. This formation of Fe molybdate and Cu molybdate significantly hinders the utilization of Mo, resulting in a considerable increase in the Mo content in the leach residue to approximately 15 %(w/w). Therefore, the efficient extraction of Mo from low-grade complex molybdenum calcine has become a critical bottleneck limiting wider application of molybdenum resources.

The molybdenum concentrate, depending on the cleaning and concentration scheme implemented in the selective flotation plant, may contain a proportion of copper and iron between 1.5% and 6%, acting as impurities.

With this copper content it can be sent to the maquila facility for processing and transformation into molybdenum trioxide (MoO_3) for commercial purposes. However, as the amount of copper and iron present in the concentration increases, processing costs increase. For many years, chloride-based leaching, particularly $FeCl_3$, has been applied to extract various metals from sulfide minerals. [14-15] Commonly, the ferric ion (Fe^{3+}) is the most effective oxidant with a redox potential of 0.77 mV in acidic media; the high solubility of the metal allows Mo to be extracted more quickly than with other oxidants. [16-17]

$FeCl_3$ is often used as an oxidant for sulfur in copper sulfides by the leaching method, and the efficiency is lower when no additional reagent is included.

Work to develop new leaching parameters has often involved bench-scale experiments testing a matrix of conditions. While important, especially in determining kinetic parameters, these efforts can be labor-intensive, time-consuming, and sophisticated thermodynamics.

Therefore, in this work, we resort to the application of leaching with hydrochloric acid with the addition of ferric salts, mainly ferric chloride ($FeCl_3$) with pH control with the purpose of reducing the concentration of copper and iron in the material, in order to find the optimal recovery parameters of the desired metal (Mo).

2 Experimental methodology

The sample used is a flotation concentrate of copper, iron and molybdenum from a deposit in northern Argentina. To obtain an idea of the nature of the sample, structural and chemical characterizations are carried out. Subsequently, a portion is separated for experimental testing.

2.1 Chemical analysis

The analytical technique for determining Mo is through acid digestion with H_2S and $HClO_4$, with an organic catalyst and subsequent determination in acid solution with Perkin Elmer ICP-OES (optical emission spectrometer), model 7300 DV, the standards used for measurement are certified, and using measurement blank. The measurements of the samples were carried out in triplicate and the average measurement was obtained as a result.

For the other elements, an analytical technique consisting of acid digestion is used, specifically for a multi-acid attack (HF, HCl, HNO_3, $HClO_4$) of the concentrated sample. All the reagents used were of analytical grade.

2.2 Structural analysis

The mineralogical characterization was carried out with the objective of identifying and describing the minerals present in the sample and thus knowing their physical and chemical properties. The mineralogical characterization was carried out through a number of techniques and methods including:

Macroscopic observation: mineral samples were visually examined, describing their appearance, color, brightness, among others.

Optical microscopy: a microscope is used to examine thin sections of mineral samples. The equipment utilized was an Olympus SZ61 TR stereoscopic magnifier and an Olympus GX 51 optical microscope with a Leco IA 32 image analysis system.

Electron microscopy: A SEM scanning electron microscope is utilized, employing the energy disperse spectroscopy (EDS) technique using Phoenix software to analyze the samples. Before observation under the microscope, these samples were coated with a conductive layer of gold palladium alloy

X-ray diffraction. This technique allows us to identify the minerals present in a sample and determine its chemical composition. The equipment utilized was a Philips WP 1011 Diffractometer.

2.3 Laboratory testing methodology

The method used to carry out leaching is via agitation. That is, acid leaching is carried out by stirring the samples where the acid reacts with the present minerals, dissolving the metal of interest and producing metal ions in the solution.

This medium allows us to evaluate important parameters, such as leaching rate, extraction efficiency and the influence of several variables such as lixiviant concentration, particle size, temperature and pH, all useful data to optimize and design leaching processes.

The steps followed in the agitation leaching tests in the laboratory were as follows:

Weighing samples: carried out on Mettler Toledo analytical scale.

- Preparation of the leaching solution and catalysts.
- Working pH conditioning.
- Mixing and stirring: The mineral samples and the

leaching solution are placed in a beaker (400 ml) and subjected to constant stirring using magnetic stirrers to ensure uniform distribution of the leaching solution. A "Fisatom, model 752A" magnetic stirrer was used, which allows to control both stirring speed and temperature.

- Contact Time Control: The sample is shaken for a certain period.
- pH control: by repeatedly measuring the pH value, it is carried out using a "Hanna, model HI 8424" pH meter.
- Temperature control: by repeatedly measuring the value, it is carried out with a "GERMAN" digital spike thermometer.
- Sampling: 20 ml rich solution samples are taken every 1 hour.
- Analysis: the resulting solution is analyzed to determine the concentration of the metals of interest via both AA and ICP techniques (after acid digestion).

A series of tests are diagrammed varying certain operational conditions of importance in the leaching process, to determine the influence of said variables, as well as determine the optimal conditions for it.

3 Tests results

3.1. Chemical analysis results

To carry out the instrumental determination after acid digestion, an Inductively Coupled Plasma Optical Emission (ICP-OES) device was used. Measurements are carried out as mentioned in 2.1 Obtaining the results of Table 1.

3.2. Mineralogical analysis results

In both optical and electronic microscopes, Figs. 1 and 2; it was possible to observe; the presence of fairly predominant grains of chalcopyrite as the predominant species and other elements present that were corroborated with quantitative chemical analysis.

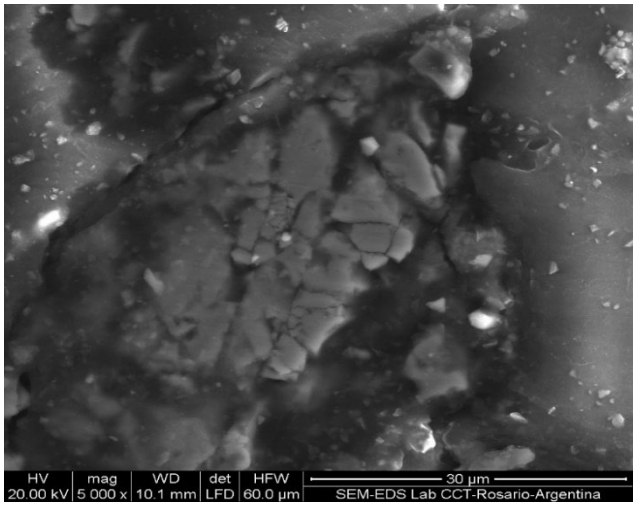

Figure 1. Scanning electron microscope (SEM) images of sample 1. Molybdenite with metal incrustation
Source: Bazan, Medina and Orozco, 2024.

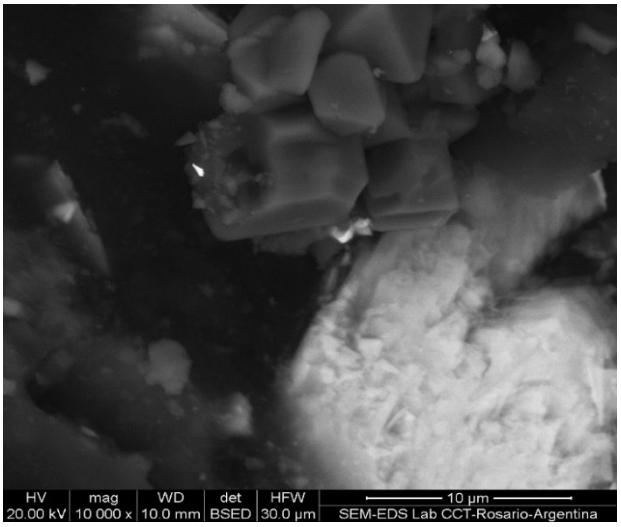

Figure 2. Scanning electron microscope (SEM) images of sample 2. Molybdenite with the presence of pyrite
Source: Bazan, Medina and Orozco, 2024.

The diffractograms obtained are shown in Figs. 3 and 4. This allows us to qualitatively evaluate the differences that exist between each of the concentrates, in terms of the crystalline phases present in it.

The spectra obtained corroborate that in each sample the majority mineralogical species is chalcopyrite ($CuFeS_2$), it is also shown that the peaks are different due to the different concentrations of Molybdenite.

3.3 Experimental methodology results

According to studies carried out by Zhan-Fang Cao [18], it was concluded that the variation in the stirring rate, as well as in the amount of catalyst, does not yield significant changes in the results, so the stirring rate is maintained between 200-300 rpm and 1gr (one gram) of NaCl as catalyst. The effect of sodium chloride is attributed to the formation of stable sodium molybdate [19]

Table 1.
Chemical composition of samples.

Majority Elements	Sample	
	M1 (%)	M2 (%)
Mo	39,53	35,83
Cu	0,97	0,99
Fe	6,12	6,24
S	18,36	16,13
Trace Elements	**Sample**	
	M1 (mg/L)	**M2 (mg/L)**
Al	16,84	13,93
Na	0,62	0,56
K	0,49	0,43
Ni	0,40	0,40
Ag	0,20	0,20
Mn	0,60	0,60
Ca	25,50	25,90
Mg	6,40	6,00
Zn	0,60	0,60
Ba	3,20	2,70
Cd	0,60	0,60
As	0,13	0,14
Re	1,72	1,58

Source: Bazan, Medina and Orozco, 2024.

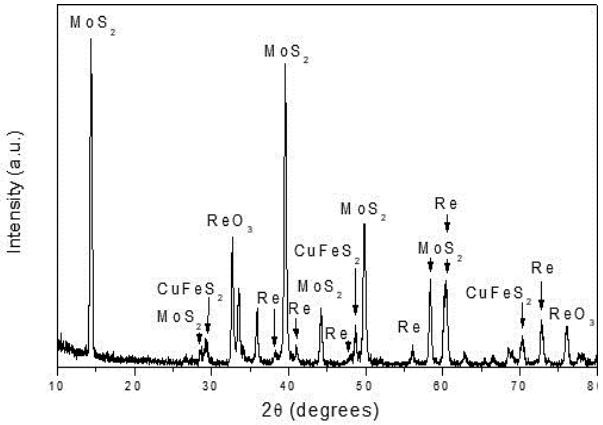

Figure 3. Diffractogram of sample M1
Source: Bazan 2024.

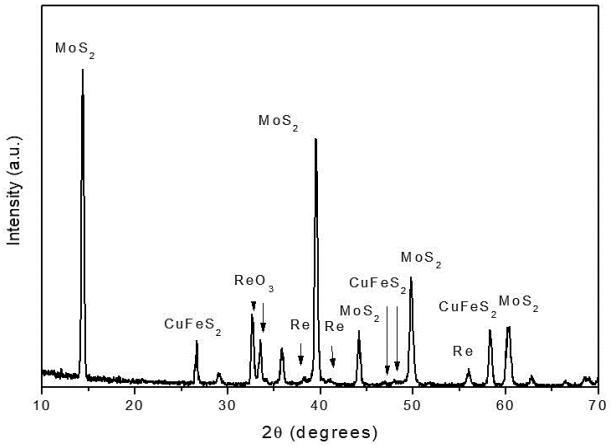

Figure 4. Diffractogram of sample M2.
Source: Bazan 2024.

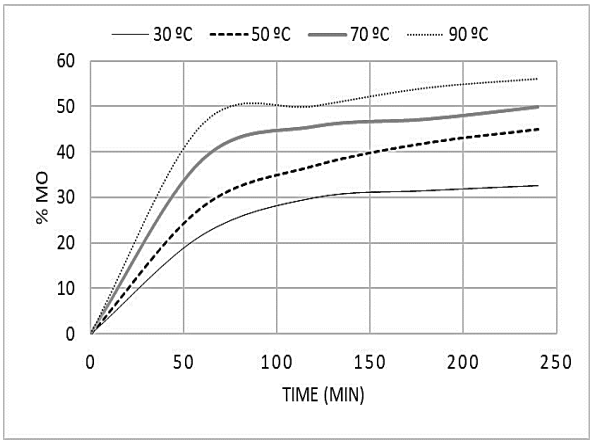

Figure 5. Mo extraction at different temperatures.
Source: Bazan, Medina and Orozco, 2024.

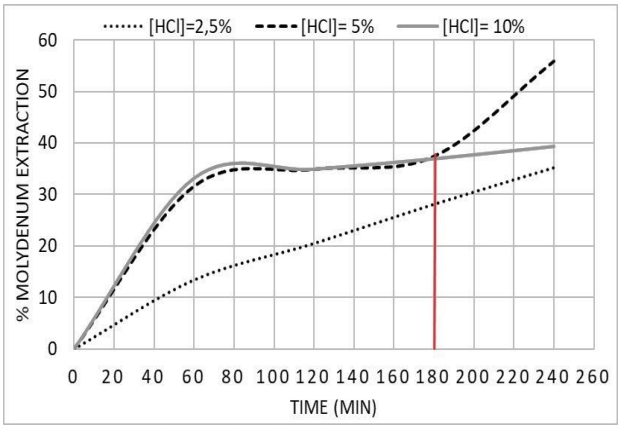

Figure 6. Mo extraction as a function of [HCl]
Source: Bazan, Medina and Orozco, 2024.

And according to Hesami [20], the pH oscillation around 8 due to the high dissolution rate of molybdenite in hypochlorite caused the production of hypochlorous acid. It seems that the presence of hypochlorous acid (strong oxidizing agent) in the pulp leads to the more extraction of molybdenum and copper.

3.3.1 Effect of operating temperature

The effect of temperature 30°C, 50°C, 70°C and 90°C has been studied with the following fixed conditions: ratio L/S:10/11 time:240 min, [HCl]=5%; pH:8.

The results obtained are shown in Fig. 5.

Temperature has an important effect on the dissolution rate of molybdenum; the highest extraction of Mo was reached at 180 minutes and 90 ºC.

For operational purposes, according to the results obtained, 50 ºC is energetically adequate to reduce energy cost. This effect of temperature on the dissolution rate of Mo tells us that increasing the reaction temperature increases the average kinetic energy of the reactants, thus accelerating the diffusion rate and the rate of the chemical reaction, which ultimately facilitates the chemical reaction.[21]

3.3.2 Effect of hydrochloric acid concentration

The next series of tests investigates the effect of the concentration of the leaching solution. Tests are carried out at different concentrations of the leach solution: 2.5%, 5% and 10% HCl, with the fixed conditions of: T.50°C, time: 240 min, L/S ratio: 10/1; pH:8. Results are shown in Fig. 6.

The highest percentage of molybdenum extraction was found at a HCl concentration of 5% for a time of 240 min.

The curve shows in Fig. 6 that for a concentration of 2.5% the rate of molybdenum dissolution is slow. The Mo extraction at the beginning of the tests for 5% and 10% shows a similar behavior until 180 min, then the Mo extraction increases rapidly for a concentration of 5% while for a concentration of 10% it remains asymptotic.

The decrease in the leaching percentage of Mo when HCl concentration was higher than 5% may be ascribed to the formation of passive film on the surface of the ores like elemental sulfur. In general, these passive films can be dissolved by a pitting mechanism in the presence of chloride ions.[22]

The lower dissolution of molybdenite (MoS_2) at a concentration of 2.5% is related to the stability of this mineral in acidic media. The quantitative extraction observed of HCl might be due to the ease with which MoO_2^{2+} is formed at high

acid concentration and the large presence of Cl^- ions required for the formation of an extractable complex. The complex might be further solved by HCl molecules thereby increasing its extractability.[23]

The graph suggests that HCl solutions in concentrations greater than 5% have no apparent effect on Mo extraction. Therefore, the dissolution of metals can be decreased by the formation of passivation layers of sulfides, metal oxides and hydroxides [24] on the surface of the mineral.

Therefore, the 5% HCl concentration is chosen as the optimal concentration for subsequent tests.

3.3.3 Effect of the liquid-solid relationship

The effect of the liquid-solid ratio (mass/volume) from 5:1 to 25:1 was studied with the following fixed conditions T:50°C, time:240 min, [HCl]=5%; pH:8.

Fig. 7 shows the effect of liquid-solid ratio on molybdenum leaching ratios. As a low liquid-solid ratio can inhibit the diffusion of ions in solution [23]. When the liquid-solid ratio is 25:1 ml/g, the maximum extraction obtained at 240 min is 41.1%. The maximum percentage of Mo extraction at 240 minutes was achieved with a solid-liquid ratio of 10:1 of 49.9%. As the percentage of solids increases, metal recoveries decrease, since there would be less hydrochloric acid available to leach a greater amount of solid.[26].

Based on bibliographic research, it has been verified that researcher Joseph D. Lessard has demonstrated that the incorporation of additional reagents, such as $FeCl_3$ (iron (III) chloride) solutions, in the acid molybdenum leaching procedure, leads to significant improvements in process effectiveness. This is because $FeCl_3$ reacts with copper (Cu) and iron (Fe) following a specific chemical reaction eq. (1):

$$CuFeS_2 + 4FeCl_3 \rightarrow CuCl_2 + 5FeCl_2 + 2S \quad (1)$$

This reaction is of the redox type where: Both S^{-2} and Cu^{+1} are oxidized to $SO4^{-2}$ and Cu^{+2} by the Fe^{+3} of $FeCl_3$. Fe is reduced to Fe^{+2} to form $FeCl_2$, whose compound is stable and does not interfere with the Mo leaching reaction.

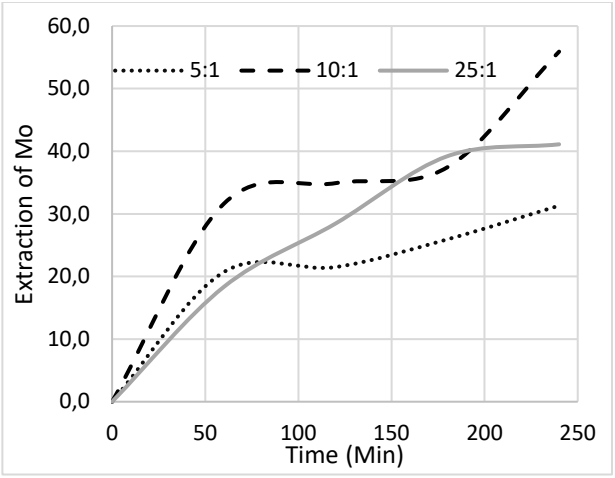

Figure 7. Mo Extraction as a Function of S/L Ratio
Source: Bazan, Medina and Orozco, 2024.

Consequently, a new series of tests are planned to use the ideal conditions previously identified, in addition to the incorporation of this specific reagent.

3.3.4 Effect of adding ferric chloride

In this series of tests, the concentration of $FeCl_3$ is varied from 2.5-5 and 10%, with the following fixed conditions: T:50°C, time: 240 min, [HCl]=5%; pH:8 and an S/L ratio= 10.1. Obtaining the results of Fig. 8.

The optimal molybdenum extraction conditions are temperature of 50°C, a HCl concentration of 5%, a $ClFe_3$ concentration of 2%, an S/L ratio of 10:1 and a reaction time of 60 minutes.

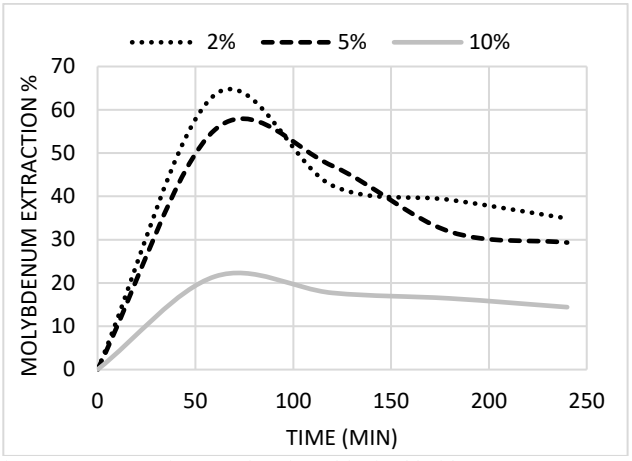

Figure 8. Mo extraction, as a function of ferric chloride ($FeCl_3$).
Source: Bazan, Medina and Orozco, 2024.

In Fig. 8 a greater recovery of Mo occurs with the addition of $FeCl_3$ at a pH greater than 8, controlling with NaOH, with a time of 60 minutes of operation, producing the following proposed chemical reaction. Eq. (2):

$$MoS_2+108FeCl_3+2NaOH+165H_20 \leftrightarrow Na_2MoO_7+36F_{e3}O_4 +324HCl+4H_2SO_4 \quad (2)$$

This can be corroborated according to the Eh-pH diagrams in Fig. 9, determined experimentally during the leaching processing where the Eh value was around =-0.127 Volt.

Although the recovery of Mo was found, under optimal operating conditions, it is important to analyze the effect of leaching on copper and iron metals in molybdenite so that it can be a marketable product.

The copper content in molybdenite concentrates is crucial since the steel industry is the primary consumer of molybdenum produced from molybdenite. Therefore, molybdenum compounds produced for the steel industry must contain very little copper to minimize the deleterious effect of this impurity on the physical properties of the resulting alloy steels [18].

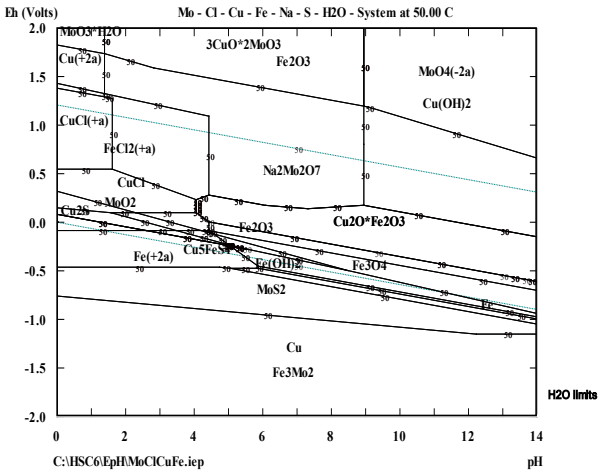

Figure 9. Eh-pH diagram of the leaching process with $FeCl_3$.
Source: Bazan, Medina and Orozco, 2024

The next stage was to focus on the percentage of iron and copper extraction. Fig. 10 shows the results obtained

Lessard investigates that the residual Cu remaining in the concentrate is found to exist as Cu_2S, lending further credence to the hypothesis that $CuFeS_2$ is decomposed and trivalent Fe is selectively reduced while most Cu, Fe, and S are removed during leaching. Increasing the $FeCl_3$ concentration also leads to an increase in the MoO_2 production, likely due to the decreased pH.[27]

3.3.5 Optimization of significant variables

To obtain maximum information from a minimum number of experiments, a Box-Behnken experimental design (BBD) was implemented using the Design-Expert software. Using the experiments mentioned above, with 2 center points of two factors (A and B) at three levels,

A: Temperature (30°C, 60°C, 90°C),

B: Time (60min, 150min and 240min).

The variables that remain fixed are:

pH ≥ 8; HCl concentration 5%; S/L ratio 10:01; stirring speed 200-300rpm.

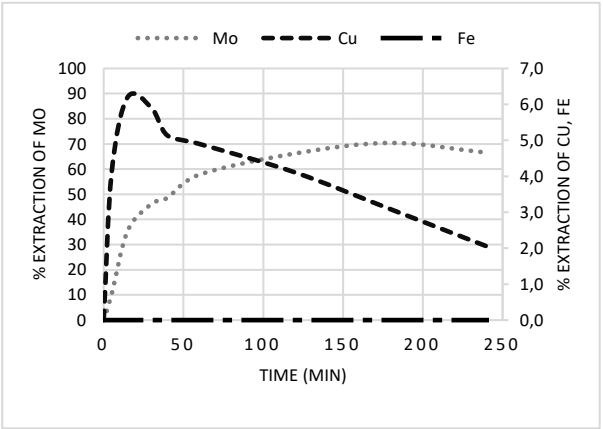

Figure 10. Mo extraction compared to Cu and Fe.
Source: Bazan, Medina and Orozco, 2024.

Table 2.
Analysis of variance (ANOVA)
Anova for Response Surface Quadractic Model

Source	Sum of Squares	df	Mean Square	F Value	p-value Prob>F
Model	422.12	5	84.42	43.36	0.0004
A-Temperature	134.26	1	134.46	69.06	0.0004
B-Tiempo	148.37	1	148.37	76.2	0.0003
AB	28.62	1	28.62	14.7	0.0122
A^2	101.7	1	101.7	52.23	0.0008
B^2	0.011	1	0.011	5.55E+00	0.9435
Residual	9.74	5	1.95		
Lack of Fit	8.7	3	2.9	5.57	0.1559
Pure Error	1.04	2	0.52		
Cor total	431.86	10			
Std Dev	1.4		R-Squared		0.9775
Mean	41.18		Adj R-Squared		0.9549
C.V. %	3.39		Pred R-Squared		0.8514
PRESS	64.17		Adeq Precision		20.738

Source: Bazan, Medina and Orozco, 2024.

Table 3.
Equation coefficients

a	-29.472720
b	1.622150
c	0.189800
d	-0.001980
e	-0.009430
f	-1.08E-05

Source: Bazan, Medina and Orozco, 2024.

The optimization criterion was to maximize Mo extraction at different temperatures and time.

The data obtained were fitted to a Quadratic vs 2FI model with regression analysis. From the analysis of variance (ANOVA) in Table 2, it can be corroborated based on F value of 43.36 that the model is significant; with an R and an adjusted R^2 of 0.9775% and 0.9549%, respectively.

In this way, the 3D response surface serves to graphically visualize the interaction effects of independent variables. Fig.11 shows that the optimal working conditions were found for a temperature of 60°C and a time of 220min. Source: Bazan, Medina and Orozco, 2024.

Resulting in a regression eq. 3 as shown below:

$$\%\text{Extraction Mo} = a + b \cdot T + c \cdot t - d \cdot T \cdot t - e \cdot T^2 - f \cdot t^2 \quad (3)$$

Where:

T is the temperature and t is the time. The coefficients are shown in the Table 3.

In Fig. 11, experiments were applied that allow the cells to move quickly; proximity to the optimum sought for the response, studying each factor at least two levels for analysis of curvature, having several points that allow estimating all the terms of the model of equation (3); providing a stable prediction error in the experimental environment. With the leaching carried out, the dissolution of molybdenum was insignificant, 100% of the iron was dissolved, but the dissolution of copper was not important or significant to meet market requirements.

An optimization of significant variables was carried out using the Design-Expert software. It can be confirmed that the model is significant since it gives an R value and an adjusted R^2 of 0.9775% and 0.9549% respectively. The optimal working conditions according to the model are a temperature of 60°C and a time of 220min.

4 Conclusions

Based on the discussion presented above, the following conclusions were reached:

Regarding the chemical and mineralogical characterization carried out, it is concluded that the data provided by the chemical analyzes (Mo, Cu and Fe) coincide with the mineralogical analysis, confirming the presence of Molybdenite (MoS_2), Pyrite (FeS_2), Chalcopyrite ($CuFeS_2$), Bornite (Cu_5FeS_4) and Covelline (CuS), minerals of said elements.

The high proportion of sulfur S confirms that these are sulfide mineral species.

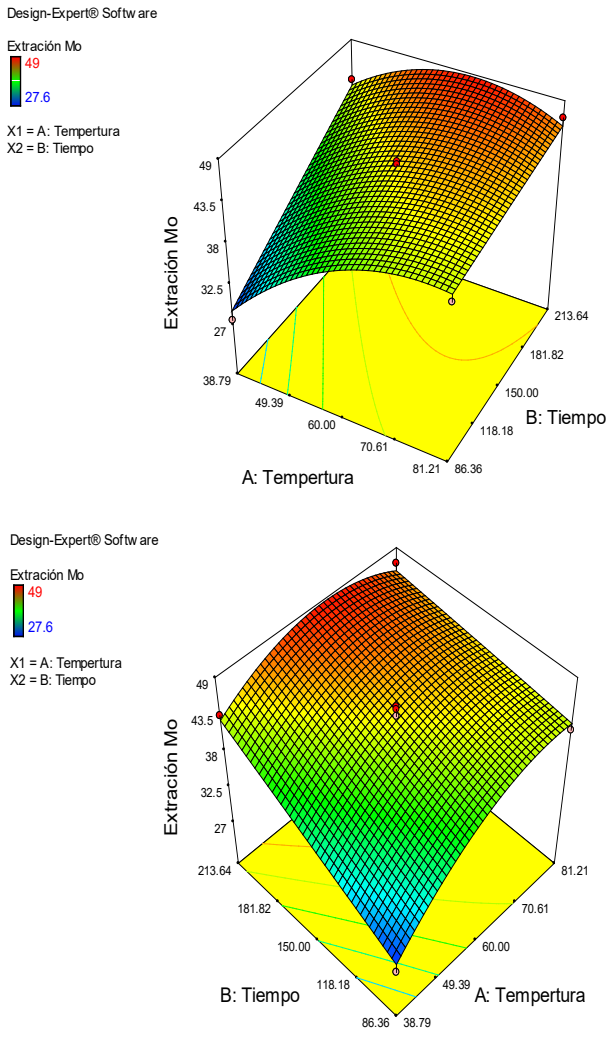

Figure 11. 3D response surface plots for Mo extraction at different temperatures and times.
Source: Bazan, Medina and Orozco, 2024.

It is also evident that the concentrations of the elements present in each sample are similar, corroborating good homogenization and quartering of the sample. The novel molybdenum extraction process was developed from a concentrate of molybdenite and chalcopyrite mainly, using hydrochloric acid as a leaching solution, sodium chloride as a catalyst, sodium hydroxide as a pH regulator to be able to work in a basic environment (pH>8).

Experiments show that it is an effective technique for extracting molybdenite concentrate by using hydrochloric acid. The experimental results show that leaching time, pH, liquid-solid ratio, leaching temperature and hydrochloric acid concentration have a significant effect.

The use of $FeCl_3$ solutions produces a positive effect on leaching, since they allow better recovery of Mo to be achieved in less operating time and allows selective leaching of the desired element.

The optimal technological parameters were determined for molybdenum leaching as follows: working pH greater than 8, temperature of 50 °C, hydrochloric acid concentration of 5%, solid/liquid ratio of 10:1, stirring rate of 200-300 rpm and the addition of 2% ferric chloride. Mo leaching was 70% under experimental conditions at a time of 180 minutes.

References

[1] Salehi, H., Tavakoli, H., Aboutaleb, M.R., and Samim, H.R., Recovery of molybdenum and rhenium in scrub liquors of fumes and dusts from roasting molybdenite concentrates, Hydrometallurgy, 185, pp. 142-148, 2019. ISSN 0304-386X, DOI: https://doi.org/10.1016/j.hydromet.2019.02.004

[2] Kumar, M., Mankhand, T.R., Murthy, D.S.R., Mukhopadhyay, R., and Prasad, P.M., Refining of a low-grade molybdenite concentrate, Hydrometallurgy, 86(1–2), pp. 56-62, 2007. ISSN 0304-386X, DOI: https://doi.org/10.1016/j.hydromet.2006.11.003

[3] Lasheen, T.A., El-Ahmady, M.E., Hassib, H.B., and Helal, A.S. Molybdenum metallurgy review: hydrometallurgical routes to recovery of molybdenum from ores and mineral raw materials. Mineral Processing and Extractive Metallurgy Review, 36(3), pp. 145–173, 2014. DOI: https://doi.org/10.1080/08827508.2013.868347

[4] Bazán, V., Brandaleze, E. y Colque, E., Cinética de tostación de concentrados de baja ley de molibdenita. DYNA.80(181), pp. 146-152, 2013.

[5] Marin, T., Utigard, T., and Hernandez, C., Roasting kinetics of molybdenite concentrates. Canadian Metallurgical Quarterly, 48(1), pp. 73-80, 2009.

[6] Yang, J-G, Yang, J-Y, Tang, M-T, Tang, C-B, and Liu, W., The solvent extraction separation of bismuth and molybdenum from a low grade bismuth glance flotation concentrate, Hydrometallurgy, 96(4), pp. 342-348, 2009. ISSN 0304-386X, DOI: https://doi.org/10.1016/j.hydromet.2008.12.006

[7] Sharia, M.H., Setoodeh, N., and Atash, R., Optimizing conditions for hydrometallurgical production of purified molybdenum trioxide from roasted molybdenite of sarcheshmeh, Minerals Engineering, 14(7), pp. 815-820, 2001. ISSN 0892-6875, DOI: https://doi.org/10.1016/S0892-6875(99)00000-X

[8] Cao, Z-F., Zhong, H., Qiu, Z-H., Liu, G-Y., and Zhang, W-X., A novel technology for molybdenum extraction from molybdenite concentrate. Hydrometallurgy, 99(1–2), pp. 2-6, 2009. ISSN 0304-386X, DOI: https://doi.org/10.1016/j.hydromet.2009.05.001

[9] Behmadi, R., Mirzaei, M., Afshar, M.R., and Najafi, H. Investigation of chalcopyrite removal from low-grade molybdenite using response surface methodology and its effect on molybdenum trioxide morphology by roasting. The Royal Society of Chemistry, 13, pp. 14899-14913, 2023.

[10] Khalil, M.M.H., Al-Wakeel, K.Z., Abd El Rehim, S.S., and Abd El Monem, H., Adsorption of Fe(III) from Aqueous Medium onto Glycine-Modified chitosan resin: equilibrium and kinetic studies.

Journal of Dispersion Science and Technology, 35(12), pp. 1691–1698. 2014. DOI: https://doi.org/10.1080/01932691.2013.859624
[11] Kuma, J.A., Amarnath, D.J., Kumar, P.S., Kaushik, C.S., Varghese, M.E., and Saravanan, A., Mass transfer and thermodynamic analysis on the removal of naphthalene from aqueous solution using oleic acid modified palm shell activated carbon, Desal. Wat. Treat., 106, pp. 238–250, 2018.
[12] Elwakeel, K.Z., Aly, M.H., El-Howety, M.A. et al., Synthesis of chitosan activated carbon beads with abundant amino groups for capture of Cu(II) and Cd(II) from Aqueous Solutions. J Polym Environ 26, pp. 3590–3602, 2018. DOI: https://doi.org/10.1007/s10924-018-1243-2
[13] Khalil, M.M.H., Al-Wakeel, K.Z., Abd El Rehim, S.S. and Abd El Monem, H., Efficient removal of ferric ions from aqueous medium by amine modified chitosan resins. Journal of Environmental Chemical Engineering, 1, pp. 566-573, 2013. DOI: https:// doi.org/10.1016/j.jece.2013.06.022.
[14] Baba, A.A., Ayinla, K.I., Adekola, F.A., Ghosh, M.K., Ayanda O.S., Bale, R.B., Sheik, A.R., and Pradhan, S.R., A review on novel techniques for chalcopyrite ore processing. Int. J. Min. Eng. Miner. Process. 1(1), pp. 1-16, 2012. DOI: https://doi.org/10.5923/j.mining.20120101.01
[15] Bazan, V., Fernandez, P., Medina, M., y Lara, R., Lixiviación de concentrados molibdeno. La Revista Latinoamericana de Metalurgia y Materiales, RLMM, S8(1), pp. 1-18, 2019.
[16] Nicol, M., Miki, H., and Velásquez-Yévenes, L., The dissolution of chalcopyrite in chloride solutions: Part 3. Mechanisms, Hydrometallurgy, 103(1–4), pp. 86-95, 2010. ISSN 0304-386X, DOI: https://doi.org/10.1016/j.hydromet.2010.03.003
[17] Li, Y., Wang, F., Yang, B. et al., Experimental investigation of molybdenum disulfide purification through vacuum distillation. J. Sustain. Metall. 6, pp. 419–427, 2020. DOI: https://doi.org/10.1007/s40831-020-00284-5
[18] Cao, Z-F., Zhong, H., Qiu, Z-H., Liu, G-Y., and Zhang, W-X., A novel technology for molybdenum extraction from molybdenite concentrate, Hydrometallurgy, 99(1–2), pp. 2-6, 2009. DOI: https://doi.org/10.1016/j.hydromet.2009.05.001
[19] Shalchian Hossein, Birloaga Ionela, Bagheri Motahareh Moghaddam, Nasiri Hadi, Vegliò Francesco, A hydrometallurgical process flowsheet for recovering MoO_3 from Molybdenite, Hydrometallurgy, 228, art. 106355, 2024. ISSN 0304-386X, DOI: https://doi.org/10.1016/j.hydromet.2024.106355
[20] Hesami, R., Ahmadi, A., Hosseini, R.M., Manafi, Z., Electroleaching kinetics of molybdenite concentrate of Sarcheshmeh copper complex in chloride media, Minerals Engineering, 186, art. 107721, 2022. ISSN 0892-6875. DOI: https://doi.org/10.1016/j.mineng.2022.107721
[21] Padilla, R., Letelier, H., and Ruiz, M.C., Kinetics of copper dissolution in the purification of molybdenite concentrates by sulfidation and leaching, Hydrometallurgy, 137, pp. 78-83, 2013. ISSN0304-386X, DOI: https://doi.org/10.1016/j.hydromet.2013.05.012
[22] Nguyen, H.N.H., Nguyen, T.T.H., and Lee, M.S., Leaching of molybdenite by hydrochloric acid solution containing sodium chlorate. Resources Recycling, 31(5), pp. 26-33, 2022. DOI: https://doi.org/10.7844/kirr.2022.31.5.26
[23] Ojo, J., Ipinmoroti, K., and Adeeyinwo, C., Solvent extraction of molybdenum (VI) from diluted and concentrated hydrochloric acid. Global Journal of Pure and Applied Sciences. 14(3), pp: 289-294, 2008. DOI: https://doi.org/10.4314/gjpas.v14i3.16810
[24] Tumen-Ulzii, N., Batnasan, A., and Gunchin, B., Selective dissolution of copper and iron from molybdenite concentrate using acidic sodium nitrate solution, Minerals Engineering, 185, art. 107715. 2022. DOI: https://doi.org/10.1016/j.mineng.2022.107715
[25] Li, L.F., Cao, Z.F., Zhong, H. et al., The selective leaching and separation of molybdenum from complex molybdenite concentrate containing copper. Mining, Metallurgy & Exploration 30, pp. 233–237, 2013. DOI: https://doi.org/10.1007/BF03402467
[26] Xu, Y., Liu, X., Zhao, Z., Chen, X., Li, J., He, L., and Sun, F., Kinetics and mechanism of selective leaching of bismuth from molybdenite and bismuthinite mixed ore, Hydrometallurgy, 224, art. 106258, 2024. ISSN 0304-386X, DOI: https://doi.org/10.1016/j.hydromet.2023.106258
[27] Lessard, J.D., and Shekhte, L.N., Thermodynamic modeling of atmospheric hydrometallurgical removal of chalcopyrite from molybdenite concentrates, Hydrometallurgy, 150, pp. 9-13, 2014. ISSN 0304-386X, DOI: https://doi.org/10.1016/j.hydromet.2014.08.013

V.L. Bazan-Brizuela, is BSc. Eng. in Chemical Engineer in 1999, Dr. of Science in Extractive Metallurgy Engineering in 2006, from the University of Concepción, Chile. She is a professor at the Faculty of Engineering at the National University of San Juan, and a researcher at CONICET. since 2008. She is director of the Graduate Department of the Faculty of Engineering of the UNSJ. His research has been based on extractive metallurgy of non-ferrous minerals, focused on increasing production with clean technologies and pyrometallurgical and/or hydrometallurgical processes.
ORCID: 0000-0001-5766-6004

M.C. Medina-Arias, is BSc. Eng. in Chemical Engineer from the UNSJ, Sp. in Mineral Processing. European Mineral Engineering Course (1999-2000) and currently completing the MSc. in Extractive Metallurgy. He worked in the mining industry at Minera Alumbrera -XSTRATA Copper and Mina Veladero- Barrick Gold & Sandong Gold among others. He currently holds the position of Head of Metallurgy for the Los Azules Project -Mc Ewen Copper.
ORCID: 0009-0005-8719-5764

M.I. Orozco-Santander, is BSc. Eng. in Food Engineering, MSc. in Extractive Metallurgy and Dr. in Mineral Processing Engineering from the Faculty of Engineering of the National University of San Juan. He is a teacher and researcher at the Department of Mining Engineering. His research is based on the recovery of metal waste, circular economy, and processing of non-ferrous minerals.
ORCID: 0000-0002-9120-3609

DYNA
http://dyna.medellin.unal.edu.co/

UNIVERSIDAD NACIONAL DE COLOMBIA

Virtual tool of nonlinear model of interconnected tanks with PID control implementation using EJsS

Oscar Oswaldo Rodríguez-Diaz [a], Oscar Humberto Sierra-Herrera [a] & Mario Eduardo González-Niño [b]

[a] *Escuela de Ingeniería Electrónica, Universidad Pedagógica y Tecnológica de Colombia, Sogamoso y Tunja, Colombia. oscar.rodriguez@uptc.edu.co, oscarhumberto.sierra@uptc.edu.co*
[b] *Escuela de Ingeniería Electromecánica, Universidad Pedagógica y Tecnológica de Colombia, Duitama, Colombia. marioeduardo.gonzalez@uptc.edu.co*

Received: May 18th, 2024. Received in revised form: October 23th, 2024. Accepted: October 30th, 2024.

Abstract
This paper describes the development and implementation of a virtual tool (TANQUES EN SERIE PID) of a system of two interconnected tanks made in Easy Java/JavaScript Simulations (EJS,), a tool that seeks to motivate learning control concepts in engineering programs. The simulated model corresponds to the non-linear system of interconnected tanks, which presents graphically the behavior of tank levels on an open loop, this application allows varying physical input parameters of the process, as the cross section of the tanks, resistivity constants of the valves and the input flow of process. The system is also presented in closed loop, presenting the behavior when a PID controller is implemented to the process, controller and time constants can be modified to enter a disturbance to the model and by doing this we are verifying the time response and system reaction when subjected to a perturbation. The tool is verified comparing the results using Simulink and equilibrium equations.

Keywords: automatic control; virtual tool; teaching; nonlinear system; tanks; PID.

Implementación de una herramienta virtual del modelo no lineal de tanques interconectados con control PID utilizando EJsS

Resumen
Este articulo describe el desarrollo e implementación de una herramienta virtual (TANQUES EN SERIE PID) de un sistema de dos tanques interconectados, hecha en Easy Java/JavaScript Simulations (EJsS), herramienta que busca motivar el aprendizaje de conceptos de control en programas de ingeniería. El modelo simulado corresponde al sistema no lineal de tanques interconectados, donde se presenta de forma gráfica el comportamiento de los niveles de los tanques en lazo abierto, esta aplicación permite variar parámetros físicos de entrada del proceso, como la sección transversal de los tanques, las constantes de resistividad de las válvulas y el flujo de entrada del proceso. También se presenta el sistema en lazo cerrado, observando el comportamiento al implementar un controlador PID al proceso, en este se pueden ajustar las constantes del controlador y el tiempo para ingresar una perturbación al modelo, verificando así su respuesta en el tiempo y la reacción del sistema al ser sometido a una perturbación. La herramienta se verifica comparando los resultados obtenidos en Simulink y las ecuaciones de los puntos de equilibrio.

Palabras clave: control automático; herramienta virtual; enseñanza; sistema no lineal; tanques; PID.

1 Introduction

Over the last years there has been a significant increment in the amount of educational software, especially on undergraduate and postgraduate levels, this has taken education tools on to a next level, new learning and teaching styles has been adopted, generating in researchers, teachers, and students the autonomous and critic thinking [1]. Easy Java/JavaScript Simulations (EJsS) is a development tool, that allows the implementation of linear and nonlinear differential equations simulations, with graphs, buttons, and visual representations of the systems [2]. Allowing the

How to cite: Rodríguez-Diaz, O.O., Sierra-Herrera, O.H., and González-Niño, E., Virtual tool of nonlinear model of interconnected tanks with PID control implementation using EJsS. DYNA, 91(234), pp. 62-69, October - December, 2024.

development of complete simulations, that are interactive, and easy to use by the user. The software developed with EJS gives the user a closer experience to the real systems applications, some examples of developed software with EJS are: ball and beam system, pendulum and a tank system for the teaching the dynamic system modelling [2]. EJsS is still in developing, getting new features each year [3]. MATLAB is a matrixial software used for simulating all kind of mathematical models, is one of the most used software by researchers in all the world, it includes Simulink that allows the use of graphical elements to create simulations of linear and nonlinear models [4]. Control learning has been always a notable topic on engineering education, this due to the number of concepts involved and its close relation with real system applications, this means that is necessary a fully understanding of system modeling, control theory, instrumentation, power electronics, among others [5]. Nowadays specially in least developed countries there is a need to leave the dependency of paid software like MATLAB to carry out simulation of nonlinear systems, also there is the urgent of tools with low resource consumption and user friendly are demanded, these reasons motivated the authors to work into the development of the TANQUES EN SERIE PID simulation tool, to solve these problems, interconnected tanks system is chosen since it is one of the most used systems in system modeling.

Regarding tanks investigations, there are works like the one presented in [6] where linear and nonlinear control applications are made for a three interconnected tanks system. A notable work of control education using EJS is presented in [7] where some tools are developed using EJS for the teaching of automatic control. More recently EJS applications can be found in [8] where EJsS is integrated into the data analytics of the national Learning Management System for Singapore schools using the Moodle platform, or [9] where EJsS is used to develop physics fundamentals tools for undergraduate students.

In this paper a nonlinear interconnected tanks system in open loop and closed loop is developed using EJS, reviewed and compared against the results obtained in Simulink of MATLAB, this paper contains: introduction, interconnected tanks system modeling, nonlinear model, Equilibrium points, virtual tool TANQUES EN SERIE, development, Graphical user interface, results, and conclusions.

2 Interconnected tanks system modeling

The mathematical analysis of the system behavior is represented by nonlinear differential equations [10]. The system is shown in the Fig. 1, it includes two tanks interconnected serially, the input flow $Q_i(t)$ can be modified over time, as the tanks level increases or decreases. The tank levels are represented by $H_1(t)$and $H_2(t)$. The model is known as interconnected tanks since the liquid flow between tanks is denominated $Q_1(t)$, this is an output at the tank1 and an input at the tank 2. $Q_1(t)$ is assumed positive since the liquid flow will always be in direction from tank 1 to tank2.

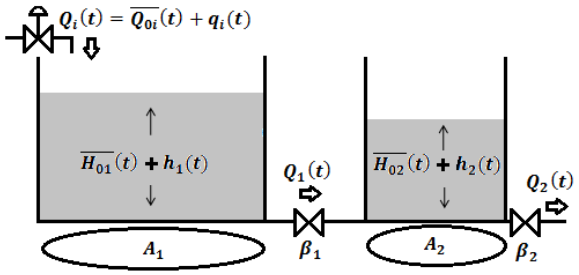

Figure 1. Interconnected tanks system.
Source: Authors.

2.1 Nonlinear model

The system model can be obtained from the conservation of mass principle, whereas the change of volume of the tank1 and tank2 relies on the variation of the input and output flows, the variation of liquid volume in tank1 can be expressed as the difference of the input flow $Q_i(t)$ and the output flow $Q_1(t)$ as it is shown in the eq. (1). Using the same reasoning of tank 1 volume for the tank2, the variation of liquid volume is show in eq. (2).

$$\frac{dV_1(t)}{dt} = Q_i(t) - Q_1(t) \tag{1}$$

$$\frac{dV_2(t)}{dt} = Q_1(t) - Q_2(t) \tag{2}$$

The flow between tanks 1 and 2 is dependent of $H_1(t)$ *and* $H_2(t)$, this means that if $H_1(t)$ is bigger, there will be more pressure. so $Q_1(t)$ will be, eq. (3).

$$Q_1(t) = \beta_1\sqrt{H_1(t) - H_2(t)} \tag{3}$$

And the flow in $Q_2(t)$ will be, eq. (4)

$$Q_2(t) = \beta_2\sqrt{H_2(t)} \tag{4}$$

The nonlinear space state representation of the tanks dynamics is given in by the differential equations show in eq. (5) and eq. (6).

$$\frac{dH_1(t)}{dt} = \frac{Q_i}{A_1} - \frac{\beta_1\sqrt{H_1(t) - H_2(t)}}{A_1} \tag{5}$$

$$\frac{dH_2(t)}{dt} = \frac{\beta_1\sqrt{H_1(t) - H_2(t)}}{A_2} - \frac{\beta_2\sqrt{H_2(t)}}{A_2} \tag{6}$$

$Q_i(t)$ input flow of tank1.
$H_1(t)$ level of liquid in tank 1.
$H_2(t)$ level of liquid in tank 2.
$\beta_1(t)$ *and* $\beta_2(t)$ are the valves constants.
$A_1(t)$ *and* $A_2(t)$ are the cross-sectional areas of the tanks.

If the input flow $Q_i(t)$ is equal to the output flow of the

tank 1 $Q_1(t)$, and the flow between the tanks is equal to the output flow $Q_2(t)$, the system become into an equilibrium point, this guarantees that there is no level variation between the tanks.

The cross-sectional areas of the tanks $A_1(t)\ and\ A_2(t)$ and the valves constants $\beta_1(t)\ and\ \beta_2(t)$ are considered constants in the software. The differential equations of the model belong to the nonlinear space state model of the system, where the state vector is composed by the tank levels $H_1(t)$ and $H_2(t)$, and the input of the system is the flow $Q_i(t)$. These variables can be visualized in the simulation tool developed.

2.2 Equilibrium points

By making nonlinear state equations (eq. (5) and eq. (6)) equal to zero, equilibrium points are obtained eq. (7) and eq. (8).

$$\frac{Q_i}{A_1} - \frac{\beta_1\sqrt{H_{01}(t) - H_{02}(t)}}{A_1} = 0 \tag{7}$$

$$\frac{\beta_1\sqrt{H_{01}(t) - H_{02}(t)}}{A_2} - \frac{\beta_2\sqrt{H_{02}(t)}}{A_2} = 0 \tag{8}$$

Solving from eq. (7), eq. (9) is obtained.

$$\sqrt{H_{01}(t) - H_{02}(t)} = \frac{Q_i}{\beta_1} \tag{9}$$

Solving from eq. (8), eq. (10) is obtained.

$$\sqrt{H_{02}(t)} = \frac{\beta_1}{\beta_2}\sqrt{H_{01}(t) - H_{02}(t)} \tag{10}$$

Replacing eq. (9) in eq. (10) and solving for $H_{02}(t)$, eq. (11) is obtained.

$$H_{02}(t) = \left(\frac{Qi(t)}{\beta_2}\right)^2 \tag{11}$$

Now from replacing eq. (11) in eq. (9), eq. (12) is obtained.

$$H_{01}(t) = \left(\frac{Q_i(t)}{\beta_1}\right)^2 + \left(\frac{Q_i(t)}{\beta_2}\right)^2 \tag{12}$$

Eq. (11) and eq. (12) represent the generalized expressions for the equilibrium points. The system has multiple equilibrium points in function of the input flow $Qi(t)$. From the equilibrium point a linear model can be obtained, eq. (13).

$$\begin{bmatrix}\dot{H}_1\\ \dot{H}_2\end{bmatrix} = \begin{bmatrix}\left.\frac{\partial f_1}{\partial H_1}\right|_{\overline{X_0}} & \left.\frac{\partial f_1}{\partial H_2}\right|_{\overline{X_0}}\\ \left.\frac{\partial f_2}{\partial H_1}\right|_{\overline{X_0}} & \left.\frac{\partial f_2}{\partial H_2}\right|_{\overline{X_0}}\end{bmatrix}\begin{bmatrix}h_1\\ h_2\end{bmatrix} + \begin{bmatrix}\left.\frac{\partial f_1}{\partial Q_i}\right|_{\overline{X_0}}\\ \left.\frac{\partial f_2}{\partial Q_i}\right|_{\overline{X_0}}\end{bmatrix} Q_i \tag{13}$$

3 The virtual tool TANQUES EN SERIE PID

3.1 Development

The virtual tool is developed using Easy Java Simulation (EJsS) software, it was created by Francisco Esquembre, it is an open-source software that allows the simulation of math models based on differential equations, wherever they are linear or nonlinear, plus the signals can be visualized in a classic manner and through didactic representations of the systems. EJsS allows the generation of .jar files that can be converted to .exe files, allowing an easy distribution of the generated software [2,11,12].

In the Fig. 2 the main window of EJsS can be seen, this window is composed by 5 sections: Work panel selector, Information panels, Workbar, Work panels, and Information messages.

The Work panel is made of 3 subpanels with the follow specific functions:

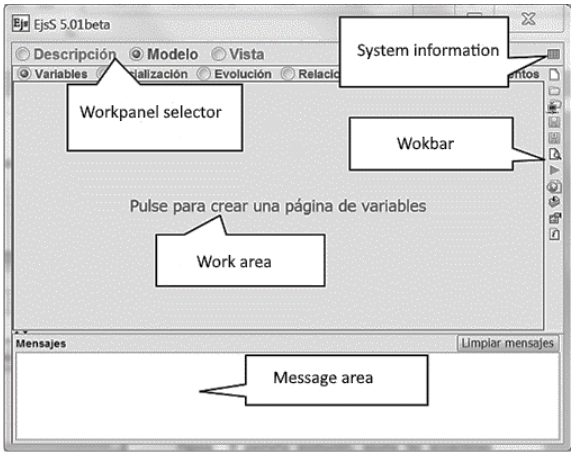

Figure 2. EJS software.
Source: Authors.

With the use of EJsS, the implementation of the nonlinear model is made using differential equations, also a closed loop is made using a PID controller, all of these using 2D graphical representations and time graphs of the most important functions, pause and play buttons are also included to control the simulation behavior, all the simulation parameters can be modified while the simulation is still running, thus resulting in a complete simulation tool.

3.2 Graphic user interface

The virtual tool has two tabs: “serie_no_lineal”, and “serie_no_lineal_controlado”, in each one of these tabs there are four sections, this can be seen in Fig. 3.

In the first section “1” there is a 2D animated graphical representation of the two interconnected tanks, there is a visual rendering of the tank levels, the input and output flows. This graph relies on the implemented differential equation of the model. The second “2” and the fourth “4” section introduce the graph of the tank1 and tank2 level functions respectively.

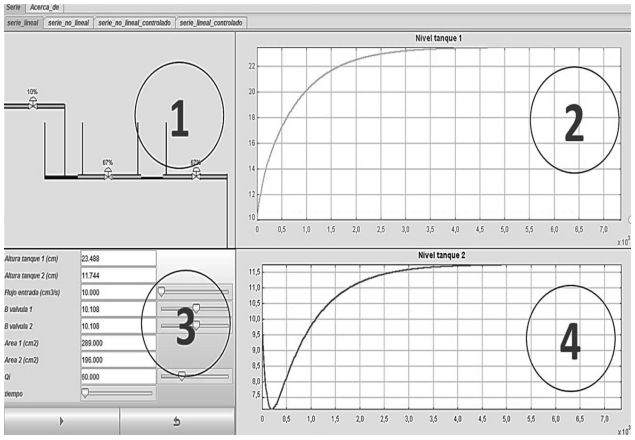

Figure 3. Interconnected tanks virtual tool sections.
Source: Authors.

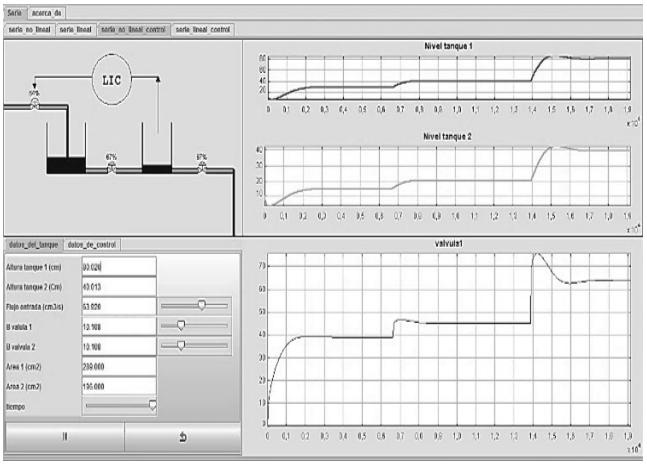

Figure 4. Nonlinear closed loop system tab.
Source: Authors.

The third "3" section display the parameters of the mathematical model that can be modified by the user, this includes A_1, A_2, β_1, β_2, and Q_i; there is a time slider, this is used to slow down or accelerate the simulation. This section also includes a play/pause and a reset button. All of this can be seen in more detail in the Fig. 5.

When the user is simulating a closed loop-controlled system in the respective tab (Fig. 4), in the third section a sub-tab appears, where the PID parameters can be modified by the user, this includes Kp, Ki, Kd and the reference, this can be seen in Fig. 6.

Note that in Fig. 4 when the user is in the "Serie_no_lineal_controlado" (closed loop system), a graph for the input valve function (controlled signal) versus time appears below the level tanks graphs.

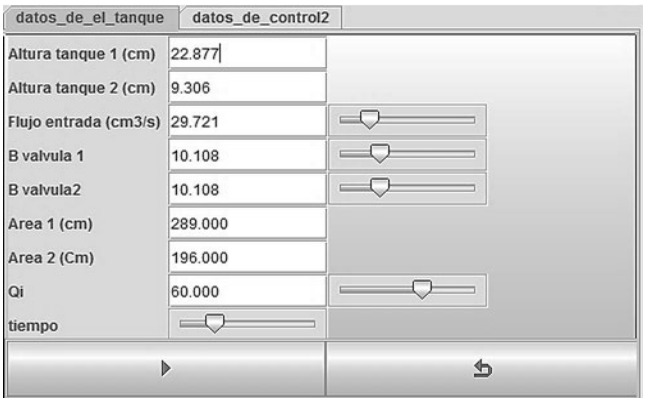

Figure 5. Model parameters modification in the virtual tool.
Source: Authors.

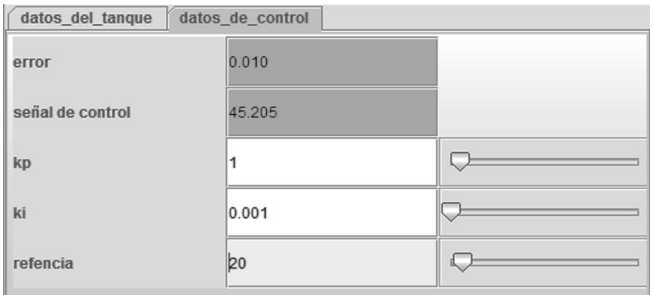

Figure 6. PID parameters modification in the virtual tool.
Source: Authors.

4 Results

4.1. Validation of the model

To validate the virtual tool results, the following parameters were used: $A_1 = 289\ cm^2$,$A_2 = 196\ cm^2$, input flow $Q_i = 60\ \frac{cm^3}{seg}$, resistivity constant of the valves $\beta_1 = \beta_2 = 10.108$. These parameters are introduced into the developed tool and set to run, after the system settles, the level in tank 1 is of 70.470cm and the level in tank 2 is of 35.235 cm, Fig. 7.

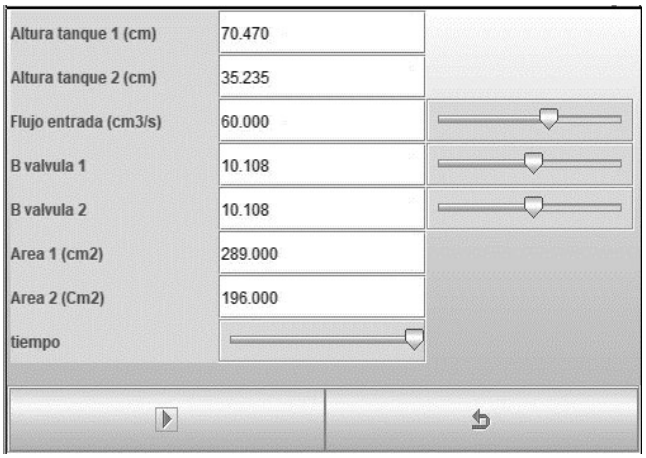

Figure 7. Parameters in the virtual tool, input flow of 60 cm3/s.
Source: Authors.

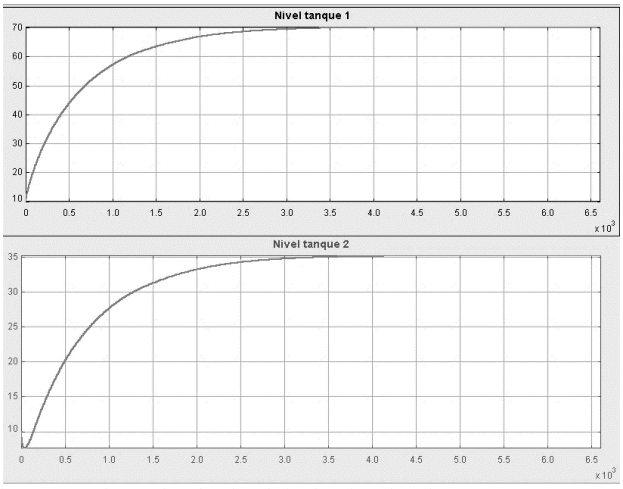

Figure 8. Tank 1 and tank 2 levels in the virtual tool.
Source: Authors.

The results are also displayed in a graphical manner in the virtual tool developed, Fig. 8.

To validate the results obtained in Fig. 7 and Fig. 8, the values are replaced into the equilibrium points equations, eq. (11) and eq. (12). The results obtained a for tank 1 and tank 2 respectively are displayed in eq. (14) and eq (15) respectively.

$$H_{01}(t) = \left(\frac{Q_i(t)}{\beta_1}\right)^2 + \left(\frac{Q_i(t)}{\beta_2}\right)^2 = 70.470 \quad (14)$$

$$H_{02}(t) = \left(\frac{Qi(t)}{\beta_2}\right)^2 = 35.235 \quad (15)$$

The results obtained through the equations and the developed software are almost the same.

To give another example using the virtual tool, the same parameters of Fig. 7 are used, then after the system settles the input flow is modified from $Q_i = 60\frac{cm^3}{seg}$ to $Q_i = 70\frac{cm^3}{seg}$, the tanks levels after the system settle are: tank 1=95.919cms and tank 2=47.957cms respectively, this can be seen in Figs. 9 and 10.

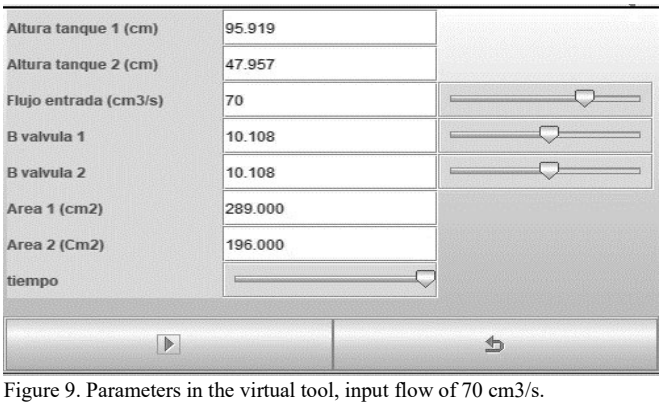

Figure 9. Parameters in the virtual tool, input flow of 70 cm3/s.
Source: Authors.

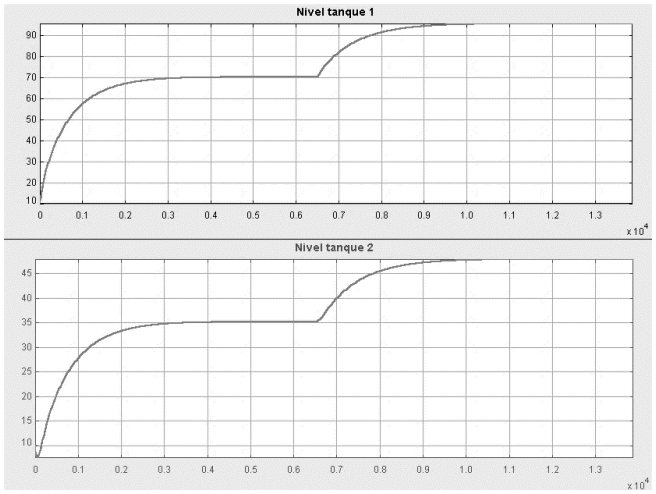

Figure 10. Tank 1 and tank 2 levels in the virtual tool.
Source: Authors.

These results are verified using eq. (11) and eq. (12), then eq. (16) and eq. (17) are obtained.

$$\boldsymbol{H_{01}(t) = \left(\frac{Q_i(t)}{\beta_1}\right)^2 + \left(\frac{Q_i(t)}{\beta_2}\right)^2 = 95.917} \quad (16)$$

$$\boldsymbol{H_{02}(t) = \left(\frac{Qi(t)}{\beta_2}\right)^2 = 47.959} \quad (17)$$

The Nonlinear differential equations are implemented in Simulink as shown in Fig. 11, the input flow is represented by a step signal, it starts at 60cm3/s then at 6600 seconds is modified to 70cm3/S, this can be seen in Fig. 12. The obtained signals for tank 1 and tank 2 levels are displayed in Figs. 12 and 13 respectively, the results obtained in Simulink match the ones obtained in the virtual tool (Fig. 10) and with the theoretical calculations, in the Table 1 a comparison

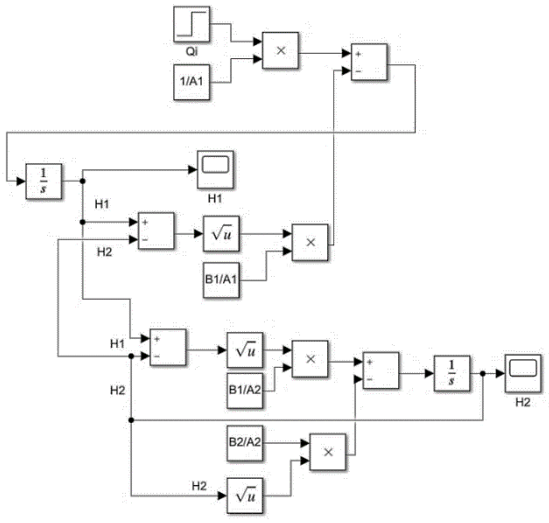

Figure 11. Nonlinear interconnected tanks model in Simulink.
Source: Authors.

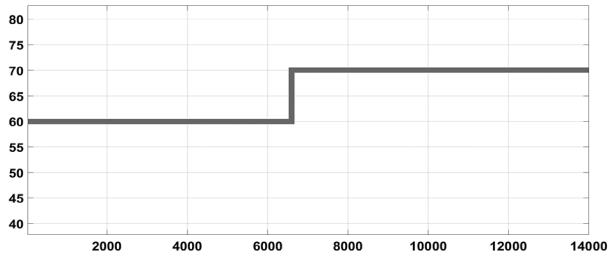

Figure 12. Input flow in Simulink.
Source: Authors

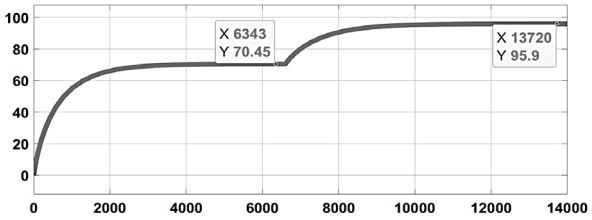

Figure 13. Tank 1 level in Simulink.
Source: Authors.

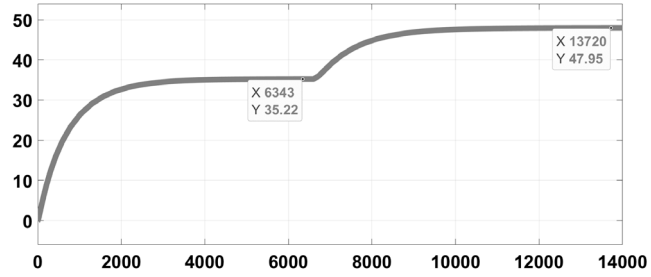

Figure 14. Tank 2 level in Simulink.
Source: Authors.

Table 1.
Obtained results.

Method	Tank 1 level (cm3/s)	Tank 2 level (cm3/s)
Equilibrium point equations Qi=60cm3/s	70.470	35.235
Virtual tool Qi=60 cm3/s	70.470	35.235
Simulink Qi=60 cm3/s	70.45	35.22
Equilibrium point equations Qi=70 cm3/s	95.917	47.959
Virtual tool Qi=70 cm3/s	95.919	47.957
Simulink Qi=70 cm3/s	95.9	47.95

Source: Authors.

between all the obtained equilibrium points is set forth. The signals obtained in the virtual tool in Fig. 10 can be directly compared with the signals obtained in Figs. 12 and 13, they are practically the same in terms of time response.

4.2 PID controller verification

As stated earlier the developed virtual tool can simulate the nonlinear model of the tanks with a PID controller in a closed loop, where the reference is the level in the tank 2 and the controlled variable is the input flow Qi. When the virtual tool is in the "serie_no_lineal_control" tab, the data panels of Figs. 5 and 6 are accessible, the tanks parameters and PID controller parameters can be modified, the subsequent parameters are used: Kp=5, Ki=0.03 and Kd=0.5, this can be seen in Fig. 15.

In Fig.16 the tank 1 and tank 2 levels obtained in the virtual tool can be seen, the variation of the input flow Qi (controlled variable) is show in Fig. 17.

To verify the results obtained in Figs. 16 and 17, a simulation in Simulink is performed, adding a PID controller and closing the loop to the system show in Fig. 11 the system of Fig. 18 is obtained.

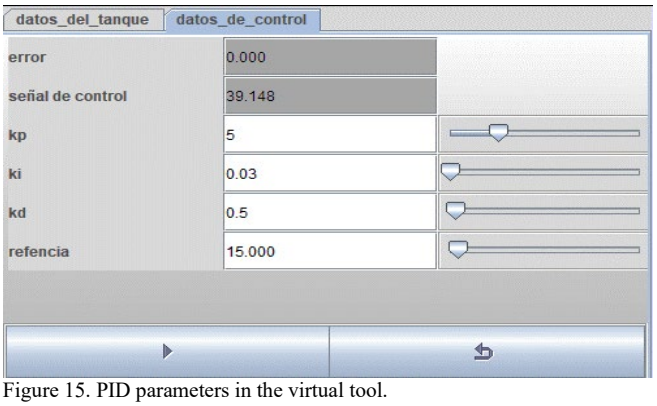

Figure 15. PID parameters in the virtual tool.
Source: Authors

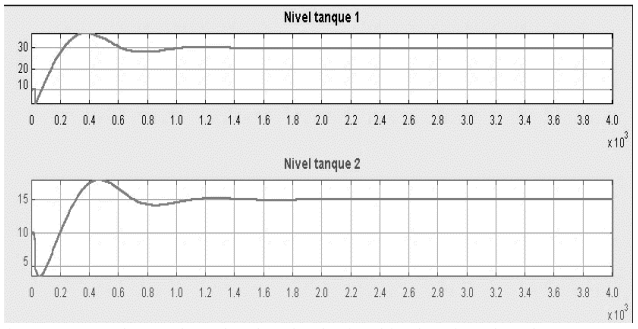

Figure 16. Tank 1 and Tank 2 levels obtained in the virtual tool.
Source: Authors

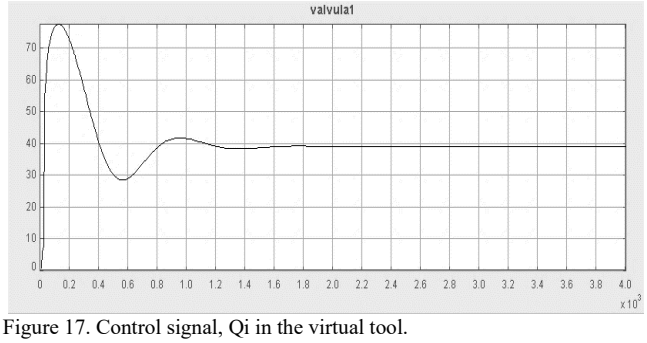

Figure 17. Control signal, Qi in the virtual tool.
Source: Authors

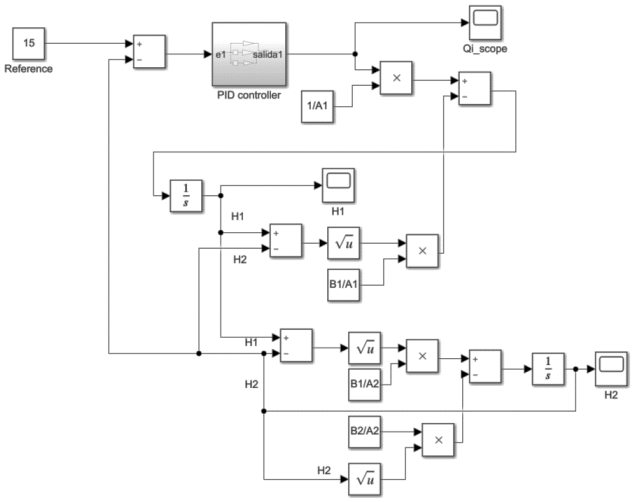

Figure 18. Closed loop simulation in Simulink.
Source: Authors

In Fig. 19 the PID controller implemented in Simulink is displayed, note that the same parameters of the Fig. 15 were used.

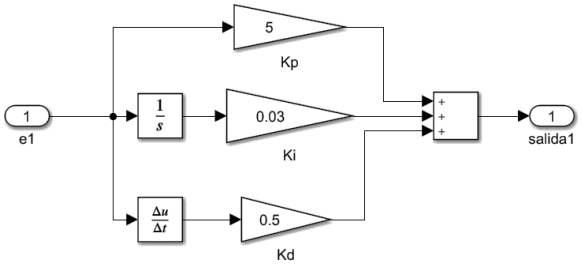

Figure 19. PID controller in Simulink.
Source: Authors

The tank 2 level signal obtained in the Simulink simulation is displayed in the Fig. 20, the signal is almost the same of the one displayed in Fig. 16, both have a maximum peak of approximately 17cm at 500 seconds, both signals settle at around 1300 seconds.

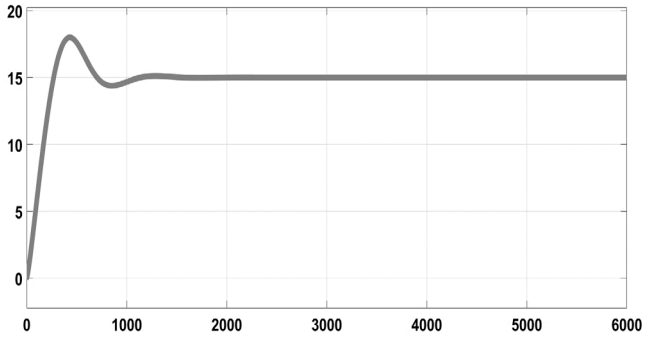

Figure 20. Tank 2 level signal in Simulink.
Source: Authors

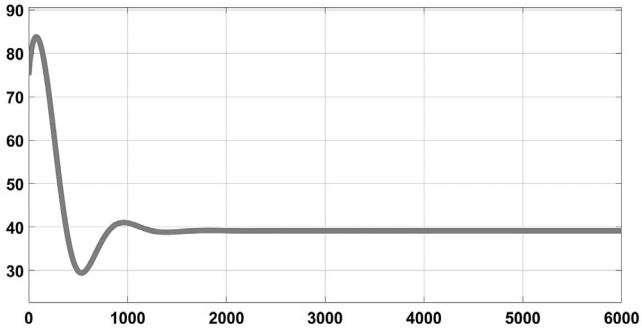

Figure 21. Control signal in Simulink.
Source: Authors

The input flow signal (control signal) obtained in Simulink is presented in Fig. 21, it is almost the same one obtained in Fig. 16, both signals have a maximum peak of almost 85, a minimum of 30, and settle at around 1300 seconds.

5 Conclusions

This work proves that the open-source software Easy Java Simulations can be used to implement fully functional, interactive and didactic simulations of nonlinear liquid level models with applied control strategies, in this case with a PID controller. Time response of tank level and valve signals can be studied in detail through the virtual tool developed, making easier the study of the nonlinear model, PID controller design, equilibrium points, and stability of continuous systems. The nonlinear model and PID parameters can be modified while the simulation is still running. The platform allows the application of PID controllers to the nonlinear model of interconnected tanks, this gives total freedom to the user, also the signals time response can be seen in time graphics or in a more didactic way in a 2D representation, this includes tanks levels, flows and valve variations.

The software results were validated using equations and simulations performed in Simulink of MATLAB. As future work, the platform is intended to be benchmarked as a teaching tool, also more functions will be added including Linear model, space state model, state variable feedback controller, among another's. TANQUES EN SERIE PID stablishes as one of the most complete user-friendly simulation tools available nowadays in the world for nonlinear PID simulation, remaining lightweight, needing few system resources, being reliable and with proved accuracy.

References

[1] Miranda, J. et al., The core components of education 4.0 in higher education: Three case studies in engineering education, Comput. Electr. Eng., 93, art. 107278, 2021, DOI: https://doi.org/10.1016/j.compeleceng.2021.107278.

[2] Esquembre, F., Using easy Java simulations to create scientific simulations in Java, IEEE Reg. 8 EUROCON 2003 Comput. as a Tool - Proc., vol. A, pp. 20–23, 2003. DOI: https://doi.org/10.1109/EURCON.2003.1247971.

[3] Chacon, J., Besada-Portas, E., Carazo-Barbero, G., and Lopez-Orozco, J.A., Enhancing EJsS with extension plugins, Electronics, 10(3), art. 242, 2021, DOI: https://doi.org/10.3390/electronics10030242
[4] Mathworks, Simulink, [online]. 2024. [accessed Mar. 24,2024]. Available at: https://es.mathworks.com/products/simulink.html
[5] Freeman, S. et al., Active learning increases student performance in science, engineering, and mathematics., Proc. Natl. Acad. Sci. U. S. A., 111(23), pp. 8410–8415, 2014, DOI: https://doi.org/10.1073/pnas.1319030111.
[6] Bistak, P., and Huba, M., Three-Tank virtual laboratory for input saturation control based on Matlab, IFAC-PapersOnLine, 49(6), pp. 207–212, 2016. DOI: https://doi.org/10.1016/j.ifacol.2016.07.178.
[7] Ramírez-Ramírez, M., Ramírez-Scarpetta, J.M., and Fernández-Samacá, L., Interactive animations for learning by playing concepts of control systems. 21st Mediterr. Conf. Control Autom. MED 2013 - Conf. Proc., pp. 573–577, 2013, DOI: https://doi.org/10.1109/MED.2013.6608779.
[8] Wee, L.K., Tan, D., Clemente, F.J.G. and Esquembre, F., Easy JavaScript Simulation (EJSS) for Singapore, J. Phys. Conf. Ser., 2693(1), art. 012017, 2024, DOI: https://doi.org/10.1088/1742-6596/2693/1/012017.
[9] Galán-Díaz, J.J., Garrido, S.F., García-Diez, A.I., Graña-López, M.Á., Filgueira-Vizoso, A., and Castro-Santos, L., Assessment of engineering undergraduates active learning experience using computer simulations, Int. J. Eng. Educ., 40(2), pp. 358–367, 2024.
[10] Grygiel, R., Bieda, R., and Blachuta, M., On significance of second-order dynamics for coupled tanks systems, 1, pp. 1016–1021, 2016.
[11] Farias, G., De Keyser, R., Dormido, S., and Esquembre, F., Developing Networked control labs: a Matlab and easy Java simulations approach, Industrial Electronics, IEEE Transactions on, 57(10), pp. 3266–3275, 2010 DOI: https://doi.org/10.1109/TIE.2010.2041130.
[12] Dormido, S., Esquembre, F., Farias, G., and Sánchez, J., Adding interactivity to existing Simulink models using Easy Java Simulations, Proc. 44th IEEE Conf. Decis. Control. Eur. Control Conf. CDC-ECC '05, 2005, pp. 4163–4168, 2005. DOI: https://doi.org/10.1109/CDC.2005.1582815.

O.O. Rodriguez-Diaz, is an associated professor at the Electronic Engineering School of the Universidad Pedagógica y Tecnológica de Colombia. He works as a researcher in the research group on digital signal processing (DSP-UPTC) in engineering education and industrial automation. He received his BSc. in Electronic Engineering from the UPTC in 2001 and holds a MSc. in Engineering-Automation from the Universidad Nacional de Colombia, in 2009. Additionally, researcher Rodríguez acquired his PhD from the Universidad del Valle with his research on control strategies in ventilation networks for underground coal mines, in 2023.
ORCID: 0000-0001-8894-6105

O.H. Sierra-Herrera, received the BSc. Eng in Electronic Engineering in 2016, and a MSc. in Electronic Engineering in 2021, from the Universidad Pedagógica y Tecnológica de Colombia. Sogamoso, Colombia. From 2019 to nowadays he is a full professor in the Escuela de Ingeniería Electrónica, Facultad de Ingeniería, Universidad Pedagógica y Tecnológica de Colombia. His research interests are control systems, microgrid, engineering education and software development.
ORCID: 0000-0003-2710-120X

M.E. Gonzalez-Niño, received the BSc. Eng in Electronic Engineering in 2016, and a MSc.in Electronic Engineering in 2021, from the Universidad Pedagogica y Tecnologica de Colombia. From 2019 to nowadays he is a full professor in the Escuela de Ingeniería Electromecánica, Facultad seccional Duitama, Universidad Pedagógica y Tecnológica de Colombia. His research interests include Power systems, Telecommunications and software development. Sogamoso, Colombia
ORCID: 0000-0002-0591-1423

DYNA
http://dyna.medellin.unal.edu.co/

UNIVERSIDAD NACIONAL DE COLOMBIA

Bibliometric analysis on current ergonomic trends in the international labor context

Jade Padrón-Sardiña, Isabela Pancorbo-Camacho, Juan Lázaro Acosta-Prieto & Yilena Cuello-Cuello

Facultad de Ingeniería Industrial, Universidad de Matanzas, Matanzas, Cuba. Padronsardinajade@gmail.com, pancorboisabela2@gmail.com, acostaprietojuanlazaro@gmail.com, yilena.cuello@gmail.com

Received: July 28th, 2024. Received in revised form: October 25th, 2024. Accepted: October 30th, 2024.

Abstract
The objective of this research is to conduct a literature review on current ergonomic current ergonomic trends in the international labor context. The Prisma method was used and a total of 160 articles from 20 high impact journals selected from the Scimago Journal & Country Rank platform were examined from 20 high impact journals selected from the Scimago Journal & Country Rank platform were examined. The most relevant results were: there is a higher concentration of publications in the year 2023 (43.75%); the journals with the highest number of publications on Ergonomics are IEE Transaction on Human Machine systems (16.25%), in which Physical Ergonomics (53.67%) studied existing Ergonomics dimensions followed by Cognitive Ergonomics (36.03%). It is concluded that the emerging trends in Ergonomics reveal the current interest in bringing automation, artificial intelligence and new technologies to all areas of the human life.

Keywords: ergonomics; human factor engineering; work environment; ergonomic trends.

Análisis bibliométrico sobre las tendencias ergonómicas actuales en el contexto laboral internacional

Resumen
El objetivo de esta investigación es realizar una revisión bibliográfica sobre las tendencias ergonómicas actuales en el contexto laboral internacional. Se utilizó el método Prisma y se examinaron un total de 160 artículos provenientes de 20 revistas de alto impacto seleccionadas de la plataforma Scimago Journal & Country Rank. Los resultados más relevantes fueron: existe una mayor concentración de publicaciones en el año 2023 (43.75%); la revistas con mayor número de publicaciones sobre Ergonomía son IEE Transaction on Human Machine sistems (16.25%), en las cuales la Ergonomía Física (53.67%) es la más estudiada entre las 3 dimensiones de la Ergonomía existente seguida de la Ergonomía Cognitiva (36,03%). Se concluye que las tendencias emergentes en la Ergonomía revelan el interés actual de llevar la automatización, la inteligencia artificial y las nuevas tecnologías a todas las áreas de la vida humana.

Palabras claves: ergonomía; ingeniería del factor humano; entorno laboral; tendencias ergonómicas.

1 Introduction

Human capital is still the main engine that drives companies and organizations around the world, for this reason it is of utmost importance that workers can have good health and all the guarantees that allow them to perform their work with all the necessary safety and comfort, without this being detrimental to their health or their physical or emotional capabilities [1].

Depending on the physical, environmental, organizational and cognitive conditions, a work activity can cause undesirable effects on the safety and health of the workers themselves. Throughout history, work has undergone major transformations in terms of structure, design, organization and technification [2].

Ergonomics is defined by the International Ergonomics Association (IEA) as the "...scientific discipline concerned with understanding the interactions between humans and

How to cite: Padrón-Sardiña, J., Pancorbo-Camacho, I., Acosta-Prieto, J.L., and Cuello-Cuello, Y., Bibliometric analysis on current ergonomic trends in the international labor context. DYNA, 91(234), pp. 70-75, October - December, 2024.

other elements of a system, and the profession that applies theory, principles, data and methods to design to optimize human and general well-being" [3].

Ergonomics presents certain guiding principles that guide its application and understanding. They represent the very basis of ergonomics and range from the adaptation of work to human capabilities to the optimization of efficiency and safety in the workplace. Among these principles are: studying the configuration of the workstation and working conditions, adapting the demands of the task to human capabilities, adapting the environment (light, noise, temperature...) to the needs of man at his workstation, and designing machines, equipment and installations with maximum performance, precision and safety [4]

The development of ergonomics is a subject of reflection for the members of its scientific and professional community at both the international and national level. In fact, the IEA in 2020 declared that its main mission is to promote the development of ergonomics as a discipline and as a profession [5,6].

Although studies concerning ergonomics have been developed for several centuries, it was not considered as a discipline until the late 1940s, when the world began to see the importance that this science attributed to the worker. Different groups were created at this time, such as the Human Factors and Ergonomics Society (HFES) in the United States, the International Ergonomics Association (IEA) in 1961 and in 1963, the French-language Ergonomics Society (ELF) was founded. Currently, more than 50 ergonomics societies from various regions of the world are an integral part of the IEA [7].

Nowadays, industrial companies have taken into account the importance of ergonomics in their work environments, because it influences the normal development of their activities, and this occurs as a result of a bad design of the tools and facilities where production work is performed. The application of ergonomics in the industry raises the performance and improves the quality of the product where the human element is the key factor to increase efficiency and effectiveness in all activities. [8].

Ergonomics simultaneously contributes to the economic health of organizations by improving the well-being, capability and sustainability of workers, maximizing performance and reducing direct and indirect costs arising from productivity losses, quality deficiencies and staff turnover [5].

Another relevant element of ergonomics is its inclusive nature, as it takes into account human variability in the design of systems. For example, some contemporary ergonomics topics include design for people with both physical and mental disabilities, as well as for the elderly population. In this way, ergonomics contributes to improving the health, safety and well-being of people, impacting public health. [7].

Therefore, even though ergonomics has had an apparently recent origin, it is in constant development and evolution to constantly offer more information on strategies and possible alternatives to facilitate and ensure the health and well-being of workers in the work environment, articulating these benefits with the projection of the achievement of organizational objectives, thus becoming a topic that is becoming increasingly relevant [4].

Consequently, the objective of this research is to conduct a literature review on current ergonomic trends in the international labor context.

2 Materials and method

In order to perform a bibliometric analysis of current trends in Ergonomics, the PRISMA method was used, following the steps outlined in the bibliographic study of [9] In order to obtain the most outstanding advances, it was decided to use information from high impact scientific journals. In order to determine the goals of this research, the following question was asked:

What are the current ergonomic trends applied in the international work context?

To proceed with the selection, abstracts and keywords associated with Ergonomics were reviewed. The results and conclusions of the articles were reviewed and those that were most related to the topic and met the inclusion criteria were selected. Information on authorship, year, abstract, results and conclusions was collected from the systematic reviews.

According to [10] the term Human Factor Engineering and therefore Human Engineering are equivalent to the term Ergonomics being the first two definitions more used in North America. Consequently, the search was performed using the descriptor *Ergonomics, Human factors* and *human engineering* to broaden the exploration system. To limit the search field, the following inclusion criteria were established:

- It was limited by year of publication in each of the journals chosen to search for updated information from January 2022 to April 2024.
- Quantitative, qualitative or mixed studies.
- English was introduced as the language of the studies.
- Open access research
- Research from high impact journals in the Q1 and Q2 quartiles during 2022 and 2023 belonging to the Scimago Journal & Country Rank platform.
- Publications that were related to the search term related to the question posed.

Therefore, as exclusion criteria, outdated articles were discarded, which were related to ergonomics, but did not contain the information and were not available for reading. The establishment of these criteria made it possible to purify the information. Fig. 1 shows the procedure for the search and selection of articles

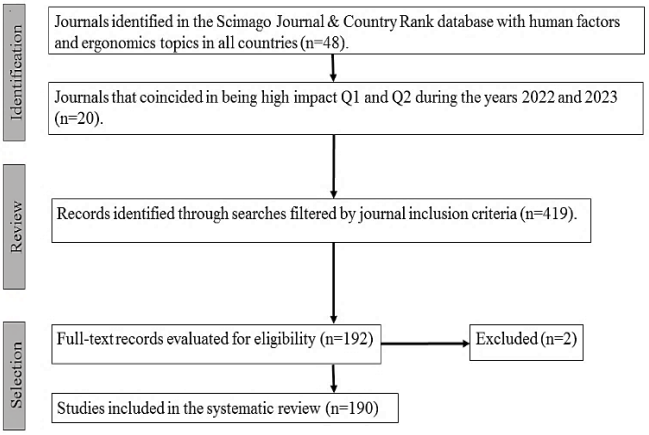

Figure 1. Procedure for the search and selection of articles.
Source: own elaboration

The articles were then classified according to the dimension of ergonomics classified by the IEA, according to the following criteria:

Physical Ergonomics: concerned with the anatomical, anthropometric, physiological and biomechanical characteristics of the worker, as they relate to physical activity. Its most relevant topics include work postures, overexertion, manual material handling, repetitive movements, work-related muscle-tendon injuries (TML), job design, occupational safety and health [11].

Cognitive Ergonomics: deals with the study of the worker's mental processes. Factors such as perception, attention, cognition, motor control, storage and memory retrieval, which are affected by mental workload, decision making, skill performance, worker interaction with the computer, stress and training. [12,2].

Organizational Ergonomics: is interested in the optimization of socio-technical systems, including their organizational structure, rules and processes. The topics covered include communication, management of collective resources, conception of work, conception of work schedules, teamwork, participatory conception, community ergonomics, cooperative work, new forms of work, organizational culture, virtual organizations, teleworking and quality management [13].

3 Results

Fig. 2 shows the quantities published per year in the period 2022-2024. The highest rate of publications in scientific journals related to ergonomic topics during the period of analysis is presented by the year 2023 (42.55%), followed by the year 2022 (30.09%) and in the months elapsed in the year 2024 (27.66%).

Table 1 identifies the journals with the number of publications per year. There are 14 journals with Human Factor and Ergonomics theme belonging to the Scimago Journal & Country Rank base that have published a total of 160 articles in the period 2022-2024. The journals with the highest number of publications on Ergonomics are IEE Transaction on Human Machine systems (16.49%), International Journal of Industrial Ergonomics (15.95%), International Journal of Human Computer Interaction (11.17%) and Theoretical Issues in Ergonomics Science (9,57%).

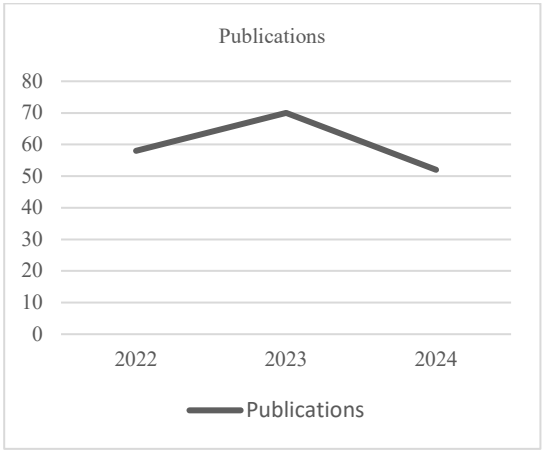

Figure 2. Accounting of publications on Ergonomics between 2022-2024.
Source: own elaboration (2024)

Table 1.
Number of publications in journals.

#	Journal	2022	2023	2024	%
1	IEE Transaction on Human Machine sistems	12	11	8	16.49
2	International Journal of Industrial Ergonomics	6	16	8	15.95
3	International Journal of Human Computer Interaction	2	13	6	11.17
4	Theoretical Issues in Ergonomics Science	8	4	6	9.57
5	Human Factors	0	6	11	9.04
6	Smart and Sustainable Built Environment	8	6	1	7.97
7	APPLIED ERGONOMIC	6	3	4	6.91
8	Ergonomics	5	6	0	5.85
9	Human Factors and Erganomics In Manufacturing	4	3	2	4,78
10	International Journal of Human Computer Studies	2	3	2	3,72
11	Facilities	2	3	1	3.19
12	Journal of Cognitive Engineering and Decision Making International	0	2	3	2.65
13	Technology in Society	1	3	0	2,12
14	New Technology, Work and Employment	0	1	0	0.53
15	Journal of Physiological Anthropology	1	0	0	0.53
16	JMIR Human Factors	1	0	0	0.53
	Total	58	80	52	100

Source: own elaboration

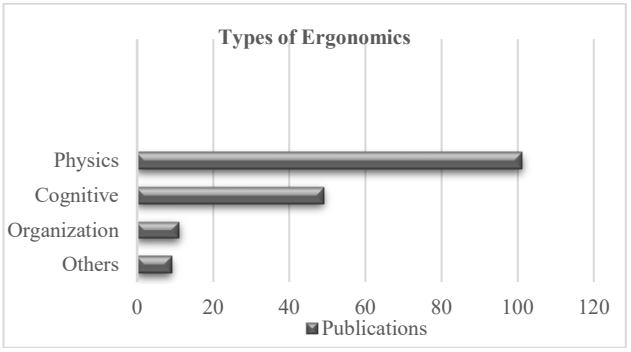

Figure 2. Types of Ergonomics.
Source: own elaboration.

Fig. 2 shows the Ergonomics dimensions used in the research works analyzed, where those studies that covered ergonomics trends in a general way are classified as others. In addition, there were researches projected to more than one dimension of Ergonomics, so they were counted equally for each criterion. Physical Ergonomics (51.53%) is the most studied among the 3 existing Ergonomics dimensions followed by Cognitive Ergonomics (32.65%).

All the data collected and evaluated show a strong tendency to research on Physical Ergonomics issues, being this the main source of future research as foreseen during all the analysis performed.

4 Discussion

The development of technologies, robotics and the world's thinking in terms of improving the working conditions of workers contribute to the evolution of Ergonomics. The following will show the current trends that are being generated in the different dimensions of Ergonomics:

Physical Ergonomics: Several works focused on the use of technologies for the physical improvement or evaluation of people such as the study by [14] on 3D mapping of the head, face and neck; or that of [15] with the creation of an evidence-based electronic training program (Sit-Stand e -Guide) and the use of assistive devices for older adults or sick people among others.

In addition, there were a considerable number of studies concerning anthropometry for the design of intelligent chairs and desks, handrails for fast and precise reactive grip when people lose their balance, as well as posture assessment in vehicles and airplane seats. Also, as the analysis of musculoskeletal disorders. Of note is the research by [16] where they developed a tool to estimate maximum acceptable manual arm forces for over-the-shoulder work with adjustments for supraspinatus tendon impingement and shoulder fatigue.

One of the areas most addressed was the health sector for research on the use of exoskeletons for stroke rehabilitation and in work areas for the reduction of fatigue and muscular activities in healthy people.

Cognitive Ergonomics: The research analyzed addressed on several occasions the use of eye tracking, eyelid marking or visualization of the maximum pupil diameter as techniques to identify mental workload supported in some cases by electroencephalography, as well as discovering usability problems and even harnessing the power of machine learning to recognize various types of emotions related to user interactions in smart applications.

A minority of papers focused on the study of smart glasses in the health area seen from the perspective it provides to patients and medical staff using them. Use of applications to promote mental health in workers and artificial intelligence to reduce the cognitive workloads of UAV operators.

One of the most visualized areas in this research has been the evaluation of the cognitive capacity of drivers in automated vehicles. Job stress due to cognitive load or simply the continued stay in an unhealthy environment was assessed in different jobs reaching conclusions such as the one offered by [17], who understand that all external environmental factors, except political factors, shape mental health management outcomes.

Organizational ergonomics: Research focused mainly on the collaboration of humans and robots to reduce the ergonomic burden on workers in the heavy automotive manufacturing industry and in the digital industry. Likewise, it happens with the study presented by [18] in which he comments on the advantages and disadvantages of incorporating supportive conversational agents (CA) in workplaces, as well as assistance for people with disabilities, which requires personalization and transparency, research commented by [19]

Research on how technology can help create a sustainable aging workforce was conducted, [20] note that digitization of workplaces, digital literacy, innovation, intergenerational collaboration and knowledge management form important elements of the international standard on age-inclusive workforce.

One of the researches in this area was that of [21] where they presented a computational model that combines all the key parameters that musicians evaluate to verify the quality of a musical instrument such as tuning, sound quality and ergonomics to predict the construction details of the instrument. In addition to the research of [22] where they analyze the hardware and software interaction interface of a smart air conditioner in order to improve the intelligence and humanization of the home environment.

Regarding the study and advancement of ergonomics the recent research by [23] comments that the impact of ergonomics and human factors (EHF) has been limited to date and that critical issues need to be resolved, such as increasing the number of appropriately qualified practitioners, resolving the gap between research and practice, and increasing awareness of EHF and its benefits. This article provides the perspectives of 18 ergonomics and human factors (EHF) professionals on the impact of EHF, current challenges and critical future directions, and changes that are needed to ensure that EHF remains relevant in the future. As such, it provides important guidance on future EHF research and practice.

[23] clarified that frequently discussed future directions include advanced emerging technologies such as artificial intelligence, developing new EHF methods, and improving the quality and scope of education and training. Most felt that there will be a need for EHF in 75 years; however, many noted that our methods will need to adapt to meet new needs.

There is a bibliographic study on Ergonomics by [24] that focused on the types of Ergonomics based on scientific publications located in the Web of Science during the years 2019 and 2022. With a sample of 69 articles it was evidenced that there is a higher concentration of publications in the journals Applied Ergonomics (29%) and Ergonomics (25%) and; where with 55% the most studied Ergonomics is physics.

The study by [24] although it does not have the same number of articles analyzed as the research presented, supports the results of the same where, combining both investigations, it can be said that during the last 5 years (2019 to mid-2024) physical ergonomics has positioned itself as the main interest of ergonomists and researchers who study safety and health at work. Therefore, it can be predicted that by the year 2025 there will also be a large number of studies on Physical Ergonomics, and from the results obtained in this research it could also be thought that studies on Cognitive Ergonomics will acquire the same fate.

5 Conclusions

From the research conducted, it can be concluded that the emerging trends in Ergonomics reveal the current interest in bringing automation, artificial intelligence and new technologies to all areas of human life. Through the bibliographic review of articles published from 2022 to 2024, it was evidenced the current interest in researching especially Physical Ergonomics, being the subject of 51.53% of the publications analyzed in this research with new visions on risk detection and protection measures involving such technological advances. In addition, there is a potential for growth in the number of researches on the area of Ergonomics, given that in 2024, 52 publications were analyzed, representing 89.66% of those reviewed in the whole year 2022.

Bibliography

[1] Chávez-Cujilán, Y.T., y Moran-Olvera, B.M., La ergonomía y los métodos de evaluación de carga postura. AlfaPublicaciones, 4(1.1), pp. 279–292, 2022. DOI: https://doi.org/10.33262/ap.v4i1.1.159

[2] Bornacelli-Orozco, D.J., Escobar-Velilla, R.J., y Velásquez-Zuluaga, M., La ergonomía y su aplicación médica a la seguridad y salud en el trabajo, [en línea]. 2021. Disponible en: https://repository.ces.edu.co/bitstream/handle/10946/5457/1140828536_2021.pdf?sequence=1&isAllowed=y

[3] Gómez-Salazar, L., Representaciones sociales de la ergonomía en personal directivo. Revista Venezolana de Gerencia, 27(98), pp. 435-451, 2022. DOI: https://doi.org/10.52080/rvgluz.27.98.4

[4] Rubio-Cano, L.P. y Florez-Alvarez, E.G., Generalidades de Ergonomía [Notas de clase]. Universidad Cooperativa de Colombia Campus Montería, [en línea]. 2023. Disponible en: https://repository.ucc.edu.co/bitstreams/60ed08fe-d581-434b-a883-ecb1da68cdf0/download

[5] Asociación Internacional de Ergonomía. Mission & Goals. [en línea]. [Recuperado: 4 de septiembre 2020]. Disponible en: https://iea.cc/about/introduction/

[6] Nouviale, L., y Giraudo, E.D.C., Perspectivas de desarrollo de la ergonomía en la Argentina: una mirada desde la Universidad Tecnológica Nacional. Ergonomía, Investigación y Desarrollo, 2(3), pp. 63-76, 2020.DOI: https://doi.org/10.29393/EID2-5PDLN20005

[7] Torres, Y., y Rodríguez, Y., Surgimiento y evolución de la ergonomía como disciplina: reflexiones sobre la escuela de los factores humanos y la escuela de la ergonomía de la actividad. Revista Facultad Nacional de Salud Pública 39(2), pp. 1-9, 2021. DOI: https://doi.org/10.17533/udea.rfnsp.e342868

[8] Bravo Honorio, D.T., Estudio del impacto negativo de la ergonomía aplicado en puestos de trabajo de plantas industriales. Un estudio de revisión sistemática. Tesis de Grado, Universidad Privada del Norte, Perú, [en línea]. 2022. Disponible en: https://repositorio.upn.edu.pe/bitstream/handle/11537/29324/Bravo%20Honorio%2c%20Daniel%20Tello.pdf?sequence=1&isAllowed=y

[9] Acosta-Prieto, J., Abrante-Leal, D., García-Dihigo, J., y Cuello-Cuello, Y., Análisis bibliométrico sobre la aplicación de indicadores fisiológicos para valorar trabajo mental. Revista Cubana de Salud y Trabajo [en línea], 25(2), 2024. Disponible en: https://revsaludtrabajo.sld.cu/index.php/revsyt/article/view/584/644

[10] Buttura-Chrusciak, C., Rodrigues-Poncini, C., Hudson-Moggio, I., Emy-Yasue, J. y Sedrez-Bitencourt, R., Ergonomía y humano factores: una descripción general de definiciones basado en literatura. Revista Ação Ergonômica, 14(1), 2020 DOI: https://doi.org/10.4322/rea.v14i1-12.es

[11] Litardo-Velásquez, C.A., Díaz-Caballero, J.R. y Perero-Espinoza, G.A., La ergonomía en la prevención de problemas de salud en los trabajadores y su impacto social. Revista Cubana de Ingeniería [en línea]. 10(2), pp. 3-15, 2019. Disponible en: https://rci.cujae.edu.cu/index.php/rci/article/view/720/0

[12] Antón-Cedeño, A.M., Ergonomía cognitiva en profesores universitarios con sobrecarga laboral. Tesis de Maestría, Dirección de Posgrado, Universidad de San Gregorio de Portoviejo, Ecuador, [en línea]. 2021. Disponible en: https://repositorio.sangregorio.edu.ec/handle/123456789/2053

[13] Carrasquero, E. y Seijo, C., La ergonomía organizacional y la responsabilidad social inclusiva y preactiva: un compromiso dentro de los objetivos de la organización. Clío América 3(6), pp. 183–192, 2009.

[14] Smulders, M., van Dijk, L.N.M., Song, Y., Vink, P., and Huysmans, T., Dense 3D pressure discomfort threshold (PDT) map of the human head, face and neck: a new method for mapping human sensitivity. Applied Ergonomics [Online], 107, art. 103919, 2023. Available at: https://www.sciencedirect.com/science/article/pii/S0003687022002423

[15] Zerguine, H., Genevieve, N.H., Goode, A.D., Abbott, A., and Johnston, V., Co-design and development of the sit-stand e-guide: an e-training program for the optimal use of sit-stand workstations. Applied Ergonomics [online], 116, art. 104207, 2024. Available at: https://www.sciencedirect.com/science/article/pii/S0003687023002454

[16] Rempel, D. y Potvin, J., Una herramienta de diseño para estimar las fuerzas manuales máximas aceptables en los brazos para trabajos por encima del hombro. Ergonomía, 65(10), pp. 1338–1351, 2022. DOI: https://doi.org/10.1080/00140139.2022.2030806

[17] Tijani, B., Jin, X., and Osei-Kyei, R., PESTEL analysis of mental health management practitioners (PMPs) in architecture, engineering and construction (AEC) project organization, Smart and Sustainable Built Environment [Online], 12(5), pp. 1002-1030, 2022. DOI: https://doi.org/10.1108/SASBE-04-2022-0074

[18] Hofeditz, L., Mirbabaie, M., and Ortmann, M., Ethical challenges for human-agent interaction in virtual collaboration at work. International Journal of Human-Computer Interaction, pp. 1–17, 2023. DOI: https://doi.org/10.1080/10447318.2023.2279400

[19] Berka, J., Balata, J., Jonker, C.M., Mikovec, Z., van Riemsdijk, M.B. y Tielman, M.L., Desalineación en la obtención de modelos semánticos de usuario a través de agentes conversacionales: un estudio de caso sobre asistencia a la navegación para personas con discapacidad visual. International Journal of Human–Computer Interaction, 38(18–20), pp. 1909–1925, 2022. DOI: https://doi.org/10.1080/10447318.2022.2059925

[20] Wissemann, A., Winona, P.S., Gebhardt, H., and Serafin, P., Strategic guidance and technological solutions for human resources management to sustain an aging workforce: review of International Standards Research, and use cases. JMIR Human Factors [Online], 9(3), art. 27250, 2022. DOI: https://humanfactors.jmir.org/2022/3/e27250

[21] Polychronopoulos, S., Bakogiannis, K., Marini, D., and Kouroupetroglou, G.T., Optimization method on the tuning, sound quality, and ergonomics of the ancient guitar using a DSP-FEM Simulation. IEEE Access 10, pp. 133574-133583, 2022. DOI: https://doi.org/10.1109/ACCESS.2022.3231616

[22] Zhou, Y., and Hu, X., Internet of things intelligent interaction technology using deep learning in public interaction desing. IEEE Access 10, pp. 3182-3191, 2022. DOI: https://doi.org/10.1109/ACCESS.2021.3135660

[23] Salmon, P.M., Burns, C., Broadbent, S., Chari, S., Clay-Williams, R., Hancock, P.A., and Young, M.S., The chartered institute of ergonomics and human factors at 75: perspectives on contemporary challenges and future directions for ergonomics and human factors. Ergonomics pp 1–16, 2024. DOI: https://doi.org/10.1080/00140139.2024.2378355

[24] Kwan-Chung, C.K., Moreno-Mareco, J. A., Díaz-Vega, M.R., Alegre-Brítez, M.Á., y González-Caballero, J.A., Revisión bibliográfica de los tipos de Ergonomía estudiadas en las publicaciones científicas localizadas en la Web of Science, 2019-2022. Ciencia Latina Revista Científica Multidisciplinar 7(2), pp. 3088-3111, 2023. DOI: https://doi.org/10.37811/cl rcm.v7i2.5556

J. Padrón-Sardiña is a student of Industrial Engineering at the University of Matanzas, Cuba. She is a member of the scientific group Ergoseg of the University of Matanzas, which develops research on ergonomics and its different versions.
ORCID: 0000-0002-8418-9028

I. Pancorbo-Camacho, is a student of Industrial Engineering at the University of Matanzas, Cuba. She is a member of the scientific group Ergoseg of the University of Matanzas, which develops research on ergonomics and its different versions.
ORCID: 0009-0003-1029-3564

J.L. Acosta-Prieto, is PhD. in Industrial Engineer from the University of Matanzas, Cuba, graduated with a degree and scientific merit award. MSc. in Ergonomics and Occupational Health and Safety and MSc. in Business Administration, Service Management module, PhD in Technical Sciences of Industrial Engineering in the research line of Cognitive Ergonomics. In 2021 he obtained the CITMA National Award as a student researcher, in 2021 the Seal of Future Shapers. In 2020 he was Vice-Dean of the Faculty of Business Sciences of the University of Matanzas, from 2021-2023 Director of the Municipal University Center of Cárdenas and from 2023-present Director of Research and Postgraduate Studies of the University of Matanzas, Cuba.
ORCID: 0000-0003-1390-2380

Y. Cuello-Cuello, is Bsc. Eng. in Industrial Engineer graduated from the University of Matanzas, Cuba since 2021. He belongs to the Cognitive Ergonomics Scientific Group, where he has developed theoretical and practical research on mental work. She is studying for a master's degree in Ergonomics and Occupational Safety and Health. She is currently a professor at the University of Matanzas, Cuba.
ORCID: 0000-0003-4589-8670

DYNA
http://dyna.medellin.unal.edu.co/

UNIVERSIDAD NACIONAL DE COLOMBIA

Comparative analysis: PVC and concrete panels and traditional masonry

Iara Lima da Silva & Renata de Oliveira Gomes

Luziânia University, UNIDESC – University Center for Development of the Central West, Goiás, Brasil. Iara.silva@sounidesc.com.br, Renata.gomes@unidesc.edu.br

Received: June 24th, 2024. Received in revised form: October 7th, 2024. Accepted: November 6th, 2024.

Abstract
This article presents a comparative analysis between the construction system using PVC panels and concrete and conventional masonry, exploring their advantages and disadvantages in the context of civil construction. The main objective is to assess the feasibility of each method, considering factors such as sustainability, cost, efficiency, and environmental impact. The study was conducted based on a literature review of the mechanical properties of PVC, its resistance to degradation, and its practical applications in various areas of construction. Characteristics such as execution speed, durability, and environmental challenges were also compared. The results indicate that the PVC system offers significant advantages in terms of construction speed, resource savings, and durability. However, it presents challenges such as the emission of toxic gases in fire situations and limited suppliers, which can increase costs. Conventional masonry, although widely used and accessible, faces problems such as waste generation and quality control. It is concluded that both systems have their place in civil construction, and the choice between them should be based on a detailed analysis of the project's needs, considering environmental impacts and long-term costs.

Keywords: civil construction; PVC system; conventional masonry; sustainability.

Análisis comparativo: paneles de PVC y concreto y albañilería tradicional

Resumen
Este artículo presenta un análisis comparativo entre el sistema constructivo utilizando paneles de PVC y concreto y la mampostería convencional, explorando sus ventajas y desventajas en el contexto de la construcción civil. El objetivo principal es evaluar la viabilidad de cada método, considerando factores como la sostenibilidad, el costo, la eficiencia y el impacto ambiental. El estudio se llevó a cabo en base a una revisión de la literatura sobre las propiedades mecánicas del PVC, su resistencia a la degradación y sus aplicaciones prácticas en diversas áreas de la construcción. También se compararon características como la velocidad de ejecución, la durabilidad y los desafíos ambientales. Los resultados indican que el sistema de PVC ofrece ventajas significativas en términos de rapidez de construcción, ahorro de recursos y durabilidad. Sin embargo, presenta desafíos como la emisión de gases tóxicos en situaciones de incendio y la limitación de proveedores, lo que puede aumentar los costos. Por otro lado, la mampostería convencional, aunque ampliamente utilizada y accesible, enfrenta problemas como la generación de residuos y el control de calidad. Se concluye que ambos sistemas tienen su lugar en la construcción civil, y la elección entre ellos debe hacerse en base a un análisis detallado de las necesidades del proyecto, considerando los impactos ambientales y los costos a largo plazo.

Palabras clave: construcción civil; sistema de PVC; albañilería convencional; sostenibilidad.

1 Introduction

The growing demand for adequate infrastructure in Brazil has driven the search for innovative solutions that overcome the challenges of traditional construction methods, such as high cost, long execution time, the need for specialized labor, and significant environmental impact [12]. In this context, the use of PVC and concrete panels emerges as a promising alternative.

The construction system using PVC and concrete panels proves to be more sustainable than traditional methods. The panels are produced from recycled materials, reducing water and energy consumption during construction [27].

How to cite: da Silva, I.L., and Gomes, R.deO., Comparative analysis: PVC and concrete panels and traditional masonry. DYNA, 91(234), pp. 76-83, October - December, 2024.

Additionally, they are highly durable and resistant to weather, fire, insects, and fungi, ensuring a long lifespan for the construction [1].

This construction system can also significantly reduce the total cost of the project compared to traditional methods due to the speed of assembly, the reduced need for specialized labor, and the optimization of material use [19]. The assembly of the prefabricated panels is quick and easy on the construction site, considerably reducing execution time [30].

Regarding electrical and plumbing installations, they follow conventional standards and are directed vertically. The pipes are inserted from the top of the wall or from the concrete base, running an internal path within the panels to accommodate different circuits. The construction process is organized into five stages: infrastructure, superstructure, roofing, finishes, and installations [32].

These objectives aim to provide a comprehensive overview of the advantages and disadvantages of construction systems using PVC and concrete panels compared to traditional masonry methods, contributing to informed decisions regarding the adoption of more efficient and sustainable construction technologies.

2 Construction system with PVC and concrete panels in civil construction

The concept of a construction system can be understood as a procedure that encompasses various levels of industrialization and organization, integrating a set of interrelated components into the construction process [28]. In the context of innovative systems, it is essential that they are based on technical qualifications related to the materials and components used, in order to meet the needs of users and the purpose of the space. Additionally, it is crucial to find efficient cost/benefit solutions, especially regarding social aspects. Fig. 1 Illustrates the cross section of the panels and the reinforcement, highlighting the integration of materials and structural elements in the construction system.

For the progress of a society, as highlighted by [25], it is essential not only to encourage the research and development of new technologies but also to establish access channels for the effective implementation of these innovations in production environments. Therefore, the next stage of this research is dedicated to the study of the concrete-PVC system, exploring theoretical references and the main contexts of application of this technology. The system, composed of structural concrete walls with integrated PVC profiles, demonstrates high productive efficiency, even when operated by a small team. These profiles are fitted together to function as concrete forms, as well as serving as cladding and final finish. This technology is primarily applied in singlestory houses and two-story houses, resulting in walls of varying thicknesses. The thickness of the PVC profile used varies according to structural loads, installations, and the manufacturer's production specifications [7]. The different modular profiles are connected through a double male and female interlock.

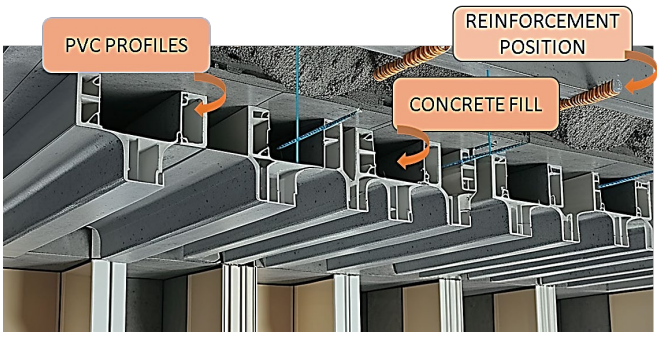

Figure 1. Illustration of the cross section of the panels and the reinforcement. Source: Author's own work.

A pioneering example in the country was the construction of 151 houses in the municipality of São Luiz do

Paraitinga/SP in 2010, aimed at sheltering families displaced by a flood. The housing complex in São Paulo was completed

after months of work. According to the Brazilian Portland Cement Association [1], which provided technical guidance for the construction, the advantages include the speed of execution, the absence of waste, and the high durability of the materials used.

Fig. 2 Illustrates a city with the basic module system of 64 mm and 100 mm. The system developed by Royal Group Technologies Limited operates through double interlocking modular profiles that are assembled vertically during construction. For the implementation of the walls, panels of different thicknesses are used: 22 mm, 64 mm, 100 mm, and 150 mm, with the latter recommended for extreme climates. The use of panels with thicknesses of 100 mm and 150 mm allows this method to be applied in the construction of buildings with different standards and purposes, such as industrial, institutional, commercial, and residential buildings of up to five stories (ground floor plus four floors) [15]. The use of structural concrete is essential, although conventional structures such as beams and columns are not necessary [26].

Initially, the site is cleared, followed by the excavation of trenches according to the alignment of the future walls. After excavation, boards are installed for framing and leveling the forms intended for concreting. It is recommended to apply a 100-micrometer polyethylene film over the entire surface of

Figure 2. Illustrates a city with the basic module system of 64 mm and 100 mm. Source: Author's own work.

the slab to ensure its waterproofing. Next, a 2.5 cm layer of gravel is added to the top of the slab, above the trenches, to serve as support for the steel bars [26].

The concrete-PVC system allows for the use of more compact foundations, such as continuous footings or strip footings. Particularly recommended is the implementation of a raft foundation, due to the speed of execution and the immediate availability of the subfloor upon completion of the foundation, resulting in a significant reduction in construction time [13].

All water and sewage points and pipes for the construction should be planned. With all previous steps completed, the concreting of the slab begins. The concrete used must have a minimum strength of 15 MPa at 28 days. During execution, it is crucial to observe to avoid unevenness in the final surface, as any irregularity in the height of the slab is reflected in the top of the PVC profiles, which are already pre-cut at the factory [13].

In cases of using other forms of foundation, such as continuous footings or strip footings, it is necessary to fill the subfloor to align it with the perimeter beams. To optimize water drainage, it is recommended to apply an internal subfloor of at least 20 mm, along with creating a sloped gradient between the external sidewalk and the structure [26].

The use of this technology does not require heavy equipment or special tools. The walls are anchored to the foundation through vertically positioned steel bars or metal channels fixed to the foundation, depending on the manufacturer's specifications. The PVC profiles are individually or collectively attached, sliding from top to bottom into the channels. In accordance with the design, vertical reinforcements are essential to strengthen the joints of the vertical walls and on the sides of doors and windows. Electrical and plumbing installations should be positioned internally to the enclosure, using specific pipelines (Fig. 3). It is crucial to position templates in the openings precisely to avoid concrete losses. From the concreting, a monolithic wall is formed, making the use of conventional fluid or selfcompacting concrete recommended for complete filling of the forms without the need for vibration [7].

Polyvinyl chloride, a synthetic polymer derived from sodium chloride and petroleum derivatives, is composed of long-chain molecules containing repeated monomers that are bonded through strong bonds. These molecules form a threedimensional network held together by considerably weaker secondary bonds [10].

In terms of composition, PVC is made up of approximately 57% chlorine and 43% ethylene, a petroleum derivative [18]. The manufacturing process of PVC involves obtaining chlorine through the electrolysis of sodium chloride, which reacts with ethylene, both in the gas phase, forming a gas. This gas, when subjected to heat, transforms into the molecule vinyl chloride monomer. Subsequent polymerization results in polyvinyl chloride, presenting itself as a very fine white powder and inert.

The polymerization of PVC is classified as addition polymerization since there is no loss of parts of the molecule. Consequently, this material is designated as thermoplastic, allowing it to be heated, cooled, molded, and reheated without losing its initial physical properties. This characteristic facilitates its reshaping through combinations of pressure and temperature, contributing to ease of recycling [10]. The general physical and chemical characteristics of PVC can be found in Table 1.

Table 1.
Main Properties of PVC.

Main properties of rigid PVC	
Average molecular weight: 20,000 to 150,000 g/mol	Melting temperature: 273°C
Specific mass: 1.40 g/cm³	Glass transition temperature: 87°C
Tensile strength: 31-60 MPa	Specific heat: 0.8 - 0.9 J/ºC

Source: Source: Author's own work.

[2] describes PVC as a material for civil construction that stands out for its versatility and durability, mentioning that, in certain cases, PVC components used in civil construction can have a lifespan of up to 50 years.

PVC (polyvinyl chloride) is one of the most widely used thermoplastics globally, as highlighted [11]. Its global demand in 2005 exceeded 35 million tons, highlighting its importance in the industry. In Brazil, PVC consumption represented about 2% of the total global demand that year, a relatively modest share compared to more industrialized countries such as China, which held a 20% share, and Japan, with 5% of global consumption.

These data underscore the significant presence and applicability of PVC in different sectors, including civil construction, packaging, healthcare, among others. In the context of civil construction, PVC is valued for its versatile properties such as durability, strength, ease of handling, and low cost, making it a common choice for a variety of applications, including innovative construction systems as mentioned in the research.

Royal Building Systems indicates that for single-story residences, any type of concrete can be used in this system. However, to ensure greater economy and performance in construction, the use of lightweight concrete is recommended. For multi-story residences, the guidance is to use structural concrete with a strength between 8 to 15 MPa and with a minimum Slump of 18 cm [26].

PVC also demonstrates remarkable tensile strength, evaluated at around 42 MPa [2], a significantly higher value compared to reinforced concrete, which has approximately 2 to 3 MPa [21].

The profiles constitute an essential part of a comprehensive construction system, with each piece meticulously identified by its height and type. Each of these pieces is strategically positioned within the previously planned layout. To determine the position of each panel, a set of plans is provided for each step of the work. Among these plans, one is dedicated to the precise identification and location of each profile. Additionally, in supplying the PVC kit for the project, pre-assembled lintels and sills for windows and doors are included, which are also meticulously identified and characterized in the engineering drawings [26].

To ensure efficient assembly, all panels are properly identified with labels or markings painted on the inner and upper part of each one. During the assembly process, the correct position of each panel is with the label or marking

facing upwards. To reduce time on-site and improve the efficiency of the workers, it is advisable to distribute the panels according to their location, meaning that all panels related to a wall should be placed near the corresponding assembly area [26].

The construction system with PVC and concrete panels represents an innovative approach in civil construction, offering a series of advantages over traditional methods. However, it also faces significant challenges that need to be addressed for its broader and more effective adoption. In this topic, both the advantages and challenges associated with this construction system will be explored.

The method involves the use of lightweight PVC panels manufactured in industries, which are easily manually fitted. The height of the profiles is determined during the project, and these panels can have various thicknesses. The modules are internally filled with concrete and structural Steel [6]. This construction system is characterized by rapid execution and offers notable advantages, especially due to PVC being used as both internal and external cladding. Watertightness, weather resistance, and long durability stand out as some of the advantages of this construction method [17].

Sustainability is one of the most striking advantages of the PVC and concrete construction system. The durability of PVC panels significantly contributes to reducing the environmental impact of construction by extending the building's lifespan, thus reducing the need for frequent material replacement. This not only minimizes resource waste but also decreases the amount of waste generated during the building's lifecycle [23].

Furthermore, the reduction of waste production during construction is an additional benefit of this construction system. The prefabrication of PVC panels allows for a cleaner and more organized construction process, maintaining a tidier and safer working environment for workers. This reduction in waste generation not only contributes to environmental preservation but also simplifies other stages of construction, such as site cleanup and waste management [17].

Another relevant point is the reduction in the use of natural resources, such as water, during construction. The use of prefabricated PVC and concrete panels can significantly decrease water consumption compared to conventional construction methods since it reduces the need for mortar and concrete preparation on-site. This saving of water resources is crucial in regions where water availability is limited or where water sustainability issues are a growing concern [14,12].

Therefore, the sustainability offered by the PVC and concrete construction system not only benefits the environment but also provides operational and economic advantages, promoting more responsible and efficient construction practices.

Another positive aspect of the PVC and concrete system is the speed of construction since the prefabrication of panels allows for quick and efficient assembly on-site, resulting in a significant reduction in construction time compared to traditional methods. This efficiency in panel assembly on-site results in a significant reduction in construction time compared to traditional methods. In many cases, building construction using this system can be completed in a substantially shorter period, which not only speeds up project delivery but also allows owners to start using the space more quickly, generating additional economic benefits [14]. Fig. 3. PVC and concrete system at the Municipal School Mônica de Fátima Meireles Pessoa in Valparaíso de Goiás. The image was taken on-site, showcasing the implementation of this construction method.

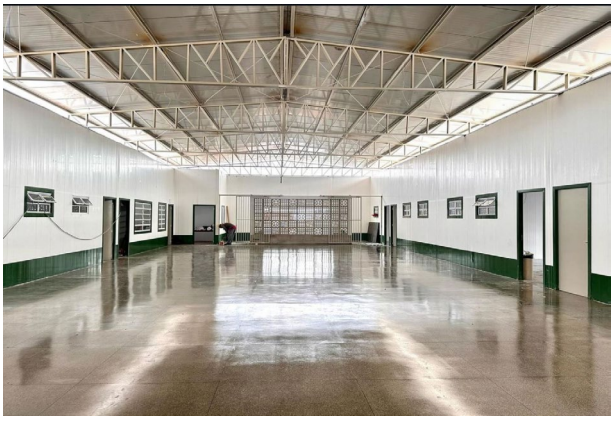

Figure 3. PVC and concrete system at the Municipal School Mônica de Fátima Meireles Pessoa in Valparaíso de Goiás.
Source: Author's own work.

Moreover, the speed of construction also has a positive impact on overall project costs, as the reduction in construction time is directly related to a decrease in labor and financing costs. This can make the PVC and concrete construction system a more attractive option for investors and developers looking to maximize return on investment and minimize risks associated with project completion delays [14].

Thus, the construction speed offered by this system not only represents an advantage in terms of schedule and operational efficiency but also can have significant positive impacts in terms of cost and project financial viability. This characteristic makes the PVC and concrete construction system an attractive choice for a wide range of applications in civil construction.

The use of PVC in construction offers several advantages, such as tensile strength, flexibility, and lightness. However, it is essential to consider the environmental and public health impacts related to the material's lifecycle, especially during its disposal or when exposed to high temperatures. When PVC is burned, it releases toxic substances like dioxins, which are highly harmful to human health and the environment. These dioxins, along with other released chemicals, are persistent pollutants, bioaccumulative, and have potentially carcinogenic effects. Moreover, exposure to these compounds can cause disruptions to the endocrine and immune systems, severely impacting public health (Rodrigues, 2010; Nakamura, 2024).

The incineration of PVC in landfills or accidental combustion during building fires also poses significant risks to air quality, contributing to atmospheric pollution with toxic substances. Therefore, proper waste management of PVC is crucial, requiring stricter recycling and disposal

policies to minimize harmful impacts on the environment and health (Acetoze, 1996; Petrucci, 1983).

The development of alternatives to PVC in construction, such as the use of less toxic materials or technological solutions that reduce the release of hazardous substances, could be an important pathway. Additionally, implementing more effective recycling practices is fundamental to reducing the risks associated with improper disposal (Silva, 2003; Júnior et al., 2006).

However, the PVC and concrete system presents challenges and some disadvantages compared to the traditional system. [17] explains that despite its ease of use, in the Brazilian context, the PVC and concrete system faces a significant limitation due to the scarcity of suppliers. This scarcity results in a limited supply of materials and services related to the PVC and concrete construction system, which, in turn, increases the product's value in the market. The price can be up to 20% higher than that of conventional masonry.

This lack of competition among suppliers can be attributed to various factors, such as the complexity of PVC and concrete panel production, the lack of government incentives for the development and dissemination of this construction system, and the historical preference for conventional construction methods. As a result, although the system offers significant benefits such as durability, safety, and construction speed, its high cost may represent an obstacle to its wider adoption in the Brazilian market.

3 Conventional construction system

All According to [16], conventional masonry is a construction system with ancestral origins, arising from the simple arrangement of materials to achieve a specific goal. This method found success over time, possibly due to a more stable economy and increasing competitiveness in the market. These factors drove the need to develop additional elements and strategies to address issues not previously considered by masonry.

Conventional construction systems, involving ceramic masonry walls or concrete blocks and concrete structural bases, have been widely used for thousands of years, recognized as safe and reliable construction methods. Conventional masonry is a construction system in which the structure's load is mainly supported by slabs, beams, columns, and foundation. In this method, walls do not have a structural function, being called non-load-bearing, and are used only to close openings and divide spaces [31].

For a long time, walls played a structural role in constructions, acting as an extension of the foundation and assuming the functions of columns and beams. This implied that walls could not be easily removed, significantly limiting renovation options. Additionally, a common challenge faced by old buildings was the additional weight that walls exerted on foundations [9].

However, with the advancement of modernism and progress in civil construction, structures began to be conceived independently of walls, which came to be known as curtain walls as well. This change represented an important innovation introduced by architects and engineers as early as the 19th century and continued to evolve throughout the 20th century [14].

According to [31], the essential element in conventional masonry construction is the brick, also known as ceramic block. This material is made from clay, which acquires a reddish hue after being subjected to high temperatures during the ceramic block manufacturing process.

According to [9] highlight that conventional masonry, also known as curtain walling, is widely used in the country due to its versatility, being able to be employed in a variety of projects, including large buildings. As it does not have a structural function, walls of conventional masonry are adaptable for the passage of hydraulic and electrical systems, providing architectural flexibility and ease of layout alteration, without the need for strict quality control in the choice of materials or in the execution of labor.

This type of masonry employs ceramic blocks with vertical holes, characterized by their low resistance compared to structural masonry blocks. As established by NBR 15270:2005, the compression strength of these blocks is 1.5 MPa [8].

Masonry, whether for curtain walls or structural purposes, is composed of natural stones, bricks, or concrete blocks, aiming to provide strength, durability, and impermeability. Bricks, especially fired clay bricks, are the most commonly used, being manufactured from clay mixed with sand. After the clay selection, the paste is molded and fired in kilns at temperatures between 900 and 1100 °C, resulting in bricks of various shades, depending on the quality of the clay used. The quality of the brick can be checked by the sound test, where a well-fired brick produces a specific sound and has a uniform color and defined edges [31].

In order to improve the speed and quality of masonry execution, the process has been divided into sub-stages, following the technical guidelines established by NBR 8545 (Execution of Masonry without structural function of bricks and ceramic blocks), in order to avoid future pathologies. These sub-stages include marking, laying, and shimming, and it is essential to respect the technical deadlines for the completion of each stage, in order to guarantee the integrity of the masonry [29].

Thus, the architectural flexibility provided by conventional masonry, combined with its adaptability for the passage of hydraulic and electrical systems, demonstrates its versatility and applicability in a variety of projects.

In conventional civil construction, the construction stages follow a sequential process involving several phases from the beginning to the completion of the work. Generally, this process is divided into distinct stages to facilitate planning, execution, and quality control.

The infrastructure constitutes the part of the construction located below ground level, where the foundations are located responsible for transmitting loads to the soil, requiring adequate strength to withstand external loads [33]. According to NBR 6122:2022 [4], foundations are categorized as deep, which transmit loads by lateral friction, and shallow, known as shallow foundations.

As explained [5], a foundation is the fundamental structure of a building, responsible for supporting the building's loads and distributing them to the soil. This base can be categorized as shallow or deep and includes elements

such as rafts, foundation beams (strip footings), footings, blocks, associated footings, among others.

The superstructure represents the portion of the building located above ground level. In this part, loads are transferred through beams and columns, ensuring the structure's stability. Beams support vertical loads and predominantly bend within the system. They also serve as support for slabs, which unload their loads onto the beams, and these, in turn, transmit the loads to the columns. The latter have the function of absorbing the vertical loads from the floors (Adapted [32]; [3] Fig. 4. Conventional Construction System. This figure illustrates the relationship between the foundation and the superstructure of a building.

For the execution of masonry, it is essential to have a complete architectural design, especially in the cross-sectional and floor plan drawings, where the dimensions to be followed during masonry construction are presented. According to [24], the procedure for executing internal and external enclosures involves several steps. Initially, it is necessary to mark the masonry modulation, starting from the corners and then marking the first row with bricks aligned in mortar. It is advisable to designate a qualified mason for this task, ensuring productivity and quality.

The construction of corners must be done with attention to leveling, perpendicularity, plumbness, and joint thickness, as they will serve as a reference for the entire work. It is important to stretch a line as a guide to ensure the correct verticality and horizontality of the rows. Each laid brick must be checked for plumbness. Vertical joints should be staggered between consecutive rows to ensure masonry stability.

As highlighted [20], during masonry execution, it is essential to observe various details: The mortar joints should have a thickness between 1.0 and 1.5 cm. Over door and window openings, lintels should be installed, which can be small wooden or concrete beams, designed to resist the masonry forces on these openings. It is important to note that wooden lintels should not be used in openings larger than 3 m or for metal frames. Concrete lintels can be precast or cast in place, should have a minimum height of 10 cm, and a width corresponding to the wall thickness.

Figure 4. Conventional Construction System.
Source: Author's own work.

In the case of constructions with an independent reinforced concrete structure, when raising the wall, it is necessary to leave a space of approximately 20 cm between the last row of bricks and the beam. This space must be filled with solid bricks laid inclined, in a procedure known as "wall tightening." This technique aims to compress the masonry raised against the concrete structure, avoiding the appearance of shrinkage cracks in the masonry. After approximately seven days of mortar curing, it is possible to perform the "masonry tightening." When one wall meets another, it is necessary to "tie" them together to avoid cracks at this junction [20].

The type of coating used varies according to the installation area. In areas subject to humidity, such as bathrooms, kitchens, service areas, and outdoor spaces, it is essential to carry out adequate waterproofing to prevent future problems [31].

According to [34], the ceiling consists of a protective or coating layer applied to the internal parts of the roofing structure, directly influencing the thermal and acoustic comfort, as well as the aesthetic aspect of the construction. The author emphasizes the importance of selecting suitable materials and elements for making the ceiling, as each requires specific installation methods. For example, in simpler residences, it is common to find ceilings made of wood or PVC.

The main purpose of the ceiling is to contribute to the aesthetic of the architectural environment while providing protection and offering acoustic and thermal insulation. A variety of materials can be used in ceiling construction, such as plaster, wood, metal, and PVC, among others. The choice of ceiling type should prioritize harmony with functionality and space comfort, also considering whether the lighting will be recessed and if the ceiling will contribute to improving thermal and acoustic comfort for occupants [5].

Before applying the floor covering, it is essential to ensure that the surface is level and properly waterproofed. The laying process follows a similar approach to that used for coating walls with ceramic tiles, using mortar and finishing with grout. There are several flooring options available, such as burnt cement, wood, stone, and the traditional ceramic tile floor, which is widely used [31].

Despite the importance of conventional construction systems, these traditional methods also have some disadvantages in terms of structural pathologies, economic issues, and environmental impacts [22]. In terms of quality, although conventional masonry is widely accepted by users and offers flexibility for changes and renovations in buildings, quality control can be compromised due to artisanal processes, often resulting in rework. Additionally, the quality of the raw materials used can vary, affecting the durability and strength of the structure [33].

Quality control is a crucial aspect in any construction project. In the case of conventional masonry, artisanal processes can pose a challenge to ensuring consistent quality standards, resulting in variations in execution and potential errors throughout construction. As a consequence, rework to correct these issues is common, increasing project costs and timelines. Additionally, the quality of the raw materials used in masonry can vary significantly, impacting the durability and strength of the structure [34].

Regarding performance, conventional masonry generally exhibits high resistance and the capacity for large spans,

which is a significant advantage. However, over time, pathologies such as cracks, fissures, and moisture may appear in conventional masonry, compromising its structural and aesthetic integrity. Additionally, the high self-weight of the structure can increase demands on foundations and affect overall stability [5].

In terms of maintenance, although costs are generally low, execution can be challenging due to significant material wastage and the need for specialized labor, which can increase costs [31,5].

In the environmental aspect, conventional masonry does not offer significant advantages, with high waste generation being a major disadvantage. This waste can pose a significant environmental problem, contributing to soil pollution and overloading landfills. Additionally, the production of construction and demolition waste has a negative impact on the use of natural resources and the carbon footprint associated with the construction industry [8].

In terms of cost, although conventional masonry generally stands out for the affordability of materials and labor, a large volume of labor is required, and material wastage can be a problem, affecting the total project cost.

4 Mechanical properties of PVC compared to other construction materials

For a comprehensive analysis between different construction systems, it is essential to compare the mechanical properties of the materials involved, such as PVC, concrete, and masonry. Below, a table compares tensile strength, modulus of elasticity, density, and the behavior of these materials under extreme temperatures, providing a clearer view of the advantages and limitations of each. Table 2. Comparison of Properties of PVC, Concrete, and Masonry (Ceramic).

Tensile Strength: PVC demonstrates a relatively high tensile strength compared to concrete and ceramic masonry, making it suitable for applications where lightness and durability are desired, but without the need to support large loads [2,21].

Modulus of Elasticity: In terms of stiffness, PVC has a lower modulus of elasticity than concrete, making it more flexible but less resistant to deformation under load. This is a limiting factor in constructions that require structural rigidity [11,31].

Table 2.
Comparison of Mechanical Properties between PVC, Concrete, and Masonry

Property	PVC	Concrete	Masonry (Ceramic)
Tensile Strength	31-60 MPa	2-5 MPa	1-1.5 MPa
Elastic Modulus	2.5-4 GPa	30-40 GPa	2-6 GPa
Density	1.40 g/cm³	2.4 g/cm³	1.8-2.0 g/cm³
Behavior at Extreme Temperatures	Resists up to 60-80°C, begins to melt above this	Resists up to 1000°C	Resists up to 900-1100°C

Source: Adapted from Acetoze (1996), Petrucci (1983), Júnior et al. (2006), Rodrigues (2010), Nakamura (2024), Silva (2003), Gorninski & Kazmierczak (2007).

Density: The density of PVC is significantly lower than that of concrete, making it lighter and consequently easier to transport and assemble in construction. However, this lightness results in lower structural strength, requiring the addition of reinforcements, such as reinforced concrete in composite systems [12,10].

Behavior in Extreme Temperatures: PVC has a clear disadvantage when exposed to high temperatures, beginning to deteriorate around 60-80ºC and emitting toxic fumes when burned. Concrete and ceramic masonry, on the other hand, are highly resistant to extreme temperatures, making them safer in the event of a fire [25,15].

5 Conclusion

This comparative analysis highlights the distinct advantages and challenges presented by the PVC and concrete system versus traditional masonry in civil construction. The PVC and concrete system offer notable benefits in terms of construction speed, sustainability, and resource efficiency. Its modular nature and ease of assembly provide significant operational advantages, reducing overall project time and costs. Additionally, the durability of PVC contributes to reducing environmental impacts over the building's lifecycle, enhancing its appeal for long-term use.

However, this system is not without its challenges. One of the major concerns is the environmental and health risks associated with the disposal or burning of PVC, which can release harmful dioxins and other toxic substances. Furthermore, the scarcity of suppliers and the potentially higher costs in some regions limit the system's widespread adoption, particularly in the Brazilian market.

On the other hand, traditional masonry, though widely accepted and cost-effective, poses its own challenges, such as waste generation, slower construction times, and quality control issues. Nonetheless, it remains a reliable and adaptable construction method, particularly suited for projects requiring flexibility and ease of renovation.

Ultimately, the decision between these two construction systems should be based on the specific needs of each project, taking into account factors like sustainability, cost, durability, and environmental impact. Both systems play a crucial role in modern civil construction and can be effectively employed depending on the priorities and requirements of the project.

References

[1] ABCP., Alvenaria estrutural: guia técnico. Associação Brasileira de Construção Predial, Brasil, 2013.

[2] Acetoze, A.L., Manual trikem de produtos de PVC utilizados na construção civil. São Paulo: Pini, 1996.

[3] Associação Brasileira de Cimento Porthland. ABPC auxilia regiões devastadas pelas enchentes. [online]. 2011. Available at: https://www.abcp.org.br/conteudo/tag/concreto-pvc

[4] NBR, ABNT. 6122: Projeto e execução de fundações. Rio de Janeiro, 2010, 91 P.

[5] Cassar, B.C., Análise comparativa de sistemas construtivos para empreendimentos habitacionais: alvenaria convencional x light steel frame. Universidade Federal do Rio de Janeiro, Rio de Janeiro, Brasil, 2018.

[6] Chanan, L.A., Análise comparativa de custos de uma residência unifamiliar executada com método construtivo convencional e concreto-PVC. 2017.
[7] Cichinelli, G., Sistema construtivo para casas e sobrados usa painéis de PVC preenchidos com concreto. Revista Téchne, São Paulo, 199, pp. 31- 34, 2013.
[8] Gonçalves, L.S., Cazella, P.H. da S., Agiado, A.C., and Pedreiro, M.R.deM., Análise comparativa entre alvenaria convencional e alvenaria estrutural. Revista Ibero-Americana de Humanidades, Ciências e Educação, 8(11), pp. 2611–2618, 2022. DOI: https://doi.org/10.51891/rease.v8i11.7851
[9] Gonzaga, A., EPS para construção civil: vantagens e desvantagens. Papo de Engenheiro. [online]. [Acesso em: 28.04.2024]. Disponível em: https://www.orcafascio.com/papodeengenheiro/eps-na-construcaocivil/
[10] Gorninski, J., and Kazmierczak, C., Microestrutura dos polímeros. In: ISAIA, G. C (Org), Materiais de construção civil e princípios de ciências e engenharia dos materiais. São Paulo, SP. IBRACON, v.1, 2007, pp.352-375.
[11] Júnior, A.R., Nunes, L.R., and Ormanji, W., Tecnologia do PVC. 2ª, ed. São Paulo: Braskem, 2006.
[12] Lira, G.K. de S., Estudo do emprego do sistema construtivo em concretoPVC em habitações de interesse social / Glacyelle Kawanna de Sousa Lira. Pombal, 2022.
[13] LTDA, T.E E. Target Normas: ABNT NBR 17077 NBR17077, Paredes estruturais. Disponível em: <https://www.normas.com.br/visualizar/abnt-nbrnm/13584/nbr17077-paredes-estruturais-constituidas-por-paineis-depvc-preenchidos-com-concreto-para-a-construcao-de-edificacoesprojeto-execucao-e-controle-requisitos-e-procedimentos>. Acesso em: 01 jun. 2024.
[14] Meireles, G.L., Comparação de desempenho entre distemas construtivos: alvenaria convencional, estrutura de metal com fechamento em PVC e paredes 100% PVC para canteiro de obras. Trabalho de Conclusão de Curso, Graduação em Engenharia Civil, Departamento de Engenharia Civil, Universidade Federal do Rio Grande do Norte, Natal, 2023.
[15] Nakamura, J., Construção plástica. Revista Techne, São Paulo, ed. 205, pp. 28-32.
[16] Nascimento, A.M., A segurança do trabalho nas edificações em alvenaria estrutural: um estudo comparativo. Dissertação de mestrado. Universidade Federal de Santa Maria, Rio Grande do Sul, Brasil, 2007.
[17] Nascimeto, M.L.S.do., Sistemas construtivos inovadores: evolução e principais materiais, Monografia graduação, Curso de Ciência e Tecnologia, Universidade Federal Rural do Semi-árido, Brasil, 2022.
[18] Nunes, L.R., et. al., Tecnologia do PVC, Braskem. Pro Editores Associados Ltda. 2a, São Paulo, Brasil, 2006.
[19] Nunes, R.C., and Nunes, A.C., A industrialização da construção civil: desafios e perspectivas para o Brasil. Revista Brasileira de Engenharia de Produção, 10(2), pp. 203-215, 2019.
[20] Penteado, P.T., and Marinho, R.C., Análise comparativa de custo e produtividade dos sistemas construtivos: alvenaria de solo-cimento, alvenaria com blocos cerâmicos e alvenaria estrutural com blocos de concreto na construção de uma residência popular. BSc. Thesis. Universidade Tecnológica Federal do Paraná, Brasil, 2011.
[21] Petrucci, E.G.R., Concreto de cimento Portland. 10ª ed. Editora Globo, Porto Alegre, Rio de Janeiro, Brasil, 1983.
[22] Queiroz, R.C., Introdução à engenharia civil: noções sobre a história, importância, principais áreas, atribuições e responsabilidades da profissão. [livro eletrônico]. –Blucher, São Paulo, Brasil, 2019.
[23] Rocha Jr., W., Análise comparativa entre os métodos construtivos de execução de vedações verticais com concreto moldado e executado in loco e convencional com blocos cerâmicos. Trabalho de Conclusão de Curso, Graduação em Engenharia Civil, Centro de Tecnologia, Universidade Federal do Rio Grande do Norte, Natal, Brasil, 2022, 53P.
[24] Rodolfo Jr., A., Nanocompósitos de PVC, argila organicamente modificada e óxidos metálicos: estudo do processo de preparação e propriedades de combustão e emissão de fumaça. Tese Doutorado em Engenharia, Universidade Estadual de Campinas, Campinas, SP, Brasil, 2010.
[25] Rodrigues, A.R., Nanocompósitos de PVC, argila organicamente modificada e óxidos metálicos: estudo do processo de preparação e propriedades de combustão e emissão de fumaça. Tese de Doutorado, UNICAMP, Brasil, 2010.
[26] Rogers, E.M., Diffusion of innovations. New York, 12, 1995, 576P.
[27] Royal do Brasil Technologies. Montagem passo a passo do Sistema RBS – 64. [online]. 2010. Disponível em: https://www.royalbrasil.com.br
[28] Royal Market Ltda., Análise do ciclo de vida do sistema construtivo em PVC e concreto. Relatório técnico, 2018.
[29] Sabbatini, F.H., Desenvolvimento de métodos, processos e sistemas construtivos – formulação e aplicação de uma metodologia. Tese Doutorado em Engenharia, Pós- Graduação em Engenharia Civil, Escola Politécnica da Universidade de São Paulo, São Paulo, Brasil, [online]. 1989, 321P. [Acesso em: fevereiro 2024]. Disponivel em: https://www.pec.poli.br/conteudo/bibliografia/_TeseSabbatini%202007- v5%20(1).pdf.
[30] Santos, E.B., Estudo comparative de viabilidade entre alvenaria de blocos cerâmicos e paredes de concreto moldadas no local com fôrmas metálicas em habitações populares. Campo Mourão, Brasil, 2013.
[31] Silva, M.A. da, Análise comparativa de sistemas construtivos para habitação popular: estudo de caso em Belo Horizonte. Dissertação de Mestrado, Universidade Federal de Minas Gerais, Belo Horizonte, MG, Brasil, 2003.
[32] Silveira, G.G., Estudo comparativo entre o sistema construtivo convencional e o sistema construtivo em EPS. RECIEC Revista Científica de Engenharia Civil. 5(2), 2022.
[33] Souza, M.I., and Murta, M.M., Patologias, recuperação e reforço estrutural em concreto armado, 2012.
[34] Villar, F.H.R., Alternativas de sistemas construtivos para condomínios residenciais horizontais: estudo de caso. Dissertação apresentada ao programa de pós-graduação em construção civil. Universidade Federal São Carlos, Brasil, 2005.
[35] Yazigi, W., A técnica de edificar, 10ª ed., Editora Pini, São Paulo, Brasil, 2009.

Silva, I.L., is BSc. Eng. in Civil Engineering, in 2024 from the Centro Universitário de Desenvolvimento do Centro-Oeste - UNIDESC. Additionally, I am the maintenance manager at the Department of Education, working in the field of Civil Engineering.
ORCID: 0009-0006-7286-3106

Gomes, R.O., is BSc. Eng. in Engineering, in 2018 from the Centro Universitário do Distrito Federal – UDF, and have specializations in various areas. I have a postgraduate degree in Traffic Management Planning from Faculdade Venda Nova do Imigrante - FAVENI (2020), in Sanitation and Environmental Health from Universidade Federal de Goiás - UFG (2020), and in Occupational Safety, also from Faculdade Venda Nova do Imigrante - FAVENI (2022). Currently, I am pursuing a master's degree in the PPG-Engineering Materials Integrity program at the University of Brasília - UNB, focusing on the physicochemical characterization of products obtained by extracting materials present in the formation of food packaging, being a scholarship holder by FAPDF (2022). Additionally, I am a professor at Centro Universitário de Desenvolvimento do Centro-Oeste - UNIDESC, working in the field of Civil Engineering.
ORCID: 0000-0002-6371-9587

DYNA
http://dyna.medellin.unal.edu.co/

UNIVERSIDAD NACIONAL DE COLOMBIA

Numerical simulation of CBR test and HS-Small parameter characterization for Bogotá soils

Camilo Ernesto Herrera-Cano [a], Juan Carlos Ruge-Cárdenas [b] & Juan Gabriel Bastidas-Martínez [a]

[a] *Universidad Piloto de Colombia, Ingeniería Civil, Bogotá, Colombia. camilo-herrrera2@unipiloto.edu.co, juan-bastidas@unipiloto.edu.co*
[b] *Universidad Militar Nueva Granada, Ingeniería Civil, Bogotá, Colombia. juan.ruge@unimilitar.edu.co*

Received: June 11th, 2024. Received in revised form: October 23rd, 2024. Accepted: November 13th, 2024

Abstract
This paper presents the determination of HS-Small constitutive model parameters for the Sabana Formation, the major deposit of Bogotá city. Mechanical parameters were obtained from index parameter of physical characterization, using correlations consulted as state-of-the-art. The characterization obtained has been validated with a numerical model of the CBR test, showing good agreement with typical values in the City of Bogotá. The methodology presented here would make possible the determination of the HS-Small parameters for the entire profile of the Sabana Formation. Once the parameter sets of the samples have been validated, a parametric analysis is performed, varying the friction angle and the shear module values. This parametric study shows that for the HS Small constitutive model, the stiffness modulus has a greater contribution in the CBR test than the friction angle, which would support the correlations between the resilient modulus and the CBR value; correlations widely used in pavement engineering. The methodology of characterization presented here would make possible the determination of the HS-Small parameters for the entire profile of the Sabana Formation. This allows for the numerical simulation of complex geotechnical works in the early stages of design when advanced mechanical laboratory tests are not available.

Keywords: FEM; HS-Small; CBR; diatomaceous soils; numerical model

Simulación numérica del ensayo CBR y determinación de los parámetros del modelo HS-Small para los suelos de Bogotá

Resumen
En este artículo se presenta la determinación de los parámetros del modelo constitutivo HS-Small para la Formación Sabana, el depósito más importante de la ciudad de Bogotá. Los parámetros mecánicos se obtuvieron a partir de propiedades índice de caracterización física, utilizando correlaciones consultadas del estado del arte para los suelos de Bogotá. La caracterización obtenida ha sido validada con un modelo numérico del ensayo monotónico de CBR, mostrando buena concordancia con valores típicos en la ciudad de Bogotá. La metodología aquí presentada haría posible la determinación de los parámetros HS-Small para todo el perfil de la Formación Sabana. Una vez validados los parámetros, se realizó un análisis paramétrico del modelo CBR variando los valores del ángulo de fricción y del módulo de corte. Este estudio paramétrico muestra que para el modelo constitutivo HS Small, el módulo de rigidez tiene una mayor contribución en el resultado del ensayo CBR que el ángulo de fricción, lo que sustentaría las correlaciones entre el módulo resiliente y el valor CBR; correlaciones ampliamente utilizadas en ingeniería de pavimentos. La metodología de caracterización aquí presentada haría posible la simulación numérica de obras geotécnicas complejas en las primeras etapas de diseño cuando no se disponga de ensayos mecánicas avanzados de laboratorio.

Palabras clave: FEM; HS-Small; CBR; suelos diatomáceos; modelo numérico

1 Introduction.

Numerical simulations are fundamental methods for understanding the phenomena within the geotechnical analysis of earthworks and other civil projects. Numerical simulation is not approximate by itself, rather, it is an implicit theoretical tool that aims to solve an engineering problem using an approximate method. The complexities of numerical

How to cite: Herrera-Cano, C.E., Ruge-Cárdenas, J.C., and Bastidas-Martínez, J.G., Numerical simulation of CBR test and HS-Small parameter characterization for Bogotá soils. DYNA, 91(234), pp. 84-92, October - December, 2024.

modeling make its implementation highly simplified, but the same is true for laboratory techniques and full-scale models in the field. Therefore, numerical methods and constitutive models have limited effectiveness and precision [1-2]. The same occurs with measurement devices used in laboratory and field tests. The constitutive equation is a key topic for the development of satisfactory numerical modeling. In geotechnical engineering, constitutive models might consider several features of the mechanical behavior of soils. Soils have properties such as stress and strain path dependence, the anisotropy of stiffness and strength, and the nonlinearity of the stress-strain relationship, which are properties commonly present in concrete and wood. However, soils also exhibit other very particular properties such as pore pressure generation, plastic deformation associated with friction by deviatoric and isotropic components, and the viscous effects associated with the speed of load application [3].

In Geotechnics, one of the advanced constitutive models available is the Hardening Soil Model or HSM. This constitutive model is offered in several commercial software packages such as PLAXIS, FACE2, Z-SOIL. The HSM incorporates the non-linearity of stiffness through a hyperbolic law and allows plastic deformation for both deviatoric and isotropic stresses [4]. This constitutive soil model was improved in 2007 when the Matsuoka-Nakai surface was introduced as a failure criterion due to a deviatoric stress component and the plastic flow rule was modified to incorporate stiffness criteria associated with small deformations, resulting in an enhanced model called the HS-Small model [5].

This paper presents the numerical modeling of a CBR test implemented with the HS-Small model included in the PLAXIS 2D software, with specific parameters for the diatomaceous soft soil of the city of Bogotá. The characterization of the model parameters was performed following the correlations presented by other authors for the soils of the city [6-7]. The results of the numerical modeling were contrasted with typical results of CBR tests, showing good agreement. To summarize, it can be inferred that the HS-Small parameters used in this study accurately represent the surface soils of Bogotá. Therefore, the variations of this set of parameters, which were adjusted following the criteria presented in this paper, could be used for modeling more complex geotechnical works such as the foundation of tall structures and deep excavations, as in the case of the city subway and other major projects. The work also delves into the discussion of the correlation between the resilient modulus and the CBR value. Through a parametric analysis where the friction angle is varied by 10 % and the stiffness modulus degradation curve by 10 %, it was found that the friction angle has an insignificant weight in the executed CBR models. In contrast, raising or lowering the modulus degradation curve by 10 % generates variations of up to 7.3 % of the original CBR value.

2 CBR test and its numerical simulation

In the 1930s, the former California Highway Agency had already included the test known today as the California Support and Expansion Ratio – CBR test as a routine test for the characterization of roadway and subgrade materials. The CBR test consisted of the penetration of a soil-material sample embedded in a metallic mold with a 3-square-inch piston at a speed of 0.05 inches per minute. Originally, the test was developed for the characterization of untreated crushed granular materials, which are indifferent to the typical tests at that rate such as the liquid limit, plastic limit, and shrinkage. The rapid reception of the test was due to the publication of easy-to-apply specifications, such as considering a granular base with a minimum support value of 80 % as acceptable. The early California Highway Agency would support its specifications in case studies where surface roughness and cracking of the treated surface course were clearly correlated with the CBR values of the subgrade [8].

Originally, the California method of design for pavements consists of designing charts to select the total thickness of the pavement for a tire load of 7,000 and 12,000 pounds from the CBR value of the subgrade. From the design of these charts, the US Corps of Engineers made theoretical extrapolations for typical aircraft loads for World War II runway construction. The improvement was favorable in civil infrastructure due to the increase in the number of vehicles in the following decades. In those years, the criterion that accepted the load ratio at 0.1 inches as the value of CBR was incorporated, unless the value at 0.2 was greater [9]. Currently, the CBR procedure is standardized by the AASHTO T-193 and ASTM D1883 standards. For Colombia, the INV E-148 standard applies. Philosophy and procedure remain the same: sample in 6-inch mold, 3-inch square flat nose piston area penetrating at 0.05 inches/min. During the test, the load must be collected at different penetrations up to 0.3 in. and the sample is tested at natural humidity (optimal in the case of compaction) and at the humidity acquired after a period of immersion during which the swelling or expansion of the material is also recorded [9].

Hight and Stevens [10] carried out a numerical study to investigate the impact of stiffness parameters on the response of clays during a simulated CBR test. The researchers employed a non-linear undrained elastic model (Poisson 0.499) varying the magnitude of the stiffness and resistance parameters. The sensitivity analysis showed that the CBR value was strongly correlated to the undrained shear resistance, and therefore, researchers concluded that the CBR test does not reflect the stiffness of saturated clays. The geometry of the used model was selected as large as possible to avoid boundary constraints as in bearing capacity problems. In fact, Finite Element models have been applied in several investigations focused on numerical simulations of small-scale bearing capacity tests, as these physical tests have strong similarities with CBR since they involve small-sized loads applied on the surface and they are strain-driven tests. The agreement between physical and numerical tests shows that the Finite Element Method is an ideal tool for simulating CBR tests as long as bearing capacity problems [11-12].

Improved Finite Element models with the detailed geometry of the CBR test, including the mold borders and the overload, have also been implemented for CBR studies as a mechanical test. Currently, several studies include both monotonic and cyclic loading. In the case of monotonic load, it is remarkable the work presented by Narzary & Ahamad [13]. The researchers ran 68 drained simulations of CBR tests incorporating the mold thickness and the annular surcharge disc, whose materials were considered linear elastic, while the soil inside the mold was a

linear elastoplastic model with Mohr-Coulomb criterion without hardening. The numerical modeling allowed researchers to find a multivariable nonlinear regression (involving friction angle, cohesion, Poisson's ratio, among other parameters) that predicts the linear elastic modulus of the sample. The equation was validated with laboratory tests showing good correspondence between the load value measured in the laboratory and that estimated in the numerical multivariable equation considering values of the resistance parameters previously estimated with direct shear tests [13].

One of the concerns in CBR testing is the draining condition during plunger penetration. In fact, the test presents heterogeneous boundary conditions (it is a boundary value problem), so the distribution of stresses and strains is not uniform within the sample. This situation implies a temporal and spatial variation of the excess pore pressure produced by the piston (and also an evolution of the degree of saturation). As is generally accepted, water flow is controlled by the permeability, which depends on several parameters such as the anisotropy of the fabric (and its evolution), the granulometry, and the void ratio. Therefore, the water permeability depends on the type of soil and the loading process itself.

Recently, Mendoza & Caicedo [14] conducted a sensitivity study of the CBR test considering drained or undrained conditions using a Finite Element numerical model. The researchers applied an elastoplastic constitutive model with a Drucker-Prager surface controlling plasticity by deviatoric loading and an elliptical cap that controls spherical compression deformation (known as the Drucker-Prager elastoplastic cap model). The results showed that for permeabilities lower than 10-6 m/s, the CBR value was influenced by the excess pore pressure located below the piston. The researchers also found that the CBR numerical model varies slightly with cohesion and friction, but it is very sensitive to pre-consolidation pressure [14].

3 Brief description of lacustrine soils of Bogotá

The largest geological deposit in the city is called the Sabana Formation. The geographical context for the city is presented in Fig. 1.

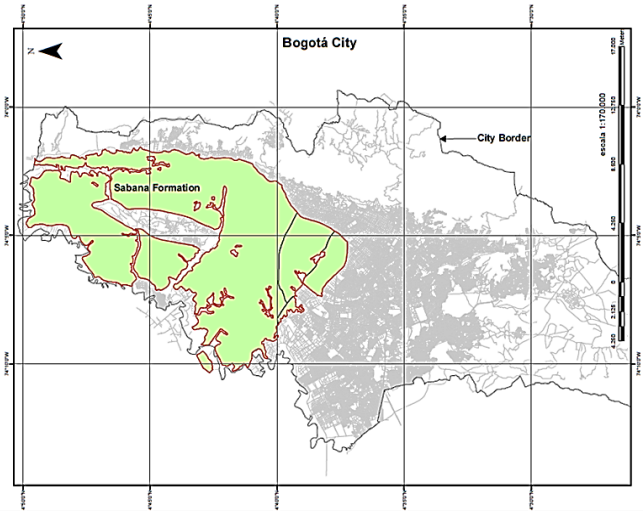

Figure 1. Geographical context of The Sabana Formation and city extension. Source: Authors.

Table 1.
Typical values of CBR undisturbed samples from Bogotá city.

CBR range (%)		Amount	Percentage	Accumulated
0.10	0.99	3	4 %	4 %
1.00	1.99	7	10 %	14 %
2.00	2.99	25	36 %	50 %
3.00	3.99	17	24 %	74 %
4.00	4.99	11	16 %	90 %
> 5.00		7	10 %	100 %

Source: Modified from Bojacá-Torres [15].

A large portion of the city is built over this Formation. According to the modern interpretation, and to generate a synthetic stratigraphic profile, this study summarizes the lithostratigraphy of the Sabana Formation as follows: from 0 to 5 meters deep, there is soil with less than 10 % organic matter, the plastic limit of 33 %, humidity of 80 % and the liquid limit of approximately 110 %. From 5 to 80 meters deep, there are unconsolidated lake sediments with a high proportion of organic matter and a very soft consistency, with a liquid limit of 140 %, water content of 70 to 140 %, and a plastic limit between 40 to 50 %. These two layers can be associated with shallow lacustrine deposits in which there was a strong presence of diatoms which are presented today as fossils that change the mechanical properties of the soil. Despite the high plasticity of these deposits, it can be noted that the Sabana Formation generally exhibits high plasticity but low clay content, and a high friction angle, both characteristics of diatomaceous soils. From 80 m, the lacustrine deposit continues with soils having less than 10 % of organic matter, a liquid limit of about 90 %, and a soft consistency ($0.5 < IC < 0.75$). In the western and northwestern parts of the city, in areas near the Bogotá river, the Sabana Formation can reach 500 m depth. In general, the water table can be found between 5 to 7 m deep. Regarding mineralogy, The Sabana Formation has kaolinite, vermiculite, illite, and fossilized diatoms. Recent publications have shown that the mechanical properties of the Sabana Formation are highly correlated with the physical properties using particular correlations.

For the city of Bogotá, several CBR-test reports can be found in public government databases. These databases have contributed to the execution of investigations such as Bojacá Torres, [15], where a series of 70 tests extracted from these databases is compiled and processed. In this study, only CBR tests that were executed on samples form The Sabana Formation were selected. Consequently, Table 1 shows some typical results from CBR tests performed on undisturbed samples extracted from different areas all over The Sabana Formation in the city of Bogotá.

4 HS-Small parameter determination

The HS-small model is developed within the theoretical framework of the theory of plasticity. The HS-small model consists of an extension of the HS model, by incorporating the degradation curve of the stiffness modulus. Both models consist of the extension of the non-linear Mohr-Coulomb failure criterion through a cap-model failure surface [3–5].

Mechanical behavior of soil is complex. Without

Table 2.
Typical (median) physical properties of superficial Sabana Formation soils.

Sample	LL (%)	OCR	LOI (%)	Ic
#1	120.0	5.0	10.0	0.70
#2	100.0	5.0	10.0	0.60
#3	80.0	6.0	10.0	0.70
#4	90.0	4.0	10.0	0.60
#5	90.0	5.0	10.0	0.50

Source: Authors.

considering solid-water phase interaction, features such as the nonlinearity caused by stress-dependent stiffness, modulus degradation by overstraining process, pre-consolidation stress memory, and non-associative plastic flow rule (related to anisotropy) are some of the most important characteristics to be considered in the numerical simulation of geotechnical problems. Another aspect is the load-failure criteria that are directional and time-dependent [16].

In this study, numerical simulations were performed with PLAXIS 2D software employing the HS-Small constitutive model. HS-Small is an elastoplastic model which incorporates nonlinearity as an elastic hyperbolic law, frictional and cap hardening to model plastic strains, and a law for modelling the decay of small-strain soil stiffness [5]. The constitutive model allows stress-dependent stiffness for loading and unloading in the elastic range until Matsuoka – Nakai yield criterion is reached. Efforts have recently been made to obtain the parameters of a similar constitutive model, such as the case of determining the parameters of the Hardening Soil model for tropical soils in the city of Brasilia [17].

HS-Small parameters might be calibrated from the Drained Triaxial Test and Consolidation test performed on undisturbed samples. However, mechanical properties can be estimated from index characteristics if well-established correlations are available for the particular site. Therefore, in this paper, HS-Small parameters are estimated from novel correlations for Bogotá soils [6-7].

For the numerical simulations, five synthetic samples were used. For this study, it is considered that the parameters presented in Table 2 are enough to determine most of the parameters of the HS-Small constitutive model. Considering that the water table would generally be below 7 m, all the synthetic samples are full unsaturated (dry).

Other considerations are the typical values of shear wave velocity V_s. For instance, the following profile by zones was considered: from 0 to 7 m deep, the average wave speed is V_s=100 m/s, from 7 to 15 m it drops to about 80 m/s, between 15 and 25 m it returns to 100 m/s, to rise to 125 m/s before 35 m and jump to 150 m/s from this depth [18].

The drained friction angle is obtained from eq. (1), proposed by B. Caicedo et al. [6]. The latter is calculated from eq. (2), a correlation proposed by Caicedo et al. [7].

$$\phi' = 18.5 + 0.112LL \quad (1)$$

$$S_u = P_{atm} \times PI \times w^{-1.8} \quad (2)$$

From the friction angle and the preselected over-consolidated ratio, the earth pressure coefficients at rest are evaluated using eq. (3) and eq. (4), as suggested by Kulhawy & Mayne, [19].

$$K_{0SC} = (0.95 - sin\,\phi)\sqrt{OCR} \quad (3)$$

$$K_{0NC} = 0.95 - sin\,\phi \quad (4)$$

Gravimetric parameters as soil unit weight and void ratio are obtained using specific gravity estimated from eq. (5), a correlation proposed by Caicedo et al. [7].

$$G_s = 2.68 - 0.019LOI \quad (5)$$

The wet unit weight, the void ratio, and the water content must be adjusted to ensure that the low strain shear modulus correspond to a shear wave velocity near 100 m/s, as noted above. With the above parameters and the average depth of the sample, the shear modulus at low deformations can be calculated by eq. (6). To evaluate horizontal effective stress, it is necessary to consider that for soils above the water table in Bogota, OCR is greater than 2 with occasional maximums close to 7.

$$G_0 = \frac{(10-e)^2}{(1+e)} \times 8.76P_{atm}\left(\frac{\sigma'_3}{P_{atm}}\right)^{0.49} \quad (6)$$

The shear modulus degradation model is obtained according to eq. (7).

$$\frac{G}{G_0} = \frac{1}{1+\alpha|\gamma|^{\lambda}} \quad (7)$$

Where λ=0.173·LL$^{0.34}$ and α=191.2$\lambda^{2.19}$, and γ is the shear strain, another mechanical parameter of HS-Small is the shear strain at 70 % of G_0 or $\gamma_{0.7}$. Making G/G_0 = 0.7, eq. (7) leads to eq. (8).

$$\gamma_{0.7} = \left[\frac{1}{\alpha}\left(\frac{1}{0.7}-1\right)\right]^{-\lambda} \quad (8)$$

The degradation of moduli for each sample is evaluated using eq. (6) and eq. (7), and those index parameters presented in Table 1. Then, the degradation of moduli is presented Fig. 2.

Shear moduli at large deformation G may be evaluated using eq. (6) considering a strain value of γ=0.04. Therefore, Young modulus at large strain levels E_{50} is estimated using eq. (9) considering a Poisson ratio ν=0.4. Although the Poisson's ratio can be variable during straining process and highly scattered, recent analyzes show that for saturated soils (e.g. without suction) the values of Poisson's ratio are the highest and relatively constant under lower scattering [20].

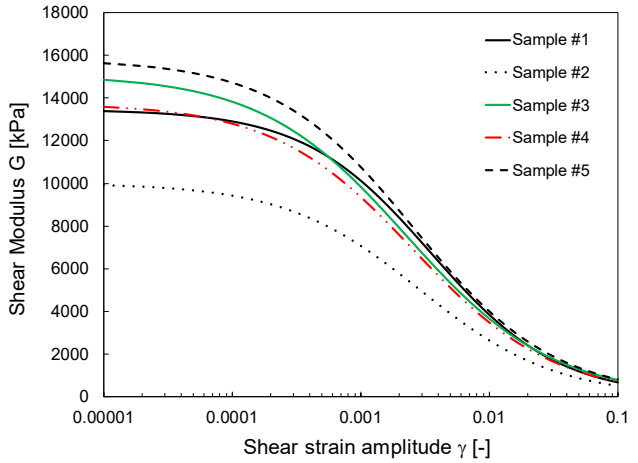

Figure 2. Shear degradation model for synthetic samples.
Source: Authors.

$$E_{50} = 2G(1 + 2v) \tag{9}$$

The initial elastic or unloading Young modulus Eur might be settled near to the model-default-value according to eq. (10).

$$E_{ur} = 2.1 \times E_{50} \tag{10}$$

The reference edometric modulus can be estimated using eq. (11), considering a vertical effective pressure of σ'_v=100 kPa.

$$E_{edo} = \frac{2.3(1+e)}{C_c} \times \sigma'_v \tag{11}$$

Compression index may be correlated using eq. (12), a correlation proposed by Caicedo et al. [7].

$$C_c = 0.01(LL - 0.58) \tag{12}$$

From the above the strength and deformation parameters for the HS-Small constitutive model from the five samples are presented in Table 3 and Table 4.

Table 3.
Strength parameters evaluated for samples.

No.	IP	w	γ	γ_{sat}	e	S_u	ϕ'	cut-off	K_0
	%	%	kN/m³	kN/m³	-	kPa	°	kPa	-
#1	82	93	13.41	14.03	2.6	33.19	31.9	12.44	0.94
#2	67	80	11.85	13.81	2.8	35.56	29.7	12.63	1.02
#3	51	60	13.8	15.05	1.9	45.43	27.5	16.61	1.2
#4	59	71	13.8	14.72	2.1	38.82	28.6	12.06	0.94
#5	59	75	14.59	14.88	2	35.17	28.6	12.15	1.05

Source: Authors.

Table 4.
Strain-Stress properties estimated for samples.

No.	λ	α	σ'_3	G_0	G	Cc	VsZ	G/G_0
	–	–	kPa	kPa	kPa	-	m/s	-
#1	1	145	44.2	13463	1417	1.19	100	10.50%
#2	1	126	30.1	10006	1021	0.99	91.9	10.20%
#3	1	107	24.8	15086	1500	0.79	105	9.90%
#4	1	117	26	13749	1384	0.89	99.8	10.10%
#5	1	117	30.8	15816	1592	0.89	104	10.10%

Source: Authors.

Table 5.
HS-Small strain-stress parameters for superficial Bogotá soils.

No.	G_0	v	E_{edo}	E_{ur}	E_{50}	$\gamma_{0.7}$
	(kPa)	-	(kPa)	(kPa)	(kPa)	–
#1	13463	0.4	1600	8333.1	3968	0.0014
#2	10005.6	0.4	1012	6003.5	2859	0.001
#3	15086	0.4	1934	8822.1	4201	0.0008
#4	13749.4	0.4	1705	8136.9	3875	0.0009
#5	15815.8	0.4	1965	9359.8	4457	0.0009

Source: Authors.

Thus, the required HS-Small moduli are presented in Table 5.

5 Numerical model and results

An axisymmetric model of the CBR molding was created in PLAXIS 2D using basic dimensions in millimeters. The thickness and material of both the mold and the upper angular ring were taken into account. The mold has an external diameter of 162.4 mm, with a thickness of 6 mm, while the charging ring has a thickness of 5 mm. The materials assigned for these elements were considered linear elastic and non-porous with Young's modulus of 110 and 200 GPa respectively, and a Poisson's ratio of 0.35 for both of them. An interface element of 0.75 value was considered for the soil-metal contact. In the numerical model, the soil sample has a diameter of 152.4 mm and a height of 172.8 mm. The modeling was performed in a drained regime with the soil inside the mold completely dry. The displacement-driven numerical test was performed until a displacement of 5.08 mm was reached uniformly at the piston area.

The triangular element of 15 nodes was used. The mesh was refined until a smoothed stress and strain distribution within the model was found. A total of 759 elements and 6433 nodes were adjusted using the automatic grid step. Fig. 3 presents the numerical model implemented in PLAXIS 2D.

Fig. 4 presents a heat map of the typical displacement distribution taken at the final stages, i.e. piston penetration over 5.08 mm. Both vertical and horizontal distribution show smooth zones thorough the sample. It is clear that beneath the piston, the vertical displacement is concentrated, which generates a vertical-displacement bulb of one piston

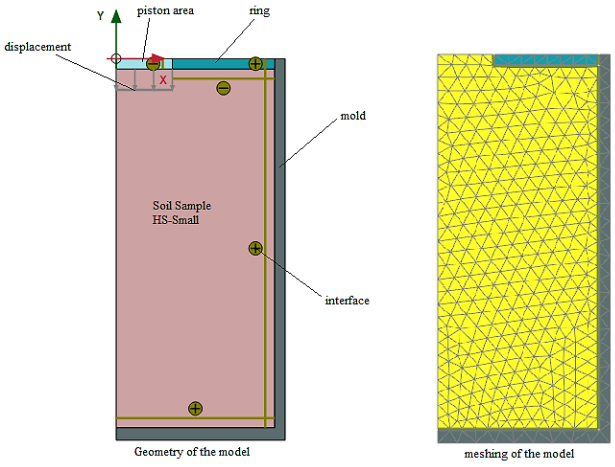

Figure 3. Numerical Model CBR test.
Source: Authors.

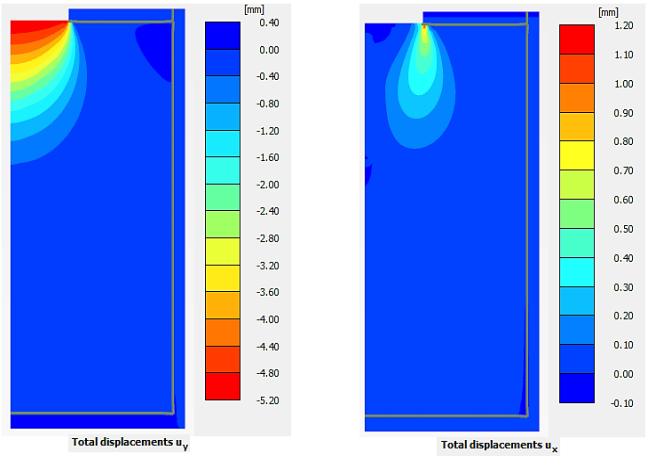

Figure 4. Typical displacement distribution at final stages (5.08 mm piston penetration).
Source: Authors.

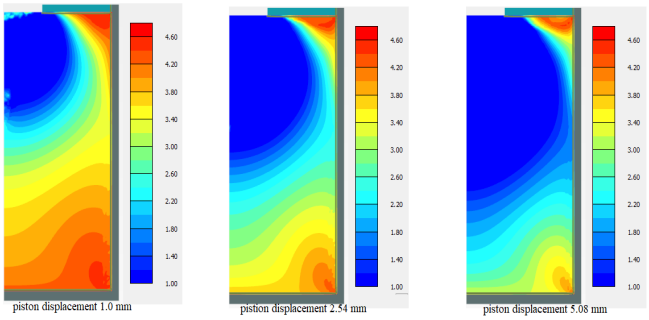

Figure 5. Typical stiffness ratio G/Gur distribution at different levels of penetration.
Source: Authors.

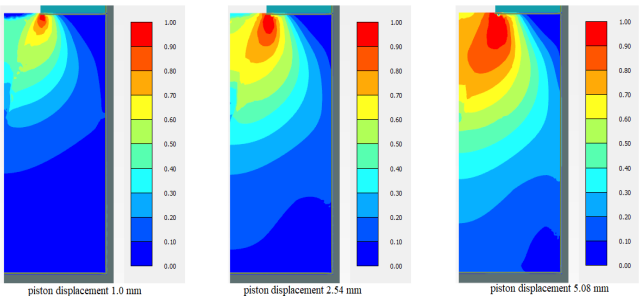

Figure 6. Typical shear ratio τ_{mob}/τ_{max} distribution at different levels of penetration.
Source: Authors.

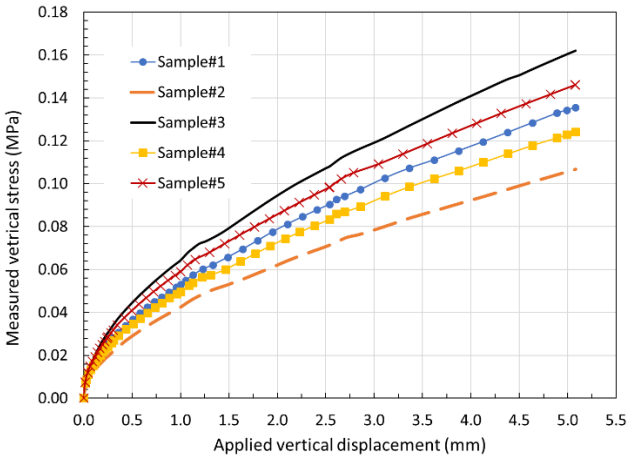

Figure 7. Numerical simulation results of the CBR test.
Source: Authors.

diameter of depth. Horizontal displacement is highly concentrated at the piston border. Horizontal-displacement bulb penetration reaches up to one piston diameter of depth. For the five samples, the numerical simulation shows a rigid triangle-shaped zone under the piston in which the soil moves almost exclusively downward. This behavior is common in bearing capacity phenomena.

Some debate has focused on whether CBR is similar to a bearing test or whether it can be correlated to a stress-strain test. The authors consider that simple constitutive models may not contribute to this type of dilemma. Therefore, some considerations can be pointed out in this regard since this research uses a constitutive equation that considers small strain and the degradation of moduli. It can be inferred in Fig. 5 that CBR tests involve a strong degradation of moduli. Critical softening in almost the entire sample occurs at 5.08 mm of piston penetration, but not at 2.54 mm which is usually the penetration level for the CBR value. It can be noted that, although at 2.54 mm the stiffness of the sample has not completely degraded, most of it has undergone some softening.

The comparison between the rate of degradation of the stiffness and the mobilization of the shear stress shows that both parameters strongly interfere with CBR response. Fig. 6 shows the typical spatial distribution of the shear ratio, i.e. the ratio between the mobilized shear stress and maximum shear, at different piston penetration levels during the simulated CBR test. The strength limit state, which occurs when mobilized shear equals available maximum shear stress, covers a small area of the sample. Furthermore, it is clear that the maximum values of shear stress are localized near the end of the piston during the entire test. At 2.54 mm of penetration, which is a typical CBR value, the vast majority of the sample exhibits relatively low shear stress ratio saturations. On the contrary, complete stiffness degradation covers more than half of the sample at the same level of penetration. These findings seem to suggest that in the case of the HS-Small constitutive model, the strength and stiffness parameters are strongly correlated to the response to CBR.

Finally, to fulfill the purpose of this study, Fig. 7 shows the CBR curves of the five synthetic soil samples whose geotechnical parameters were determined using previously presented criteria and correlations extracted from recent literature. The curves of the simulated CBR tests are not contrasted against tests executed on real samples. Instead, only the CBR values are compared with a reference or typical values for soils in the city of Bogotá. The maximum CBR values were found at a penetration of 2.54 mm. For each of the samples, the CBR value is presented in Table 6.

Table 6.
CBR results using HS-Small model (at 2.54 mm).

Sample	Vertical Stress MPa	CBR %
#1	0.197	1.31
#2	0.152	1.04
#3	0.160	1.57
#4	0.121	1.21
#5	0.142	1.42

Source: Authors.

Table 7.
Identification of samples for parametric study.

ID	Description
AF	Corresponds to sample with friction angle decreased by 10 % and recalculating the coefficients of earth pressures; remained parameters keeps the same value.
BF	Corresponds to sample with friction angle increased by 10 % and recalculating the coefficients of earth pressures; remained parameters keeps the same value.
AG	Sample with E_{edo}, E_{ur}, E_s, G_0 parameters decreased by 10 %, but keep all other parameters the same.
BG	Sample with E_{edo}, E_{ur}, E_s, G_0 parameters increased by 10 %, but keep all other parameters the same.

Source: Authors.

Considering that the HS-Small parameters of the samples used in the simulations were obtained from average index values, typical of the Sabana Formation, it is remarkable that the numerical result of the CBR will yield typical average values of the field tests consulted in the literature.

Finally, a parametric analysis for stiffness and resistance parameters is presented here to find their incidence on the CBR numerical tests. For this purpose, additional simulations were carried out with four variations of the original samples. The variations consisted of decreasing and increasing the friction angle by 10 % and decreasing or increasing the stiffness parameters by 10 %. In all cases, the overconsolidation and cohesion (and cut off) remained constant.

Type A samples consist of a 10 % decrease in the respective parameter, while type B samples correspond to an increase of said parameter by 10 %. The letters F and G correspond to the adjusted parameter: friction angle letter F, and stiffness modulus letter G. The following table summarizes the description.

Thus, from the original samples Sample 1 to Sample 5, twenty additional samples were made adjusting the resistance or rigidity parameters as described above. Table 7 presents the adjusted parameters involve in the parametric study. When a parameter keeps the same value of the original sample Table 7 calls the character # and the number of the original sample.

For the sake of brevity, Fig. 8 presents the results of the parametric analysis of the CBR test modeling by varying the stiffness or resistance parameters for sample #2. The load displacement curvature is typical of the nonlinear elastoplastic constitutive model. In Fig. 8 it can also be verified that the stiffness parameters have a greater incidence than the resistance parameters.

Table 8.
Values of parameters for parametric study.

No.	ϕ' °	E_{edo} N/mm²	E_{ur} N/mm²	G_0 N/mm²	$K_{0\,SC}$	$K_{0\,NC}$
#1	**31.94**	**1.6**	**8.3331**	**13.463**	**0.987**	**0.422**
#1AF	28.746	#1	#1	#1	1.017	0.47
#1BF	35.134	#1	#1	#1	0.946	0.375
#1AG	#1	1.44	7.4998	12.1167	#1	#1
#1BG	#1	1.76	9.1664	14.8093	#1	#1
#2	**29.7**	**1.095**	**6.0035**	**10.0056**	**1.009**	**0.455**
#2AF	26.73	#2	#2	#2	1.032	0.5
#2BF	32.67	#2	#2	#2	0.978	0.41
#2AG	#2	0.9855	5.4031	9.005	#2	#2
#2BG	#2	1.2045	6.6038	11.0061	#2	#2
#3BF	30.206	#3	#3	#3	1.101	0.447
#3AF	24.714	#3	#3	#3	1.125	0.532
#3	**27.46**	**1.934**	**8.8221**	**15.086**	**1.117**	**0.489**
#3AG	#3	1.7406	7.9399	13.5774	#3	#3
#3BG	#3	2.1274	9.7043	16.5946	#3	#3
#4BF	31.438	#4	#4	#4	0.883	0.428
#4AF	25.722	#4	#4	#4	0.942	0.516
#4	**28.58**	**1.705**	**8.1369**	**13.7494**	**0.915**	**0.472**
#4AG	#4	1.5345	7.3232	12.3744	#4	#4
#4BG	#4	1.8755	8.9505	15.1243	#4	#4
#5BG	#5	2.1615	10.2957	17.3973	#5	#5
#5AG	#5	1.7685	8.4238	14.2342	#5	#5
#5BF	31.438	#5	#5	#5	0.992	0.428
#5AF	25.722	#5	#5	#5	1.038	0.516
#5	**28.58**	**1.965**	**9.3598**	**15.8158**	**1.019**	**0.4716**

Source: Authors.

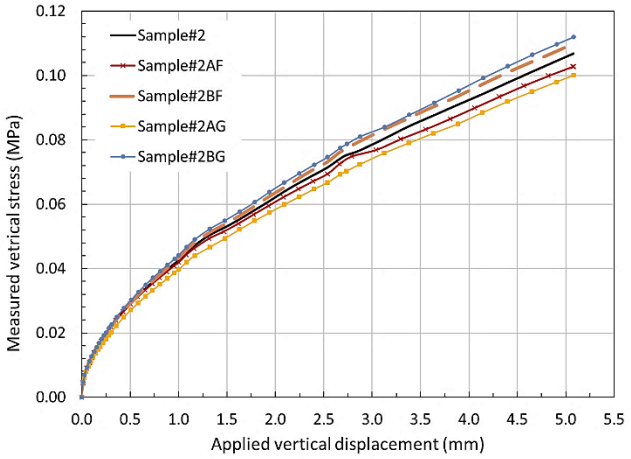

Figure 8. Numerical simulation results of the CBR for sample#2 – parametric study.
Source: Authors.

Table 9 presents the CBR results of the modeling and the variations with respect to the reference sample. Through parametric analysis It was evidenced that both the resistance parameters (and initial stress state - K0) and the stiffness parameters (G degradation curve) have an impact on the CBR result. For the samples with high friction angle and high overconsolidation ratio, the variation of the resistance parameters was not proportional. For sample#1 the symmetric variation +/-10 % of the friction angle produced an asymmetric response of CBR (-1 % and +5 %), while for sample #3 the variations produced an always positive

Table 9.
Results of CBR - parametric study.

Sample	CBR %	Variation
#1	1.31	--
#1AF	1.30	-1.09 %
#1BF	1.38	5.29 %
#1AG	1.26	-4.25 %
#1BG	1.43	8.81 %
#2	1.04	--
#2AF	1.01	-2.75 %
#2BF	1.06	2.49 %
#2AG	0.97	-6.54 %
#2BG	1.08	4.49 %
#3	1.56	--
#3AF	1.62	3.57 %
#3BF	1.74	11.03 %
#3AG	1.60	2.40 %
#3BG	1.65	5.34 %
#4	1.21	--
#4AF	1.17	-3.26 %
#4BF	1.24	2.41 %
#4AG	1.13	-6.48 %
#4BG	1.28	6.14 %
#5	1.42	--
#5AF	1.38	-3.37 %
#5BF	1.47	3.01 %
#5AG	1.35	-5.24 %
#5BG	1.49	4.71 %

Source: Authors.

variation in the CBR. For samples #2, #4 and #5, which coincide with the lowest friction angles and overconsolidation ratios the responses were proportional. For these samples, it was found that varying the friction angle by 10 % causes a variation that does not exceed 3.3 % of the CBR value of the reference samples, while raising or lowering the modulus degradation curve vertically in a ratio of 10 % causes sensitive variations in the CBR result, with ratios of change ranging between 2.4 and 6.5 % compared to the reference samples.

6 Conclusion

Different criteria and correlations have been developed in recent years for the largest soil deposit in the city of Bogotá. These criteria and correlations can be used to estimate the set of resistance and stiffness parameters of the HS-Small constitutive model with appropriate precision. This paper shows how to perform this characterization from index properties and others considerations.

A set of five synthetic samples was elaborated based on typical index properties of Bogotá soil. The soils are representative of the most superficial part by assigning high OCR values. However, the same set of parameters could represent soils at other depths by adjusting this ratio.

To show reliability, numerical CBR tests were performed in drained conditions. Although an inspection of the curves does not exactly match that of tests with samples from the site, the numerical CBR values at 2.54 mm are in the midrange of the typical values for soils in the City.

Additionally, a short discussion is presented on the applicability of the CBR as a test to determine the deformation properties of soils. Simulations show that the HS-Small constitutive model could contribute to this discussion by showing that even at low piston displacements, the degradation of the stiffness modulus occurs in a large part of the sample.

This work confirms that the set of parameters of the HS-Small model of the city of Bogotá can be determined with high accuracy from quick and inexpensive tests. Therefore, it contributes to the implementation of complex numerical analyzes for specific urban projects, even in early instances, when mechanical tests are not available.

The HS small constitutive model allows obtaining CBR values by simulating controlled displacement tests under axisymmetric conditions. In the present study it was possible to verify that, for dry tests, of over-consolidated soils with low cohesion, variations in the friction angle lead to slight variations in the CBR result. In contrast, variations in the stiffness parameters cause significant variations in the final result of the simulated CBR.

It can be inferred that the HS Small constitutive model, by incorporating a shear modulus degradation curve, generates a response in the CBR model that is more correlated with material stiffness than with friction angle, which may imply that the test of CBR if it would be correlated with the resilient modulus of the soil rather than with the resistance parameters.

In this study, the drained cohesion c' intercept is estimated from undrained shear strength S_u as suggested in eq. (13) and making ξ=5.

$$c' = \frac{1}{\xi}(S_u)OCR^{sin\phi} \tag{13}$$

This expression follows recommendation from Norwegian Geotechnical Institute – NGI – and involves the fact that drained cohesion appears on overconsolidated soils, so it is related to overconsolitation ratio - OCR.

References

[1] Alkhorshid, N.R., Araújo, G.L.S., and Palmeira, E.M., Geosynthetic Encased Column: comparison between numerical and experimental results. Soils and Rocks, 44, art. 073121, 2021. DOI: https://doi.org/10.28927/SR.2021.073121

[2] Simpson, B., (). Retaining structures: displacement and design. Géotechnique, 42(4), pp. 541-576, 1992. DOI: https://doi.org/10.1680/geot.1992.42.4.541

[3] Ti, K.S., Huat, B.B., Noorzaei, J., Jaafar, M.S., and Sew, G.S., A review of basic soil constitutive models for geotechnical application. Electronic Journal of Geotechnical Engineering, 14, pp. 1-18, 2009.

[4] Schanz, T., Vermeer, P.A., and Bonnier, P.G., The hardening soil model: formulation and verification. In: Beyond 2000 in Computational Geotechnics, Brinkgreve (ed). Balkema. Rotterdam, 1999, pp. 281-296.

[5] Benz, T., Small-strain stiffness of soils and its numerical consequences. Doctoral Dissertation, Stuttgart University, Germany, 2007.

[6] Caicedo, B., Mendoza, C., Lizcano, A., and Lopez-Caballero, F., Behavior of diatomaceous soil in lacustrine deposits of Bogotá, Colombia. Journal of Rock Mechanics and Geotechnical Engineering, 10, pp. 367-379, 2018. DOI: https://doi.org/10.1016/j.jrmge.2017.10.005

[7] Caicedo, B., Mendoza, C., Lizcano, A., and Lopez-Caballero, F., Some contributions to mechanical behaviors of lacustrine deposit in Bogotá, Colombia. Journal of Rock Mechanics and Geotechnical Engineering, 11, pp. 837-849, 2019. DOI: https://doi.org/10.1016/j.jrmge.2018.12.016

[8] Porter, O.J., The preparation of subgrades. In Highway Research Board

Proceedings, Vol. 18,1939.
[9] Standard Method of Test for The California Bearing Ratio, AASHTO Designation: T 193-22 UL, 2022.
[10] Hight, D.W., and Stevens, M.G.H., An analysis of the California Bearing Ratio test in saturated clays. Geotechnique, 32(4), pp. 315-322, 1982. DOI: https://doi.org/10.1680/geot.1982.32.4.315
[11] Yetimoglu, T., Wu, J.T., and Saglamer, A., Bearing capacity of rectangular footings on geogrid-reinforced sand. Journal of Geotechnical Engineering, 120(12), pp. 2083-2099, 1994. DOI: https://doi.org/10.1061/(ASCE)0733-9410(1994)120:12(2083)
[12] Thomé, A., Donato, M., Consoli, N.C., and Graham, J., Circular footings on a cemented layer above weak foundation soil. Canadian geotechnical Journal, 42(6), pp. 1569-1584, 2005. DOI: https://doi.org/10.1139/t05-069
[13] Narzary, B.K., and Ahamad, K.U., Estimating elastic modulus of California bearing ratio test sample using finite element model. Construction and Building Materials, 175, pp. 601-609, 2018. DOI: https://doi.org/10.1016/j.conbuildmat.2018.04.228
[14] Mendoza, C., and Caicedo, B., Elastoplastic framework of relationships between CBR and Young's modulus for fine grained materials. Transportation Geotechnics, 21, art. 100280, 2019. DOI: https://doi.org/10.1016/j.trgeo.2019.100280
[15] Bojacá-Torres, D.C., Módulo resiliente de suelos blandos de subrasante de la zona lacustre de Bogotá a partir del ensayo CBR cíclico, Doctoral Dissertation, Escuela Colombiana de Ingeniería Julio Garavito, Colombia, 2020.
[16] Brinkgreve, R.B., Selection of soil models and parameters for geotechnical engineering application. In Soil constitutive models: evaluation, selection, and calibration 2005, pp. 69-98. DOI: https://doi.org/10.1061/40771(169)4
[17] Rebolledo, J.F.R., León, R.F.P., and Camapum-de Carvalho, J., Obtaining the mechanical parameters for the hardening soil model of tropical soils in the city of Brasília. Soils and Rocks, 42(1), pp. 61-74, 2019. DOI: https://doi.org/10.28927/SR.421061
[18] Barón-Castro, M.A., Calibración del ensayo CPTu para el depósito lacustre de Bogotá. Master's Dissertation, Universidad Nacional de Colombia, 2021.
[19] Kulhawy, F.H., and Mayne, P.W., Manual on estimating soil properties for foundation design (No. EPRI-EL-6800). Electric Power Research Inst., Palo Alto, CA (USA), Geotechnical Engineering Group. Cornell Univ., Ithaca, NY, USA, 1990.
[20] Oh, W.T., and Vanapalli, S.K., Influence of Poisson's ratio on the stress vs. settlement behavior of shallow foundations in unsaturated fine-grained soils. Soils Rocks, 39(1), pp. 71-79, 2016. DOI: https://doi.org/10.28927/SR.2021.066521

C.E. Herrera-Cano, is BSC. Eng. in Civil Engineer in 2005, from the Universidad Industrial de Santander, Colombia. MSc. in Geotechnics in 2012, from the Universidad de Los Andes, and PhD in Dynamics of Pavements in 2021. from the Universidad de los Andes. Consultant in geotechnics and pavements. He currently works as a full-time professor at Universidad Piloto de Colombia.
ORCID: 0000-0002-4154-8705.

J.C. Ruge-Cardenas received the BSc. Eng in Civil Engineering in 2002 from the Universidad Francisco de Paula Santander (UFPS), Colombia; MSc. in Civil Engineering with emphasis on Geotechnics in 2005 from the Universidad de Los Andes, Colombia, and a PhD in Geotechnics in 2014 from the University of Brasilia (UnB), Brazil. Formerly postdoctoral researcher fellow in the Civil and Agricultural Department, at the Universidad Nacional de Colombia.
ORCID: 0000-0002-9100-6058

J**.G. Bastidas-Martinez**, received the BSc. Eng in Civil engineer in 2010, from the University of Cauca, Colombia. MSc. in Geotechnic in 2014, and Dr. in Geotechnic in 2017 from the University of Brasilia, Brazil. Diodoro National Engineering Award Sanches by the Colombian Society of Engineers in 2021. He currently works as an full time professor at Universidad Piloto de Colombia.
ORCID: 0000-0002-6818-0322

DYNA
http://dyna.medellin.unal.edu.co/

UNIVERSIDAD NACIONAL DE COLOMBIA

Waste-based consumable for hardfacing by welding: a look from the Circular Economy

Azucena Elizabeth Bernal-Gutiérrez [a], Carmen Isabel Ulloa-Méndez [b], Rodolfo Najarro-Quintero [c], Amado Cruz-Crespo [d], Lorenzo Perdomo-González [d] & Alejandro Duffus-Scott [d]

[a] *Facultad de Ciencias de la Ingeniería, Universidad Técnica Estatal de Quevedo, Ecuador. abernal@uteq.edu.ec*
[b] *Facultad de Ciencias Administrativas, Universidad Técnica de Cotopaxi, Ecuador. carmen.ulloa@utc.edu.ec*
[c] *Facultad de Ciencias de la Ingeniería y Aplicadas, Universidad Técnica de Cotopaxi, Ecuador. ing.rnajarro@gmail.com*
[d] *Centro de Investigaciones de Soldadura, Facultad de Ingeniería Mecánica e Industrial, Universidad Central "Marta Abreu" de Las Villas, Santa Clara, Cuba. amadocruz393@gmail.com, lperdomo@uclv.edu.cu, aduffus@uclv.edu.cu*

Received: May 6th, 2024. Received in revised form: November 8th, 2024. Accepted: November 18th, 2024.

Abstract
In the present work, the obtaining of a consumable for the restore parts by welding from the perspective of the circular economy is addressed, using industrial solid residuals (slag from steel production, graphite from fragments of electrodes of arc furnaces) and agroindustrial residuals (ash from the combustion of biomass (rice husk)) and conceiving the non-generation of new solid residuals in the hardfacing process. The conceptual scheme of obtaining a sustainable consumable for hardfacing by Submerged Arc Welding (SAW) is proposed, establishing the internal symbiosis between the obtaining and application processes, as well as the symbiosis of these with external processes and the possibility of introduction to industrial practice. The obtaining of a flux based on residuals and its application in the hardfacing of pieces are experimentally validated, confirming the possibility of recycling the resulting slag.

Keywords: steel slag; rice husk ash; SAW fluxes; hardfacing by welding; circular economy.

Consumible basado en residuales para recargue por soldadura: una mirada desde la Economía Circular

Resumen
En el presente trabajo, se aborda la obtención de un consumible para la recuperación de piezas por soldadura desde la perspectiva de la economía circular, empleando residuales sólidos industriales (Escorias de la producción de acero, grafito de fragmentos de electrodos de hornos de arco) y agroindustriales (cenizas de la combustión de biomasa (de cascarilla del arroz)) y concibiendo la no generación de nuevos residuales sólidos en el proceso de recargue. Se propone el esquema conceptual de la obtención sustentable de un consumible para el recargue por Soldadura por Arco Sumergido (SAW, por sus siglas en inglés), estableciéndose la simbiosis interna entre los procesos de obtención y aplicación; así como, la simbiosis de estos con procesos externos y la posibilidad de introducción a la práctica industrial. Se valida experimentalmente la obtención de un fundente a base de residuales y su aplicación en el recargue de piezas, confirmándose la posibilidad del reciclado de la escoria resultante.

Palabras clave: escorias de acería; cenizas de cascarilla del arroz; fundentes SAW; recargue duro por soldadura; economía circular.

1 Introduction

The production of consumables for hardfacing by SAW, to restoring parts or manufacturing new cheaper or more durable parts, is carried out fundamentally based on natural minerals, implicitly carry an environmental cost due to the deterioration of ecosystems caused by mining activity [1]. However, the use of solid waste is reported in obtaining new consumables for welding surfacing [2-8], and even the AWS A 5.17 standard [9] declares the reuse of slags in SAW joint welding of carbon steels.

How to cite: Bernal-Gutiérrez, A.E., Ulloa-Méndez, C.I., Najarro-Quintero, R., Cruz-Crespo, A., Perdomo-González, L., and Duffus-Scott, A., Waste-based consumable for hardfacing by welding: a look from the Circular Economy. DYNA, 91(234), pp. 93-99, October - December, 2024.

Surfacing to restore worn parts and return them to service, extending their useful life, or to manufacture new highly durable parts, implies a sustainable approach. This becomes even more evident if a consumable made from waste is used. However, to date, there is only one report on the application of the Circular Economy concept when addressing part hardfacing by SAW [8]. In this work, the non-generation of a new solid residual was not set as a goal (it was not planned to apply the slag resulting from welding overlay).

The Circular Economy is proposed as the logical and viable alternative, which corrects the main problems of linearity (production, use and disposal of goods) and aims for products, components and resources in general to maintain their usefulness and value at all times or which is the same, zero residues [10-13]. In this sense, several authors validate the conception of the Circular Economy, based on the 3R model (Reduce, Reuse, Recycle) or the 4R (Reduce, Reuse, Repair, Recycle), as sustainable solution in sectors with high consumption of natural mineral resources and that produce large volumes of solid waste [14-16].

Based on what has been discussed, the objective of this work is to obtain a consumable based on residuals to restore pieces by welding, from the Circular Economy perspective.

2 Materials y methods

2.1 Scheme for obtaining and applying a consumable for hardfacing parts by welding from the circular economy perspective

Fig. 1 shows the conceptual scheme of sustainable obtaining and application of a consumable for the restore of parts by SAW, from the Circular Economy perspective. The scheme considers the symbiosis of two processes, obtaining a flux (a) and parts hardfacing (b). It also considers symbiosis with external processes, while conceiving the non-generation of a new residual.

2.2 Obtaining the consumable

According to the diagram in Fig. 1 (Process framed by (a)), a flux was obtained to hardfacing parts subjected to abrasion. The composition of the flux matrix was established in a previous study (72.99 % slag from steel refining in the ACINOX Las Tunas ladle furnace, 20.44 % ash from the combustion of rice husk and 6.57 % of fluorite) [5]. In the present work it was decided to prepare the mixture of the flux matrix without flourite, since the slag from the fusion of said matrix, even without CaF_2, satisfies the requirements, having a location in the pseudowallastonite region of the system CaO-SiO_2-MgO, with melting temperatures around 1400 ºC [5,7]. The non-addition of fluorite favorably leads to a decrease in the flux/wire consumption ratio in hardfacing. In this way, the composition of the flux matrix to be produced is as follows: 78.12 % slag from steel refining in a ladle furnace and 21.88 % ash of rice husks.

According to previous results [6,7], the flux is composed of 83 % matrix and an alloy system (7% graphite and 10 % FeCrMn). The total dry mass to obtain the flux is composed

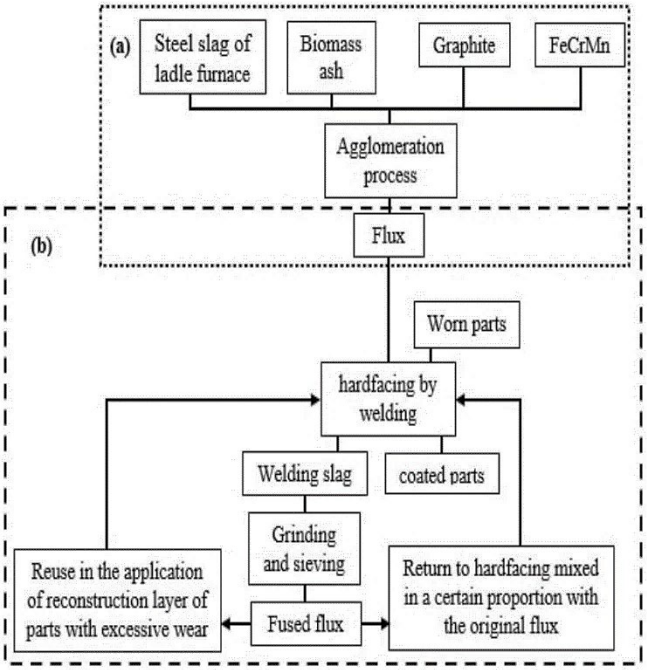

Figure 1. Scheme for obtaining and sustainable application of a consumable for parts hasrfacing by welding from the Circular Economy perspective. Source: Own elaboration

of: 64.84 % ladle furnace slag, 18.16 % rice husk ash, 7 % graphite and 10 % FeCrMn. Compositions of raw materials; as well as the procedures followed for its preparation and for obtaining the flux were previously reported [7].

The matrix components were sieved to a grain size less than 0.25 mm (steel refining slag and rice husk ash are fine granulated materials, that do not require grinding for use in welding consumables [5,7]); while FeCrMn and graphite were ground and sieved in a range between 0.1 mm and 0.25 mm. To obtain the flux, a mixture of 1 kg of dry mass was prepared. The components were mixed for 30 min in a rotating drum with an inclination of 5°, to ensure the homogeneity of the mixture. The components to the drum were added in increasing order of their densities, to facilitate counterflow mixing.

The flux was manufactured by pelletization, using sodium silicate as a binder, in a proportion of 30 % in relation to the dry mass. The flux was air dried for 24 h, then it was sieved to a particle size between 0.25 mm and 2.5 mm and finally it was calcined in a muffle furnace for 120 min at 350 °C.

2.3 Obtaining and characterization of weld deposits

With the flux, using a Mansfeld Submerged Arc Welding machine at the UCLV Welding Research Center (CIS), a bead-on-plate deposit was obtained. As in previous works [7], a 150x80x8 mm AISI 1020 steel plate was used as the base metal. The 3 mm EL12 electrode wire was used, using a current of 400 A, with normal polarity. The welding speed was 30 m/h, the arc voltage was 30 V. To guarantee cooling conditions, similar to the hardfacing of real parts, and to avoid deformations of the sheet, it was fixed on a device to perform the deposition. (Fig. 2).

Figure 2. Deposition on fixed plate to achieve heat extraction and prevent deformation
Source: Own elaboration

Two overlapping beads were deposited, positioning the electrode above the edge of the first bead to make the second, in such a way that a sufficient area was covered for the subsequent extraction of the specimens and the dilution with the base metal was attenuated.

From the deposit, the samples were extracted by means of transverse cuts on a metallographic cutting machine, for determination of chemical composition by Optical Emission Spectral Analysis and another for metallographic characterization and determination of hardness. The chemical analysis sample was roughed off at the top of the deposit, by grinding, to achieve a sufficient area for the incidence of the arc in the analysis. The metallographic sample was prepared in the cross-sectional part of the deposit. The sample was grinded and polished, in accordance with the ASTM E3 standard [17]. The attack was carried out by immersion with 2 % nital reagent, according to the ASTM E407 standard [18]. Fig. 3 shows the macrograph of the deposit, captured with a low magnification microscope.

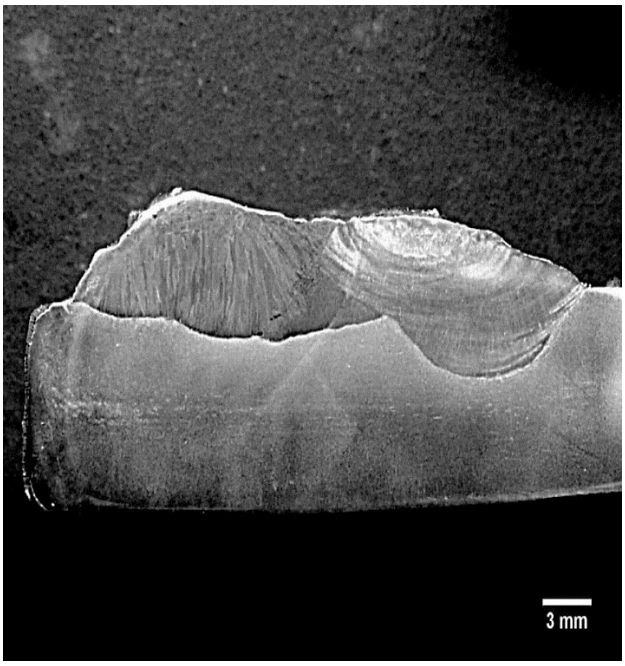

Figure 3. Macrograph of the deposit.
Source: Own elaboration

The metallographic observation was carried out by optical microscopy, in the upper center area of the second deposited bead (right bead in Fig. 3). In that same region, the Vickers hardness was measured with a microhardness tester, using a load of 1000 g and an indentation time of 10 s.

3 Results and discussion

3.1 Analysis of the circular economy perspective in obtaining a consumable for hard facing using residuals

Obtaining the consumable (Process (a) in Fig. 1) is based on the use of three residuals, slag from steel refining in a ladle furnace, graphite from electrode fragments from the steelmaking furnace, and ashes from the combustion of biomass (In this work, rice husk ash was used). This process of obtaining the flux (Process (a) in Fig. 1) has external symbiosis with the process of obtaining steel, because ladle furnace slag and graphite from fragments of electrodes are used. Has external symbiosis too with agroindustry through the use of ashes from the combustion of biomass and with the production of FeCrMn by aluminothermy [19].

Internally, obtaining the consumable (Process (a) in Fig. 1) has symbiosis with the parts hardfacing process (Process (b) in Fig. 1). In Process (b) in Fig. 1, internal symbiosis is carried out by recycling the slag in the same parts hardfacing process.

Externally, the hardfacing process (Process (b) in Fig. 1) has symbiosis with the repair and maintenance processes of equipment and facilities, since it returns worn parts to service or manufactures parts on a cheaper substrate.

According to what was discussed, in the scheme of Fig. 1, the conception of the Circular Economy is validated [10-16], since a marked emphasis is placed on the use of residuals and the non-generation of new residuals; as well as, because worn parts are returned to service (the useful life is extended). That is, residuals are reduced (slag from steel production and biomass ash), graphite is reused, worn parts are restored and the slag generated in the hardfacing is recycled. Additionally, the matrix components (steel refining slag and rice husk ash) do not require grinding, which means energy savings compared to the use of natural minerals in the flux matrix.

If the symbiosis of processes in Fig. 1 is integrated into the analysis of the possibility of obtaining and applying the consumable in industrial practice, four possibilities are noted:

1. Produce the hardfacing consumable (Flux for SAW) (Process (a) in Fig. 1) in a metal-mechanical company

whose object is the hardfacing of parts (Process (b) in Fig. 1).

2. Produce the hardfaciong consumable (Process (a) in Fig. 1) in a company that has infrastructure for the processing of granular materials and the production of agglomerates (company that produce clay elements, for example). This would supply the consumable to companies that perform hardfacing of parts by welding (Process (b) in Fig. 1).
3. Produce the hardfacing consumable (Process (a) in Fig. 1) in the steel producing company, where the slag, that constitutes the majority raw material to produce said consumable, is generated. The steel company would supply the manufactured consumable to metalworking companies that perform hardfacing of parts by welding (Process (b) in Fig. 1).
4. Produce the consumable (Process (a) in Fig. 1) in the steel producing company, where the slag is generated. Unlike the previous variant, this entity would also perform the parts hardfacing process (Process (b) in Fig. 1) for itself and for other companies.

Variants 2 and 3 consider producing the consumable (Process (a) in Fig. 1) in one company and performing the hardfacing in another (Process (b) in Fig. 1). There are the least viable, since recycling the slag from the hardfacing would be more difficult. In this case, the user of the consumable must also have equipment for crushing and sieving the slag from the hardfacing. In this sense, variant 1 is more viable than the previous ones, but requires that the company dedicated to the processes of manufacturing and restoring parts (Process (b) in Fig. 1) diversify, integrating operations of crushing, grinding, sieving, agglomeration, etc., to manufacture the consumable (Process (a) in Fig. 1).

Variant 4 is considered the most comprehensive solution, since the fundamental raw material for the manufacture of the consumable (Process (a) in Fig. 1) is the slag from steel refining in a ladle furnace. The steel production industry itself generates graphite electrode fragments as waste, this being another component to manufacture the consumable (flux). In turn, the ashes from the combustion of rice husks are used in steel company as a thermal insulating coating powder for liquid steel. The volumes of ash to be consumed, to satisfy the demand for the hardfacing consumable, would be insignificant compared to the frequent consumption of this agroindustrial residual (ash) in steel production. On the other hand, FeCrMn is an alloy also developed from waste, with mill scale being used to obtain it [19]. Therefore, obtaining FeCrMn could be integrated with the production of the hardfacing consumable (flux), especially because it does not require specialized equipment and facilities, while at the same time it would give application to another waste product from steel production (the mill scale [14,15]). FeCrMn to obtain the consumable for hardfacing parts can be replaced by commercial FeCr and FeMn, which are frequently used in steel production.

Additionally, steel production is related to the manufacturing and use of hardfacing consumables. The steel mill has the infrastructure (available areas, connections, laboratory equipment for grinding, sieving, mixing, etc.), which are often underutilized and which have the appropriate dimensions for the production of the hardfacing consumable (flux). At the same time, the steel industry has mechanical workshops that allow parts to be restored, since maintenance and repairs are required within the company itself.

3.2 Analysis of the deposited metal characterization

Table 1 shows the chemical composition of the deposited metal. This is characterized by C, Cr and Mn contents typical of hardfacing deposits to abrasive wear, according to AWS A 5.13 [20]. The silicon content (Table 1) is much higher than what is provided of this element in the wire-flux system (is provided by the wire and FeCrMn). This is a result of the fact that, in the high temperature zone (in the drop and the front area of the weld pool), the endothermic oxidation reaction of the metal in the weld pool by the SiO_2 of the flux develops intensely (Eq. 1), while C and Mn act as deoxidizers (Eq. 2-3), releasing iron and favoring the silicon reduction reaction by eq. (1) [7].

$$2Fe + (SiO_2) \rightarrow [Si] + 2\,[FeO] \quad (1)$$

$$[Mn] + [FeO] \rightarrow (MnO) + Fe \quad (2)$$

$$[C] + [FeO] \rightarrow CO + Fe \quad (3)$$

According to the high cooling rates and the preferential orientation of heat extraction in the surfacing by arc welding; as well as, the chemical composition of the deposited metal (Table 1), the microstructure (Fig. 4) is characterized by a high predominance of martensite (with possible some presence of bainite) and with austenite in the interdendritic region. This microstructure is appropriate for low stress abrasion conditions [3,5-7,20]. After deposition, the liquid metal cools, undergoing a primary crystallization of austenite in dendritic form, which, under conditions of high cooling rates, undergoes the non-diffusive transformation to martensite in the solid state. In the primary crystallization process, there is a certain tendency for the alloying elements to segregate, without reaching equilibrium conditions due to the high cooling rates. Austenite remains in the interdendritic region, which crystallizes last and does not undergo transformation.

Table 1 shows the average hardness of the deposited metal. According to the hardness value (about 57 HRc), the predominance of martensite in the dark dendritic region is confirmed (Fig. 4) [3,5-7,20]. The elements C, Cr and Mn influence hardenability, since they favor the transformation from austenite to martensite by shifting the pearlitic transformation curves to the right. These elements reduce the starting temperature of the martensitic transformation, which leads to a certain presence of retained austenite [6,7]. Carbon is responsible for the tetragonality of martensite, which consequently influences the hardness.

Table 1.
Chemical composition (% mass) and Vickers hardness of the metal deposited with the experimental flux

C	Mn	Cr	Si	HV_{1000}
1,68	1,61	0,52	1,44	621,4

Source: Own elaboration

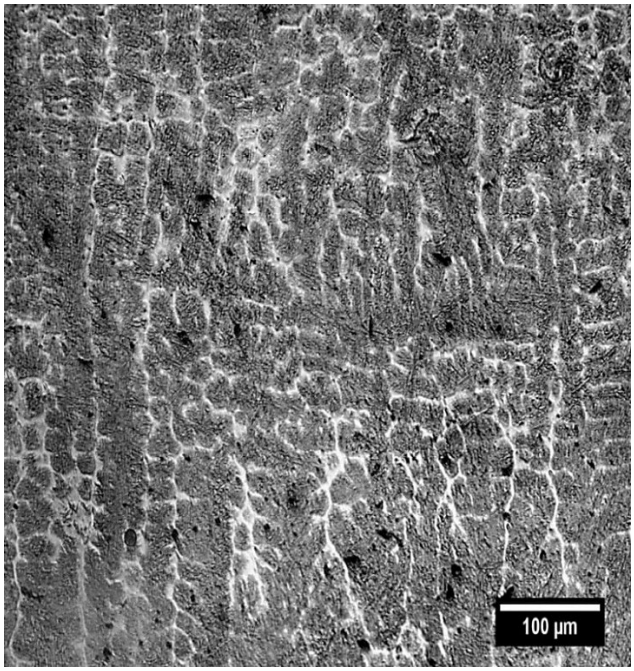

Figure 4. Microstructure of the deposited metal.
Source: Own elaboration

The AWS A 5.13 standard [20] reports the classification of EFe5 hardfacing deposits, whose composition is similar to the deposit obtained (Table 1). This standard declares that this EFe5 classification corresponds to a tool steel for cold work, with a hardness between 50 and 55 HRc, suitable for work with high compression stresses, moderate abrasion and metal-to-metal wear. Previous works [3,5-7] report, as suitable for abrasive wear, hardfacing deposits with composition and microstructure similar to those of the present (Tables 1 and 2, Fig. 4). Haiko et al. [21] even validate the adequate abrasive wear behavior of a lower hardness steel, with a predominance of bainite.

3.3 Analysis of slag formation in the hardfacing process to evaluate its recycling

As stated in section 2.2, the flux matrix is containing 78.12 % slag from steel refining in a ladle furnace and 21.88 % ash from the combustion of rice husks; while in the flux, the matrix represents 83 % and the rest corresponds to the alloy system (7% graphite and 10 % FeCrMn). Thus, the components of the dry mass of the flux represent 64.84 % slag from steel refining in a ladle furnace, 18.16 % rice husks ash, 7 % graphite and 10 % FeCrMn. When agglomerating with sodium silicate (the composition of sodium silicate is [7]: SiO_2- 29.39%; Na_2O- 10.10% and H_2O- 60.51%), at 30% in relation to the dry mass of 1 kg (648.4 g of ladle furnace slag, 181.6 g of rice husk ash, 70 g of graphite and 100 g of FeCrMn), this provided 88.2 g of SiO_2 and 30.3 g of Na_2O, since the water evaporated during the drying and calcination of the flux. Then the percentage ratio of the slag-forming flux components, considering the contribution of SiO_2 and Na_2O from the silicate is: 66.96 % of steel refining slag, 19.79 % of rice husk ash and (9.89 % SiO_2 + 3.39 Na_2O) provided by sodium silicate.

Based on the aforementioned percentage ratio of the slag-forming components in the flux and the compositions of the ladle furnace slag and rice husks ash, reported in a previous work [7], the composition of the slag, that is formed in the hardfacing with the experimental flux, was calculated (Table 2). It is observed that the formed slag is characterized by the majority CaO, SiO_2, MgO system, which represents 90.73 % of the total slag composition and, therefore, the ternary phase equilibrium system (Fig. 5) can be used to evaluated the phase composition and fusibility of the slag that is formed in the hardfacing with the flux [1,5,7,22].

The composition in Table 2, recalculated to 100 % of the CaO-SiO_2-MgO ternary system, corresponds to: 43.32% CaO, 50.53% SiO_2 and 6.15% MgO. Fig. 5 shows the location of this composition, showing that it´s localized in the pseudowalastonite region, around the melting temperature of 1400 °C. This location satisfices the basic flux behavior, melting before the electrode wire and the base metal, which have a fusion temperature around 1500 °C, thus guaranteeing the protection of the molten metal. Such localization in the pseudowallastonite zone (Fig. 5) coincides with the literature [1,2,5,7], which means a clear indication that it´s possible to recycle the slag in the same hardfacing process.

Table 2.
Composition of the slag that is formed in hardfacing with the experimental flux (% mass).

NiO	Cr_2O_3	MnO	FeO	CaO	MgO	SiO_2
0,06	0,03	0,64	0,77	39,30	5,58	45,85
Al_2O_3	**P_2O_5**	**SO_3**	**TiO_2**	**V_2O_5**	**Na_2O**	**K_2O**
3,50	0,02	0,56	0,20	0,02	3,46	0,01

Source: Own elaboration

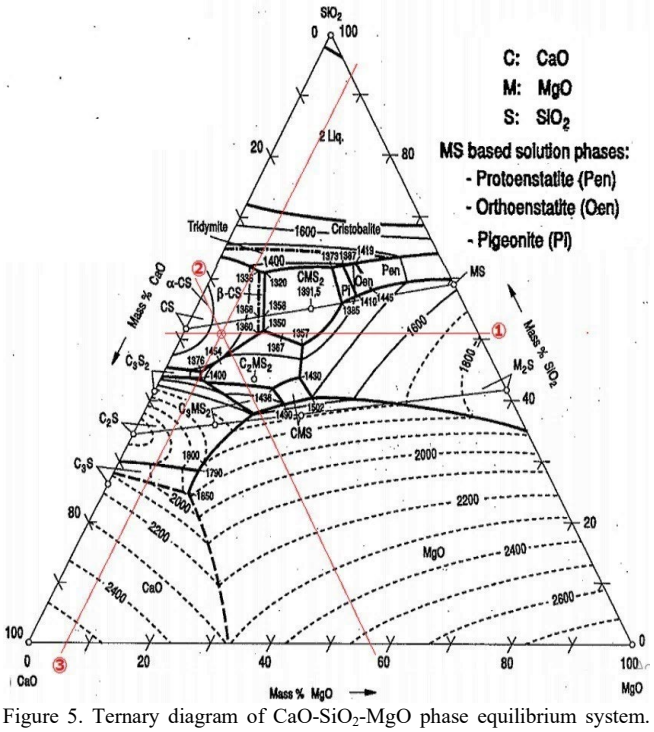

Figure 5. Ternary diagram of CaO-SiO_2-MgO phase equilibrium system. (The lines, identified with the numbers 1, 2 and 3 inside a circle, represent the contents of SiO_2, CaO and MgO and their intersection corresponds to the location of the composition)
Source: Allibert, 1995.

4 Conclusions

- The obtaining of a consumable (Flux) based on residuals for the parts hardfacing by welding is validated, from the Circular Economy perspective, conceiving the non-generation of new residual.
- The proposed scheme for sustainable obtaining and application of a hardfacing consumable (flux), shows the symbiosis between the processes of obtaining the consumable and parts hardfacing; as well as the external symbiosis of these with other processes such as obtaining steel and agribusiness.
- The most sustainable and comprehensive variant of introduction to industrial practice of the obtained consumable consists of: Obtaining the consumable in the steel producing company, where the slag, that is the majority raw material, is generated, and carrying out the parts hardfacing in the same company to satisfy internal demand and for others companies.
- The experimental consumable makes it possible to obtain a deposited metal, appropriate for parts working in abrasive wear. The deposited metal, corresponding to high carbon and low alloy steel, with a predominance of martensite in the microstructure and, consequently, which a high hardness (57 HRc).
- The slag from hardfacing with the experimental flux corresponds to the CaO-SiO_2-MgO ternary system, located in the pseudowallastonite region, being appropriate for recycling in the same hardfacing process.

References

[1] Quintana-Puchol, R., Gómez-Pérez, C.R., Cruz-Crespo, A. y Perdomo-González, L., Evaluación de matrices vítreas del sistema SiO_2-Al_2O_3-CaO-MgO para fundentes aglomerados a través la basicidad óptica y criterios estructuro-químicos. Soldagem and Inspeção [online]. 16(2), pp. 137-145, 2011. Available at: https://www.scielo.br/j/si/a/KcpttTsRS7ch5njXNwGx4WN/?lang=es&format=pdf

[2] Jerez-Pereira, R., Cruz-Crespo, A., Quintana, R., and Perdomo, L., Aprovechamiento de escorias de fundición de empresas del sector azucarero en la obtención de matriz de un fundente aglomerado para recuperación de piezas del propio sector. Centro Azúcar [online]. 34(2), pp. 43-49, 2007. Available at: http://centroazucar.uclv.edu.cu/index.php/centro_azucar/article/view/555

[3] Cruz-Crespo, A., Perdomo, L., Fernández, R., y Scotti, A., Composición química y microestructura del metal depositado con fundentes obtenidos con empleo de escorias del sistema MnO-SiO_2-CaO. Centro Azúcar [online], 44(3), pp. 43-52, 2017. Available at: http://scielo.sld.cu/scielo.php?script=sci_arttext&pid=S2223-48612017000300005

[4] Cruz-Crespo, A., Perdomo-González, L., Quintana-Puchol, R., and Scotti, A., Fundente para recargue por soldadura con arco sumergido a partir de ferrocromo-manganeso y escoria de la reducción simultánea de cromita y pirolusita., Soldagem and Inspeção, 24, art. 2424, 2019. DOI: https://doi.org/10.1590/0104-9224/SI24.24

[5] Najarro-Quintero, R., Cruz-Crespo, A., Perdomo, L., Ramírez Torrez, J., and López, R.J., Potencialidades de las escorias de afino del acero en la obtención de un fundente para recargue por soldadura. Centro Azúcar [online]. 45(4), pp. 32-40, 2018. Available at: http://scielo.sld.cu/scielo.php?script=sci_arttext&pid=S2223-48612018000400004

[6] Najarro-Quintero, R., Cruz-Crespo, A., Perdomo-González, L., Duffús-Scott, A., Ramírez-Torres, J., Fernández-Fuentes, A., y Morales-Torres, M., Efecto de los contenidos de matriz, grafito y ferrocromo- manganeso en fundentes SAW, obtenidos con escorias de acería y cenizas de cascarilla del arroz, sobre la composición química y dureza del metal depositado en una camada. Soldagem and Inspeção, 27(1), pp. 1-10, 2022. DOI: https://doi.org/10.1590/0104-9224/SI27.11

[7] Najarro-Quintero, R., Desarrollo de un fundente para el recargue por SAW de piezas sometidas a desgaste abrasivo a baja tensión en base a escorias de afino del acero y cenizas de cascarilla del arroz, PhD dissertation, Centro de Investigaciones de Soldadura, Universidad Central "Marta Abreu" de Las Villas, Santa Clara, Cuba, 2023.

[8] Jadán-Solís, K.P., Cruz-Crespo, A., Najarro-Quintero, R., y Perdomo-González, L., Enfoque de economía circular en la obtención de fundentes para el recargue con empleo de escorias. Centro Azúcar [online]. 50(1), pp. 1-9, 2023. Available at: http://centroazucar.uclv.edu.cu/index.php/centro_azucar/article/view/743/847

[9] AWS A5.17. Specification for carbon steel electrodes and fluxes for Submerged Metal Arc Welding. American Welding Society [online]. [online]. 2019. Available at: https://pubs.aws.org/Download_PDFS/A517_A517M_2019_Web_PV.pdf

[10] Arroyo, F.R., La Economía Circular como factor de desarrollo sustentable del sector productivo, INNOVA Research Journal [online]. 3(12), pp. 78-98, 2018. Available at: https://dialnet.unirioja.es/servlet/articulo?codigo=6828555

[11] Rodríguez-Martín, J., López-Errasti, O., and Ruiz-de A.L.P., Analysis of the impact of eco-design on the circular economy: a bibliometric analysis of publications in Spain. DYNA, 89(224), pp. 140-147, 2022. DOI: https://doi.org/10.15446/dyna.v89n224.102669

[12] Cardozo-Munar., C.E., Monroy-Perdomo, L., Flórez-Forero, D.F., Rodríguez-Bolivar, L.M. y Alarcón-Pinilla, Y.M., Conceptos de economía circular aplicados al sector agropecuario cundiboyacense Saponina en la provincia de Ubaté, Revista Universidad y Sociedad [online]. 15(1), pp. 269-276, 2023. Available at: https://rus.ucf.edu.cu/index.php/rus/article/view/3539/3482

[13] Romero-Perdomo, F., Carvajalino-Umaña, J.D., López-González, M., Ardila, N., and González-Curbelo, M.A., The private sector's role in Colombia to achieving the circular economy and the Sustainable Development Goals. DYNA, 90(228), pp. 9-16, 2023. DOI: https://doi.org/10.15446/dyna.v90n228.107721

[14] Guadagnino, P., Cantone, L., Conte, P., Pocina, G., Matarazzo, A., and Bertino, A., Techniques of reuse for slags and flakes from the steel industry: a circular economy perspective. Procedia Environmental Science, Engineering and Management [online]. 5(2), pp. 93-99, 2018. Available at: http://www.procedia-esem.eu/pdf/issues/2018/no2/11_Guadagnino_18.pdf

[15] Branca, T.A., Colla, V., Algermissen. D., Granbom, H., Martini, U., Morillon, A., Pietruck, R., and Rosendahl, S., Reuse and recycling of by-products in the steel sector: recent achievements paving the way to circular economy and industrial symbiosis in Europe. Metals, 345(10), pp. 2-18, 2020. DOI: https://doi.org/10.3390/met10030345

[16] Sithole, N.T., Tsotetsi, N.T., Mashifana, T., and Sillanpaa, M., Alternative cleaner production of sustainable concrete from waste foundry sand and slag. Journal of Cleaner Production, 336, art. 130399, pp. 1-11, 2022. DOI: https://doi.org/10.1016/j.jclepro.2022.130399

[17] ASTM E3. Standard guide for preparation of metallographic specimens. American Society for Testing and Materials [online]. 2011. Available at: https://www.academia.edu/35989703/ASTM_E_3_01_Standard_Guide_for_Preparation_of_Metallographic_Specimens_1

[18] ASTM E407. Standard practice for microetching metals and alloys, American Society for Testing and Materials [online]. 1999. Available at: https://edisciplinas.usp.br/pluginfile.php/4313805/mod_resource/content/1/NORMA_ASTM_ATAQUE_E407-99.28400.pdf

[19] Perdomo-González, L., Rodríguez-Pérez, M., Quintana-Puchol, R., Cruz-Crespo, A., Gómez-Ríos, I., Alfonso-López, I., González-Cabrera, O., Gómez- Pérez, C., and Herrera-Artiles, A., Procesamiento pirometalúrgico de minerales y desechos sólidos industriales para la obtención de productos de utilidad industrial. Anales de la Academia de Ciencias de Cuba [online]. 12(2), pp. 118-125, 2022. Available at: http://www.revistaccuba.cu/index.php/revacc/article/view/1118/1372

[20] AWS A 5.13. Specification for surfacing electrodes for shielded metal arc welding. American Welding Society [online]. 2010. Available at: https://pubs.aws.org/Download_PDFS/A5.13-A5.13M-2010PV.pdf

[21] Haiko, O., Kaikkonen, P., Somani, M., Valtonen, K., and K€omi, J.

Characteristics of carbide-free medium-carbon bainitic steels in high-stress abrasive wear conditions. Wear, 456–457, art. 203386, 2020. DOI: https://doi.org/10.1016/j.wear.2020.203386

[22] Allibert, M., Gaye, H., Geiseler, J., et al., Slag atlas. Verein Deutscher Eisenhuttenleute (VDEh), Germany, [online]. 1995. Available at: https://dokumen.tips/download/link/slag-atlas-55d475ae27209.html

A.E. Bernal-Gutierrez, is a BSc. Eng in Agro-industrial Engineering and the MSc. in Production Management from the Technical University of Cotopaxi-La Maná, Ecuador. Professor and researcher at the Engineering Science Faculty of the State Technical University of Quevedo (UTEQ), Ecuador. She is carrying out her doctoral work in the Food Engineering Program at the University of Havana, Cuba. Her research interest includes the artisanal production of leaf cheese. She has several academic and scientific awards. She is Career Director of Agroindustry and Director of undergraduate research projects.
ORCID: 0000-0003-2917-6408

C.I. Ulloa-Méndez, is a BSc. in Economic and BSc. in Accounting and Auditing. and MSc. in Accounting and Auditing, from the Quevedo State Technical University, Ecuador. PhD in Economic Sciences from Andres Bello Catholic University, Venezuela. Professor and researcher at the Faculty of Administrative and Economic Sciences of the Technical University of Cotopaxi-La Mana. She brings 11 years of teaching experience in undergraduate and postgraduate courses in Social Science, and strong sense of academic integrity. Motivated professional in economic and accounting. Adds value to any organization in need of great collaboration, interpersonal and organizational skills in various environment, such us Academic Subdirector, Director of career and Zone Auditor. She has led several research projects.
ORCID: 0000-0001-9138-887X

R. Najarro-Quintero, is a BSc. Eng. in Mechanical Engineering from the Technological University of Havana, Cuba, and MSc. in Computer Connectivity and Networks from the State Technical University of Quevedo, Ecuador, as well as, PhD in Mechanical Engineer from Central University "Martha Abreu" of Las Villas, Cuba. Professor and researcher at the Faculty of Engineering Sciences of the Technical University of Cotopaxi-La Maná. His research interest includes the obtain and evaluation of consumables for hardfacing and wear studies. He has several awards, including one from the Cuban Academy of Sciences. He has been the tutor of several BSc and MSc theses. He has led scientific research and extension projects and has held positions of academic responsibilities
ORCID: 0000-0002-6760-4269

A. Cruz-Crespo, is a BSc. Eng. and MSc. in Ferrous Metals from the Moscow Institute of Steel and Alloys, Russia. MSc. in Mechanical Engineering "Mention Welding" from the Central University “Martha Abreu” of Las Villas (UCLV), Cuba. PhD in Metallurgy from the Mining-Metallurgical Institute of Moa, Cuba. Professor and researcher at the Welding Research Center of the Central University "Marta Abreu" of Las Villas (UCLV). He has made several postdoctoral stays in Brazil and has been Visiting Professor at Universities in Nicaragua, Chile and Brazil. He is a Member of the Doctoral Committee “Metallurgy and Material” and “Mechanical Engineer” Programs of Moa University and UCLV, respectively. He is Executive Secretary of the Territorial Program of Industries of the Ministry of Sciences, Technology and Environment of Villa Clara, Cuba. He has been the tutor of several doctoral and master's theses about the development of ferroalloys and consumables for welding and hardfacing, the development of alloys and studies of weldability of armor steels. He has led several research projects. He is the author of several invention patents. He has several awards, including five annuals from the Cuban Academy of Sciences. He teaches undergraduate and postgraduate courses in materials science, welding metallurgy and tribology.
ORCID: 0000-0003-0227-9853

L. Perdomo-Gonzales, is a BSc. Eng. in Chemical Engineer and MSc. from UCLV. PhD in Metallurgy from the Mining-Metallurgical Institute of Moa, Cuba. is researcher at the Welding Research Center of the "Marta Abreu" Central University of Las Villas (UCLV). He has made several postdoctoral stays in Brazil. He is a member of the Doctoral Committee “Metallurgy and Material” Program of Moa University. He has been the tutor of several doctoral, master and graduate theses, about the development of ferroalloys and consumables for hardfacing. He is the author of several invention patents. He has led several research and technology transfer projects to the industry. He has several awards, including five annual awards from the Cuban Academy of Sciences. He teaches undergraduate and postgraduate courses in Corrosion.
ORCID: 0000-0002-3425-1487

A. Duffus-Scott, is a BSc in Physics from the UCLV, Cuba. PhD in Phisycs of Metals from the Kiev Polytechnic Institute, URSS. Professor of the Welding Research Center of the Central University "Marta Abreu" of Las Villas (UCLV). He has made several postdoctoral stays in Brazil and has been visiting professor at several universities in Mexico, Nicaragua, Colombia and Venezuela. He is a member of the Doctoral Committee “Building Engineer” Program of UCLV. He has been the tutor of several doctoral, master and graduate theses about the Failure Analysis and the characterization of welded joints and metallic structures. He has led several research and technology transfer projects to the industry and has directed the materials research line at UCLV. He has Annual Awards from the Cuban Academy of Sciences. He is an emeritus professor from UCLV. He teaches undergraduate and graduate courses in materials science and engineering, fracture mechanics, and predictive and diagnostic technologies. He has held various academic responsibilities, including head of the physics department and director of the welding research center.
ORCID: 0000-0001-9959-5697

DYNA
http://dyna.medellin.unal.edu.co/

UNIVERSIDAD NACIONAL DE COLOMBIA

Electromechanical flight stabilization system for CubeSat nanosatellites

Fausto R. Freire & Karla E. Mora

Facultad de Ciencias de la Ingeniería e Industrias, Universidad UTE, Quito, Ecuador. ffreire@ute.edu.ec, karla,mora@ute.edu.ec

Received: July 24th, 2024. Received in revised form: November 12th, 2024. Accepted: November 18th, 2024.

Abstract
The objective of the research was to design and simulate a stabilization system for attitude control of CubeSat nanosatellites in LEO orbit. The electronic system was inside the mechanical system, designed in Proteus. The mechanical system was designed in SolidWorks, then a CubeSat 3U CAD was downloaded for simulation and finally, all CAD designs were assembled. These data were used for the analysis of the spatial environmental perturbations of aerodynamic drag, gradient, gravity and magnetic field. Attitude representation was done by analyzing the Euler, Poisson and Quaternions equations. Then, a fuzzy logic control was created with two cases for automatic control. The analysis and virtual reality simulation revealed the correct attitude control on the CubeSat 3U nanosatellite, considering the perturbations of the space environment and a new 25° orientation of each axis.

Keywords: fuzzy control; simulation; virtual reality; electromechanical stabilization system; LEO orbit.

Sistema electromecánico de estabilización de vuelo para nanosatélites CubeSat

Resumen
El objetivo de la investigación fue diseñar y simular un sistema de estabilización para el control de actitud de nanosatélites tipo CubeSat en la órbita LEO. El sistema electrónico estaba dentro del sistema mecánico, diseñado en Proteus. El sistema mecánico se diseñó en SolidWorks, luego se bajó un CubeSat 3U CAD para la simulación y finalmente, se ensamblaron todos los diseños CAD. Estos datos se utilizaron para el análisis de las perturbaciones ambientales espaciales de arrastre aerodinámico, gradiente, campo gravitatorio y magnético. La representación de la actitud se hizo mediante el análisis de las ecuaciones de Euler, Poisson y Quaternions. A continuación, se creó un control de lógica difusa con dos casos para el control automático. El análisis y la simulación de realidad virtual revelaron el correcto control de actitud en el nanosatélite CubeSat 3U, considerando las perturbaciones del entorno espacial y una nueva orientación de 25° de cada eje.

Palabras clave: control difuso; simulación; realidad virtual; sistema electromecánico de estabilización; órbita LEO.

1 Introduction

The satellite is a natural or artificial object which turn around a planet on a specific orbit. The artificial satellites are vehicles, would was manned or unmanned, they transport and retransmit information [1,2]. Many satellites orbit the earth, they provide us of instant communication, internet or television signal, GPS signals and the most advanced satellites provide us of weather conditions of Earth [3,4].

Since putting a satellite into orbit has been very expensive, the nanosatellites have been an alternative because they are unmanned vehicles, without much weight, size, and cost [5,6].

There are many types of nanosatellites such us CubeSat, generally these are putting into orbit LEO (Low Earth Orbit), and the characteristics like weight and useful load are defined depending on the mission [7]. The development of nanosatellites is a trend in space science and research engineering area because they enable the study of nanosatellites subsystems and new technologies. The CubeSats are an example of the maximum use of electronic systems and technological advances [8]. Therefore, a lot of universities around the word, work with these nanosatellites.

A large part of CubeSat's tasks needs and excellent

How to cite: Freire, F.R. and Mora, K.E., Electromechanical flight stabilization system for CubeSat Nanosatellites. DYNA, 91(234), pp. 100-106, October - December, 2024.

attitude control because much of the tasks performed by nanosatellites in space require precise guidance and accuracy (attitude) to meet mission objectives; considering that the constructional characteristics such as total mass and power of nanosatellites are limited and many of them lack attitude control systems [9].

The nanosatellites have a wide range of attitude control systems. Some control systems have 3-axis magnetometers and 3-axis gyroscopes to measure relative rotations to determine absolute orientation [10], others incorporate sun sensors, star sensors or GPS to measure rotational speed [11].

For the change of orientation, the actuators are the components that produce the necessary torques to achieve the desired attitude, among the most used are, reaction wheels, torsion bars and thrusters [12], but the most accurate actuators are the reaction wheels, these respond to external disturbances that are present around the nanosatellite, generating corrective torques to change the angular acceleration.

An actuator alternative is the BLDC (Brushless Direct Current) brushless DC motor, where an electronic controller replaces the brushes, thus improving the reliability of the motor.

To achieve attitude control of a nanosatellite in the three axes (x, y, z), at least three reaction wheels, placed in three directions in different typologies, are necessary [13].

The present work consists of the design and simulation of a stabilization system to control the rotation and orientation of a CubeSat type nanosatellite.

It is designed and tested the operation of the subsystems: mechanical, electronic and control of the stabilization system considering the earth's gravity and the conditions in the low LEO orbit.

2 Methodology

For the development of the work, the V methodology was used, applied to the development of mechatronic devices, through which the functional requirements of the system were determined, such as system measurements, maximum weight allowed, type of material for the structure, type of working orbit of the nanosatellite, speed of rotation about the center of masses, angle of inclination, altitude, among others.

2.1 Conceptual design

A cubic carbon fiber structure was designed to support and protect the components. The motors are controlled by a PIC microcontroller, to which the MPU6050 sensor signals are input, consisting of a gyroscope and accelerometer; the sensor takes simulated data from a space environment in LEO orbit. The power supply is responsible for the power supply for the operation of the entire stabilization system.

A cubic carbon fiber structure was designed to support and protect the components. The motors are controlled by a PIC microcontroller, to which the MPU6050 sensor signals are input, consisting of a gyroscope and accelerometer; the sensor takes simulated data from a space environment in LEO orbit. The power supply is responsible for the power supply for the operation of the entire stabilization system as shown in Fig. 1.

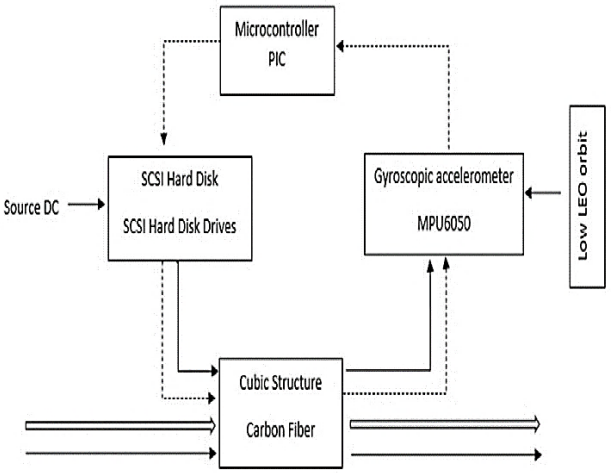

Figure 1. Conceptual design of the stabilizer system structure.
Source: the authors

In the Fig. 2 shows the flowchart of the simulation of the stabilizer system for a nanosatellite, where the MATLAB program collects information from other software packages such as SolidWorks and Proteus, then by means of VR Sink it is possible to simulate the behavior of the system in virtual reality.

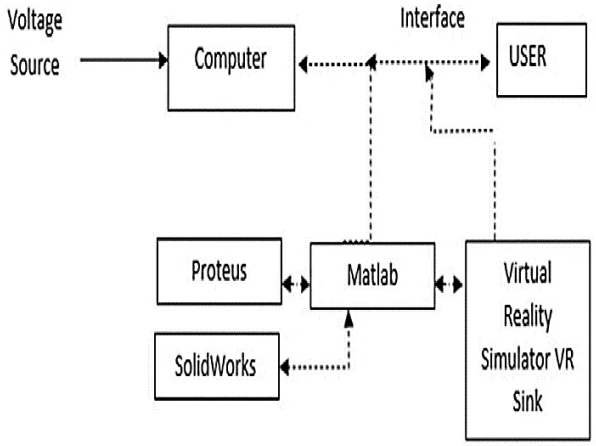

Figure 2. Simulation diagram of the stabilizer system.
Source: the authors

2.2 Mechanical design

To achieve control in the three axes of the CubeSat type nanosatellite, four reaction wheels were installed, one in the "x" axis, one in the "z" axis and two in the "y" axis; these motors have the capacity to rotate the nanosatellite around the axis of its center of mass, since they have flywheels that cause the acceleration of the rest of the satellite in the opposite way to the rotation.

For the selection of the material for the structure, different materials used in the aerospace industry were analyzed, after which carbon fiber was chosen because it has properties such as: high resistance, low weight, flexibility, tolerance to high temperatures and low thermal expansion.

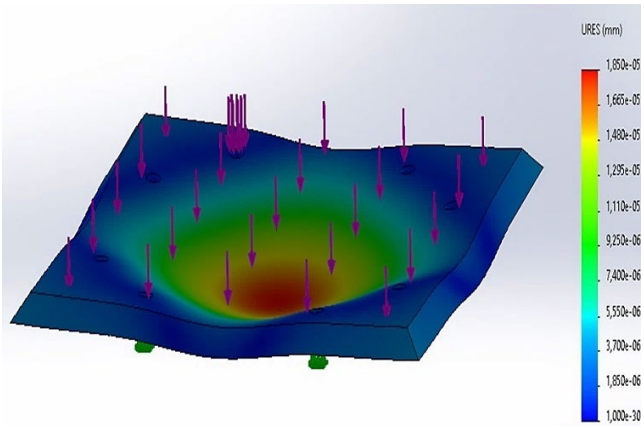

Figure 3. Base plate deformation analysis.
Source: the authors

The analysis of deflection and deformation forces to which each carbon fiber plate of the structure will be subjected was carried out, considering a thickness of 3 mm, y 8x8 cm^2 area; for the base plate it was considered that it must also support the weight of the control system, and for the side and top plates the analysis was performed considering the weight of each actuator (Fig. 3).

2.3 Electronic design

The control system board is made of 78x78 mm^2 and consists of a PDB-XT60 power regulation board, a MPU6050 sensor, a PIC16F877A microcontroller and the actuator controllers. For the PCB board design, the track size was calculated based on the IPC-2221 standards, obtaining a track width of 0,146 mm Fig. 4.

In space applications it is essential to eliminate all types of mechanical contacts such as bearings, gears, and motor brushes, for this reason we used BLDC motors of the ATA hard disk type (Fig. 5), which stand out for their torque characteristics, wide speed range (7200 a 8000 rpm), and unsurpassed service life. Fig. 6 shows the assembled stabilization system, with all components, mechanical and electronic.

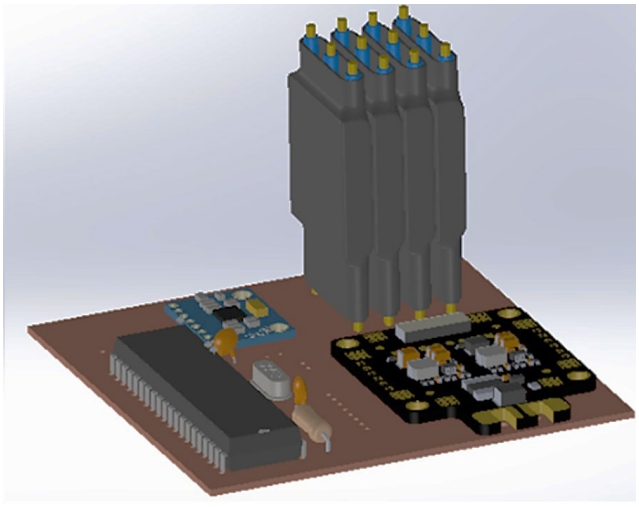

Figure 4. Electronic system exported to SolidWorks.
Source: the authors

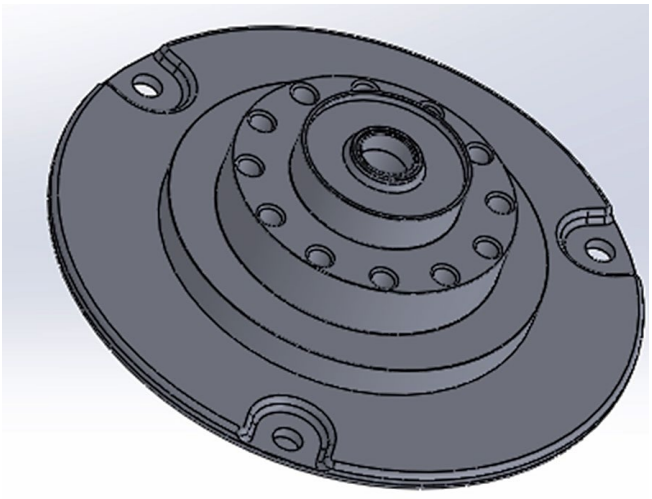

Figure 5. Hard disk motor.
Source: the authors

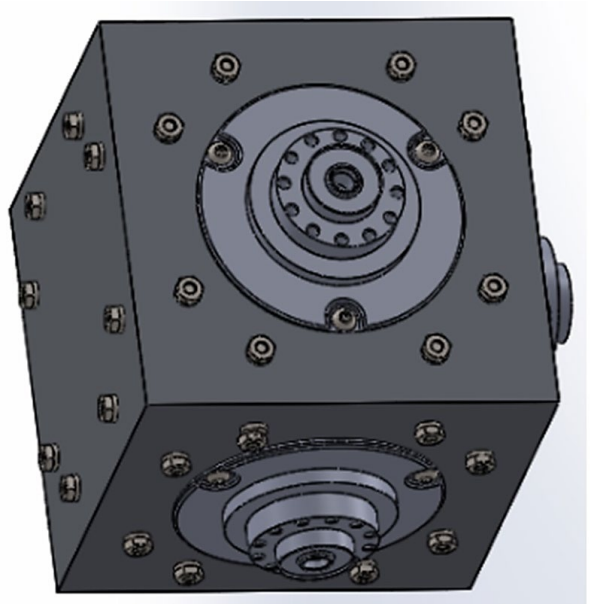

Figure 6. Mechanical stabilization system.
Source: the authors

To make the attitude control system of the nanosatellite we considered the motion of celestial bodies and laws of orbital motion, considering some elements such as: Eccentricity, Inclination, Altitude, Orbital velocity and the shape and physical characteristics of the nanosatellite. Their values were calculated with respect to locations of UTE nanosatellite previously sent to space (Table 1.).

Table 1.
Orbit elements.

Orbit elements	Value
Eccentricity	e=0
Inclination	i=90°
Altitude	h=629 km
Orbital velocity	V=27169.20 km/h

Source: the authors

Table 2.
Disturbances at 620 km of altitude.

Disturbance	Value [Nm]
Gravitational Gradient	3.117×10^{-10}
Magnetic Fields	4.645×10^{-7}
Atmospheric Drag	8.572×10^{-11}
Solar Radiation	0

Source: the authors

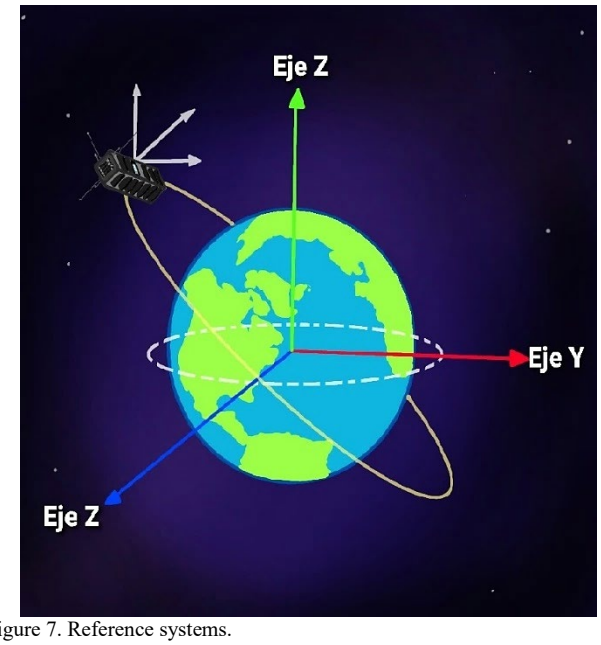

Figure 7. Reference systems.
Source: the authors

In the space environment there are disturbances to which the CubeSat is subjected, and which affect its orbit and attitude, among the disturbances considered are: aerodynamic drag, gravitational gradient, magnetic field, and solar radiation [14], the latter is stronger at higher altitudes so in LEO orbits it has a negligible value and was not considered. Table 2 shows the calculations performed for the perturbations at an altitude of 620 km which will simulate the space environment.

The orientation of the nanosatellite is usually analyzed with respect to a reference system, as shown in Fig. 7, which can be expressed by means of director vectors or angles. For this case, the orientation was analyzed, and the attitude representation was performed using Euler, Poisson, and Quaternion kinematic equations, which will simulate the attitude of the nanosatellite.

2.3.1 Euler equations

The system analyzes the rotations performed around the principal axes, to which rotation angles are associated for the axes (x, y, z), by means of the angular velocities of the sensor [15]. This is represented in eq. (1).

$$\dot{\phi} = \begin{bmatrix} 1 & sin\,\Phi\ tan\,\Theta & cos\,\Theta\,tan\,\Theta \\ 0 & cos\,\Phi & -sin\,\Phi \\ 0 & sec\,\Phi\ \ sin\,\Phi & cos\,\Phi\ \ sec\,\Theta \end{bmatrix} . \bar{\omega}_{b/v} \qquad (1)$$

2.3.2 Poisson equations

It is represented by the cosine direction matrix and takes the time of the rate of change as a function of (p, q, r) [16]. As seen in eq. (2).

$$\dot{c_{b/v}} = -\begin{bmatrix} 0 & -r & q \\ r & 0 & -p \\ -q & p & 0 \end{bmatrix} . c_{b/v} \qquad (2)$$

2.3.3 Quaternions

It is obtained from the angles provided by the sensor, and the attitude representation is defined by the vector and the angle representing the twist [17]. It is defined in eq. (3).

$$Q = \begin{bmatrix} q_0 \\ q_1\hat{\imath} \\ q_2\hat{\jmath} \\ q_3\hat{k} \end{bmatrix} = \begin{bmatrix} \cos\left(\frac{\delta}{2}\right) \\ V_{(x,y,z)}\ sin\left(\frac{\delta}{2}\right) \end{bmatrix} \qquad (3)$$

For testing and simulation purposes, the assembled stabilization system was exported to Simulink together with a standard CubeSat 3U design (t. 8). the assembled system reached a total weight of 3.808 kg.

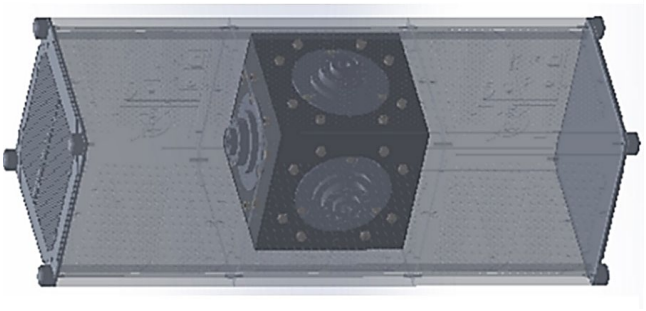

Figure 8. Stabilizer and CubeSat System Assembly.
Source: the authors

The automatic control system provided with a fuzzy controller and the simulation result using virtual reality elements are presented in Fig. 9.

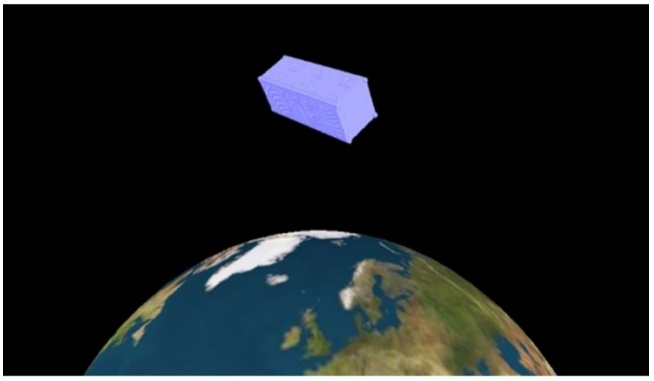

Figure 9. Virtual Reality Simulation.
Source: the authors

3 Results and discussion

In the Fig. 10 shows the design and control flowchart for a CubeSat type nanosatellite stabilization system.

The process started with the creation of the structure of the stabilizer system in the SolidWorks software, then a printed circuit board was designed in the Proteus software for the connections of the hard disk controllers and motors, the MPU6050 sensor, the PIC microcontroller, and other components.

The PCB design was exported in CAD format to SolidWorks software, to assemble the mechanical system and the electronic system of the stabilizer, for this purpose a fixed subassembly was made and, for the motors a flexible subassembly; then the assembled system was exported to MATLAB software and the project was saved in Simulink to test the operation of the motors.

To start with the tests in Simulink, a Gimbal Join was added which functioned as a sensor between the CubeSat 3U and the stabilizer system. Afterwards, several angular velocities were applied to the motors of the system and the working units were established in the connections, which generated a correct reading of the values of angular velocities, position, torque and acceleration of the nanosatellite; the turns and orientation change of the CubeSat were evaluated with the creation of a rotational kinematics subsystem using the Poisson, Quaternion and Euler equations, which established the most appropriate technique for the simulation and obtained a correct attitude representation.

A spatial perturbation subsystem was added, and two fuzzy control subsystems were created to evaluate the performance of the actuators; the first case: the stabilizer system performed a correct attitude control when the CubeSat was exposed to spatial perturbations, the second case: the stabilizer system performed a correct attitude control when the CubeSat was exposed to spatial perturbations and a new orientation of 25° for each axis. Finally, a Virtual Reality simulator was created, the results were sent, and the CubeSat 3U motion video was generated.

The CubeSat 3U and the stabilizer system have a total weight of 3.808 kg for the tests, an altitude of 620 km was determined, an orbital velocity of 27169.2 km h-1 and the perturbations calculated for each axis.

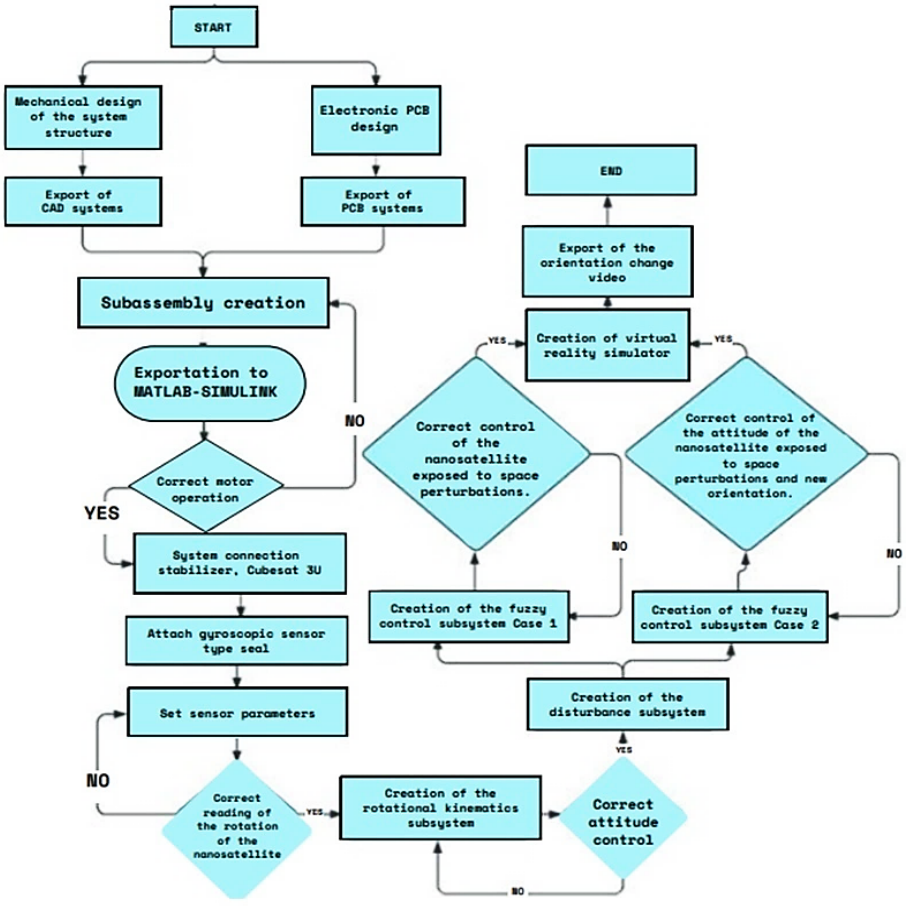

Figure 10. Flow diagram of the design and operation of the stabilizer system.
Source: the authors

Table 3.
Velocity and torque generated by the perturbations for each axis of the CubeSat.

Axis	Disturbance [Nm]	Disturbance [rpm]
X	-2.378×10^{-10}	0
Y	4.645×10^{-7}	0.516
Z	5.495×10^{-10}	0

Source: the authors

Table 4.
Velocity and touch generated by the stabilizer system for each CubeSat axis.

Axis	Torque [Nm].	Angular speed [rpm].
X	1.723×10^{-3}	0
Y	23.198×10^{-3}	21.43
Z	0.803×10^{-3}	0

Source: the authors

The maximum torque and maximum angular velocity provided to the nanosatellite by the environmental perturbations are shown in Table 3 below.

To test the stabilization system, the 4 motors were activated and an input from 0 to 8000 rpm was provided for each motor in the two directions of rotation, the maximum torque and maximum angular velocity provided to the nanosatellite, is observed in the following Table 4.

A fuzzy controller was developed, which receives information from the angles provided by the gyroscope, with which the operating ranges of inputs for control are defined. Two scenarios were created for the attitude control of the nanosatellite.

Case 1, the initial orientation was defined as the desired orientation at a rotation angle of 0° for each axis, and the perturbations were activated to evaluate the performance of the fuzzy control. At the start of the simulation the stabilizing system controlled the attitude and stabilized the nanosatellite at 0.03s, with an oscillation of 0.001˚.

Case 2, the desired orientation was defined with change of rotation angle from 0° a 25° for each axis of the nanosatellite and the environmental perturbations were activated. At the start of the simulation the stabilizer system controlled the attitude and stabilized the nanosatellite at 1.85s, with an oscillation of 0˚.

1 Conclusion

A stabilization system was designed for the attitude control of CubeSat 3U type nanosatellites, with a total weight of 0.808 kg, being the support structure a cube-shaped base of 80 mm on each side, with a thickness of 3 mm and carbon fiber material.

It was determined that "BLDC motor" type reaction wheels are the most accurate actuators for attitude control.

The arrangement of the wheels in the stabilizer system is, one for each axis (x, y, z) and an extra one on the y-axis, which provided a higher torque and angular velocity for the nanosatellite, with respect to the other axes.

The matrix of the Euler kinematic equations was evaluated and determine infinite values when the nanosatellite is directed from 90° a 270° (from top to bottom), this produced errors in the attitude reading; therefore, the Poisson and Quaternion equations are established as optimal for the attitude representation in simulation.

The fuzzy logic controller was accurate to validate the performance of the stabilizer system and performed a correct attitude control of the CubeSat 3U was exposed to spatial perturbations and different orientations.

Bibliography

[1] Maral, G., Michel, B., and Zhili, S., Satellite communications systems: systems, techniques and technology, John Wiley & Sons, Hoboken, NJ, USA, 2020. DOI: https://doi.org/10.1002/9781119673811

[2] Fourati, F., and Alouini, M.S., Artificial intelligence for satellite communication: a review. Intelligent and Converged Networks, 2(3), pp. 213-243. 2021. DOI: https://doi.org/10.23919/ICN.2021.0015

[3] Kodheli, O., Lagunas, E., Maturo, N., Sharma, S.K., Shankar, B., Montoya, J.F.M., and Goussetis, G., Satellite communications in the new space era: a survey and future challenges. IEEE Communications Surveys & Tutorials, 23(1), pp. 70-109, 2020. DOI: https://doi.org/10.1109/COMST.2020.3028247.

[4] Prol, F.S., Ferre, R.M., Saleem, Z., Välisuo, P., Pinell, C., Lohan, E. S., ... and Kuusniemi, H., Position, navigation, and timing (PNT) through low earth orbit (LEO) satellites: a survey on current status, challenges, and opportunities. IEEE Access, 10, pp. 83971–84002. 2022. DOI: https://doi.org/10.1109/ACCESS.2022.3194050

[5] Malisuwan, S., and Kanchanarat, B., Small satellites for low-cost space access: launch, deployment, integration, and in-space logistics. American Journal of Industrial and Business Management, 12(10), pp. 1480-1497, 2022. DOI: https://doi.org/10.4236/ajibm.2022.1210082

[6] Murugan, P., and Agrawal, Y., Small satellites applications, classification and technologies. International Journal of Science and Research (IJSR), 9(7), pp. 1682-1687, 2020. DOI: https://doi.org/10.21275/SR20723213825

[7] İnce, F., Nano and micro satellites as the pillar of the "new space" paradigm. Journal of Aeronautics and Space Technologies, [online]. 13(2), pp. 235-250, 2020. Available at: https://jast.hho.msu.edu.tr/index.php/JAST/article/view/420

[8] Saeed, N., Elzanaty, A., Almorad, H., Dahrouj, H., Al-Naffouri, T.Y., and Alouini, M.S., CubeSat communications: recent advances and future challenges. IEEE Communications Surveys & Tutorials, 22(3), pp. 1839-1862, 2020. DOI: https://doi.org/10.1109/COMST.2020.2990499.

[9] Freire, F., Shilenkov, E., Titenko, E., Frolov, S., and Shitov, A., Mathematical model of the earth's magnetic anomalies. Revista Técnica de la Facultad de Ingeniería Universidad del Zulia, [online]. 43(S1), pp. 35-39, 2020. Available at: https://produccioncientificaluz.org/index.php/tecnica/article/view/31066/47095

[10] Wailand, A., and Bauer, R., Investigation of gain tuning and sensor noise for CubeSat B-dot detumbling and 3-axis PD magnetic attitude control, Proceedings of the Canadian Society for Mechanical Engineering International Congress, [online]. 2020. Available at: https://library.upei.ca/islandora/object/csme2020%3A31/datastream/PDF/download/csme2020%3A31.pdf

[11] Gaber, K., El Mashade, M.B., and Aziz, G.A.A., A hardware implementation of flexible attitude determination and control system for two-axis-stabilized cubesat. Journal of Electrical Engineering & Technology, 15, pp. 869-882, 2020. DOI: https://doi.org/10.1007/s42835-020-00352-6

[12] Yang, Y., Spacecraft modeling, attitude determination, and control: quaternion-based approach, Rockville, Maryland, USA: CRC Press, 2019.

[13] Wang, Z., Smart attitude control system for small satellites, Doctoral dissertation, Faculty of Engineering, School of Aerospace Mechanical and Mechatronic Engineering, The University of Sydney, Australia, 2022. DOI: https://hdl.handle.net/2123/29905

[14] Shehzad, M.F., Asghar, A.B., Jaffery, M.H., Naveed, K., and Čonka, Z., Neuro-fuzzy system based proportional derivative gain optimized attitude control of CubeSat under LEO perturbations, Heliyon, 9(10), art. 20434, 2023. DOI: https://doi.org/10.1016/j.heliyon.2023.e20434

[15] Gordon, R., Worrall, K., and Ceriotti, M., Attitude control of a nanosatellite using inverse simulation, Proceedings of 72nd International Astronautical Congress 2021, pp. 833-847. Attitude

Control of a Nanosatellite using Inverse Simulation. In: 72nd International Astronautical Congress 2021, Dubai, United Arab Emirates, 25-29 Oct 2021, pp. 833-847.

[16] Liu, H.L., Wu, Y.S., Wan, L.C., Pan, S.J., Qin, S.J., Gao, F., and Wen, Q.Y., Variational quantum algorithm for the Poisson equation. Physical Review A, 104(2), art. 022418, 2021. DOI: https://doi.org/10.1103/PhysRevA.104.022418

[17] Krishna, A.B., Sen, A., and Kothari, M., Super twisting algorithm for robust geometric control of a helicopter. Journal of Intelligent & Robotic Systems, 102 art. 61, 2021. DOI: https://doi.org/10.1007/s10846-021-01366-6

F.R. Freire-Carrera, is a BSc. Eng. in Computer Systems Engineer with a MSc. in Engineering Sciences in 1995, and a PhD. in Dynamics, Strength, Apparatus, and Devices in 2007, all of them from the Kursk State Technical University in the Russian Federation. He also holds a MSc. in Information Technologies for Manufacturing and is a Specialist in Robotics in 2001 from the Polytechnic University of Madrid, Spain. Since 1998, he has been a lecturer at various universities and currently works in the Mechatronics program at the Faculty of Engineering and Industry of the UTE University. His research interests include fields such as: satellite technology, automatic control, mathematical modeling and simulation, dynamics, mobile robotics, artificial intelligence, distributed systems, telematics, programming languages, and quantum computing.
ORCID: 0000-0003-4307-5048

K.E. Mora-Cajas, is a BSc. Eng in Mechatronics Engineering in 2021 from the University UTE, and MSc. in Data Science and Machine Learning with a specialization in Artificial Intelligence in 2024 from the International University of Ecuador (UIDE), Quito, Ecuador. From 2021 she currently works as an educational advisor at UIDE and since 2020 conducting independent mechatronics projects for various companies. Additionally, she is the point of contact in Ecuador through the Space Generation Advisory Council (SGAC) for aerospace matters since 2024. Her research interests include nanosatellites, LEO orbit stabilization, automatic control, artificial intelligence, data analysis and predictions, and electronics.
ORCID: 0009-0003-5778-7350

DYNA
http://dyna.medellin.unal.edu.co/

UNIVERSIDAD NACIONAL DE COLOMBIA

Design and fabrication study of a small remote-controlled bionic butterfly flapping-wing flying machine

Yaozeng Mao, Fan Wu, Junjie Lao & Minglei Li *

School of Intelligent Manufacturing, Jiangnan University, Wuxi, China.
jyxy@jiangnan.edu.cn, 1046220226@stu.jiangnan.edu.cn; 13965192332@163.com; laojunjie126@126.com,
** Corresponding author, lml18888071473@163.com*

Received: May 21st, 2024. Received in revised form: October 23rd, 2024. Accepted: November 18th, 2024.

Abstract
This research is devoted to simulating the flight characteristics of real butterflies, and a small remote-controlled bionic butterfly flying machine is designed and manufactured. We analyze the principle of butterfly wing flight, which provides a theoretical basis for bionic design. Then, through 3D modeling and finite element analysis, an innovative design scheme of small bionic butterfly flight vehicle was proposed and verified, and its lift force was analyzed after assembly. This study not only demonstrates the feasibility of the design and implementation of small bionic butterfly aircraft, but also emphasizes its potential application value in the execution of small space missions, providing a new perspective for the design and optimization of bionic aircraft in the future.

Keywords: flying machine; bionic machinery; butterfly flight characteristics; remote-controlled.

Estudio de diseño y fabricación de una pequeña máquina voladora biónica de alas batientes de mariposa teledirigida

Resumen
Esta investigación se dedica a simular las características de vuelo de mariposas reales, y se diseña y fabrica una pequeña máquina biónica teledirigida para volar mariposas. Analizamos el principio del vuelo de las alas de mariposa, que proporciona una base teórica para el diseño biónico. A continuación, mediante modelado 3D y análisis de elementos finitos, se propuso y verificó un innovador esquema de diseño de un pequeño vehículo biónico de vuelo de mariposa, y se analizó su fuerza de sustentación tras el ensamblaje. Este estudio no sólo demuestra la viabilidad del diseño y la implementación de pequeños aviones mariposa biónicos, sino que también pone de relieve su valor de aplicación potencial en la ejecución de pequeñas misiones espaciales, proporcionando una nueva perspectiva para el diseño y optimización de aviones biónicos en el futuro.

Palabras clave: máquina voladora; maquinaria biónica; características de vuelo de mariposa; teledirigida.

1 Introduction

Many of the current flight devices are based on the principle of bionics, modeled after the structure and flight mode of insects. Compared with fruit flies, mosquitoes, and other insects with flutter frequency above 100Hz, butterflies with flutter frequency below 10Hz have a more special way of fluttering, and this low-frequency fluttering feature gives it the advantages of low noise and low energy consumption. Therefore, in the implementation of narrow space reconnaissance and close-range monitoring tasks, imitation butterfly wing flapping machines can play an important role.

Most of the bionic butterflies developed so far have the problems of oversized design and limited path planning. Accordingly, we would like to control the size to about five times by improving the design and material, and at the same time control the movement path by remote control device and motor, to make it closer to the movement process of a real butterfly. Our research is based on the principle of bionics to design and fabricate a wing-fluttering flying machine that

How to cite: Mao, Y., Wu, F., Lao, J., and Li, M., Design and fabrication study of a small remote-controlled bionic butterfly flapping-wing flying machine. DYNA, 91(234), pp. 107-115, October - December, 2024.

mimics the way butterflies fly and looks in nature. It can integrate the process of climbing, propulsion, and hovering, and has high aerodynamic efficiency within a certain speed range, which prolongs the range and sailing time; at the same time, it has very low requirements for the environment of the take-off site, which is very convenient and has a very good prospect in military reconnaissance and environmental monitoring.

To further improve the performance of the current bionic butterfly flapping-wing aircraft, we designed and manufactured a new type of bionic butterfly flapping-wing aircraft. The contributions of this article are as follows:

- Based on the physiological characteristics of the butterfly itself, a new transmission mechanism was developed. This transmission mechanism enables the aircraft to achieve stable flight while keeping its size and weight as close as possible to that of a butterfly.
- Through simulation analysis of butterfly wing movements, specially distributed wing veins were designed. Experiments show that the wing veins are reasonably distributed and can achieve stable flight.
- Designed a high-performance, highly integrated, and intelligent flight control board, which allows for more subsequent application scenarios.

2 Related works

With the in-depth study of bionic machinery and the development of aerodynamic theory, it has been found that fluttering wing flight has the advantages of low noise and low energy consumption relative to other flight modes [1-5]. However, the inability to hover and the lack of a bird's broad tail for flight direction and attitude control are also obvious defects, which is also the current research direction of researchers on the bionic butterfly flyer. At the same time, due to the low-frequency characteristics of butterfly fluttering wings, it is difficult for researchers to design a bionic butterfly with 1:1 size and stable flight under the limitation of material and process.

In order to solve these problems, predecessors have conducted extensive and useful research. Yue Zhu et al. designed a new flap mechanism and conducted mathematical modeling to provide guidance at the theoretical level [6]. In addition, Yixin Zhang and others used high-speed photography to capture the butterfly's abdominal swing, wing movement and body pitching during free flight, further proving that there is a dynamic coupling effect between the wings and body of the butterfly in different flight modes [7]. In the field of manufacturing new structures, researchers have also made innovative attempts. Leng et al. conducted in-depth research on Festo's bionic butterfly and independently designed a new butterfly-shaped flapping aircraft structure scheme based on this prototype. The USButterfly produced by Huang Haifeng and others is a new milestone in bionic butterfly design, but its size is too different from that of a real butterfly [8]. In recent years, most bionic butterflies have been designed to be more than ten times the size of a butterfly, with wings proportionally larger to increase lift as much as possible without increasing mass.

In this design, the ailerons of the aircraft are cleverly designed as flexible hinge structures, with the main wings located above the ailerons. During downward flapping, the main wing drives the entire wing to complete downward flapping through the overlap with the aileron, maximizing the windward area; on the contrary, during the upward flapping process, the aileron is placed under the active wing and communicates with the active wing through a flexible hinge. The wings are connected, and a phase difference occurs between the main aileron and the active wing, which gradually reduces the windward area, eventually forming an upward net lift. This series of innovative designs further advances the research on bionic butterflies in aircraft structural design.The small bionic butterfly flapping wing aircraft is currently showing good prospects, but the rudder drive and other methods are very demanding on the hardware equipment, and so far there is no energy source with sufficiently high energy density or sufficiently efficient rudder to drive the small flying machine. The small imitation butterfly flier designed in this study uses a motor drive and an innovatively designed transmission mechanism that allows for greater energy efficiency.

3 Detailed program design and production

3.1 Bionic butterfly working principle

Based on biological research, butterflies mainly rely on the "principle of drag" to carry out flapping flight, and their lifting force to balance the gravity of the body and the thrust force to overcome the body resistance are mainly provided by the drag force generated by the wings. When the butterfly starts its downbeat movement, the left and right wings start flapping symmetrically from a small angle (about 50°) to both sides. At this time, strong leading-edge vortices and wing end vortices were formed at the leading edge and end of the two wings, respectively, while vortices formed during the downbeat and upbeat, respectively, of the previous beat cycle were also present downstream of the wings. In the subsequent flapping motion, the leading-edge vortex and the wing end vortex developed into a "vortex ring" in a short time, and a strong downward flow, i.e., jet, was formed in the area between the two wings under the action of the "vortex ring". Subsequently, the vortex on the wing surface starts to become loose and move backward and fall off due to the reduction of the flapping speed and the larger forward incoming flow. In the upbeat process, no new vortex formation on the upper fin surface, while the "vortex ring" generated in the downbeat continues to fall off backward, and gradually dissipates under the viscous effect of the fluid. After the start of the upbeat movement, the lower wing surfaces of the left and right wings also produce leading-edge vortices and wing end vortices, and they are obviously much weaker than the vortices produced on the upper wing surfaces during the downbeat. This is because the angle between the two wings at the beginning of the upbeat is larger (about 150°), and the angle between the direction of beat movement and the direction of incoming flow becomes smaller due to the upward tilt of the body. As a result, the peak in drag is much smaller in the upbeat than in the downbeat. Similarly, the vortex on the lower wing surface moves backward in

subsequent motions and flips off from the end of the wing onto the upper wing surface as a result of the reduced flapping speed and the incoming flow.

3.2 Bionic butterfly total solution

Our bionic butterfly wing flutterer has an overall weight of 11.4g in a 30cm diameter circle, a double wing flapping rate of 4 Hz, and a full battery life of up to 4 min.

This small bionic butterfly flutter abandons less efficient drive methods such as rudders, chooses motors to control the wing movement, and increases the torque by gear reduction, and uses a linkage mechanism to convert the rotary motion of the gears into reciprocating oscillation of the wings. In addition, we simplify the principle of wing flutter and try to reduce the weight of the whole aircraft from the perspective of materials, batteries, etc., so that the lifting force is enough to overcome the gravity of the whole aircraft and the resistance of the flight, and at the same time, we can also reduce the power consumption and improve its stability and endurance during flight.

The small imitation butterfly aircraft designed in this study mainly consists of three parts: the main torso, the wing assembly, and the driving device. The wing assembly is divided into left and right parts, which are each mounted on the wing drive assembly on both sides of the front end of the main structure, and presents a mirror image symmetric layout. Each wing assembly consists of five parts: the outer profile bar, the main drive bar, the wing veins, the wing root connectors, and the elastic membrane. Specifically, the wing root connector adopts a fan-like cross-sectional structure; the outer contour rod forms the outer contour of the wing assembly, and the end of the main drive rod is connected to a blind hole. The structure sketch is shown in Fig. 1.

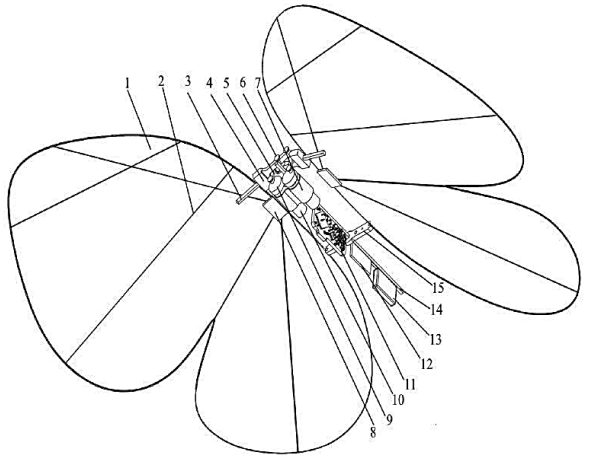

1. Fin	2. Fin vein	3. Main drive rod	4. Drive linkage	5. Linkage
6. Shaft cover	7. Motor bracket	8. Fin root	9. Eccentric disc	10. Motor
11. Flight control board	12. Receiver	13. Battery	14. Main rod	15. Rear fin bracket

Figure 1. Bionic butterfly structure sketch.
Source: own elaboration

The middle section of the outer contour rod is fitted with a wing vein connection member along its length direction, so as to connect the wing veins and realize the concave in the middle of the outer contour of the wings through the wing veins, thus replicating the typical form of a butterfly wing. In addition, the front end of the outer contour rod is fitted with a main drive rod connector, one end of which is firmly connected to the main drive rod connector, and the other end of which passes through the through-hole provided in the wing vein connector and is ultimately secured to the drive motor rocker arm in the wing drive assembly. The trailing edge of the wing is connected to an articulating member in the center of the main body. Instead of a kite cloth, this flying machine utilizes a polyethylene terephthalate (PET) material, which covers the outer contour of the wings.

With the above construction, the small bionic butterfly flyer proposed in this study aims to achieve a more efficient and responsive flight performance by simulating the natural fluttering pattern of butterfly wings.

3.3 Bionic butterfly body torso design

The constituent elements of the main torso section include the carbon main rod, motor bracket, flight control board fixing bracket, battery connection bracket, and rear fin bracket as shown in Fig. 2. The main stem is a hollow carbon fiber rod with a cross-section of 1.5 mm side length and a length of 113 mm. the motor bracket, flight control board fixing bracket, battery connection bracket and rear fin bracket are all polylactic acid (PLA) structural components. The motor bracket has a bracket mounting hole in the center that matches the cross-section of the main rod, through which the bracket is set on the front end of the main rod to be fixed with a tight fit, and at the same time there are motor mounting holes designed along the axial direction of the main rod at the symmetric positions under the left and right sides, as shown in Fig. 3. The rear wing bracket is in a zigzag shape, with a mounting hole designed to match the cross-section of the main rod at the center, through which the rear wing bracket is put on the front of the main rod to be fixed in a tight fit, with the fixing position close to the center of the main rod, and at the same time there is a wing connecting hole designed for connecting the left wing assembly and the right wing assembly, respectively, as shown in Fig. 4. On this basis, the rear wing bracket and the wing drive mounting bracket are adjustable in the main torso axial direction to enable adjustment of the position of the left-wing assembly, the right-wing assembly, the flight control board, and the power supply unit. The adjustment is generally made with reference to a combination of factors such as the aerodynamic forces to which the left-wing assembly and the right-wing assembly are subjected and their own gravity.

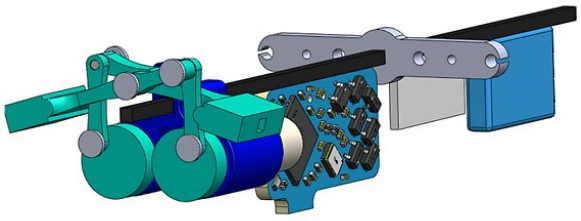

Figure 2. Main torso assembly drawing.
Source: own elaboration

Figure 3. Motor bracket.
Source: own elaboration

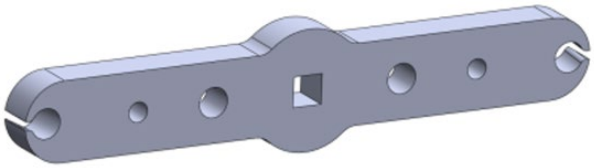

Figure 4. Rear fin bracket. (source: own elaboration)

3.4 Bionic Butterfly Drive System Design

The bionic butterfly drive system includes paired and symmetrically mounted motors and their transmission mechanisms on both sides of the main pole. The motors are 3V, 6mm, 242rpm hollow-cup motors with high precision, ultra-miniature, and lightweight metal cases. This motor can meet the speed and torque required for flight while dramatically reducing the overall mass of the machine.

To transform the rotation of the motor into the oscillation of the wing, we carefully designed a set of high-precision and lightweight drive mechanisms, as shown in Fig. 5. The motor is tightly connected to the eccentric disk through a D-shape shaft, the connecting rod is connected to the eccentric disk through an optical shaft and is positioned through the shaft cover, and the connecting rod is connected to the driving rod through an optical shaft to drive the wing movement. After the transmission mechanism, the wings swing at 63°. The axes of motor output axes of the two sets of wings are kept in the same plane with the axes of the main rods of the main torso of the bionic butterfly, toward the end of the main torso, and form an angle of 10° with the main rods, which is a key design parameter that determines that the forward swept angles of the left and right-wing assemblies are in a reasonable range.

The following is a detailed calculation description of the design of the four-bar mechanism of the drive system.

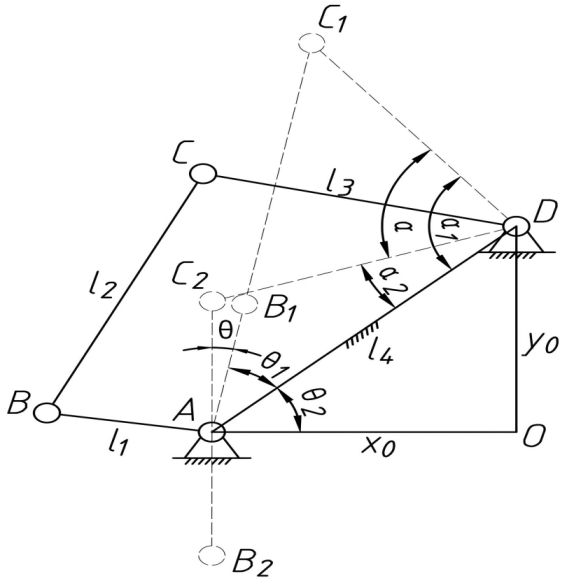

Figure 5. Schematic diagram of wing drive linkage mechanism.
Source: own elaboration

The schematic diagram of the wing drive linkage mechanism is shown in Fig. 8, where l_1=3mm, l_2=6mm, l_3=5.439mm, l_4=7.029mm, x_0=5.25mm, y_0=4.941mm.

When l_1 and l_2 coincide and $AC_1=AB_1+BC_1=l_1+l_2$=9mm, rod l_3 swings to the highest point.

In $\triangle AC_1D$, from the cosine theorem:

$$\alpha_1 = \arccos\frac{(l_1+l_2)^2-l_3^2-l_4^2}{2l_3l_4} = \frac{9^2-5.439^2-7.029^2}{2\times 5.439\times 7.029} = 88.493^\circ$$
$$\theta_1 = \arccos\frac{l_3^2-(l_1+l_2)^2-l_4^2}{2(l_1+l_2)l_4} = \frac{5.439^2-9^2-7.029^2}{2\times 9\times 7.029} \quad (1)$$

When l_1 and l_2 coincide, $AC_2=B_2C_2-AB_2=l_2-l_1$=3mm, and rod l_3 swings to the lowest point.

In $\triangle AC_2D$, from the cosine theorem:

$$\alpha_2 = \arccos\frac{(l_1-l_2)^2-l_3^2-l_4{}^2}{2l_3l_4} = \frac{3^2-5.439^2-7.029^2}{2\times 5.439\times 7.029} = 23.743^\circ \quad (2)$$

Therefore, the swing angle of one wing of the bionic butterfly is

$$\alpha = \alpha_1 - \alpha_2 = 88.492^\circ - 23.743^\circ = 64.749^\circ \quad (3)$$

In Rt$\triangle ADO$

$$\theta_2 = \arctan\frac{y_0}{x_0} = \arctan\frac{4.941}{5.25} = 43.263^\circ \quad (4)$$

Therefore, the angle between the pole positions of the four-bar mechanism is

$$\theta = 90^\circ - \theta_1 - \theta_2 = 90^\circ - 37.165^\circ - 43.263^\circ = 9.572^\circ \quad (5)$$

The emergency return characteristics are

$$K = \frac{180° + \theta}{180° - \theta} = \frac{180° + 9.572°}{180° - 9.572°} = 1.112 \quad (6)$$

This bionic butterfly has obtained the most efficient movement mode through experimental tests of pitch attitude and propulsion efficiency, that is, flapping its wings at a frequency of 4 times per second. The starting position of flapping is at an angle of approximately 40° with the horizontal plane where the main trunk is located. position, flutter down to a position with an angle of about -25°, then flutter up, and flutter up and down in this manner. After estimation, this design intends to achieve the effect: the maximum speed of the bionic butterfly aircraft can reach 1.5m/s.

3.5 Bionic butterfly wing structure design

The left fin assembly and the right fin assembly have the same structural and dimensional parameters and are set symmetrically on the left and right sides of the main torso. They consist of an outer contour bar, a main drive bar, a fin vein, a fin root connector, and a PET fin surface, as shown in Fig. 6. Among them, the wing root connectors adopt a fan-shaped structure with a thickness of 0.5 mm. the outer contours of the wings of the left-wing assembly and the right-wing assembly are formed by the bending of the outer contour rod, which is made of carbon fiber rods, and the front and rear ends of which are glued to the front and rear positions of the wing root connectors. The middle part of the outer contour rod is bonded to three wing veins in sequence from front to back, and the length of the three wing veins decreases in sequence from front to back, and the lengths of the three wing veins are all smaller than the length of the main drive rod. By means of the fin veins in the rear part, a concave structure can be formed in the middle part of the carbon fiber rod, and this structure can make the front part and the rear part of the outer contour rod convex. By means of the wing veins in the middle and the front portion, the middle structure of the outer contour of the wing can be stabilized and the transition between the front and the rear convex portions of the outer contour of the wing can be smoothed. The main drive rod connector with a blind hole structure fixed in the front part of the outer contour rod is located in the front convex part to connect the main drive rod. Through our optimized design, it is possible to make the output power of the drive motor, which is transmitted to the drive arm through the cam linkage mechanism, drive the wing assembly to realize the fluttering motion.

The wing vein connector, the main drive rod connector, the wing root connector, and the wing vein and main drive rod parts are all made of carbon fiber. In the design of the wing, the rear part of the outer contour is specially designed as a U-shape structure, which not only optimizes the stability of the wing but also the convex part of the wing at the rear, we cleverly fix it to the wing connection holes within the end of the middle and rear wing brackets of the main torso, which is an innovative innovation that makes the wing assembly securely fastened to the main torso part. Through this precise design, the stability of the wing assembly during the tumbling movement is finally realized, and the flopping phenomenon during the movement is avoided.

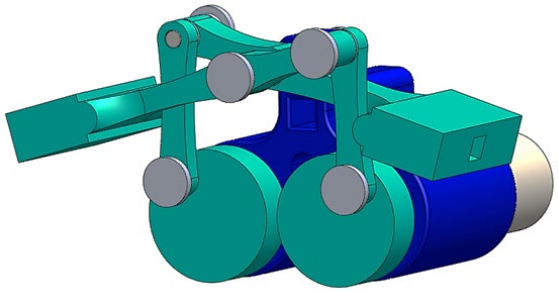

Figure 6. Transmission mechanism.
Source: own elaboration

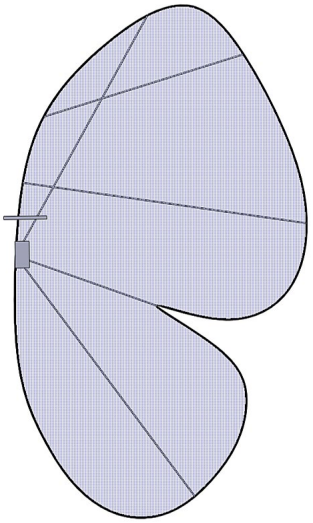

Figure 7. Butterfly wings design.
Source: own elaboration

3.6 Bionic butterfly control system design

The control circuit of our small bionic butterfly wing flutterer uses the STM32F401 microcontroller as the main control chip. The chip has a dynamic power consumption adjustment function, which can achieve a power consumption as low as 128μA/MHz in the operation mode, and at the same time, it has a strong performance and high integration degree, which enables us to ensure the processing speed and at the same time, reduce the burden of the whole machine and optimize the power consumption of the whole machine. The control circuit can independently control the speed of the two motors, and through mechanical transmission can realize the differential motion of the wings to realize the turn. The control circuit also integrates a voltage regulator circuit using a PW2057 voltage regulator chip to adapt to different specifications of the power supply. In order to meet the needs of the remote-control track, we have also reserved the pins required for remote control reception in the control circuit. Our solution provides a control circuit schematic diagram as shown in Fig. 8 and a PCB diagram as shown in Fig. 9.

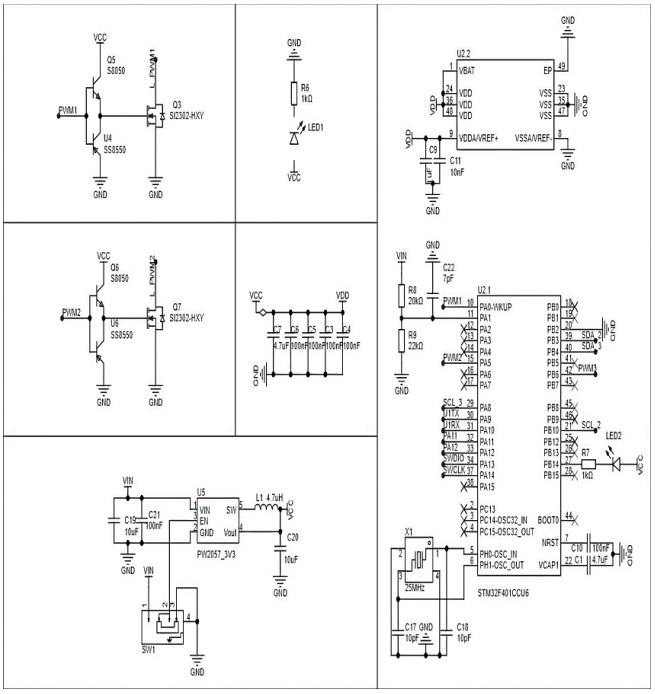

Figure 8. Control system schematic.
Source: own elaboration

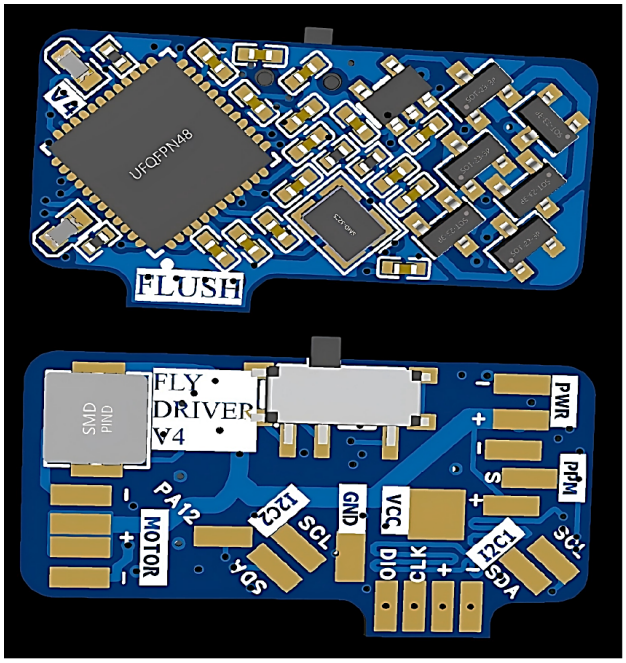

Figure 9. Control system PCB diagram.
Source: own elaboration

The flight control board is 25mm long, 12mm wide, and weighs only 0.9g, with redundant structures such as through holes and rows of pins removed, the integration level is quite high. It is worth mentioning that the flight control board also integrates a burn-in Debug interface and two IIC interfaces. The dual IIC interfaces can be interconnected with external modules such as WIFI/BT module, GPS module, IMU module, etc., reflecting the idea of intelligence.

At the level of the control algorithm, we use pulse width modulation (PWM) output to achieve accurate and stable control of the motor.

The power supply unit of our Bionic Butterfly Puffer is a 100mAh, 3.7V Li-Polymer battery, which operates at 15C and up to 30C. It can ensure excellent performance and sufficient endurance under a lighter mass and can be used for the Bionic Butterfly Puffer to fly for 3-4 minutes.

4 Simulation

4.1 Stress analysis

The Abaqus finite element numerical simulation technique was used to investigate the bending performance of the butterfly wing model under the reaction force as the point force, in which the material properties were assigned to the wing membrane and the wing veins separately. According to the results in Fig. 10, the butterfly wings have the most concentrated stress at the wing root, which suffers the most serious load damage, and the stress is transferred from the wing root to the wing edge along the wing vein; the load application position obviously affects the stress distribution of the wings, with the load at the edge of the wing vein, where the overall stress is more uniform, and the load in the middle of the wing vein, where the stress is concentrated in the application position with the position of the wing root; and the stress distribution increases with the increase of load.

According to the simulation results, we carry out several iterations of the wing structure, and the main optimization directions are the strengthening design of the wing root connection, the effect of different wing vein distribution on the stress distribution, the effect of spraying and dispensing process on the stress distribution of the wing, and the selection of the wing vein and wing surface materials.

4.2 Flow field analysis

The motion analysis of our bionic butterfly flutter aircraft is carried out using the Fluent module of ANSYS. The transient overlapping mesh method is used, and the simulation parameters are as follows: the wing flapping frequency is 4Hz, the flight speed is 0.3m/s, the air inlet velocity is 1m/s, and the gravitational acceleration is 9.81m/s. After the simulation analysis, the pressure and velocity clouds on the yz-plane at different moments in a cycle are obtained as in Fig. 11. It can be seen in Fig. 10 that when the wing is flapping down, the lower surface pressure of the fin is greater than the upper surface pressure of the fin, and there is a wing end vortex generated. surface pressure is greater than the upper surface pressure of the fin, and this pressure difference generates the lift of the fin, and there is a vortex generated at the end of the fin. The velocity of the flow field on the upper surface of the wing is greater than that on the lower surface of the wing, and a vortex is formed on the upper surface of the wing. The flow field generated by the fin during uptake is just the opposite of downtime, there is drag generated to provide forward thrust, and the vortices generated at the end of the wing are weaker than during downtime.

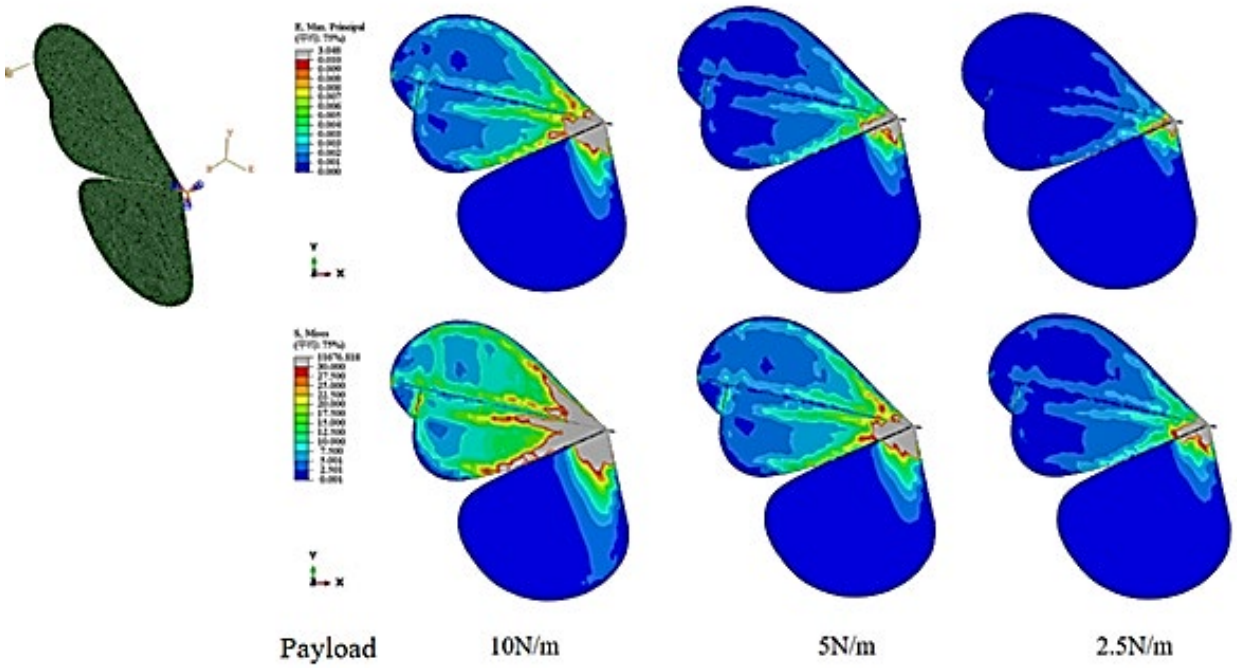

Figure 10. Stress analysis.
Source: own elaboration

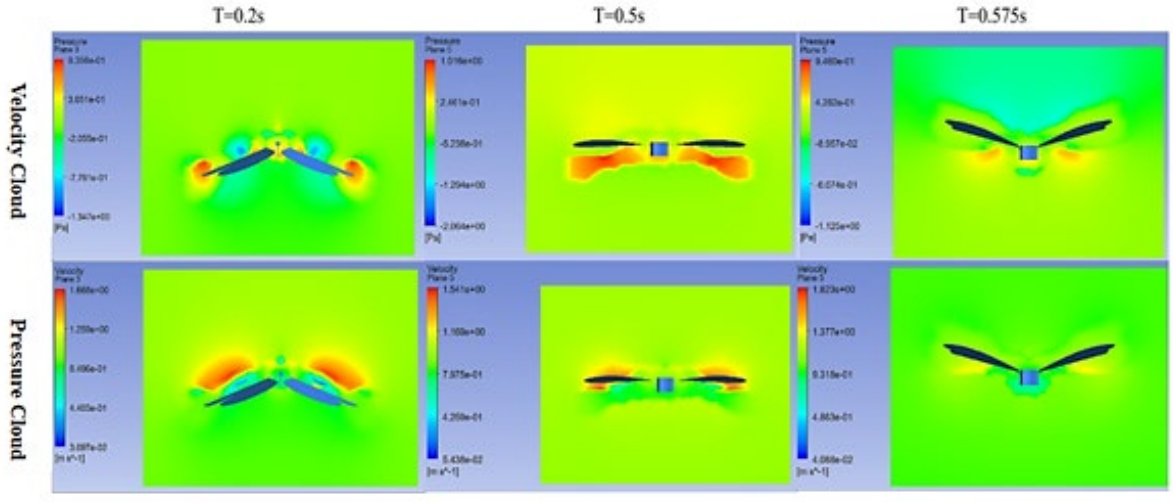

Figure 11. Flow field analysis.
Source: own elaboration

1 Data computation and analysis

v is the velocity of the butterfly as it swings its wings upward, F_q is the thrust on the wings, and F_f is the drag on the wings, according to the theory of the swashplate effect:

$$F_q = 2C_c \sin\theta \cos\theta \rho k v^2 \quad (7)$$

$$F_f = 2C_c \sin^2\theta \rho k v^2 \quad (8)$$

From the equation it can be seen that θ is near maximum thrust at about 45°, and drag is close to zero.

$$\Delta v = v \sin\theta \quad (9)$$

$$v_a = \Delta v \cos\theta = v \sin\theta \cos\theta \quad (10)$$

$$v_c = \Delta v \sin\theta = v \sin^2\theta \quad (11)$$

$$\xi = \frac{v_a}{v_c} \tag{12}$$

Since different beat angles φ correspond to different headway angles θ, the headway angle is a function of the beat angle, and the total resistance after integration can be written as:

$$F_f = 2c\rho\int_{r0}^{R} k\int_{-\varphi}^{\varphi} v^2 \sin\,\theta\cos\,\theta dr d\varphi \tag{13}$$

Total lift is:

$$\begin{aligned} F_q &= 2c\rho\int_{r0}^{R} k\int_{-\varphi}^{\varphi} r v^2 \sin^2\,\theta dr d\varphi \\ &= 4c\varphi(R^2 - r0^2)\rho k v^2 \sin^2\,\theta \end{aligned} \tag{14}$$

where, c is the air viscosity coefficient taken as 17.9×10^{-6}, flapping angle $\varphi = 75°$, distance from the tip of the wing to the symmetry plane of the butterfly's body R = 285mm, distance from the root of the wing to the symmetry plane of the butterfly's body r_0 = 40mm, wing area k=10563, and θ is the angle of approach taken as 30-45°.

When the flight speed is v=4m/s, F_p is about 0.34N, and this lift is the lift that a single wing can provide, so the total lift F=0.68N.

2 Photograph of the real object

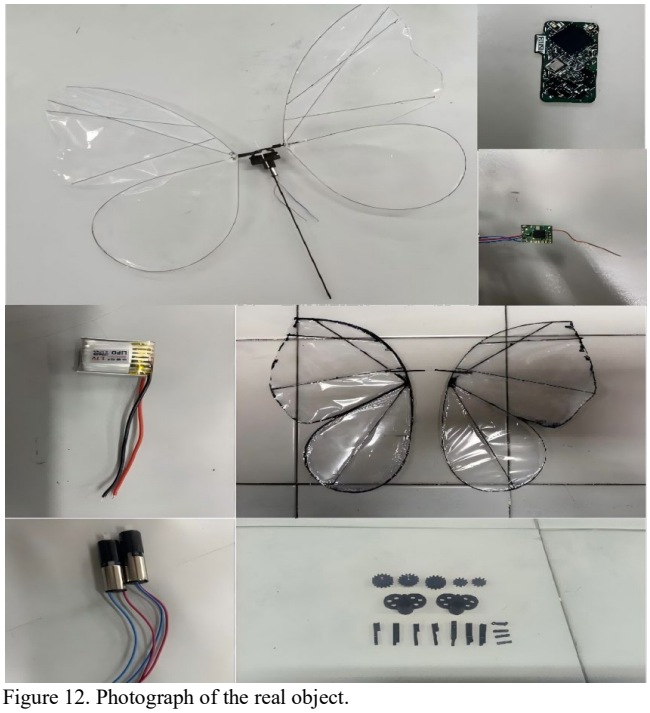

Figure 12. Photograph of the real object.
Source: own elaboration

3 Conclusion

Inspired by the excellent maneuverability, agility, and adaptability shown in the flight of butterflies, this study proposes the design of a small remote-controlled bionic butterfly flyer. This paper is devoted to simulating the flight characteristics of butterflies, including maneuverability and adaptability. At the theoretical level, the forces on the wings in the flapping and gliding states are analyzed in detail, and the lift force in the gliding state is calculated. Subsequently, the design proposal was modeled by 3D modeling software, and the strength of the wing was verified using finite element analysis software to ensure the reasonableness of the design. Further, a prototype of a small remote-controlled bionic butterfly flyer was fabricated by selecting appropriate materials and designing the drive structure and hardware circuit. The prototype is controlled by a remote controller to control the flight path and driven directly by a servo, with a wingspan of 29.8 cm, an overall length of 17.9 cm, and an overall weight of 11.4 g. The experimental results show that the lifting force of the prototype reaches 0.68 N, and the flapping frequency is stable at about 4 Hz, with a maximum flapping angle of 65°.

References

[1] Huang, H., He, W., Fu, Q., He X., and Sun, C., A Bio-Inspired Flapping-Wing robot with cambered wings and its application in autonomous airdrop, in: IEEE/CAA Journal of Automatica Sinica, 9(12), pp. 2138-2150, 2022. DOI: https://doi.org/10.1109/JAS.2022.106040.

[2] Fu, Q., Wang, X., Zou, Y., and He, W., A miniature video stabilization system for flapping-wing aerial vehicles, Guid. Navigation Control, 2(1), 2022. DOI: https://doi.org/10.1142/S2737480722500017.

[3] He, W., Mu, X., Zhang, L., and Zou, Y., Modeling and trajectory tracking control for flapping-wing micro aerial vehicles, in: IEEE/CAA Journal of Automatica Sinica, 8(1), pp. 148-156, 2021. DOI: https://doi.org/10.1109/JAS.2020.1003417.

[4] Huang, H., Wu, X., Wang, T., Sun Y., and Fu, Q., Reinforcement learning control for a flapping-wing micro aerial vehicle with output constraint, Assem. Automat., 42(6), pp. 730-741, 2022. DOI: https://doi.org/10.1108/AA-05-2022-0140

[5] Qiao, H., Wu, Y.-X., Zhong, S.-L., Yin P.-J., and Chen, J.-H., Brain-inspired intelligent robotics: theoretical analysis and systematic application, Mach. Intell. Res., 20(1), pp. 1-18, 2023. DOI: https://doi.org/10.1007/s11633-022-1390-8

[6] Zhu, Y., Huang, H., Wang, Y., Han Z., and Zhong, J., Structure design and mathematical modeling of bionic butterfly flapping wing aircraft, in: 2021 IEEE International Conference on Mechatronics and Automation (ICMA), Takamatsu, Japan, 2021, pp. 1249-1254. DOI: https://doi.org/10.1109/ICMA52036.2021.9512601.

[7] Zhang, Y., Wang, X., Wang, S., et al., Kinematic and aerodynamic investigation of the butterfly in forward free flight for the butterfly-inspired flap wing air vehicle[J]. Applied Sciences, 2021, 11(6), pp. 2620. DOI: https://doi.org/10.3390/app11062620

[8] Huang, H., He, W., Zou, Y., and Fu, Q., USTButterfly: a servo-driven biomimetic robotic butterfly, in: IEEE Transactions on Industrial Electronics, 71(2), pp. 1758-1767, 2024. DOI: https://doi.org/10.1109/TIE.2023.3260355.

Y. Mao, is currently pursuing the BSc. degree in Robotic Engineering at Jiangnan University, Wuxi, China. His research interests include computer vision and robot control.
ORCID: 0009-0000-2842-1761

J. Lao is currently pursuing the BSc. degree in Mechanical Engineering at Jiangnan University in Wuxi, China. His research focus on motion simulation and mechanics.
ORCID: /0009-0003-5749-6297

F. Wu, is currently pursuing the BSc. degree in Mechanical Engineering at Jiangnan University, Wuxi, China. His research interests include exoskeletons, robot control, and bionic devices.
ORCID: 0009-0005-6454-2540

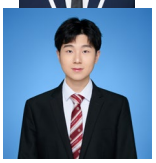

M. Li, is currently pursuing the BSc. degree in Robotic Engineering at Jiangnan University, Wuxi, China. His research interests include SLAM, autonomous driving, and robot control.
ORCID: 0009-0007-3454-8073

DYNA
http://dyna.medellin.unal.edu.co/

UNIVERSIDAD NACIONAL DE COLOMBIA

Analysis of scientific production on environmental risk assessment in ecosystems with a circular economy

Yasniel Sánchez-Suárez [a], José Armando Pancorbo-Sandoval [b], Sonia Emilia Leyva-Ricardo [c] & Verenice Sánchez-Castillo [d]

[a] *Facultad de Ingeniería Industrial, Universidad de Matanzas. Centro de Estudios Futuro, Matanzas, Cuba. yasnielsanchez9707@gmail.com*
[b] *Facultad de Derecho, Ciencias Administrativas y Sociales, Universidad UTE Sede Santo Domingo, Santo Domingo de los Tsáchilas, Ecuador. jose.pancorbo@ute.edu.ec*
[c] *Facultad de Ciencias de la Ingeniería e Industrias, Universidad UTE Sede Santo Domingo, Santo Domingo de los Tsáchilas, Ecuador. sonia.leyva@ute.edu.ec*
[d] *Facultad de Ingeniería, Universidad de la Amazonia, Florencia, Colombia. ve.sanchez@udla.edu.co*

Received: June 3rd, 2024. Received in revised form: November 8th, 2024. Accepted: November 18th, 2024.

Abstract
Ecosystems are currently at risk, and scientific methods have been developed to assess these impacts. In this scenario, the circular economy makes it possible to reuse raw materials and reduce waste. The objective of the research is to analyze the scientific production related to the evaluation of environmental risks in ecosystems with a circular economy approach. Quantitative research was carried out, with a retrospective and descriptive approach, from a bibliometric study in the SCOPUS database in the period 2014 - 2024. The peak of research was 4, where research articles predominated with 7 in 12 areas of knowledge. The most producing country was the United States. The most producing journal was Thunderbird International Business Review with 159. four research lines and their gaps were identified. Environmental risk assessment is much more than a legal requirement; it is an opportunity to demonstrate an organization's commitment to sustainability.

Keywords: bibliometric analysis; circular economy; ecosystems; quantitative research; environmental risks.

Análisis de la producción científica sobre la evaluación de riesgos ambientales en ecosistemas con enfoque de economía circular

Resumen
Los ecosistemas en la actualidad se encuentran en riesgo, por lo que se han desarrollado métodos científicos para evaluar estos impactos. En este escenario, la economía circular permite reutilizar materias primas y reducir los residuos. El objetivo de la investigación es analizar la producción científica relacionada con la evaluación de riesgos ambientales en ecosistemas con enfoque de economía circular. Se llevó a cabo una investigación cuantitativa, con un enfoque retrospectivo y descriptivo, a partir de un estudio bibliométrico en la base de datos SCOPUS en el período 2014 – 2024. El pico de investigaciones fue 4, donde predominaron los artículos de investigación con 7 en 12 áreas del conocimiento. El país más productor fue Estados Unidos. La revista más productora fue Thunderbird International Business Review con 159. Se identificaron 4 líneas de investigación y sus brechas. La evaluación de riesgos ambientales es mucho más que un requisito legal; constituye una oportunidad para demostrar el compromiso de una organización con la sostenibilidad.

Palabras clave: análisis bibliométrico; economía circular; ecosistemas; investigación cuantitativa; riesgos ambientales.

1 Introduction

The evolution and formation of diverse ecosystems on our planet was due to its physical, geological and geographical conditions [1]. An ecosystem is a functional unit of nature [2], which includes living organisms (biocenosis) [3] and their physical environment (biotope) [4], interacting as a closed system [5]. The main characteristics of an ecosystem

How to cite: Sánchez-Suárez, Y., Armando Pancorbo-Sandoval, J.A., Leyva-Ricardo, S.E., Sánchez-Castillo, V., Analysis of scientific production on environmental risk assessment in ecosystems with a circular economy. DYNA, 91(234), pp. 116-125, October - December, 2024.

include species diversity [6], trophic structure [7], nutrient [8] and energy cycling [9], and interactions between species and their environment [10].

Ecosystems are dynamic and subject to constant change due to internal and external factors [11]. They are classified into terrestrial of various types, including forests, grasslands, deserts, tundra's, mountains and aquatic ecosystems are divided into freshwater (rivers, lakes, marshes and wetlands) [12] and marine (oceans, seas, coral reefs and estuaries) ecosystems, these cover more than 70% of the earth's surface and harbor a great diversity of marine life [13].

All ecosystems play a crucial role in climate regulation [14] and habitats for a wide range of species [15]. They have unique characteristics in terms of climate, soil, flora and fauna [16]. For example, forests are rich in biodiversity and act as carbon sinks [17], deserts are extreme ecosystems with arid conditions and a diversity of life adapted to such conditions [18], while seas contain high dissolved salt content, with producer, consumer and decomposer organisms forming food chains [19].

Environmental risks are factors that can damage the natural environment [20], either by natural phenomena or by human action. These risks can be of various kinds, from air, water and soil pollution (depending on the type of ecosystem and its characteristics) [21], to the generation of hazardous waste. Environmental risks can be classified into natural and anthropogenic [22]. Natural environmental risks are caused by natural phenomena that are beyond our control, but that cause great damage to the ecosystem [23], while anthropogenic environmental risks are those caused by human action [24].

Environmental risk assessment is a critical process used to estimate the probability of an adverse outcome from environmental changes caused by natural and human activities [25]. This process follows the scientific method of determining the hazard and risks to the health and welfare of species associated with exposure to pollution [26]. There are several methodologies for conducting environmental risk assessments, including:

- Failure Mode and Effects Analysis (FMEA) [27],
- Fault Tree Analysis (FTA) [28],
- Checklists [29],
- Functional Analysis of Operability (FAO) [30],
- Layer of Protection Analysis (LOPA) [31],
- Ishikawa Diagram or Cause and Effect Diagram [32],
- Theory of Constraints [33].

Environmental risk assessment has a significant impact on business management today [34]. It allows organizations to identify and assess the impacts of their activities on the environment, in turn facilitating informed decision making to minimize their environmental footprint [35]. In addition, it is considered crucial to comply with government regulations and improve the company's reputation in order to achieve greater competitiveness [36,37].

In this scenario, and with the aim of reducing the consumption of raw materials that affect ecosystems through a change in the current model (linear model of production and consumption), the circular economy paradigm [38-40] arises in order to promote the generation of environmental impacts [39] and sustainable spaces based on cultural diversity [41].

Among the objectives of this management approach are: to generate economic prosperity, protect the environment and prevent pollution [42]. This economic model, while proposing the reuse of waste and its utilization as new resources, focuses on an innovative change in the design of each phase of the process, which allows the adoption of new ideas that enhance regeneration and eco-design [43].

It is a method that seeks not only sustainable production, but also responsible consumption, which implies creating environmental quality, economic prosperity and social equity, for the benefit of current and future generations [42]. In this sense, the assimilation of this management philosophy by the different business systems in terms of expanding their responsible practices and respect for the environment, will increasingly reduce ecosystemic risks directly or indirectly, and will become a competitive advantage due to its alignment with the objectives of sustainable development.

Consequently, the objective of this research is to analyze the scientific production related to the evaluation of environmental risks in ecosystems with a circular economy approach.

2 Methodology

Research was conducted under the quantitative paradigm [44,45], with a retrospective and descriptive approach, based on a bibliometric study with the aim of analyzing indicators that allow describing science and its triangulation in order to identify lines of research and possible future work agendas [46,47].

2.1 Selection and exclusion criteria

For the selection of the documents, a set of criteria were established with the aim of ensuring the impact, relevance and quality of the research found [48]. Inclusion criteria focused on the identification and collection of the most relevant articles in English and Portuguese language in the period 2014 - 2024 (last 10 years), in the databases: SCOPUS (https://www.scopus.com/), for its impact at international level grouping mainstream journals and Lens (https://www.lens.org/) for its extensive library of research.

The exclusion criteria were to eliminate all those studies that did not address environmental risks in ecosystems and that in turn these analyses did not have a focus on the circular economy, as well as all those articles that were duplicated after the integration of both databases in the EndNote X8 bibliographic manager. This review was carried out independently by two researchers, who initially applied the strategies, presented and discussed the results together as feedback until reaching the final version.

2.2 Search strategy

The main thematic descriptors identified for the search strategy were: "environmental risks", "ecosystems" and "circular economy". The search formula was: TITLE-ABS-KEY (("environmental risks" OR "environmental griess") AND ("ecosystems" OR "ecosystems") AND ("circular economy" OR "economic circular")).

Table 1
Search results

Parameters	Quantity
SCOPUS	15
Lens	152
Total	167
Duplicates	0

Source: Own elaboration.

It was conducted on April 4, 2024. Table 1 shows a summary of the search results. The information was downloaded in a ".RIS" format for analysis and processing.

2.3 Bibliometric indicators

In the analysis of bibliometric indicators, the source of information was combined between both databases and is described below:

2.3.1. Trend indicators

- Scientific production per year: the behavior of the research was studied, its frequency over time, and the trend line adjusted to the highest R2 value was plotted to determine the confidence level of the function.

2.3.2. Production indicators

- Scientific production by type of document: documents were classified according to their type (articles, books, etc.) and quantified.
- Scientific production by area of knowledge: the amount of research by area of knowledge was quantified.
- Scientific production by country: the amount of research by country was quantified.
- Scientific production by institutional affiliation: the amount of research by institutional affiliation was quantified, these were related to countries based on a binary matrix (affiliation versus country), which was processed in the UCINET for Windows - Version 6 software and a network of institutional affiliation and its frequency was created.

Source of information: Obtained from the SCOPUS database. The .XLSX files were downloaded in Excel format and further processed using Microsoft Excel software. The country map was generated with the Lens platform, the density corresponds to the introduction and assimilation of results.

2.3.3. Impact indicators

The impact analysis was focused on indicators of quality and positioning of the journals in which the research was published; only SCOPUS journals were taken into account, as they were the ones with the highest impact during the period. Table 2 summarizes the main impact indicators analyzed.

Source of information: The QC are obtained from the file in ".RIS" format processed in the EndNote X8 bibliographic manager in the "Notes" section, where the sum of the number of citations of the articles of a journal, are the total citations. The IF, Q and H-index indicators were obtained from the SCImago Journal & Country Rank site (https://www.scimagojr.com/).

Table 2
Journal impact indicators

	Acronym	Description
Journal rankings	QC	Number of citations (QC): evaluates the number of citations received by the journal in the period analyzed.
	IF	Impact Factor (IF): analyzes the ratio between the number of citations received by a journal's articles during the previous two years and the number of articles published in those years.
	Q	Quartile (Q): analyzes the relevance of a journal within all journals in the area of knowledge, divided into four quartiles Q1, Q2, Q3 and Q4.
	H-index	Measures the productivity of a journal in correlation with the citation impact of publications.

Source: Own elaboration.

2.4 Building knowledge maps

- Keyword co-occurrence analysis: network, overlay and word cloud knowledge maps were constructed to compare the results in both databases, the most predominant terms and the clusters in which they are grouped. From the cluster analysis, possible lines of research are determined.

Specifications of each of the maps according to the analysis:

Network bibliometric map: an analysis of the relationship of keywords was performed based on the network study and the identification of main clusters.

Bibliometric overlay map: the temporal evolution of keywords was studied in order to identify the most recent and novel terms.

Word cloud map: the frequency of occurrence of keywords and those of greater relevance in the Lens database were analyzed for comparative analysis.

- Analysis of collaboration between countries: knowledge maps were constructed with the objective of analyzing collaboration or not between countries, alliances or clusters on the subject and possible inferences of knowledge transfer between regions, with emphasis on the role of Latin America.
- Author relationship analysis: the relationships or not between authors were studied based on the study of co-citations and alliances in publications through inter-institutional collaboration.
- Citation analysis: an analysis of the level of citations per author / publications was made, where the level of citations per period and the possibility of access (open access) or not were contrasted to compare these citation levels.

Table 3.
Sources of knowledge maps

Analysis - Maps	Sources of procurement
Keyword co-occurrence analysis	
Network bibliometric map Overlay bibliometric map	Vosviewer
Word cloud map	Lens
Analysis of cross-country collaboration	
Network bibliometric map	Vosviewer
Author relationship analysis	
Overlay bibliometric map	Vosviewer
Citation analysis	
Citation map	Lens

Source: Own elaboration.

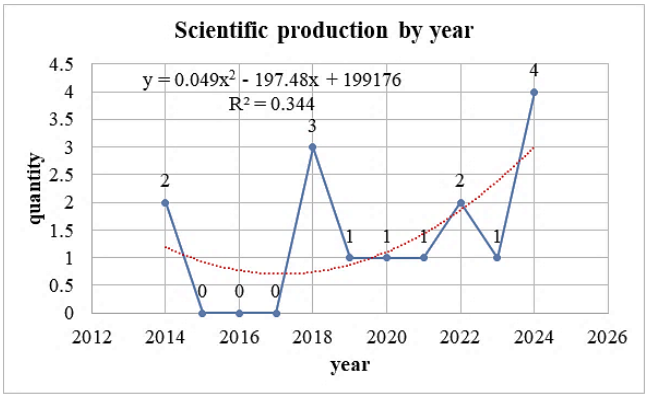

Figure 1. Scientific production by year.
Source: Own elaboration.

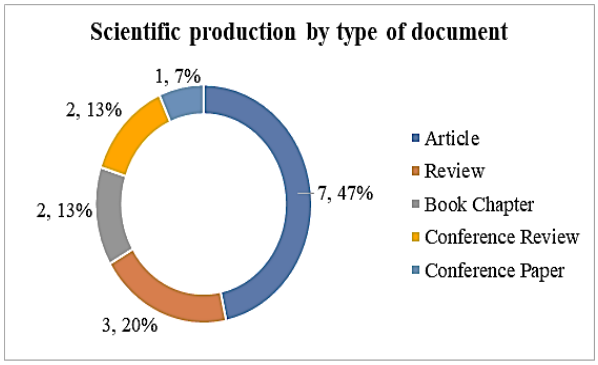

Figure 2. Scientific production by type of document.
Source: Own elaboration.

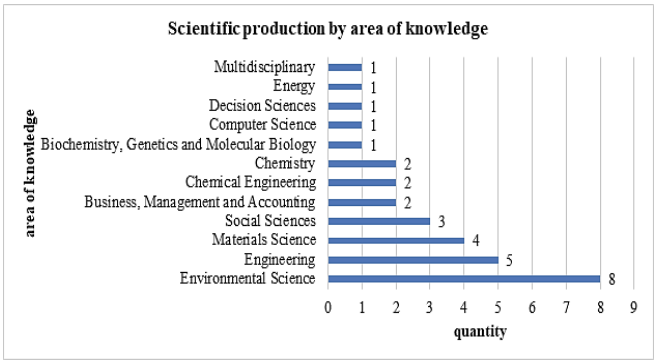

Figure 3. Scientific production by area of knowledge.
Source: Own elaboration.

Table 3 shows the relationship between the analyses and knowledge maps described and the platforms or ways of obtaining them.

3 Discussion of results

The behavior of the investigations was heterogeneous (Fig. 1), its behavior was between zero and four investigations, in the period 2015 - 2017 no investigations were found, while the trend is towards increase characterized by a polynomial function with a confidence level of 34.4 % with a maximum peak of four investigations in the year 2024.

Fig. 2 shows the distribution by type of research documents, where research articles predominated, representing 47 % of the total, followed by research papers with 20 %. Two book chapters and three events were found, two at the 2013 International Conference on Manufacture Engineering and Environment Engineering, MEEE 2013 and one at the 2022 8th International Engineering, Sciences and Technology Conference, IESTEC 2022, both with emphasis on environmental policies and their assimilation in industrial processes [49,50].

Research was identified in 12 areas of knowledge (Fig. 3), with a predominance of environmental sciences with eight investigations, followed by engineering and materials science with five and four investigations, respectively, where innovations related to the reuse of resources and water treatment to reduce environmental risks in ecosystems stood out [51-53].

Fig. 4 shows the analysis of scientific production by country, initially analyzing the amount of research by region, in the Americas the most productive country was the United States, with two studies, followed by Panama and Brazil, both with one study. The region with the highest results was Europe, where Spain and France led with two publications. In Asia, India was the country with the highest number of publications, with three articles.

On the other hand, when analyzing the assimilation and introduction of the results in the area of knowledge, it became evident that the most representative country was China through the creation of capacities to carry out an efficient transfer of this knowledge in terms of sustainable development and the adoption of social responsibility strategies in its actions for the protection of the environment [54,55]. Countries such as the United Kingdom, the United States, Australia and Russia also stood out.

Research was identified in 35 institutional affiliations, all on an equal footing with one research each; these were associated with their countries of origin by means of affinity diagrams that resulted in the preparation of the binary matrix and from its processing the institutional affiliation network was obtained (Fig. 5). The countries with the highest production by institutional affiliation were India and the United States with seven and six investigations, respectively, while in Latin America, Panama stood out with three institutions.

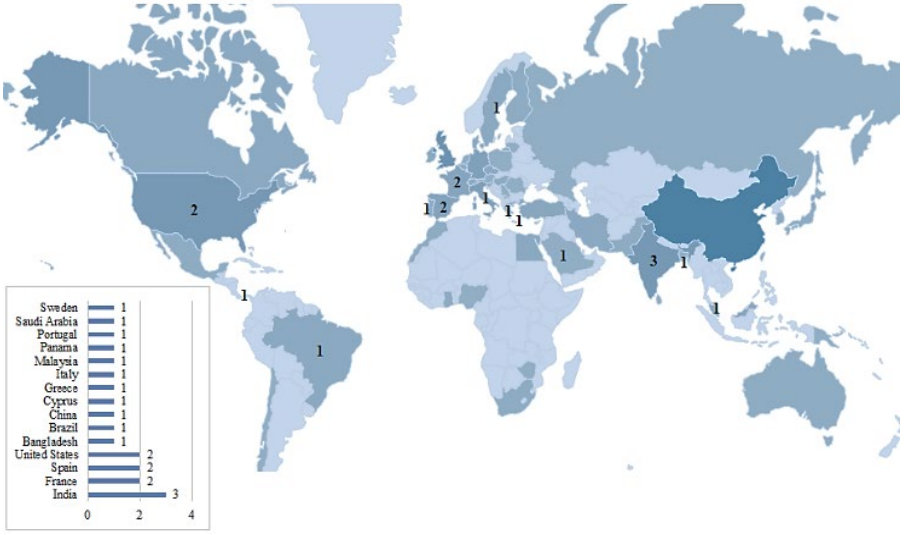

Figure 4. Scientific production by country.
Source: Own elaboration.

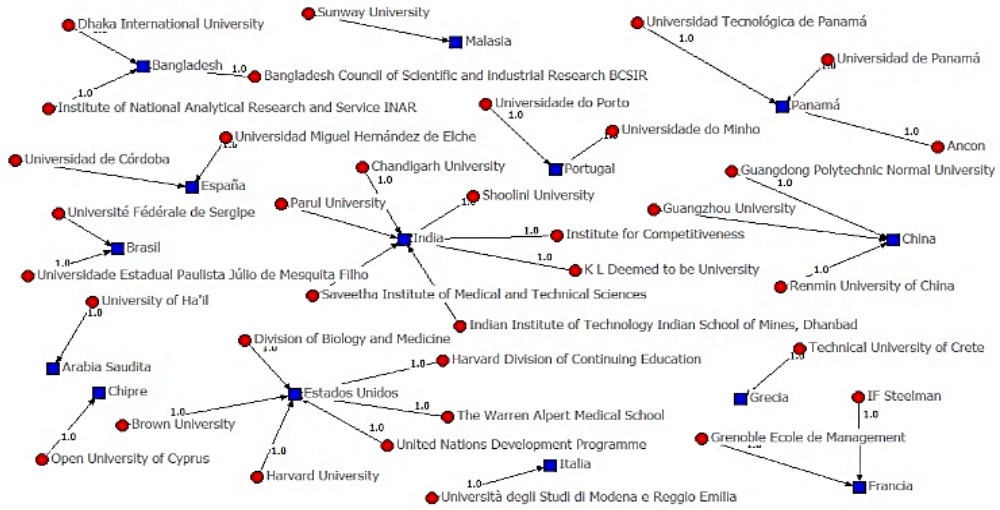

Figure 5. Institutional affiliation network.
Source: Own elaboration.

Research was identified in 14 journals, including one that published two papers resulting from events, the journal WIT Transactions on Engineering Sciences. Table 4 shows the ranking of the seven most cited journals, where the one that accumulated the highest number of citations during the period analyzed was Thunderbird International Business Review with 159 (n = 159) corresponding to the article "Circular economy business models in developing economies: Lessons from India on reduce, recycle, and reuse paradigms".

Journal of Hazardous Materials was the journal with the highest impact factor and h-index with a value of 2.95 (IF = 2.95) and 352 (H-index = 352) respectively. Regarding the quartile of the seven journals analyzed, one is not in any quartile, five are in quartile 1 (Q1) representing 71.43 % of the total and one is in quartile 3 (Q3).

Table 4
Journals ranking.

Journal	QC	IF	Q	H-index
1. Thunderbird International Business Review	159	0.51	Q1	51
2. Journal of Hazardous Materials	73	2.95	Q1	352
3. Environmental Science and Pollution Research	26	-	-	-
4. Water Alternatives	15	0.71	Q1	53
5. Sustainability (Switzerland)	5	0.67	Q1	169
6. Materiaux et Techniques	4	0.29	Q3	13
7. International Journal of Biological Macromolecules	3	1.25	Q1	191

Source: Own elaboration.

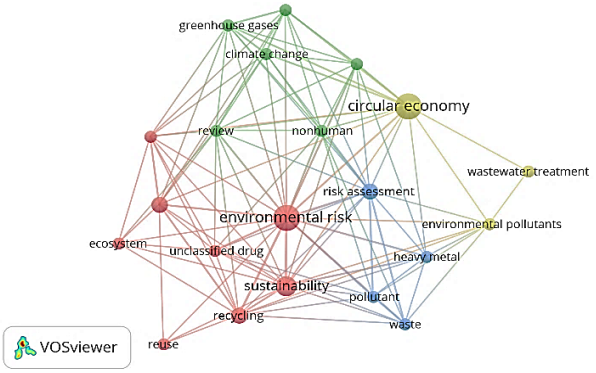

Figure 6. Word concurrency network map.
Source: Own elaboration.

Fig. 6 shows the map of cooccurrence of key words network, where four clusters and 21 items were identified, from the analysis of the interrelation between the items, four possible lines of research were identified:

- Cluster 1 (8 items) colored red focused on environmental risk assessment from a sustainable approach to ecosystems affected by misuse and deficient recycling strategies for unclassified drugs.
- Cluster 2 (6 items) in green focused on comprehensive reviews of existing studies on the impact of greenhouse gases on climate change, with a particular focus on non-human perspectives. How climate change affects non-human species, ecosystems and biodiversity in general will be investigated.
- Cluster 3 (4 items) in blue focused on environmental risk assessment and heavy metal waste management from an integrated approach to pollution mitigation in ecosystems.
- Cluster 4 (3 items) in yellow focused on the use of innovative strategies for the elimination of environmental pollutants with a circular economy approach for wastewater treatment.

An analysis of the most recently used keywords in the literature was carried out based on the study of the overlay keyword cooccurrence map (Fig. 7). The most recent research focused their studies on wastewater treatment from governance strategies focused on environmental management at local, regional and global levels [56], on applications in agriculture in support of germination [57,58], focus on sustainable innovation in water use [59] and strategies for water desalination and obtaining energy from chemical reactions [60].

On the other hand, research has also focused on fertilizer applications in agriculture [61], in addition to other research focused on the challenges and potentials in new precision agriculture systems [62].

Fig. 8 shows the keyword cloud map, with the objective of contrasting the results obtained from the network keyword co-occurrence map and the frequency of occurrence in the Lens database. The keyword with the highest frequency was environmental sciences with a frequency equal to 65 (n = 65), followed by biology with 63 (n = 63) and, ecology and business both with a frequency of 57 (n = 57).

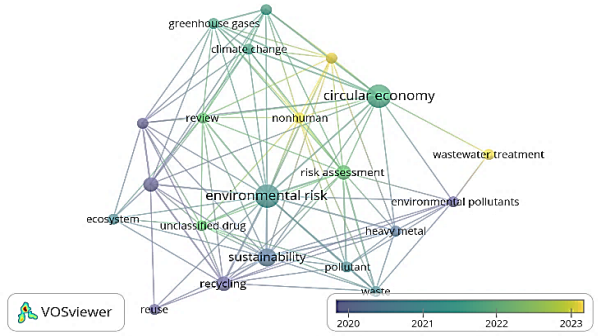

Figure 7. Word concurrency overlay map.
Source: Own elaboration.

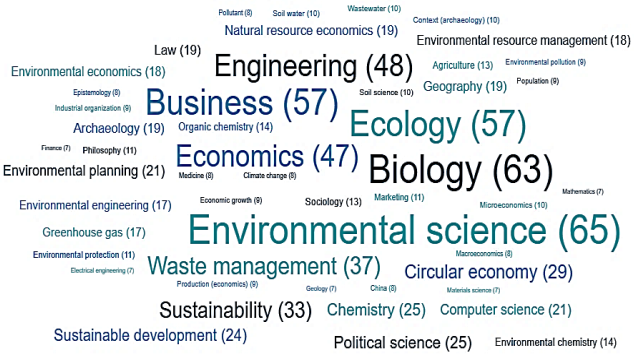

Figure 8. Word cloud map.
Source: Own elaboration.

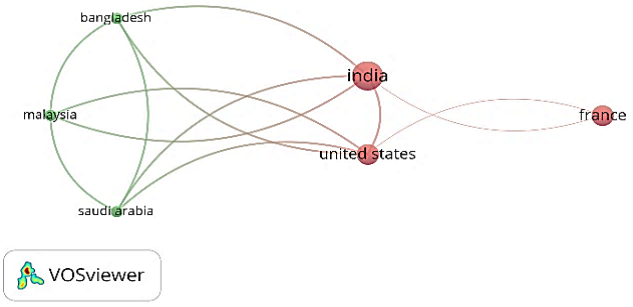

Figure 9. Country network.
Source: Own elaboration.

An analysis of the collaboration network between countries was carried out (Fig. 9), where two main clusters and six items were identified, three for each cluster:

- Cluster 1: green color with the countries Bangladesh, Malaysia and Saudi Arabia.
- Cluster 2: red color with the countries India, United States and France.

An analysis of authorial collaboration was performed (Fig. 10), where the overlay collaboration map was constructed to identify the authors who have published most recently in 2024, including: Trivedi, R., Upadhyay, T.K., Kha; Chang, K.F., Lin, C. and Bin, Y; Martins, M., Sousa, F and Soares, C and Olivera, R.V. and Maia, H.B. In isolation, 58 authors were found in the research, all with only one publication.

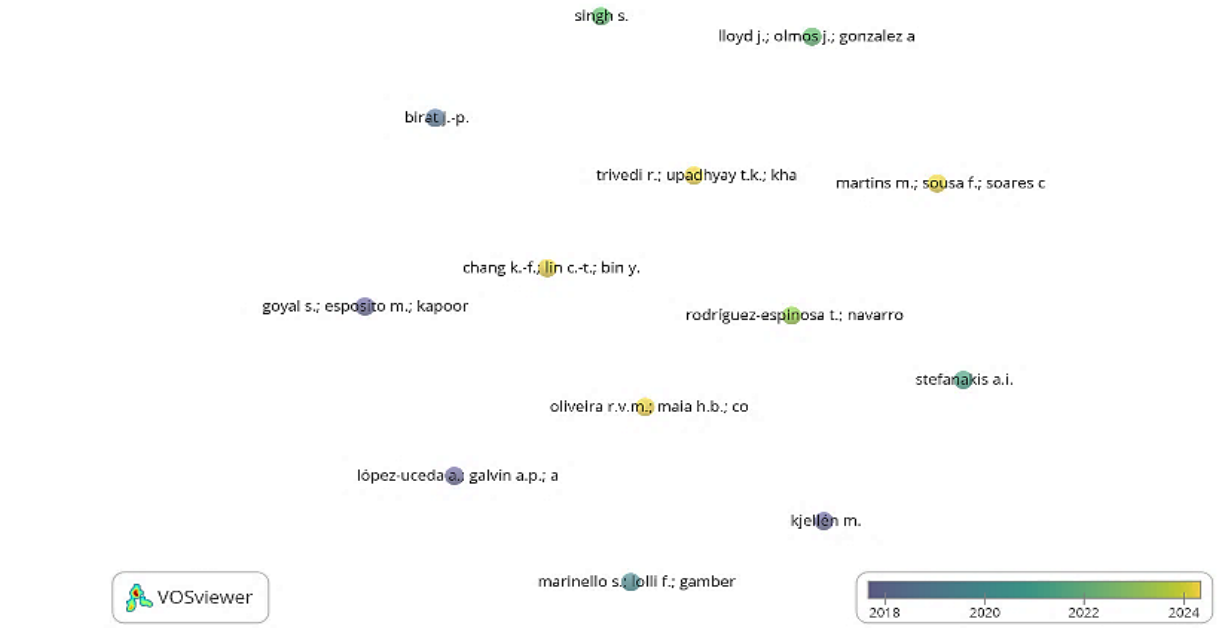

Figure 10. Author overlay network.
Source: Own elaboration.

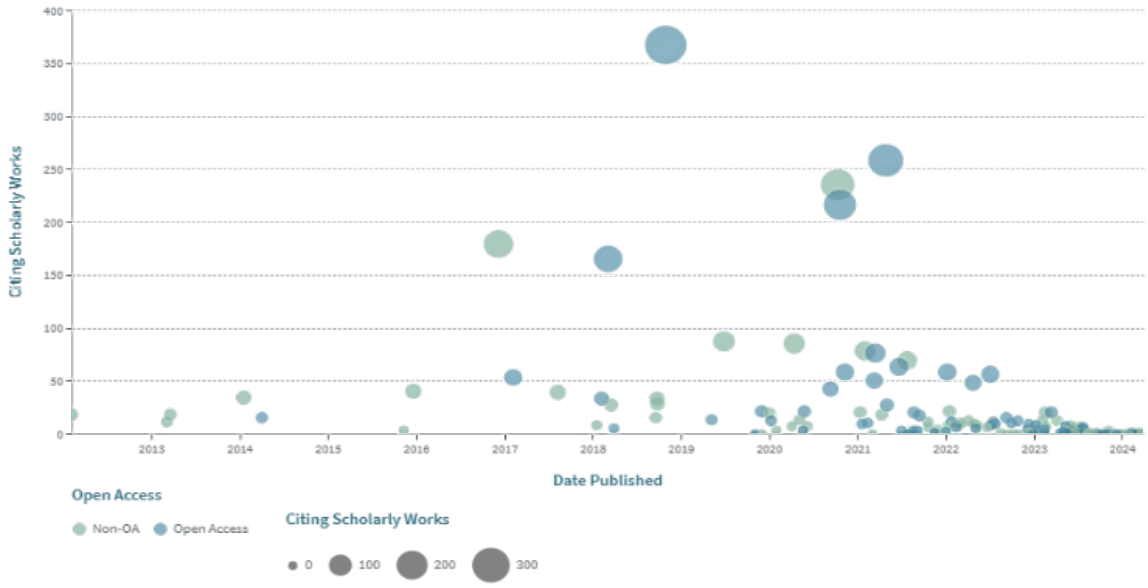

Figure 11. Citation map.
Source: Own elaboration.

Fig. 11 shows an analysis of the citation levels of the papers from the citation map generated in the Lens database, during the period 2013 - 2017 the citation levels did not exceed 50 citations and the papers that are not in open access predominated, while from 2017 these levels increased and the citations were balanced towards papers in open access, an element that demonstrates the transit of different publishers towards open science, with a maximum peak of more than 350 citations in the year 2019.

1 Conclusions

Environmental risk assessment is much more than a legal requirement; it is an opportunity to demonstrate an organization's commitment to sustainability and the well-being of the planet, through a focus on sustainable development and the fulfillment of the Sustainable Development Goals. In order to reduce environmental risks,

Table 5.
Agenda for future research.

Research cluster	Future research objectives
Cluster 1	• Identify and classify unclassified drugs that represent a significant environmental risk. • Study the impact of these drugs on different ecosystems. • Develop methods to measure and quantify this impact. • Investigate reuse and recycling strategies for these medicines. • Propose sustainable policies and practices for the management of unsorted drugs.
Cluster 2	• Review and synthesize existing literature on greenhouse gases and climate change. • Analyze the impact of climate change on non-human species and ecosystems. • Identify gaps in current research and suggest areas for future research. • Develop a framework for assessing the impact of climate change from a non-human perspective. • Propose mitigation strategies based on the findings of the review.
Cluster 3	• Develop methods to assess the risks associated with exposure to heavy metals in waste. • Research on how heavy metals act as contaminants in different environments. • Develop strategies and technologies for the safe and efficient management of waste containing heavy metals.
Cluster 4	• Investigate how the principles of the circular economy can be applied to wastewater treatment. • Study existing and emerging technologies for wastewater treatment. • Research on the different types of pollutants present in wastewater, including their origin, their behavior in the environment and their effects on human and ecological health.

Source: Own elaboration.

different initiatives have been developed, reflected in the 2030 agenda and the sustainable development goals; in this context, the circular economy plays an important role through the reuse of resources that optimizes the generation of waste to the environment.

The behavior of the research was heterogeneous with a maximum peak of four, research articles in the area of environmental sciences predominated. In the geographical area of the Americas, the main results were published in the United States, Panama and Brazil. The most productive journal was Thunderbird International Business Review with 159, while the Journal of Hazardous Materials had the highest impact with a value of 2.95.

From the keyword co-occurrence analysis, four lines of research were identified: environmental risk assessment from a sustainable ecosystem approach, the impact of greenhouse gases on climate change, environmental risk assessment and heavy metal waste management from an integrated approach, and the use of innovative strategies for the elimination of environmental pollutants.

1.1 Future research

In future work, we recommend generalization to other databases such as Web of Science, Sciencedirect or Scielo, the development of other bibliometric indicators, including the Price index, as well as the analysis of collaboration maps between institutions. On the other hand, to develop research that analyzes the visibility indicators of research and journals to maximize their impact and that in turn constitute the starting point for conducting bibliographic or systematic reviews of the literature. In this sense, an agenda for future research is proposed where specific objectives are identified for each of the research clusters identified (Table 5).

References

[1] Reyes-Fornet, A., Saabedra-García, J.F., Zúñiga-Igarza, L.-M., and Fornet-Hernández, E.B., Modelo conceptual del patrimonio natural en la gestión ambiental para la conservación de ecosistemas. Ecosistemas, 29(2), pp. 2003-2003, 2020. DOI: https://doi.org/10.7818/ECOS.2003

[2] Ao, A., Changkija, S., and Tripathi, S.K., Patterns of forest community diversity, regeneration potential and carbon storages along an altitudinal gradient in Eastern Himalaya, India. Environmental and Sustainability Indicators, 22, art. 100399, 2024. DOI: https://doi.org/10.1016/j.indic.2024.100399

[3] Zou, K., Zhu, Y., Jiang, Y., Ma, S., Li, M., Zhao, W., and Wang, J. Distinct stochastic processes drive bacterial community assembly and co-occurrence patterns with common antibiotic resistance genes in two highly urbanised coastal ecosystems of the Pearl River Estuary. Journal of Hazardous Materials, 459, art. 132161, 2023. DOI: https://doi.org/10.1016/j.jhazmat.2023.132161

[4] Buda, J., Łokas, E., Pietryka, M., Richter, D., Magowski, W., Iakovenko, N.S., Porazinska, D.L., Budzik, T., Grabiec, M., and Grzesiak, J., Biotope and biocenosis of cryoconite hole ecosystems on Ecology Glacier in the maritime Antarctic. Science of The Total Environment, 724, art. 138112, 2020. DOI: https://doi.org/10.1016/j.scitotenv.2020.138112

[5] Robert, J., Kubler, S., and Ghatpande, S., Enhanced lightning Network (off-chain)-based micropayment in IoT ecosystems. Future Generation Computer Systems, 112, pp. 283-296, 2020. DOI: https://doi.org/10.1016/j.future.2020.05.033

[6] Kassa, G., Bekele, T., Demissew, S., and Abebe, T., Plant species diversity, plant use, and classification of agroforestry homegardens in southern and southwestern Ethiopia. Heliyon, 9(6), art. e16341, 2023. DOI: https://doi.org/10.1016/j.heliyon.2023.e16341

[7] Giraldo, C., Cresson, P., Mackenzie, K., Fontaine, V., Loots, C., Delegrange, A., and Lefebvre, S., Insights into planktonic food-web dynamics through the lens of size and season. Scientific Reports, 14(1), pp., 2024. DOI: https://doi.org/10.1038/s41598-024-52256-4

[8] Bekchanova, M., Campion, L., Bruns, S., Kuppens, T., Lehmann, J., Jozefczak, M., Cuypers, A., and Malina, R., Biochar improves the nutrient cycle in sandy-textured soils and increases crop yield: a systematic review. Environmental Evidence, 13(1), art. 3, 2024. DOI: https://doi.org/10.1186/s13750-024-00326-5

[9] Zheng, Y., Li, G., Xing, Y., Xu, W., and Yue, T., Adsorption removal of mercury from flue gas by metal selenide: a review. Journal of Environmental Sciences (China), 148, pp. 420-436, 2025. DOI: https://doi.org/10.1016/j.jes.2023.02.034

[10] Chappell, J., and Thorpe, S.K.S., The role of great ape behavioral ecology in One Health: implications for captive welfare and re-habilitation success. American Journal of Primatology, 84(4-5), pp., 2022. DOI: https://doi.org/10.1002/ajp.23328

[11] Basole, R.C., Park, H., and Seuss, C.D., Complex business ecosystem intelligence using AI-powered visual analytics. Decision Support Systems, 178, art. 114133, 2024. DOI: https://doi.org/10.1016/j.dss.2023.114133

[12] Cui, M., Bao, B., Wu, Y., Hui, N., Li, M.-H., Wan, S., Han, S., Ren, F., and Zheng, J., Light grazing alleviates aeolian erosion–deposition effects on microbial communities in a semi-arid grassland. Ecological Processes, 13(1), art. 00510-y, 2024. DOI: https://doi.org/10.1186/s13717-024-00510-y

[13] Li, Q., Liu, R., Jing, Z., Wei, Y., Tu, S., Yu, H., Gao, H., and Yuan, P., High potential in synergizing the reduction of dissolved organic carbon concentration and carbon dioxide emissions for submerged-vegetation-

covered river networks. Journal of Environmental Sciences (China), 151, pp. 298-309, 025. DOI: https://doi.org/10.1016/j.jes.2024.04.007
[14] Zhang, X., Liu, L., Zhao, T., Wang, J., Liu, W., and Chen, X., Global annual wetland dataset at 30 m with a fine classification system from 2000 to 2022. Sci Data, 11, art. 310, 2024. DOI: https://doi.org/10.1038/s41597-024-03143-0
[15] Findlay, C.R., Aleynik, D., Farcas, A., Merchant, N.D., Risch, D., and Wilson, B., Auditory impairment from acoustic seal deterrents predicted for harbour porpoises in a marine protected area. Journal of Applied Ecology, 58(8), pp. 1631-1642, 2021. DOI: https://doi.org/10.1111/1365-2664.13910
[16] Soleimani, N., Rahimnejad, M., and Ezoji, H., An overview of electrochemical sensing strategies for methylparaben analysis. Journal of the Taiwan Institute of Chemical Engineers, 159, pp. 105457, 2024. DOI: https://doi.org/10.1016/j.jtice.2024.105457
[17] Ipinza, R., Barros, S., De la Maza, C.L., Jofré, P., and González, J., Bosques y Biodiversidad. Ciencia & Investigación Forestal, 27(1), pp. 101-132, 2021. DOI: https://doi.org/10.52904/0718-4646.2021.475
[18] Hernández-García, M., Granados-Sánchez, D., and Sánchez-González, A. Productividad de los ecosistemas en las regiones áridas. Revista Chapingo. Serie Ciencias Forestales y del Ambiente, [online]. 9(2), pp. 113-123, 2003. Available at: http://www.redalyc.org/articulo.oa?id=62913142002
[19] Palacios-Luis, F.J., and Solorzano-Tarazona, D.C., Determinación de plomo y cadmio en plancton de la playa de Pucusana durante el 2018, Tesis para optar el Título Profesional de Toxicólogo, Universidad Nacional Mayor de San Marcos Lima, Perú, 2024.
[20] Hryhorczuk, D., Levy, B.S., Prodanchuk, M., Kravchuk, O., Bubalo, N., Hryhorczuk, A., and Erickson, T.B., The environmental health impacts of Russia's war on Ukraine. Journal of Occupational Medicine and Toxicology, 19(1), art. 00398-y, 2024 DOI: https://doi.org/10.1186/s12995-023-00398-y
[21] Wang, X., and Wu, L., Intergenerational differences in the environmental concerns of plastic waste business owners: environmental knowledge, environmental risk exposure, and community connection as mediators. Humanities and Social Sciences Communications, 11(1), art. 03018-0, 2024. DOI: https://doi.org/10.1057/s41599-024-03018-0
[22] Navarro-Falcón, V.M., Jiménez-González, Y., Vera-Carroza, R., and Villa-Janeiro, M., Situación de la contaminación ambiental de un sector de Cienfuegos (Cuba) para el manejo integrado de zonas costeras. Ciencia en su PC, [online]. 1(3), pp. 1-15, 2022. Available at: https://www.redalyc.org/journal/1813/181374718001/181374718001.pdf
[23] Guo, Z., Hong, M., Shi, J., Zhang, Y., Qian, L., and Li, H., Risk assessment of unmanned underwater platforms in the South China Sea marine environment based on two-dimensional density-weighted operator and cloud barycentric Bayesian combination. Ocean Engineering, 283, art. 115184, 2023. DOI: https://doi.org/10.1016/j.oceaneng.2023.115184
[24] Sotelo-Pérez, I., Sotelo-Pérez, M., and Sotelo-Navalpotro, J.A., Riesgos antrópicos y tecnológicos, el turismo como alternativa? estudio de caso. Cuadernos de turismo (49), pp. 261-288, 2022. DOI: https://doi.org/10.6018/turismo.521911
[25] Lee, K.C., Guiney, P.D., Menzie, P.D., and Belanger, S.E., Advancing the weight of evidence approach to enable chemical environmental risk assessment for decision-making and achieving protection goals. Integrated Environmental Assessment and Management, 19(5), pp. 1188-1191, 2023. DOI: https://doi.org/10.1002/ieam.4803
[26] Singh, M., Periasamy, A., Goyal, P., Goswami, S., and Yadav, A., Environmental risk assessment for Zika, Nipah virus and Scrub typhus disease in a district of north India: first step towards one health. Journal of Zoonotic Diseases, 6(1), pp. 25-32, 2022. DOI: https://doi.org/10.22034/JZD.2022.14408
[27] González-Villanueva, L., Gutiérrez-Quintana, Y., Gutiérrez-Anillo, J.M., Baños-Paiffer, N., Bolaños-Queral, G.M., Hall-Puebla, N., Troya-Jiménez, Y., and Benítez-Zamora, J.D., Risk management for changing working seed lots at finlay Vaccine Institute. VacciMonitor, [online]. 31(1), pp. 15-24, 2022. Available at: https://www.medigraphic.com/pdfs/vaccimonitor/vcm-2022/vcm221d.pdf
[28] Wang, F., Zheng, P., Dai, J., Wang, H., and Wang, R., Fault tree analysis of the causes of urban smog events associated with vehicle exhaust emissions: a case study in Jinan, China. Science of the Total Environment, 668, pp. 245-253, 2019. DOI: https://doi.org/10.1016/j.scitotenv.2019.02.348
[29] Fatemi, F., Dehdashti, A., and Jannati, M., Implementation of chemical health, safety, and environmental risk assessment in laboratories: a case-series study. Frontiers in Public Health, 10, art. 898826, 2022. DOI: https://doi.org/10.3389/fpubh.2022.898826
[30] Montaño, A., Torres, Y., Herrera, E., Rincon, J., Velasquez, P., and Santis, A., Analysis of the operational risk of the process pasteurization and mixing in a dairy processing plant, using the Hazop Methodology. Chemical Engineering Transactions, 82, pp. 97-102, 2020. DOI: https://doi.org/10.3303/CET2082017
[31] Generowicz, A., and Iwanejko, R., Environmental risks related to the recovery and recycling processes of waste electrical and electronic equipment (WEEE). Problemy Ekorozwoju/Problems of Sustainable Development, [online]. 12(2), pp. 181-192, 2017. Available at: https://papers.ssrn.com/sol3/papers.cfm?abstract_id=3000872
[32] Machado, T.S.S., Leal, P.H.A.daC., Cardoso, T.A.S., Borges, L.daS., Santos, C.J.deM., and Oliveira, A.M.Sant'A., Risk and safety assessment in the foundry process in the metallurgical industry. Revista Produção Online, 23(3), pp. 5104-5104, 2023. DOI: https://doi.org/10.14488/1676-1901.v23i3.5104
[33] Mishra, J.L., Chiwenga, K.D., Mishra, N., and Choudhary, S., Extending dynamic capabilities towards lean thinking in humanitarian supply chains. Production Planning & Control, 33(6-7), pp. 655-675, 2022. DOI: https://doi.org/10.1080/09537287.2020.1834136
[34] Pavlova, A., Daniliuk, M., Pavlov, A., Savoskula, V., and Bendenko E., Applying a risk-based approach to the analysis of environmental aspects (on the example of dairy industry enterprise), in: International Multidisciplinary Scientific GeoConference Surveying Geology and Mining Ecology Management, SGEM, 2020, 2020, pp. 67-74. DOI: https://doi.org/10.5593/sgem2020/5.2/s21.008
[35] Nogueira-López, A., La huella ecológica. El establecimiento de indicadores ambientales y su significación para el derecho. Revista Catalana de Dret Ambiental, 10(1), pp. 1-25, 2019. DOI: https://doi.org/10.17345/rcda2589
[36] Pawlowski, S., Luetjens, L.H., Preibisch, A., Acker, S., and Petersen-Thiery, M., Cosmetic UV filters in the environment—state of the art in EU regulations, science and possible knowledge gaps. International Journal of Cosmetic Science, 45(S1), pp. 52-66, 2023. DOI: https://doi.org/10.1111/ics.12898
[37] Tajima, G., Huh, S., Schmidt, N.A., Macdonald, J.C., Fleischmann, T., and Wonnacott, K.M., Impact of genetically modified organism requirements on gene therapy development in the EU, Japan, and the US. Molecular Therapy Methods and Clinical Development, 26, pp. 74-83, 2022. DOI: https://doi.org/10.1016/j.omtm.2022.05.012
[38] Prieto-Sandoval, V., Jaca-García, C., and Ormazabal-Goenaga, M., Economía circular: relación con la evolución del concepto de sostenibilidad y estrategias para su implementación. Memoria Investigaciones en Ingeniería, [online]. 17, pp. 85-95, 2017. Available at: https://dadun.unav.edu/bitstream/10171/53653/1/Economia_Circular.pdf
[39] Ridaura, G., La Economía circular en Ecuador: perspectivas de cumplimiento de los ODS en la era Post COVID-19. CienciAmérica, 9(4), pp. 19-26, 2020. DOI: https://doi.org/10.33210/ca.v9i4.339
[40] Raudales-Garcia, E.V., Acosta-Tzin, J.V., and Aguilar-Hernández, P.A., Economía circular: una revisión bibliométrica y sistemática. Región Científica, 3(1), art. 2024192, 2024. DOI: https://doi.org/10.58763/rc2024192
[41] Sanabria, M., Construir nuevos espacios sostenibles respetando la diversidad cultural desde el nivel local. Región Científica, 1(1), art. 20222, 2022. DOI: https://doi.org/10.58763/rc20222
[42] Sánchez-Suárez, Y., Trujillo-García, L., Hernández-Nariño, A., Cuervo-Saiz, L., Sablón-Cossío, N., and Marqués -León, M., Una aproximación a la economía circular y su contribución en el contexto de la pandemia. Infodir [Online]. (40), art. e1336, 2023. Available at: https://scielo.sld.cu/pdf/infd/n40/1996-3521-infd-40-e1336.pdf
[43] Almeida-Guzmán, M., and Díaz-Guevara, C., Economía circular, una estrategia para el desarrollo sostenible. Avances en Ecuador. Estudios de la Gestión: Revista Internacional de Administración, 8(8), pp. 34-56, 2020. DOI: https://doi.org/10.32719/25506641.2020.8.10
[44] Sánchez-Suárez, Y., Marqués-León, M., Hernández-Nariño, A., and Suárez-Pérez, M., Metodología para el diagnóstico de la gestión de

trayectorias de pacientes en hospitales. Región Científica, 2(2), art. 2023115, 2023. DOI: http://doi.org/10.58763/rc2023115
[45] Tápanes-Suárez, E., Bosch-Nuñez, O., Sánchez-Suárez, Y., Marqués-León, M., and Santos-Pérez, O., Sistema de indicadores para el control de la sostenibilidad de los centros históricos asociada al transporte. Región Científica, 2(1), art. 202352, 2023. DOI: https://doi.org/10.58763/rc202352
[46] Sánchez-Suárez, Y., Pérez-Castañeira, J.A., Sangroni-Laguardia, N., Cruz-Blanco, C., and Medina-Nogueira, Y.E., Retos actuales de la logística y la cadena de suministro. Ingeniería Industrial, [online]. XLII(1), pp. 1-12, 2021. Available at: https://rii.cujae.edu.cu/index.php/revistaind/article/download/1079/992
[47] Sánchez-Suárez, Y., Pérez-Gamboa, A., Hernández-Nariño, A., Díaz-Chieng, L., Marqués-León, M., Pancorbo-Sandoval, J., and Rodríguez-Torres, E., Cultura hospitalaria y responsabilidad social: un estudio mixto de las principales líneas para su desarrollo. Salud, Ciencia y Tecnología-Serie de Conferencias, 2, pp. 451-451, 2023. DOI: https://doi.org/10.56294/sctconf2023451
[48] Sarmentero-Bon, I., Sánchez-Suárez, Y., Rodríguez-Sánchez, Y., Bravo-Macías, C.C., and Torrens-Pérez, M.E., Bibliometría sobre cultura organizacional en el sector de la salud, ante la Covid-19. Universidad y Sociedad, [online]. 14(S6), pp. 427-436, 2022. Available at: https://rus.ucf.edu.cu/index.php/rus/article/download/3474/3418
[49] Flores-Hidalgo, B.L., and Hurtado-Moreno, J.J., Impact of industrial maintenance on the supply chain in a textile company in times of pandemic, in: 2022 8th International Engineering, Sciences and Technology Conference (IESTEC), Panama, Panama, 2022, pp. 1-8. DOI: https://doi.org/10.1109/IESTEC54539.2022.00010
[50] Gonzales-Romero, A., Huamani-Martinez, I.J., Quiroz-Flores, J.C., and Diaz-Garay, B.H., Production management model based on Lean and DDMRP tools to increase the rate of project compliance in manufacturing SMEs in the metalworking sector, in: 2022 8th International Engineering, Sciences and Technology Conference (IESTEC), Panama, 2022, pp. 38-45. DOI: https://doi.org/10.1109/IESTEC54539.2022.00015
[51] Raheem, A., Sikarwar, V.S., He, J., Dastyar, W., Dionysiou, D.D., Wang, W., and Zhao, M., Opportunities and challenges in sustainable treatment and resource reuse of sewage sludge: a review. Chemical Engineering Journal, 337, pp. 616-641, 2018. DOI: https://doi.org/10.1016/j.cej.2017.12.149
[52] Luukkonen, T., and Pehkonen, S.O., Peracids in water treatment: a critical review. Critical Reviews in Environmental Science and Technology, 47(1), pp. 1-39, 2017. DOI: https://doi.org/10.1080/10643389.2016.1272343
[53] Gamito, G., Monteiro, C.J., Dias, M.C., Oliveira, H., Silva, A.M., Faustino, M.A., and Silva, S., Impact of Fe_3O_4-porphyrin hybrid nanoparticles on wheat: physiological and metabolic advance. Journal of Hazardous Materials, 471, art. 134243, 2024. DOI: https://doi.org/10.1016/j.jhazmat.2024.134243
[54] Yi, J., Li, J., and Chen, L., Ecosystem social responsibility in international digital commerce. Journal of International Business Studies, [online]. 54(1), pp. 24-41, 2023. Available at: https://link.springer.com/article/10.1057/s41267-022-00561-3
[55] Lu, Y., and Abeysekera, I., Do investors and analysts value strategic corporate social responsibility disclosures? Evidence from China. Journal of International Financial Management & Accounting, 32(2), pp. 147-181, 2021. DOI: https://doi.org/10.1111/jifm.12126
[56] Kjellén, M., Wastewater governance and the local, regional and global environments. Water Alternatives, [online]. 11(2), pp. 219-237, 2018. Available at: https://www.scopus.com/inward/record.uri?eid=2-s2.0-85048136033&partnerID=40&md5=3cad4fcac7c2afa1a5bf582a1383d302
[57] Lúcio, D.S.G., Menegassi, L.C., Lima, A.C.M., Gomes, T.M., and Tommaso, G., Assessing the phytotoxicity of wastewater from the structured-bed hybrid baffled reactor (SBHBR) for agricultural reuse during the germination phase. Science of the Total Environment, 918, art. 170449, 2024. DOI: https://doi.org/10.1016/j.scitotenv.2024.170449
[58] Lloyd, J., Olmos, J., González, A., Hernández, C., Deago, E., James, A., Salazar, E., and Broce, K., Occurrence of organochlorine compounds in biosolids from wastewater treatment plants in Panama city, in: Proceedings - 2022 8th International Engineering, Sciences and Technology Conference, IESTEC 2022, pp. 602-607. DOI: https://doi.org/10.1109/IESTEC54539.2022.00100
[59] Marczak, D., Lejcuś, K., Lejcuś, I., and Misiewicz, J., Sustainable innovation: turning waste into soil additives. Materials, 16(7), pp., 2023. DOI: https://doi.org/10.3390/ma16072900
[60] Shokri, A., and Sanavi-Fard, M., Water-energy nexus: cutting edge water desalination technologies and hybridized renewable-assisted systems; challenges and future roadmaps. Sustainable Energy Technologies and Assessments, 57, pp., 2023. DOI: https://doi.org/10.1016/j.seta.2023.103173
[61] Martins, M., Sousa, F., Soares, C., Sousa, B., Pereira, R., Rubal, M., and Fidalgo, F., Beach wrack: discussing ecological roles, risks, and sustainable bioenergy and agricultural applications. Journal of Environmental Management, 356, pp., 2024. DOI: https://doi.org/10.1016/j.jenvman.2024.120526
[62] Panday, D., Bhusal, N., Das, S., and Ghalehgolabbehbahani, A., Rooted in nature: the rise, challenges, and potential of organic farming and fertilizers in agroecosystems. Sustainability (Switzerland), 16(4), art. 16041530, 2024. DOI: https://doi.org/10.3390/su16041530

Y. Sánchez-Suárez, is BSc. Eng. in Industrial Engineering, MSc. of Business Administration and PhD. in Science, Industrial Technical Engineering, all of them from the University of Matanzas, Matanzas, Cuba in 2021 and 2024 respectively. He is currently a trainee in the Quality Department of the University of Matanzas. His main research interests include operations management, management, business, supply chain management and hospital management.
ORCID: 0000-0003-1095-1865.

J.A. Pancorbo-Sandoval, is Lic. Accounting in 1983, PhD. in Business Administration and Management. Leader of the Study Group on Planning and Intelligent Territorial Development (GEPDIT) UTE University Ecuador Representative of the UTE University Santo Domingo Headquarters in the Santo Domingo Network Investigates Member of the Network of Latin American Studies in Administration and Business Mexico Guest Professor Institute Technologic Superior de Cajeme México Guest Professor University of León, Spain Collaborator of the Institute Mesías Marca España Member of the Spanish Association of Academic and Professional Marketing (AEMARK). His main research Interests include Marketing, business administration, territorial planning, logistics and circular economics.
ORCID: 0000-0002-8082-6720

S.E. Leyva-Ricardo, is BSc. Eng. in Industrial Engineering. MSc. in Environmental Pollution Mention Environmental Management and protection of Natural Resources Member of the Research Group of Studies in Planning and Intelligent Territorial Development (GEPDIT) UTE University Member of the Network of Latin American Studies in Administration and Business Mexico Research Coordinator at the University UTE headquarters Santo Domingo de los Tsáchilas. Ecuador Guest professor at universities in Mexico. His research interest is in business administration, logistics and circular economy, environmental engineering, industrial engineering.
ORCID: 0000-0002-4556-2301.

V. Sánchez-Castillo, is BSc. Eng. in Agroecological Engineer from the Universidad de la Amazonia (Colombia), Master in Regional Studies in Environment and Development from the Universidad Iberoamericana de Puebla (Mexico), PhD in Anthropology from the Universidad del Cauca (Colombia). Professor linked to the Universidad de la Amazonia; Associate Researcher at Minciencias. Director of the GIADER Research Group, category A in Minciencias-Colombia.
ORCID: 0000-0002-3669-3123.

DYNA
http://dyna.medellin.unal.edu.co/

UNIVERSIDAD NACIONAL DE COLOMBIA

Use of end-of-life tires for the production of a waterproofing agent as a strategy to promote the circular economy

Valentina Salcedo-Mojica [a] & Jaime Arturo-Calvache [a*] & Cristina Ramírez-Meneses [b]

[a] *Departamento de Química y Ambiental, Universidad América, Bogotá, Colombia. Facultad de Ingenierías, Grupo de procesos sostenibles, laura.salcedo@estudiantes.uamerica.edu.co, * jaime.arturo@profesores.uamerica.edu.co*
[b] *Servicio Nacional de Aprendizaje SENA, Centro de Gestión de Mercados, Logística y Tecnologías de la Información, Bogotá, Colombia, cramirezm@sena.edu.co*

Received: August 5th, 2024. Received in revised form: November 12th, 2024. Accepted: November 20th, 2024.

Abstract
This paper develops a formulation to produce a laboratory-scale waterproofing for exterior walls and roofs using recycled tires. It begins by identifying its chemical composition using Fourier transform infrared spectroscopy and selects a technology using the ELECTRE method. It uses a reticular simplex mixing design of experiments to adjust the resin proportions according to their mechanical properties. In addition, it evaluates the critical pigment volume content and parameters such as water absorption, permeability, total solids content and mechanical properties for quality assurance. Acrylic emulsions were found to be favorable in cost, application, safety, and efficiency; the flexible resin offers better elongation and the rigid one better tensile strength, with less than 10% tire reducing porosity. The results support the competitiveness of the product and confirm the effective use of recycled tires in waterproofing, offering a favorable and functional approach to construction

Keywords: waste tire; circular economy; waterproofing; waterborne coating

Aprovechamiento de neumáticos al final de su vida útil para la producción de impermeabilizante como estrategia de promoción de la economía circular

Resumen
Este trabajo desarrolla una formulación para producir un impermeabilizante a escala de laboratorio para paredes exteriores y cubiertas utilizando neumáticos reciclados. Inicia identificando la composición química mediante espectroscopia infrarroja por transformada de Fourier y selecciona una tecnología mediante el método ELECTRE. Utiliza un diseño de experimentos de mezcla simple reticular para ajustar las proporciones de resina en función de sus propiedades mecánicas. Además, evalúa el contenido crítico de volumen de pigmento y parámetros como la absorción de agua, permeabilidad, contenido total de sólidos y las propiedades mecánicas para el aseguramiento de la calidad. Las emulsiones acrílicas resultaron favorables en coste aplicación, seguridad y eficacia; la resina flexible ofrece mejor alargamiento y la rígida mejor resistencia a la tracción, con menos de un 10% de porosidad reductora del neumático. Los resultados apoyan la competitividad del producto y confirman el uso eficaz de neumáticos reciclados en la impermeabilización, ofreciendo un enfoque favorable y funcional para la construcción.

Palabras clave: neumáticos usados; economía circular; impermeabilización; recubrimientos base agua

1 Introduction

Building materials formulations and selection have evolved over the past few decades in response to greater energy efficiency goals and a greater understanding of building science [1]. Although conventional coatings derived from fossil feedstocks and based on solvents exhibit superior physical and mechanical properties [2,3], their use increases environmental damage and extraction costs, especially in the face of dwindling supplies of resources such as oil and natural gas [4]. Consequently, the materials industry has undergone a significant transformation toward the integration

How to cite: Salcedo-Mojica, V., Arturo-Calvache, J., and Ramírez-Meneses, C., Use of end-of-life tires for the production of a waterproofing agent as a strategy to promote the circular economy. DYNA, 91(234), pp. 126-134, October - December, 2024.

of renewable raw materials and emerging technologies, with a particular focus on sustainability through the use of water as a liquid vehicle in formulations [5]. This move towards a circular economy reflects the sector's persistent efforts to innovate and reduce environmental impact, contributing to sustainable development goals [6,7]. Within this trend, the incorporation of recyclable materials as additives seeks not only to reduce costs but also to improve key mechanical properties, such as tensile strength and durability [8-13].

The production of efficient and low-cost waterproofing has become a crucial breakthrough for building protection [14] and whose formulations are based on polymeric compounds in a liquid vehicle, either solvent or emulsion in water, together with viscosity-reducing additives, fillers, and fibers [15] highlighting the use of a waste with high recoverability potential such as end-of-life tires as a promising solution [16]. Currently these wastes represent a major environmental problem [17]. It is estimated that the annual generation of tires amounts to 1.5 billion whole tires worldwide [18]. In Colombia, between 5,5 and 6,7 million units of tires are imported to meet the growing demand for mobility [19] identifying that in the capital around 4,000 tires are collected weekly by the Mayor's Office that are not destined for any method of reuse [20]. They are not considered a hazardous waste; however, they are highly bulky, and their composition makes their degradation almost impossible [21-23].

The reuse of these tires is therefore a practical and economical solution supported by studies suggesting that tire rubber powder is suitable for the industrial production of waterproofing coatings [17,24].

This article focuses on designing a formulation to produce a waterproofing agent that, through the correct selection and dosage of compounds together with the physicochemical transformation of the tires, reincorporates this waste into the production chain as a secondary raw material. The main objective of the project is to offer an alternative to the current problem of managing these wastes, contributing to sustainability and the extended life cycle of the materials. This approach not only helps preserve natural resources and mitigate negative environmental impacts, but also supports three sustainable development goals: SDG 9 (innovation and infrastructure), improving the properties of construction materials; SDG 11 (sustainable cities and communities), properly managing waste and improving infrastructure; and SDG 12 (responsible production and consumption), reducing the environmental impact of waste and improving the production of waterproof construction materials.

2 Materials and methods

2.1 Characterization of the waste Tire

Tire dust particle size registered by the manufacturer of ≤0,71mm was used to analyze the possible chemical composition of the residue by Fourier transform infrared spectroscopy (FTIR) using the Spectrum Two equipment™ and comparing the spectra with the library available in the Spectrum software™ 10.

2.2 Technology selection

The ELECTRE (Elimination Et Choix Traduisant la Realitè) multi-criteria decision-making methodology was applied to evaluate and select the most favorable technology. First, low cost, trouble-free application, waterproofing efficiency and low chemical risk were defined as the criteria for evaluating the different available technologies. Second, a weight was assigned to each criterion by means of a survey of 37 people, who indicated their order of preference when purchasing a waterproofing product. Finally, each alternative was rated according to the information available in the literature and provided by the manufacturers, normalizing the values on a scale of 0 to 1 with correspondence intervals of 0,25. This allowed obtaining the initial decision matrix used to run the ELECTRE method and thus identify the hierarchy of technologies.

The ELECTRE method considers the relationship between the alternatives considering both the absolute values of performance and the significant differences between them and thus determine the dominance between technologies. Therefore, once this matrix was obtained, we proceeded to create the concordance and discordance matrix whose indexes were calculated with eq. (1), (2) respectively.

$$\mathbf{C_{ik}} = \sum_{\mathbf{j:c_j(A_i)>c_j(A_k)}} \mathbf{w_j} + \frac{\mathbf{1}}{\mathbf{2}} \sum_{\mathbf{j:c_j(A_i)=c_j(A_k)}} \mathbf{w_j} \tag{1}$$

$$\mathbf{D_{ik}} = \frac{\mathbf{max}\left|\mathbf{c_j(A_i)} - \mathbf{c_j(A_k)}\right|_{\mathbf{j:c_j(A_i)<c_j(A_k)}}}{\mathbf{max}\left|\mathbf{c_j(A_i)} - \mathbf{c_j(A_k)}\right|_{\mathbf{j:c_j(A_i)>(A_k)}}} \tag{2}$$

Subsequently, the concordance and discordance thresholds, c and d, were calculated from a simple average with the values of their respective matrices, which allowed the creation of the concordant and discordant dominance matrices, such that if $C_{ik} > c = 1$if, if $C_{ik} < c = 0$ and that if $D_{ik} > d = 0$ and if $C_{ik} < d = 1$. Finally, the two dominance matrices were multiplied to obtain the aggregate dominance matrix and thus obtain the ELECTRE graph that allowed the identification of the most favorable technology.

2.3 Sample preparation

Sample preparation was conducted in three stages. The first consists of the preparation, in a paddle stirrer the water was mixed with the wetting agent, the dispersant and the thickener for 2 minutes before adjusting the pH to 8 and continued mixing until a gel was formed, then a third part of the defoamer was added. The second stage is the dispersion stage, in which the pigment (titanium dioxide) and tire powder are added to the previous mixture. This stage is the most important, so it was left to mix for 15 minutes. Finally, the second part of the defoamer is added. The final phase is the adjustment phase; in this stage the polymeric dispersions were added together with the coalescent agent, the rheology modifier, the acrylic thickener, the biocide and finally what was left of the defoamer.

2.4 Tensile test

To prepare the specimens, a mold was used with the dimensions defined by the ASTM D638 standard for a type IV specimen, which is used when a comparison between soft polymers and other more rigid polymers is sought. The specimens were molded with acrylic sheets and kept for 4 days under standard laboratory conditions, then placed in a drying oven at 40°C for 2 days before the tensile test.

2.5 Experimental design

An experimental design of simple cross-linked mix was conducted, considering as response variables the maximum stress (MPa), elongation at break (%) and maximum force (N) obtained from tensile tests performed in a SHIMADZU universal testing machine, with a maximum capacity of 50 kN and 10 kg, following the ASTM D2370 standard. Additionally, a design of experiment with simplex reticular (2,4) mixtures was used for two components, rigid resin and flexible resin, with two levels 70/30 and 90/10, obtaining two replicates for each response variable. The results were analyzed by analysis of variance using Minitab with quadratic adjustment to determine the impact of resin proportions on the mechanical properties of the final product.

2.6 Quality test

Viscosity, density, volume of solids and weight of solids tests were conducted according to standards D2196, D1475, D2697 and D1644, respectively, for the liquid material. Additionally, the capacity of the already applied and dry waterproofing was determined in an extreme situation of water presence, allowing it to pass through it without altering its internal structure, that is, without suffering deterioration, by means of the permeability test calculated from the measurement of the amount of water passing through the dry waterproofing film for one week. On the other hand, water absorption was evaluated to determine how well the product performs under extreme humidity conditions, immersing the test specimens in distilled water for seven days. At the end of this period, the percentage of water absorption of each specimen was calculated by weight difference. Finally, the elongation at break and tensile strength were measured. All tests were compared to the range required by ASTM D6083/D6083M - 21 "Standard Specification for Liquid-Applied Acrylic Coating Used in Roofing".

3 Results and discussion

3.1 Chemical composition of the waste

Tires are complex materials containing various components to function in various environments, their end-of-life properties are determined by the particle size according to the grinding technology and composition, which influences their mechanical behavior and longevity. All tires contain four groups of fundamental materials: natural (polyisopropene) and synthetic rubbers such as butadiene (BR) hydrogenated nitrile-butadiene (HNBR), styrene-butadiene (SBR) and ethylene-propylene-diene (EPDM), carbon blacks and silicas, reinforcing materials such as metals and/or textiles, and chemical additives [24] as vulcanizing agents whose objective is to facilitate the irreversible cross-linking of rubber macromolecules [25]. They are all selected and dosed to improve properties such as abrasion resistance in the tread, flexural strength in the sidewall and impermeability of the inner liner [26]. In addition to increasing resistance to biodegradation, photochemical decomposition, chemical reagents and thermal degradation [27]. Fourier transform infrared spectroscopy was used to identify various compounds present in the recycled material sample.

Fig. 1 shows the % transmission of infrared light as a function of wavelength in cm^{-1}, which is presented in such a way that the higher frequencies are on the left and the lower frequencies on the right. In the stretching region comprising frequencies between 1400 and 4000 cm^{-1}, two types of bands are identified, a strong one between 2800 and 2950 cm^{-1} corresponding to stretching vibrations between C-H bonds with sp3 hybridization carbons, suggesting the presence of the methyl group and aliphatic structures. Another moderate band between 1500 and 1550 cm^{-1} is found within the double bond region which may suggest the presence of 1 carbonyl group. Fig. 1 also contrasts the spectrum of the recycled tire with the known spectrum of zinc stearate which presented the highest coincidence with 66.1%, this means that the chemical characteristics of zinc stearate can coincide with several other substances present in the tire dust, generating a coincidence in the spectral bands and/or that the transmittance bands of zinc stearate can be very intense, dominating the spectrum even if it is present in a minor proportion within the sample.

Between 550 and 1400 cm^{-1} is the fingerprint region, it means, characteristic vibrations of each molecule, so reference spectra of different polymers were used to identify the identity of the sample. The weak bands 1, 2, 3 and 4 of the bending regions in Fig. 1 have a possible identification at frequencies 1461 cm^{-1}, 960 cm^{-1}, 722 cm^{-1} and 699 cm^{-1} of the functional groups' propylene, butadiene, ethylene and styrene [23,28-30] respectively, present in EDPM, SBR and NR rubber polymers.

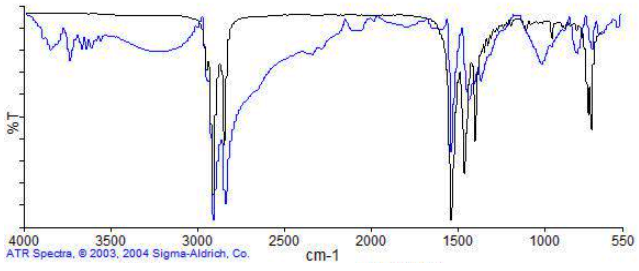

Figure 1. Comparison of tire FTIR spectrum (blue line) with zinc stearate FTIR spectrum (black lines) from the library available in SpectrumTM 10 software. Source: Own elaboration

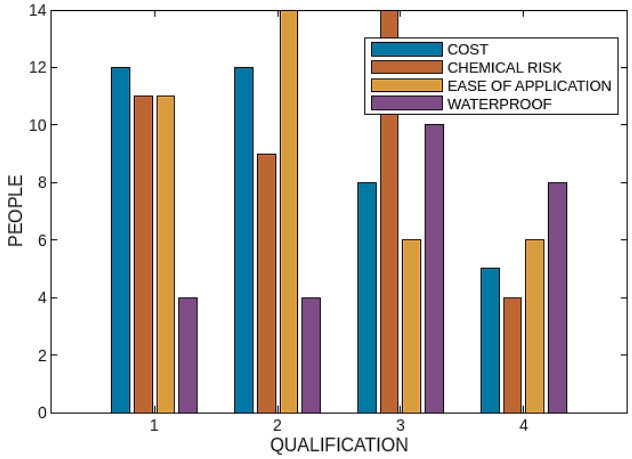

Figure 2. Consumer preference results
Source: Own elaboration

3.2 Selection of technology

Waterproof coatings are complex materials that contain binders. These are especially important in heterogeneoussystems, such as emulsions and dispersions, where their main function is to maintain a firm and stable structure [31]. The wide variety of available waterproofing systems allows the selection of a wide range of materials and techniques thatprovide and ensure product performance and durability. Some of the most commonly used water-based waterproofing systems in construction are silicone, polyurethane, acrylic, and asphalt emulsions.

Fig. 2 shows the survey results, determining that the most important criterion when acquiring a waterproofing product is its efficiency in waterproofing, while cost has the least weight.

The weights assigned to each criterion are detailed in Table 1 shows the normalized ratings for each alternative based on the information available in the literature. Additionally, Table 1 presents the standardized ratings of various waterproofing technologies according to the literature. Considering that siliconized resins are hydrophobic and resistant, but costly [32]; polyurethane membranes are durable and adhesive, but expensive and toxic [33]; acrylic technologies are inexpensive and UV-resistant [34]; and asphaltic emulsions, derived from petroleum, are consistent, adhesive and durable, in addition to being low-cost [35].

Once the alternatives were compared with each other, the Electre method was run and the hierarchy of preference in the alternatives studied was obtained together with the identification of their net flows. Fig. 3 illustrates the outflows in which one alternative is preferred over others, and the inflows in which other alternatives are preferred over these.

Once the alternatives were compared with each other, the Electre method was run and the hierarchy of preference in the alternatives studied was obtained together with the identification of their net flows. Fig. 3 illustrates the outflows in which one alternative is preferred over others, and the inflows in which other alternatives are preferred over these.

Table 1.
Normalized decision matrix

Alternatives	Criteria			
	Cost	Ease of application	Chemical risk	Water resistance
Silicone	0,20	0,75	0,50	0,55
Polyurethane	0,10	0,50	0,35	1,00
Acrylic	0,60	0,70	0,60	0,60
Asphalt	0,70	0,50	0,20	0,70
Criteria weight	0,1	0,2	0,3	0,4

Source: Compiled by the author

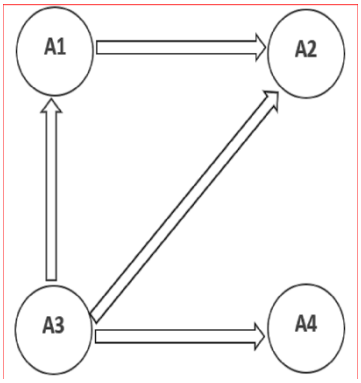

Figure 3. ELECTRE network, net flows of each alternative
Source: Own elaboration

In the case of polyurethane emulsions (A2), it is a technology that does not have outflows, that is, it is not considered preferable with respect to the others, in spite of having excellent waterproofing efficiency, other criteria such as cost and its components that reduce its chemical safety make other technologies stand out, as is the case of acrylic (A3), which was positioned in first place as the most preferable, balancing each of the criteria. Therefore, it was chosen as the base technology on which the tire-based waterproofing was formulated.

3.3. Additive study

The incorporation of additives improves the miscibility of polymer blends by lowering their interfacial tension, which is called compatibilization. The wetting agent forms an envelope around the pigment particles and the dispersant improves the incorporation of pigments and fillers into a coating, ensuring its stability [36]. The pH regulator neutralizes the coating to prevent pigment shock, the rheology modifier controls viscosity and provides a suitable texture for application [37,38]. The defoamer reduces foaming during emulsion manufacture and application [39]. The biocide prevents the growth of microorganisms in the emulsion and prolongs its shelf life. The thickener optimizes the flow behavior by adjusting the viscosity for storage, processing and application and the coalescing agent acts as a film former [40]. Table 2 shows the additives that were selected in order to achieve good stability and excellent coating properties.

Table 2.
Base formulation and function of additives

Additive	Type	%
Moisturizer	Indole, nonionic wetting agent	0,1
Dispersant	Sodium polyacrylate	1,2
pH Regulator	Sodium silicate	0,1
Rheology modifier	Monoethylene glycol	0,4
Defoamer	Polyacrylate defoamer	1,2
Biocide	Stabilized aqueous solution of isothiazolinones with bromine derivatives.	0,2
Thickener	Hydroxy-propoxymethylcellulose	0,4
Coalescing agent	Haltane isobutyrate	1,2

Source: Compiled by the author

3.4. Formulation adjustment

3.4.1 Percentage change (%) of tire

As pigment volume content (PVC) increases and approaches critical volume content (CPVC), properties such as gloss and blistering decrease, while permeability, susceptibility to oxidation, and viscosity increase [37]. This abrupt change is observed experimentally, so the percentage of tires was varied first. Fig. 4 shows that at 0% tire, the porosity is low and the structure is compact. At 5%, porosity increases slightly, improving shock absorption without compromising strength. At 10%, a significant increase in porosity is observed, with more prominent particles and pigments beginning to agglomerate, indicating proximity to the critical pigment volume content, and at 23%, the lack of binder increases pores, resulting in low quality. Therefore, formulations with PVC below CPVC, such as 5% tire, are preferred. And although incorporating as little as 10% by weight of tire in polymeric matrices would mean a large consumption of scrap tires [41] even a smaller percentage, such as 5%, can represent a significant impact. Incorporating 5% by weight of recycled tire is still beneficial because, on an industrial scale, it translates into large volumes of recycled material. This approach not only helps reduce the volume of tire waste that ends up in landfills but also allows it to flow continuously into production cycles, as well as maintaining the desired properties of the final material.

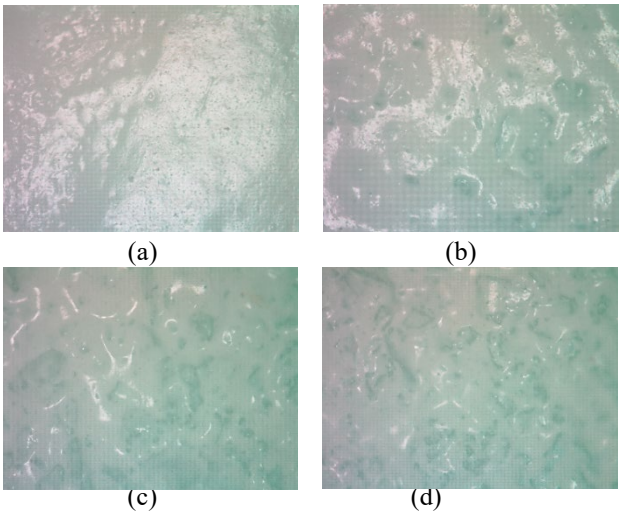

Figure 4. Porosity of different tires % a) 0%, b) 5%, c) 10% and d) 23%
Source: Own elaboration

Table 3.
Results of mechanical tests for different proportions of rigid and flexible resin

Rigid resin	Flexible resin	Maximum force (N)	Maximum stress (MPa)	Elongation at break (%)
70	30	10,8322 11,4759	0,7952 0,7332	450,0765 402,3961
30	70	5,0068 4,1564	0,3599 0,2832	294,5056 198,8111
90	10	9,7116 9,7672	0,9502 0,9429	295,5902 267,4216
10	90	3,8068 3,1710	0,2973 0,2343	191,8667 183,8111

Source: Own elaboration

Once it is determined that 5% of the total weight of the formulation corresponds to recycled tire powder and 35% is made up of additives, solvent (water), and pigment, the remaining 60% is attributed to the acrylic resin, which is further divided into rigid and flexible resin.

Selecting an optimal resin ratio that satisfies 60% of the formulation results in improved mechanical properties, impermeability, and resistance to environmental conditions of the coating, ensuring efficient protection for terraces and exterior walls. It is expected that increasing the proportion of flexible resin will improve the elasticity and adaptability of the material, while increasing the proportion of rigid resin can improve tensile strength and therefore durability.

The results of varying the resin ratio are shown in Table 3, where it can be observed that as the proportion of rigid resin increases, the maximum tension tends to increase in the same way. However, the behavior for the other response variables is not similar. Regarding elongation at break, it would be expected that a higher percentage of flexible resin would result in a higher percentage, however, the highest value is for 70R/30F. This behavior can be visualized in Fig. 5, corresponding to the contour plots for the response variables of maximum strength and elongation at break. It can be observed that for higher force values, the proportion of rigid resin is between 60 and 100, and for higher elongation at break percentages, the optimal proportion of rigid resin is between 60 and 80.

Before selecting the proportion to use, a statistical analysis of the data was performed. First, the goodness of fit was identified to determine how well the statistical model fits the data. For maximum stress, maximum force, and elongation at break, the R2 values are 99,0%, 98,24%, and 90,64% respectively, indicating that the model explains the variability of the data better for maximum stress compared to the other response variables. On the other hand, to determine the level of confidence in the obtained results, it is analyzed whether the results are statistically significant, which indicates an insignificant risk of being due to chance.

First, the "p" values shown in Fig. 6 were evaluated, corresponding to the probability against the null hypothesis for lack of fit, in order to determine if the model required more terms or data transformation. For the three response variables, the "p" values are greater than 0,05 indicating that no lack of fit was detected and that the model explains the relationship between the predictors and the response.

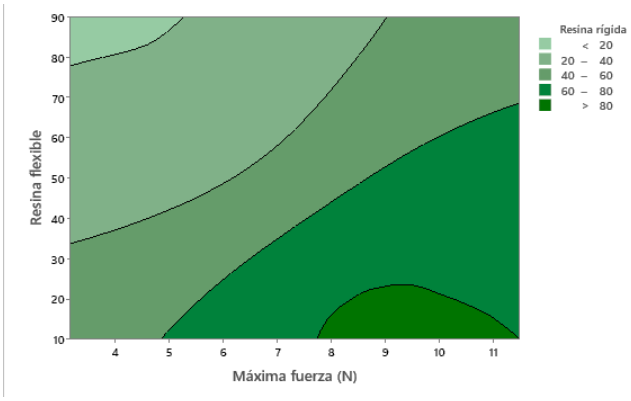

(a)

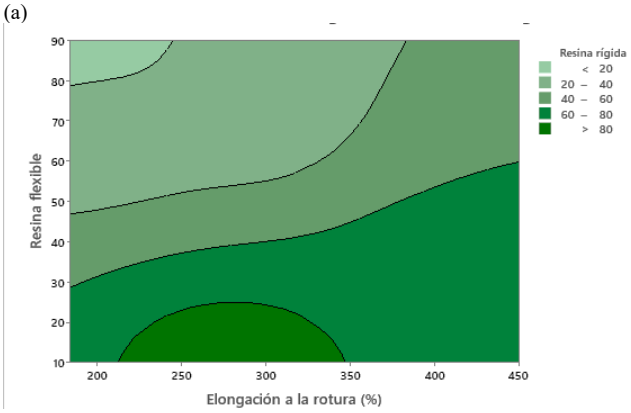

(b)

Figure 5. Contour charts for (a) maximum strength and (b) elongation at break. Source: Own elaboration

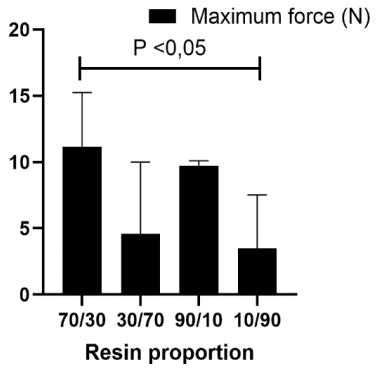

(a)

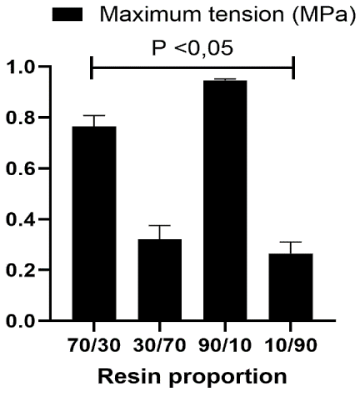

(b)

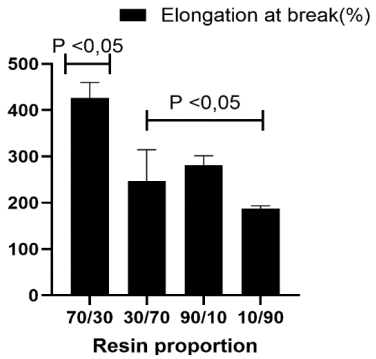

(c)

Figure 6. Probability results against the null hypothesis for each of the studied mechanical properties evaluated with alpha 0,05. (a) Maximum force, (b) Maximum tension and (c) Elongation at break. Source: Own elaboration
Source: Own elaboration

Additionally, the "p" values for the interaction between resins were examined, which were found to be less than 0,05, indicating a statistically significant difference when working with a significance level of 95%. This indicates that at least one of the terms in the group has an effect on the response, leading to the rejection of the null hypothesis

Finally, the regression coefficients for each response variable presented in Table 4 were analyzed. The coefficients explain that for maximum stress, the rigid resin has a significantly higher coefficient (0,9412) compared to the flexible resin (0,3716), and the interaction has a negative coefficient (-0,0551), indicating that an excess of flexible resin can reduce maximum stress. For maximum force, the interactions between the rigid and flexible resins are statistically significant and balanced proportions can be managed. The rigid resin has a higher coefficient (6,052) compared to the flexible resin (4,877), indicating a greater contribution of the rigid resin to maximum force. Lastly, in terms of elongation at break, the flexible resin has a much higher coefficient (310,8) than the rigid resin (21,6) and the interaction is positive (779), suggesting that a higher proportion of flexible resin increases elongation at break.

Since the model shows that maximum stress is more closely related to the rigid resin, a higher proportion of this in the mixture is preferable. Therefore, a 95/5 ratio of rigid resin to flexible resin would be a suitable choice to maximize maximum stress.

Table 4.
Results of estimated regression coefficients for each response variable

Term	Maximum stress Coefficient	Maximum force Coefficient	Elongation at break
Rigid resin	0,9412	6,052	21,6
Flexible resin	0,3716	4,877	310,8
Rigid resin* Flexible resin	-0,551	12,28	779

Source: Own elaboration

3.5. Quality test

Quality tests are performed to obtain the technical specifications of the finished product and their values are recorded in Table 5. The waterproofing agent is white with slight black particles, which is beneficial for exterior walls and roofs as it reduces heat accumulation by reflecting light. The viscosity of the product at 12500 cps is suitable for trouble-free application. On the other hand, the solids volume exceeds 50% and the solids weight is greater than 60%, ensuring that a larger portion of the applied product remains on the surface. Thanks to the water-based formulation, the curing time is longer, however, a low content of volatile organic compounds is guaranteed.

A pH around 8,5 ensures optimal dispersion efficiency [37]. In terms of the mechanical properties of the material, they exhibit an elongation at break percentage greater than 100%, indicating high flexibility and adaptability to movements and deformations of the building, along with sufficient tensile strength to support pedestrian traffic in the case of being used on terraces, ensuring greater durability of the material and better resistance to external loads and environmental stresses, resulting in more effective protection of the building against aging and weathering.

Finally, the efficiency of the waterproofing is reflected in the properties of permeability and water absorption. The material's permeability is 12 Perms, which is a convenient value and reflects proper formulation and selection of tire percentage by avoiding particle agglomeration and pore formation. However, the water absorption of 20% indicates that the material can absorb a moderate amount of water, so it is recommended to apply the material where there is not a high and prolonged accumulation of water, or a good drainage system is suggested.

The obtained formulation shows good physical and mechanical properties, as well as high efficiency in waterproofing. This not only ensures that the product is competitive in terms of performance but also demonstrates that tires can undergo an extended life cycle by transforming into valuable materials that enhance the properties of products used in the construction industry.

Table 5.
Quality test results

Property	ASTM	Units	Value
Color	-	-	*White*
Viscosity	D2196	cps	12500
Density	D1475	g/mL	1,39
Volume of solids	D2697	%	>50
Weight of solids	D1644	%	>60
pH	-	-	8,9
Curing time	-	hours	96
Elongation at break	D2370	%	295,59
Tensile strength	D2370	MPa	1,37
Permeability	D1653	Perms	12
Water absorption	D471	%	20

Source: Own elaboration

4 Conclusions

An appropriate process for collecting and processing tires at the end of their useful life is crucial to identify the compounds present in the waste and effectively select additives that ensure their compatibility and stability. Simultaneously, the application of a multicriteria analysis method like ELECTRE has allowed determining the favorability of available alternatives. This study has highlighted acrylic emulsions as the most convenient option, balancing criteria of cost, ease of application, efficiency, and chemical safety.

The statistical analysis revealed that the ratio between rigid and flexible resins directly impacts the mechanical properties, and to improve weather resistance, a formulation with a 90/10 ratio in favor of rigid resin was chosen. Additionally, controlling the volume content of critical pigment has been crucial to avoid particle agglomeration and pores that could compromise the quality of the final product; a content below 10% has shown improvements in physical properties, as evidenced in the final product quality tests. These tests guarantee good stability, with a pH that facilitates particle dispersion, a color that reduces heat accumulation, and a solids content that ensures optimal performance by retaining over 60% of the product on the surface once applied.

In conclusion, transforming tires at the end of their useful life into loads for waterproofing emulsions not only effectively extends their lifespan but also significantly improves the mechanical properties of the coating. After their useful life as a waterproofing agent, these materials can be recovered and reused in new products, thus completing their life cycle, minimizing waste without a destination, and maximizing the value of the resources used. This strategy not only addresses the environmental problem of tire disposal but also actively promotes the circular economy, standing out as an innovative and sustainable solution for the construction materials industry.

Acknowledgements

This work was supported by the Universidad de America (Grant No. IIQ-003, 2021)

References

[1] Casini, M., Advanced technology, tools and materials for the digital transformation of the construction industry, cap. 1.3, Low-Carbon and sustainable cities. [online]. 2022. Available at: https://app.knovel.com/hotlink/khtml/id:kt012RPNH3/construction-4-0-advanced/low-carbon-sustainable

[2] Gijsbertus, E., Catarina, C., and Leendert, G., Polymer coatings - A guide to chemistry, characterization, and selected applications, Cap 4. Coating compositions in general. [online], John Wiley & Sons. 2018, Available at: https://app.knovel.com/hotlink/khtml/id:kt011QZ3L2/polymer-coatings-guide/coating-compositions

[3] Casini, M., Advanced technology, tools and materials for the digital transformation of the construction industry, cap 7. Nanocomposite concrete. [Online]. 2022. Available at: https://app.knovel.com/hotlink/khtml/id:kt012RPSK1/construction-4-0-advanced/nanocomposite-concrete

[4] Höfer-Rainer, M., Green chemistry principles and global drivers for sustainability - An introduction. Royal Society of Chemistry (RSC).

[Online]. 2019. Available: https://app.knovel.com/hotlink/khtml/id:kt012VYN26/green-chemistry-surface/green-chemistry-principles.
[5] Gündüz, G., Chemistry, materials, and properties of surface coatings - Traditional and evolving technologies, cap 1. Future forecast. [Online]. 2015. Available at: https://app.knovel.com/hotlink/khtml/id:kt0132BATP/chemistry-materials-properties/future-forecast.
[6] Koleske, J.V., Paint and coating testing manual - Fifteenth edition of the Gardner-sward Handbook, cap 78. Ultraviolet radiation systems. [Online]. 2012. Available at: https://app.knovel.com/hotlink/pdf/id:kt00B7Y83A/paint-coating-testing/curing-equ-ultraviolet
[7] Pacheco-Torgal, F., Introduction to the environmental impact of construction and building materials, in: Eco-efficient construction and building materials, Pacheco-Torgal, F., Cabeza, L.F., Labrincha, J., and Magalhães, A., Eds. Woodhead Publishing, 2014, pp. 1–10. DOI: https://doi.org/10.1533/9780857097729.1
[8] Leon, A., Chen, Q., Palaganas, N., Palaganas J., Manapat J., and Advincula, R., High performance polymer nanocomposites for additive manufacturing applications, React Funct Polym, 103, pp. 141–155, 2016. DOI: https://doi.org/10.1016/j.reactfunctpolym.2016.04.010
[9] Dixit, S., Goel, R., Dubey, A., Shivhare, P., and Bhalavi, T., Natural fibre reinforced polymer composite materials - A review. Polymers from Renewable Resources, 8(2), pp. 71–78, 2017, DOI: https://doi.org/10.1177/204124791700800203
[10] Hejna, A., Korol, J., Przybysz-Romatowska, M.Ł., Zedler, B., and Chmielnicki, F.K., Waste tire rubber as low-cost and environmentally-friendly modifier in thermoset polymers – A review. Waste Management, 108, pp. 106–118, 2020, DOI: https://doi.org/10.1016/j.wasman.2020.04.032
[11] Zabalza-Bribián, I., Valero-Capilla, A., and Aranda-Usón, A., Life cycle assessment of building materials: comparative analysis of energy and environmental impacts and evaluation of the eco-efficiency improvement potential, Build Environ, 46(5), pp. 1133–1140, 2011. DOI: https://doi.org/10.1016/j.buildenv.2010.12.002
[12] Na, O., and Xi, Y., Mechanical and durability properties of insulation mortar with rubber powder from waste tires, J Mater Cycles Waste Manag, 19(2), pp. 763–773, 2017, DOI: https://doi.org/10.1007/S10163-016-0475-2/METRICS
[13] Wang, Q., Cui, Y., and Xue, J., Study on the improvement of the waterproof and mechanical properties of hemihydrate phosphogypsum-based foam insulation materials, Constr Build Mater, 230, art. 117014, 2020. DOI: https://doi.org/10.1016/J.CONBUILDMAT.2019.117014
[14] Al-Jabari, M., Al-Rashed, R., Ayers M.E., and Clement, D., Materials selection and proportioning for watertight and durable concrete, in: Integral waterproofing of concrete structures, Al-Jabari, M., Ed., Woodhead Publishing Series in Civil and Structural Engineering, Woodhead Publishing, 2022, pp. 109–134. DOI: https://doi.org/10.1016/B978-0-12-824354-1.00004-0
[15] Al-Jabari, M., Waterproofing coatings and membranes, in: Integral waterproofing of concrete structures, Al-Jabari, M., Ed., in Woodhead Publishing Series in Civil and Structural Engineering. Woodhead Publishing, 2022, pp. 393–435. DOI: https://doi.org/10.1016/B978-0-12-824354-1.00012-X
[16] Edun, A., and Hachem-Vermette, C., Energy and environmental impact of recycled end of life tires applied in building envelopes, Journal of Building Engineering, 39, art. 102242, 2021. DOI: https://doi.org/10.1016/j.jobe.2021.102242
[17] Kim-Jin K.S. Introduction, 2019, Royal Society of Chemistry (RSC). [Online]. Available at: https://app.knovel.com/hotlink/khtml/id:kt011IVUD2/rubber-recycling-challenges/thermoplas-introduction
[18] Martínez, J.D., An overview of the end-of-life tires status in some Latin American countries: proposing pyrolysis for a circular economy, Renewable and Sustainable Energy Reviews, 144, art. 111032, 2021. DOI: https://doi.org/10.1016/J.RSER.2021.111032.
[19] Park, J., Díaz-Posada, N., and Mejía-Dugand, S., Challenges in implementing the extended producer responsibility in an emerging economy: the end-of-life tire management in Colombia, J. Clean Prod, 189, pp. 754–762, 2018. DOI: https://doi.org/10.1016/j.jclepro.2018.04.058.
[20] Denguir, Y., Estudio del uso de neumáticos fuera de uso (NFU) como material para la construcción de terraplenes. Aplicación a la ampliación del vertedero de residuos controlado de les Borges Blanques (Lleida). [Online]. 2021. [Accessed: Jun. 03, 2024] Available at: https://riunet.upv.es:443/handle/10251/173175
[21] Sienkiewicz, M., Janik, H., Borzędowska-Labuda, K., and Kucińska-Lipka, J., Environmentally friendly polymer-rubber composites obtained from waste tyres: aq review, J Clean Prod, 147, pp. 560–571, 2017. DOI: https://doi.org/10.1016/j.jclepro.2017.01.121.
[22] Mohajerani, A., Recycling waste rubber tyres in construction materials and associated environmental considerations: a review, Resour Conserv Recycl, 155, art. 104679, 2020. DOI: https://doi.org/10.1016/j.resconrec.2020.104679.
[23] Das Gupta, S., Mukhopadhyay, R., Baranwal, K.C., and Bhowmick, A., Reverse engineering concepts, in: Engineering of rubber products, Taylor & Francis Group, Boca Ratón, USA, 2013, pp. 194–199.
[24] Araujo-Morera, J., Verdejo, R., López-Manchado, M., and Hernández Santana, M., Sustainable mobility: the route of tires through the circular economy model, Waste Management, 126, pp. 309–322, 2021. DOI: https://doi.org/10.1016/J.WASMAN.2021.03.025
[25] Valentini, F., and Pegoretti, A., End-of-life options of tyres. a review. Advanced Industrial and Engineering Polymer Research, 5(4), pp. 203–213, 2022, DOI: https://doi.org/10.1016/j.aiepr.2022.08.006
[26] Ramarad, S., Khalid, M., Ratnam, C.T., Chuah, A.L, and Rashmi, W., Waste tire rubber in polymer blends: a review on the evolution, properties and future, Prog Mater Sci, 72, pp. 100–140, 2015, DOI: https://doi.org/10.1016/j.pmatsci.2015.02.004.
[27] Fazli, A., and Rodriguez, D., Waste rubber recycling: a review on the evolution and properties of thermoplastic elastomers. Materials, 13(3), art. 782, 2020. DOI: https://doi.org/10.3390/ma13030782.
[28] Mengistu, D., Nilsen, V., Heistad, A., and Kvaal, K., Detection and quantification of tire particles in sediments using a combination of simultaneous thermal analysis, Fourier Transform Infra-Red, and parallel factor analysis. Int J Environ Res Public Health, 16(18), 2019. DOI: https://doi.org/10.3390/ijerph16183444.
[29] Gunasekaran, S., Natarajan, R.K., and Kala, A., FTIR spectra and mechanical strength analysis of some selected rubber derivatives. Spectrochim Acta A Mol Biomol Spectrosc, 68, pp. 323–330, 2007. DOI: https://doi.org/10.1016/j.saa.2006.11.039.
[30] Lee, Y.S., Lee, W.-K., Cho, S.-G., Kim, I., and Ha, C.-S., Quantitative analysis of unknown compositions in ternary polymer blends: a model study on NR/SBR/BR system. J Anal Appl Pyrolysis, 78(1), pp. 85–94, 2007, DOI: https://doi.org/https://doi.org/10.1016/j.jaap.2006.05.001.
[31] Al-Jabari, M., Fundamentals and categorizations of waterproofing technologies, in: Integral waterproofing of concrete structures, Al-Jabari, M., Ed., in Woodhead Publishing Series in Civil and Structural Engineering, Woodhead Publishing, 2022, pp. 165–198. DOI: https://doi.org/10.1016/B978-0-12-824354-1.00006-4.
[32] Gündüz, G., Chemistry, materials, and properties of surface coatings - Traditional and evolving technologies, cap 9. Silicon resins. [Online]. 2015. Available at: https://app.knovel.com/hotlink/khtml/id:kt0132BATP/chemistry-materials-properties/future-forecast.
[33] Jones, F.N., Polyurethanes and Polyisocyanates, John Wiley & Sons. [Online]. 2017. Available at: https://app.knovel.com/hotlink/khtml/id:kt011JHDH1/organic-coatings-science/polyurethanes-polyisocyanates
[34] Gündüz, G., Chemistry, materials, and properties of surface coatings - Traditional and evolving technologies. cap 11. Acrylic and vinyl resins [Online]. 2015. Available at: https://app.knovel.com/hotlink/khtml/id:kt0132BATP/chemistry-materials-properties/future-forecast.
[35] Ronald, M., and Luis, F.P., Asphalt emulsions formulation: state-of-the-art and dependency of formulation on emulsions properties. Constr Build Mater, 123, pp. 162–173, 2016. DOI: https://doi.org/10.1016/j.conbuildmat.2016.06.129
[36] Kleinsteinberg, F., Wetting- and dispersing additives, in: Additives for waterborne coatings, Vincentz Network, Hannover, Germany, 2014. pp. 20–38. DOI: https://doi.org/10.1515/9783748602187-003.

[37] Gijsbertus, E., and Catarina, C., Leendert, G., Polymer coatings - A guide to chemistry, characterization, and selected applications. Cap 5. Additives and particulates. John Wiley & Sons. [online], 2018, Available at: https://app.knovel.com/hotlink/khtml/id:kt011QZ3Z4/polymer-coatings-guide/additives-particulates
[38] Müller, B., and Poth, U., Coatings formulation, 2nd Revised Edition. Vincentz Network, Hanover, 2011.
[39] Kirchner, J., Defoaming of coating systems, in Additives for waterborne coatings, Vincentz Network, Hannover, Germany, 2014. pp. 39–55. DOI: https://doi.org/10.1515/9783748602187-004.
[40] Koleske J.V., Paint and coating testing manual – cap 32. Coalescing aids 15th Ed., Gardner-Sward Handbook, [Online] 2012. Available at: https://app.knovel.com/hotlink/khtml/id:kt00B7X494/paint-coating-testing/coalescing-aids
[41] Fazli, A., and Rodriguez, D., Effect of Ground Tire Rubber (GTR) particle size and content on the morphological and mechanical properties of recycled High-Density Polyethylene (rHDPE)/GTR Blends, Recycling, 6(3), 2021. DOI: https://doi.org/10.3390/recycling6030044.

L.V. Salcedo-Mojica, received the BSc. Eng. in Chemical Engineering in 2024, from the Universidad América. Bogotá, Colombia. Since 2023, she has been working as a quality control analyst, performing physicochemical analysis, gas chromatography and sensory analysis of finished products and raw materials for use and/or dispatch decisions, in addition to conducting research on non-conformity and compounding errors in the weighing of formulations.
ORCID: 0009-0002-2965-9848

J Arturo-Calvache, received the BSc. Eng. in Chemical Engineering from the Universidad Nacional de Colombia (Manizales, Colombia) and a MSc. in Chemical Engineering from the Universidad Nacional de Colombia (Bogotá, Colombia), currently pursuing a doctoral degree in materials engineering at the Federal University of Rio de Janeiro (Brazil). He is a research professor of the Sustainable Processes Group of the chemistry and environmental program at Universidad de América (Bogotá, Colombia). His research interests include simulation and intensification of chemical processes, molecular dynamics, energy efficiency and waste utilization.
ORCID: 0000-0002-4267-3399

C Ramirez-Meneses, received the BSc. Eng. in Industrial Engineering from the National School of Engineers of Metz, France in 2008, Technology in Industrial Production Management from the National Learning Service SENA, Bogotá D.C. Colombia in 2008, Industrial Engineering in 2013 from the Central University, and Master in Industrial Engineering in 2019 from the Colombian School of Engineering Julio Garavito in Bogotá, Colombia. Currently Research Group Leader and teacher in Logistics and Transportation programs of the National Learning Service SENA. His research interests include: Design and optimization of logistics strategies for supply chains through 4.0 technologies and metaheuristics, digital transformation and Supply Chain Sustainability. She works as a consultant in planning, execution and supervision of research, technological development and innovation projects for companies in the logistics sector.
ORCID: 0000-0003-3891-6949

DYNA
http://dyna.medellin.unal.edu.co/

UNIVERSIDAD NACIONAL DE COLOMBIA

Numerical simulation of waste landfill biodegradation: Fitting experimental data

Vladimir Buelvas-Hernandez [a,b], Juliana Lucía Moreno-Medina [b] & Marcela Mercado-Montoya [b c]

[a] *Coppe, Universidade Federal do Rio de Janeiro, Rio de Janeiro, Brasil. vladimir.buelvas@coc.ufrj.br*
[b] *Semillero In Silico – UdeA, In Silico STEM SAS, Universidad de Antioquia, Medellín, Colombia. jlucia.moreno@udea.edu.co*
[c] *In Silico STEM SAS, Medellín, Colombia. marcela.mercadom@insilicostem.com*

Received: April 11th, 2024. Received in revised form: November 12th, 2024. Accepted: November 20th, 2024.

Abstract
Landfill remains economically viable for the disposal of Municipal Solid Waste (MSW), however, experiences of failure in several Colombian and global locations, lead to soil, water, and air pollution, harming ecosystems, and biodiversity. Numerical models can help improve the design by considering biodegradation, hydraulic, thermal, and mechanical phenomena involved in landfills. This paper presents a simulation of the landfill biodegradation, calibrating parameters to make results match experimental data from previous references. COMSOL Multiphysics was used to implement McDougall's biodegradation model, tracking organic matter transformation into volatile fatty acids (VFA) and methane (CH4) production via acetogenesis. Parameters taken from previous references were recalibrated to fit data from six US landfills. The results for the concentration variation with time for organic matter, VFA and CH4 successfully follows the expected behavior and fits the experimental data. McDougall's 2007 model, successfully implemented in COMSOL, can be calibrated for data from Colombian and global landfills.

Keywords: waste landfill, biodegradation; mathematical modeling; methane generation.

Simulación numérica de la biodegradación en rellenos sanitarios: ajuste de datos experimentales

Resumen
Los rellenos sanitarios siguen siendo económicamente viables para la disposición de Residuos Sólidos Urbanos (RSU), sin embargo, experiencias de fallas en varios lugares de Colombia y el mundo, conducen a la contaminación del suelo, agua y aire, perjudicando los ecosistemas, y la biodiversidad. Los modelos numéricos pueden ayudar a mejorar el diseño considerando los fenómenos de biodegradación, hidráulicos, térmicos y mecánicos involucrados en los rellenos sanitarios. Este trabajo presenta una simulación de la biodegradación en rellenos sanitarios, calibrando los parámetros para que los resultados coincidan con los datos experimentales de la literatura técnica. Se utilizó COMSOL Multiphysics para implementar el modelo de biodegradación de McDougall, siguiendo la transformación de la materia orgánica en ácidos grasos volátiles (AGV) y la producción de metano (CH4) vía acetogénesis. Los parámetros tomados de referencias anteriores se recalibraron para ajustarlos a los datos de seis vertederos estadounidenses. Los resultados de la variación de la concentración con el tiempo para la materia orgánica, los AGV y el CH4 siguen satisfactoriamente el comportamiento esperado y se ajustan a los datos experimentales. El modelo de McDougall de 2007, implementado con éxito en COMSOL, puede calibrarse para datos de rellenos colombianos y mundiales.

Palabras clave: relleno sanitario; biodegradación; modelado matemática; generación de metano

1 Introduction

Utilizing stratified waste placement continues as an economically viable approach for the disposal of Municipal Solid Waste (MSW) in numerous countries. However, experiences of failure in several Colombian locations, including Bucaramanga (Carrasco, 2017), Cali (2001), and Bogota (1998), have underscored the need for heightened scrutiny and research on MSW management within the country.

How to cite: Buelvas-Hernandez, V., Moreno-Medina, J., and Ramírez-Meneses, M., Numerical simulation of waste landfill biodegradation: fitting experimental data. DYNA, 91(234), pp. 135-139, October - December, 2024.

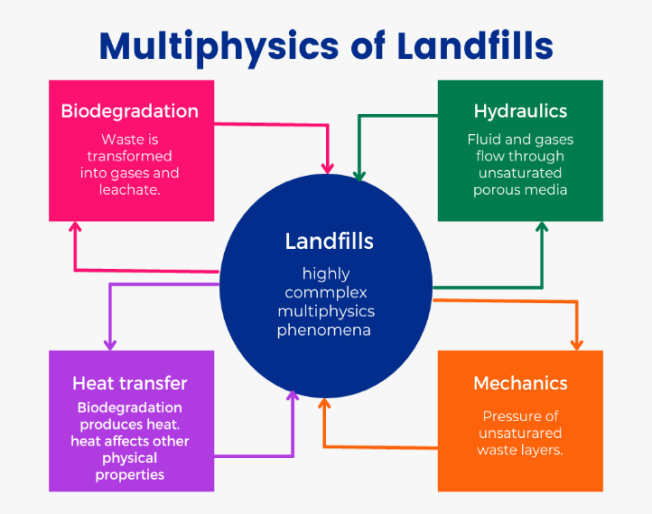

Figure 1. The Multiphysics phenomena influencing landfill design.
Source: Own

One of the primary challenges in MSW landfill management revolves around the accurate estimation of settlement, given that landfills naturally undergo settling processes over time. The final settlement can amount around to 30% of the initial landfill height according to [1]. The intricate interplay of waste biodegradation significantly influences this settling phenomenon. As waste materials biodegrade, they generate byproducts such as gas and leachate, initiating a cascade of complex processes that involve biochemical, mechanical (settlement, stresses, etc.), hydraulic (flow, pressure), and thermal phenomena (temperature rise). Fig. 1 illustrates the multiphysics phenomena intricately interwoven in landfill design and performance [2].

Introducing a Multiphysics simulation of biodegradation in landfill waste is crucial for understanding the long-term behavior of municipal solid waste (MSW) and its environmental impact. Landfill settlement estimation and the complex processes involved are of significant concern in landfill management. To address these challenges, innovative models have been developed, such as hydro-mechanical [3-8], bio-mechanical [3-11], hydro-bio-mechanical [3-8,11], hydro-thermal [12,13], gas generation [3-5,9,11], and hydro-bio-thermal models [13-15].

The degradation model encompasses various stages, from organic matter coming from solid degradable fraction (SDF) transforming into volatile fatty acids (VFA) through hydrolysis and acidogenesis to the formation of methanogenic biomass (MB), which leads to methane (CH4) and carbon dioxide (CO2) production, Fig. 2 [2]. Methane generation is an environmental concern that further emphasizes the study of biodegradation in landfills [8].

Different methods, such as one-state, two-state, and multi-state, can be used to classify anaerobic biodegradation models based on the number of chemical and bacterial reaction paths. The two-state method is the most widely used and relies on variables such as Solid Degradable Fraction (SDF), VFA, and MB.

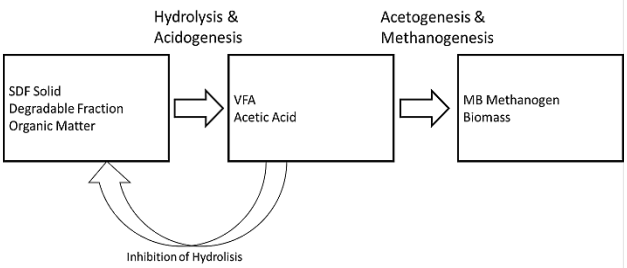

Figure 2. Biodegradation process.
Source: Own

Several mathematical models have been proposed to describe the depletion rate of SDF in MSW. A mathematical model proposed by McDougall [3] based on a chemical equation has served as a foundation for subsequent studies. [16] proposed a bio-thermal (BT) model validated through six laboratory experiments conducted by [5] and [17]. As a result of calibrating the model, the author applied it to a typical full-scale landfill cell geometry to examine the long-term spatial and temporal variation over time. A laboratory test performed by [18] achieved similar results using a biodegradation model based on McDougall of approach.

Estimating MSW properties for numerical modeling requires empirical measurements. Studies by [5] and [17] conducted laboratory tests to characterize biodegradation potential and measure key byproducts such as VFA and MB. These studies provide valuable insights into the behavior of MSW under different conditions.

A series of laboratory tests were performed and carried out to characterize anaerobic biodegradation potential of fresh MSW, using two large-scale Consolidating Anaerobic Reactors (CARs). The CARs contained waste material of the same composition as that used in BMP tests in other laboratory test performance by the authors. Two levels of constant vertical overburden pressures were applied on the top of the waste sample during the entire course of the experiment (CAR1: 150 kPa and CAR2: 50 kPa) to simulate representative overburden stresses experienced in landfills [5].

[17] run out laboratory tests to investigate the biochemical and physical characteristics of MSW under leachate recirculation-enhanced conditions. Waste samples were extracted from different waste landfills around USA, with duration ranging approximately 850 to 1500 days (namely, Michigan MI – 1,100 days, Texas TX – 1,500, Arizona AZ – 885, and California CA – 850 days).

Correlations of Methane generation potential (L0) and a percentage of biodegradable waste prior to degradation, parameter B0, were obtained. In the same way, correlations of methane generation rate (r_{CH4}), L_0 and maximum soluble chemical oxygen demand in leachate were developed.

The articles by [19] and [4] present mathematical models for predicting the biodegradation of organic matter in landfills. [19] model considered factors like moisture content, temperature, and pH levels, accurately predicting degradation rates. [4] focused on biochemical processes, including hydrolysis, acidogenesis, acetogenesis, and methanogenesis, validating the model with empirical data and using it to predict waste degradation rates and methane production.

Understanding biodegradation processes and modeling them is crucial for landfill management and reducing greenhouse gas emissions. The processes can provide valuable insights and optimization strategies.

This paper presents the modeling and simulation of landfill biodegradation using the mechanistic biodegradation model [3], widely used in technical literature. The analysis is based on model parameter values reported in the literature [5,17,20,21]. In addition, the basis is laid for future comparison with laboratory measurements to corroborate the theory and calibrate the model parameters.

2 Methodology

2.1 Mathematical Model

The most used model for biodegradation in landfills is that of [3], which was implemented in this study by means of COMSOL Multiphysics software. According to the McDougall model, the three main mechanisms involved in biodegradation (Fig 1) can be simplified by eq. (1).

$$\overbrace{\underbrace{C_6H_{10}O_5}_{162\ g}}^{SDF} + \underbrace{H_2O}_{18g} \rightarrow \overbrace{CH_3COOH}^{VFA} + 8H_2 + 4CO_2 \rightarrow \overbrace{\underbrace{3CO_2}_{132g} + \underbrace{3CH_4}_{48g}}^{MB} \quad (1)$$

The Solid Degradable Fraction (SDF), Volatile Fatty Acids (VFA) and Methanogenic Biomass (MB) are represented chemically in eq. (1) by cellulose, acetic acid, and carbon dioxide plus methane, respectively. The VFA accumulation rate r_g in gVFA m-3aqueous day-1, is expressed mathematically by eq. (2). where kVFA is the production inhibition rate constant, c is the concentration of VFA in the aqueous phase in gVFA m-3aqueous, S is the solid degradable fraction at any instant of time, SO is the initial solid degradable fraction (SDF) b is the maximum VFA growth rate (gVFA m-3aqueous day-1), n is the structural transformation parameter, $\theta_e = \frac{\theta - \theta_r}{\theta_s - \theta_r}$ is the effective volumetric moisture content, and θ, θ_r and θ_s are respectively the volumetric, residual and saturation moisture contents.

$$r_g = \theta_E b \left[1 - \left[\frac{S_O - S}{S_O}\right]^n\right] * e^{-k_{VFA}(c))} \quad (2)$$

The MB production/growth rate (r_j) represents methanogenic substrate depletion and methanogen growth, which are described by Monod kinetics according to eq. (3). Where k0 is the specific growth rate (day-1), m is the concentration of MB in aqueous phase (g[VFA] m-3[aqueous]) and kMC is the half-saturation constant (g[VFA] m-3[aqueous]).

$$r_j = \frac{k_0 c}{(k_{MC} + c)} m \quad (3)$$

The terms $r_h = \frac{r_j}{Y}$, and $r_k = k_2 m$ depict the VFA consumption rate and the MB decay/death rate respectively. VFA consumption rate is associated to the MB growth rate r_j through a substrate yield coefficient Y. The methanogenic decay rate is related to k2, the MB decay rate constant (day-1). Finally, it is possible to set up a system of ordinary differential equations to describe the accumulation rates of SDF (S), VFA (c) and MB (m) by equations Eq. 4 to 6 respectively.

$$\frac{\partial S}{\partial t} = -\theta \frac{162}{60} r_g \quad (4)$$

$$\frac{\partial c}{\partial t} = [r_g - r_h] \quad (5)$$

$$\frac{\partial m}{\partial t} = [r_j - r_k] \quad (6)$$

The model was proved with different combinations of parameters and initial conditions as shown in Table 1, as reported in [20,21], which refers to measurements in different landfills in the USA. The parameters were further optimized for better adjustment of the simulation with the field data.

Table 1.
Parameter values for different landfill data cases

Parameter	CAR1	CAR2	MI	TX	AZ	AC
Initial volumetric moisture content (%)	56.3	64.3	27.0	49.0	38.0	42.0
Volumetric residual moisture content (%)	11.0	11.0	7.7	15.0	12.0	16.0
Percentage of degradable solids (%)	55.0	55.0	30.2	11.7	24.0	9.0
Degradable solids density (kg m^{-3})	745.0	745.0	882.0	1044.0	955.0	1338.0
Inert solids phase density (kg m^{-3})	1735.0	1735.0	895.0	1727.0	1716.0	1660.0
Initial SDF concentration (kg m^{-3})	240.6	196.6	93.4	70.1	111.6	57.4
Initial VFA concentration (g$_{[VFA]}$ m^{-3}$_{[aqueous]}$)	300.0	300.0	0.0	0.0	8500.0	0.0
Initial MB concentration (g$_{[VFA]}$ m^{-3} $_{[aqueous]}$)	1000.0	1000.0	300.0	100.0	1200.0	10.0
Maximum hydrolysis rate (g$_{[VFA]}$ m^{-3}$_{[aqueous]}$ day^{-1})	18000.0	24000.0	9000.0	2000.0	5200.0	2000.0
Product inhibition factor (m^{3}g^{-1}) kVFA	1×10^{-4}	1×10^{-5}	8.5×10^{-4}	4.2×10^{-4}	1.2×10^{-4}	6.3×10^{-3}
Structural transformation parameter (-) n	0.06	0.06	1.00	0.70	1.00	0.70
Maximum specific growth rate for MB k(day^{-1})	0.047	0.047	0.128	0.150	0.070	0.70
Methanogen death rate (day^{-1})	0.0040	0.0040	0.0050	0.0005	0.0040	0.0005
Half saturation constant kMC(g m^{-3} aq.)	4000	4000	1000	1500	3500	700
Cell to substrate yield coefficient	0.08	0.08	0.30	0.40	0.40	0.30

Source: taken from [20]

3 Results and Discussion

Fig 2 illustrates the biodegradation process, wherein degradable waste undergoes hydrolysis, acidogenesis/acetogenesis, and methanogenesis to transform SDF material into VFA and MB. Over time, Figs. 3 to 5 display the concentrations of SDF, VFA, and MB. A comparison between field data and model results from six experiments conducted across various waste landfills is available for analysis.

As shown in Fig. 3, a non-linear drop in SDF is presented as the initial fraction consumed by chemical processes under anaerobic conditions. The comparison between field data and model results for MI, TX, AZ and CA samples shows a very similar behavior of SDF over time, suggesting the model parameters are well calibrated. The experimental results are not available for CAR 1 and CAR2, but the simulated results are like the other samples in trend. In the case of CAR2, the results suggest additional parameter refinement could be done to improve the results, as other references suggest the decay time of SDF is shorter for this sample [16].

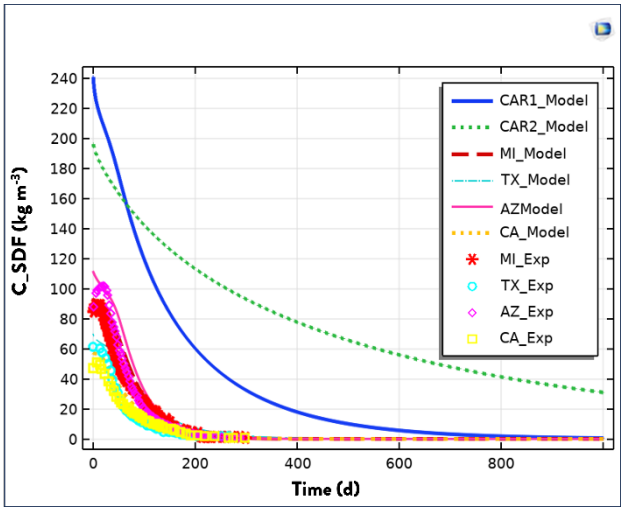

Figure 3. Concentration of Solid Degradable Fraction (C_SDF) as a function of time. Source: Own

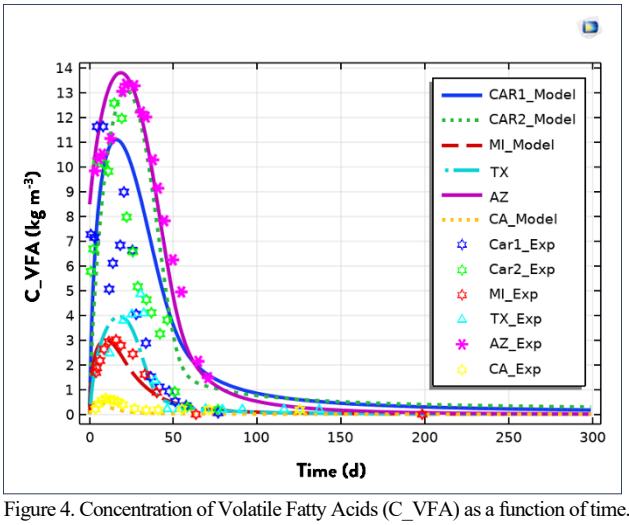

Figure 4. Concentration of Volatile Fatty Acids (C_VFA) as a function of time. Source: Own

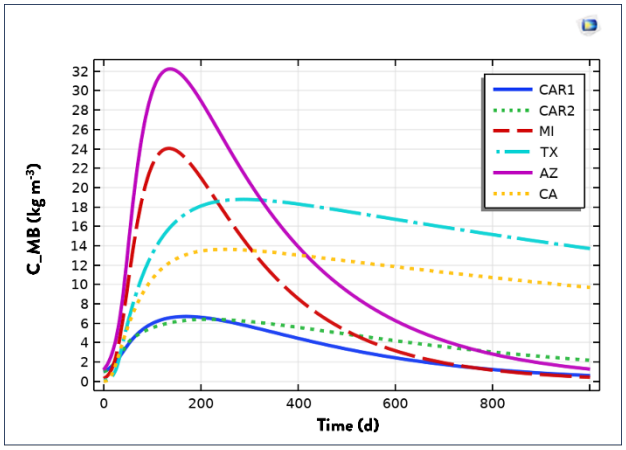

Figure 5. Concentration of Methanogenic Biomass (C_MB) as a function of time. Source: Own

Fig. 3 presents only simulated results available for CAR1 and CAR2 samples. For MI, TX, AZ, and CA samples, the comparison of experimental and simulated results is available.

The VFA behavior over time is shown in Fig. 4. Fig. 4 presents all the samples (CAR1, CAR2, MI, TX, AZ, and CA), the comparison of experimental and simulated results is available. The comparison between field and simulated data shows a good agreement for all the samples. As SDF is consumed, the maximum VFA peaks after 25 to 50 days, then decays exponentially leading to MB generation. For all the samples, 150 to 200 days are required to consume all the VFA.

On the other hand, Methane production/consumption occurs slower (Fig. 5), reaching a peak after 150 days just when the VFA has been depleted, controlled by the specific decay rate (k2). For all the samples (CAR1, CAR2, MI, TX, AZ, and CA), only simulated results are available.

The numerical results spanning 1000 days of simulation, as depicted in Figs. 3-5, align closely with the anticipated outcomes based on the chemical processes inherent to the waste site. Moreover, the model accurately reproduces curve trends, with peak values closely resembling those reported by the authors [20,21].

4 Conclusion

The mathematical model proposed by McDougall in 2007 has been successfully implemented in COMSOL. Its validation was achieved through comparison with biochemical data collected from six laboratory experiments conducted on samples sourced from real MSW landfills in both the United States and the United Kingdom. In summary, the model delineates the biodegradation process within a bioreactor landfill, comprising three phases transitioning from SDF to MB via intermediate VFA stages. Graphical representations underscore the correlation between the consumption of the VFA phase and the subsequent increase in the MB phase, offering insights into the dynamics of the system.

Upon calibration of the model, we have successfully determined biodegradation parameters. These parameters exhibit strong agreement with laboratory experimental data, particularly concerning variations in biochemical parameters such as volatile

fatty acids and degradable solids within the waste samples. This alignment underscores the model's reliability in capturing the intricate dynamics of the biodegradation process. These refined parameters serve as a foundation for executing coupled Multiphysics models in subsequent analyses.

Integrating thermal dynamics, mechanical settlement, and hydraulic processes is essential for advancing the present waste backfill model. Thermal dynamics account for temperature's impact on biodegradation, while considering mechanical settlement ensures structural stability and deformation analysis. Hydraulic processes govern fluid flow, gas migration, and leachate transport. By incorporating these physics, we develop a comprehensive model that predicts temperature variations, structural integrity, and fluid dynamics within landfill systems, enhancing our management strategies.

Acknowledgements

We extend our sincere thanks to Semillero In Silico UdeA for their invaluable support in promoting sustainability through STEM disciplines. Vladimir would like to greatly acknowledge the financial supports by ¨Pasaporte a la ciencia¨-ICETEX-Colfuturo.

Bibliography

[1] Krase, V., Bente, S., Kowalsky, U., and Dinkler, D., Modelling the stress-deformation behaviour of municipal solid waste, Geotechnique, 61(8), pp. 665–675, 2011. DOI: https://doi.org/10.1680/geot.8.P.140.

[2] Hubert, J., Liu, X. F. and Collin, F., Numerical modeling of the long term behavior of Municipal Solid Waste in a bioreactor landfill, Comput Geotech, 72, pp. 152–170, 2016. DOI: https://doi.org/10.1016/j.compgeo.2015.10.007

[3] McDougall, J., A hydro-bio-mechanical model for settlement and other behaviour in landfilled waste. Comput Geotech, 34(4), pp. 229–246, 2007. DOI: https://doi.org/10.1016/j.compgeo.2007.02.004.

[4] White, J., Robinson, J., and Ren, Q., Modelling the biochemical degradation of solid waste in landfills, Waste Management, 24(3), pp. 227–240, 2004. DOI: https://doi.org/10.1016/j.wasman.2003.11.009.

[5] Ivanova, L.K., Richards, D.J., and Smallman, D.J., Assessment of the anaerobic biodegradation potential of MSW, Proceedings of Institution of Civil Engineers: Waste and Resource Management, 161(4), pp. 167–180, 2008. DOI: https://doi.org/10.1680/warm.2008.161.4.167.

[6] Hettiarachchi, H., Meegoda, J., and Hettiaratchi, P., Effects of gas and moisture on modeling of bioreactor landfill settlement, Waste Management, 29(3), pp. 1018–1025, 2009. DOI: https://doi.org/10.1016/j.wasman.2008.08.018.

[7] Chen, Y., Xu, X., and Zhan, L., Analysis of solid-liquid-gas interactions in landfilled municipal solid waste by a bio-hydro-mechanical coupled model. Sci China Technol Sci, 55(1), pp. 81–89, 2012. DOI: https://doi.org/10.1007/s11431-011-4667-7.

[8] Staub, M.J., Gourc, J.-P., Drut, N., Stoltz, G., and Mansour, A.A., Large-scale bioreactor pilots for monitoring the long-term hydromechanics of MSW. J Hazard Toxic Radioact Waste, 17(4), pp. 285–294, 2013. DOI: https://doi.org/10.1061/(ASCE)HZ.2153-5515.0000160.

[9] Machado, S.L., Carvalho, M.F. and Vilar, O.M., Constitutive model for municipal solid waste. Journal of Geotechnical and Geoenvironmental Engineering, 128(11), pp. 940–951, 2002. DOI: https://doi.org/10.1061/(ASCE)1090-0241(2002)128:11(940).

[10] Babu, G.L.S., Reddy, K.R., Chouskey, S.K., and Kulkarni, H.S., Prediction of long-term municipal solid waste landfill settlement using constitutive model. Practice Periodical of Hazardous, Toxic, and Radioactive Waste Management, 14(2), pp. 139–150, 2010. DOI: https://doi.org/10.1061/(ASCE)HZ.1944-8376.0000024.

[11] Liu, X., Shi, J., Qian, X., Hu, Y., and Peng, G., One-dimensional model for municipal solid waste (MSW) settlement considering coupled mechanical-hydraulic-gaseous effect and concise calculation. Waste Management, 31(12), pp. 2473–2483, 2011. DOI: https://doi.org/10.1016/j.wasman.2011.07.013.

[12] Garg, A., and Achari, G., A comprehensive numerical model simulating gas, heat, and moisture transport in sanitary landfills and methane oxidation in final covers. Environmental Modeling & Assessment, 15(5), pp. 397–410, 2010. DOI: https://doi.org/10.1007/s10666-009-9217-3

[13] Gholamifard, S., Eymard, R., and Duquennoi, C., Modeling anaerobic bioreactor landfills in methanogenic phase: long term and short term behaviors. Water Res, 42(20), pp. 5061–5071, 2008. DOI: https://doi.org/10.1016/j.watres.2008.09.040

[14] Gawande, N.A., Reinhart, D.R., and Yeh, G.-T., Modeling microbiological and chemical processes in municipal solid waste bioreactor, Part I: development of a three-phase numerical model BIOKEMOD-3P. Waste Management, 30(2), pp. 202–210, 2010. DOI: https://doi.org/10.1016/j.wasman.2009.09.009

[15] Hanson, J.L., Yeşiller, N., Onnen, M.T., Liu, W.L., Oettle, N.K., and Marinos, J.A., Development of numerical model for predicting heat generation and temperatures in MSW landfills. Waste Management, 33(10), pp. 1993–2000, 2013. DOI: https://doi.org/10.1016/j.wasman.2013.04.003

[16] Kumar, G., Reddy, K.R., and McDougall, J., Numerical modeling of coupled biochemical and thermal behavior of municipal solid waste in landfills. Comput Geotech, 128, art. 103836, 2020. DOI: https://doi.org/10.1016/j.compgeo.2020.103836

[17] Fei, X., and Zekkos, D., Coupled experimental assessment of physico-biochemical characteristics of municipal solid waste undergoing enhanced biodegradation. Géotechnique, 68(12), pp. 1031–1043, 2018. DOI: https://doi.org/10.1680/jgeot.16.P.253

[18] Datta, S., and Zekkos, D., The influence of waste composition on biogas generation model parameters. Environmental Geotechnics, 10(7), pp. 443-454, 2021. DOI: https://doi.org/10.1680/jenge.20.00058

[19] Haarstrick, A., Hempel, D.C., Ostermann, L., Ahrens, H., and Dinkler, D., Modelling of the biodegradation of organic matter in municipal landfills. Waste Management & Research: the Journal for a Sustainable Circular Economy, 19(4), pp. 320–331, 2001. DOI: https://doi.org/10.1177/0734242X0101900409.

[20] Datta, S., Zekkos, D., Fei, X., and Mcdougall, J., Waste-composition-dependent 'HBM' model parameters based on degradation experiments, Environmental Geotechnics, 8(2), pp. 124-133, 2018. DOI: https://doi.org/10.1680/jenge.18.00014

[21] Kumar, G., Reddy, K.R., and McDougall, J., Numerical modeling of coupled biochemical and thermal behavior of municipal solid waste in landfills, Comput Geotech, 128, 2020. DOI: https://doi.org/10.1016/j.compgeo.2020.103836.

V. Buelvas-Hernandez received the BSc. Eng in Civil Engineering in 2001 from the Universidad Nacional de Colombia. Medellin campus, Colombia, had an MSc. in Geotechnical Engineering in 2008 from the Universidad Polytechnical de Catalunya, Spain, and currently he is pursuing his PhD. in Geotechnical Engineering from the Universidade Federal do Rio de Janeiro, Brazil. Mr. Buelvas has been working as a consultor and professor in some universities of. His research interests include simulation, modeling, and behavior of soil mechanic.
ORCID: 0009-0006-2556-9473

J.L. Moreno-Medina, is an undergraduate student in Bioengineering at the University of Antioquia, Colombia. She has been a member of the research incubator In Silico UdeA since 2022, where she has participated in projects involving Multiphysics Simulation related to areas such as landfills, geothermal energy, and hyperthermia in breast cancer treatments.
ORCID: 0009-0008-6924-9695

M. Mercado-Montoya, is the co-founder and CEO of In Silico STEM SAS and Semillero In Silico UdeA. Is a BSc. Eng. in Bioengineer and MSc. in Engineering from UdeA. She possesses extensive expertise in numerical modeling and simulation applied to sustainable physical innovations. Marcela has served as a consultant on simulation projects across various industries including biomedical, energy, chemical, and civil engineering, among others. Additionally, she has contributed to academia as a university lecturer in the same field.
ORCID: 0000-0002-1453-4690

DYNA
http://dyna.medellin.unal.edu.co/

UNIVERSIDAD NACIONAL DE COLOMBIA

Trends in the use of biomass for energy generation for a province in the Central Region of Argentina

Agostina Lucía Quicchi [a], Mariana Del Valle Bernard [a], Diego Martín Ferreyra [a] & Gustavo Alejandro Schweickardt [b]

[a] *Facultad Regional San Francisco, Universidad Tecnológica Nacional, San Francisco, Argentina. aquicchi@facultad.sanfrancisco.utn.edu.ar, mbernard@facultad.sanfrancisco.utn.edu.ar, dferreyra@facultad.sanfrancisco.utn.edu.ar*
[b] *Facultad Regional Concepción del Uruguay, Universidad Tecnológica Nacional, Concepción del Uruguay, Argentina. gustavoschweickardt@conicet.gov.ar*

Received: August 28th, 2024. Received in revised form: November 19th, 2024. Accepted: November 25th, 2024.

Abstract
In this work, analyses are performed on international reports applicable to Argentina regarding the use of biomass for energy generation. More specific trends in the national context are also analyzed, and then a more detailed study is performed for Córdoba, one of the three provinces in the so-called Central Region. Córdoba was chosen not only due to its large availability of biomass and wide range of agricultural production, but also because of its favorable regulation promoting energy generation with regional biomass. It becomes clear that projects using dry biomass are very limited in number and scale in this province. Considering previous studies, including articles by the authors on energy applications of regional biomass such as sorghum, esparto grass or corn, it can be hinted that the use of dry biomass resources for energy generation is well below the capacity in the chosen province.

Keywords: energy crops; biofuels; biomass residue; bioenergy; biomass energy.

Tendencias en el uso de biomasa para generación de energía en una provincia de la Región Centro de Argentina

Resumen
En este trabajo, se evalúan informes internacionales sobre el uso de biomasa para generación de energía en Argentina. También se analizan tendencias específicas del contexto nacional y luego se estudia más detalladamente Córdoba, una de las tres provincias de la denominada Región Centro. Se elige Córdoba no solo por su gran disponibilidad de biomasa y amplia variedad de producción agrícola, sino también por su normativa favorable para promover la generación de energía con biomasa regional. Resulta evidente que los proyectos con biomasa seca son muy limitados en cantidad y escala en esta provincia. Teniendo en cuenta estudios previos, incluso artículos de los autores sobre aplicaciones energéticas de biomasa regional como sorgo, espartillo o maíz, se revela que el aprovechamiento de los recursos de biomasa seca para generación de energía está muy por debajo de la capacidad de la provincia seleccionada.

Palabras clave: cultivos energéticos; biocombustibles; residuo biomásico; bioenergía; energía de la biomasa.

1 Introduction

Biomass is understood as all organic matter of biological origin, including materials resulting from its natural or artificial transformation. It is one of the most reliable and adaptable renewable energy sources and can be stored, which facilitates its conversion into thermal and electrical energy [1].

In recent years, the use of biomass for energy purposes has been included as one of the priorities in several countries. However, there are still certain difficulties associated with

How to cite: Quicchi, A.L., Bernard, M.dV., Ferreyra, D.M., and Schweickardt, G.A., Trends in the use of biomass for energy generation for a province in the Central Region of Argentina. DYNA, 91(234), pp. 140-146, October - December, 2024.

the political, institutional, economic, sociocultural and environmental context that have a direct impact on the advancement of biomass for energy purposes [1].

Globally, bioenergy is the largest renewable resource available, accounting for 12 % of total energy consumption for various uses. Nevertheless, the traditional use of solid biomass such as firewood, charcoal and crop residues accounts for more than 50 % of total bioenergy consumption [2]. As a result, the growth in the production and use of modern bioenergy is crucial for the energy transition, since it not only involves different technologies of higher efficiency such as gasification, cogeneration plants, and biogas systems, but also employs different types of fuels, including pellets, biogas, biomethane, and agricultural and forestry residues. The modern use of biomass allows for a better use of energy and reduces greenhouse gas emissions, but it is important for its development to be managed sustainably and with appropriate policies. This article will analyze the use of biomass for energy generation, particularly electricity, first from a global point of view, then focusing on Argentina, and finally on a particular region of this country.

2 International trends

From 2009 to 2019, electricity from bioenergy doubled and, according to the current forecast by the IEA (International Energy Agency), this trend will continue between 2020 and 2030, although its growth is very gradual compared to the contribution of other renewable energies. Based on IRENA's data (International Renewable Energy Agency), in 2020, 29 % of the world's total electricity generation will come from renewable energies, mainly hydroelectric, wind and solar power. In 2020, bioenergy accounted for only about 2 % of the total installed electric power and contributed about 3 % of the total electrical energy generated, although it is noted that electricity from bioenergy increased by 6.7 % that year compared to 2019. In IRENA's reports, the term "bioenergy" includes three different categories: biogas, liquid biofuels, and solid biofuels and renewable waste [2, 3].

Currently, biomass continues to grow steadily in electricity generation, but with a relatively low share and practically constant values, with China, India, the United Kingdom, Brazil, the United States, and the European Union having the largest installed capacity [2].

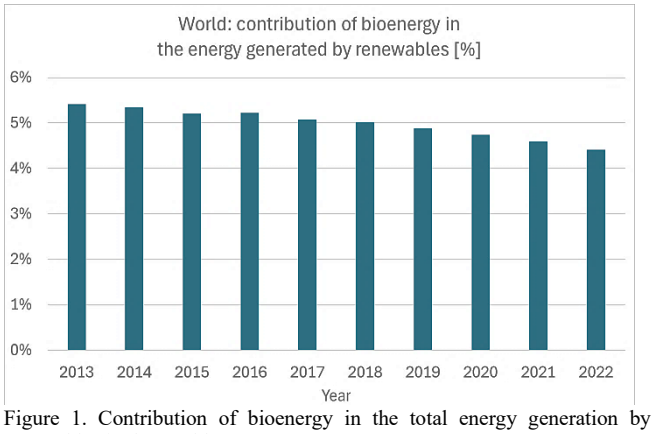

Figure 1. Contribution of bioenergy in the total energy generation by renewables in the world [%].
Source: The authors, based on public data from the IRENA, 2023 [4].

Fig. 1 shows the contribution of bioenergy to global electricity generation from renewable sources over the years.

It can be seen that biogas, solid biofuels and renewable waste represent almost all the bioenergy used for electricity generation, while a marginal percentage corresponds to liquid biofuels. This figure shows a decreasing trend in the percentage contribution of bioenergy in recent years [4]. This means that, although the total electricity generation from biomass increases annually in the world, the other renewable sources grow at a higher rate.

Of the 3 % of electricity generated from bioenergy, 90 % corresponds to the use of solid biofuels such as pellets, bagasse, and renewable municipal waste. It is interesting to note that the use of pellets has increased recently, although they are mostly used for heating: Russia, Vietnam and the United States are the main exporters of biofuels [2].

It is important to mention that, in Europe, the final cost of wood pellets for domestic use in 2018 was about 16 USD/GJ. This shows that it is a fully competitive option compared to natural gas, whose price ranged in the same year between 14 USD/GJ and 35 USD/GJ, depending on the levels of VAT and other taxes [2]. It is curious that, despite this clear economic sustainability even in the residential market, there is not a greater development of projects involving dry biomass.

3 National trends

According to IRENA's most recent report, in Argentina the percentage contribution of bioenergy in the generation of electricity from renewable sources in 2023 decreased by 48 % compared to 2013, even higher than the 35 % reduction recorded as a global trend for the same period [4].

It should be noted that, in Argentina, energy generation from biomass is mainly for thermal uses. However, some solid biofuels, renewable residues, bagasse, and biogas are mainly used for electricity generation, all of them in low proportions, almost insignificant compared to countries in other regions of the world [4].

According to the final WISDOM report 'Analysis of the Biomass Energy Balance in Argentina' from 2009, the national potential for dry biomass is around 37 200 kTEP, but current use is only about 5000 kTEP [5]. In addition, this analysis was updated in 2020 with the report 'Update of the Biomass Balance for Energy Purposes in Argentina,' which determined a physically and legally accessible biomass supply of 51 408 235 tons per year available nationwide, with a demand of approximately 10 131 736 tons annually.

This means that the balance between potential supply and consumption results in an annual excess of 40 421 220 tons of biomass resources available for energy use [1]. Considering that this figure does not include crop residue from extensive agricultural activities, both references show the great potential in Argentina, which is currently not being exploited, since progress is gradual and, in recent years, there is no clear trend of growth.

In Argentina, CAMMESA (Compañía Administradora del Mercado Mayorista Eléctrico SA), the Argentine Wholesale Electricity Market Clearing Company, is a private company with objectives regarding the public energy sector. It operates the Argentinian wholesale energy market since 1992 and issues regular reports regarding the national electricity sector. The most regular reports are specifically made available to the operators in

the interconnected system and deal with energy dispatch, energy capacity planning, and short-term market monitoring. There are also monthly and yearly reports which are available to the public, where wholesale figures on energy consumption and generation are broken down into different categories. The information for Figs. 2-5 in this section was obtained from ten consecutive public yearly reports issued by CAMMESA, focusing specifically on renewable energy sources and, among those, on data related to bioenergy sources [6].

In Fig. 2, the total energy generated in GW·h within Argentina is itemized by source for this period. Up to and including the 2017 report, the raw "Renewables" item included only wind power and photovoltaics, and other renewable sources were detailed separately in each report; therefore, the figures for all these renewable sources were retrieved and included in the current analysis. Also as from 2018, the net imported energy was recorded in a different way in the reports; however, for all the reports under analysis, Argentina's energy imports were left out, so as to focus solely on the national energy generation sources. As a reference, a grand total of 141 398 GW·h was generated in 2023 in the country, considering all the sources [7-16].

In Fig. 3, the evolution of the percentage contribution of renewables in the total energy generation within Argentina is shown for this period.

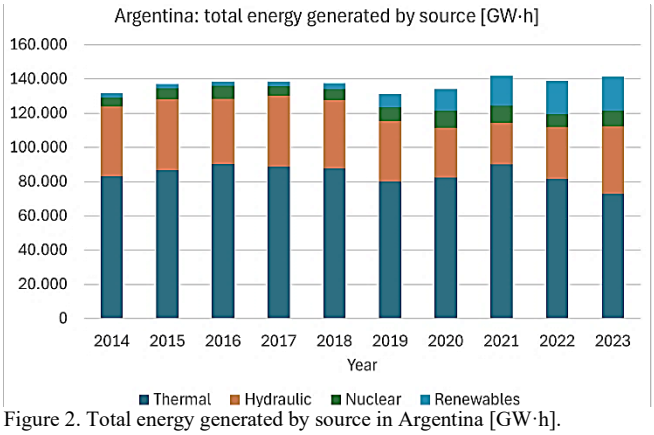

Figure 2. Total energy generated by source in Argentina [GW·h].
Source: The authors, based on public data from CAMMESA, 2015-2024 [7-16].

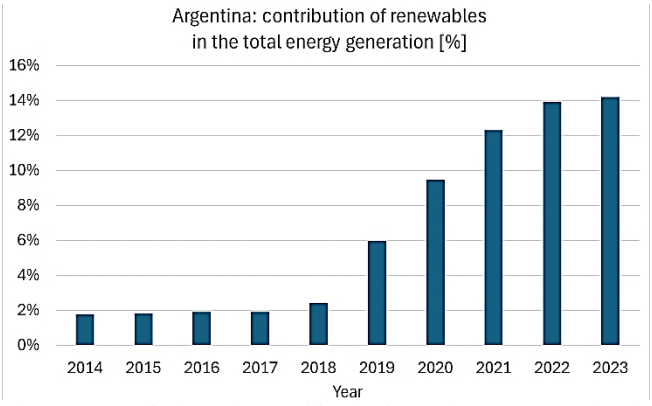

Figure 3. Contribution of renewables in the total energy generation in Argentina [%].
Source: The authors, based on public data from CAMMESA, 2015-2024 [7-16].

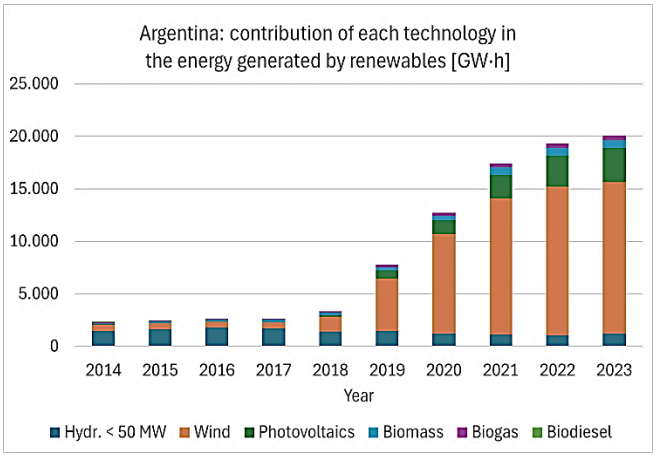

Figure 4. Contribution of each technology in the energy generated by renewables in Argentina [GW·h].
Source: The authors, based on public data from CAMMESA, 2015-2024 [7-16].

As a reference, in 2023 renewables contributed 14.20 % of the total energy generation in the country [7-16].

In Fig. 4, the evolution of the contribution for each technology in the energy generated by renewables within Argentina is shown for this period. In comparison with IRENA reports, it must be noted that CAMMESA distinguishes biomass from biogas and biodiesel, the latter being only marginal for a few years (only 2 GW·h in 2014 and 1 GW·h in 2016) [7-16].

In Fig. 5, the evolution of the energy generated using biomass within Argentina is shown for this period. As a reference, in 2023 biomass accounted for 723 GW·h of energy generation in the country [7-16].

In Fig. 6, the evolution of the percentage contribution of biomass in the energy generation by renewables within Argentina is shown for this period. As a reference, in 2023 biomass accounted for 3.64 % of the energy generation by renewables in the country [7-16].

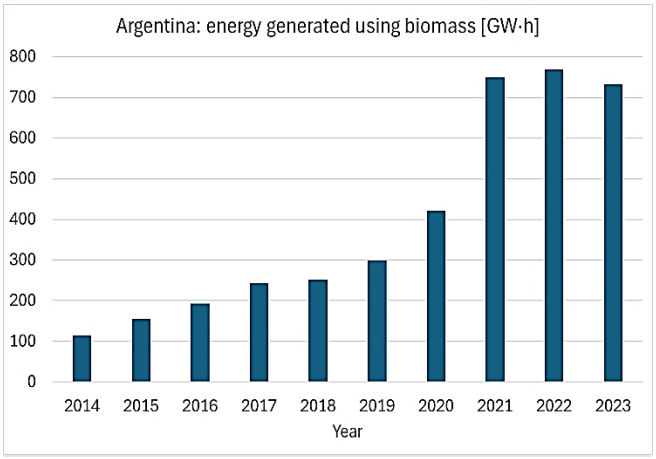

Figure 5. Energy generated using biomass in Argentina [GW·h].
Source: The authors, based on public data from CAMMESA, 2015-2024 [7-16].

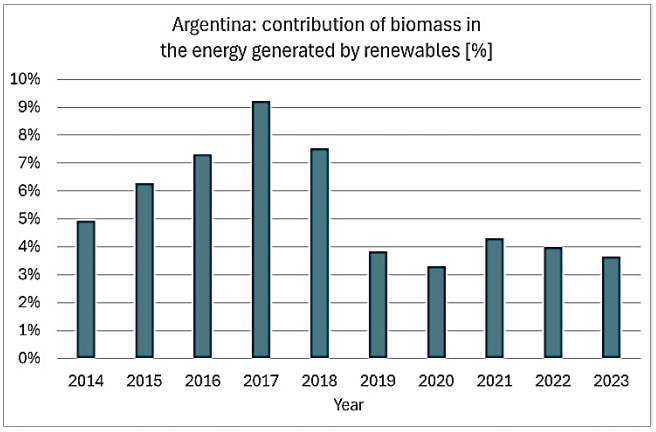

Figure 6. Contribution of biomass in the energy generated by renewables in Argentina [%]
Source: The authors, based on public data from CAMMESA, 2015-2024 [7-16].

For the 2019-2023 period, it can be seen in Fig. 6 that the percentage contribution of biomass among renewables remained at an almost constant level, 3.81 % on average. This might look incoherent with the net growth in the energy generation by biomass as seen in Fig. 5, mainly from 2020 to 2021. However, Fig. 4 helps explain that other renewable technologies, especially photovoltaics, were the ones that drove the general increase in renewable energy, which made biomass contribution remain approximately constant.

4 Regional trends

Fig. 7 highlights the three provinces included in the so-called “Región Centro” (Central Region) of Argentina: Córdoba (CBA), Santa Fe (SFE) and Entre Ríos (E.R).

Figure 7. Provinces in the Central Region of Argentina
Source: public data from website [17]

Together, in the Argentinian context, they account for 55 % of the total grain crop production, 38 % of the country’s exports, and 70 % of the dairy farming.

These proportions are the main reason for considering Córdoba, one of the provinces in this region, for the analysis in this article [17].

In order to identify Córdoba in the national context regarding biomass availability balance, a piece of graphical information can be shown. As for the offer-demand balance regarding biomass for energy, Fig. 8 shows a comparative description of the overall values in tons per year for the whole country, where administrative departments account for the minimum unit of geographic division. It must be emphasized that the balance is consistently positive in most jurisdictions, and it can also be noted that the values in Córdoba tend to be around the average values for the country [18].

In addition, it is important to mention that, within the Central Region, Córdoba is one of the provinces that is most advanced in terms of energy transition regulations and policy. For this reason, the analysis in this section is mainly based on this province. In this context, CAPEC (Córdoba Advisory Council on Energy Policies) committed to working with different energy issues, including bioenergy and biofuels, achieving several regulatory advances in the province [19]. For example, in November 2020, Law 10721 on 'Promotion and Development for the Production and Consumption of Biofuels and Bioenergy' came into force, which establishes a program of encouragement, exemptions, subsidies and incentives to promote the production and consumption of bioenergy and biofuels [20].

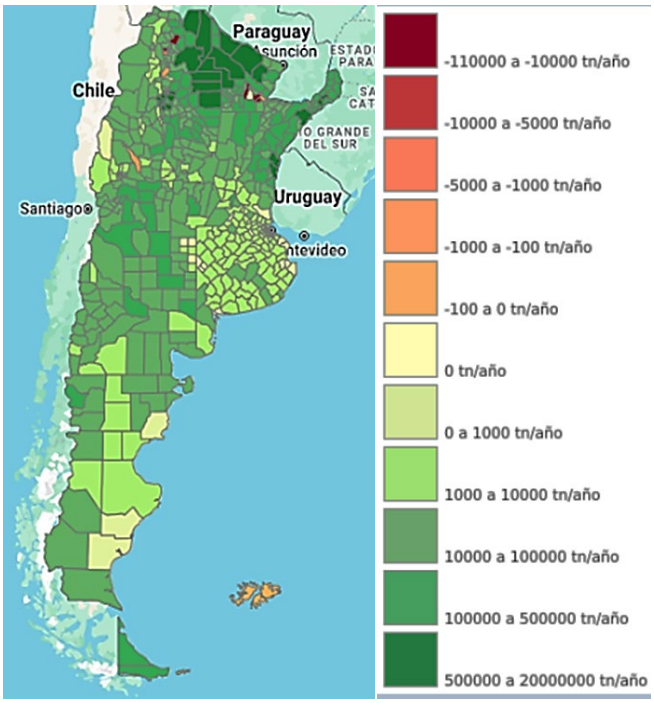

Figure 8. Balance of biomass for energy in Argentina (values in tons/year)
Source: public data from website [18]

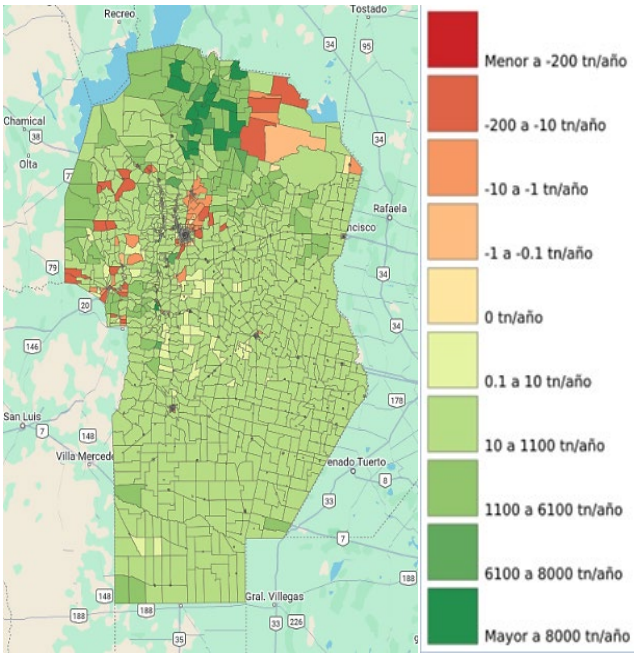

Figure 9. Balance of biomass for energy in the province of Córdoba (values in tons/year)
Source: public data from website [18]

Similarly, Fig. 9 shows the same description as in Fig. 8 in tons per year, particularly for all the departments in the province of Córdoba. These data correspond to PROBIOMASA ('Project for the Promotion of Biomass Derived Energy') whose main objective is to increase the production of thermal and electrical energy derived from biomass at a local, provincial and national level [18].

It can be confirmed that there is an overall evenly distributed positive biomass balance all over the province, which implies a considerably favorable biomass potential [18].

In terms of land cover, according to data obtained from IDECOR ('Spatial Data Infrastructure of the Government of the Province of Córdoba') more than 50 % of the area is covered by annual extensive crops: corn, soybean, sunflower and sorghum, among others [21]. This shows that several agricultural residues from different crops could be used for energy purposes.

For example, in the case of corn, which is one of the main crops, the area planted in the 2022-2023 season was 2 533 203 ha [22]. Considering that an average of 8 t/ha corresponds to corn stubble, the latter represents an interesting source of energy generation from agricultural residues. It is important to note that in recent years several producers have resorted to no-tillage as a sustainable practice. This involves direct seeding on top of the stubble of the previous crop in order to favor soil organic amendment. However, even with no-till, the soil can incorporate up to 40 % of the remaining material as nutrients, so it is possible to remove up to 25 % of the corn stubble for energy use without affecting the soil protection scheme [23]. On the other hand, in drier and colder regions, degradation processes are slower, so the accumulated stubble can interfere with subsequent planting or encourage the proliferation of pathogenic microorganisms [24,25].

In addition to crop stubble, there are different types of biomass available for energy generation [26]. There are naturally growing species such as 'espartillo' (esparto grass or *Spartina argentinensis*) or *Arundo donax*, and energy crops such as *Sorghum saccaratum* variety M81 typical of the region [27, 28], that can be exploited for energy use through different alternatives: obtaining synthesis gas (syngas) [29] for electrical energy generation, and production of hybrid pellets [23] for both thermal and electrical energy [26].

It is important to note that the biomass mentioned is lignocellulosic, meaning that it has a high lignin content, which is associated with a good calorific value for both syngas and pellets.

However, despite the large biomass availability in the province, the electrical energy generation facilities are very scarce: CAMMESA identifies only three biomass-based thermal plants in the province of Córdoba. The following are the nominal powers and locations of said power plants: 9 MW in General Cabrera (Prodeman SA), 3 MW in Ticino (Ticino Biomasa SA), and 0.5 MW in Las Junturas (Emerald Resources SRL). As a reference for 2023, the plant in General Cabrera produced 50.9 GW·h and the one in Ticino generated 22.8 GW·h; no generation records were found for the plant in Las Junturas. Together, they add up to 73.7 GW·h. Comparing this with the information in Fig. 5, it can be seen that Córdoba supplies only 10.19 % of the total biomass energy in the country. Taking into account the agricultural resources in the region, it could be suggested that this contribution could be increased remarkably [6].

5 Discussion

Due to Argentina's favorable agro-ecological conditions and the competitive advantages of the agricultural sector, it can be confirmed that the country has a huge potential regarding energy generation with biomass. However, this has still not been leveraged on a large scale, even though there are several regional or provincial initiatives and policies promoting the use of biomass for energy purposes.

Currently, there are some technical, economic, legal, institutional, and sociocultural barriers and challenges that need to be overcome to increase the share of bioenergy in the national energy matrix [30]. The proliferation of biomass as an energy resource must involve a productive strategy that is attractive to producers. Currently, the profitability from traditional crops in the region is high, so the introduction of new species should be economically competitive with the production of commodities. On the other hand, the demand for solid fuels in the country for energy production is, at best, limited, so the production of pellets or briquettes involves costs and logistics that producers are not willing to adopt unless justified by the demand. Successful experiences in generating electrical energy with dry biomass emerge as a solution to disposal problems involving peanut residues, at the same time providing a solution to local grid power quality issues. However, for the typical crops in the region explored in this work, crop residues do not cause any such problems, making them unattractive for added-value generation. In this context, producers lose interest in energy generation because the economic competition is not only against the replacement

of fossil fuels but also against the profitability of other crops [30]. However, local energy production brings other benefits into focus, such as energy self-sufficiency, decreasing grid demand, adding value to crop residues, developing skilled labor, and creating job opportunities. It would be inadequate to attribute to producers the responsibility of diversifying the productive matrix over the profitability of their agricultural businesses. Therefore, it may be necessary to discuss cross-sectoral policies that promote the continuous and long-term development of the biomass sector. This includes energy strategies that create an attractive market for fuel production and encourage the incorporation of sustainable and distributive economies [31], based on technological development and economic growth [32]. Such strategies should integrate energy-vulnerable communities, generate new job opportunities, and attract investments that add value to residues through new business ventures.

Energy derived from biomass is of particular interest because it helps protect the environment by reducing greenhouse gas emissions and converting waste into resources. Additionally, it provides a storable fuel that can be used with existing generation technology in thermal power plants with minimal modifications. This presents an interesting possibility in this stage of energy transition, with the additional possibility of supplying thermal needs for domestic heating mainly in areas distant from population centers, with no accessibility to the gas network. While this alternative is viable and is already exploited in European countries, it still needs to be explored in Latin America, and specifically in Argentina. To this effect, resources should be managed applying comprehensive, long-term energy transition policies with sustainable criteria and a focus on the profitability of the agricultural sector and a socio-productive perspective. This approach would benefit rural communities, protect productivity, and ensure resource conservation to support energy independence.

6 Conclusions

In recent years, according to international reports, Argentina follows the global trend of slow or almost zero growth in the use of biomass for energy. This situation is replicated in the specific context of Córdoba, one of the three provinces of the so-called Central Region, despite its great availability of biomass, wide variety of agricultural production, and favorable regulations for the generation of energy with regional biomass. It is evident from the literature that projects using dry biomass are very limited in quantity and scale in the mentioned province of Córdoba. Besides, an analysis on previous studies including those conducted by the authors on energy applications of examples of regional biomass such as sorghum, 'espartillo' (esparto grass), or corn, demonstrates that dry biomass resources are very poorly exploited for energy generation in the selected province. Considering all the above, it becomes evident that there are still several technical, economic, legal, and especially local sociocultural challenges impacting the advancement of this type of energy.

References

[1] Denaday, F., Escartín, C., Parodi, G., and Spinazzola, E., Actualización del balance de biomasa con fines energéticos en la Argentina, Buenos Aires, FAO, Argentina, 2020, 126 P.

[2] IRENA (International Renewable Enery Agency), Bioenergy for the energy transition: ensuring sustainability and overcoming barriers, Abu Dhabi, 2022, 128 P.

[3] IEA (International Energy Agency), Renewables 2020. Analysis and forecast to 2025, Paris, IEA Publications, France, 2020, 172 P.

[4] IRENA (International Renewable Energy Agency), Renewable Capacity Statistics, Abu Dhabi, 2023, 69 P.

[5] Trossero, T.J.M., Drigo, R., Anschau, A., Carballo, S., Flores-Marco, N., and Beaumont-Roveda, E., Análisis del balance de energía derivada de biomasa en Argentina WISDOM Argentina, Rome, FAO Departamento Forestal, Dendroenergía [FAO Forest Departament, Dendroenergy], Italy, 2009, 118 P.

[6] CAMMESA (Compañía Administradora del Mercado Mayorista Eléctrico SA), CAMMESA | Sitio web de CAMMESA, Ciudad Autónoma de Buenos Aires, CAMMESA, Argentina, [en línea]. 2024. Disponible en: https://cammesaweb.cammesa.com

[7] CAMMESA (Compañía Administradora del Mercado Mayorista Eléctrico SA), Informe anual 2014, Ciudad Autónoma de Buenos Aires, CAMMESA, Argentina, 2015, 69 P.

[8] CAMMESA (Compañía Administradora del Mercado Mayorista Eléctrico SA), Informe anual 2015, Ciudad Autónoma de Buenos Aires, CAMMESA, Argentina, 2016, 67 P.

[9] CAMMESA (Compañía Administradora del Mercado Mayorista Eléctrico SA), Informe anual 2016, Ciudad Autónoma de Buenos Aires, CAMMESA, Argentina, 2017, 72 P.

[10] CAMMESA (Compañía Administradora del Mercado Mayorista Eléctrico SA), Informe anual 2017, Ciudad Autónoma de Buenos Aires, CAMMESA, Argentina, 2018, 85 P.

[11] CAMMESA (Compañía Administradora del Mercado Mayorista Eléctrico SA), Informe anual 2018, Ciudad Autónoma de Buenos Aires, CAMMESA, Argentina, 2019, 71 P.

[12] CAMMESA (Compañía Administradora del Mercado Mayorista Eléctrico SA), Informe anual 2019, Ciudad Autónoma de Buenos Aires, CAMMESA, Argentina, 2020, 110 P.

[13] CAMMESA (Compañía Administradora del Mercado Mayorista Eléctrico SA), Mercado Eléctrico Mayorista. Informe Anual 2020, Ciudad Autónoma de Buenos Aires, CAMMESA, Argentina, 2021, 111 P.

[14] CAMMESA (Compañía Administradora del Mercado Mayorista Eléctrico SA), Mercado Eléctrico Mayorista. Informe Anual 2021, Ciudad Autónoma de Buenos Aires, CAMMESA, Argentina, 2022, 111 P.

[15] CAMMESA (Compañía Administradora del Mercado Mayorista Eléctrico SA), Mercado Eléctrico Mayorista. Informe Anual 2022, Ciudad Autónoma de Buenos Aires, CAMMESA, Argentina, 2023, 111 P.

[16] CAMMESA (Compañía Administradora del Mercado Mayorista Eléctrico SA), Mercado Eléctrico Mayorista. Informe Anual 2023, Ciudad Autónoma de Buenos Aires, CAMMESA, Argentina, 2024, 111 P.

[17] Infraestructura – Región Centro. Región Centro, [en línea]. 13 May 2024, dispnible en: https://www.regioncentro.gob.ar/infraestructura/

[18] Argentina.gob.ar, Probiomasa. [en línea]. 2024. Disponible en: https://sig.energia.gob.ar/visor/visorsig.php?t=19

[19] CAPEC (Consejo Asesor de Políticas Energéticas de Córdoba), Transición energética 2050, Córdoba, Secretaría de Biocombustibles y Energías Renovables, Ministerio de Servicios Públicos, Gobierno de la provincia de Córdoba, Argentina, 2022, 34 P.

[20] Ley Nro. 10721, Ley de Promoción y Desarrollo para la Producción y Consumo de Biocombustibles y Bioenergía. [en línea]. 2020, Boletín Oficial de la Provincia de Córdoba. Disponible en: https://boletinoficial.cba.gov.ar/wp-content/4p96humuzp/2020/11/1_Secc_271120.pdf

[21] IDECOR (Infraestructura de Datos Espaciales de la Provincia de Córdoba), Mapa de Cobertura y Uso de Suelo de la Provincia de Córdoba 2022-2023, Gobierno de la Provincia de Córdoba, Argentina, 2023, 33 P.

[22] IDECOR (Infraestructura de Datos Espaciales de la Provincia de Córdoba), Mapa de Área Sembrada, Rindes y Producción de Soja y Maíz, Campaña 2022/, Gobierno de la Provincia de Córdoba, Argentina, 2023, 46 P.
[23] Balangione, A., Gallará, R., Ortmann, V., and Bernard, M., Obtención de pellets híbridos de maíz/espartillo para generación de energía. X Congreso de Investigaciones y Desarrollos en Tecnología y Ciencia IDETEC 2022, Villa María, Argentina, [en línea]. 2022. Disponible en: https://ria.utn.edu.ar/handle/20.500.12272/8416
[24] Cerrotta, A., Siembra directa en el sur del país: ¿qué hacer con el exceso de rastrojo? AAPRESID [Online], 2023. [date of reference April 25th of 2023]. Available at: https://www.aapresid.org.ar/blog/siembra-directa-sur-pais-exceso-rastrojo
[25] Madariaga, R., Rastrojos y su relación con las enfermedades del trigo. Rastrojo de Cultivos y Residuos Forestales, Programa de Transferencia de Prácticas Alternativas al Uso del Fuego en la Región del Biobío. Boletín INIA [Online]. 308, 2015. [date of reference May of 2015]. Available at: https://bibliotecadigital.ciren.cl/server/api/core/bitstreams/d2836e3d-df00-4eef-b299-fbbb3057ef4c/content
[26] Quicchi, A., Balangione, A., Belmonte, L., Gallará, R., Mariotta, A., Ortmann, V., Ferreyra, D., and Bernard, M., Análisis de biomasa lignocelulósica regional de origen herbáceo para la generación de energía. IV Simposio de Residuos Agropecuarios y Agroindustriales, Mendoza, Argentina, [en línea]. 2023. Disponible en: https://ria.utn.edu.ar/handle/20.500.12272/10006
[27] Belmonte, L., Mariotta, A., Binotto, N., Quicchi, A., and Bernard, M., Análisis comparativo de cultivos lignocelulósicos con alto potencial energético: Arundo Donax L. y Sorghum Saccharatum. Jornadas de Ciencia y Tecnología 2023 de la UTN San Francisco, San Francisco, Argentina, [en línea]. 2023. Disponible en: https://ria.utn.edu.ar/handle/20.500.12272/9266
[28] Ortmann, V., Balangione, A., Gallará R., Quicchi, A., Ferreyra D.M., and Bernard, M., Cuantificación preliminar del consumo de energía en el proceso de obtención de pélets de rastrojo de sorgo. Jornadas de Ciencia y Tecnología 2023 de la UTN San Francisco, San Francisco, Argentina, [en línea]. 2023. Disponible en: https://ria.utn.edu.ar/handle/20.500.12272/9266
[29] Bernard, M., Goiran, A.R., Quicchi, A.L., and Ferreyra, D.M., Optimización preliminar del peletizado de sorgo lignocelulósico para generación de gas de síntesis, Ingenio Tecnológico, 4, pp. 1-10, 2022.
[30] De La Torre-Ugarte, D.G., Bioenergía y Agricultura-Promesas y Retos: desarrollo de bioenergía: asuntos económicos y sociales, Enfoque, International Food Policy Research Institute, 14, pp 5-6, 2020.
[31] FAO 2000, La energía en la economía mundial, in: El nexo entre la agricultura y la energía, Documento de trabajo sobre medio ambiente y recursos naturales No. 4. [en línea]. 2000. Disponible en: https://www.fao.org/4/x8054e/x8054e00.htm#P-1_0
[32] Trivelli, C., y Berdegué, J.A., 2019. Transformación rural. Pensando el futuro de América Latina y el Caribe. 2030. Alimentación, agricultura y desarrollo rural en América Latina y el Caribe, No. 1. Santiago de Chile. FAO. 76 P. Licencia: CC BY-NC-SA 3.0 IGO.

A.L. Quicchi, received the Bs. Eng in Chemical Engineering in 2019. She is an Assistant Professor both in Calculus II and in Thermodynamics and Thermal Machinery in the San Francisco Regional Faculty of the UTN (Universidad Tecnológica Nacional) in Argentina. She is currently pursuing her PhD in Industrial Engineering at the Santa Fe Regional Faculty of UTN. She also works in the biomass area of the UTN R&D group CIDEME in her Faculty.
ORCID: 0000-0001-6369-1046

M. Bernard, received the Bs. Eng in Chemical Engineering in 2010 and the PhD in Chemical Sciences in 2020. She has worked in several research programs and projects related to biomaterials with several applications, and in the last few years turned her focus to energy efficiency and biomass for energy generation, with emphasis on gasification of regional materials. She is currently a tenured full-time Research Professor in Thermodynamics in the San Francisco Regional Faculty of the Universidad Tecnológica Nacional (UTN) in Argentina and coordinates the biomass area of the UTN R&D group CIDEME in her Faculty.
ORCID: 0000-0003-2525-9089

D.M. Ferreyra, received the Bs. Eng in Electromechanical Engineering in 2001, the MS degree in Engineering Sciences with a mention in Electrical Engineering in 2014, and the PhD degree in Electrical Engineering in 2018. After working for several years in metalworking and electromechanical companies, he developed his university career and is currently a tenured full-time Research Professor in Electrical Machinery in the San Francisco Regional Faculty of the Universidad Tecnológica Nacional (UTN) in Argentina. There, he has worked in several R&D projects related to electrical machines, power quality, energy management, and distributed generation using renewable sources. He is currently the Director for the UTN R&D group CIDEME in his Faculty.
ORCID: 0000-0003-2251-2819

G.A. Schweickardt, received the Bs. Eng in Electrical Engineering in 1989 and the PhD degree in Engineering/Energy Economics in 2002. He also obtained an MS degree in Energy Economics and Environmental Energy Policy in 2005, as well as different SP degrees in Environmental Impact Assessment, Energy Economics, and Software Engineering-Data Science. He is a Senior Researcher for the National Scientific and Technical Research Council (CONICET), Argentina. His research interests include energy economics, computational artificial intelligence, soft computing optimization, renewable energies, distributed generation, smart grids, and electrical power distribution systems planification and operation. As a Professor in the Concepción del Uruguay Regional Faculty of the Universidad Tecnológica Nacional (UTN), he is the Director of the Research Group on Computational Economics of Regulation and Renewable Energies (GIECRRER), and the Director of the Master Program in Renewable Energies.
ORCID: 0000-0002-0843-2946

DYNA
http://dyna.medellin.unal.edu.co/

UNIVERSIDAD NACIONAL DE COLOMBIA

Development of financial and administrative management strategies for business sustainability

William Alberto Guerrero [a], Stefanny Camacho-Galindo [a], Laura Estefanía Guerrero-Martin [a], John Carlos Arévalo[a], Fernando Antônio da Silva Fernandes [b,c], Edinelson Saldanha Correa[b] & Camilo Andrés Guerrero-Martin [b,c,d]

[a] *Fundación de Educación Superior San José, Bogotá, Colombia. waguerrero@hotmail.com, setefa110992@gmail.com, guerrero.laura.9705@gmail.com, john.c.arevalo@gmail.com*

[b] *Federal University of Pará – Campus Salinópolis - Department of Engineering (FAE), Salinópolis, Brazil. fernandesfernando27@gmail.com, fernandofernandes@ufpa.br, camilo.guerrero@poli.ufrj.br, edinelsonsaldanha@ufpa.br*

[c] *Grupo de pesquisa em Energia e Mar, Universidade Federal do Pará.*

[d] *Universidade Federal do Pará, Programa de Pós-Graduação em Engenharia Mecânica. Belém, PA, Brasil*

Received: June 20th, 2024. Received in revised from: November 13th, 2024. Accepted: December 3rd, 2024.

Abstract
This article explores how financial and administrative management strategies aligned with ESG (environmental, social and governance) criteria foster corporate sustainability. Using a mixed methodology, it combined literature review, analysis of financial data from Colombian companies such as Grupo Sura, Nutresa and Davivienda, and surveys applied to 351 business leaders. The results highlight that the integration of ESG practices optimizes resources, reduces operating costs and improves competitiveness, as evidenced by a 13.3% growth in revenues and a 26.3% increase in operating profits. However, significant challenges were identified, such as the lack of clear metrics and limited financial resources. Companies that adopt these strategies are able to strengthen their organizational resilience, improve their economic performance and consolidate sustainable competitive advantages. The article concludes that corporate sustainability is not only an ethical imperative, but also an opportunity to balance economic growth with social and environmental responsibility

Keywords: corporate sustainability; financial management; management strategies; social responsibility; operational efficiency.

Desarrollo de estrategias de gestión financiera y administrativa para la sostenibilidad empresarial

Resumen
Este artículo explora cómo las estrategias de gestión financiera y administrativa alineadas con criterios ESG (ambientales, sociales y de gobernanza) fomentan la sostenibilidad empresarial. Utilizando metodología mixta, se combinó revisión de literatura, análisis de datos financieros de empresas colombianas como Grupo Sura, Nutresa y Davivienda, y encuestas aplicadas a 351 líderes empresariales. Los resultados destacan que la integración de prácticas ESG optimiza recursos, reduce costos operativos y mejora la competitividad, evidenciado en un crecimiento del 13,3% en ingresos y un aumento del 26,3% en ganancias operativas. Sin embargo, se identificaron desafíos significativos, como la falta de métricas claras y recursos financieros limitados. Las empresas que adoptan estas estrategias logran fortalecer su resiliencia organizacional, mejorar su desempeño económico y consolidar ventajas competitivas sostenibles. El articulo concluye que la sostenibilidad empresarial no solo es un imperativo ético, sino también una oportunidad para equilibrar el crecimiento económico con la responsabilidad social y ambiental.

Palabras clave: sostenibilidad empresarial; gestión financiera; estrategias administrativas; responsabilidad social; eficiencia operativa.

1 Introducción

La sostenibilidad empresarial se ha convertido en un componente estratégico esencial para las organizaciones que buscan equilibrar el desempeño económico con las crecientes demandas sociales y ambientales [1]. En un contexto global

How to cite: Guerrero, W.A., Camacho-Silva, S., Guerrero-Martin, L.E., Arévalo, J.C., Fernandes, F.A.daS., Correa, E.S., and Guerrero-Martin, C.A., Development of financial and administrative management strategies for business sustainability DYNA, 91(234), pp. 147-156, October - December, 2024.

marcado por crisis climáticas, expectativas de transparencia y la creciente importancia de los criterios ESG (ambientales, sociales y de gobernanza), las empresas enfrentan presiones para implementar prácticas sostenibles que minimicen su impacto ambiental, fortalezcan su competitividad y aseguren su viabilidad a largo plazo [2,3].

Estudios recientes evidencian que la adopción de estrategias sostenibles no solo mejora los resultados financieros, como incrementos en ingresos y utilidades, sino que también fortalece la reputación corporativa y la eficiencia operativa [4,5]. Estrategias como la reducción en el consumo de recursos, la inversión en tecnologías limpias y la implementación de políticas de responsabilidad social se destacan como prácticas clave para construir organizaciones resilientes [6,7]. Sin embargo, la transición hacia modelos sostenibles presenta barreras significativas, entre ellas, la falta de métricas claras, la disponibilidad limitada de recursos financieros y la resistencia al cambio organizacional [8,9].

En este contexto, la integración de criterios ESG en la gestión financiera y administrativa emerge como un enfoque prometedor para alinear objetivos económicos con compromisos sociales y ambientales. Este artículo analiza cómo empresas líderes en Colombia, como Grupo Sura, Nutresa y Davivienda, han logrado implementar estrategias sostenibles que impactan positivamente su desempeño organizacional [10]. A través del estudio de casos, se exploran las oportunidades y desafíos asociados con estas prácticas, destacando la importancia de medir y reportar el impacto ambiental y social, diversificar fuentes de financiamiento, e invertir en tecnologías verdes [11,12].

La hipótesis central de este trabajo plantea que la sostenibilidad empresarial, más allá de un imperativo ético, representa una oportunidad para generar ventajas competitivas sostenibles y fortalecer la resiliencia organizacional. Asimismo, este estudio contribuye al campo académico al proporcionar evidencia empírica que conecta las estrategias ESG con el desempeño económico, ofreciendo una hoja de ruta para organizaciones que buscan prosperar en un entorno empresarial dinámico y globalizado [13].

2 Marco teórico

El marco teórico de este estudio está fundamentado en conceptos clave de la gestión financiera, administrativa y la sostenibilidad empresarial, integrando perspectivas teóricas y prácticas. Se estructura en tres áreas principales:

2.1 Gestión financiera y sostenibilidad empresarial

La gestión financiera desempeña un papel fundamental en la sostenibilidad empresarial. Según *Principles of Managerial Finance*, el principal objetivo es maximizar el valor para los accionistas mediante decisiones estratégicas y el uso eficiente de recursos [11]. En este contexto, las estrategias financieras deben adaptarse a las condiciones cambiantes del mercado y considerar criterios ESG para garantizar sostenibilidad a largo plazo. Además, *Cost Accounting: A Managerial Emphasis* enfatiza que una gestión rigurosa de costos no solo mejora la rentabilidad, sino que también fomenta la eficiencia en el uso de recursos, un aspecto crucial en la sostenibilidad empresarial [14].

Estudios recientes subrayan que la integración de criterios ESG en la gestión financiera genera beneficios tangibles, como la optimización de recursos y la reducción de costos operativos. Por ejemplo, empresas que adoptan prácticas de sostenibilidad logran un desempeño financiero superior al de sus competidores, evidenciado en indicadores como incremento de ingresos y mejora en la rentabilidad operativa [15].

2.2 Gestión administrativa y resiliencia organizacional

La gestión administrativa es fundamental para estructurar estrategias que promuevan la sostenibilidad empresarial. Según *Principles of Management*, las funciones de planificación, organización, dirección y control son pilares esenciales para la implementación de estrategias sostenibles [15]. En un entorno dinámico, las organizaciones deben adoptar procesos administrativos ágiles que les permitan responder eficazmente a los cambios en el mercado [16].

La planificación estratégica desempeña un rol crítico en la alineación de objetivos sostenibles con metas organizacionales. *Modern Management* sugiere que la resiliencia organizacional se fortalece cuando las empresas integran criterios ESG en sus decisiones administrativas [16]. Además, *Strategic Management and Business Policy* destaca cómo la sostenibilidad no solo responde a demandas regulatorias y sociales, sino que también mejora la competitividad al fortalecer las relaciones con las partes interesadas y reducir riesgos operativos [17].

2.3 Responsabilidad social corporativa y competitividad

La responsabilidad social corporativa (RSC) es un componente clave de la sostenibilidad empresarial. Según *Business and Society: Ethics, Sustainability, and Stakeholder Management*, la RSC promueve la creación de valor compartido al abordar desafíos ambientales y sociales mientras genera beneficios económicos [18]. Las prácticas sostenibles, como la inversión en tecnologías limpias y la reducción de la huella ambiental, contribuyen directamente a la reputación corporativa y la fidelidad del cliente [19].

Investigaciones publicadas en el *Journal of Cleaner Production* muestran cómo las empresas que adoptan prácticas sostenibles no solo reducen su impacto ambiental, sino que también obtienen ventajas competitivas al diferenciarse en mercados globales altamente competitivos [19]. Además, *Making Sustainability Work* enfatiza la importancia de medir y reportar los avances en sostenibilidad mediante herramientas como el reporte integrado, que conecta la sostenibilidad con los objetivos organizacionales y fortalece la transparencia [20].

3 Métodos

El desarrollo sostenible es una estrategia que las organizaciones utilizan para promover el crecimiento y la sostenibilidad a largo plazo. Para lograr esta perdurabilidad financiera, es esencial planificar, ser competitivo y tomar decisiones racionales. Por ello, el enfoque de la investigación consideró los recursos disponibles y los objetivos del estudio, estructurándose en los siguientes pasos:

3.1 Revisión de literatura

Se llevó a cabo una exhaustiva revisión bibliográfica sobre sostenibilidad empresarial, gestión financiera y administrativa, y estrategias específicas relacionadas con la sostenibilidad. Esta revisión permitió construir un marco teórico sólido que sirvió como base para analizar cómo la integración de criterios ESG contribuye al desempeño organizacional [21].

3.2 Análisis de datos financieros

Se recopilaron y analizaron datos financieros de empresas colombianas reconocidas por implementar estrategias sostenibles. El análisis se enfocó en evaluar el desempeño financiero a largo plazo mediante indicadores clave como activos, ingresos, costos, utilidades y patrimonio. Las empresas estudiadas fueron:

3.2.1. Grupo Sura

Grupo SURA, un conglomerado financiero colombiano con presencia en 11 países de América Latina, basa su estrategia en la gestión equilibrada de capital económico, social, humano y natural. Destacan sus inversiones en Suramericana, SURA Asset Management, Bancolombia y participaciones en Grupo Argos y Grupo Nutresa. Este enfoque le ha valido su inclusión en el Índice Global de Sostenibilidad Dow Jones desde 2011 [21].

3.2.2. Grupo Nutresa

Grupo Nutresa, fundado en 1920 como Compañía Nacional de Chocolates Cruz Roja, ha evolucionado hasta convertirse en un referente en la industria de alimentos, priorizando la salud, el bienestar y la sostenibilidad. Su estrategia de diversificación e inversiones estratégicas en la región refuerza su compromiso con prácticas responsables y sostenibles [22].

3.2.3. Banco Davivienda

Banco Davivienda, con más de 40 años de experiencia en el desarrollo financiero de Colombia, forma parte del Grupo Empresarial Bolívar. Se distingue por su innovación tecnológica y su compromiso con la sostenibilidad, gestionando un portafolio de productos financieros adaptados a diversos sectores. Desde 1973, su emblemático símbolo, la Casita Roja, representa su visión de banca cercana y responsable [23, 24].

3.3 Encuestas

Se diseñaron y aplicaron encuestas a una muestra de 351 líderes empresariales, gerentes y profesionales del sector financiero y administrativo. Estas encuestas evaluaron las percepciones sobre los desafíos en la integración de criterios ESG, las prácticas actuales relacionadas con la sostenibilidad y sus opiniones sobre la contribución de estas estrategias al desempeño organizacional. Los datos recopilados, combinados con los análisis financieros y la revisión de literatura, permitieron obtener resultados representativos y profundizar en el impacto de las estrategias sostenibles en la gestión empresarial.

4 Resultados

Los indicadores de sostenibilidad financiera y los posibles resultados de una investigación científica sobre el desarrollo de estrategias de gestión financiera y administrativa para la sostenibilidad empresarial pueden agruparse de la siguiente manera:

4.1 Revisión de literatura

El desarrollo de estrategias de gestión financiera y administrativa para la sostenibilidad empresarial busca integrar criterios ESG para mejorar el rendimiento, reducir riesgos y crear valor a largo plazo. [25,26] destacan la gestión eficiente de recursos y el enfoque al cliente, mientras que [27] promueve una visión sistémica. La gestión de riesgos ambientales [28] y la atención a los stakeholders [29,30] mejoran los resultados financieros. Los marcos de responsabilidad social [31,32] y la transparencia en la divulgación ambiental [33] son claves. Herramientas como el reporte integrado [34] y la triple línea de resultados [35] vinculan sostenibilidad y competitividad [36-38]. [39] aporta evidencia empírica de estos beneficios. La responsabilidad corporativa [40] y la medición del impacto social y ambiental [41] promueven valor y resiliencia organizacional. Empresas como Sura, Argos y Nutresa destacan por combinar éxito económico, responsabilidad social y cuidado ambiental [42,1,2]. Persisten desafíos como falta de recursos y métricas claras [43]. La literatura subraya la necesidad de indicadores clave y herramientas como el Balanced Scorecard [44,45] para alinear estrategias sostenibles y financieras, promoviendo confianza entre los grupos de interés [46].

4.2. Análisis de datos financieros

Se recopilo y analizo datos de estados financieros de empresas que han implementado estrategias de sostenibilidad y se evaluó el desempeño financiero a largo plazo, tales como Grupo Sura, Nutresa y Davivienda, los cuales se presentan a continuación.

4.2.1. Resultado del análisis de los estados financieros del Grupo Sura mencionados a continuación según Tablas 1, 2, 3, y 4

Tabla 1.
Estado de situación financiera Grupo Sura

Estados Financieros Grupo Sura					
Estado de Situación Financiera Miles de millones de pesos	**2023**	**2022**	**2021**	**2020**	**2019**
Total Activos	93.505	98.393	75.902	70.941	69.037
Total Pasivos	61.070	62.612	47.290	42.400	40.946
Total Patrimonio	32.435	35.782	28.612	28.541	28.091

Fuente: Los autores

Tabla 2.
Estado de resultados Grupo Sura

Estados Financieros Grupo Sura					
Estado de Resultados	2023	2022	2021	2020	2019
Total Ingresos	35.529	31.350	24.803	20.837	21.328
Total Costos y Gastos	30.881	27.669	22.220	19.230	18.445
Ganancia operativa	4.648	3.681	2.583	1.607	2.883
Resultado Financiero	1.047	993	593	811	625
Ganancias antes de Impuesto	3.602	2.689	1.990	796	2.256
Impuestos	1.569	363	470	453	650
Ganancia operaciones discontinuas	97	20	5	-6	112
Ganancias Netas	1.935	2.345	1.525	336	1.718

Fuente: Los autores

Tabla 3.
Análisis estado de situación financiera Grupo Sura

Estado de Situación Financiera	Análisis			
En miles de millones de pesos	2022-2023	2021-2022	2020-2021	2019-2020
Total Activos	-4,97%	29,63%	6,99%	2,76%
Total Pasivos	-2,46%	32,40%	11,53%	3,55%
Total Patrimonio	-9,35%	25,06%	0,25%	1,60%

Fuente: Los autores

Tabla 4.
Análisis estado de resultados Grupo Sura

	Análisis			
Estado de Resultados	2022-2023	2021-2022	2020-2021	2019-2020
Total Ingresos	13,33%	26,40%	19,03%	-2,30%
Total Costos y Gastos	11,61%	24,52%	15,55%	4,26%
Ganancia operativa	26,27%	42,51%	60,73%	-44,26%
Resultado Financiero	5,44%	67,45%	-26,88%	29,76%
Ganancias antes de Impuesto	33,95%	35,13%	150,00%	-64,72%
Impuestos	332,23%	-22,77%	3,75%	-30,31%
Ganancia operaciones discontinuas	385,00%	300,00%	-183,33%	-105,36%
Ganancias Netas	-17,48%	53,77%	353,87%	-80,44%

Fuente: Los autores

El análisis financiero del Grupo Sura 2022-2023 mostró fluctuaciones destacadas, como una disminución en activos (-4,97%) y patrimonio (-9,35%), posiblemente por ajustes o desinversiones, junto con una leve reducción de pasivos (-2,46%), sugiriendo un enfoque en la reducción de deuda. En 2021-2022, el crecimiento en activos y pasivos reflejó una expansión que no incrementó proporcionalmente el patrimonio. Los ingresos crecieron un 13,33% en 2022-2023, aunque moderadamente en comparación con años anteriores, mientras que el control de costos y gastos permitió un alza de la ganancia operativa del 26,27%. La volatilidad del resultado financiero, con un incremento del 67,45% en 2021-2022, y las oscilaciones en las ganancias antes de impuestos, afectadas por un incremento del 332,23% en impuestos, señalaron la necesidad de estrategias financieras más sólidas. Los resultados resaltaron cómo las estrategias de gestión financiera y administrativa para la sostenibilidad empresarial optimizaron recursos, mitigaron riesgos y alinearon la rentabilidad con objetivos de sostenibilidad a largo plazo, promoviendo eficiencia, resiliencia y competitividad organizacional.

4.2.2. Resultado del análisis de los estados financieros del Grupo Nutresa mencionados a continuación según tablas 5, 6, 7 y 8.

Tabla 5.
Estado de situación financiera Grupo Nutresa

En miles de millones de pesos	2023	2022	2021	2.020	2.019
Total Activos	15.689	20.757	16.956	15.537	15.659
Total Pasivos	9.245	9.953	7.914	7.280	6.977
Total Patrimonio	6.444	10.805	9.042	8.257	8.682

Fuente: Los autores

Tabla 6.
Estado de resultados Grupo Nutresa

En miles de millones de pesos	2023	2022	2021	2020	2019
Total Ingresos	18.906	17.038	12.738	11.127	9.958
Total Costos y Gastos	17.178	15.531	11.633	10.108	9.002
Ganancia operativa	1.728	1.507	1.105	1.019	956
Ganancias antes de Impuesto	1.002	1.261	988	815	732
Impuestos	262	357	263	231	222
Ganancias Netas	740	904	693	583	510

Fuente: Los autores

Tabla 7.
Análisis estado de situación financiera Grupo Nutresa

	Análisis			
En miles de millones de pesos	2022-2023	2021-2022	2020-2021	2019-2020
Total Activos	-24,42%	22,42%	9,13%	-0,78%
Total Pasivos	-7,11%	25,76%	8,71%	4,34%
Total Patrimonio	-40,36%	19,50%	9,51%	-4,90%

Fuente: Los autores

Tabla 8.
Análisis estado de resultados Grupo Nutresa

	Análisis			
En miles de millones de pesos	2022-2023	2021-2022	2020-2021	2019-2020
Total Ingresos	10,96%	33,76%	14,48%	11,74%
Total Costos y Gastos	10,60%	33,51%	15,09%	12,29%
Ganancia operativa	14,66%	36,38%	8,44%	6,59%
Ganancias antes de Impuesto	-20,54%	27,63%	21,23%	11,34%
Impuestos	-26,61%	35,74%	13,85%	4,05%
Ganancias Netas	-18,14%	30,45%	18,87%	14,31%

Fuente: Los autores

El análisis financiero de Nutresa en 2022-2023 reflejó una notable reducción en activos (-24,42%) y patrimonio (-40,36%), junto con una disminución de pasivos (-7,11%), lo que podría deberse a estrategias de ajuste y optimización financiera. Este enfoque, en contraste con el crecimiento en 2021-2022, evidencia una reestructuración orientada a una mayor eficiencia. Aunque los ingresos crecieron un 10,96%, los costos y gastos aumentaron de manera similar (10,60%), lo que, sin embargo, permitió mejorar la ganancia operativa en un 14,66%. Las caídas en ganancias antes de impuestos (-20,54%) y netas (-18,14%) reflejan el impacto de costos financieros y ajustes estratégicos, mitigado parcialmente por una reducción de impuestos (-26,61%). En conjunto, estas fluctuaciones sugieren que las estrategias de gestión financiera y administrativa se centraron en mantener la sostenibilidad operativa y financiera a largo plazo, promoviendo eficiencia, resiliencia y un equilibrio entre sostenibilidad y competitividad.

4.2.3. Resultado del análisis de los estados financieros de Davivienda mencionados a continuación según tablas 9, 10, 11 y 12

El análisis financiero de Davivienda durante el periodo 2022-2023 mostró una ligera disminución en activos (-3,21%) y pasivos (-2,60%), mientras que el patrimonio cayó un -9,46%, sugiriendo ajustes financieros enfocados en optimizar la estructura de capital. Aunque en años previos (2021-2022) se evidenció un crecimiento importante en activos y pasivos, no fue sostenido. El Estado de Resultados evidenció un notable crecimiento de ingresos (99,98%) en 2022-2023, pero acompañado de un fuerte aumento en costos y gastos (139,61%), afectando la rentabilidad. Las ganancias antes de impuestos y las netas presentaron caídas significativas (-3537,50% y -662,50%), agravadas por una elevada volatilidad en impuestos. Esto sugiere que las estrategias de gestión financiera y administrativa aplicadas buscaban estabilidad y sostenibilidad, con un enfoque en crecimiento de ingresos y reducción de costos; sin embargo, los desafíos operativos, financieros y de costos resaltaron la necesidad de estrategias más efectivas para mantener la competitividad y la sostenibilidad a largo plazo.

Tabla 9.
Estado de situación financiera Davivienda

Miles de millones de pesos	**2023**	**2022**	**2021**	**2020**	**2019**
Total Activos	178.218	184.128	152.680	136.413	122.222
Total Pasivos	163.466	167.835	138.401	123.693	109.571
Total Patrimonio	14.752	16.293	14.279	12.720	12.651

Fuente: Los autores

Tabla 10.
Estado de resultados Davivienda

Miles de millones de pesos	**2023**	**2022**	**2021**	**2020**	**2019**
Total Ingresos	9.999	5.000	5.574	11.447	10.725
Total Costos y Gastos	9.491	3.961	4.456	10.971	8.798
Ganancias antes de Impuesto	-550	16	402	476	1.927
Impuestos	280	-32	69	68	444
Ganancias Netas	-270	48	333	408	1.483

Fuente: Los autores

Tabla 11. Análisis estado de situación financiera Davivienda

	Análisis			
Miles de millones de pesos	2022-2023	2021-2022	2020-2021	2019-2020
Total Activos	-3,21%	20,60%	11,92%	11,61%
Total Pasivos	-2,60%	21,27%	11,89%	12,89%
Total Patrimonio	-9,46%	14,10%	12,26%	0,55%

Fuente: Los autores

Tabla 12.
Análisis estado de resultados Davivienda

Estado de Resultados	**Análisis**			
Miles de millones de pesos	2022-2023	2021-2022	2020-2021	2019-2020
Total Ingresos	99,98%	-10,30%	-51,31%	6,73%
Total Costos y Gastos	139,61%	-11,11%	-59,38%	24,70%
Ganancias antes de Impuesto	-3537,50%	-96,02%	-15,55%	-75,30%
Impuestos	-975,00%	-146,38%	1,47%	-84,68%
Ganancias Netas	-662,50%	-85,59%	-18,38%	-72,49%

Fuente: Los autores

4.3 Encuestas

La elaboración de encuestas se respalda en autores clave que garantizan la calidad y validez de los instrumentos de recolección de datos. [47], en Survey Methodology, aborda cómo mejorar la precisión y reducir el sesgo mediante un diseño riguroso. [48], en Improving Survey Questions, destaca la importancia de preguntas claras y escalas de medición coherentes. [49] propone un enfoque adaptado al contexto y público objetivo en The Tailored Design Method. La escala Likert, desarrollada por [50], es esencial para medir actitudes y percepciones. [51] subrayan la relevancia del proceso de recopilación de datos y las interacciones encuestador-encuestado. [52], en The Practice of Social Research, enfatiza la formulación de preguntas válidas y el diseño de muestras, mientras que [53], en Research Design, resalta la integración de métodos cuantitativos y mixtos para asegurar claridad y fiabilidad en las encuestas. Estos enfoques proporcionan una base teórica robusta para diseñar encuestas representativas y útiles.

Las respuestas a la pregunta 1. ¿Cómo describiría la importancia de la sostenibilidad en la gestión financiera y administrativa de una empresa? Se muestran en la Fig. 1.

La encuesta muestra que la sostenibilidad en la gestión financiera y administrativa es crucial para las empresas. El 57% de los encuestados considera que es clave para minimizar riesgos financieros y operativos a largo plazo, mientras que el 22.5% resalta su papel en la generación de valor y en la construcción de relaciones sólidas con las partes interesadas. Un 15.1% menciona los desafíos en su

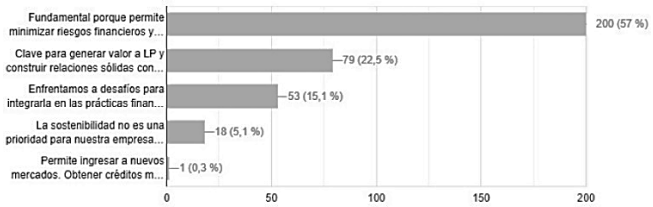

Figura 1. Resultados de encuesta a la pregunta 1.
Fuente: Los autores

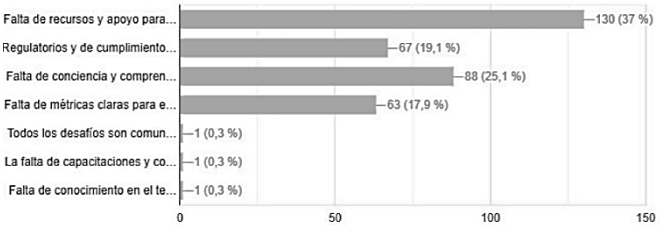

Figura 2. Resultados de encuesta a la pregunta 2.
Fuente: Los autores

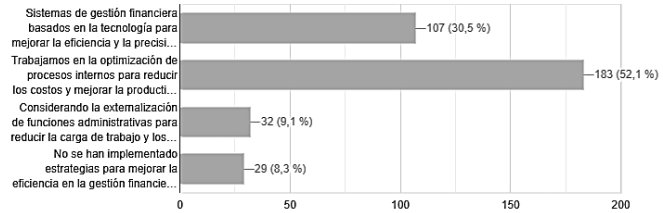

Figura 3. Resultados de encuesta a la pregunta 3.
Fuente: Los autores

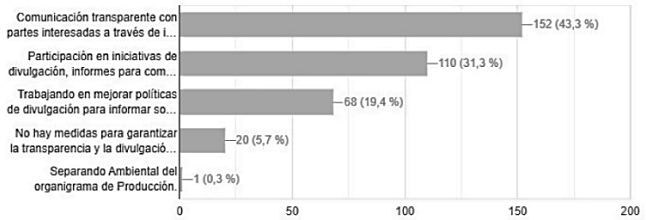

Figura 4. Resultados de encuesta a la pregunta 4.
Fuente: Los autores

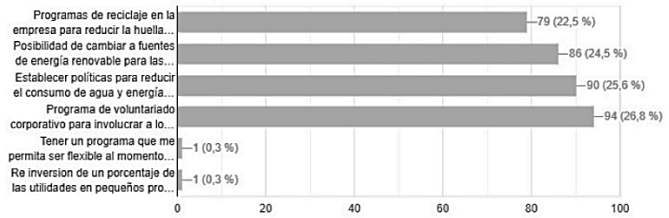

Figura 5. Resultados de encuesta a la pregunta 5.
Fuente: Los autores

integración en las prácticas financieras y administrativas, y un 5.1% no la considera una prioridad en este momento. Estos hallazgos subrayan la necesidad de abordar la sostenibilidad de manera integral, reconociendo tanto sus beneficios como sus obstáculos.

Las respuestas a la pregunta 2. ¿Cuáles son los principales desafíos que enfrenta al intentar integrar prácticas sostenibles en las operaciones financieras y administrativas? Se muestran en la Fig. 2.

La integración de prácticas sostenibles enfrenta desafíos como la escasez de recursos (37%), regulaciones (19.1%), y falta de conciencia sobre sus beneficios (25.1%). Además, el 17.9% mencionó la ausencia de métricas claras. Superar estas barreras es esencial para una implementación efectiva en el ámbito empresarial. Estos resultados subrayan la importancia de superar estos obstáculos para una integración más efectiva de la sostenibilidad en el ámbito empresarial.

Las respuestas a la pregunta 3. ¿Qué estrategias ha implementado o está considerando implementar para mejorar la eficiencia en la gestión financiera y administrativa de la empresa? Se muestran en la Fig. 3.

Los encuestados proponen medidas como implementar tecnología para la gestión financiera (30.5%), optimizar procesos internos (52.1%) y externalizar funciones administrativas (9.1%). Sin embargo, el 8.3% señala que no se han tomado acciones, evidenciando áreas de mejora en algunas organizaciones.

Las respuestas a la pregunta 4. ¿Qué medidas toma para garantizar la transparencia y la divulgación en la gestión financiera y administrativa, especialmente en lo que respecta a las prácticas sostenibles? Se muestran en la Fig. 4.

En la gestión financiera y administrativa, el 43.3% de los encuestados resalta la importancia de informes transparentes para las partes interesadas, mientras que el 31.3% participa en iniciativas de divulgación sobre sostenibilidad. Un 19.4% trabaja en políticas de divulgación y un 5.7% aún está en la fase de diseño de medidas, mostrando la necesidad de estrategias más efectivas.

Las respuestas a la pregunta 5. ¿Qué oportunidades identifica al integrar consideraciones ambientales, sociales y de gobierno en la toma de decisiones financieras y administrativas? Se muestran en la Fig. 5.

Los encuestados adoptan diversos enfoques en decisiones administrativas y financieras con criterios ESG. Un 26.8% impulsa voluntariado corporativo en proyectos de sostenibilidad, un 25.6% aplica políticas para reducir agua y energía, un 24.5% apuesta por energía renovable, y un 22.5% implementa programas de reciclaje para minimizar el impacto ambiental. Estas estrategias reflejan el compromiso de las organizaciones con la sostenibilidad y destacan la importancia de considerar múltiples aspectos en sus decisiones administrativas y financieras.

Las respuestas a la pregunta 6. ¿Qué obstáculos encuentra al tratar de convencer a los accionistas o partes interesadas de la importancia de adoptar prácticas sostenibles en la gestión empresarial? Se muestran en la Fig. 6.

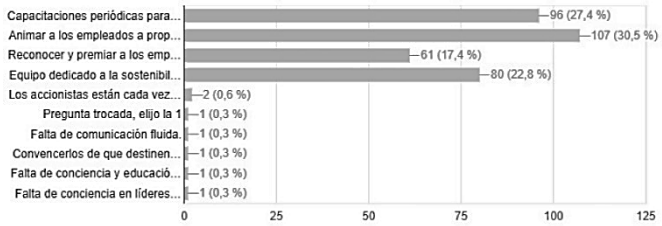

Figura 6. Resultados de encuesta a la pregunta 6.
Fuente: Los autores

La implementación de prácticas sostenibles enfrenta desafíos, pero estrategias como fomentar propuestas de empleados (30.5%), capacitaciones (27.4%), equipos dedicados (22.8%) y reconocimiento a empleados comprometidos (17.4%) resultan clave. Estos enfoques no solo educan y motivan a los empleados, sino que también fomentan una cultura organizacional que valora y promueve la sostenibilidad, fundamental para impulsar el cambio hacia la sostenibilidad empresarial.

Las respuestas a la pregunta 7. ¿Qué iniciativas de sostenibilidad específicas ha implementado en el pasado o planea implementar en el futuro en la empresa? Se muestran en la Fig. 7.

Las iniciativas de sostenibilidad han avanzado en persuadir a accionistas mediante informes detallados y casos de éxito (32.2%), y un 29.1% muestra mayor interés en estas prácticas. Sin embargo, un 21.4% prioriza resultados financieros a corto plazo y un 15.1% señala la falta de evidencia concreta sobre beneficios económicos. Estos hallazgos resaltan la necesidad de fortalecer la argumentación y presentar evidencia sólida para fomentar una mayor aceptación y compromiso hacia modelos de negocio más sostenible.

Las respuestas a la pregunta 8. ¿Cómo involucra a los empleados y otros miembros del equipo en la promoción de prácticas sostenibles en la gestión financiera y administrativa? Se muestran en la Fig. 8.

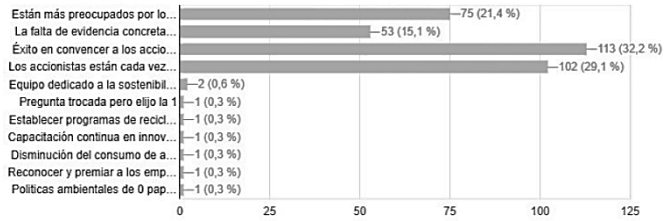

Figura 7. Resultados de encuesta a la pregunta 7.
Fuente: Los autores

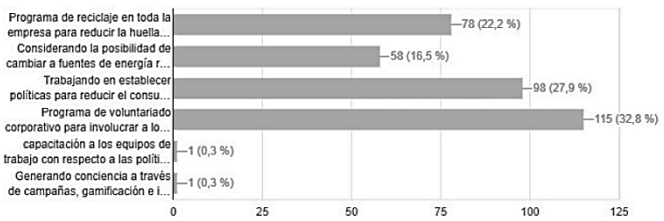

Figura 8. Resultados de encuesta a la pregunta 8.
Fuente: Los autores

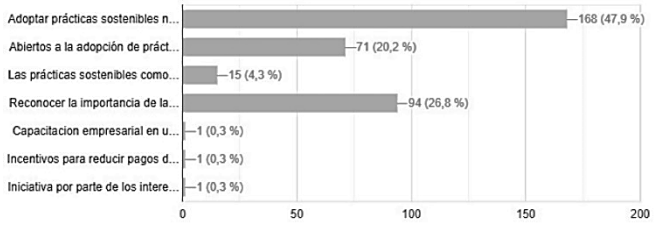

Figura 9. Resultados de encuesta a la pregunta 9.
Fuente: Los autores

Para fomentar prácticas sostenibles, se destacan programas de voluntariado corporativo (32.8%), políticas para reducir el consumo de agua y energía (27.9%), y programas de reciclaje empresarial (22.2%). Además, un 16.5% apoya la transición a fuentes de energía renovable en las operaciones. Estas iniciativas reflejan un compromiso activo hacia la sostenibilidad e involucran a todos los miembros de la organización en la búsqueda de soluciones ambientalmente responsables.

Las respuestas a la pregunta 9. ¿Qué cree que se necesita para que más empresas adopten prácticas sostenibles en su gestión financiera y administrativa? Se muestran en la Fig. 9.

La adopción de prácticas sostenibles combina beneficios y desafíos. Un 47.9% las ve como una ventaja competitiva que atrae clientes y talentos, mientras un 26.8% enfrenta limitaciones de recursos. Un 20.2% es cauteloso, aceptándolas solo si no afectan los objetivos financieros, y un 4.3% duda de su valor a largo plazo. Estas percepciones destacan la complejidad de la adopción de prácticas sostenibles y la necesidad de abordarlas de manera estratégica e integral.

Las respuestas a la pregunta 10. ¿Cómo evalúa el impacto de las prácticas de sostenibilidad en la rentabilidad y el rendimiento financiero de la empresa? Se muestran en la Fig. 10.

El análisis muestra que un 29.1% percibe un impacto positivo en la reputación y lealtad del cliente, mientras un 38.5% destaca beneficios financieros como reducción de costos y mayor eficiencia. No obstante, un 18.5% trabaja en establecer métricas para medir la rentabilidad, y un 14% aún no evalúa formalmente estos impactos, evidenciando la necesidad de mayor estructuración en la medición de resultados. Estos hallazgos destacan la complejidad de la relación entre sostenibilidad y rendimiento financiero y la

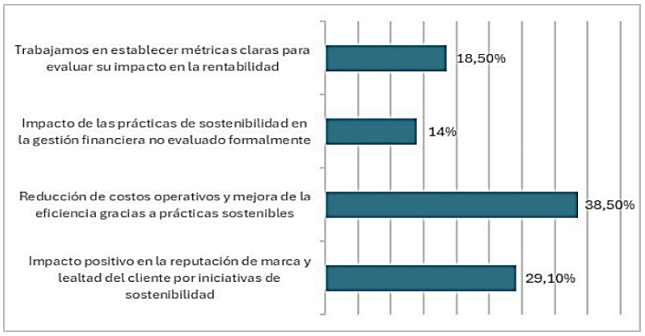

Figura 10. Resultados de encuesta a la pregunta 10.
Fuente: Los autores

necesidad de seguir investigando para desarrollar estrategias que maximicen sus beneficios económicos

5 Discusión

La discusión del artículo en aborda cómo la integración de estrategias sostenibles la gestión financiera y administrativa puede mejorar el rendimiento empresarial, reducir riesgos y generar valor a largo plazo. Los hallazgos de los análisis realizados sobre empresas como Grupo Sura, Nutresa y Davivienda, junto con encuestas a líderes empresariales, revelan que la sostenibilidad puede ser un importante motor de competitividad y resiliencia organizacional. Las estrategias aplicadas por estas compañías han optimizado recursos, mejorado la eficiencia y fortalecido su compromiso con las partes interesadas y el entorno. No obstante, persisten desafíos, como la limitación de recursos financieros y la ausencia de métricas claras para evaluar el impacto económico de estas prácticas. El marco teórico respalda la alineación de decisiones financieras con criterios ESG (ambientales, sociales y de gobierno corporativo), destacando enfoques integrales para el diseño de encuestas representativas y eficaces, que contemplan el impacto social y ambiental.

El marco teórico establece una base sólida para abordar la gestión financiera, administrativa y de sostenibilidad empresarial, haciendo referencia a contribuciones de diversos autores reconocidos. Se subraya la importancia de maximizar el valor para los accionistas, gestionar recursos financieros de manera eficiente, controlar costos, adaptarse a cambios del mercado y considerar aspectos económicos, sociales y ambientales en la toma de decisiones. Los resultados de la investigación evidencian un impacto positivo de las prácticas sostenibles en la reputación de marca, la lealtad del cliente y la eficiencia operativa. No obstante, persisten dificultades, como la carencia de métricas claras para evaluar el impacto financiero y la necesidad de una evaluación más exhaustiva. Tanto el marco teórico como la investigación resaltan la importancia de considerar factores sociales y ambientales en las decisiones empresariales, apoyándose en evidencia empírica sobre el desempeño financiero de estas prácticas.

El análisis de los resultados incorpora perspectivas de académicos y expertos en el tema. Por ejemplo, [54] subraya la relevancia de entender las tendencias históricas para prever el futuro de la gestión empresarial, mientras que [55] analiza la perspectiva de los inversores sobre indicadores clave de desempeño ambiental, social y de gobernanza en relación con la sostenibilidad financiera. Autores como [1] enfatizan la relación entre responsabilidad social empresarial y ventaja competitiva, destacando el papel de la estrategia empresarial en la sostenibilidad a largo plazo. Además, [56-59] aborda la gobernanza corporativa como elemento crucial para integrar prácticas sostenibles en la gestión financiera y administrativa, proporcionando una base teórica para enfrentar desafíos y aprovechar oportunidades en este ámbito.

Los resultados reflejan que las estrategias sostenibles no solo incrementan la rentabilidad, sino que también fortalecen relaciones con las partes interesadas y mitigan riesgos operativos y financieros. Sin embargo, la transición hacia un modelo de gestión sostenible enfrenta obstáculos, como la escasez de recursos y el escepticismo de algunos actores clave. Las encuestas revelan que el compromiso con la sostenibilidad varía según la percepción de su valor e impacto. A medida que las organizaciones evolucionen, será fundamental desarrollar herramientas de medición más precisas y estrategias de comunicación que demuestren los beneficios económicos y sociales de la sostenibilidad. En conjunto, estos elementos subrayan la importancia de una gestión financiera y administrativa estratégica que promueva un equilibrio entre éxito económico, responsabilidad social y cuidado del entorno.

6 Conclusiones

La investigación reafirma que el desarrollo de estrategias de gestión financiera y administrativa para la sostenibilidad empresarial, basado en la integración de criterios ESG (ambientales, sociales y de gobernanza), genera un impacto positivo y significativo en el desempeño económico, la competitividad y la resiliencia de las organizaciones. Las empresas que implementan prácticas sostenibles, como la reducción del consumo de recursos, inversiones en tecnologías limpias, promoción de la responsabilidad social corporativa y políticas de transparencia, logran mejorar su reputación, fidelización de clientes, eficiencia operativa y reducción de riesgos. Casos como los de Grupo Sura, Nutresa y Davivienda demuestran que estas estrategias pueden generar beneficios tangibles, aunque enfrentan desafíos como la escasez de recursos financieros, la falta de métricas claras y la necesidad de conciencia en algunos sectores.

El análisis teórico y empírico realizado valida la hipótesis de que la integración de estrategias financieras y administrativas sostenibles mejora el desempeño económico, la competitividad y la resiliencia organizacional. La revisión de la literatura y el análisis de estados financieros confirman que las estrategias que consideran criterios ESG contribuyen a optimizar recursos, reducir costos y fortalecer el compromiso de las partes interesadas. Las encuestas a líderes empresariales revelaron que, si bien existen barreras significativas, como la falta de recursos y escepticismo sobre el retorno de la inversión en sostenibilidad, hay un claro potencial para que esta se convierta en un motor de competitividad.

La adopción de prácticas sostenibles no solo genera beneficios financieros, sino que promueve un compromiso ético y social, creando una ventaja competitiva a largo plazo. Para superar obstáculos, las empresas deben implementar políticas de comunicación efectivas, métricas claras y mecanismos que integren objetivos financieros, sociales y ambientales. Un enfoque integral hacia la sostenibilidad equilibra el crecimiento económico con la responsabilidad social y ambiental, destacando la importancia de transparencia, medición del impacto y comunicación para fortalecer la confianza y resiliencia organizacional.

Este enfoque integral de sostenibilidad, que combina criterios ESG, optimiza la gestión financiera y administrativa mediante la reducción de costos, la mitigación de riesgos y la adopción de tecnologías limpias. El resultado es una mejora continua en la resiliencia organizacional, eficiencia operativa

y ventaja competitiva. En conjunto, las estrategias sostenibles impulsan la competitividad, el equilibrio entre crecimiento económico, responsabilidad social y viabilidad a largo plazo en un entorno empresarial dinámico.

La integración de prácticas sostenibles enfrenta desafíos como la falta de métricas claras para medir su impacto económico y recursos financieros adecuados. Superar estos obstáculos requiere comunicación efectiva, transparencia y marcos de sostenibilidad como el Balanced Scorecard, que alineen metas financieras y sociales, promoviendo la resiliencia organizacional y una ventaja competitiva sostenible.

Para validar la hipótesis de que la integración de estrategias de gestión financiera y administrativa sostenibles, alineadas con criterios ESG (ambientales, sociales y de gobernanza), mejora el desempeño económico, la competitividad, la resiliencia organizacional y las relaciones con las partes interesadas, se llevó a cabo un enfoque analítico basado en múltiples métodos de recolección de datos y análisis. La revisión de la literatura reveló que la adopción de criterios ESG se asocia con un mejor rendimiento empresarial, optimización de recursos, reducción de costos y compromiso de las partes interesadas. Esta base teórica demostró que las estrategias sostenibles pueden aportar ventaja competitiva y resiliencia. Asimismo, el análisis de estados financieros de empresas como Grupo Sura, Nutresa y Davivienda evidenció un impacto positivo en ingresos, ganancia operativa y eficiencia operativa, respaldando que la sostenibilidad fortalece la competitividad. Las encuestas a 351 líderes empresariales también confirmaron que integrar criterios ESG fomenta una cultura organizacional resiliente y competitiva, con un 57% destacando su relevancia para mitigar riesgos.

Los casos de éxito analizados mostraron que las estrategias sostenibles mejoran la reputación de marca y la lealtad del cliente, pero enfrentan barreras como la falta de métricas claras y recursos financieros limitados. La evidencia general respalda la hipótesis de que las estrategias sostenibles mejoran el desempeño económico y la resiliencia organizacional. Sin embargo, su efectividad depende de superar obstáculos financieros, implementar políticas de comunicación eficaces y desarrollar herramientas de evaluación adecuadas. La integración de estas estrategias debe ser continua y personalizada para maximizar su impacto económico, social y ambiental, fomentando una cultura empresarial inclusiva y sostenible.

Referencias

[1] Porter, M.E., and Kramer, M.R., Strategy and society: the link between competitive advantage and corporate social responsibility. Harvard Business Review, 84(12), pp. 78-92. 2006.

[2] Lozano, R., A holistic perspective on corporate sustainability drivers. Corporate Social Responsibility and Environmental Management, 22(1), pp. 32-44. 2015. DOI: https://doi.org/10.1002/csr.1325

[3] Kaplan, R.S., and Norton, D.P., The balanced scorecard: translating strategy into action. Harvard Business Press, 1996.

[4] Margolis, J.D., and Walsh, J.P., Misery loves companies: rethinking social initiatives by business. Administrative Science Quarterly, 48(2), pp. 268-305, 2003. DOI: https://doi.org/10.2307/3556659

[5] Hillman, A.J., and Keim, G.D., Shareholder value, stakeholder management, and social issues: What's the bottom line? Strategic Management Journal, 22(2), pp. 125-139, 2001. DOI: https://doi.org/10.1002/smj.163

[6] Lankoski, L., Corporate governance and corporate social responsibility disclosure: evidence from the EU. Managerial Auditing Journal, 27(6), pp. 532-549, 2012. DOI: https://doi.org/10.1108/02686901211236444

[7] McWilliams, A., and Siegel, D., Corporate social responsibility and financial performance: Correlation or misspecification? Strategic Management Journal, 21(5), pp. 603-609. 2000. DOI: https://doi.org/10.1002/(SICI)1097-0266(200005)21

[8] Sen, S., and Bhattacharya, C.B., Does doing good always lead to doing better? Consumer reactions to corporate social responsibility. Journal of Marketing Research, 38(2), pp. 225-243, 2001. DOI: https://doi.org/10.1509/jmkr.38.2.225.18838

[9] Hooghiemstra, R., Corporate communication and impression management—New perspectives why companies engage in corporate social reporting. Journal of Business Ethics, 27(1-2), pp. 55-68, 2000. DOI: https://doi.org/10.1023/A:1006400707757

[10] Schaltegger, S., and Burritt, R., Corporate sustainability: assessing environmental, social, and economic impacts. Environmental Management, 36(1), pp. 14-26, 2005. DOI: https://doi.org/10.1007/s00267-004-0275-2

[11] Gitman, L.J., Principles of corporate finance. Pearson Education, 2016.

[12] Van-Marrewijk, M., Concepts and definitions of CSR and corporate sustainability: between agency and communion. Journal of Business Ethics, 44(2-3), pp. 95-105, 2003. DOI: https://doi.org/10.1023/A:1023331212247

[13] Sachs, J.D., The age of sustainable development. Columbia University Press, 2015. DOI: https://doi.org/10.7312/sach17314

[14] Horngren, C.T., Datar, S.M., and Rajan, M.V., Cost accounting: a managerial emphasis. 16th ed. Pearson Education, 2018.

[15] Daft, R.L., Management. 12th ed. Cengage Learning, 2015.

[16] Jones, G.R., Organizational theory, design, and change, 8th ed. Pearson Education, 2019.

[17] Wheelen, T.L., and Hunger, J.D., Strategic management and business policy: globalization, innovation and sustainability,15th ed. Pearson Education, 2017.

[18] CarrCarroll, A.B., Brown, J.A., and Buchholtz, A.K., Business and society: ethics, sustainability, and stakeholder management, 10th ed. Cengage Learning, 2018.

[19] Balzarova, M.A., Bamber, C.J., McCambridge, S., and Sharp, J.M., Key success factors in implementing ISO 14001 in the UK. Journal of Cleaner Production, 16(16), pp. 1717-1726, 2008. DOI: https://doi.org/10.1016/j.jclepro.2007.11.036

[20] Epstein, M.J., Buhovac, A.R., and Yuthas, K., Making sustainability work: best practices in managing and measuring corporate social, environmental, and economic impacts, 2nd ed. Greenleaf Publishing, 2014.

[21] Grupo Sura. Quiénes somos, [en línea]. 2024. Disponible en: https://www.gruposura.com/nuestra-compania/sobre-grupo-sura/

[22] Grupo Nutresa. Su historia, [en línea]. 2024. Disponible en: https://gruponutresa.com/quienes-somos/historia/

[23] Davivienda. ¿Quiénes Somos?, [en línea]. 2024. Disponible en: https://www.davivienda.com/wps/portal/personas/nuevo/personas/quienes_somos/sobre_nosotros

[24] Grupo Empresarial Bolívar. Banco Davivienda: Historia y compromiso. [Descripción institucional]. 2024. Recuperado de los documentos corporativos del Grupo Empresarial Bolívar.

[25] Latorre-Guillem, M.Á., Insurance Brokers' behaviour: the effect of policy collection on management decisions. International Humanities Review, 13(3), pp. 1-10, 2022.

[26] Latorre-Guillem, M.A., The customer orientation service of spanish brokers in the insurance industry: The advisory service of the insurance distribution channel bancassurance. Sustainability, 12(7), pp. 2970. 2020.

[27] Ackoff, R.L., The future of operational research is past. Journal of the Operational Research Society, 30(2), pp. 93-104, 1979. DOI: https://doi.org/10.1057/jors.1979.22

[28] Alexander, C., and van 't Hof, S., Managing risk: a framework for risk management, Pearson Education, 2000.

[29] Berman, S.L., Wicks, A.C., Kotha, S., and Jones, T.M., Does stakeholder orientation matter? The relationship between stakeholder management models and firm financial performance. Academy of

Management Journal, 42(5), pp. 488-506, 1999. DOI: https://doi.org/10.2307/256972
[30] Donaldson, T., and Preston, L.E., The stakeholder theory of the corporation: concepts, evidence, and implications. Academy of Management Review, 20(1), pp. 65-91, 1995. DOI: https://doi.org/10.5465/amr.1995.9503271992
[31] Clarkson, M.B.E., A stakeholder framework for analyzing and evaluating corporate social performance. Academy of Management Review, 20(1), pp. 92-117, 1995. DOI: https://doi.org/10.5465/amr.1995.9503271994
[32] Freeman, R.E., Strategic management: a stakeholder approach. Pitman. 1984.
[33] Darnall, N., Ji, H., and Potoski, M., Managing stakeholder influences: the adoption of environmental management practices. Journal of Public Administration Research and Theory, 20(3), pp. 591-615, 2010. DOI: https://doi.org/10.1093/jopart/mup024
[34] Eccles, R.G., and Krzus, M.P., One report: integrated reporting for a sustainable strategy. John Wiley & Sons, 2010. DOI: https://doi.org/10.1002/9781119199964
[35] Elkington, J., Towards the sustainable corporation: Win-Win-Win business strategies for sustainable development. California Management Review, 36(2), pp. 90-100, 1994. DOI: https://doi.org/10.2307/41165746
[36] Esty, D.C., and Winston, A.S., Green to gold: how smart companies use environmental strategy to innovate, create value, and build competitive advantage. John Wiley & Sons. 2009.
[37] Garriga, E., and Melé, D., Corporate social responsibility theories: mapping the territory. Journal of Business Ethics, 53(1-2), pp. 51-71, 2004. DOI: https://doi.org/10.1023/B:BUSI.0000039399.90587.34
[38] Godfrey, P.C., Merrill, C.B., and Hansen, J.M., The relationship between corporate social responsibility and shareholder value: an empirical test of the risk management hypothesis. Strategic Management Journal, 30(4), pp. 425-445, 2009. DOI: https://doi.org/10.1002/smj.750
[39] Orlitzky, M., Schmidt, F.L., and Rynes, S.L., Corporate social and financial performance: a meta-analysis. Organization Studies, 24(3), pp. 403-441, 2003. DOI: https://doi.org/10.1177/0170840603024003910
[40] KPMG International. KPMG International Survey of Corporate Responsibility Reporting 2011. KPMG International Cooperative.
[41] Moneva, J.M., Archel, P., and Correa, C., GRI and the camouflaging of corporate unsustainability. Accounting Forum, 30(2), pp. 121-137, 2006. DOI: https://doi.org/10.1016/j.accfor.2006.02.001
[42] Van Marrewijk, M., Concepts and definitions of CSR and corporate sustainability: between agency and communion. Journal of Business Ethics, 44(2-3), pp. 95-105, 2003. DOI: https://doi.org/10.1023/A:1023331212247
[43] Schaltegger, S., and Burritt, R., Corporate sustainability: assessing environmental, social, and economic performance. Greenleaf Publishing, 2005.
[44] Horngren, C.T., Datar, S.M., and Rajan, M.V., cost accounting: a managerial emphasis, 16th ed. Pearson Education, 2018.
[45] Kaplan, R.S., and Norton, D.P., The balanced scorecard: translating strategy into action. Harvard Business Press, 1996.
[46] Sachs, J.D., The age of sustainable development. Columbia University Press, 2015. DOI: https://doi.org/10.7312/sach17314
[47] Groves, R.M., et al., Survey Methodology. 2nd Edition, Wiley-Interscience, 2009
[48] Fowler, F.J., Improving survey questions: design and evaluation. SAGE Publications, 1995
[49] Dillman, D.A. Internet, Phone, Mail, and Mixed-Mode surveys: the tailored design method. 4th Edition, Wiley, 2014.
[50] Likert, R., A technique for the measurement of attitudes. Archives of Psychology, 140, pp. 1–55, 1932.
[51] Cannell, C.F., and Kahn, R.L., Interviewing. In Lindzey, G., and Aronson, E. (Eds.), The Handbook of Social Psychology, 2nd ed., Addison-Wesley. 1968
[52] Babbie, E., The Practice of Social Research. 12th Edition. Wadsworth Publishing, 2010.
[53] Creswell, J.W., Research design: qualitative, quantitative, and mixed methods approaches. 3rd Edition, SAGE Publications, 2009.
[54] Ackoff, R.L., The art of problem solving: accompanied by Ackoff's Fables. Wiley, 1979.
[55] Bassen, A., and Kovacs, A M., Environmental, social and governance aspects in corporate valuation. International Journal of Business Environment, 2(1), pp. 51-68, 2008.
[56] Mallin, C.A., Corporate Governance, 3rd ed. Oxford University Press, 2010.
[57] Guerrero-Martin, C.A., Fernández-Ramírez, J.S., Arturo-Calvache, J.E., Milquez-Sanabria, H.A., da Silva Fernandes, F.A., Costa Gomes, V.J., ..., and Lucas, E.F., exergy load distribution analysis applied to the dehydration of ethanol by extractive distillation. Energies, 16(8), art. 3502, 2023. DOI: https://doi.org/10.3390/en16083502
[58] Vanegas, P.A.V., Ruiz, T.Y.Z., Macualo, F.H.E., y Martin, C.A.G., Metodología para la formulación de proyectos de recuperación química mediante analogías, 2019. DOI: https://doi.org/10.18273/revfue.v17n1-2019003
[59] Ibañez-Gómez, L.F., Albarracín-Quintero, S., Céspedes-Zuluaga, S., Montes-Páez, E., Ando Junior, O.H., Carmo, J.P., ..., and Guerrero-Martin, C.A., Process optimization of the flaring gas for field applications. Energies, 15(20), art. 7655, 2022. DOI: https://doi.org/10.3390/en15207655

W.A. Guerrero, es Economista, Administrador de Empresas y Contador, Esp. en Finanzas y MSc. en Educación, se desempeña actualmente como instructor técnico y contable en el Servicio Nacional de Aprendizaje (SENA), y docente investigador de la Fundación de Educación Superior San José (Usanjose).
ORCID: 0000-0002-8826-5307

L.E. Guerrero-Martin, es Ing. Ambiental, de la Universidad Distrital Francisco José de Caldas. Actualmente, se desempeña como docente investigadora en la Fundación de Educación Superior San José (Usanjose), donde aplica su amplia experiencia en sistemas de gestión integrados y evaluación de impactos ambientales.
ORCID: 0000-0002-8563-6977

S. Camacho-Galindo, es Abogada, Esp. en Derecho Administrativo. Actualmente se desempeña como Vicerrectora Financiera de la Fundación de Educación Superior San José (Usanjose).
ORCID:0009-0007-2552-8978

J.C. Arévalo, es Ing. de Telecomunicaciones de la Universidad Abierta y a Distancia (UNAD) y cuenta con un Diplomado en Radio Enlaces. Experiencia en empresas contratistas para Ecopetrol. Actualmente, se desempeña como profesor investigador en la Fundación de Educación Superior San José (Usanjose).
ORCID: 0000-0002-8195-5196

F.A. da Silva Fernandes, es Dr. en Ingeniería, Esp. en Ciencia y Tecnología de los Materiales por la Universidade Federal do Rio Grande do Sul (UFRGS), Brasil. Profesor de la Universidad Federal do Pará del Campus Salinópolis.
ORCID: 0000-0003-4718-3230

E. Saldanha Correa, es Dr. en Ciencias Ambientales por la Universidad Federal del Oeste de Pará (UFPOPA) Brasil. Profesor Adjunto de la Universidad Federal de Pará (UFPA).
ORCID: 0000-0002-4162-4296

C.A. Guerrero-Martin, es Ing. de Petróleos de la UIS e Ing. Industrial de la Usanjosé. MSc. en Ciencia y Tecnología de Polímeros (UFRJ) y Dr. en Planeamiento Energético (UFRJ). Profesor de la Universidad Federal de Pará.
ORCID: 0000-0002-5979-8542

DYNA
http://dyna.medellin.unal.edu.co/

UNIVERSIDAD NACIONAL DE COLOMBIA

Cybersecurity in the maritime industry: an analysis of emerging threats and challenges

Alexander Palma-Chipana, Juan Villantoy-Echegaray, Javier Ccapcha-Cabrera & Carlos Neyra-Rivera

Facultad de Ingeniería de Sistemas e Informática, Universidad Tecnológica del Perú, Lima, Perú, U21219084@utp.edu.pe, U20307124@utp.edu.pe, c24878@utp.edu.pe, c29136@utp.edu.pe

Received: July 24th, 2024. Received in revised form: October 7th, 2024. Accepted: November 8th, 2024.

Abstract
The maritime industry faces increasing cyber threats that jeopardize the safety and efficiency of its operations. Therefore, the present study aims to analyze cybersecurity in this industry. We used SCOPUS databases and the PRISMA methodology, applying rigorous inclusion and exclusion criteria to select relevant articles. The results of these articles show that the most common threats include attacks on navigation systems and manipulation of cargo data. The reviewed studies indicate growing concern over insufficient regulations and lack of cybersecurity training. Additionally, it highlighted the need to improve cyber defenses through robust policies and international cooperation. In conclusion, the maritime industry must adopt a proactive and coordinated stance to address these challenges and ensure the resilience of its operations within the digital environment.

Keywords: cyber-attack; cyber-threat; maritime industry; risks; vessels.

Ciberseguridad en la industria marítima: un análisis de las amenazas y desafíos emergentes

Resumen
La industria marítima enfrenta crecientes amenazas cibernéticas que ponen en riesgo la seguridad y eficiencia de sus operaciones. Por ello, el presente estudio tiene como objetivo analizar la ciberseguridad en la industria. Se utilizó la base de datos de SCOPUS y la metodología PRISMA aplicando criterios rigurosos de inclusión y exclusión para seleccionar los artículos relevantes. Los resultados de estos artículos muestran que las amenazas más comunes incluyen ataques a sistemas de navegación y manipulación de datos de carga. Los estudios revisados indican una preocupación creciente por la insuficiencia de normativas y la falta de formación en ciberseguridad. Además, se destaca la necesidad de mejorar las defensas cibernéticas mediante políticas robustas y cooperación internacional. Como conclusión, la industria marítima debe adoptar una postura proactiva y coordinada para enfrentar estos desafíos y asegurar la resiliencia de sus operaciones en el entorno digital.

Palabras clave: buques; ciberataque; ciber amenaza; industria marítima; riesgos.

1 Introduction

La industria naviera lleva consigo un rol importante para el desarrollo económico de los países en cuestión de mejores rendimientos de exportación tal como ocurrió con el crecimiento de exportaciones de Vietnam al permitirle a la empresa naviera Maersk operar en su territorio [1], para la modelización de la agitación marítima como una herramienta importante para ayudar al diseño de obras marítimas [2], para el desarrollo turístico [3,4], para definir la onda de diseño de un proyecto marítimo [5], para la mejora de la ingeniería naval [6] así como también podría tener un impacto en trabajos vinculados al submarinismo [7]. La ciberseguridad juega un rol importante en la resiliencia cibernética de las entidades, por ello, las organizaciones buscaron modelos y marcos de referencia que le ayuden a implementar una gestión de ciberseguridad dentro de sus estrategias [8]. A pesar de los aportes de la industria marítima para la economía de los países hay varias investigaciones que

How to cite: Palma-Chipana, A., Villantoy-Echegaray, J., Ccapcha-Cabrera, J., and Neyra-Rivera, C., Ciberseguridad en la industria marítima: un análisis de las amenazas y desafios emergentes DYNA, 91(234), pp. 157-162, October - December, 2024.

manifiestan que hay problemas en materia de ciberseguridad que se presentan en los diversos sistemas a bordo de los buques y aunque algunas proponen posibles soluciones se requiere de una mayor profundización sobre estos [9-13].

Mientras que los constructores y stakeholders invierten en innovación tecnológica para mejorar las operaciones y la progresiva cimentación e integración de los buques autónomos a los mares aparece una creciente preocupación sobre la seguridad cibernética que compromete el progreso de la industria naviera [9,13]. En este sentido, se necesita de una revisión de toda evidencia y fuentes bibliográficas actuales que ayuden a entender la situación actual de la industria respecto a la seguridad de su infraestructura tecnológica, considerando los riesgos que se pueden presentar, las vulnerabilidades de los sistemas, las soluciones que se han propuesto y las recomendaciones que se han brindado. Existe un reducido número de artículos que tratan el tema de la ciberseguridad dentro de la industria naviera pero en los que existen se destaca la necesidad de mejorar la ciberseguridad marítima desde bases costeras, puertos, barcos y la comunicación satelital, la falta de preparación y sensibilización de la tripulación y agencias internacionales, federales e industriales que realizaron proyectos, investigaciones, guías y estándares de administración de ciber riesgos [14,15]. Actualmente, el problema se agrava considerando que nuevos riesgos y ciberataques se incrementarán a medida que la industria marítima dependa cada vez más de las tecnologías de la información y comunicación (TICs). El éxito de los ciberataques y la materialización de los riesgos en esta industria pueden conducir a catástrofes financieras y ambientales y esto hace incierto la inclusión de buques autónomos que hacen uso del ciberespacio ya que podrían ser más vulnerables a distintos tipos de ciberataques [13].

En la presente investigación, se identificaron revisiones sistemáticas de literatura respecto a la actividad marítima y los retos para la navegación marítima y la integración de barcos autónomos en puertos de contenedores que concluyen en que la industria marítima no es inmune a los ciberataques y que no está preparada para combatir los riegos del uso de sistemas obsoletos a lo que proponen establecer medidas de seguridad e integrar sistemas específicos para el aseguramiento de la navegación [16,17]. Estos hallazgos indican que hay una necesidad de conocer las vulnerabilidades, riesgos y soluciones que nos den un panorama de la situación actual de la industria naviera en ciberseguridad, a lo que se propone realizar una recopilación de estos.

Por lo indicado anteriormente, el objetivo de la presente Revisión Sistemática de Literatura (RSL) es identificar y clasificar las amenazas y desafíos en la ciberseguridad de los buques y agencias navieras y sintetizarlas, haciendo un acercamiento especial hacia los ataques de malware para conocer la naturaleza de estos y apoyar el diseño de soluciones informáticas sobre ciberseguridad que se ajusten a los requerimientos del sector naviero.

2 Metodología

Para el desarrollo de la presente RSL en el periodo 2020-2024 para identificar y clasificar las amenazas y desafíos en la ciberseguridad de los buques y agencias navieras. Para ello se se aplicó la metodología PRISMA [18]. La estrategia de búsqueda se realice en base a la pregunta PICO (Problema, Intervención, Comparador y Resultados) permitiendo realizar una búsqueda más rigurosa en la base de datos seleccionada.

La pregunta de investigación que guio el estudio fue ¿Qué amenazas y desafíos afectan a las operaciones principales de las empresas navieras? En base a la pregunta de investigación se genera la siguiente ecuación de búsqueda: (threats OR menance OR cyberdanger OR cyberrisk OR cybermenance OR cyberattack OR cybervulnerability OR cyberhazard OR cyberintrusion OR cyberperil OR cyberthreat OR cybersecurity OR "information security" OR "cyber defense" OR "cyber protection" OR "digital security" OR "computer security" OR "malicious software" OR "malicious code" OR malware OR "malicious program" OR "malicious script" OR "malicious application" OR "malicious payload") AND (shipping OR shipment OR freight OR carriage OR conveyance OR ship OR vessel OR watercraft OR seacraft OR harbor OR docks OR terminals OR wharve OR marina OR berth OR quay). Dicha búsqueda se realizó en la base de datos Scopus durante los meses de abril-junio del 2024 definiendo los criterios “year, subject area, document type, y open access con los valores 2020 – 2024, Engineering y Computer Science, Article, y All open access y Green”. Para la selección de artículos se establecieron los siguientes criterios de selección:

Criterios de Inclusión: CI-1 Estudios referente a malwares en la industria naviera, CI-2 Estudios que aborden la seguridad tecnológica en la industria naviera, CI-3: Estudios referente a navieras internacionales.

Criterios de Exclusión: CE-1 Estudios provenientes de entornos simulados, CE-2 Estudios de activos afectados diferentes de los procesos principales de las navieras y compañías de cruceros, CE-3 Estudios que se encuentren en un idioma diferente al español e inglés, CE-4: estudios anteriores al año 2020.

Luego de aplicar la ecuación de búsqueda se identificaron 529 publicaciones las que siguieron el diagrama de flujo PRISMA y los criterios de inclusión y exclusión seleccionándose finalmente 6 artículos (Figura 1).

3 Resultados

Los resultados de la presente RSL se han dividido en análisis descriptivo de datos bibliométricos y análisis detallado de las características de interés según el objetivo de la presente investigación.

3.1. Análisis bibliometrico

En la Tabla 1 se resumen los principales datos bibliométricos de las publicaciones identificadas en la temática de estudio. Hasta junio del 2024 solo se identificaron 6 publicaciones que cumplían con los criterios de inclusión y exclusión indicados en la presente RSL. El artículo que tuvo mayor cantidad de citas fue el de Caprolu et al. [24] mientras que el que tuvo menor cantidad de citaciones fue el de Pawelski [20].

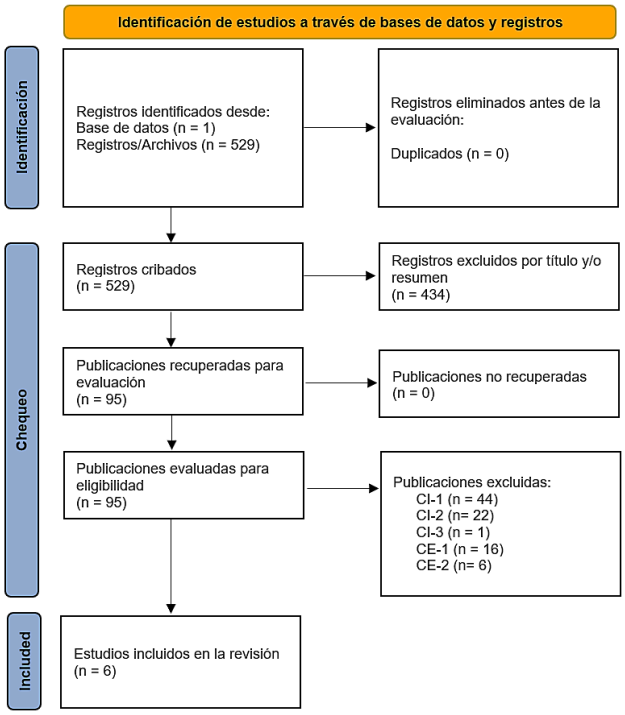

Figura 1. Flujograma PRISMA para la filtración y selección de fuentes. Fuente: [18].

Tabla 1.
Datos bibliometricos de artículos seleccionados

Ref.	Título	Año	Revista	Citas
[19]	Quantifying potential cyber-attack risks in maritime transportation under Dempster–Shafer theory FMECA and rule- based Bayesian network modelling	2024	Reliability Engineering and System Safety	15
[20]	Cyber Threats for Present and Future Commercial Shipping	2023	TransNav	0
[21]	Ensuring Cyber Resilience of Ship Information Systems	2022	TransNav	23
[22]	Discussing cybersecurity in maritime transportation	2022	Maritime Technology and Research	2
[23]	Maritime Cyber(in) security: A Growing Threat Imperils EU Countries	2021	Connections	1
[24]	Vessels Cybersecurity: Issues, Challenges, and the Road Ahead	2020	IEEE Communicati ons Magazine	61

Fuente: Elaboración propia

3.2 Ciber amenazas y ciberataques en sistemas a bordo

Pawelski [20] indica que los barcos actuales llevan consigo una gran variedad de sistemas a bordo y cada uno tiene sus respectivos propósitos. Acerca de los sistemas digitalizados se pueden categorizar en dos grupos, las tecnologías de información y tecnologías de operaciones. Algunas de las redes (sistemas) a bordo de los barcos se encuentran las redes de comunicaciones, los sistemas de control industrial, red y carga y estabilidad, sistemas de seguridad de barcos, sistemas de protección de barcos y sistemas de navegación integrado (INS). Los sistemas AIS (Sistema de Identificación Automática) son vulnerables ante amenazas como accesos no autorizados; spoofing; DoS, por medio de la inundación de la red AIS con sobrecarga de tráfico o interferencia de las señales de radio; o ataques de malware, infectando la red con virus o gusanos, causando la interrupción o destrucción de sistemas y/o datos críticos. Uflaz et al. [19] menciona que los mensajes transmitidos por el sistema AIS son planos y no están encriptados, generando más problemas como técnicas de eavesdropping, inyección de información falsa sobre el tráfico marítimo, y la eliminación y modificación de mensajes. El protocolo de comunicación que usa el sistema AIS no posee propiedades de seguridad como la autenticación y la confidencialidad, y no posee mecanismos de verificación de datos [23,24].

Acerca de los equipos GPS (Sistema de Posicionamiento Global), Bielawski et al. [22], mencionan que son vulnerables ante ataques de spoofing, que consisten en la transmisión de señales GPS falsas para que los receptores a bordo de los barcos reciban información incorrecta sobre el posicionamiento del barco. Uflaz et al. [19] mencionan que otro tipo de ataque es jamming de señales GPS, que consiste en la saturación de las señales GPS con ruido excesivo o interferencia de radio para que los receptores GPS pierdan la señal o la capacidad de obtener información precisa y se identificaron ataques DoS que sobrecargan las señales con tráfico excesivo para interrumpir la navegación y comunicación, y accesos no autorizados, que implican la extracción o modificación de datos críticos como las variables de ubicación, velocidad y curso.

Bielawski et al. [22] estudiaron el ECDIS (Sistema Electrónico de Navegación), siendo un sistema que se encarga de la recolección de información proveniente de varios sistemas instalados en el barco y muestran los mapas digitales para asistir a los oficiales en la navegación. Para hacer uso de estos mapas el sistema necesita estar conectado a internet para poder descargar las últimas versiones más actuales, aunque también se puede hacer uso de dispositivos USB. Es por esta característica que este sistema es vulnerable ante infecciones de malware. Otras amenazas identificadas son los ataques de repudio, tampering, spoofing y DoS. Pawelski [20] encuentra que estos componentes funcionan en computadoras con sistemas operativos comerciales propensos a ciberataques inclusive si están actualizados o protegidos con software anti-malware. Además, se encontró que la mayoría de los sistemas operativos empleados para correr el software de ECDIS, eran antiguos, tales como Windows NT y menciona que el GNSS (Sistema Global de Navegación por Satélite) permite el control de datos de

navegación y mostrar el estado y datos de navegación. Este es el pilar de los INS y que permite el funcionamiento de los demás componentes. En contraste, Caprolu et al. [24], indican que puede ser atacado por métodos de spoofing por medio de SDR'S comerciales, que aprovechan las vulnerabilidades propias del sistema. Las señales legítimas son débiles y los mensajes falsos pueden superponerse, haciendo que los receptores de señal estimen localizaciones falsas. Los ataques de jamming son también otra amenaza que se realiza aproximando dispositivos que emitan ruido en las frecuencias de comunicación GNSS. Este sistema carece de propiedades de seguridad como la confidencialidad, autenticación y disponibilidad.

Bielawski et al. [21] indican que el GMDSS (Sistema Mundial de Socorro y Seguridad Marítimos) es un sistema diseñado para la obtención de asistencia temprana en casos de emergencia. Sus potenciales amenazas son los ataques de repudio, spoofing, tampering y divulgación de información (information disclosure). Según Uflaz et al. [19], otras amenazas identificadas son los accesos no autorizados, DoS, spoofing, y ataque de malware, que consiste en la infección del sistema con software malicioso generando mal funcionamiento o entrega de datos no precisos.

Respecto a los componentes PLC, Pawelski [20] menciona que las primeras generaciones de malware tenían como objetivo a las tecnologías de operaciones OT y se llevaban a cabo en sistemas SCADA basados en Windows, debido a que los componentes PLC fueron considerados por largo tiempo seguros contra malwares, estos eran fabricados con características básicas de seguridad. En pocos años los investigadores descubrieron un hack de PLC que les permitiría obtener información importante y enviarlo por frecuencia de radio originadas por el PLC mismo. También se desarrollaron puertas traseras (rootkits) que se alojan en memorias dinámicas con el que se puede manipular los dispositivos PLC. Con esto se logra afectar el control de los procesos industriales.

Todorov [23] indica que los sistemas ESD (Emergency Shut Down System) sirven para el bloqueo de la gestión de la propulsión y maquinaria del marco en casos de emergencia. Se identificó que su única vulnerabilidad es que es accesible desde la costa.

3.3 Niveles de impacto

Pawelski [20], menciona que los ataques de malware en los sistemas ECDIS pueden hacer que este se vuelva inservible y afectar de la misma manera a los demás equipos conectados debido a la expansión de la infección de malware. Todorov [23] destaca que falta de propiedades de autenticación puede conducir a la alteración de rutas de navegación.

Los ataques dirigidos al componente GPS termina en una mayor dificultad de navegación y compromete la seguridad de la navegación del barco [3].

Si no se logran superar las vulnerabilidades de los sistemas AIS la introducción de los buques autónomos en la industria naviera demorará [9]. Afectan a la confidencialidad, integridad, disponibilidad, posesión, autenticidad y facilidad para la utilización de información, así se pueden generar desviación del curso de los barcos [21]. También puede conducir a la alteración de rutas de navegación [23].

La materialización de las amenazas en GNSS comprometería a los barcos no tripulados, puesto estos dependerían del GNSS, por lo que se haría imposible la inclusión de este nuevo tipo de barcos [9]. Además, las operaciones de estos barcos se verían comprometidos [22].

Pawelski [20] indica que los ataques dirigidos tanto a líneas navieras y compañías que ocurrieron en los últimos años originaron pérdidas financieras a pesar de que las compañías posean profesionales de red e IT, que los problemas en la comunicación pueden repercutir seriamente en las operaciones del barco y acceso a los equipos de OT, y que en caso las tecnologías usadas a bordo no se vuelven lo suficientemente resilientes la introducción de buques autónomos tardará [20]. Según Uflaz et al. [19], otras consecuencias son el incremento de la vulnerabilidad de los sistemas hacia ataques físicos, pérdidas de información comercial o militar valiosa, daño a propiedad, contaminación ambiental y, la pérdida de vidas humanas, incremento de los riesgos de accidentes y colisiones, pérdida de la funcionalidad e incremento de los costos de operaciones y mantenimientos, toma de decisiones equivocadas, disminución de la alerta situacional, y demora en la respuesta a situaciones de emergencia.

3.4 Desafíos identificados

Uflaz et al. [19] revela que los componentes del INS, como el AIS y el GPS son altamente vulnerables y los modos de falla críticos incluyen el spoofing de AIS y GPS así como la manipulación de datos del VDR (Registrador de Datos del Buque).

Pawelski [20] destaca cómo varios componentes de la red de los barcos, como los PLC, que se creían seguros, pueden ser afectados por rootkits indetectables, que los sistemas de navegación críticos como AIS, GPS y ECDIS son susceptibles a ataques de malware, y que pueden propagarse a través de la red de la nave.

Onishchenko et al. [21] enfatizan la falta de atención que las empresas navieras otorgan a la defensa contra ciber amenazas y la filtración de información confidencial, como bajos niveles de conocimiento entre los profesionales a bordo sobre la complejidad de las redes de los barcos, la incapacidad del personal para detectar correos electrónicos de phishing y la mala gestión de los sistemas pueden abrir puertas a los hackers, como conectar un teléfono al terminal ECDIS, permitiendo el acceso a sistemas críticos.

Bielawski [22] discuten que los problemas potenciales asociados con tendencias emergentes en el transporte marítimo como la alta vulnerabilidad de los sistemas AIS, GPS y ECDIS, con este último especialmente propenso a infecciones de malware tanto a través de la red como de conexiones USB, e indican que las amenazas pueden ser indiscriminadas, apuntando a los sistemas sin un objetivo específico, usando técnicas comunes como el malware.

Caprolu et al. [24] señalan la falta de armonización y estandarización en los marcos de ciberseguridad marítima como una vulnerabilidad significativa, indica la necesidad de un código global de ciberseguridad marítima para mejorar la

resiliencia y seguridad, enfocándose en la compartición de información, aumento de la alerta, certificaciones y resiliencia, y resalta la importancia de establecer normas y guías técnicas coherentes para los sistemas de buques.

3.5 Ataques de malware y evidencias

Uflaz et al. [19] mencionan que los ataques de malware son parte de los modos de falla del INS pero no son los más destacados en términos de criticidad ya que sus valores de riesgo y consecuencias son comparables a otros riesgos significativos. Pawelski [20] identificó que los sistemas de navegación como ECDIS son vulnerables a ataques de malware ya que pueden desplegarse a través de la red de la embarcación resultando en consecuencias similares a las que ocurren en sistemas informáticos personales. Onishchenko et al. [21] reportan casos reales donde empresas navieras fueron víctimas de ataques de malware debido a la falta de conocimiento y capacitación del personal y al mal uso de los sistemas como la conexión de dispositivos no autorizados.

Bielawski et al. [22] subrayan la vulnerabilidad de sistemas como AIS, GPS y ECDIS a infecciones de malware, que pueden ocurrir a través de la red o mediante dispositivos USB conectados. Todorov [23] menciona numerosos incidentes de malware en sistemas GNSS, AIS y GMDS1S, indicando que los tripulantes desprevenidos suelen ser la fuente de estos ataques.

4 Discusión

La RSL ha revelado una variedad de desafíos y vulnerabilidades en la ciberseguridad de la industria naviera. A través del análisis de múltiples estudios y artículos se destacan varios puntos clave que merecen ser discutidos en profundidad.

Los sistemas de navegación y comunicación a bordo de los barcos, como AIS, GPS y ECDIS [12], presentan vulnerabilidades significativas. Estos sistemas, que son cruciales para la operación segura y eficiente de los barcos son susceptibles a ataques de spoofing, jamming y malware [20]. Los ataques a estos sistemas pueden resultar en la manipulación de datos críticos, pérdida de señales y en última instancia en la navegación incorrecta o pérdida de control del barco [13]. La investigación muestra que estas vulnerabilidades son consecuencia tanto de la falta de encriptación y autenticación en los protocolos de comunicación así como también del uso de sistemas operativos obsoletos que son más propensos a ser explotados [21].

La creciente digitalización y conectividad de los sistemas de TI y OT a bordo de los barcos han aumentado las vulnerabilidades cibernéticas [19]. La integración de redes y sistemas digitales, mientras mejora la eficiencia operativa, también abre nuevas vías para los ciberataques. El uso de dispositivos USB y la conectividad a Internet para actualizaciones de software son ejemplos de cómo el malware puede introducirse en los sistemas críticos del barco [11]. Este fenómeno se ve exacerbado por la falta de medidas de seguridad robustas y actualizadas en muchos de estos sistemas [16].

La falta de conciencia y capacitación en ciberseguridad entre el personal marítimo es otro desafío crítico identificado [13]. La revisión indica que los profesionales a bordo a menudo no están suficientemente entrenados para identificar y responder a ciber amenazas [14]. Esta falta de preparación puede llevar a errores humanos que facilitan los ciberataques, como la apertura de correos electrónicos de phishing o la conexión de dispositivos no seguros a los sistemas del barco. Por lo tanto, es crucial implementar programas de capacitación y sensibilización que aborden estas deficiencias [13].

La industria marítima no solo enfrenta amenazas actuales, sino también futuras tendencias que pueden agravar las vulnerabilidades existentes. La adopción de buques autónomos, por ejemplo, depende en gran medida de la robustez de los sistemas de ciberseguridad [22]. Sin una ciberseguridad adecuada la operación de estos buques puede estar comprometida poniendo en riesgo no solo las operaciones comerciales sino también la seguridad y el medio ambiente. Las tendencias emergentes en ciberataques también sugieren que los atacantes están desarrollando técnicas cada vez más sofisticadas para explotar las vulnerabilidades marítimas [23].

La falta de regulación y estandarización en ciberseguridad marítima representa un desafío significativo [8]. Aunque existen marcos y guías para la ciberseguridad, la revisión señala la necesidad de un código global y armonizado que establezca estándares claros y coherentes para la protección cibernética en la industria naviera. Un enfoque estandarizado permitiría una mejor coordinación internacional, intercambio de información y respuesta a incidentes, aumentando la resiliencia cibernética del sector.

Los ataques de malware en la industria naviera han demostrado tener un impacto significativo, desde la interrupción de las operaciones hasta pérdidas financieras y daños ambientales [10]. Los estudios revisados documentan casos donde el malware ha comprometido sistemas críticos, resultando en fallos operativos y riesgos para la seguridad marítima. La discusión destaca la necesidad de adoptar medidas preventivas y de respuesta eficaces para mitigar estos riesgos y proteger tanto los activos físicos como digitales de las navieras.

Para futuras investigaciones, sería crucial abordar varias áreas que aún no han sido completamente exploradas. Por ejemplo, sería beneficioso investigar más sobre la efectividad a largo plazo de las soluciones de ciberseguridad implementadas en la industria marítima. Estudios longitudinales podrían proporcionar insights sobre cómo estas soluciones evolucionan con el tiempo y cómo responden a nuevas amenazas emergentes. Además, explorar la integración de tecnologías emergentes como la inteligencia artificial y el machine learning en los sistemas de ciberseguridad marítima podría mejorar significativamente la detección temprana y la respuesta a amenazas avanzadas. También sería crucial investigar más sobre la efectividad y la viabilidad de estrategias de concientización y capacitación en ciberseguridad para el personal marítimo.

5 Conclusiones

Los hallazgos principales indican que los sistemas AIS, GPS y ECDIS son susceptibles a ataques de spoofing, jamming y malware, lo que puede resultar en navegación incorrecta o pérdida de control del barco. La creciente

digitalización y conectividad de los sistemas a bordo han incrementado las vulnerabilidades, facilitando la introducción de malware a través de redes y dispositivos USB. El personal a bordo destaca como una vulnerabilidad importante y que requieren capacitaciones sobre ciberseguridad. Por último, no existe un marco regulatorio global y estandarizado en ciberseguridad marítima, dificultando la coordinación internacional y la respuesta eficaz a incidentes.

Se proporcionar una visión comprensiva de las vulnerabilidades actuales en la ciberseguridad marítima y al resaltar la necesidad de una mayor estandarización y regulación. Se enfatiza la importancia de la capacitación continua del personal y la adopción de nuevas tecnologías para mejorar la resiliencia cibernética.

Referencias

[1] Krase, V., Bente, S., Kowalsky, U., and Dinkler, D., Modelling the stress-deformation behaviour of municipal solid waste, Geotechnique, 61(8), pp. 665–675, 2011. DOI: https://doi.org/10.1680/geot.8.P.140.

[2] Hansen, M., and Wendelboe, M., The role of shipping and logistics MNCs in economic development: a case study of how Maersk contributed to Vietnam's ascendence to an export-oriented economy. Journal of Shipping and Trade, 9(4), pp. 1-30, 2024. DOI: https://doi.org/10.1186/s41072-023-00161-w

[3] Gonçalves, R.S., Camacho, R.F., Lousada, S., Castanho, R.A., Modeling of maritime agitation for the design of maritime infraestructures: the case study of Madeira Archipelago. Revista Brasileira de Planejamento e Desenvolvimento, 7(1), pp. 29-50, 2018. DOI: https://doi.org/10.3895/rbpd.v7n1.7136

[4] Lousada, S., Castanho R.A., The role of ports in tourism: Porto Santo Harbour. Water, 14(19), art. 3176, 2022. DOI: https://doi.org/10.3390/w14193176

[5] Lousada, S., and Castanho, R.A., Port Structures, Maritime Transport, and Tourism. Water, 15, 3898, 2023. https://doi.org/10.3390/w15223898.

[6] Lousada, S.A.N., and Gonçalves, R., Metodologias de determinação de alturas de onda. Dimensionamento de obras marítimas. Novas Edições Acadêmicas, Portugal, 2019, 253 P. ISBN 978-613-9-61105-8,

[7] Lousada, S.A.N., and Hassan, N.M.S., New innovations in engineering education and naval engineering. Ed. IntechOpen, Inglaterra, 2020, 164 P. ISBN: 978-1- 78984-037-7

[8] Lousada, S.A.N., Underwater Work., Ed. Intech Open, Inglaterra, 2021, 88 P. ISBN: 978-1- 78985-229-5

[9] Valkenburg, B., and Bongjovanni, I., Unravelling the three lines model in cybersecurity: a systematic literature review. Computers and Security, 139, art. 103708, 2024. DOI: https://doi.org/10.1016/j.cose.2024.103708

[10] Pawelski, J., Cyber threats for present and future commercial shipping. The International Journal on Marine Navigation and Safety of Sea Transportation, 17(2), pp. 261-267, 2023. https://doi.org/10.12716/1001.17.02.01

[11] Soner, O., Kayisoglu, G., Bolat, P., and Tam, K., Risk sensitivity analysis of AIS cyber security through maritime cyber regulatory frameworks. Applied Ocean Research, 142, art. 103855, 2024. DOI: https://doi.org/10.1016/j.apor.2023.103855

[12] Beradi, D., Giallorenzo, S., Melis, A., Melloni, S., Onori, L., and Prandini, M., Data flooding against ransomware: concepts and implementations. Computers & Security, 131, pp.1-15, 2023. DOI: https://doi.org/10.1016/j.cose.2023.103295

[13] Oruc, A., Kavallieratos, G., Gkioulos, V., and Katsikas, S., Cyber Risk Assessment for Ships (CRASH). TransNav, 18(1), pp. 115- 124, 2024. DOI: https://doi.org/10.12716/1001.18.01.10

[14] Oruc, A., Chowdhury,N., and Gkioulos, V., A modular cyber security training programme for the maritime domain. International Journal of Information Security, 23(2), pp. 1477-1512, 2024. DOI: https://doi.org/10.1007/s10207-023-00799-4

[15] McGillivary, P., Why maritime cybersecurity is an ocean policy priority and How it can be addressed. Maritime Technology Society Journal, 52(5), pp. 44-57, 2018. DOI: https://doi.org/10.4031/MTSJ.52.5.11

[16] Cabuya, D., Alvarado, C., Carrascal, R., Escandón, S., Riola, J., and Fajardo-Toro, C., Ciberseguridad y ciberdefensa marítima: análisis bibliométrico años 1990 – 2021. Risti Revista Iberica de Sistemas r Tecnologias de Informacao, 49(4), pp.197-210, 2022. DOI: https://doi.org/10.17013/risti.43.314-326

[17] Hirata, E., and Hansen, A.S., identifying key issues in integration of autonomous ships in container ports: a Machine-Learning-Based systematic literature review. Logistics, 8(1), pp. 1-15, 2024. DOI: https://doi.org/10.3390/logistics8010023

[18] Androjna, A., Brcko, T., Pavic, I., and Greidanus, H., Assessing cyber challenges of maritime navigation. Journal of Marine Science and Engineering, 8(10), pp. 1-21, 2020. DOI: https://doi.org/10.3390/jmse8100776

[19] Page, M.J., McKenzie, J.E., Bossuyt, P.M., Boutron, I., Hoffmann, T.C., Mulrow, C.D., Shamseer, L., Tetzlaff, J.M., Akl, E.A., Brennan, S.E., Chou, R., Glanville, J., Grimshaw, J.M., Hróbjartsson, A., Lalu, M.M., Li, T., Loder, E.W., Mayo-Wilson, E., McDonald, S., McGuinness, L.A., … Moher, D., Declaración PRISMA 2020: una guía actualizada para la publicación de revisiones sistemáticas. Revista Panamericana de Salud Pública, 46, art. 112, 2020. DOI: https://doi.org/10.26633/RPSP.2022.112

[20] Olapoju, O., Autonomous ships, port operations, and the challenges of African ports. Maritime Technology and Research, 5(1), pp. 1-16, 2023. DOI: https://doi.org/10.33175/mtr.2023.260194

[21] Uflaz, E., Sezer, S., Tunçel, A., Aydin, M., Akyuz, E., and Arslan, O., Quantifying potential cyber-attack risks in maritime transportation under Dempster-Sahafer theory FMECA and rule-based Bayesian network modelling. Reliability Engineering and System Safety, 243, art. 109825, 2024. DOI: https://doi.org/10.1016/j.ress.2023.109825

[22] Onishchenko, O., Shumilova, K., Volyanskyy, S., Volyanskaya, Y., and Volianskyi, Y., Ensuring cyber resilience of ship information systems. TransNav, 16(1), pp. 43-50, 2022. DOI: httpS://doi.org/10.12716/1001.16.01.04

[23] Bielawski, A., and Lazarowska, A., Discussing cybersecurity in maritime transportation. Maritime Technology and Research, 4, art. 252151, 2022. DOI: https://doi.org/10.33175/mtr.2022.252151

[24] Caprolu, M., Di Pietro, R., Raponi, S., Sciancalepore, S., and Tedeschi, P., Vessel's cybersecurity: issues, challenges, and the road ahead. IEEE Communications Magazine, 58(6), pp. 1-8, 2020. DOI: https://doi.org/10.1109/MCOM.001.1900632

[25] Todorov, Y., Maritime Cyber(in) security: a growing threat imperils EU countries. Connections QJ, 20(3-4), pp. 73-93, 2021. DOI: https://doi.org/10.11610/Connections.20.3-4.04

A. Palma-Chipana, es estudiante de último ciclo de la carrera de Ingeniería de Sistemas de la Universidad Tecnológica del Perú.
ORCID: 0009-0001-0992-1805

J. Villantoy-Echegaray, es estudiante de último ciclo de la carrera de Ingeniería de Sistemas e Informática de la Universidad Tecnológica del Perú.
Orcid: 0009-0004-7033-1160

J. Ccapcha-Cabrera, es MSc. en Ing. de Sistemas e Informática con Mención en Tecnologías de la Información. Ing. de Sistemas y Cómputo. Coordinador Especialista en Asistencia y Asesoramiento Tecnológico. Docente tiempo parcial de la carrera de Ingeniera de Sistemas y Redes en la Universidad Tecnológica del Perú.
ORCID: 0000-0003-1713-0648

C. Neyra-Rivera, Dr. en Biología Molecular y Biotecnología. Investigador en el área de Ciencias de la Salud, Ciencias Básicas y Ciencias Forenses. Ha desarrollado proyectos de investigación a nivel nacional (Perú) e internacional y es docente universitario tanto a nivel de pregrado como de posgrado en asignaturas relacionadas con Biología Celular, Bioquímica e Investigación.
ORCID: 0000-0003-1594-4947

DYNA
http://dyna.medellin.unal.edu.co/

UNIVERSIDAD NACIONAL DE COLOMBIA

Analysis of EPS and PVC-U reinforced concrete block for structures

Andy Oblitas-Torres, Wily Yuan Torres-Muñoz, Boris Enrique Oblitas-Gastelo & Fiorela Anaí Fernández-Otoya

Facultad de Ingeniería, Universidad Tecnológica del Perú, Chiclayo, Perú; U20102761@utp.edu.pe, U20102744@utp.edu.pe, C18740@utp.edu.pe, C21106@utp.edu.pe

Received: August 3rd, 2024. Received in revised form: October 11th, 2024. Accepted: October 23th, 2024.

Abstract
Currently, recycling materials is one of the solutions to combat pollution. This research reused EPS (expanded polystyrene) and PVC-U (rigid polyvinyl chloride) in mixtures to manufacture structural concrete blocks, analyzing their behavior in compressive strength. Substitution percentages of 10% and 20% were used, where EPS replaced the fine aggregate and PVC-U replaced the coarse aggregate. The results of physical properties (warping, absorption, suction, dimensional variability) complied with RNE E.070 (National Building Regulations - masonry) and NTP 399.602 (Peruvian Technical Standard - masonry units). The compressive strength of the block with EPS decreased by 14% and 21.63%, while that of the block with PVC-U decreased by 12.69% and 21.79%, but both values remained within the requirements of NTP 399.602.

Keywords: block; concrete; expanded polystyrene; PVC-U y compressive strength.

Análisis del bloque de concreto reforzado con EPS y PVC-U para estructuras

Resumen
En la actualidad, el reciclaje de materiales es una de las soluciones para combatir la contaminación. Esta investigación reutilizó EPS (poliestireno expandido) y PVC-U (cloruro de polivinilo rígido) en mezclas para fabricar bloques de concreto estructural, analizando su comportamiento en la resistencia a la compresión. Se emplearon porcentajes de sustitución del 10% y 20%, donde el EPS reemplazó al agregado fino y el PVC-U al agregado grueso. Los resultados de propiedades físicas (alabeo, absorción, succión, variabilidad dimensional) cumplieron con las normas RNE E.070 (Reglamento Nacional de Edificaciones – albañilería) y NTP 399.602 (Norma Técnica Peruana – Unidades de albañilería). La resistencia a la compresión del bloque con EPS se redujo en un 14% y 21.63%, mientras que la del bloque con PVC-U disminuyó un 12.69% y 21.79%, pero ambos valores se mantuvieron dentro de lo establecido en la NTP 399.602.

Palabras clave: bloque; concreto; poliestireno expandido; PVC-U y resistencia a la compresión.

1 Introducción

El sector de construcción tiene alto consumo en energía y de materias primas, esto genera un importante desperdicio de residuos generados de sus procesos [8]. En las construcciones se generan escombros derivado de las demoliciones del proceso constructivo los cuales no poseen lugares donde puedan verter sus desperdicios por lo que estos van a parar a lugares donde no son para ese fin, estos desperdicios conllevan a la contaminación del suelo y las aguas superficiales, los cuales son problemas ambientales [9]. Por ello, se ha transformado en un problema tanto ambiental como social en todas las ciudades. La necesidad que existe de reciclar esta materia para disminuir la contaminación ambiental es de mucha importancia en la actualidad. Por eso es necesario poder

How to cite: Oblitas-Torres, A., Torres-Muñoz, W.Y., Oblitas-Gastelo, B.E., Fernández-Otoya, F.A., Análisis del bloque de concreto reforzado con EPS y PVC-U para estructuras. DYNA, 91(234), pp. 163-171, October - December, 2024.

reutilizar dichos desperdicios que se generan a diario en nuevas estructuras. En la capital del Perú en promedio al día se generan 19 toneladas de desmonte las cuales van a parar al mar, ríos entre otros lugares [14]. Por otro lado, es importante la reducción de la extracción de agregados debido a que esto disminuiría el impacto al ambiente y el acabamiento de las reservas de los materiales pétreos de las canteras [2]. La demanda de los materiales naturales en la construcción ha aumentado debido a la demanda que se tiene en este sector, lo que está llevando a un desequilibrio ecológico. Por esto existen diversas propuestas de investigaciones que buscan utilizar materiales de desperdicio para la fabricación de unidades de albañilería ecológicos [10].

Existen investigaciones relacionadas al poliestireno como reemplazo para el agregado fino en un bloque de concreto, uno de estos estudios menciona que remplazo el agregado fino por PET (Tereftalato de polietileno) que utilizó para la mezcla de concreto fue de 5%, 10% y 15%; y también remplazo 15% de cemento por cenizas volantes la resistencia a la compresión que obtuvo fue que disminuyo en 34.15%; 52.22%; y 56.53% [4]. Por otra parte, un estudio donde se remplazó 10%, 20% y 30% de agregado fino por plástico PET (Tereftalato de polietileno) en relación con el peso, los resultados que obtuvieron fueron que el adoquín con remplazo del 20% y 30%, la resistencia a la compresión disminuyó en 28.62% y 85.85%, esto debido al abundante plástico presente en la mezcla era considerable, pero en el remplazo del 10% los resultados obtenidos de la resistencia son aceptables [3].

En este trabajo buscamos analizar las propiedades tanto mecánicas y físicas del bloque de concreto, sustituyendo en porcentajes de 10% y 20% al agregado fino y grueso por poliestireno expandido(EPS) y cloruro de polivinilo rígido (PVC-U), se realiza estas sustituciones con el objetivo de disminuir el peso del elemento debido a que ayudaría a su trabajabilidad pero sin experimentar disminución en su resistencia requerida, además que el bloque de concreto cumpla con las normas que lo rigen para su utilización en Perú como es la NTP 399.602 y NTP 399.604. También se realizará una comparación con un bloque patrón el cual está elaborado sin ninguna sustitución de sus agregados.

Tabla 1.
Características químicas del cemento Portland

Ensayos	Tipo	Valor	Unidad	Norma de Ensayo	Resultados
MgO	Máximo	6	%	NTP 334.086	1.7
SO2	Máximo	3	%	NTP 334.086	2.82
Alcalis equivalente	-	-	%	NTP 334.086	0.8
Pérdida por ignición	Máximo	3.5	%	NTP 334.086	2.8
Residuo inoxidable	Máximo	1.5	%	NTP 334.086	0.6

Fuente: Pacasmayo, 2023

2 Materiales y métodos

2.1 Materiales

2.1.1 Cemento Portland

Se utilizo en la presente investigación un cemento Portland de uso general tipo I. En la Tabla 1 se presentan los requisitos químicos [15].

2.1.2 Agregados

En la mezcla de concreto los agregados que se utilizó fueron obtenidos en la región de Lambayeque-Perú.

2.1.3 Poliestireno expandido (EPS)

Es un plástico espumoso que está compuesto por un 98% aire lo cual le brinda el notorio bajo peso que posee, además puede absorber impactos, también es un buen aislante térmico y acústico. Por estas propiedades es utilizado en diversos ámbitos, uno de ellos es la construcción. Para la recolección del material se visitó los desmontes de las construcciones como proceso de reciclaje.

2.1.4 Cloruro de polivinilo rígido (PVC-U)

Es un plástico que se puede mezclar o adherirse a otros materiales, según la fabricación puede tener propiedades flexibles o regidas, lo podemos encontrar en los tubos de fontanería. Para la obtención del cloruro de polivinilo se recurrió a un establecimiento de reciclaje.

2.2 Método

La investigación es de tipo experimental., por ende, se realizaron distintas pruebas de laboratorio para obtener los distintos resultados de la resistencia para luego comparar las resistencias de todas las sustituciones que se realizaron al bloque de concreto respecto a la resistencia de un bloque patrón.

Para su fabricación del bloque de concreto se realizó en una máquina que fabrica este tipo de elemento, para ello se debe de tener las proporciones que se utilizaran de material de agregados y la proporción de agua para una bolsa de cemento la cual tiene un peso de 42.5 kg, debido que estos mismos se mezclaran en al tambor donde después de un tiempo determinado son trasladados por una cinta trasportadora hacia la maquina fabricadora de bloques la cual tiene como capacidad de fabricar 6 bloques por vuelta, según el diseño de mezcla se pueden fabricar 42 bloques por cada bolsa de cemento de 42.5 kg. Para cada combinación se deberá realizar el mismo procedimiento, esto nos dará la cantidad de muestra para poder ensayar.

La máquina utilizada está conformada por cuatro partes, la primera es el almacén donde llega la mezcla de concreto por la cinta trasportadora para el bloque, la segunda es la plancha vibradora la cual al llegar la mezcla vibra para que

esta entre al molde, como tercer parte se tiene el molde del bloque con las medidas de ancho, largo y alto de 12-39-19 cm que corresponde a un bloque de tipo 12, con doble tronco-piramidal centradas los que permiten que se realice los huecos del bloque y como última parte se tiene la compresora el que se encarga de compactar la mezcla para que no queden vacíos en el bloque.

Una vez que el bloque sale del molde se le traslada al patio donde estará en temperatura ambiente por los siguientes días hasta que llegue la edad de ensayo, donde se le estará curando progresivamente para que el bloque pueda llegar a su máxima resistencia. El número de bloques por ensayo por cada porcentaje de sustitución fue 3 para alabeo, absorción, succión y variabilidad dimensional y 30 para cada porcentaje de sustitución para la resistencia a la compresión. La muestra fue de un total de 132 bloques.

Se utilizó combinaciones de dosificación para cada tipo de bloque a fabricar: bloque patrón, bloque con poliestireno expandido 10% y 20%, bloque con cloruro de polivinilo 10% y 20%. Las proporciones que se utilizaron fue en baldes, que podemos observar en la Tabla 2.

Tabla 2.
Diseño de mezcla

Insumos para 6 bloques de concreto	Cantidad		Altura de la lata	
Arena gruesa	1.333	Latas	44	cm
Arena fina	1.333	Latas	44	cm
Agua	8.061	Litros	14	cm
Cemento portland tipo i	7.083	Kilogramos	11	cm = 1/3 lata

Fuente: Elaboración propia.

Figura 1. Modo de fallo de ruptura del bloque de concreto.
Fuente: Autor.

3 Resultados y discusión

3.1 Propiedades físicas

3.1.1 Variabilidad dimensional

La variación dimensional del bloque de concreto se evalúo con respecto a la NTP 399.604 [11], los resultados que se obtuvieron del ensayo se observan en las Tablas 3-7.

Tabla 3.
Bloque patrón

Bloque normal tipo 12	19	12	39
n° bloque de concreto	**Altura (cm)**	**Ancho (cm)**	**Largo (cm)**
1	18.6	12.1	39.3
2	18.7	12	39.4
3	18.9	12.1	39.4
Promedio	18.73	12.07	39.37
Variación dimensional:	1.40%	-0.56%	-0.94%
Norma	-+2%	-+3%	-+2%
	Cumple		

Fuente: Elaboración propia.

Tabla 4.
Poliestireno expandido (EPS) 10%

Bloque normal tipo 12	19	12	39
n° bloque de concreto	**Altura (cm)**	**Ancho (cm)**	**Largo (cm)**
1	19.2	12.1	39.2
2	19.4	12	39.2
3	19.5	12.2	39.2
Promedio	19.37	12.10	39.20
Variación dimensional:	-1.93%	-0.83%	-0.51%
Norma	-+2%	-+3%	-+2%
	Cumple		

Fuente: Elaboración propia.

Tabla 5.
Poliestireno expandido (EPS) 20%

Bloque normal tipo 12	19	12	39
N° bloque de concreto	**Altura (cm)**	**Ancho (cm)**	**Largo (cm)**
1	19.4	12.1	39.2
2	19.2	12.1	39.1
3	19.1	12	39.3
Promedio	19.23	12.07	39.20
Variación dimensional:	-1.23%	-0.56%	-0.51%
Norma	-+2%	-+3%	-+2%
	Cumple		

Fuente: Elaboración propia.

Tabla 6.
Cloruro de polivinilo rígido (PVC-U) 10%

Bloque normal tipo 12	19	12	39
n° bloque de concreto	**Altura (cm)**	**Ancho (cm)**	**Largo (cm)**
1	19	12	39.2
2	18.7	12.1	39.3
3	18.5	12	39.3
Promedio	18.73	12.03	39.27
Variación dimensional:	1.40%	-0.28%	-0.68%
Norma	-+2%	-+3%	-+2%
	Cumple		

Fuente: Elaboración propia.

Tabla 7.
Cloruro de polivinilo rígido (PVC-U) 20%

Bloque normal tipo 12	19	12	39
N° bloque de concreto	**Altura (cm)**	**Ancho (cm)**	**Largo (cm)**
1	18.6	12.1	39.2
2	19.1	12.1	39.3
3	18.8	12	39.3
Promedio	18.83	12.07	39.27
Variación dimensional: (mm)	0.88%	-0.56%	-0.68%
Norma	-+2%	-+3%	-+2%
	Cumple		

Fuente: Elaboración propia.

Tabla 8.
Bloque patrón

N° bloque de concreto	Cara (mm) a	lado 1 (mm) b	Cara (mm) a'	Lado 2 (mm) b'	Promedio (mm)
1	2	2	3	4	2.75
2	3	3	4	3	3.25
3	3	2	3	4	3
			Promedio (mm)		**3.0**
				Norma	**4**
					Cumple

Fuente: Elaboración propia.

Tabla 9.
Poliestireno expandido (EPS) 10%

N° bloque de concreto	Cara (mm) a	Lado 1 (mm) b	Cara (mm) a'	Lado 2 (mm) b'	Promedio (mm)
1	2	4	0	1	1.75
2	1	1	3	2	1.75
3	2	3	2	2	2.25
			Promedio (mm)		**1.9**
				Norma	**4**
					Cumple

Fuente: Elaboración propia.

Tabla 10.
Poliestireno expandido (EPS) 20%

N° bloque de concreto	Cara (mm) a	Lado 1 (mm) b	Cara (mm) a'	Lado 2 (mm) b'	Promedio (mm)
1	1	2	4	2	2.25
2	2	2	3	2	2.25
3	3	3	5	1	3
			Promedio (mm)		**2.5**
				Norma	**4**
					Cumple

Fuente: Elaboración propia.

Tabla 11.
Cloruro de polivinilo rígido (PVC-U) 20%

N° bloque de concreto	Cara (mm) a	Lado 1 (mm) b	Cara (mm) a'	Lado 2 (mm) b'	Promedio (mm)
1	2	3	1	0	1.5
2	1	4	1	3	2.25
3	1	2	2	2	1.75
			Promedio (mm)		**1.8**
				Norma	**4**
					Cumple

Fuente: Elaboración propia.

3.1.2 Alabeo

El ensayo de alabeo se evaluó con respecto a la RNE E0.70 y NTP 399.613 para los bloques que tenían los diferentes porcentajes de sustitución. Los resultados que se obtuvieron se presentan en las Tablas 8-12.

3.1.3 Succión

El ensayo de succión que se realizó a los bloques de concreto teniendo en cuenta la RNE E0.70 de albañilería y NTP 399.602, se pudo obtener los valores que muestran las Tablas 13-17 los cuales están dentro del límite permitido.

Tabla 12.
Cloruro de polivinilo rígido (PVC-U) 20%

N° bloque de concreto	Cara (mm) a	Lado 1 (mm) b	Cara (mm) a'	Lado 2 (mm) b'	Promedio (mm)
1	5	1	2	2	2.5
2	1	2	5	1	2.25
3	3	1	2	3	2.25
			Promedio (mm)		**2.3**
				Norma	**4**
					cumple

Fuente: Elaboración propia.

Tabla 13.
Bloque patrón

N° de bloque de concreto	1	2	3
P. Seco (kg)	12.17	11.92	12.55
P. Seco (gr)	12170	11920	12550
P. Succión (kg)	12.2	11.95	12.58
P. Succión (gr)	12200	11950	12580
Largo (cm)	39.3	39.4	39.4
Ancho (cm)	12.1	12	12.1
Área (cm2)	475.53	472.8	476.74
Succión (gr-200cm2/min)	12.618	12.690	12.585
	Promedio =		**12.631**
		Norma	**<20**
	Cumple		

Fuente: Elaboración propia.

Tabla 14.
Poliestireno expandido (EPS) 10%

N° de bloque de concreto	1	2	3
P. Seco (kg)	11.835	11.485	11.565
P. Seco (gr)	11835	11485	11565
P. Succión (kg)	11.865	11.545	11.595
P. Succión (gr)	11865	11545	11595
Largo (cm)	39.2	39.2	39.2
Ancho (cm)	12.1	12	12.2
Área (cm2)	474.32	470.4	478.24
Succión (gr-200cm2/min)	12.650	25.510	12.546
	Promedio =		**24.604**
		Norma	**<20**

Al momento se asentar los bloques, pasar con brocha a la cara de asentado o rociarlas; para evitar succionar el agua del mortero y perder su resistencia.
Fuente: Elaboración propia.

Tabla 15.
Poliestireno expandido (EPS) 20%

N° de bloque de concreto	1	2	3
P. Seco (kg)	10.965	11	11.25
P. Seco (gr)	10965	11000	11250
P. Succión (kg)	11.09	11.08	11.28
P. Succión (gr)	11090	11080	11280
Largo (cm)	39.2	39.1	39.3
Ancho (cm)	12.1	12.1	12
Área (cm2)	474.32	473.11	471.6
Succión (gr-200cm2/min)	52.707	33.819	12.723
Promedio =		46.503	
		Norma	<20

Al momento se asentar los bloques, pasar con brocha a la cara de asentado o rociarlas; para evitar succionar el agua del mortero y perder su resistencia.
Fuente: Elaboración propia.

Tabla 16.
Cloruro de polivinilo rígido (PVC-U) 10%

N° de bloque de concreto	1	2	3
P. Seco (kg)	11.39	11.83	11.54
P. Seco (gr)	11390	11830	11540
P. Succión (kg)	11.475	11.87	11.58
P. Succión (gr)	11475	11870	11580
Largo (cm)	39.2	39.3	39.3
Ancho (cm)	12	12.1	12
Área (cm2)	470.4	475.53	471.6
Succión (gr-200cm2/min)	36.139	16.823	16.964
Promedio =			16.931
		Norma	<20
	Cumple		

Fuente: Elaboración propia.

Tabla 17.
Cloruro de polivinilo rígido (PVC-U) 20%

N° de bloque de concreto	1	2	3
P. Seco (kg)	11.22	11.265	11.235
P. Seco (gr)	11220	11265	11235
P. Succión (kg)	11.3	11.345	11.315
P. Succión (gr)	11300	11345	11315
Largo (cm)	39.2	39.3	39.3
Ancho (cm)	12.1	12.1	12
Área (cm2)	474.32	475.53	471.6
Succión (gr-200cm2/min)	33.733	33.647	33.927
Promedio =	33.769		
		Norma	<20

Al momento se asentar los bloques, pasar con brocha a la cara de asentado o rociarlas; para evitar succionar el agua del mortero y perder su resistencia.
Fuente: Elaboración propia.

3.1.4 Absorción

Al realizar el ensayo de absorción se toma como consideración la NTP E0.70 [13], donde establece que la absorción de un bloque de concreto debe ser menor que 12%. Como se puede observar en las Tablas 18-22, tanto el bloque patrón como los bloques con sustitución de EPS y PVC-U cumple con la norma.

Tabla 18.
Bloque patrón

N° de bloque	Masa de la muestra seca (kg)	Masa de la muestra húmeda (kg)	Absorción (%)
1	12.17	13.03	7.07%
2	11.92	12.73	6.80%
3	12.55	13.365	6.49%
		Prom=	6.79%
		Norma	<12%
	Cumple		

Fuente: Elaboración propia.

Tabla 19.
Poliestireno expandido (EPS) 10%

N° de bloque	Masa de la muestra seca (kg)	Masa de la muestra húmeda (kg)	Absorción (%)
1	11.835	12.67	7.06%
2	11.485	12.44	8.32%
3	11.565	12.33	6.61%
		Prom=	7.33%
		Norma	<12%
	Cumple		

Fuente: Elaboración propia.

Tabla 20.
Poliestireno expandido (EPS) 20%

N° de bloque	Masa de la muestra seca (kg)	Masa de la muestra húmeda (kg)	Absorción (%)
1	10.965	11.95	8.98%
2	11	11.89	8.09%
3	11.25	12.21	8.53%
		Prom=	8.54%
		Norma	<12%
	Cumple		

Fuente: Elaboración propia.

Tabla 21.
Cloruro de polivinilo rígido (PVC-U) 10%

N° de bloque	Masa de la muestra seca (kg)	Masa de la muestra húmeda (kg)	Absorción (%)
1	11.39	12.395	8.82%
2	11.83	12.63	6.76%
3	11.54	12.45	7.89%
		Prom=	7.82%
		Norma	<12%
	Cumple		

Fuente: Elaboración propia.

Tabla 22.
Cloruro de polivinilo rígido (PVC-U) 20%

N° de bloque	Masa de la muestra seca (kg)	Masa de la muestra húmeda (kg)	Absorción (%)
1	11.22	12.29	9.54%
2	11.265	12.19	8.21%
3	11.235	12.145	8.10%
		Promedio =	8.62%
		Norma	<12%
	Cumple		

Fuente: Elaboración propia.

Tabla 23.
Pesos del bloque de concreto

	Peso seco (kg)	Peso húmedo (kg)	Promedio (kg)	
Bloque patrón	12.213	13.042	12.628	**KG-diferencia**
Eps 10%	11.628	12.480	12.054	**0.573**
Pvc-u 10%	11.587	12.492	12.039	**0.588**
Pvc-u 20%	11.240	12.208	11.724	**0.903**
Eps 20%	11.072	12.017	11.544	**1.083**

Fuente: Elaboración propia.

3.1.5 Peso del bloque de concreto

Respecto al ensayo realizado los resultados obtenidos se muestran que el peso del bloque con poliestireno expandido y PVC-U respecto al bloque patrón disminuye siendo 1.083 kg su máxima disminución, la Tabla 23 muestra los valores.

3.2 Propiedades mecánicas

3.2.1 Resistencia a la compresión

Los valores que se obtuvieron del ensayo de la resistencia a la compresión se observan en las Tablas 24-32 podemos observar la probabilidad de ocurrencia. Además, en las figuras 2-5 se tiene la campana de gauss de cada una de las sustituciones. Los resultados si cumplen con lo establecido en la NTP 399.602 donde se indica que la resistencia mínima de un bloque de concreto de uso estructural debe ser de 75 kg/cm2 [12], sin embargo, se muestra que al sustituir el agregado fino por poliestireno expandido en porcentajes de 10% y 20% la resistencia disminuyo en 14% y 21.63% y al sustituir el agregado grueso por cloruro de polivinilo rígido (PVC-U) en porcentajes de 10% y 20% su resistencia disminuyo en 12.69% y 21.79%. En otro estudio se sustituyó el agregado fino por EPS en 20%, 30%, 40% y 50% tuvo como resultado que se redujo su resistencia has un 64% en el último remplazo [1]. Otro estudio que tiene los mismos porcentajes de remplazo de EPS con 20%, 30%, 40% y 50% sus resultados dieron que la máxima disminución de resistencia fue del 57% con respecto a la muestra [7]. Por otra parte, se sustituyó a la piedra por plástico (PEAD) en porcentajes de 25 y 50 obteniendo como resultado una disminución en peso de 9,7% y 12,02% pero en cambio su resistencia bajo en 29,17% y 48,5% [5]. En cambio, [6] quien realizo un adoquín sustituyendo el agregado fino por plásticos menciona que el porcentaje que se debería de usar debe de estar entre 20% y 30% debido a que con estas cantidades de sustitución la resistencia disminuye en un 20% pero se encuentra dentro de la resistencia mínima.

Tabla 24. Bloque patrón

N° de bloque	Resistencia (kg/cm2)	F (x)
1	142.610	0.068
2	145.430	0.100
3	150.350	0.057
Promedio/media =	**146.130**	

Fuente: Elaboración propia.

Tabla 25.
Bloque - EPS 10%

N° de bloque	Resistencia (kg/cm2)	F (x)
1	87.57	0.002
2	94.495	0.005
3	96.88	0.006
4	99.15	0.007
5	101.42	0.008
6	107.93	0.012
7	109.77	0.013
8	116.545	0.018
9	121.32	0.020
10	122.66	0.020
11	123.02	0.020
12	125.16	0.021
13	125.235	0.021
14	126.76	0.021
15	127.155	0.021
16	128.670	0.021
17	129.150	0.021
18	130.860	0.020
19	133.805	0.020
20	137.135	0.018
21	143.410	0.015
22	144.145	0.014
23	144.880	0.014
24	146.290	0.013
25	147.275	0.012
26	148.260	0.012
27	148.260	0.012
28	149.410	0.011
29	153.940	0.008
30	158.470	0.006
Promedio/media =	**127.634**	
Desv-estandar (kg/cm2)	**19.244**	

Fuente: Elaboración propia.

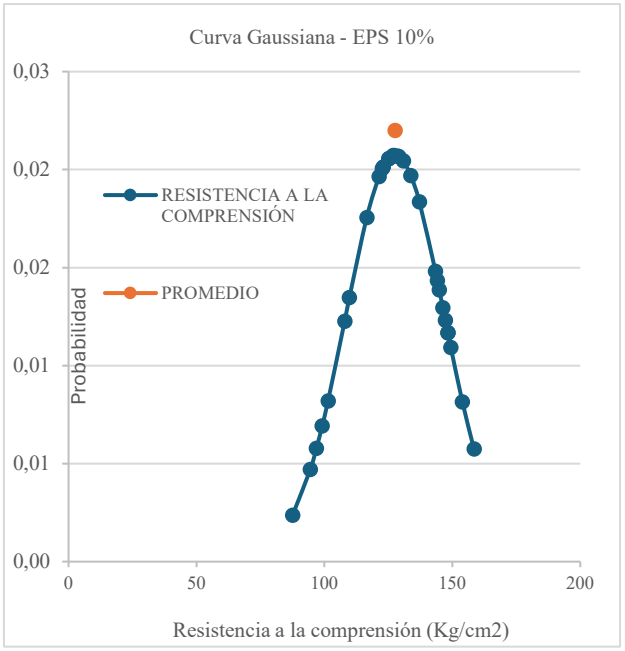

Figura 2. Curva Gaussiana - EPS 10%
Fuente: Elaboración Propia.

Tabla 26.
Probabilidad de ocurrencia EPS-10%

Probabilidad	Resistencia		
68.20%	114.280	a	137.913
95.20%	100.925	a	148.191
100.00%	87.570	a	158.470

Fuente: Elaboración propia.

Tabla 27.
Bloque - EPS 20%

N° de bloque	Resistencia (kg/cm2)	F (x)
1	87.53	0.005
2	90.17	0.007
3	91.55	0.009
4	92.81	0.010
5	99.2	0.019
6	100.025	0.020
7	102.84	0.024
8	106.6	0.029
9	106.695	0.029
10	107.03	0.029
11	107.46	0.029
12	108.5	0.030
13	109.685	0.031
14	110.87	0.031
15	111.9	0.031
16	113.760	0.031
17	114.155	0.031
18	114.200	0.031
19	114.650	0.031
20	115.100	0.030
21	116.375	0.029
22	117.560	0.028
23	120.135	0.025
24	120.850	0.024
25	120.920	0.024
26	121.840	0.023
27	125.170	0.018
28	131.940	0.009
29	133.605	0.007
30	142.040	0.002
Promedio/media =	111.839	
Desv-estandar (kg/cm2)	12.7497	

Fuente: Elaboración propia.

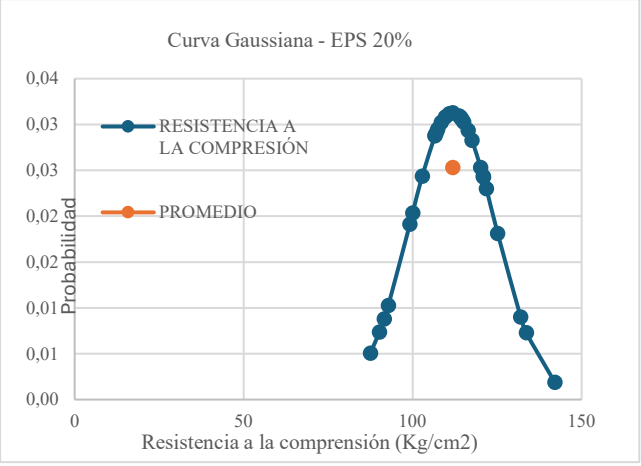

Figura 3. Curva Gaussiana - EPS 20%
Fuente: Elaboración Propia.

Tabla 28.
Probabilidad de ocurrencia EPS-20%

Probabilidad	Resistencia		
68.20%	103.736	a	121.906
95.20%	95.633	a	131.973
100.00%	87.530	a	142.040

Fuente: Elaboración propia.

Tabla 29.
Bloque - PVC-U 10%

N° de bloque	Resistencia (kg/cm2)	F (x)
1	91.98	0.004
2	94.18	0.005
3	96.525	0.006
4	101.07	0.009
5	105.405	0.011
6	111.91	0.016
7	112.52	0.016
8	115.555	0.018
9	116.23	0.018
10	116.63	0.018
11	119.77	0.019
12	120.55	0.020
13	122.51	0.020
14	123.92	0.020
15	125.135	0.021
16	126.755	0.021
17	127.630	0.021
18	129.720	0.020
19	130.040	0.020
20	131.110	0.020
21	132.500	0.020
22	132.680	0.020
23	135.320	0.019
24	139.420	0.016
25	139.615	0.016
26	151.210	0.009
27	156.905	0.006
28	161.530	0.004
29	161.530	0.004
30	162.600	0.004
Promedio/media =	126.415	
Desv-estandar (kg/cm2)	19.3793	

Fuente: Elaboración propia.

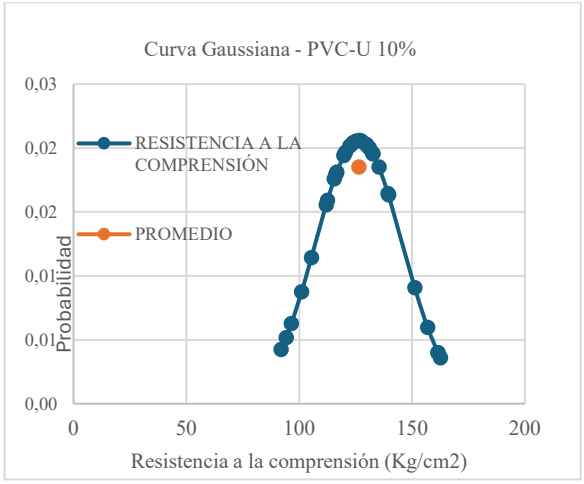

Figura 4. Curva Gaussiana - PVC-U 10%
Fuente: Elaboración Propia.

Tabla 30.
Probabilidad de ocurrencia PVC-U-10%

Probabilidad	Resistencia		
68.20%	114.937	a	138.477
95.20%	103.458	a	150.538
100.00%	91.980	a	162.600

Fuente: Elaboración propia.

Tabla 31.
Bloque - PVC-U 20%

N° de Bloque	Resistencia (kg/cm2)	F (X)
1	96.57	0.006
2	104.07	0.009
3	104.14	0.009
4	105.61	0.010
5	107.08	0.010
6	109.005	0.011
7	110.2	0.012
8	110.985	0.012
9	111.56	0.012
10	113.87	0.013
11	115.85	0.014
12	116.46	0.014
13	117.41	0.014
14	117.8	0.014
15	119.05	0.015
16	120.775	0.015
17	124.620	0.016
18	125.400	0.016
19	130.550	0.016
20	137.765	0.015
21	144.980	0.014
22	145.000	0.014
23	153.270	0.010
24	153.270	0.010
25	154.945	0.010
26	157.775	0.009
27	162.280	0.007
28	170.810	0.004
29	179.340	0.002
30	185.930	0.001
Promedio/media =	130.212	
Desv-estandar (kg/cm2)	24.6177	

Fuente: Elaboración propia.

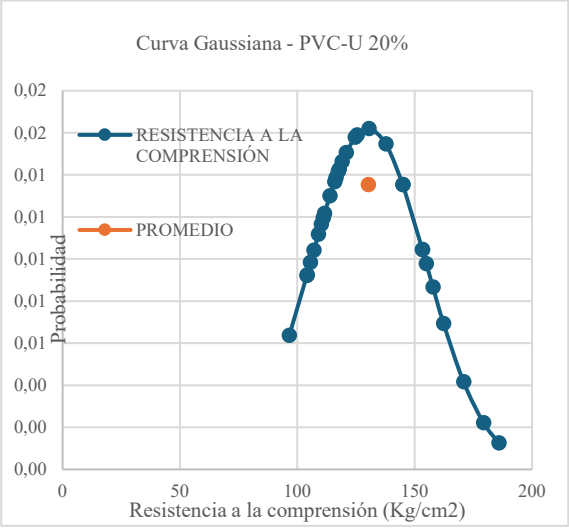

Fig. 5. Curva Gaussiana - PVC-U 20%
Fuente: Elaboración Propia.

Tabla 32.
Probabilidad de ocurrencia PVC-U-20%

Probabilidad	Resistencia		
68.20%	118.998	a	148.785
95.20%	107.784	a	167.357
100.00%	96.570	a	185.930

Fuente: Elaboración propia.

4 Conclusiones

Al sustituir a uno de los agregados por EPS o PVC-U el peso del bloque de concreto disminuye en promedio 900gr con respecto al bloque patrón.

En términos de propiedades físicas y mecánicas, cumplen con todas las especificaciones. Sin embargo, hay una observación en el ensayo de succión por parte del PS en 10% y 20% y por parte del PVC-U en 20%. Por ello, se recomienda humedecer más el lado del asentamiento del bloque de concreto para evitar que succione agua del mortero, lo que evita la pérdida de resistencia del mortero y mejora la adherencia del asentamiento.

La resistencia a la compresión entre el bloque de EPS y PVC-U se observa que la sustitución de estos agregados disminuye su resistencia respecto al bloque patrón, además el bloque con EPS disminuya más su resistencia a comparación del bloque PVC-U.

Se aconseja que en trabajos posteriores de investigación se utilice un aditivo para que la resistencia a la compresión del bloque de concreto no disminuya, de esta manera se pueda sustituir un porcentaje mayor de un material que ayude a reducir el peso del bloque.

Bibliografía

[1] Nurain-Izzati, M.Y., Suraya-Hani, A., Shahiron, S., Sallehuddin-Shah, A., Mohamad-Hairi, O., Zalipah, J., Noor-Azlina, A.H., Mohamad-Nor-Akasyah, W.A., and Nurul-Amirah, K., Strength and water absorption properties of lightweight concrete brick. IOP Conference Series: Materials Science and Engineering, 513, art. 012005, 2019. DOI: https://doi.org/10.1088/1757-899X/513/1/012005

[2] Rakshvir, M. y Barai, S.V., Estudios sobre hormigón a base de áridos reciclados. Waste Management Research, 24, pp. 225-233, 2006. DOI: https://doi.org/10.1177/0734242X06064820

[3] Cabanillas, H.B., Influencia del PET reciclado en la resistencia a la compresión de adoquines convencionales en la ciudad de Trujillo. Tesis de licenciatura. Repositorio de la Universidad Privada del Norte. 2020. Disponible en: https://hdl.handle.net/11537/24147

[4] Fauzan, Zakaria, R.F., Nugraha, D.A.M., and Jauhari, Z.A., The effect of pet and Ldpe plastic wastes on the compressive strength of paving blocks. International Journal of GEOMATE, 24(101), pp. 94-101, 2023. DOI: https://doi.org/10.21660/2023.101.g12250

[5] Mendoza, V., Pérez, C., Rodríguez, M., y Ortiz, S., Bloques de concreto con sustitución de residuos sólidos de polietileno de alta densidad. [en línea]. 2020. Disponible en: https://www.redalyc.org/articulo.oa?id=605772532005

[6] Arif, S., Ovy, S., and Tan, N., Strength of paving block by replacing up to 40% of fine aggregate by weight with plastic waste, E3S Web of Conferences 429, art. 05027, 2023. DOI: https://doi.org/10.1051/e3sconf/202342905027

[7] Suraya, H., A., Nurain-Izzati, M.Y., Sallehuddin-Shah, A., Shahiron, S., Mohamad-Hairi, O., Mohd-Sufyan, A., Mohamad-Luthfi, A.J., Zalipah, J., Mohamad-Nor Akasyah, W.A., and Nurul-Amirah, K., Strength and water absorption properties of lightweight concrete brick containing expanded polystyrene and palm oil fuel ash. IOP

Conference Series: Materials Science and Engineering, 513, art. 012004, 2019. DOI: https://doi.org/10.1088/1757-899X/513/1/012004

[8] Luciano, A., Cutaia, L., Altamura, P., y Penalvo, E., Cuestiones críticas que obstaculizan una práctica generalizada de reciclaje de residuos de construcción y demolición (RCD) en los países de la UE y acciones a emprender: la perspectiva de las partes interesadas. Sostenible Química y Farmacia, 29, art. 100745, 2022. DOI: https://doi.org/10.1016/j.scp.2022.100745

[9] Devaki, H., y Shanmugapriya, S., ACV sobre enfoques de gestión de residuos de construcción y demolición: una revisión. Materiales hoy: Actas, 65(2), pp. 764-770, 2022. DOI: https://doi.org/10.1016/j.matpr.2022.03.286

[10] Ceballos-Medina, S., González-Rincón, D.C., y Sánchez, J.D., Reciclaje de residuos de construcción y demolición (RC&D) generados en la Universidad del Valle Sede Meléndez para la fabricación de adoquines. Revista Ion, 34(1), pp. 27-35, 2021. DOI: https://doi.org/10.18273/revion.v34n1-2021003

[11] NTP 399.604, Unidades de Albañilería. Métodos de muestreo y ensayo de unidades de albañilería de concreto., 1ra ed., Comisión de Reglamentos Técnicos y Comerciales-INDECOPI, [en línea]. 2002. Disponible en: https://es.scribd.com/document/557527189/22136-399-604

[12] NTP 399.602, Unidades de Albañilería|. Bloques de concreto para uso estructural. Requisitos., 1ra ed., Comisión de Reglamentos Técnicos y Comerciales-INDECOPI, [en línea]. 2002. Disponible en: https://es.scribd.com/document/450875231/393015147-NTP-399-602-pdf-pdf

[13] RNE E.070., Albañilería, Reglamento Nacional de Edificaciones, Ministerio de Vivienda, Construcción y Saneamiento, [en línea]. 2019. Disponible en: https://drive.google.com/file/d/15N2ZQwZGegdoui4rrjTR6uq5blTu7uyv/view

[14] León, J.P., En Lima se generan 19 mil toneladas de desmonte al día y el 70% va al mar o ríos. El Comercio Perú. [en línea]. agosto 26, 2017. Disponible en: https://elcomercio.pe/lima/sucesos/lima-generan-19-mil-toneladas-desmonte-dia-70-mar-rios-noticia-453274-noticia/

[15] Pacasmayo. (2023). Cemento Tipo I “Estructural”. [en línea]. Disponible en: https://ecosaco.cementospacasmayo.com.pe/wp-content/uploads/2023/10/FICHA-INFORMATIVA-TIPO-I-.pdf

A. Oblitas-Torres, estudiante del décimo ciclo de la carrera de Ingeniería Civil en la Universidad Tecnológica del Perú, Chiclayo, Perú.
ORCID: 0009-0005-9528-4476

W.Y. Torres-Muñoz, es BSc. en Ingeniería Civil en la Universidad Tecnológica del Perú, Chiclayo, Perú.
ORCID: 0009-0008-1381-0180

B.E. Oblitas-Gastelo, MSc. en Administración de Empresas con mención en Finanzas: Proyectos de Inversión por la Universidad ESAN. Ing. Civil por la Universidad Nacional Pedro Ruiz Gallo de Lambayeque. Auditor en la Contraloría General de la República del Perú desde el 2006. Jefe de OCI en la Municipalidad Provincial de Chiclayo y anteriormente en Zona Registral II - Chiclayo - SUNARP, Gerencia Regional de Salud Lambayeque y Gobierno Regional Lambayeque. Docente de postgrado en la Universidad Cesar Vallejo y Señor de Sipán en Gestión Pública y de pregrado en diversas universidades de Lambayeque como Ingeniería Civil. Ha recibido reconocimientos por su labor destacada y ha participado como ponente en conferencias y congresos sobre control en obras públicas.
ORCID: 0000-0001-6791-4016

F.A. Fernández-Otoya, Dra. en Ciencias de la Educación por la Universidad de Málaga en España. Esp. en Gestión y Didáctica de Programas de Educación a Distancia otorgado por la PUCP. Esp. en Educación Virtual graduada de la UNED en Madrid, España. Esp. en Administración y Planificación de la Educación a Distancia, graduada de la UNAM en México. Esp. en Enseñanza a Distancia por medio de la Red Interamericana de Formación en Educación y Telemática en Canadá. Participa en eventos académicos. Coordinadora Académica para Programas de Formación Continua. Coordinadora del Grupo de Investigación e Informática Educativa y TIC. Consultora externa de Proyectos de Investigación otorgados por el FONDECYT en Chile. Participa en eventos académicos como miembro del Comité Científico. Autora de artículos en revistas científicas. Realiza Estancias de Investigación y Académicas en naciones de Europa, América del Norte y Latinoamérica.
ORCID: 0000-0003-0971-335X

DYNA

DYNA 91 (234), October - December, 2024
is an edition consisting of 100 printed issues
which was finished printing in the month of December of 2024
in Todograficas Ltda. Medellín - Colombia

The cover was printed on Propalcote C1S 250 g,
the interior pages on Propal Beige 90 g.
The fonts used are Times New Roman, Imprint MT Shadow

- Production of hydroxyapatite from phosphoric rock
- Synthesis and evaluation of the antibacterial activity of Cu(II) and Ni(II) complexes with mixed ligands based on glycine and dicarboxylic acids
- Colombian monthly energy inflows predictability
- Relationship between climate variability and mass removal processes. Tunja-Páez case study
- Structure of the production module, production factors and economic performance in Brazilian coffee growth
- Extraction of molybdenite concentrates by leaching
- Virtual tool of nonlinear model of interconnected tanks with PID control implementation using EJsS
- Bibliometric analysis on current ergonomic trends in the international labor context
- Comparative analysis: PVC and concrete panels and traditional masonry
- Numerical simulation of CBR test and HS-Small parameter characterization for Bogotá soils
- Waste-based consumable for hardfacing by welding: a look from the Circular Economy
- Electromechanical flight stabilization system for CubeSat nanosatellites
- Design and fabrication study of a small remote-controlled bionic butterfly flapping-wing flying machine
- Analysis of scientific production on environmental risk assessment in ecosystems with a circular economy
- Use of end-of-life tires for the production of a waterproofing agent as a strategy to promote the circular economy
- Numerical simulation of waste landfill biodegradation: Fitting experimental data
- Trends in the use of biomass for energy generation for a province in the Central Region of Argentina
- Development of financial and administrative management strategies for business sustainability
- Cybersecurity in the maritime industry: an analysis of emerging threats and challenges
- Analysis of EPS and PVC-U reinforced concrete block for structures

- Obtención de hidroxiapatita a partir de roca fosfórica
- Síntesis y evaluación de la actividad antibacteriana de complejos de Cu(II) y Ni(II) con ligandos mixtos basados en glicina y ácidos dicarboxílicos
- Predictibilidad de los aportes mensuales de energía en Colombia
- Relación entre la variabilidad climática con procesos de remoción en masa. Caso de estudio Tunja-Páez
- Estructura del módulo de producción, factores de producción y desempeño económico en el crecimiento del café brasileño
- Extracción de concentrados de molibdenita por lixiviación
- Implementación de una herramienta virtual del modelo no lineal de tanques interconectados con control PID utilizando EJsS
- Análisis bibliométrico sobre las tendencias ergonómicas actuales en el contexto laboral internacional
- Análisis comparativo: paneles de PVC y concreto y albañilería tradicional
- Simulación numérica del ensayo CBR y determinación de los parámetros del modelo HS-Small para los suelos de Bogotá
- Consumible basado en residuales para recargue por soldadura: una mirada desde la Economía Circular
- Sistema electromecánico de estabilización de vuelo para nanosatélites CubeSat
- Estudio de diseño y fabricación de una pequeña máquina voladora biónica de alas batientes de mariposa teledirigida
- Análisis de la producción científica sobre la evaluación de riesgos ambientales en ecosistemas con enfoque de economía circular
- Aprovechamiento de neumáticos al final de su vida útil para la producción de impermeabilizante como estrategia de promoción de la economía circular
- Simulación numérica de la biodegradación en rellenos sanitarios: ajuste de datos experimentales
- Tendencias en el uso de biomasa para generación de energía en una provincia de la Región Centro de Argentina
- Desarrollo de estrategias de gestión financiera y administrativa para la sostenibilidad empresarial
- Ciberseguridad en la industria marítima: un análisis de las amenazas y desafíos emergentes
- Análisis del bloque de concreto reforzado con EPS y PVC-U para estructuras